**Computational and Experimental Study of Two Phase Flow in Pressure**

**Swirl Atomizer**

**By**

Sherry Kwabla Amedorme

BSc, MSc (Mech)

**Submitted in accordance with the requirements**

**for the degree of Doctor of Philosophy**

**UNIVERSITY OF LEEDS**

**School of Mechanical Engineering**

September 2018

The candidate confirms that the work submitted is his own, except where work which has formed part of jointly authored publications has been included. The contribution of the candidate and the other author to this work has been explicitly indicated. The candidate confirms that appropriate credit has been given within the thesis where reference has been made to the work of others.

## ACKNOWLEDGEMENT

## DEDICATION

This work is dedicated to my children Judith, Eugene and Evans Amedorme. To my late parents who had always encouraged and inspired me to do my best in education.

**Section based on jointly authored paper**

1. Amedorme, S. K., & Burluka, A. A. (2017). Numerical Prediction of Sauter Mean Diameter from Pressure Swirl Atomizer using Eulerian Model, International Journal of Engineering and Technology, 7(3), 484-494.

The contributions by the candidate and the co-author to this paper are as follows

The introduction to the paper was written by the candidate in which the existing atomization models and the accompanying difficulties in modelling them were reviewed.

The co-author, A. A. Burluka, developed, reviewed and contributed the new Eulerian model called the $\Sigma - Y_{liq}$ atomisation model to the paper and did the final proofreading.

The choice of numerical procedure in implementing this entirely Eulerian $\Sigma - Y_{liq}$ atomization model in the pressure swirl atomizer using commercial CFD code was written by the candidate.

The results and discussion section which leads largely to the numerical prediction of the droplet Sauter Mean Diameter (SMD) on the spray centre line and radial axis of the pressure swirl atomizer was contributed by the candidate.

The conclusion of the paper was written by the candidate.

2. University of Leeds, School of Mechanical Engineering Poster Event, January 19, 2018, 5th Floor Design Studio (Mech Eng). Poster titled 'Numerical Prediction of Sauter Mean Diameter (SMD) from Pressure Swirl Atomizer using Entirely Eulerian Model'

**ABSTRACT**

Atomizers are used in many engineering applications including spray combustion in furnaces, diesel engines, direct injection petrol engines and gas turbine engines. They are also commonly used in applying agricultural chemicals to crops, paint spraying, food processing and cooling of nuclear cores. Pressure swirl atomizers occupy a special position amongst other atomizers because they differ in quality of atomization, simplicity of construction, reliability and low pumping power requirements. Turbulent mixing of the liquid and gas in these atomizers is indispensable consideration in the process of atomization. This thesis presents a recent Eulerian modelling of two-phase flow in a pressure swirl atomizer using Computational Fluid Dynamics (CFD) STAR-CD code and assesses its capabilities and validation. In this novel $\Sigma - Y_{liq}$ atomisation model, an Eulerian description is applied to solve the two-phase flow assuming both liquid and gas phases as a single continuum with high-density variation at large Reynolds and Weber numbers. The transport equations for the liquid mass fraction and interfacial surface density as well as the average density of the liquid and gas phases are modelled, liquid dispersion correctly captured and their numerical results presented. The results also show atomization characteristics such as droplet velocity and predicted droplet Sauter Mean Diameter (SMD) with reasonable order-of-magnitudes. The predictions show good agreement with experimental results obtained from a laser-diffraction-based drop size analyser (Malvern Spraytec). Different RANS turbulence models are evaluated in order to achieve the best configuration in comparison with experimental measurements and the standard k-ε turbulence model has shown the best performance. Parametric studies were conducted to analyse the influence of the liquid viscosity, surface tension, liquid and gas velocities, liquid and gas densities and pressure on the spray droplet SMD at different locations on the spray centre line and radial distances from the symmetry line of the atomizer. A combination of CFD modeling and the statistical Design of Experiments (DoE) technique known as modified Latin Hypercube Designs (LHD) is applied in order to improve SMD predictions from $\Sigma - Y_{liq}$ atomisation model. With 4-factor DoE, eighty-seven (87) cases were simulated with the variations and combinations in the design variables such as liquid viscosity 0.31 to 200 mPa.s, surface tension 20 to 75 mN/m, nozzle exit orifice diameter 1.5 to 3.5 mm and liquid velocity from 1 to 6 m/s. The results for the SMD at the axial distances along the spray centreline were obtained. Combinatorial optimization was performed to identify and obtain the optimal nozzle exit orifice diameters, operating conditions and fluid properties that give the most minimum droplet (SMD) at the spray centreline. The results show remarkable improvement SMD and new SMD correlation for the model.

# TABLE OF CONTENTS

# LIST OF FIGURES

xi

xiii

## LIST OF TABLES

## NOMENCLATURE

$C_d$     Discharge coefficient

$D$     Drop diameter     m

$d$     Initial jet diameter     m

$D_o$     Nozzle exit orifice diameter     m

$d_{32}$     Sauter mean diameter     m

$D_t$     Turbulent diffusivity

$\dot{m}$     Mass flow rate of liquid     kg/s

$m_{\text{vap}}$     Mean rate of vaporization     kg/s

$N$     Rotational speed     rpm

$Oh$     Ohnesorge number

$r_{eq}$     Equilibrium drop size     m

$Re$     Reynolds number

$Sc_{liq}$     Turbulent Schmidt number

$SMD$     Sauter Mean Diameter     m

$\tilde{u}$     Mean velocity     m/s

$u$     Velocity     m/s

$\check{Y}$     Mean mass fraction of liquid

$W_e$     Weber number

## Greek Symbol

$\bar{\rho}$     Average density     kg/m$^3$

$\rho_l$     Liquid density     kg/m$^3$

$\mu_l$     Liquid dynamic viscosity     Pa-s

$\nu_l$     Liquid kinematic viscosity     m$^2$/s

$\lambda_{opt}$     Optimum wavelength     m

$\sigma$     Surface tension     N/m

$\tau_c$     Turbulence time scale     s

$\theta$     Cone angle     deg

$\bar{\Sigma}$     Mean interfacial surface density     m$^{-1}$

$\Sigma_{eq}$     Equilibrium interface area per unit mass     m$^2$/kg

**Subscripts and Superscripts**

*g*    gas

*l*    liquid

**Abbreviations**

*CFD*    Computational Fluid Dynamics

*DoE*    Design of Experiments

*LHD*    Latin Hypercube Designs

*PSA*    Pressure-Swirl Atomizers

*RANS*    Reynolds Averaged Navier-Stokes

*RSM*    Reynolds Stress Model

*SMD*    Sauter Mean Diameter

# CHAPTER 1 INTRODUCTION

## 1.1 General introduction

Atomizers are used in many engineering applications including spray combustion in furnaces, diesel and direct injection petrol engines, and gas turbine engines. They are also commonly used in applying agricultural chemicals to crops, paint spraying, and spray drying of wet solids, food processing and cooling of nuclear cores. Atomizers are special nozzles designed to produce a rapid break-down of liquid in a two-phase flow. They are used to increase the specific surface area of the fuel and thereby achieving high rate of mixing and evaporation. In most combustion systems, reduction in mean drop size leads to higher volumetric heat release rate, easier ignition, a wide burning range and lower exhaust concentrations of the pollutant emissions. Atomizers are known to affect combustion stability limits, combustion efficiency, smoke generation and carbon monoxide and unburned hydrogen-carbon levels[1, 2].

There are different types of atomizers. Generally, they are classified based on the source of energy used for atomization. These nozzles include jet, swirl and jet-swirl atomizers. Pneumatic atomizers use gas energy for atomization while rotary atomizers break the liquid sheet into particles using mechanical energy. Atomisers using vibration or electric energy include acoustic, ultrasonic and electrostatic atomizers. Within these, pressure driven swirl atomizers occupy a unique operating space due to the quality of atomization, simplicity of construction, reliability of operation, low clogging and low expenditure of energy [3]. They are also the most common type found in the industry [4]. However, the greatest disadvantages of these atomizers are that they require very high injection pressure and consequently low discharge coefficient owing to the fact the air core covers the majority of the atomizer orifice.

Horvay and Leuckel [5] credited the invention of pressure atomizers to Korting in 1902. The atomizer designed by Korting was for use in an oil burner but it could also be used in other applications, such as fire suppression, oil-fired combustors, such as those used in power stations, aerosol nozzles for pharmaceutical and cosmetics, agricultural to administer chemicals such as fertilizers, pesticides and herbicides, spray drying such as in the production of powdered milk, fuel injection systems, and many chemical processes. By now these nozzles have been manufactured from a wide range of materials depending on the applications. These materials include plastics such as

nylon, PVC and Teflon, metals such as brass, stainless steel, tungsten carbide and aluminium, and ceramics such as silicon carbide.

Pressure atomizers have different designs such as plain orifice, simplex, duplex, dual-orifice, fan spray and spill return. Pressure swirl atomizers also called simplex atomizers are the most versatile among them. The basic principle of fluid flow through the swirl atomizer as shown in Figure 1.1 **i**s that, the liquid is introduced through tangential or helical passages into a swirl chamber from which it emerges through an exit orifice with tangential velocity components. As a result of the vortex flow, a hollow air core is formed which is concentric with the nozzle axis. The outflowing thin conical liquid sheet attenuates rapidly becoming unstable and disintegrates into ligaments and then drops in the form of a well-defined hollow cone spray.
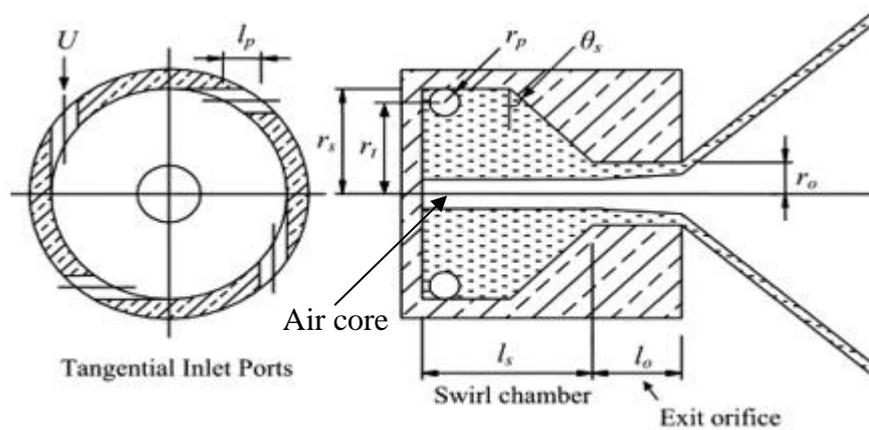


Figure 1.1 Schematic of pressure swirl atomizer[6]

Dombrowski and Hasson [4], Wang and Lefebvre [7] indicated that the motion in the swirl chamber is complex and the mechanisms of flow within the chamber and the resultant spray outside are not fully understood and therefore further research needs to be conducted on this atomizer. This unsatisfactory situation is due to several causes such as the great complexity of the atomisation process, differences in the design, size, and operating conditions of the nozzles tested and the inaccuracies and limitations associated with drop-size measurement techniques. However, the impact of certain geometrical dimensions of swirl nozzles on the sprays produced has been studied by Rizk and Lefebvre [8] and indicates that the pressure swirl atomizer essentially consists of three main elements inlet tangential ports, swirl chamber and exit orifice. The exit orifice is preceded by a swirl chamber with a certain contraction or convergence. The

inlet is one or more cylindrical or rectangular channels positioned tangentially to the swirl chamber. The circular grooves are easier to drill to within specified limits of accuracy, this advantage is outweighed by the practical difficulties in obtaining holes which are truly tangential to the chamber therefore noncircular grooves are preferred in some atomizers [4]. The groove length to width ratio must be sufficiently large to ensure that the liquid enters the chamber tangentially and not as a diffuse flow. However, it must also not be too large since the gain in circulation may be offset by frictional losses. The swirl chamber contains a strong swirl motion of the liquid fuel and the central air core. Study of the swirl effect on the atomization of a liquid sheet has been performed by Rho et al.[9]. In the chamber, a portion of the swirl energy is converted into axial velocity and the liquid flows out of the nozzle in the form of a hollow cone. The exit orifice serves as the discharge outlet for the atomizer and contains holes in which the liquid is discharged. The size of the hole is usually of the order of a tenth of millimetre or less.

Some of the most important parameters in pressure swirl atomizer are the pressure exerted by the fluid on the walls, the axial and the tangential components of the velocity and air core characteristics. These characteristics significantly influence the discharge coefficient at the exit orifice, the mean drop sizes and distribution, the spray cone angle and the liquid film thickness. The influence of injection pressure on spray angle has been investigated by several workers including, De Corso and Kennedy [10], Neya and Sato[11], Ortman and Lefebvre [12], Dodge and Biaglow [13]. The results obtained by De Corso and Kennedy and Neya and Sato show that over a wide range of injection pressures from 0.17 to 2.7 MPa, the equivalent spray angle is an inverse function of the change in pressure. Ortman and Lefebvre also show that starting from atmospheric pressure, increases in liquid pressure cause the spray angle to first widen and then contract. The most common research in a pressure-swirl atomizer is the influence on the mean drop size. Several researchers including Lefebvre and Wang [7], Belhadef et al [14] and Emekwuru et al [15] did extensive works in this regard. They show that the mean drop sizes emanating from the pressure-swirl atomize decrease with increasing pressure. The pressure on the internal walls of the atomizer also influences the swirling motion and the initiation of the central air core. Horvay and Leukel [5] experimentally observed that the pressure in a swirl atomizer is almost constant in the swirl chamber, drops sharply in the contraction zone and further decreases in the exit orifice. The liquid velocity is an essential factor that affects the degree of atomization

3

and primarily depends on the injection pressure and has three components: the axial, tangential and the longitudinal.

The formation of a central air core is one of the important characteristics of the flow in a simplex nozzle. The size of the air core determines the effective flow area at the discharge orifice and thus controls the coefficient of discharge. Som et al [16] determine the influences of nozzle geometry and nozzle flow on the size of the fully developed air core and recognize that below a certain Reynolds number at the inlet to the nozzle, liquid flows full through the nozzle without the formation of an air core while above a certain Reynolds number at the inlet to the nozzle, the formation of a fully developed central air core of cylindrical shape takes place in the nozzle.

The internal characteristics and the nozzle dimensions are not the only factors that govern atomization performance. Liquid properties and ambient gas properties can significantly alter the mean droplet size and distribution. The liquid surface tension and viscosity tend to prevent breakup and instabilities, whereas the gas density will promote instability and breakup due to aerodynamic interaction. The ambient gas into which liquid spray is injected can vary widely in pressure and temperature. This is especially true for liquid fuel-fired combustion systems [17]. The ambient gas density has a strong influence on the mean drop sizes produced by the pressure-swirl atomizer. Not only that it affects the spray angle too such that the spray angle decreases sharply with increase in the ambient gas density until a maximum value of spray angle is reached beyond which any further increase in the ambient gas density does not affect the spray angle. Liquid density, while having a smaller overall effect on the flow can also alter performance as the higher inertia of the liquid phase. In fact, a modest amount of available data on the effects of liquid density on the mean drop size suggests that the influence is quite small [1]. In many respects, the liquid viscosity is the most important liquid property. As pointed out by Lefebvre although in an absolute sense its influence on atomization is no greater than the surface tension, its importance stems from the fact that it does not only affect the drop size and distributions but also the nozzle flow rate and the spray pattern. An increase in viscosity reduces the Reynolds number and also prevents the development of any natural instability in the jet or sheet. The combined effect is that it delays the disintegration of the liquid sheet and increase the size of the droplets in the spray. However, in a hollow-cone nozzle, a modest increase in the viscosity can actually increase the flow rate. It does this by thickening the liquid film in

the discharge orifice, thereby raising the effective flow area. At high viscosities, however, the flow rate diminishes with increasing liquid viscosity [1].

In addition to fluid properties, different instability mechanisms are paramount to the atomization process. These instability mechanisms include the Kelvin-Helmholtz instability arising from the interfacial shear across the liquid-gaseous boundary and the Rayleigh-Taylor instability that forms due to the different densities of the two fluids. The Kelvin-Helmholtz instability mechanisms are prevalent mostly in the primary atomization process while the Rayleigh-Taylor instability model is suitable for predicting the secondary breakup regime. Though these models in some aspects provide reasonable predictions of the liquid atomization, they do not account for the liquid turbulence motion observed in certain sprays. Recent experimental investigations and physical modelling studies have indicated that turbulence behaviours within a liquid jet have considerable effects on the atomization process. Such turbulent flow phenomena are encountered in most practical applications of common liquid spray devices[18].

In Computational Fluid Dynamics (CFD), two-phase flows are commonly modelled using two different approaches: The Eulerian method where the spray is considered a continuum across the whole flow domain and the Lagrangian method where the paths taken by the droplets are tracked through the domain. A combination of an Eulerian k-$\varepsilon$ turbulence model to describe the interaction between droplets and gas phase in the secondary break-up with the Lagrangian method to model the disperse droplet phase was carried out by Lin et al.[19] and Xiong et al.[20] in a non-swirling effervescent atomisation spray. In these related works, the droplet velocity is finally calculated in the spray far field by a one-phase model initially developed for variable density jets.

Within Eulerian methods, the two-phase model solves state equations for each fluid and takes into account the interactions between phases [21, 22]. Drawbacks of this method include the interfacial terms requiring complex modelling and the high number of equations as each fluid is transported. This work focuses on the entirely one-fluid Eulerian model and potentially brings the advantage to compute only the transport of one single fluid with a high-density variation [14]. This entirely Eulerian and general mathematical model developed and presented by Vallet et al [23] called the $\Sigma - Y_{liq}$ atomization model has the potential for all the basic necessary capabilities. It describes the atomization from the first principle. However, its validation is insufficient and has

not been demonstrated well enough in the pressure swirl atomizer at the time being and therefore needs further research and improvement.

## 1.2 The objectives of the research

The aim of this research is to validate and assess the capabilities of the $\Sigma - Y_{liq}$ atomisation model in the pressure swirl atomizer and study the spray parameters, turbulence fields and effects arising in these two-phase flows. This will be achieved through the following objectives

a. To perform numerical studies using STAR-CD code in order to model the effects of spray parameters and turbulence occurring inside the liquid jet to its atomization.

b. To model the interfacial surface density for the liquid and gas for $\Sigma - Y_{liq}$ atomisation model in the STAR-CD code

c. To evaluate the transport equation for the liquid mass fraction and average density for liquid and gas phase for turbulence and flow fields to be generated.

d. To perform qualitative comparisons of the spray parameters, the turbulence and flow fields under varying conditions for the $\Sigma - Y_{liq}$ atomisation model.

e. To measure the droplet Sauter Mean Diameter (SMD) at different axial distances from the hollow-cone nozzle and different radial distances from the spray centreline using a laser-diffraction-based drop size analyser (Malvern Spraytec).

f. To compare the measured droplet sizes to the predicted values of the droplet Sauter Mean Diameter (SMD) in order to validate the $\Sigma - Y_{liq}$ atomisation model.

g. To perform parametric studies in order to assess the capabilities of the $\Sigma - Y_{liq}$ atomisation model.

h. To perform optimization technique in order to identify the optimal nozzle exit design parameter, operating conditions and fluid properties that perform at or give the most minimum drop sizes (SMD) at the spray centre line.

i. To establish a SMD correlation for the model and compare it to the existing correlations.

## 1.3 The thesis outline

This thesis is organized into eight chapters. The introduction, which is the subject of chapter one, consists of the background, the specific objectives which the research seeks to achieve and the organization of the report. Chapter two contains the review of atomization mechanisms, numerical atomization modelling techniques, theoretical and experimental research into pressure swirl atomizer as well as the turbulence modelling techniques. The atomization model and computational fluid dynamics techniques used in modelling sprays in the Star-CD software code are described in chapter three. Chapter four presents the experimental methods and techniques for measuring mean drop sizes in the sprays emanating from pressure-swirl atomizer using Malvern Spraytec. Chapter five focuses on the computational analysis of the results where the qualitative comparisons of flow and turbulence fields are evaluated. This chapter also presents the numerical prediction of the droplet Sauter Mean Diameter on the spray centre line and radial positions. The experimental result analyses are performed in chapter six and chapter seven compares the numerical and experimental results in order to validate the $\Sigma - Y_{liq}$ atomisation model. Parametric studies are also undertaken in chapter seven in order to assess the capabilities and influence of spray parameters, operating and fluid properties on the droplet Sauter Mean Diameter (SMD). This chapter also presents the optimization techniques carried out on the nozzle and the model in order to identify the most minimum and optimal droplet Sauter Mean Diameter at the spray centre line. In addition, this chapter also undertakes an in-depth description of the reationship between the Design of Experiments (DoE) and the resulting droplet Sauter Mean Diameter (SMD). Chapter eight gives the detailed discussions and conclusions of the study and also summarises the overall assessment of the model.

# CHAPTER 2 LITERATURE REVIEW

## 2.1 Introduction

Atomizers have many applicable uses in internal combustion engines, agricultural and chemical processes. Most of these engineering applications and processes require two-phase flow and thus require the dispersion of liquids into a gaseous medium. The liquid fuels used in these processes have relatively low volatility and therefore could not achieve the required combustion in these systems. Therefore, atomizers are required to break the liquid fuels into fine droplets in order to achieve easier evaporation and efficient combustion as well as reduce the pollutants in the exhaust emissions [7]. Most atomizers achieve these through various complex processes and stages but largely it is due to a high relative velocity or the interaction between the liquid and surrounding gas phase. Numerous atomizers are in use but the most widely used is the pressure swirl atomizer which is designed to produce a hollow cone spray [1].

## 2.2 Atomizer classification

Many types of atomizers are used in practice such as pressure atomizers, rotary atomizers and twin-fluid atomizers. Others are electrostatic, acoustics, ultrasonic atomizers [24]. Lefebvre [17, 25] summarized that the ideal atomizer should possess the following characteristics: 1.Ability to provide good atomization over wide ranges of fuel rates, 2. Provide rapid response to changes in fuel flow rates 3. Freedom from flow instabilities, 4. Low power requirements 5. Capability for scaling to provide design flexibility 6. Low cost, light in weight, ease of maintenance, and ease of removal for servicing, 7. Low susceptibility to damage during manufacture and installation, 8. Low susceptibility to blockage by contaminants in the fuel and to carbon build up on the nozzle face 9. Low susceptibility to gum formation by heat 10. Uniform radial and circumferential fuel distribution.

## 2.3  Pressure atomizers

Pressure atomizers utilise the pressure energy in the liquids and convert it into the kinetic energy by subjecting the liquid to a high applied pressure through a small orifice. This creates a relatively high velocity between the liquid and the surrounding gas and makes the liquid sheet disintegrates into ligaments and then to droplets. In terms of the direction to which the liquid is fed into the swirl chamber, pressure

atomizers can be classified as axial and tangential flow designs. The tangential designs are also called the "true" swirl atomizer because no special insert is used and liquid flows directly into the swirl chamber. On the other hand, the axial design requires the swirl insert for the liquid flow so that swirling motion can be created in the chamber. The schematic diagrams for both designs are shown in Figure 2.1(a) and (b) [26]. Pressure atomizers include plain-orifice, pressure-swirl (simplex), square spray, duplex, dual orifice, spill return and fan spray nozzles as shown in Figure 2.2 [17]. Plain-orifice atomizer shown in Figure 2.2a discharges liquid from a circular hole into the surrounding air and has narrow spray cone angles of about 10° which are disadvantageous for many spraying applications. The difficulties in keeping liquids free from impurities limit the minimum exit orifice to around 0.3mm and the maximum depends on the applications. The pressure swirl nozzle which has much wider cone angles of between 30° to 150° achieve these spray angles by imparting a swirling motion to the liquid in the swirl chamber. As the centrifugal force increases, it discharges from the exit orifice as an annular liquid sheet and spreads radially outward to form a conical spray which is disintegrated into ligaments and then into droplets. A full cone design can also be achieved by either using axial jet or other devices to introduce droplets into the core of the conical sprays. The hollow cone spray is more often used than the full cone because of its ability to create finer and small droplets. Pressure-swirl atomizers (PSA) shown in Figure 2.2b have the following advantages inter alia; they are simply constructed, low cost, require small amount energy for atomization and have high reliability. A problem with this nozzle is that it has a wide dispersion of droplet size [1, 26].
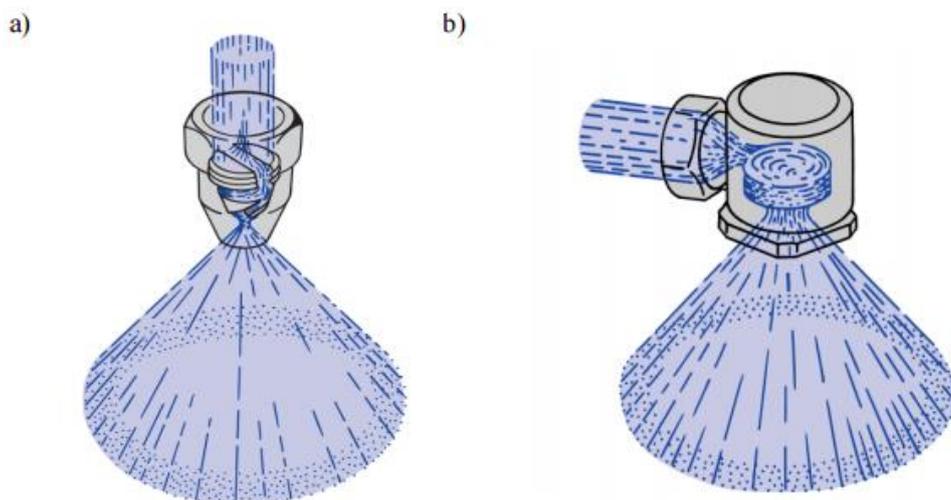


Figure 2.1 a) Schematic of (a) axial  and (b) tangential flow atomizers [26]

Another disadvantage is an exponential relation between the liquid flow rate and the injection pressure. That is before the liquid flow rate can be doubled it requires a fourfold increase in the injection pressure. However, since pressure swirl nozzles are designed to operate within certain pressure regimes, this invariably affect the choice of liquid flow rate for a given pressure atomizer. This basic limitation necessitated the development of various "wide range" of pressure atomizers which can accommodate maximum to minimum flow rate ratio in excess of 20 with good quality atomization without impractical limitations imposed by the injection pressure. The dual-orifice nozzle shown schematically in Figure 2.2c, is one of the most common wide range atomizers and are mostly used in aircraft and industrial gas turbines. This atomizer basically consists of the combination of two simplex nozzles fitted concentrically inside each other designated primary and secondary nozzles. The primary nozzle which has small flow passages allows low liquid flow rate through it and gives better and quality atomization since high injection pressure is required. When a maximum pressure is reached due to the increase in the flow rate a pressurizing valve opens and allows liquid through the secondary nozzle. The liquid flow rate requires in the secondary nozzle is high due to large orifices compared to the primary nozzle passages without excessively using high injection pressures [1].
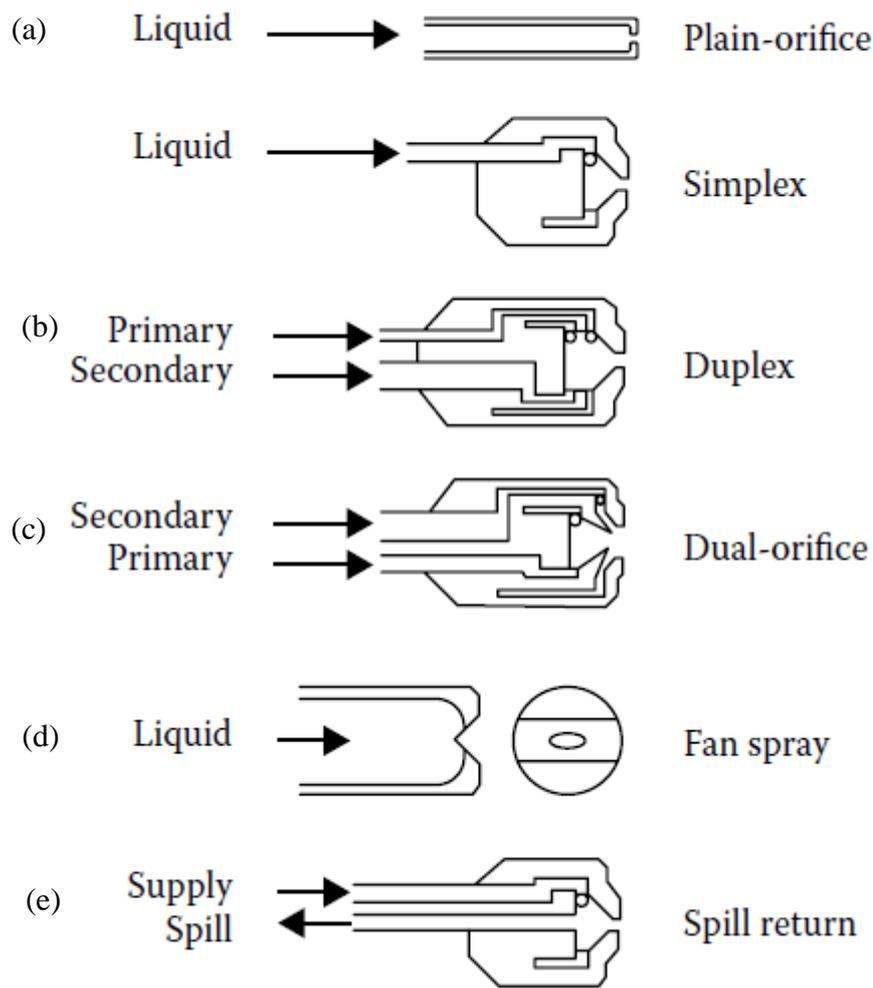
Figure 2.2 Classification of pressure atomizers [1]

## 2.4 Atomization mechanisms

This involves the process in converting a bulk liquid into either jet or sheet and its disintegrating into ligament and then into drops as well as the mechanisms underpinning the growth of disturbances on the liquid sheet. This process affects the shape, structure and penetration of the resulting sprays as well as its droplet velocity and size distribution. The geometrical size, physical properties of the liquid and gaseous medium, turbulence in the liquid and cavitation in the nozzle all have strong influence on these atomization characteristics. The relevant liquid properties to atomization are surface tension, viscosity and density [27-29]. The surface tension and viscosity tend to have a consolidating influence on the sprays as against the disruptive actions of the various internal and external aerodynamic forces on the sprays. Basically, atomization occurs when the disruptive forces just exceed the stabilizing surface

11

tension forces. The initial large droplets produced at this stage are unstable and undergo further break-ups into small droplets which is called secondary atomization. Thus atomization mechanism encompasses the process leading to the initial large droplet which is the primary atomization and the secondary atomization [1].

### 2.4.1 **Non-dimensional Parameters of Atomization**

In order to analyse liquid flows having an interface between two fluids some parameters are used to define its nature and atomization properties. To predict the influence of each atomization mechanism, it has been found that the momentum flux ratio provides a good estimation for atomization rate [30].

For incompressible flows the momentum flux ratio is written as

$$M = \frac{\rho_l V_l^2}{\rho_g V_g^2}$$

where g and l refers to the gas and liquid respectively, $\rho$ is the density and V the velocity.

Additional non-dimensional parameters in the description of the primary atomization are the fluids Reynolds number.

$$Re_l = \frac{\rho_l V_l D_c}{\mu_l}$$

where $D_c$ is the characteristic length and is usually taken as the diameter of the nozzle and $\mu_l$ the dynamic viscosity of liquid.

The influence of the surface tension effects on the liquid surface also play an important role in the atomization mechanics. Due to this, the Weber number is also commonly employed:

$$We = \frac{\rho_l V_l D_c}{\sigma}$$

where $D_c$ is the characteristic length and is taken as the diameter of the droplets for a dispersed phase description and $\sigma$ is the surface tension of the fluid.

Ohnesorge number (Oh) on the other hand relates the viscous forces to the inertial and surface tension forces. It is given according to the relation as

$$Oh = \frac{\mu_l}{\sqrt{\rho_l \sigma D_c}}$$

2.4.2 **Breakup of liquid jets**

The phenomenom of jet break up has been a subject of research for decades. The earliest studies on jet disintegration were those of Plateau and Rayleigh at low Reynolds numbers [31]. Rayleigh studied theoretically the breakup of laminar liquid jets issuing from a circular orifice and concluded that all disturbances on the jet with wavelengths greater than the circumference will grow and that breakup occurs when the fastest growing disturbance attains an optimum wavelength $\lambda_{opt}$ of 4.51d, where d is the initial jet diameter shown by Figure 2.3 and Figure 2.4a.
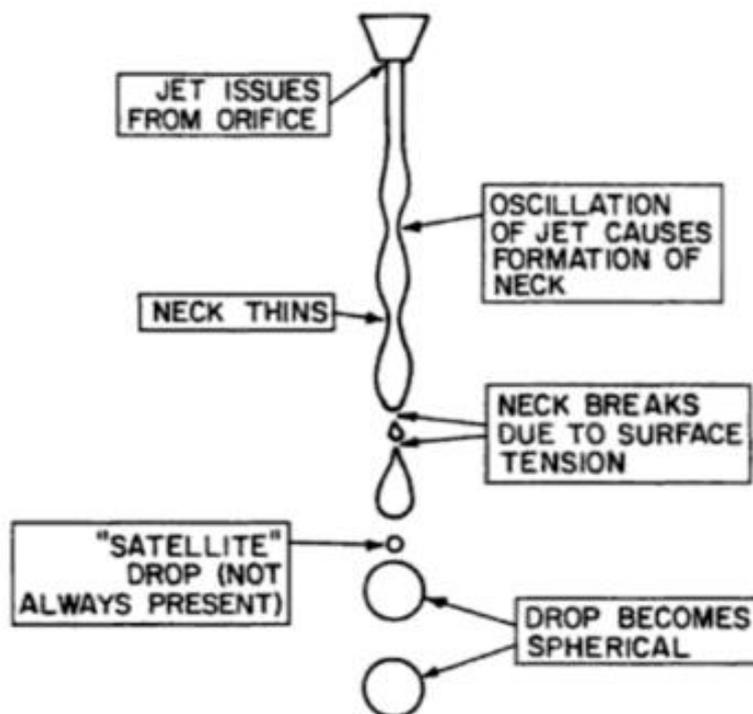


Figure 2.3 Droplet breakup of plain circular jet [17]

After break-up, the cylinder of length *4.51d* becomes a spherical drop, so that

$$4.51d \times (\pi/4)d^2 = (\pi/6)D^3$$

and the drop diameter, *D*, is obtained as

13

$$D = 1.89d$$

Weber [32] later examined Rayleigh's work to include the effect of air resistance on the disintegration of jets into drops and found that the air friction reduces the optimum wavelength $\lambda_{opt}$ and the minimum wavelength $\lambda_{min}$ for the drop formation. For zero air velocity he found that $\lambda_{opt} = 3.14d$ and $\lambda_{min} = 4.44d$ and at relative velocity of 15 m/s, the optimum and minimum wavelengths were found to be $\lambda_{opt} = 2.2d$ and $\lambda_{min} = 2.8d$ respectively with the drop diameter reducing from $1.88d$ to the value of $1.61d$. Weber also examined liquid viscosity on the jet break and found the maximum wavelength $\lambda_{opt}$ to be

$$\lambda_{opt} = 4.44d(1 + 3Oh)^{0.5}$$

where Ohnesorge number $Oh$ $\mu_l$= liquid viscosity, $\rho_l$= liquid density, $\sigma$ = surface tension, $d$ = initial jet diameter.

In terms of relative velocity between the jet and the surrounding air in generating the wave motion, low relative velocities cause the droplets to disintegrate into a fairly uniform drops which are far larger than the initial jet diameter as shown Figure 2.4a. At higher jet velocities, break up is caused by the oscillations or waviness of the whole jet with respect to the jet axis shown in Figure 2.4b. At even higher velocities, due to the enhanced interaction between the surface of the jet and the surrounding air, the waves become detached from the surface to from ligament and subsequently into drops as illustrated in Figure 2.4c. As the jet velocity increases, the diameter of the ligaments decreases. When they collapse, smaller droplets are formed in accordance with Rayleigh's theory [17].



(a) Rayleigh mechanism

(b) Sinuous

(c) Surface breakup
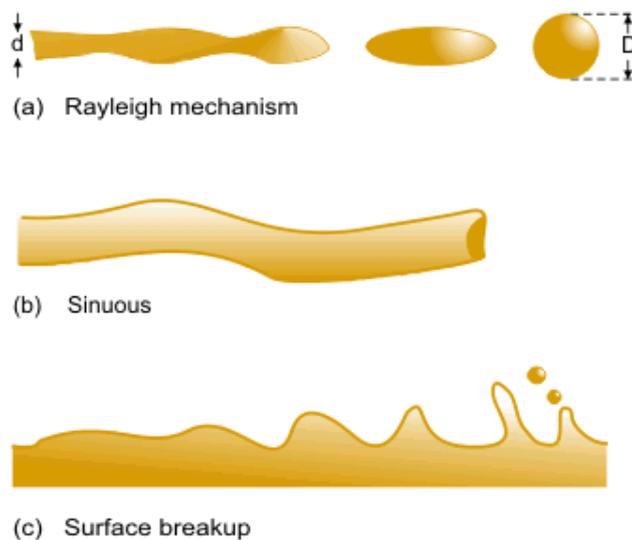
Figure 2.4 Breakup of liquid jets [1]

### 2.4.3 **Regimes of liquid jet break-up in pressure-assisted atomisation**

Four major different regimes for round liquid jet break-up in ambient or stagnant gases have been considered which are normally referred to as (with increasing jet Reynolds number from 1 to 4):

1. Rayleigh break-up regime

2. First wind-induced regime

3. Second wind-induced regime

4. Atomisation or spray regime

The Rayleigh regime can be observed when a liquid jet of diameter $D_l$ and velocity $u_l$, is injected into a stagnant gas, if the jet diameter is small and the jet Reynolds' number $Re_l = \rho_l u_l D_l / \mu_l$ is of the order $10^2$. However, the maximum possible Reynolds number for this regime is dependent upon the Ohnesorge number $Oh = \mu_l / (\rho_l \sigma D_l)^{1/2}$ shown in Figure 2.5 Boundaries of four different jet disintegration regimes based on Reynolds and Ohnesorge numbers according to Reitz [35]. where $\mu_l$, $\rho_l$ and $\sigma$ are the liquid viscosity, liquid density and the surface tension respectively. The drops formed are larger than the jet diameter. At larger Reynolds numbers the jet shape becomes irregular and wavy. This regime is known as the non-axisymmetric Rayleigh break-up or the first wind-induced regime. These drop sizes equal approximately the jet diameter.

Further increasing the Reynolds number leads to a stage where the shear stresses at the liquid jet surface induced by mean velocity difference between the jet and the ambient gas, and also by the turbulent eddies in both the gas and the liquid start to detach some droplets from the jet surface. This regime is called the second wind-induced regime and drops are smaller than $D_l$. This is where break-up is taking place under the influence of both 'waves and instabilities' and 'turbulence and mean flow shear'. Further increase in Reynolds numbers around $10^5$ leads to full atomisation of the jet [33, 34]. This is known as spray or atomisation regime. Drop sizes in this regime are much smaller than $D_l$. The limits and transition criteria for these regimes based on Reynolds and Ohnesorge numbers are given in Figure 2.5 from Reitz as straight lines in a log-log scale of the parameter space of Ohnesorge and Reynolds numbers. However, it should be noted that these limits are not definitive and they are only indicating approximate regions for the parameter space of Oh-Re. An illustration of the jet shape and the break-

up process for each of the aforementioned four regimes is given in the schematics of Figure 2.6.
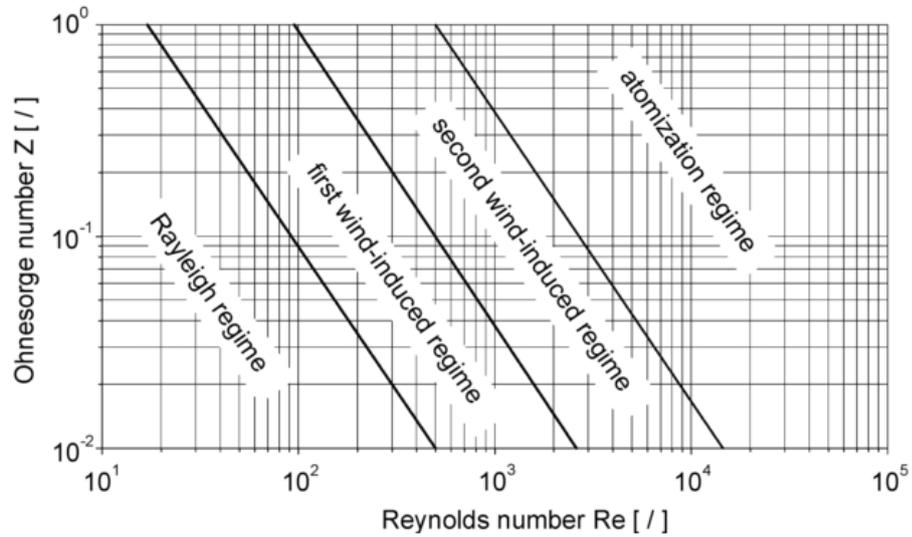


Figure 2.5 Boundaries of four different jet disintegration regimes based on Reynolds and Ohnesorge numbers according to Reitz [35].
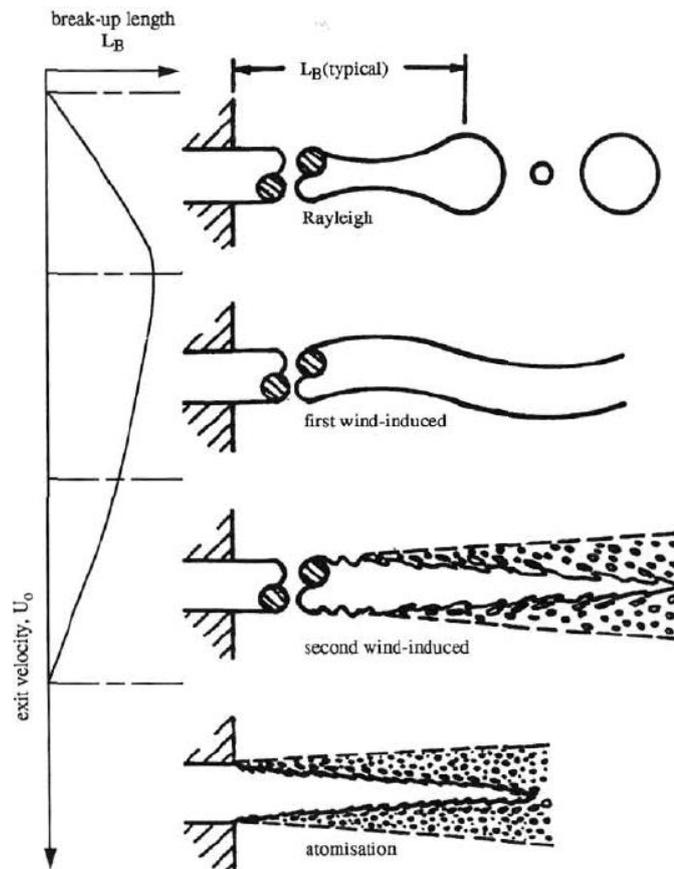


Figure 2.6 Liquid jet shape and qualitative variation of the break-up length in the four jet disintegration regimes with increasing velocity [35].

The same classification of the regimes with their boundaries defined by Weber and Ohnesorge numbers are given in Table 2.1 with the criteria for evaluating the nature of cylindrical liquid jet break-up regimes. The values of the gaseous Weber number, $We_G$, liquid Weber number, $We_L$, and Ohnesorge number, $Oh$, should be calculated to evaluate the Rayleigh and first-induced regimes. However, the gaseous Weber number, the liquid-to-gas density ratio, and the Taylor parameter, T, are involved in the second wind-induced and atomization regimes. These numbers are as follows.

$$We_L = \frac{\rho_l u_l^2 D}{\sigma}, We_G = \frac{\rho_g u_l^2 D}{\sigma}, Re_L = \frac{\rho_l u_l D}{\mu_l}, Oh = \frac{\mu_l}{\sqrt{\rho_l \sigma D_c}}, T = \frac{\rho_l}{\rho_g}\left(\frac{Re_L}{We_G}\right)^2$$

$\mu_l$ is the liquid dynamic viscosity, $u_l$ is the liquid average velocity, $\sigma$ is the surface tension coefficient, $D$ is the nozzle diameter, and $\rho_l$ and $\rho_g$ are the liquid and gas densities respectively.

Table 2.1. Criteria used in evaluating the regimes of cylindrical liquid jet breakup [35-39].

| Break-up regime | Criteria |
|---|---|
| Dripping regime | $We_L < 8$ |
| Rayleigh regime | $We_L > 8, We_G < 0.4 \ or \ 1.2 \ + 3.41 Oh^{0.9}$ |
| First wind-induced regime | $1.2 \ + 3.41 Oh^{0.9} < We_G < 13$ |
| Second wind-induced regime | $13 < We_G < 40.3$ |
| Atomization regime | $40.3 < We_G$ $$\frac{\rho_g}{\rho_l} > \frac{(\sqrt{A} - 1.15)}{744} f(T)^{-2}, f(T)$$ $$= \frac{\sqrt{3}}{6}[1 - \exp(-10T)]$$ |

The boundaries are mostly straight lines of constant Weber numbers unless for transition from Rayleigh to wind-induced regime where according to two different

correlations two boundaries of $We_G = 0.4$ or $We_G = 1.2 + 3.41Oh^{0.9}$ with $Oh < 0.4$ can be considered. According to Besheshti [40] transition between the first and second wind-induced regimes cannot be easily defined with these two parameters. Transition to atomisation regime is gradual and according to two different correlations the criterion for this transition is $We_G < 13$ and $We_G < 40.3$.

### 2.4.4 **Liquid sheet breakup**

The basic mechanisms of sheet disintegration are broadly the same as those responsible for jet break up. According to Frazer et al.[41] if the relative velocity between the liquid sheet and the surrounding air is fairly low, a wave motion is generated on the sheet which causes rings of the liquid to break away from its leading edge. The volume of liquid contained in the rings can be estimated as the volume of a ribbon cut out of the sheet with a thickness equal to that of the sheet at the breakup distance and a width equal to one-half wavelength of the oscillation ($\lambda_{opt}/2$). These cylindrical ligaments then disintegrate into drops of uniform size according to the Rayleigh mechanism as illustrated in Figure 2.7[17].
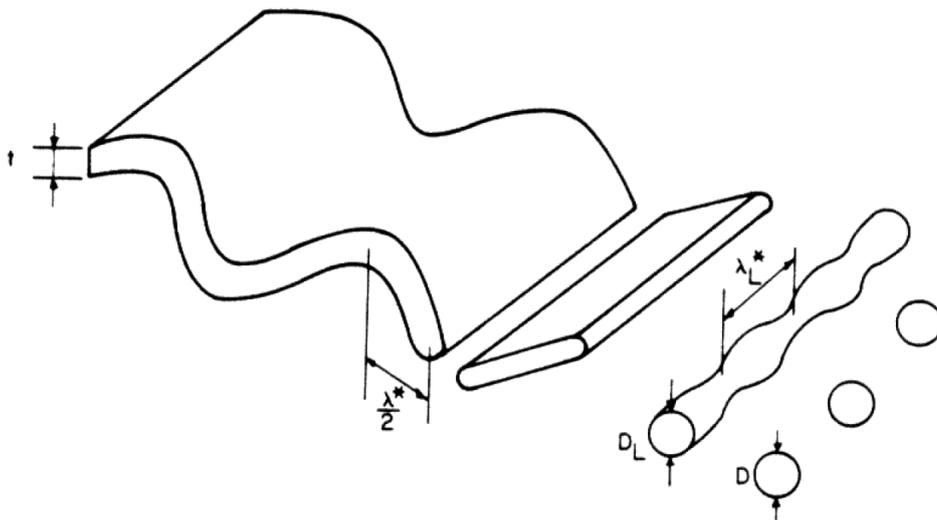


Figure 2.7 The successive stages in the idealized break-up of a wavy sheet [41]

For pressure-swirl atomizers (PSA), a conical liquid sheet is generated as shown in Figure 2.8. In contrast to the plain-orifice breakup, a wave motion is generated on the liquid sheet, which causes the primary breakup. This process is called classical atomization. With increasing inlet pressure and thus relative velocity, sheet breakup occurs closer to the atomizer. At very high relative velocities, atomization starts at the atomizer exit orifice. In this case, the liquid sheet has no time to develop a wavy structure, but is immediately torn into ligaments. This mode is called prompt

18

atomization. For high Weber number prompt atomization is dominant whereas for a low Weber number the classical model is dominant [2].
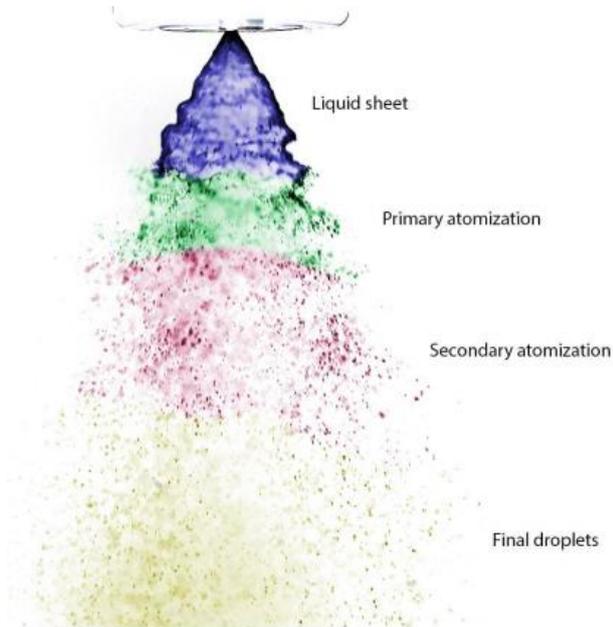


Figure 2.8 Liquid sheet break up, generated by pressure-swirl atomizer [42]

### 2.4.5 Break-up length and the liquid core length in round liquid jets

The break-up length or the intact length $L_b$ is the length where break up begins on the jet surface. The dense spray region shown in Figure 2.6 in second wind induced and atomisation regimes include a liquid core similar to the potential core in single-phase jets which is surrounded by a two-phase mixture of large droplets. The length of this liquid core is called the liquid core length $L_c$. It is also considered as the length that continuous liquid exists on the jet axis. This core length $L_c$ equals the break-up length $L_b$ in the Rayleigh regime but is much longer than $L_b$ in the other three regimes and it reaches in the atomization regime. A qualitative illustration of the break-up length for each of the four regimes of jet break-up against jet velocity is shown on the left hand side of Figure 2.6.

### 2.4.6 Effect of density ratio and injection velocity on the liquid core length

Grant & Middleman [43] performed liquid core length measurements in the atomisation regime with $\rho_l/\rho_g > 500$ and proposed a correlation in the form of:

$$L_c/D_l = 8.51\,We^{0.32}$$

Since the gas density is much smaller than the liquid density, the correlation only depends on the liquid properties and the injection velocity. However, other researchers, Hiroyasu et al. [44], Chehroudi et al. [45] and Andrews [46] have proposed the following correlation for experiments when $\rho_l/\rho_g > 500$:

$$L_c/D_l = C_c\left(\rho_l/\rho_g\right)^{1/2}$$

with different values of 15.8, 7.0 and 5 for $C_c$ respectively. The wide range of values for $C_c$, given by different researchers from different experiments, can be related to the fact that the primary break-up is very much affected by the flow conditions in the nozzle such as vorticity and turbulence which are not taken into account in these correlations. However, Chehroudi et al. [45] relate their much lower value of $C_c$ to some uncertainties in the measurements of Hiroyasu at al.[44].

This dependency of the liquid core on $\left(\rho_l/\rho_g\right)^{1/2}$ is the same as predicted by the theories based on the growth and instability of the surface waves with most unstable wavelength [47]. When the jet surface has become wavy or irregular typical of the first break up regime the pressure forces exerted by gas as a result of the motion of the jet on this irregular surfaces which will be unequal on each side of the surface because of the different diameters and shapes that it attains, can cause further disruption to the jet. These effects are generally referred to as aerodynamic effects in the literature. However, these effects are expected to be non-existent in the atomization regime since the jet surface is subject to strong mean flow shear and small-scale turbulent eddies that do not leave much room for waves or significant irregularities like the other regimes to develop or remain on surface.

Tseng et al.[48] argue that the so-called aerodynamic effects are negligible for liquid to gas density ratios of above 500 and become important only for values of this ratio below 500. Hence they relate the lack of gas properties in the Grant & Middleman's correlation to negligibility of the aerodynamic effects because of very high density ratios in their experiments and the rather strong dependency on the liquid to gas density ratio in the other correlations to smaller density ratios in the related experiments.

### 2.4.7 **Mean drop size**

The mean droplet diameter is a very important parameter used to characterize the distribution of a spray. For most engineering purposes, the distribution of drop sizes may be described in terms of two parameters, one of them is the representative diameter and the other one is a measure of the range of drop sizes. There are several measures to define it, e.g., mass median droplet diameter, $D_{0.5}$, arithmetic mean diameter, $D_{10}$, the surface area mean diameter, $D_{20}$, the volume mean diameter, $D_{30}$, the Sauter mean diameter, $D_{32}$ etc.

In combustion and fuel injection, it is only the mean or average diameter and in particular the most important Sauter mean diameter (SMD) named after Josef Sauter in 1924 which is used instead of the complete drop size distribution. Generally, a combustor with larger SMD will produce more pollution (oxides of nitrogen, carbon monoxide) [49]. Table 2.2 shows the basic definitions for the average diameters [1].

Table 2.2 Mean diameters

| Common name | Definition | Used for |
|---|---|---|
| Arithmetic mean diameter | $$D_{10} = \frac{1}{N}\sum_{i=1}^{N_i} n_i D_i$$ | General comparison and calculating evaporation rates |
| Area mean diameter | $$D_{20} = \left(\frac{1}{N}\sum_{i=1}^{N_i} n_i D_i{}^2\right)^{\frac{1}{2}}$$ | Monitoring surface applications |
| Area-length mean diameter | $$D_{21} = \frac{\sum_{i=1}^{N_1} n_i D_i{}^2}{\sum_{i=1}^{N_1} n_i D_i}$$ | Absorption studies |
| Volume mean diameter | $$D_{30} = \left(\frac{1}{N}\sum_{i=1}^{N_i} n_i D_i{}^3\right)^{\frac{1}{3}}$$ | Hydrology and mass flux application |
| Mean evaporative diameter | $$D_{31} = \left(\frac{\sum_{i=1}^{N_1} n_i D_i{}^3}{\sum_{i=1}^{N_1} n_i D_i}\right)^{\frac{1}{2}}$$ | Evaporation and molecular diffusion applications |
| Sauter mean diameter (SMD) | $$D_{32} = \frac{\sum_{i=1}^{N_1} n_i D_i{}^3}{\sum_{i=1}^{N_1} n_i D_i{}^2}$$ | Mass transfer and reaction |
| De Broukere diameter | $$D_{43} = \frac{\sum_{i=1}^{N_1} n_i D_i{}^4}{\sum_{i=1}^{N_1} n_i D_i{}^3}$$ | Combustion applications |

2.4.8 **Drop size distributions**

A critical parameter in atomization study is the distribution of droplet size within the spray. It is an essential element to understand the atomization process. Some of the most widely used empirical droplet size distribution functions in spray atomization are the Rosin-Rammler volume distribution function, the log-normal distribution function, root-normal, log-hyperbolic and the Nukiyama-Tanasawa distribution functions.

The Rosin-Rammler volume distribution function is widely used to express the droplet size distribution from nozzles especially for pressure nozzles. It is empirical and relates the volume percent oversize to droplet diameter. The atomization process produces droplets with random and chaotic size. Usually, atomizers produce droplets in the size range from a few microns up to several hundred microns. A simple method of illustrating the distribution of drop size in a spray is to plot a histogram, where each bin represents count percent of droplets of a given size class. A histogram sample is shown in Figure 2.9. Because the graphic representation of drop size distribution is experimental, several mathematic models were introduced in an attempt to reduce the intensity of experimental measurements. The Rosin and Rammler [50, 51] expression used to describe drop size distribution is given by:

$$1 - Q = \exp\left(-\frac{D}{X}\right)^q \qquad\qquad 2.1$$

where Q is the fraction of the total volume contained in drops of diameter less than D and X and q are constants that are determined experimentally [1, 7].
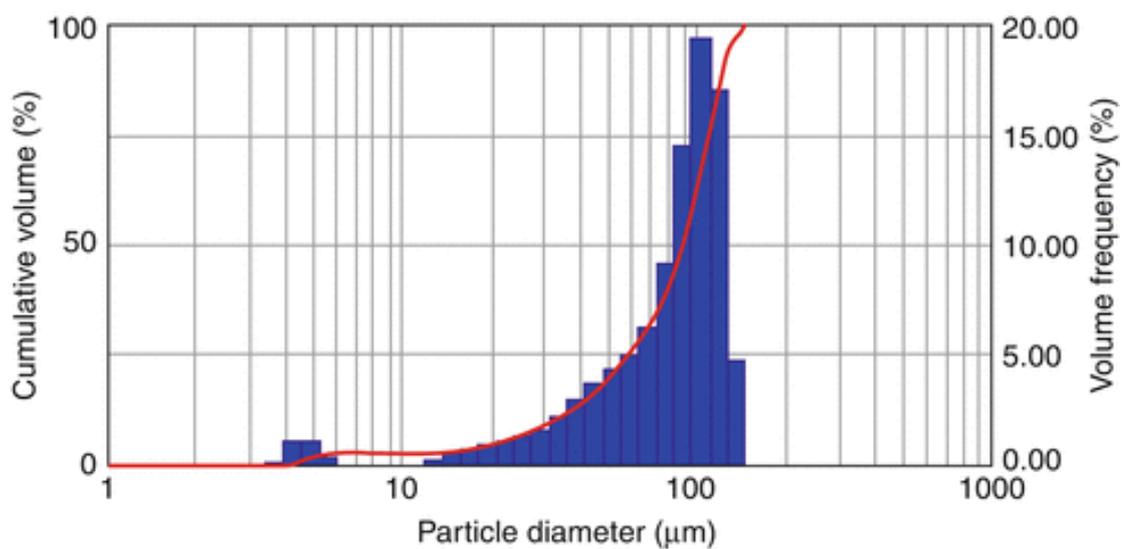


Figure 2.9 Drop size distribution from pressure-swirl atomizer, inlet pressure 10 bar, axial distance from exit orifice 50 mm, in center line of spray[1]

The problem with this empirical approach is the difficulty of extrapolating the data to operating regimes outside the experimental range. Without additional experimentation, one can never be certain whether the extrapolated empirical correlation applies to the regime of interest. Unfortunately, additional experimentation is often impractical, impossible, or prohibitively expensive [52].

Alternative to the empirical approach are two analytical approaches to the problem of modelling drop size distribution. These are the maximum entropy (ME) method, and the discrete probability function (DPF) method. The ME method, pioneered by Sellens and Brzustowski [53] and Li and Tankin [54], views spray formation as a completely non-deterministic process that can be modelled using the principle of entropy maximization subject to a set of global constraints. The ME method assumes that the most likely drop size distribution is the one that maximizes an entropy function under a set of physical constraints (e.g. conservation of spray mass, minimization of surface energy, etc.). The most important part of applying the maximum entropy principle to predict drop size distribution is the correct formulation of the constraints. After approximately a decade of research, it appears that various formulations have converged to a commonly accepted form. The constraints contain 'source terms', which can be expressed in terms of representative diameters of the drop size distribution (eg. SMD, $D_{21}$, $D_{30}$, $D_{10}$). It appears that at least two such diameters are needed to predict the drop size distribution. In principle, they can be obtained by other means such as an instability analysis. However, an instability analysis can provide only one such representative diameter; at present, there are no means of obtaining two or more. This makes the maximum entropy method less useful for practical applications because at present experimental measurement is the only way of obtaining more than one representative diameter [52].

The DPF method applied to modelling drop size distributions in Newtonian sprays by Sovani et al.[55, 56] and developed originally by Sivathanu and Gore [57] divides the spray formation process into deterministic and non-deterministic portions. It is assumed that spray formation involves a series of breakup stages of the initial fluid structure (flat sheet, annular sheet, jet, conical sheet, etc.). A fluid mechanic instability analysis such as the ones of Rayleigh [58], Weber [32], Sterling and Sleicher [37], Goren and Gottlieb [59], or Panchagnula et al.[60] can be used to describe the relevant breakup processes. It is stated that the DPF method is not tied to any particular instability

analysis and that any number of linear or non-linear analyses that acceptably describe the relevant breakup physics may be used [52].

### 2.4.9 Sauter Mean Diameter (SMD) predictions

Sauter mean diameter abbreviated SMD or $D_{32}$ is one of the most discussed atomizer characteristics and plays an important role in the combustion process. The goal is to keep SMD as low as possible due to higher efficiency and lower production of pollutions in combustion. A list of the best known empirical correlations of SMD is shown in Table 2.3 ordered from the oldest to the newest[1].

Table 2.3 SMD correlations

| N | Author | Equation | Year | Liquid | Comment |
|---|--------|----------|------|--------|---------|
| I | Ohnesorge[61] | $SMD = 0.61\dot{m}_1^{0.318}\Delta p_1^{-0.53}$ | 1936 | water | |
| II | Radcliffe[62] | $SMD = 7.3\vartheta^{0.2}\sigma^{0.6}\dot{m}_1^{0.25}\Delta p_1^{-0.4}$ | 1960 | | $\vartheta$=0.5-20 mm$^2$/s $\rho_l$=750-1600 kg/m$^3$ |
| III | Jasuja[63] | $SMD = 4.4\vartheta^{0.16}\sigma^{0.6}\dot{m}_1^{0.22}\Delta p_1^{-0.43}$ | 1979 | Kerosene Gas oil Residual fuel oil | |
| IV | Simmons[64] | $SMD = \Delta p_1^{0.275}We^{-0.43}$ $SMD = 170.824\dfrac{FN^{0.64291}}{\Delta p^{0.22565}}$ | 1981 | Water Kerosene | We<1 |
| V | Babu[65] | $SMD = 198.515\dfrac{A_0^{0.3888}A_1^{0.32114}}{A_C^{0.05414}\Delta p^{0.2565}}$ $SMD = 66.898\dfrac{FT^{0.50939}D_0^{1.00546}V_E^{1.0}}{U_E^{0.0809}\Delta p^{0.72844}}$ | 1982 | Kerosene | Pressure up to 27.6 bar |

| VI | Kennedy[66] | $SMD = 10^{-3}\sigma(6.11 + 0.32$ $* 10^5 FN\sqrt{\rho_l}$ $- 6.973$ $\times 10^{-3}\sqrt{\Delta p_1}$ $+ 1.89$ $* 10^{-6}\Delta p_l)$ | 1986 | 25 types of liquid-Kerosene ,oil etc | We>10 |
|---|---|---|---|---|---|
| VII | Lefebvre[67] | $SMD$ $= 2.25\mu^{0.25}\sigma^{0.25}\dot{m}_1^{0.22}\Delta p_1^{-0.5}$ $\rho_A^{-0.25}$ | 1987 | Kerosene Gas oil Residual fuel oil | |
| VIII | Wang, Lefebvre[68] | $SMD$ $= 4.52\left[\dfrac{\sigma\mu^2}{\rho_A\Delta p_1^2}\right]^{0.25}[t\cos\theta]^{0.25}$ $+ 0.39\left[\dfrac{\sigma\rho_1}{\rho_A\Delta\rho_1}\right]^{0.75}[t\cos\theta]^{0.75}$ | 1987 | Diesel oil water | |
| IX | Couto[69] | $SMD$ $= 1.817\cos\theta\left(\dfrac{h_0^4\sigma^2}{U_0^4\rho_a\rho_1}\right)^{\frac{1}{6}}\left[1\right.$ $+ 2.6\mu_1\cos\theta\left.\left(\dfrac{h_0^2\rho_a^4 U_0^7}{72\rho_1^2\sigma^5}\right)^{1/3}\right]^{0.2}$ | 1997 | Water Diesel oil | |
| X | Musemic[70] | $SMD = \left[\dfrac{k}{We}\right]^{0.44}\left[\dfrac{\rho_l}{\rho_a}\right]^{0.08}$ | 2011 | Water Water-glycerol | |

$$t = 3.66\left(\frac{d_0\dot{m}_l\mu_1}{\rho_1\Delta P_1}\right)^{0.25} \quad h_o = \frac{0.00805 FN\sqrt{\rho_1}}{D_0\cos\theta} \quad U_o = \sqrt{\frac{2\Delta P_1 Cd}{\rho_1}} \quad k = \frac{\mu}{2\pi\varphi\sin\left(\frac{\theta}{2}\right)}$$

$$\varphi = \frac{v_{eff}}{v_{pot}}$$

The simplest correlations were empirical formulas in the general form

$$SMD \sim \sigma^a \vartheta^b \dot{m}_1^c \Delta p_1^d \qquad\qquad 2.2$$

where a, b, c, d are experimental constants. Due to a disparity in the listed formulas (I, II, III, VII), it is not possible to define one universal correlation based on this model. The first correlation (I) in Table 2.3 was probably the first correlation of SMD in swirl atomization. It was published by Ohnesorge [61] in 1936. He set SMD to be a function

of injection pressure and mass flow, but did not include any of the liquid properties. Further correlations were made by Radcliffe [62] (II) and Jasuja[63] (III). They are both very similar to each other. They put in the correlation liquid properties such as viscosity and surface tension. According to the more convenient Lefebvre´s correlation [67] (VII), they have a bigger influence on surface tension and do not involve liquid and air density. These correlations are based on the model empirical formula in eq. (2.2), their advantage is the simplicity of creation and application, but more complex correlations (VIII, IX, X) are more accurate. Simmons[64] in 1981 investigated six swirl atomizers of small flow rates with water and kerosene and correlated the Weber number with inlet pressure. His correlation (IV) is valid only for small atomizers, with a Weber of number less than 1. Babu [65] in 1982 used eight different atomizers for pressure up to 27.6 bar, all with kerosene. He defined three equations (V), which are based on the atomizers dimensions. He also correlated equations for pressure above 27.6 bar, but in his thesis they are not classified. Kennedy [66] derived his equation (VI) using six different atomizers with 25 types of liquids. He correlated mass flow rate, surface tension and inlet pressure under the condition that the Weber number is larger than 10. The SMD was found to be independent of liquid viscosity. Probably one of the most complex, semi-empirical correlation was introduced by Wang and Lefebvre[68] in 1987. The correlation (VIII) was based on the theory

$$SMD = SMD_1 + SMD_2 \qquad\qquad 2.3$$

where $SMD_1$ represents the first stage in the atomization process and $SMD_2$ represents the final stage of atomization. They used several liquids to provide a range of viscosity from 1 mm$^2$/s to 18 mm$^2$/s and range of surface tension from 27 to 73 mN/m. Nowadays more than quarter-century later, it is taken as a reference for other corrections. Couto et al [69] derived a theoretical formula (IX) based on a hypothesis regarding the thickness of a plane disintegrating liquid sheet. They compared their results with other empirical correlations in their work. They correlated liquid properties with atomizer dimensions and with properties of surrounding air. Recent investigation was made by Musemic [70] (X) by testing 20 atomizers with water-glycerol mixture with a dynamic viscosity of up to 5 mPas. He observed that higher swirl ratio led to a smaller drop size. A higher swirl ratio means a higher ratio of the tangential velocity components to the axial velocity [1]. Apart from these general correlations some

specific correlations are used for some specific atomizers. According to Elkotb [71] the SMD for plain orifice nozzles is determined using

$$SMD = 3.08 \vartheta_L^{0.385} (\sigma \rho_L)^{0.737} \rho_A^{0.06} \Delta p_L^{-0.54}$$

For pressure-swirl nozzles, mean drop sizes are usually correlated using empirical equations of the form

$$SMD = 2.25 \sigma^{0.25} \mu_L^{0.25} \dot{m}_L^{0.25} \Delta p_L^{-0.5} \rho_A^{-0.25}$$

For rotary atomizers, any equation for mean drop size should take into account the effects of variations in disc or cup diameter and rotational speed, in addition to liquid properties and liquid flow rate. For atomization by direct drop formation, Tanasawa et al. [72] obtained a good correlation between their experimental data and the following expression for mean drop size

$$SMD = \frac{0.45}{N} \left[ \frac{\sigma}{d \rho_L} \right]^{0.5} \left[ 1 + 0.003 \frac{\dot{m}_L}{d \mu_L} \right]$$

For atomization by ligament formation, these same workers proposed the following equation

$$SMD = \frac{0.50}{N} \left[ \frac{\sigma}{d \rho_L} \right]^{0.5} \left[ \frac{\dot{m}_L}{\mu_L} \right]^{0.1}$$

An interesting feature of this equation is that it predicts the mean droplet size to increase slightly with increase in liquid viscosity [1].

The mean drop sizes produced by twin-fluid atomizers are usually correlated in terms of the Weber and Ohnesorge numbers and the air/liquid mass ratio (ALR), as illustrated below

$$\frac{SMD}{L_c} = (A. We^{-0.5} + B. Oh) \left[ 1 + \frac{1}{ALR} \right]^C$$

where A, B, and C are constants whose values depend on atomizer design and must be determined experimentally. Lc is a characteristic dimension of the atomizer. For prefilming types of airblast atomizer the correlation is [73]

$$\frac{SMD}{D_h} = \left[ 0.33 \left( \frac{\sigma}{\rho_A U_A^2 D_p} \right)^{0.6} \left( \frac{\rho_L}{\rho_A} \right)^{0.1} + 0.68 \left( \frac{\eta_L}{\rho_L \sigma D_p} \right)^{0.5} \right] \left[ 1 + \frac{1}{ALR} \right]$$

where $D_h$ is the hydraulic mean diameter of the atomizer air duct at its exit plane, and $D_p$ is the prefilmer diameter.

## 2.5 Theoretical studies on pressure swirl atomizer

Early studies of simplex atomizers employed analytical and/or experimental methods to predict the internal and external spray characteristics of the atomizer [3, 28-32]. Taylor in 1948 did the earliest work on the internal analyses of the simplex atomizer. He proved that there is a difference between the values of the air-core radii at the top of the swirl chamber and in the outlet and in 1950 investigated the growth of the boundary layer adjacent to a cone which represented the convergence of a swirl atomizer from the edge of the cone to the vertex. He also investigated the velocity distribution within the boundary layer. Giffen and Muraszew [74] undertook treatments of the inviscid theory of the pressure swirl atomizer (PSA). It was a classical quasi-one-dimensional inviscid analysis that may be used by those wishing to design swirl atomizers. The analysis of Giffen and Muraszew has been re-presented in the major works on atomization by Lefebvre [1]. The purpose of the analysis was to develop expressions in terms of the atomizer dimensions only for: (a) the air-core radius in the outlet, or discharge orifice, (b) the discharge coefficient and (c) the spray cone angle. Bayvel and Orzechowski [3] also did analytical analysis on the atomizer similar to Giffen and Muraszew but in addition gave a novel analysis of the axial and tangential velocities along with the air-core radius at the exit cross-section where the static pressure is zero throughout. The boundary layer analysis to determine the air-core diameter in the outlet was undertaken by Som and Biswas [75]. They made it clear from the outset that the flow was analysed according to three distinct zones of flow: (a) a central air-core near the axis (b) a boundary layer near the surface of the nozzle (c) an inviscid zone between the latter two zones where the tangential velocity behaves in the manner of a free vortex. Rizk and Lefebvre [8, 33] investigated the internal flow characteristics of simplex swirl atomizers using approximate analytical treatment of the flow. They investigated the effects of variation of the individual swirl atomizer geometrical dimensions on the thickness of the annular liquid film at the nozzle exit and the effects of the variation of the fluid properties on the values of the discharge coefficient, the spray angle and the liquid film thickness. They developed a general expression for the liquid film thickness at the exit of the swirl atomizer and stated that the air-core diameter increases with increasing pressure, decreasing inlet area, increasing swirl chamber diameter, decreasing swirl chamber length, increasing orifice length, decreasing liquid viscosity and decreasing liquid density. Moradi [76] developed a theoretical model for pressure swirl atomizer using integral conservation methods to

predict the SMD for fully developed atomization conditions. The results showed the model predicted the droplet sizes with high accuracy for wide range of operating conditions. However, the model overestimated the SMD for very low injection velocities, Weber numbers and cone angles. Theoretical model such as the semi-empirical model developed from the surface wave breakup theory was also established by Xiao and Huang [77] to predict the SMD for combustors. They concluded that three geometrical parts such as tangential inlets, swirl chamber and the discharge orifice have significant effect on the SMD for pressure swirl atomizer.

## 2.6 Experimental studies on pressure swirl atomizer

One of the earliest pioneers who studied experimentally the velocity profiles within a pressure swirl atomizer was Horvay and Leuckel [5]. The experiments were conducted using three different convergence configurations (standard, concave, and plain conical) and two different inlet/swirl chamber configurations (four 20 x 10 mm and four 20 x 5 mm rectangular inlet slots). The atomizers were manufactured from Plexiglas(Perspex) and shared many of the overall dimensions: radius of swirl chamber $r_s$ = 50 mm, length of swirl chamber $l_s$ = 25 mm, radius of orifice $r_o$ = 10 mm and length of orifice lo = 20 mm as shown in Figure 2.10.
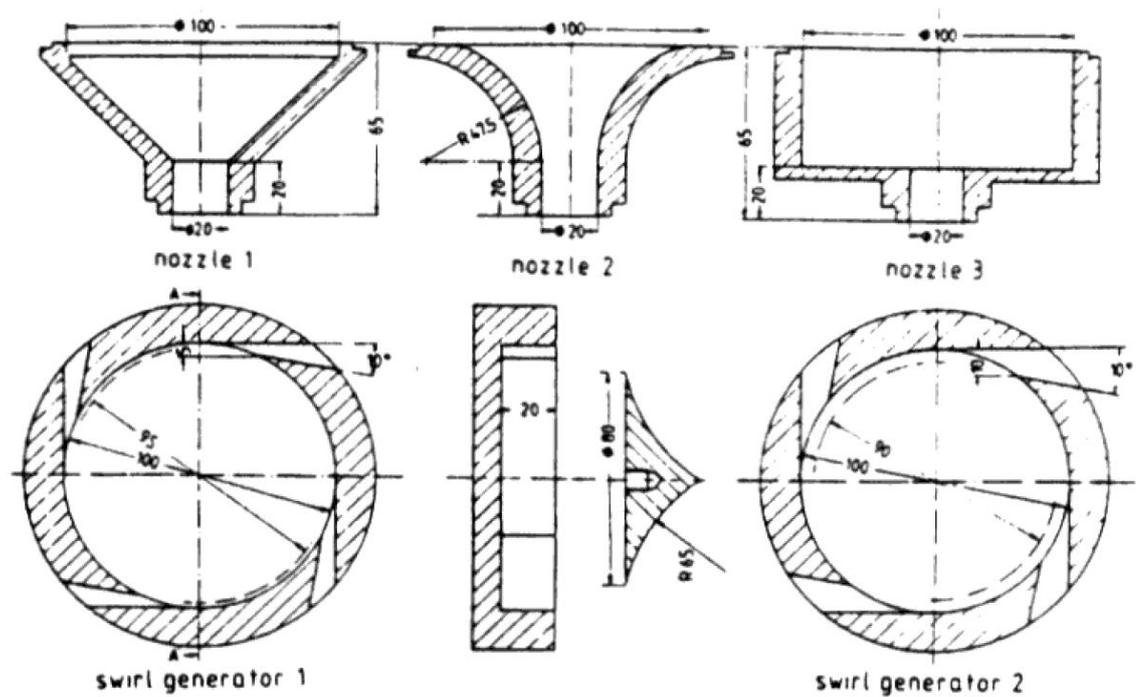
Figure 2.10 The different atomizer designs and dimensions employed in the velocity measurement experiment of Horvay and Leuckel [5]

The measurements of the liquid velocity components within the atomizer were carried out using the 'no contact' method of Laser-Doppler Anemometry (LDA). The refractive index of the operating liquid was adapted to that of the perspex by the use of mixtures of tetraline, turpentine and castor oil. The seeding particles needed to scatter the laser light were small air bubbles that were entrained at the intake pump that supplied the operating liquid to the experimental rigs. Radial profiles of the axial and tangential velocities were taken at six different cross-sections through the atomizer. De Keukelaere [78] conducted tests on a large perspex atomizer using water as the operating liquid. The flow rate was measured for different inlet pressures. Static pressure measurements were conducted on the internal walls of the atomizer using an electrical transducer providing wall pressure profiles for different inlet pressures. Measurements of the air-core diameter were undertaken employing a video system providing a clear view of the air-core topology within the convergence and outlet of the atomizer. To observe the velocities and nature of flow occurring within an atomizer Hsieh and Rajamani [79] investigated the flow in the body of a hydrocyclone separator which bears close similarities with that of a swirl atomizer. They suggested that the flow may be turbulent but admitted that *"The correlation between the turbulence and*

30

*the Reynolds number has not been established for vortical flow yet it is generally believed that turbulent conditions exist within the body of the hydrocyclone especially as the Reynolds number is as high as $10^5$ to $10^6$ for most practical applications''*. Other numerous experiments have been performed in order to determine a functional relationship between the SMD and the relative parameters such as surface tension, film thickness, viscosity, discharge coefficient, spray angle and liquid and gas densities [8, 67, 80]. Rizk and Lefebvre [80] explained using Figure 2.11 that the film thickness t increases with increasing kinematic viscosity $v_L$ for any given pressure while it does appear to decrease with liquid density but stated that the effect was minimal and that the influence of pressure differential $\Delta p$ on the film thickness was more pronounced.
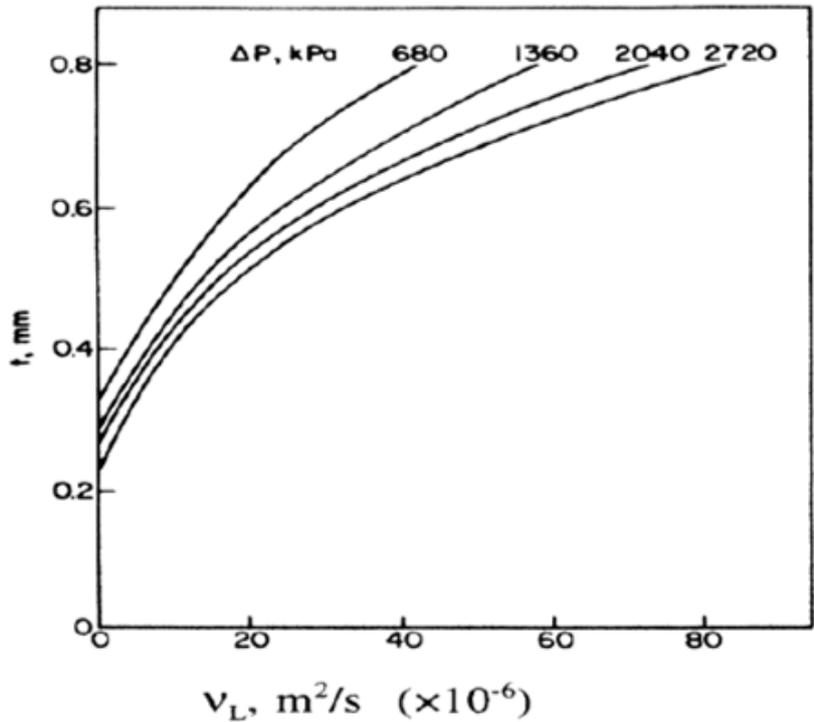
a) Variation of film thickness, t with kinematic viscosity $v_L$
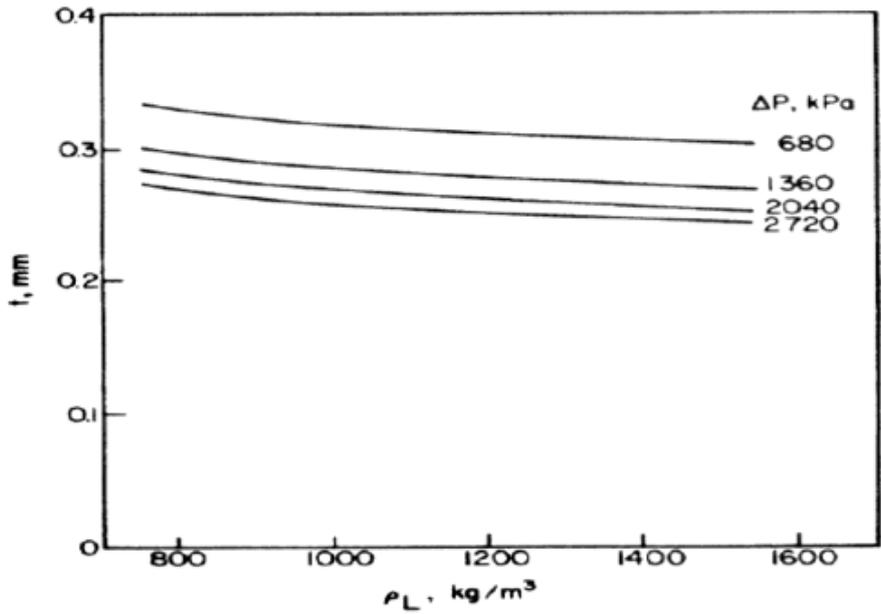


b) Variation of film thickness t with liquid density $\rho_L$

Figure 2.11 Variation of film thickness t with kinematic viscosity $\boldsymbol{v_L}$ and liquid density $\boldsymbol{\rho_L}$ observed by Rizk and Lefebvre [80]

Rizk and Lefebvre [80] also presented a graph of variation of discharge coefficient $C_D$, cone angle α with kinematic viscosity $v_L$ as shown in Figure 2.12 and explained that the maximum value of discharge coefficient was reached when the air-core disappeared entirely and the flow became predominantly axial. Further increase in viscosity then

has a retarding influence on the axial velocity which then causes the discharge coefficient to decrease. They also noted that there was a sharp decline in spray cone angle with an increase in viscosity and that the increase in the pressure differential across the nozzle tended to widen the spray angle to the extent that the value of viscosity at which the swirl component became effectively zero was almost doubled for a four-fold increase in pressure differential.
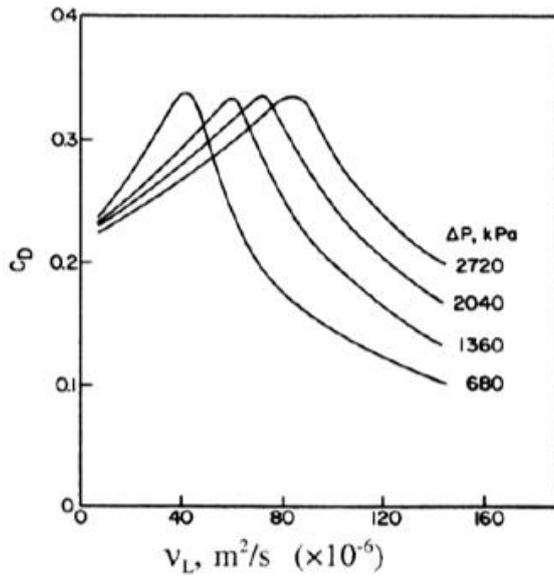
a) Variation of discharge coefficient CD with kinematic viscosity $v_L$
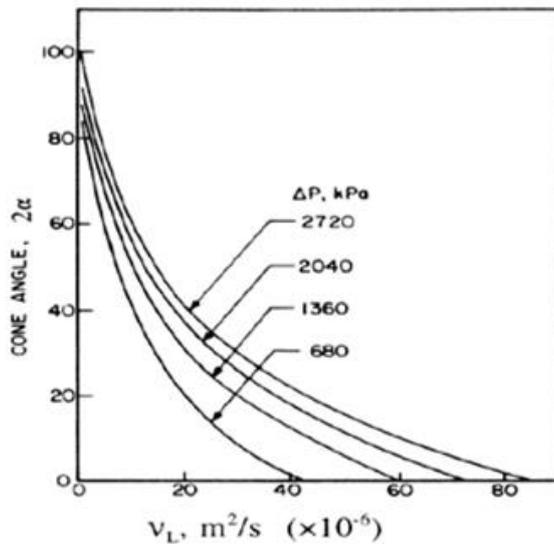
b) Variation of cone angle 2α with kinematic viscosity $v_L$

Figure 2.12 Variation of discharge coefficient, cone angle with kinematic viscosity observed by Rizk and Lefebvre [80]

Wang and Lefebvre[68] conducted an experiment in which they utilized two pressure-swirl atomizers with different flow numbers to determine the proportionality of the SMD with the surface tension σ of the liquid. They discovered that SMD scales proportional to $\sigma^{0.25}$. Similar results were found by Jones [81] and Simmons [82] with slight variation in the constant power. Saha et al.[83] attempted to quantify the average droplet diameters and velocities due to the breakup and subsequent coalescence of the droplets from two different simplex atomizers utilizing Phase Doppler Particle Analyzer (PDPA) and shadowgraph techniques. They discovered that, regardless of the injector diameter used, the droplet diameters and velocities all converged to the same value at axial distances far from the injector orifice. The final droplet velocities seem to vary only with respect to the injection pressure near the nozzle; however, far enough downstream all the droplet velocities converged to the same value along the center axis. They also discovered that even though the simplex nozzles were of the hollow-cone type, they still had significant number of droplets along the center axis. This was attributed to the fact that smaller droplets are going to be carried inwards by the entrained gas whereas the larger droplets would continue along their path at the sheet breakup point. They also observed appreciable coalescence effects downstream of the nozzle. Muhammad at al [84] experimentally study the effect of geometric parameters on the spray cone angle and the SMD for twelve (12) atomizers for three geometrical ratios of $D_s/D_o$, $L_o/D_o$ and $L_s/D_s$ varied from 3 to 7.5, 0.81 to 2.69 and 1.25 to 5.0 respectively where $D_s$ is the diameter of the swirl chamber, $D_o$ diameter of exit orifice, $L_o$ height of exit orifice, $L_s$ combined vertical height of contraction part and swirl chamber. The experiment was performed at two injection pressures of 0.8 and 1.2MPa using Malvern instruments and water as the test liquid. It was observed that the spray cone angle continuously decreases with the increase in ratio $D_s/D_o$, however, optimum value of 3.75 was obtained for the measurement of SMD. It was also shown that the SMD continuously increase with increase in $L_o/D_o$ while 1.44 optimal value was obtained for the measurement of the spray cone angle.

## 2.7 Numerical studies on pressure swirl atomizer

Computational fluid dynamics (CFD) research has been developed to produce simulations of spray characteristics in pressure swirl atomizer. Chinn et al.[85], Cooper et al. [86] and Yule and Chinn [87] are pioneers in the simulation of two-phase flow in the simplex atomizers. They predicted numerically the air core shape in the pressure-swirl atomizer. Belhadef et al.[14] performed numerical studies using FLUENT to model the sprays characteristics within and outside the pressure swirl atomizer. He developed one-fluid Eulerian model to predict liquid sheet atomization with high Weber and Reynolds numbers. The model considered a single phase of liquid-gas mixture to represent the turbulent mixing of the liquid sheet with the ambient gas. As the flow was highly swirled and highly anisotropic, the Reynolds stress model was used for the turbulence. The mean liquid–gas interface density balance equation was solved to get the Sauter Mean Diameter of droplets. Experimental data was obtained using Phase Doppler Anemometry (PDA). Atomization characteristics such as the axial velocity and droplet Sauter Mean Diameter were determined experimentally and were compared with the modeling results. The agreement was reasonably good between predictions and measurements as shown in Figure 2.13.
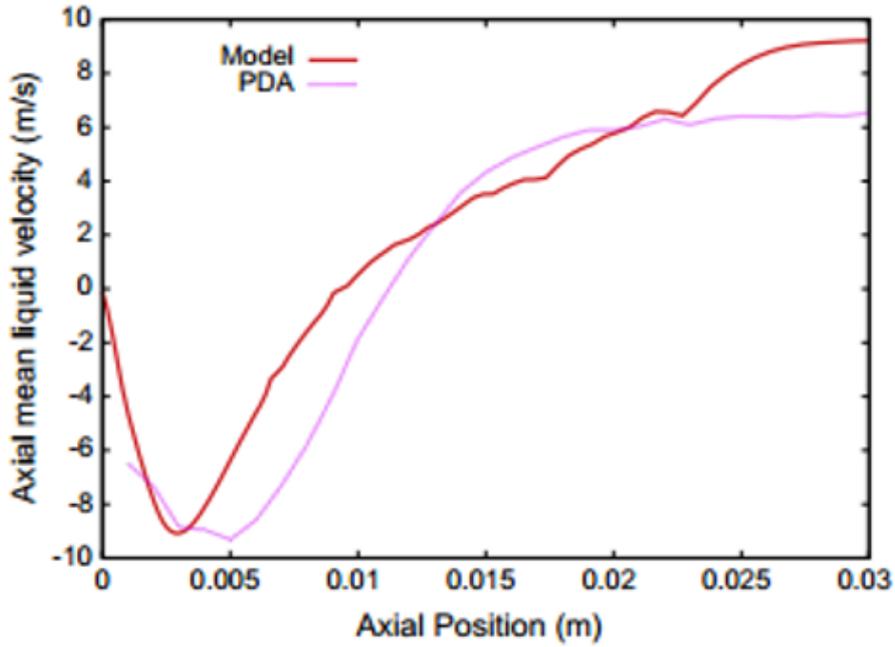
a) Axial profile of the axial mean liquid velocity, modeling and experimental
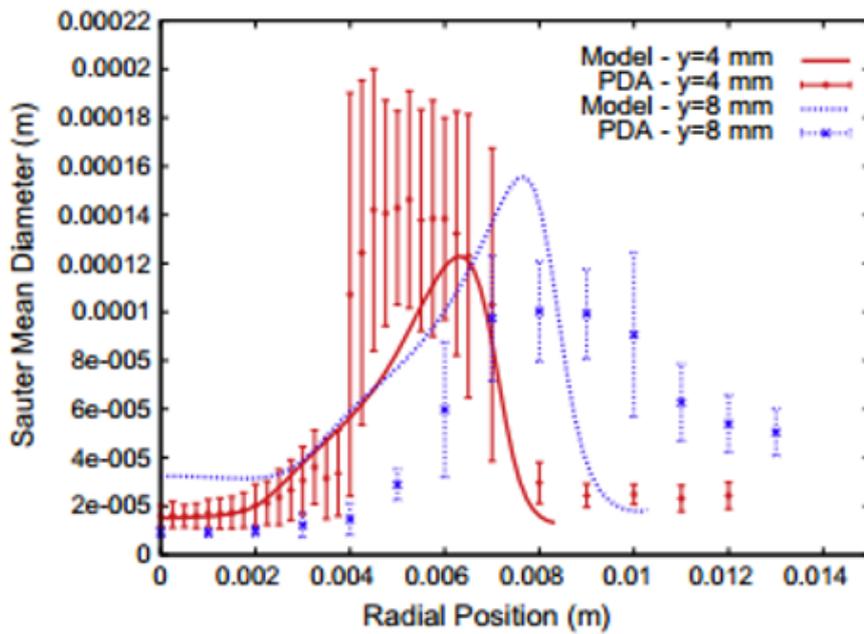


b) Radial profile of the Sauter Mean Diameter(SMD), modelling and experimental comparison

Figure 2.13 Validation of numerical results in terms of axial mean liquid velocity and Sauter Mean Diameter [14]

36

Numerical simulation of laminar and turbulent two-phase flow in pressure-swirl atomizers was also carried out by Nouri-Borujerdi [88]. He coupled the laminar and turbulent Navier–Stokes equations with the explicit algebraic Reynolds stress model as well the level set model to simulate the air-water two-phase flow inside the pressure-swirl atomizer. Applying a high-order compact upwind finite difference scheme with the level set equation culminated to capture the interface between air-liquid two-phase flow and decreasing the mass conservation error in the level set equation showed that some recirculation zones were observed close to the wall in the swirl chamber and to the axis. The proposed model showed that some improvements were obtained compared with the previous numerical solutions, especially in the laminar flow, so that the discharge coefficient, film thickness, and spray cone angle were satisfactory with the previous experimental data as shown in Table 2.4

Table 2.4 Comparison of air core diameter, discharge coefficient, and spray cone angle

| Author | Type of data | $d_{air}/d_o$ | $C_D$ | $\theta$ |
|---|---|---|---|---|
| (Laminar flow) | Numerical | 0.70 | 0.388 | 68.22 |
| (Turbulent flow) [88] | Numerical | 0.64 | 0.428 | 71.23 |
| Datta [16] | Numerical | 0.45 | 0.448 | 74.30 |
| Taylor[89] | Analytical | 0.632 | - | - |
| Rizk [8] | Experimental | 0.59 | 0.39 | - |
| Rizk [8, 90] | Experimental | - | - | 69.63 |
| Suyari & Lefebvre [91] | Experimental | 0.697 | - | - |
| Jones[81] | Experimental | - | 0.382 | - |

He also showed the result of turbulent kinetic energy versus the radius cross section at the locations of z = 6.13 mm, $r_s$=1.8 mm, and z = 12.58 mm, $r_s$=1 mm respectively as shown in Figure 2.14a, b and indicates that the intensity of the kinetic energy increases drastically near the interface between the air core and the liquid. The comparison between the two figures indicates that the maximum turbulent kinetic energy increases as the flow approaches the nozzle outlet, i.e., when the fluid flows from z =6.13 to 12.58 mm.
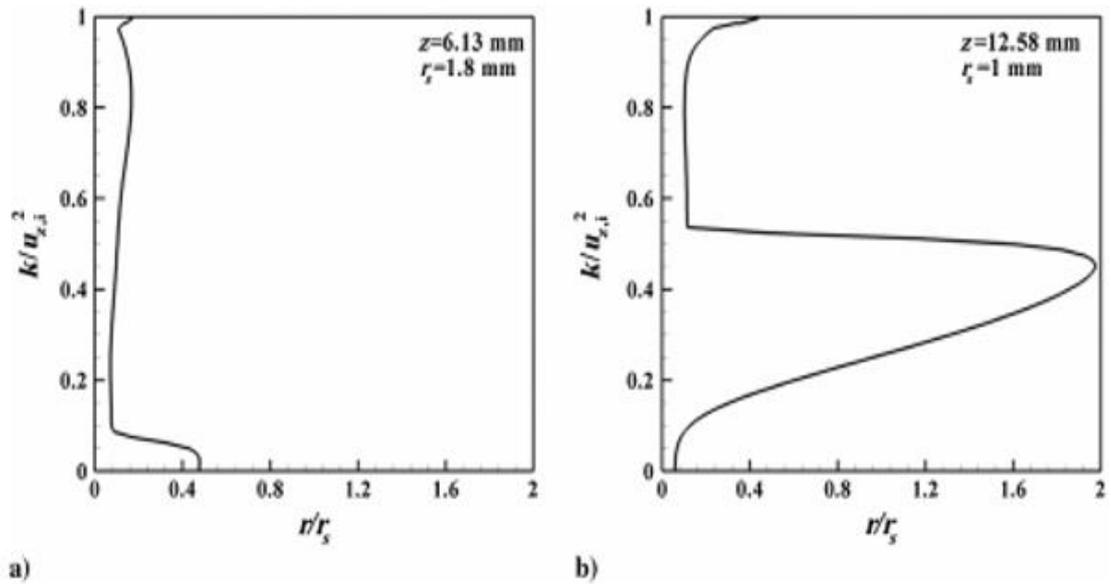
Figure 2.14 Turbulent kinetic energy in the cone region at different axial locations of the nozzle

Hansen [92] also studied and simulated the flow in a scaled model of a Danfoss pressure-swirl atomizer through commercially available CFX-4.3 code. The main objective of his work was to investigate whether it was possible to model the internal gas-liquid flow of an atomizer by use of the commercial code CFX-4.3. Special emphasis was given to the flow of the liquid phase. Two approaches were used in the simulations: A Large Eddy Simulation (LES) based on the work of [93] and a simulation where the flow was modelled as being laminar. The simulations were performed in a three-dimensional curvilinear grid representing the swirl chamber of the atomizer and managed to capture the overall flow characteristics of a pressure-swirl atomizer with the formations of an air-core and a thin liquid film in the exit region of the swirl chamber. The results from LES and simulations assuming laminar flow were verified against experimental findings from LDA and pressure measurements. Yule and Chinn [94] conducted a numerical study in pressure atomizer by treating the entire computational domain as single phase and then guessing the interface by joining grid points where pressure is found to be atmospheric. The solution was re-calculated by creating a new grid using the calculated interface and treating the interface as a "with-slip" boundary. However, the condition of normal stress balance was not applied at the interface. The velocity and pressure distribution in the atomizer were calculated and discharge coefficient and spray angle were predicted. Steinthorsson and Lee [95] conducted three-dimensional simulations of internal, free-surface flow in a pressure-swirl atomizer via commercial software FLUENT. The atomizer used in the

simulations is a large-scale atomizer. The Volume of Fluid (VOF) method was adopted to capture the formation of the air-core and Reynolds Stress Turbulence model was used to model the effects of turbulence. The results were compared to experimental data given by Wang et al. [96]. They concluded that the effect of the discrete inlet slots disappears before the liquid enters the orifice. Sakman et al.[97] studied the effects of simplex nozzle geometry on its performance numerically. They concluded that when designing a nozzle particular attention should be given to optimum values of the performance variables like the local maximum of spray cone half angle at Ds/ Do = 4.1 and extreme caution should be taken when designing a simplex nozzle. The performance variables are dependent on the actual 18 physical dimensions since these may determine whether the flow is laminar or turbulent and may change the trends of the performance parameters.

The numerical simulation of two-phase flow was also undertaken by Saha et al [98] whose research involves modelling the internal and near-nozzle flows in the Gasoline Direct Injection (GDI) injector. The Engine Combustion Network (ECN) Spray G condition and Spray G injector were considered for the simulation of the two-phase flow. The results showed that the predicted mass flow rate reasonably agreed with the experimental data available in the ECN database for peak needle lift and was also observed that the flow patterns and vapour formation were largely affected by very low needle lift for both flashing and non-flashing scenarios. A comprehensive review of various models for Sauter Mean diameter (SMD) prediction was also undertaken by Vijay et al [99]. They revealed that the SMD was greatly influenced by the breakup mechanism and that the droplet size was minimized as the perforated instability converted into a surface wave breakup mechanism due to higher inertia collisions. They also indicated that viscosity downplayed the surface tension force and supported larger sized droplets and suggested experimental validation for SMD findings for higher ambient conditions. When the influence of fuel injection pressure and fuel temperature on SMD were analysed, it was observed that the temperature effect dominates in reducing the droplet size. Since spray flow fields are difficult to predict due to the topology and irregularities of the dense break-up region, Gin and Loth [100] used inflow boundary condition approach to characterise it where the droplets are computationally injected at 9 mm downstream of the orifice and combined this with empirical relations for turbulent kinetic energy and dissipation. The approach described the spatial distribution of the gas and the droplet velocity and found the droplet velocity

to be consistent with the turbulent diffusion theory based on the local Stokes numbers and turbulent kinetic energy. In the recent works by Stevenin at al [101] to model the atomization and dispersion of an irrigation water jet from the nozzle outlet to the region of the full development of the spray, an Eulerian model developed for large Reynolds and Weber numbers was used to treat the two phase mixture as a single continuous process. The mean velocity, turbulent kinetic energy, liquid volume fraction and Sauter Mean Diameter (SMD) were determined numerically and compared to experimental measurements. It was observed that the model successfully predicted the volume fraction and mean droplet size profiles but overestimated the decrease of the longitudinal velocity on the axis.

## 2.8 Turbulence modelling

A turbulence model is a computational procedure to close the system of mean flow equations so that a more or less wide variety of flows problems can be calculated. For most engineering problems it is unnecessary to resolve the details of the turbulent fluctuations. Only the effects of the turbulence on the mean flow are usually analysed. For turbulence model to be useful in a general-purpose CFD code it must have wide applicability, be accurate, simple and economical to run. The most common turbulence models are classified below. The classical models use the Reynolds Averaged Navier–Stokes (RANS) equations which was proposed by Reynolds in 1895 [102] which provided an approximate time-averaged solution method to the Navier–Stokes (NS) equations and form the basis of turbulence in currently available commercial CFD codes.

Table 2.5 Classification of turbulence models

| Classical models | Based on (time–averaged) Reynold equations (RANS) |
|---|---|
|  | 1. Algebraic models or zero equation models |
|  | 2.One-equation models- Prandtl's mixing length model |
|  | 3.Two equation models- *k-ε, k-ω* model |
|  | 4.Reynolds stress model (RSM) |
|  | 5.Algebraic stress model |
| Large eddy simulation (LES) | Base on space-filtered equations |
| Direct Numerical Simulation (DNS) | Navier-Stokes equations are numerically solved without any turbulence model |
| Detached eddy simulation (DES) | Combine the best aspects of RANS and LES methodologies in a single solution strategy |

The three different two-equation turbulence models commonly used in RANS modelling are briefly described below [103-105].

### 2.8.1 **Standard k-ε turbulence model**

The standard k-ε is a classical model which is based on transport equations for the turbulence kinetic energy ($k$) and its dissipation rate ($\varepsilon$): The k- $\varepsilon$ model is the most widely used and validated turbulence model. It has achieved notable successes in calculating a wide variety of thin shear layer and recirculating flows without the need for case-by-case adjustment of the model constants. The model performs particularly well in confined flows where the Reynold shear stresses are important. This includes a wide range of flows with industrial applications which explains its popularity. In spite of the numerous successes the standard k- $\varepsilon$ model shows only moderate agreement in unconfined flows. The model is reported not to perform well in weak shear layers and spreading rate of axisymmetric jets in stagnant surroundings is severely overestimated. A summary of performance assessment of the standard k-epsilon model is given below

**Advantages**

- Simplest turbulence model for which only initial and/or boundary conditions need to be supplied
- Excellent performance for many industrial relevant flows
- Well established; the most widely validated turbulence model

**Disadvantages**

- Most expensive to implement than mixing length model (two extra PDEs)
- Poor performance in a variety of important case such as
    i.    some unconfined flows
    ii.   flows with large extra strains(e.g. curved boundary layers, swirling flows)
    iii.  rotating flows
    iv.   fully developed flows in non-circular ducts [103]

For turbulence kinetic energy ($k$) and its dissipation rate ($\varepsilon$):

$$\frac{\partial}{\partial t}(\rho k) + \nabla.\rho k\vec{u} = \nabla\left[\left(\mu + \frac{\mu_t}{\sigma_k}\right)grad\ k\right] + G_k - \rho\varepsilon$$

$$\frac{\partial}{\partial t}(\rho\varepsilon) + \nabla.\rho\varepsilon\vec{u} = \nabla\left[\left(\mu + \frac{\mu_t}{\sigma_\varepsilon}\right)grad\ \varepsilon\right] + C_{1\varepsilon}\frac{\varepsilon}{k}G_k - C_{2\varepsilon}\rho\frac{\varepsilon^2}{k}$$

where the turbulent (or eddy) viscosity, $\mu_t$, and the production of turbulence kinetic energy, $G_k$, are given as

$$\mu_t = \rho C_\mu \frac{k^2}{\varepsilon}$$

$$G_k = -\rho\overline{u_i'u_j'}\frac{\partial u_j}{\partial x_i}$$

The model constants $C_{1\varepsilon}, C_{2\varepsilon}, C_\mu$ and the turbulent Prandtl numbers $\sigma_k$ and $\sigma_\varepsilon$ are determined as follow to accommodate a variety of flow problems [106-108].

$C_{1\varepsilon} = 1.44,\ C_{2\varepsilon} = 1.92,\ C_\mu = 0.09,\ \sigma_k = 1.0$ and $\sigma_\varepsilon = 1.3$

### 2.8.2 Renormalization Group (RNG) k-ε model

RNG k-ε is a more refined model than the standard k-ε model, developed using a statistical technique. The differences between the two models are:

- An additional term is introduced in the dissipation equation to improve the accuracy in rapidly strained flows.
- The accuracy of the swirl flow is improved.
- An analytical formula for turbulent Prandtl numbers (inverse effective Prandtl numbers, $\sigma_k$ and $\sigma_\varepsilon$) is added where the standard k-ε uses adjustable constants
- Effective viscosity, $\mu_{eff}$, is also analytically derived to handle the low-Reynolds number case

The equations for the RNG k-ε model are:

$$\frac{\partial}{\partial t}(\rho k) + \frac{\partial}{\partial x_i}(\rho k u_i) = \frac{\partial}{\partial x_j}\left[\left(\mu + \frac{\mu_t}{\sigma_k}\right)\frac{\partial k}{\partial x_j}\right] + P_k - \rho\varepsilon$$

$$\frac{\partial}{\partial t}(\rho\varepsilon) + \frac{\partial}{\partial x_i}(\rho\varepsilon u_i) = \frac{\partial}{\partial x_j}\left[\left(\mu + \frac{\mu_t}{\sigma_\varepsilon}\right)\frac{\partial\varepsilon}{\partial x_j}\right] + C_{1\varepsilon}\frac{\varepsilon}{k}P_k - C_{2\varepsilon}^*\rho\frac{\varepsilon^2}{k}$$

where

$C_{2\varepsilon}^* = C_{2\varepsilon} + \frac{C_\mu \eta^3 (1-\eta/\eta_0)}{1+\beta\eta^3}$ and $\eta = Sk/\varepsilon$, $S = \left(2S_{ij}S_{ij}\right)^{1/2}$ with the turbulent viscosity being calculated in the same manner as with the standard k-epsilon model.

The model constants of the RNG k-ε model, $C_{1\varepsilon}, C_{2\varepsilon,} C_\mu,\ \sigma_k,\ \sigma_\varepsilon,\ \eta_0, and\ \beta$ are given below.

$C_{1\varepsilon} = 1.42$, $C_{2\varepsilon} = 1.68$, $C_\mu = 0.0845$, $\sigma_k = 0.7194$, $\sigma_\varepsilon = 0.7194$, $\eta_0 = 4.38, \beta = 0.012$[109].

### 2.8.3 Standard k-ω turbulence model

The standard k-ω model is another two-equation RANS turbulence model which replaces the rate of dissipation of turbulent kinetic energy in the k-ε model by the turbulence frequency (or specific dissipation rate), $\omega = \varepsilon/k$. The equations have forms similar to the k-ε model:

Kinematic Eddy Viscosity $v_T$

$$v_T = \frac{k}{\omega}$$

Turbulence Kinetic Energy k

$$\frac{\partial k}{\partial t} + u_j\frac{\partial k}{\partial x_j} = \tau_{ij}\frac{\partial u_i}{\partial x_j} - \beta^* k\omega + \frac{\partial}{\partial x_j}\left[(v + \sigma^* v_T)\frac{\partial k}{\partial x_j}\right]$$

Specific Dissipation Rate, $\omega$

$$\frac{\partial\omega}{\partial t} + u_j\frac{\partial\omega}{\partial x_j} = \alpha\frac{\omega}{k}\tau_{ij}\frac{\partial u_i}{\partial x_j} - \beta\omega^2 + \frac{\partial}{\partial x_j}\left[(v + \sigma v_T)\frac{\partial\omega}{\partial x_j}\right]$$

Closure coefficients and auxiliary relations

$\alpha = \frac{5}{9}, \beta = \frac{3}{40}, \beta^* = \frac{9}{100}, \sigma = \frac{1}{2}, \sigma^* = \frac{1}{2}$ and $\varepsilon = \beta^*\omega k$ [110, 111]

In aaplying these variants of k- ε turbulence models to the spray characteristics in the pressure swirl stomizer, Baharanchi et al [112] investigated the influence of variants of K-e turbulence model and Reynolds Stress Model (RSM) on the atomization characteristics and swirl strength of the internal flow of a pressure swirl atomizer. They used the Volume of Fluid (VOF) multiphase model in Fluent 6.3 to simulate the flow in the atomizer and used the implicit scheme to calculate the interface between the two phases. The results showed that RNG k-epsilon turbulence model performed satisfactorily with the experimental data when an effective inlet Weber number was introduced into the flow and also reduced the computational cost when compared to SST K-ω and RSM.

### 2.8.4 **Direct Numerical Simulation (DNS) atomization modelling**

The only means to exactly describe the atomization process numerically is through the use of Direct Numerical Simulation (DNS) where the full Navier-Stokes equations are solved exactly for all relevant length and time scales. For a fully turbulent multiphase flow, this involves discretizing the domain at a resolution on the scale of both the smallest turbulent velocity fluctuation (the Kolmogorov length scale) and the smallest liquid structure within the flow [113]. Gorokhovski and Herrmann [114] summarize the challenges involved in applying this strategy to study primary atomization as

- Spatial and temporal scales span many orders of magnitude.

In addition to resolving the Kolmogorov length scale η, it is also necessary to resolve the length scale of the smallest liquid structures. As topological change occurs, this length scale approaches zero as the liquid structure undergoes pinch-off. This necessitates a model to track topological changes.

- Discontinuities in material properties at the interface must be resolved

While some methods are able to approach a discontinuity in fluid properties well (for example a level set method) some approaches such as a finite difference method will introduce numerical smearing along the interface.

- Surface-tension presents a singular force at the interface.

Surface tension effects are crucial to accurate resolution of breakup in the case of small local Weber number. A typical approach to this problem is the continuum surface force method in which a local point force is applied proportional to the interfacial curvature.

- Both turbulence and turbulent atomization are inherently 3D rendering 2D simulation inaccurate.
- The interface undergoes rapid topological distortion as shown in Figure 2.15

Although DNS remains the only true way to resolve all atomization processes exactly its prohibitive cost restricts its use to primarily academic applications. Nonetheless, DNS results provide an invaluable tool for verifying models of primary atomization phenomenon for which no experimental data is available [114].
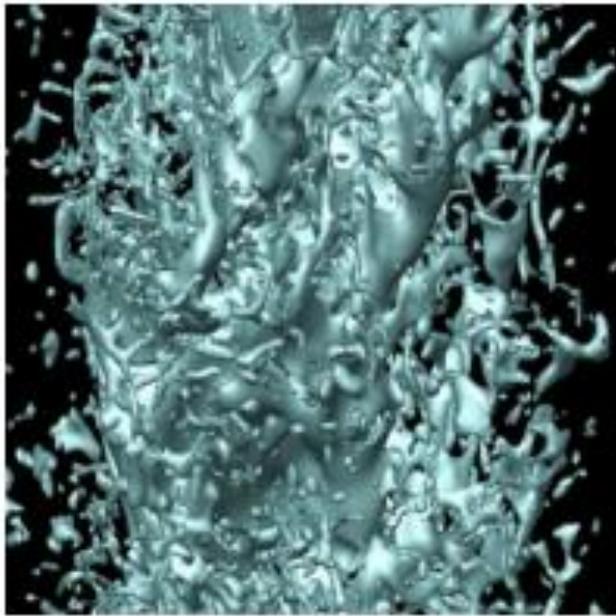


Figure 2.15 Direct Numerical Simulation (DNS) liquid structures downstream of injector [113]

### 2.8.5 Large Eddy Simulation (LES)

Large Eddy Simulation (LES) is an approach in which the larger three-dimensional unsteady turbulence is explicitly resolved while the small scale eddies are modeled. The smaller eddies which are responsible for the majority of the energy dissipation but contain only a small amount of energy are assumed to have a more universal isotropic character making them easier to model than the large eddies which are directly affected by the flow geometry and may have an unsteady character. This eases the turbulent resolution restriction significantly and has been used successfully to simulate single phase flow. Current LES approaches to resolving primary atomization either [114]

- Incorporate a coupled LES/DNS technique, performing a DNS calculation in regions containing multiple phases and LES in single-phase regions. This technique reduces the computational demand of DNS but is still expensive.
- Develop a sub-grid scale atomization model. Several attempts have been made to couple a near DNS scale Eulerian simulation to a Lagrangian droplet formulation removing stripped-off ligaments from the domain and replacing them with Lagrangian droplets with appropriate secondary atomization models.
- Neglect sub-grid atomization terms.

### 2.8.6 Turbulence model for two-phase flow

Elgbobashi et al [115] developed a two-equation turbulence model for predicting two-phase flows. His two equations described the conservation of turbulence kinetic energy and dissipation rate of that energy for the carrier fluid in a two-phase flow. These equations have been derived vigorously from the momentum equations of the carrier fluid. Closure of the time-mean equations was achieved by modeling the turbulent correlations up to third order. The new model eliminates the need to simulate in adhoc manner the effect of the dispersed phase on turbulence structure. Preliminary testing indicates that the model is successful in predicting the main features of a round gaseous jet laden with uniform-sized solid particles however the model is not implemented in most of the available commercial CFD codes.

The model conservation equations of the turbulence kinetic energy and the dissipation rate of that energy for the carrier fluid in a steady incompressible turbulent two-phase round jet are presented below.

(i)     The  turbulent kinetic energy k equation

$$\underbrace{\rho_1\varphi_1 U_1 k_{,1} + \rho_1\varphi_1 U_2 k_{,2}}_{convection} - (1/r)\underbrace{[\rho_1\varphi_1 r(v_t/\sigma_k)k_{,2}]_{,2}}_{Diffusion} - \underbrace{\rho_1\varphi_1 v_t U^2_{1,2}}_{production\ P}$$

$$+\begin{bmatrix} \dfrac{4}{3}C_{\varphi5}\rho_1(k^2/\epsilon)[(v_t/\sigma_\varphi)\varphi_{1,2}]_{,2}U_{2,2} - c_{\varphi5}\rho_1\,v_t \\[2mm] \left((k\big/\epsilon)[\underbrace{(v_t/\sigma_\varphi)\varphi_{1,2}]_{,2}}_{Extra\ Production}\,U^2_{1,2} - (v_t/\sigma_\varphi\right)\varphi_{1,2}p_{,2} \end{bmatrix} + \underbrace{\rho_1\varphi_1\epsilon}_{Dissipation}$$

$$+\left[F\varphi_2 k\left[1 - \int_0^\infty \left(\dfrac{\Omega_1 - \Omega_R}{\Omega_2}\right)f(\omega)d\omega\right] - \underbrace{F\,(U_2 - V_2)\left(\dfrac{v_t}{\sigma_\varphi}\varphi_{1,2}\right)}_{Extra\ Dissipation}\right.$$

$$\left.+\ C_{\varphi5}F\dfrac{k^2}{\epsilon}\left[1 - \int_0^\infty \left(\dfrac{\Omega_1 - \Omega_R}{\Omega_2}\right)f(\omega)d\omega\right]\left(\dfrac{v_t}{\sigma_\varphi}\varphi_{1,2}\right)_{,2}\right] = 0$$

(ii)    The turbulent dissipation rate $\epsilon$ equation

$$\underbrace{\rho_1\varphi_1 U_1\epsilon_{,1} + \rho_1\varphi_1 U_2\epsilon_{,2}}_{convection} - (1/r)\underbrace{[\rho_1\varphi_1 r(v_t/\sigma_\epsilon)\epsilon_{,2}]_{,2}}_{Diffusion} - \underbrace{C_{\epsilon1}(\epsilon/k)(P + P_e)}_{Total\ production}$$

$$+ \rho_1\varphi_1 \underbrace{(\epsilon/k)(C_{\epsilon2}\epsilon + C_{\epsilon3}\epsilon_e)}_{Total\ Dissipation} = 0$$

The subscripts 1 and 2 denote the fluid and dispersed phase respectively,    $U_i$ = the velocity components of the fluid, $V_i$= velocity components of the dispersed phase, $\rho$ = material density, $p$ = is the pressure, $\varphi$ = volume fraction, the symbol $(\ )_{,1}$ means $\partial(\ )/\partial x$ and, $(\ )_{,2}$ means $\partial(\ )/\partial r$, where x and r  are the distances along the axial and radial directions respectively.

The values of the constants are

$C_{\epsilon1} = 1.43,\ C_{\epsilon2} = 1.92, C_{\epsilon3} = 1.2,\ C_{\varphi5} = 0.1, \sigma_k = 1.0,\ \ \sigma_\epsilon = 1,3\ \sigma_\varphi = 1.0$  [115]

**2.9 Design Optimization**

Optimization is a tool used to obtain the optimum value of a certain function. For a given application and models, several engineering projects are possible. However, due to economic costs and input requirements, it is important to find the best configuration, which represents the optimum. The basic concepts of optimization are the objective functions and the constraints. The objective functions define a mathematical expression of some value to be optimized. It can either be maximized or minimized depending on the goal. As indicated by many researchers, in real engineering problems there will always be constraints. There are equality and inequality constraints [116] which are embodied in the deterministic and stochastic methods of optimization. In generating the design variables and the distributions, a statistical Design of Experiments (DoE) technique known as Latin Hypercube Designs (LHD) which is used in this work to obtain an optimum set of parameters for the model is also discussed.

### 2.9.1 **Deterministic methods**

These are methods with strong mathematical background. Thus, it is possible to prove that the minimum of a function under certain conditions was found. Because they require the computation of the gradient of the vector, which is the vector of the first derivatives of the object function, this is also called gradient-based methods. Steepest descent method, the conjugate gradient method, the Newton–Raphson, and the quasi-Newton method are examples of deterministic methods [116].

### 2.9.2 **Evolutionary and stochastic methods**

Evolutionary methods, in contrast to the deterministic methods, generally do not rely on strong mathematical basis and do not make use of the gradient nor second derivative of the objective function as a direction of descent. The evolutionary optimization algorithms attempt to mimic nature in order to find the minimum of the objective function. However, there is no proof of convergence to a global minimum, although they usually converge. These methods require more function evaluations than the gradient-based ones. Genetic algorithm, differential evolution, particle swarm and simulated annealing are examples of evolutionary methods [116, 117].

### 2.9.3 **Hybrid optimization**

A hybrid optimization is a combination of the deterministic and the evolutionary or stochastic methods, in the sense that it utilizes the advantages of each of these methods.

The hybrid optimization method usually employs an evolutionary or stochastic method to locate a region where the global extreme point is located and then automatically switches to a deterministic method to get to the exact point faster. The hybrid optimization method is quite simple conceptually, although its computational implementation is more involved [118].

### 2.9.4 **Response surface methods**

A statistical Design of Experiments (DoE) technique known as Response Surface Method (RSM) is used in order to obtain an optimum set of modelling parameters. The design of experiments (DoE) methodology has been applied to different knowledge fields because of its high reliability and accuracy in the results [119-122]. The other great advantage of this statistical analysis is the huge reduction in the number of simulations needed to achieve the optimum set of values for the input parameters, which predefine exactly the number of iterations, in comparison with evolutive methods in which the number of iterations is unknown forehand since the termination point is arbitrary in order not to obtain a local optimum [123].

Response surfaces methods significantly accelerate the entire design optimization process and are often used to replace very complicated physical models, to generate correlations of experimental data and to reduce the computational cost involved [124]. Response surfaces are mathematical functions used to simulate the behavior of processes, experiments, and complex engineering analysis techniques. They allow optimization techniques to be feasibly applied to classes of problems outside of computer evaluated objective functions. This occurs because a properly constructed response surface that captures the behavior of a complex, computationally intense objective can be used to speed up the optimization process. Also, a properly constructed response surface can be used to optimize a process, or experimental work, where only discrete, empirical samples of the underlying system's response to process parameters can be evaluated [117, 125]. There are a lot of different methods for generating response surface models. A popular, rapid, and accurate response surface method is to use Radial Basis Functions (RBF) as the foundation of creating a response surface[116]. It constructs an interpolation scheme with favorable properties such as high efficiency, good accuracy, and capability of dealing with scattered data, especially for higher dimension problems [117]. Another response surface model which uses interpolation method is Kriging and represents a relationship between objective

function (output) and design variables (input) using a stochastic process. The Kriging model drastically reduces the computational time required for objective function evaluation in the optimization (optimum searching) process[126]. This method is based on the assumption that the parameter being interpolated can be treated as a regionalized variable. A regionalized variable is intermediate between a truly random variable and a completely deterministic variable in that it varies in a continuous manner from one location to the next and therefore points that are near each other have a certain degree of spatial correlation, but points that are widely separated are statistically independent. In optimization, this method is very accurate when the number of design variables is small [116].

### 2.9.5 **Latin Hypercube Designs**

Latin hypercube designs abbreviated LHD is a rich class of designs that are suitable for computer experiments and numerical integration. They are easy to generate and achieve maximum stratification in each of the univariate margins of the design region[127]. McKay et al.[127] and Iman and Conover [128] proposed Latin-hypercube designs. These authors and Stein [129] showed that LHD is generally useful and efficient for computer experiments. It has some advantages in that it is computationally cheap to construct and covers the design region well without replications. One other good reason is that it allows the creation of experimental designs with as many points as needed or desired. Another good reason for the Latin hypercube popularity is flexibility. For example, if few dimensions have to be dropped out the resulting design is still a Latin hypercube design. This is because in Latin hypercube samples are non-collapsing i.e orthogonality of the sampling points. Although Latin hypercube designs have good uniformity with respect to each dimension individually, however, desirable properties such as space filling, or column-wise orthogonality come at the cost of very expensive optimization [130, 131].

In a computer experimental design with $p$ points in $d$ dimensions is written as a $p \times d$ matrix

$$X = \begin{bmatrix} x_1 & x_2 & \cdots x_p \end{bmatrix}^T$$

where each column represents a variable and each row $x_i = \begin{bmatrix} x_i^{(1)} & x_i^{(2)} & \cdots & x_i^{(d)} \end{bmatrix}$ represents a sample. A Latin hypercube design is constructed in such a way that each of the dimensions is divided into equal levels and that there is only one point (or sample)

at each level. As originally proposed, a random procedure is used to determine the point locations.

Figure 2.16 shows two examples of Latin hypercube designs with good and poor space filling properties. A better choice is shown in Figure 2.16 (a) where the points are more uniformly distributed over the domain [132].
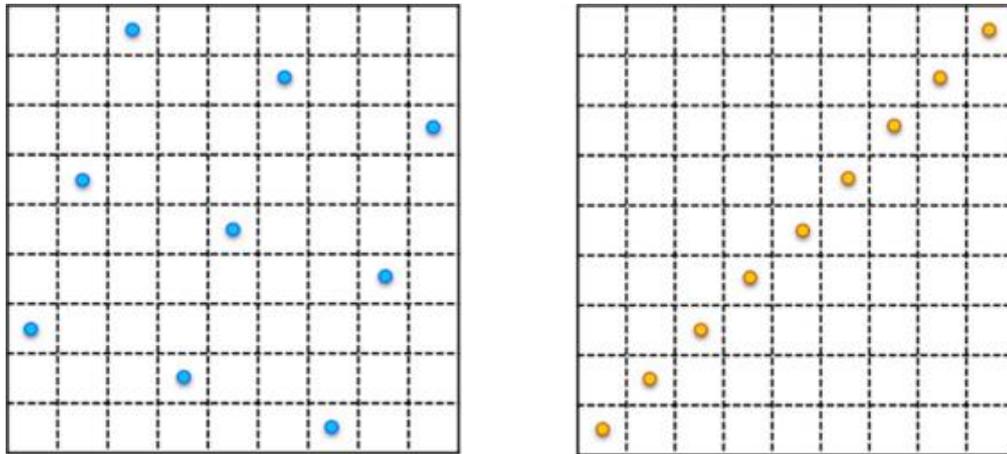


a.Design with good space filling properties    b.Design with poor space filling properties

Figure 2.16 Latin hypercube designs with good and poor space filling properties

Modified Latin hypercube designs used in this work is a modification of the Matlab Statistics function lhsdesign (code) for LHD which provides a Latin hypercube sample of n values of each of p variables and the variables can range between any minimum and maximum numbers specified by the user, whereas the original LHD only provide data between 0 and 1 which is not very helpful in this practical problem where the design range is not bound to 0 and 1. To identify the number design points to be generated Felipe et al [133] presented in Table 2.6 a set of configurations that covers the typical application range of the LHD.

Table 2.6 Table Latin hypercube design configurations

| No. of variables | | No. of points | | |
| --- | --- | --- | --- | --- |
| | | Small designs | Medium designs | Large designs |
| 2 | | 12 | 20 | 120 |
| 4 | | 30 | 70 | 300 |
| 6 | | 56 | 168 | 560 |
| 8 | | 90 | 330 | 900 |
| 10 | | 132 | 572 | 1320 |
| 12 | | 182 | 910 | 1820 |

Rajaram et al. [134] carried out a study on the optimization of spray characteristics of biodiesel using response surface method of Design of Experiments (DoE). They considered three influencing factors such as the injection pressure, fuel temperature and fuel blends and indicated that the injection pressure and fuel temperature are the most important factors affecting the spray tip penetration (S), spray angle (θ) and Sauter mean diameter (SMD) since they have greater influence in the sheet disintegration and atomization. They chose three levels of factors for fuel injection pressure varies from 180 to 220 bars, fuel temperatures 50°C, 60°C and 70°C and biodiesel fuel blends namely KB20, KOME and COME for the three levels respectively although the constituents of these blends were not specified. With these parameters, 27 design of experiment points were developed using full factorial design approach. The spray emanating from the multi-hole nozzle of diameter 0.33mm was captured using a high speed digital camera and the spray cone angles and the spray penetration tip were measured from the images captured by the camera for each respective DOE point. The SMD was calculated using $SMD = 500D^{1.2}\vartheta^{0.2}/V_{inj}$ and $V_{inj} = \sqrt{2\Delta P/\rho}$, where D= diameter of orifice of nozzle, V= kinematic viscosity of fuel $V_{inj}$ = fuel injection velocity, $\Delta P$ = (injection pressure − atmospheric pressure), $\rho$ = density of fuel. When the SMD was considered for finding the optimized conditions, it was realised from the response surface methodology that KOME oil at 210 bar injection pressure and 62°C fuel temperature were the optimized conditions and these conditions were used to test the engine performance and calculate the pollutants in the emission.

## 2.10 Summary

This chapter covers many types of atomizers used in practice such as pressure atomizers, rotary atomizers and twin-fluid atomizers. Atomization processes such as break up of liquid jets and sheets as well as its break up regimes were discussed. The Sauter Mean Diameter (SMD) which is the main focus of this work was also described along aside the best known empirical SMD correlations for pressure swirl nozzles. The current state in the theoretical, experimental and numerical studies of flow inside and spray charateristics outside the pressure swirl atomizer were thoroughly reviewed. The various general turbulence models currently available in commercial CFD codes were also looked at and in particular the Reynolds Averaged Navier–Stokes (RANS) equations which provided an approximate time-averaged solution method to the Navier–Stokes (NS) equations. A brief review of variants of k-epsilon turbulence models on the spray characteristics in the pressure swirl atomizer were also presented. The design optimization techniques were also reviewed in order to identify the optimal nozzle exit design parameter, operating conditions and fluid properties that give the most minimum drop sizes (SMD) at the spray centre line. In order to select the appropriate technique to generate the design variables a statistical Design of Experiments (DoE) techniques known as Latin Hypercube Designs (LHD) which is used in this work to obtain an optimum set of parameters for the model was also adequately discussed.

# CHAPTER 3 COMPUTATIONAL FLUID DYNAMICS (CFD) CODE SELECTION

## 3.1 Introduction

This section gives a brief overview of the CFD solver used in this study. There are several major commercial CFD software packages available now including STAR-CCM+[135], ANSYS FLUENT[136], CFX[137], OpenFOAM[138], STAR-CD[139], etc. Generally, these packages can provide basic functions about flow calculation, two-phase flow, and other applications based on different mathematical models and mesh generation strategies. A commercial STAR-CD code is used in this study because it provides a wide range of mathematical models for different physical transport problems like spray and atomization, droplet evaporation, combustion, heat transfer, particle mixing, etc., and can be applied in various categories like automotive (internal combustion engines), mechanical, nuclear, and chemical, etc. The flow in STAR-CD study can be compressible or incompressible, laminar or turbulent, single phase or multiphase, and the geometry can be a simple tube or a complex domain. In addition, it makes uses of various types of boundaries such as porous media, solid wall, moving or periodic in steady or unsteady flow fields. STAR-CD also provides a powerful set of meshing, pre and post-processing data tools to analyse interested physical parameters on certain locations in the simulated geometry which can enhance the understanding of complex physical phenomenon.

## 3.2 Basic conservation equations

An essential task in CFD is to resolve the conservation equations of mass flow and momentum to obtain the velocity and pressure fields in the domain. After that other models can be started using this basis of velocity and pressure distribution for different applications.

The mass and momentum conservation equations (the 'Navier-Stokes' equations) [140] solved by STAR-CD for general incompressible and compressible fluid flows in Cartesian tensor notation are shown in equations 3.1 and 3.2 respectively[139] :

$$\frac{\partial \rho}{\partial t} + \frac{\partial}{\partial x_j}\left(\rho u_j\right) = S_m \qquad\qquad 3.1$$

$$\frac{\partial \rho u_i}{\partial t} + \frac{\partial}{\partial x_j}\left(\rho u_j u_i - \tau_{ij}\right) = -\frac{\partial p}{\partial x_i} + S_i \qquad\qquad 3.2$$

where $t$ — time

$x_i$          — Cartesian coordinate (i = 1, 2, 3)

$u_i$          — absolute fluid velocity component in direction $x_i$

$p$          — piezometric pressure $p_s - \rho_0 g_m x_m$ where $p_s$ is static pressure, $\rho_0$ is reference density, the $g_m$ are gravitational acceleration components and the $x_m$ are coordinates relative to a datum where is defined

$\rho$          — density

$\tau_{ij}$          — stress tensor components

$S_m$          — mass source

$S_i$          — momentum source components and repeated subscripts denote summation.

The specialisation of the above equations to a particular class of flow involves

- Specification of a constitutive relation connecting the components of the stress tensor $\tau_{ij}$ to the velocity gradients.

- Specification of the 'source', $S_i$ , which represents the sum of the body and other external forces, if present

- Application of ensemble or time averaging if the flow is turbulent

For Newtonian turbulent flows

$$\tau_{ij} = 2\mu S_{ij} - \frac{2}{3}\mu \frac{\partial u_k}{\partial x_k}\delta_{ij} - \bar{\rho}\overline{u_i'u_j'}$$        3.3

where the $u'$ are fluctuations about the ensemble average velocity and the overbar denotes the ensemble averaging process. The rightmost term in the above represents the additional Reynolds stresses due to turbulent motion. These are linked to the mean velocity field via the turbulence models. In principle, STAR-CD can accommodate any form of user-specified momentum source field $S_i$, but it does contain built-in provision for two common kinds of body forces, arising from buoyancy and rotation, respectively[139]. The relevant expressions are:

Buoyant forces

$$S_i = g_i(\rho - \rho_0)$$        3.4

where $g_i$ is the gravitational acceleration component in direction $x_i$ and $\rho_0$ the reference density.

Rotational forces

$$S_i = f(u_k, \omega_k, r_k) \tag{3.5}$$

where $f( )$ is a function involving components of the rotation vector $\omega_k$ and radius vector $r_k$ about a user-specified axis[139].

## 3.3 Thermophysical properties

The modelling framework of STAR-CD provides for variations of all the thermophysical properties of fluid(s), namely density, viscosity, thermal conductivity, species diffusivities and specific heats, as functions of temperature, mass fraction and other variables. In some cases, optional built-in dependencies are provided. In all cases, facilities are available for user-specified property functions to be inserted. The in-built function relevant to this research for the equation of state (density) for incompressible multicomponent mixtures is given by

$$\rho = \left[ \sum_m \left( \frac{Y_m}{\rho_m} \right) \right]^{-1} \tag{3.6}$$

where $Y_m$ and $\rho_m$ are the mass fraction and density of component m, respectively [139].

## 3.4 Generic variables

STAR-CD offers an additional facility for solving an arbitrary number of transport equations for user-defined variables needed for special-purpose applications as well as solving the basic flow equations. The generic form of the transport equation for these variables can be written as:

$$\frac{d}{dt} \underbrace{\int_V T_\phi \phi dV}_{\text{Transsient}} + \underbrace{\int_S C_{\phi 1} \phi (u - u_c). dS}_{\text{Convection 1}} + \underbrace{\int_S C_{\phi 2} \phi (u_{gc} - u_c). dS}_{\text{Convection 2}} = \underbrace{\int_S D_\phi \text{grad}\phi. dS}_{\text{Diffusion}} +$$
$$\underbrace{\int_V S_\phi dV}_{\text{Source}} \tag{3.7}$$

where $\phi$ is a transported scalar or vector component, u the fluid velocity, $u_c$ the control volume surface velocity (grid velocity). The second convection term in the above equation allows for the possibility that the generic variable property is convected by a velocity $u_{gc}$ different from the fluid velocity, where $u_{gc}$ is specified by the user. The user-specified coefficients $T\phi$, $C\phi 1$, $C\phi 2$, $D\phi$ and $S\phi$ can be either constants or arbitrary functions defined via user subroutines. Existence of any of the transient, convection, diffusion or source terms is optional [139].

### 3.5 Turbulence modelling options in STAR-CD

STAR-CD offers a wide variety of turbulence modelling capabilities. These may be subdivided into four categories as eddy Viscosity models, Reynolds Stress models, Large Eddy Simulation models and Detached Eddy Simulation models.

It is generally recognised that all existing turbulence models, including those mentioned here, are inexact representations of the physical phenomena of turbulence. The degree of approximation in a given model depends on the nature of the flow to which it is being applied, and the characterisation of the circumstances which give rise to 'good' and 'bad' performance must unfortunately be based mainly on experience[139].

### 3.5.1 **The k-ε turbulence models**

The main options currently available in STAR-CD for the well-known k-ε models for general applications are the 'standard' k-ε model [108, 141, 142], the 'Renormalisation Group' (RNG) version of the k-ε model [109, 143], the 'realizable' k-ε model [144]. In these models, k and ε turbulent kinetic energy and its dissipation rate are chosen as typical turbulent velocity scale and length scale respectively. The options differ from each other in one of the following respects such as the form of the equations, the treatment of the near-wall region or the relation between Reynolds stresses and the rates of strain. The Standard k-ε model is employed in this study because it is the most widely used, one recommended fo the atomization model and validated turbulence model with varied applications[40].

### 3.5.2 **Standard k-ε model**

The 'standard' model in which the high Reynolds number forms of the k and ε equations are used in STAR CD in conjunction with algebraic law-of-the-wall representations of flow, heat and mass transfer. The transport equations for standard k-ε modelare as follows

Turbulent kinetic energy k

$$\frac{\partial}{\partial t}(\rho k) + \frac{\partial}{\partial x_j}\left[\rho u_j k - \left(\mu + \frac{\mu_t}{\sigma_k}\right)\frac{\partial k}{\partial x_j}\right] = \mu_t(P + P_B) - \rho\varepsilon - \frac{2}{3}\left(\mu_t\frac{\partial u_i}{\partial x_i} + \rho k\right)\frac{\partial u_i}{\partial x_i} + \mu_t P_{NL}$$

$$3.8$$

where

$$P = S_{ij}\frac{\partial u_i}{\partial x_j}$$

$$P_B = -\frac{g_i}{\sigma_{k,t}}\frac{1}{\rho}\frac{\partial \rho}{\partial x_i}$$

$$P_{NL} = -\frac{\rho}{\mu_t}\overline{u_i'u_j'}\frac{\partial u_i}{\partial x_j} - \left[P - \frac{2}{3}\left(\frac{\partial u_i}{\partial x_i} + \frac{\rho k}{\mu_t}\right)\frac{\partial u_i}{\partial x_i}\right]$$

$P_{NL} = 0$ for linear models and $\sigma_k$ is the turbulent Prandtl number. The first term on the right-hand side of equation 3.8 represents turbulent generation by shear and normal stresses and buoyancy forces, the second viscous dissipation, and the third amplification effects. The last term accounts for the non-linear contributions.

Turbulent dissipation rate $\varepsilon$

$$\frac{\partial}{\partial t}(\rho\varepsilon) + \frac{\partial}{\partial x_j}\left[\rho u_j\varepsilon - \left(\mu + \frac{\mu_t}{\sigma_\varepsilon}\right)\frac{\partial \varepsilon}{\partial x_j}\right] = C_{\varepsilon 1}\frac{\varepsilon}{k_t}\left[\mu_t P - \frac{2}{3}\left(\mu_t\frac{\partial u_i}{\partial x_i} + \rho k\right)\frac{\partial u_i}{\partial x_i}\right] + C_{\varepsilon 3}\frac{\varepsilon}{k}\mu_t P_B -$$

$$C_{\varepsilon 2}\rho\frac{\varepsilon^2}{k} + C_{\varepsilon 4}\rho\varepsilon\frac{\partial u_i}{\partial x_i} + C_{\varepsilon 1}\frac{\varepsilon}{k}\mu_t P_{NL} \hspace{3cm} 3.9$$

where $\sigma_\varepsilon$ is the turbulent Prandtl number and $C_{\varepsilon 1}, C_{\varepsilon 2}, C_{\varepsilon 3},$ and $C_{\varepsilon 4}$ are coefficients whose values are given in Table 3.1[108]. The first term on the right-hand side of equation (3.9) represents the contribution to the production of dissipation due to linear stresses and dilatation effects, the second the contribution due to buoyancy, the fourth the contribution due to temporal mean density changes (of importance in combustion models), and the fifth the contribution due to non-linear stresses. The third term in the equation accounts for the dissipation destruction [139].

Table 3.1 Coefficients of the Standard k-ε Turbulence Model

| $C_\mu$ | $\sigma_k$ | $\sigma_\varepsilon$ | $\sigma_h$ | $\sigma_m$ | $C_{\varepsilon 1}$ | $C_{\varepsilon 2}$ | $C_{\varepsilon 3}$ | $C_{\varepsilon 4}$ | K | E |
|---|---|---|---|---|---|---|---|---|---|---|
| 0.09 | 1.0 | 1.22 | 0.9 | 0.99 | 1.44 | 1.92 | 1.44 | -0.33 | 0.419 | 9.0 |

### 3.6 SIMPLE algorithm

The SIMPLE (Simple Implicit Method of Pressure-Linked Equation) algorithm gives a method of calculating pressure and velocities. The method is iterative and when other scalars are coupled to the momentum equations, the calculation need to be done sequentially. The sequence of operations in CFD procedure which employs the SIMPLE algorithm is given in Figure 3.1.



START

Initial guess $p^*, u^*, v^*, \phi^*$

STEP 1: Solve discretised momentum equations

$$a_{i,j}u^*_{i,j} = \sum a_{nb}u^*_{nb} + \left(p^*_{i-1,j} - p^*_{i,j}\right)A_{i,j} + b_{i,j}$$
$$a_{i,j}v^*_{i,j} = \sum a_{nb}v^*_{nb} + \left(p^*_{i,j-1} - p^*_{i,j}\right)A_{i,j} + b_{i,j}$$

$u^*, v^*$

STEP 2: Solve pressure correction equation

$$a_{i,j}p'_{i,j} = a_{i-1,j}p'_{i-1,j} + a_{i+1,j}p'_{i+1,j} + a_{i,j-1}p'_{i,j-1} + a_{i,j+1}p'_{i,j+1} + b'_{i,j}$$

$p'$

Set
$p^* = p, u^* = u$
$v^* = v, \phi^* = \phi$

STEP 3: Correct pressure and velocities
$$p_{i,j} = p^*_{i,j} + p'_{i,j}$$
$$u_{i,j} = u^*_{i,j} + d_{i,j}\left(p'_{i-1,j} - p'_{i,j}\right)$$
$$v_{i,j} = v^*_{i,j} + d_{i,j}\left(p'_{i,j-1} - p'_{i,j}\right)$$

$p, u, v, \phi^*$

STEP 4: Solve all the other discretised transport equations

$$a_{i,j}\phi_{i,j} = a_{i-1,j}\phi_{i-1,j} + a_{i+1,j}\phi_{i+1,j} + a_{i,j-1}\phi_{i,j-1} + a_{i,j+1}\phi_{i,j+1} + b\phi_{i,j}$$

$\phi$

No         Convergence?

Yes

STOP

Figure 3.1 Flow chart of the SIMPLE algorithm [103, 108]

### 3.7 PISO algorithm

PISO algorithm (Pressure implicit with splitting of operator) was proposed by Issa in 1986 without iterations and with large time steps and a lesser computing effort. It is an extension of the SIMPLE algorithm used in CFD computational fluid dynamics to solve the Navier-Stokes equations. PISO is a pressure-velocity calculation procedure for the Navier-Stokes equations developed originally for non-iterative computation of unsteady compressible flow, but it has been adapted successfully to steady-state problems. PISO involves one predictor step and two corrector steps and is designed to satisfy mass conservation using predictor-corrector steps [103, 145] as shown in Figure 3.2.
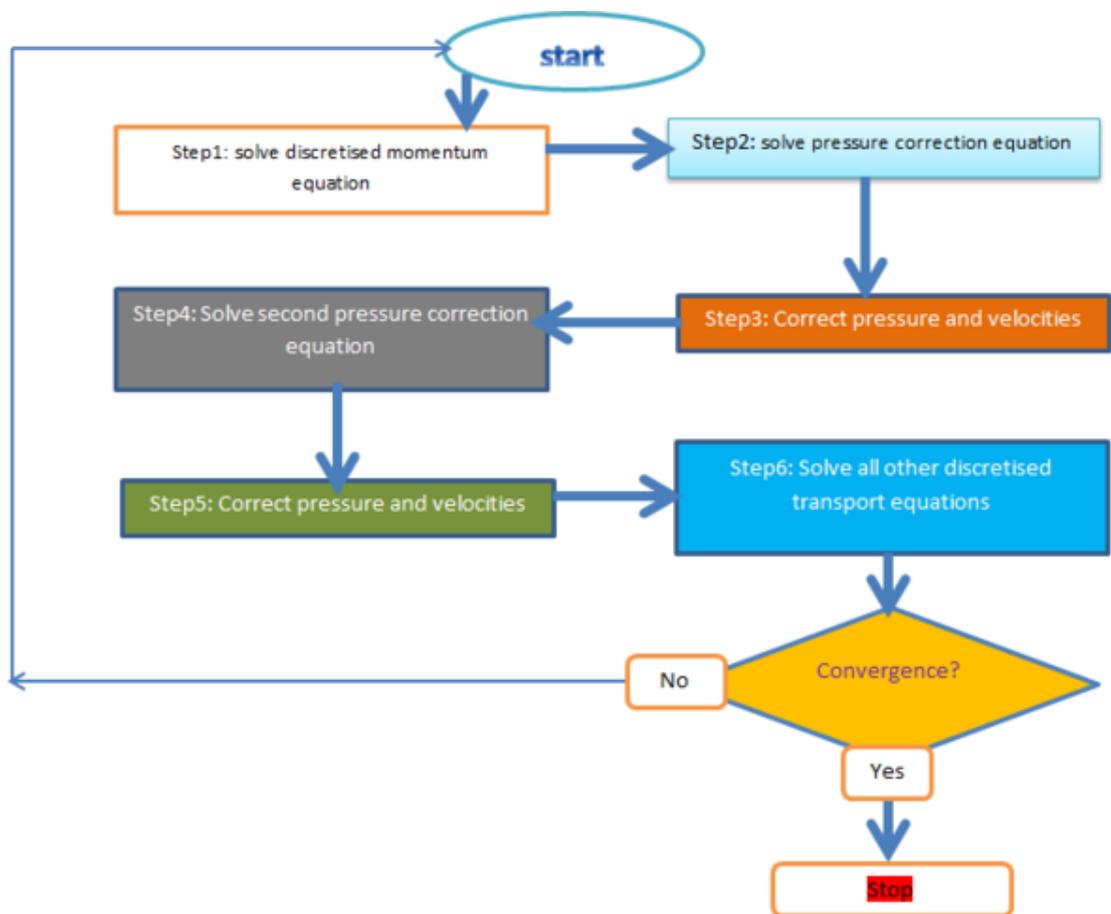


Figure 3.2 Flow chart of PISO algorithm[145]

PISO generally gives more stable results and takes less CPU time but not suitable for all processes[145]. For laminar backward facing step PISO is faster than SIMPLE but it is slower concerning flow through heated fin and if momentum and scalar equation have weak or no coupling then PISO is better than SIMPLEC[103].

60

### 3.8 Geometry and computational mesh capabilities

The versatility and accuracy of an industrial continuum mechanics analysis system are very much tied to the flexibility of the computational mesh structure it employs. This determines both the level of geometrical complexity it can handle and the degree of control it offers over resolution of flow features. The function of the mesh is to fit the boundary surface of the computational domain and subdivide its volume into subdomains or 'cells', used in the numerical solution of the differential conservation equations of the mathematical model. STAR-CD employs a highly flexible mesh system that is probably unique in its combination of features[139]. At its heart lies the STAR-CD solver's ability to perform a numerical analysis in a mesh consisting of arbitrary polyhedral cells, which may be used for fitting local geometrical features to a high degree of fidelity or for facilitating further mesh generation or optimization. Special cell shapes within this general category include hexahedra, tetrahedra, triangular prisms and pyramids, all of which may be generated using pro-STAR's basic meshing capabilities. More complex, polyhedral cells may be created by pro-STAR's advanced Auto Meshing module of the same volume. Further still, grids containing cells of arbitrary shape may be created in third-party packages and then imported into STAR-CD. The 3D model geometry shown in Figure **3.3** which is used to perform full 3D steady state simulations  has 100mm by 150mm  for the diameter and vertical height of the computational domain. Other important geometrical parameters are exit orifice diameter 3.5 mm, diameter of swirl chamber 12 mm, exit orifice height 8mm and vertical height of contraction portion 3mm. These dimesions were chosen to suit the nozzle used in the experimental validation and to accommodate all the axial and radial distances considered in the spray.  The mesh imported into STAR-CD is shown and Figure 3.4. The mesh sizes were varied to determine whether the solution was grid dependent or not since it has been shown that a fine mesh produces better or accurate results and predictions than a coarse mesh though a fine grid increases the computational time.  Therefore, an optimal mesh configuration is required that provides a balance between computational time and solution accuracy. It was realized after various refinements of the mesh in relation to the simulation results that a final non-uniform mesh grid composed of 1,894,340 polyhedral cells with base size 0.03mm produced better results than the base size of 0.05mm. The distribution of the mesh was done such that the swirl chamber and the middle of the cylinder have fine cells and coarse meshes on the remaing part of the cylinder.  The refined grid spacing on the

swirl chamber was about 0.015 mm and coarse mesh of 0.03 mm on the computation domain with a growth factor of 2.0. This is to reduce the computational time.
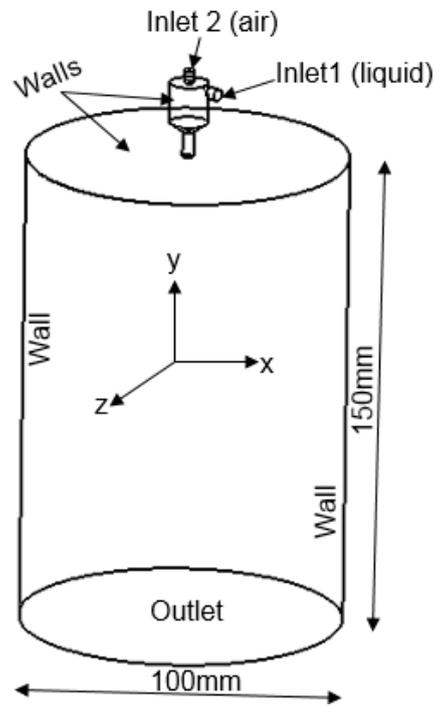


Figure 3.3 The computational domain and boundary conditions
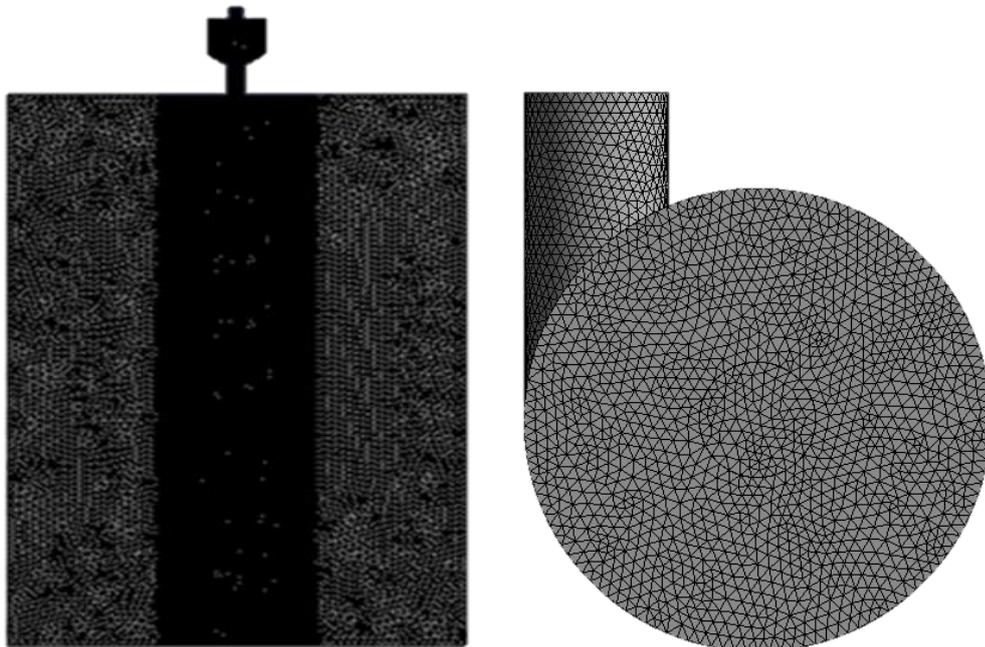


Figure 3.4 Mesh on vertical and cross section planes through the atomizer model

### 3.9 Discretization practices in STAR-CD

The differential equations governing the conservation of mass, momentum, energy, etc. within fluid systems are discretised by the finite volume (FV) method [146, 147]. Thus, they are first integrated over the individual computational cells and then approximated in terms of the cell-centred nodal values of the dependent variables. This approach has the merit, amongst others, of ensuring that the discretised forms preserve the conservation properties of the parent differential equations.In STAR-CD, only implicit schemes for time advancement are used. This means that diffusive and convective fluxes and source terms are computed at each time step. Two options for approximating the time derivative are offered. The choice depends on the solution algorithm used. In the case of SIMPLE, predominantly used for steady flows but under some conditions also recommended for transient flow simulations. The available options are the first order, fully-implicit Euler scheme and the second order, fully-implicit scheme with three time levels also called 'quadratic backward implicit'. In the case of PISO, which is optimized for transient flow simulations, no choice is available: a special implicit scheme is used, based on the fully-implicit Euler scheme and explicit deferred correctors, which results in a formal accuracy lying between first and second order. In terms of spatial discretization, the differencing schemes available in STAR-CD for all types of mesh are the upwind differencing (UD), linear upwind differencing (LUD), central differencing (CD) scheme, monotone advection and reconstruction scheme (MARS) and blended differencing. The upwind differencing (UD) which may be low (first)-order scheme or second-order scheme selects the nearest upwind neighbour value for the transport quantity and also prevents the formation of artificial maxima in the solution. This form of interpolation preserves the correct physical bounds on transport quantity under all conditions, but can lead to numerical diffusion [148, 149]. Linear upwind differencing (LUD) which is the second-order accurate scheme formulated for non-structured meshes and derived from a scheme originally proposed for structured meshes. It results in less numerical smearing than the UD scheme, but can produce solutions that are outside the physical bounds on transport quantity (i.e. numerical dispersion) and central differencing (CD) scheme, which is also second-order, simply interpolates linearly on nearest neighbour values, irrespective of flow direction. This scheme also produces less numerical diffusion, but can be dispersive. It is particularly recommended for use in direct and large-eddy simulation of turbulent flows [103].

### 3.10 Boundary conditions

STAR-CD contains built-in boundary condition options that cover the majority of practical situations. These options are selected using pro-STAR which provides a level of spatial selection resolution ranging from individual cell faces through to entire surfaces. Any physically-consistent mix of boundary conditions is admissible. The available options used in the research are inlet (prescribed flow) boundary, outlet boundary, impermeable wall boundary and the symmetry plane. The inlet (prescribed flow) which is at an inlet or 'free' boundary, where the distributions of mass flux and fluid properties are known. The outlet boundary treatment is suitable for locations where the flow is everywhere outwards-directed, but the conditions are otherwise unknown. They are, of course, mainly determined by what is happening upstream. In impermeable wall the usual no-slip prescriptions for velocity is either applied directly or, in the case of turbulent flow calculations with certain turbulence models, via 'wall functions'. These also include provision for wall roughness. Symmetry plane denotes a surface such that all field quantities on one side of it are a mirror image of those on the other side. The various boundary locations and conditions for the model are shown in Figure 3.3. The following quantities and values are defined as material properties for the inlet boundary regions. Liquid of density ($\rho_l = 997.5 \, kg/m^3$) flows through the velocity inlet1 of 3.7mm diameter with air of density ($\rho_g = 1.30 kg/m^3$) passing through the other 3mm diameter inlet2. The inlet boundary conditions used to perform the calculations for the liquid are one (1) for liquid mass fraction, 10% for turbulence intensity, 0.005m for turbulent length scale and 5.0 m/s for the velocity magnitude. The air inlet conditions remain the same except for the velocity magnitude and mass fraction which are 1 m/s and zero respectively. The outlet boundary conditions are 10% for turbulent intensity, mass fraction of one for both liquid and air and 0.0024 m for the turbulent length scale. The walls represent the solid walls of the nozzle and the computation domain and standard wall functions are used to model the near-wall regions with no-slip conditions.

### 3.11 Atomization modelling

Spray and atomization modelling refers to a subset of discrete phase particle modelling that describes the breakup of a continuous liquid into droplets. A number of industrial processes and applications such the internal combustion engines require turning of quantities of liquid into vapour. To burn such stable liquid fuels in an engine, the fuel droplets must be finer for intimate mixing to occur between the fuel and the oxidizer in a gaseous state. This gaseous mixing entails turning the liquid into a vapour and promoting mixing of the resulting gases. There are two general categories of spray modelling and these are primary atomization and secondary atomization. Primary atomization makes assumptions about the physics inside the nozzle and computes an initial drop size in the region near the nozzle [150]. On the other hand, secondary atomization models droplets that traverse the domain where they become hydrodynamically unstable and break into smaller droplets. Droplets can interact with each other directly through collision, creating larger droplets and changing the dynamics of the spray plume [1, 7]. There are a number of mixed approaches used to characterise the spray in the primary and the secondary atomization regions. Spray atomization models such as the Langragian or Discrete Droplet Model (DDM), Eulerian Model, Eulerian-Eulerian model and Eulerian-Langrangian Spray Atomization (ELSA) models are briefly reviewed with special focus and in-depth review of the entirely Eulerian model proposed by Vallet et al called $\Sigma - Y$ atomization model [23].

### 3.11.1 Lagrangian atomization model

Lagrangian spray method also called Discrete Droplet Model (DDM) derived from stability analysis of the Kelvin-Helmholtz and Rayleigh instabilities have been in use for the past twenty years and used to characterise the spray in the secondary atomization regime. These methods have achieved this popularity due to their computational efficiency and ability to match experimental spray angles and penetrations [151]. The assumption is typically made that the liquid phase has negligible volume fraction in comparison to the gas phase rendering such simulations to be accurate only in predicting secondary breakup in the far-field of the flow. As such, many applications require tuning of model constants based on empiricism. The main drawback of this method is that it requires the first cell to be two or three times bigger than the nozzle diameter and makes the profile of the velocity at the inlet to be lost [152] There have been significant attempts to generalize the Lagrangian formulation to

accommodate accurate resolution of primary atomization. Gorokhovski et al. [153] generalized the stochastic approach traditionally used to model secondary atomization to predict primary air-blast atomization.

### 3.11.2 Eulerian modelling

Vallet et al [23] proposed an entirely Eulerian model called $\Sigma - Y$ atomization model which treats two phase flow as a single continuous flow with variable density at high Reynolds and Weber numbers. This model which is analogous to the model used in calculating the flame front in combustion captures the features of primary atomization and mainly characterise the droplet Sauter Mean Diameter (SMD) and the number density. The model makes assumption similar to Kolmogorov hypothesis of turbulence that at large Reynolds and Weber numbers the flow is independent of surface tension and viscosity. To capture the rate at which the surface energy is created the transport equation for the interfacial surface density is developed. This equation contains the production and destruction terms accounting for the physical phenomenon of interface stretching and collapse. The second transport equation for the liquid mass fraction controls the liquid dispersion and models the turbulent mixing of the liquid. The mean density of the two fluids is linked to the liquid mass fraction. With the knowledge of the interfacial surface density, liquid mass fraction and the mean density the droplet SMD is then determined for the primary atomization. This will then be used as an input for the secondary break up in the Lagrangian formulation and will in turn be used to predict liquid vaporization and subsequent in the combustion calculations [113, 154]. The $\Sigma - Y$ model has been successfully applied and validated for a variety of coaxial and diesel jet type injectors [40].

### 3.11.3 Governing equations

An entirely Eulerian approach proposed by Vallet et al.[23] treats a two- phase medium as a single continuum where the dense phase is described similarly to a species in a multi-component reactive mixture.

Let $\tilde{Y}_{liq}$ be the liquid mass fraction per unit mass of the two-phase medium, then

Conservation equation for liquid mass fraction [40]

$$\frac{\partial \bar{\rho}\,\tilde{Y}_{liq}}{\partial t} + \frac{\partial \bar{\rho}\,\tilde{u}_j \tilde{Y}_{liq}}{\partial x_j} = \frac{\partial}{\partial x_j} \bar{\rho}\,\frac{D_t}{Sc_{liq}}\frac{\partial \tilde{Y}_{liq}}{\partial x_j} - \dot{m}_{vap}\bar{\rho}\tilde{\Sigma} \tag{3.10}$$

where $\bar{\rho}$ is the Reynold-average density, $\tilde{u}_j$ is the Favre-averaged velocity of both phases,

The mean density $\bar{\rho}$ is related to the Favre averaged liquid mass fraction $\tilde{Y}$ by

$$\frac{1}{\bar{\rho}} = \frac{\tilde{Y}_{liq}}{\rho_l} + \frac{1 - \tilde{Y}_{liq}}{\rho_g}$$

3.11

where $\rho_l$ and $\rho_g$ are the constant liquid and gas densities respectively. It is assumed that the pressure acting upon both phases is equal.

$\dot{m}_{vap}$ is the mean rate of vaporization per unit surface of the liquid $\tilde{\Sigma}$ is the mean surface area of the gas-liquid interface per unit of two-surface media. Dispersion of the liquid by the turbulence is expressed in the equation by using the turbulent diffusivity $D_t$ and the turbulent Schmidt number as constant $Sc_{liq} = 0.7$

Let $\tilde{\Sigma}$ be the average surface area of the liquid-gas interface per unit mass of two-phase medium. The transport equation for the $\tilde{\Sigma}$ can be written as [40]

$$\frac{\partial \bar{\rho} \tilde{\Sigma}}{\partial t} + \frac{\partial \bar{\rho} \tilde{u}_j \tilde{\Sigma}}{\partial x_j} = \frac{\partial}{\partial x_j} \bar{\rho} \frac{D_t}{Sc_\Sigma} \frac{\partial \tilde{\Sigma}}{\partial x_j} + \frac{\bar{\rho}\tilde{\Sigma}}{\tau_c}\left[1 - \frac{\tilde{\Sigma}}{\Sigma_{eq}}\right]$$

3.12

where $D_t$ is the turbulent diffusivity, $Sc_\Sigma$ is turbulent Schmidt number and is a constant $Sc_\Sigma = Sc_t = 0.7$, $\tau_c$ is the rate of surface production and is proportional to turbulence time scale given by

$$\tau_c = C_1 \frac{\tilde{k}}{\tilde{\varepsilon}}$$

3.13

$\Sigma_{eq}$ is equilibrium interface area and is related to equilibrium drop size $r_{eq}$ [23, 40] by:

$$\Sigma_{eq} = \frac{3\tilde{Y}_{liq}}{\rho_l r_{eq}}, \qquad r_{eq} = C_r \left(\frac{\bar{\rho}\tilde{Y}_{liq}}{\rho_{liq}}\right)^{2/15} \frac{\mathfrak{y}^{2/5}}{\tilde{\varepsilon}^{2/5}\rho_{lig}^{3/5}}$$

3.13

where $C_r$ is a constant $\mathfrak{y}$ is the surface tension of the liquid.

The atomization model eqs.(3.10) and (3.12) require a turbulent diffusivity and an integral scale $\tau_c$ and the standard k-$\varepsilon$ turbulence model was used to calculate these variables as well as providing closure of the fluid dynamics transport equations[155].

Once $\tilde{\Sigma}$ is calculated, the Sauter mean diameter (SMD) $d_{32}$ and the number density $n$ can be found as:

$$d_{32} = \frac{6\bar{\rho}\tilde{Y}_{liq}}{\rho_{liq}\tilde{\Sigma}} \qquad n = \frac{\rho_{liq}{}^2 \tilde{\Sigma}^3}{36\pi\bar{\rho}^2\tilde{Y}_{liq}{}^2}$$

2.27

### 3.11.4 **Evaluation of $\Sigma - Y$ Model**

Beheshti et al [40] assessed $\Sigma - Y$ model's ability to predict the effects of liquid properties and injection regimes on the atomisation quality in air-assisted atomizer. Air-assisted atomisation for which extensive experimental data are available was chosen as a test case. It was shown that a good agreement was observed between the predictions and the experiment for a wide range of liquid properties such as density and surface tension for the various injection regimes defined for the liquid and gas velocities. They noted however that the model is limited in the fact that it only attempts to resolve the Sauter mean diameter (SMD) and as such is unable to resolve effects caused by the droplet size distribution in polydispersed sprays such as ballistic drop spreading. They concluded that this is acceptable in the current application because existing experimental data for gaseous and aerosol jets show a lower spreading rate for an increasingly heavy central jet suggesting that variable density effects are more dominant than ballistic spreading [40, 113, 156].

Figure 3.5 and Figure 3.6 show two of their results that predicted SMD along the symmetry axis of the air-assisted atomizer for a range of gas velocities. The only discrepancy they noted was that below a critical momentum ratio a recirculation zone was formed and within this range the model under-predicted the SMDs [40].
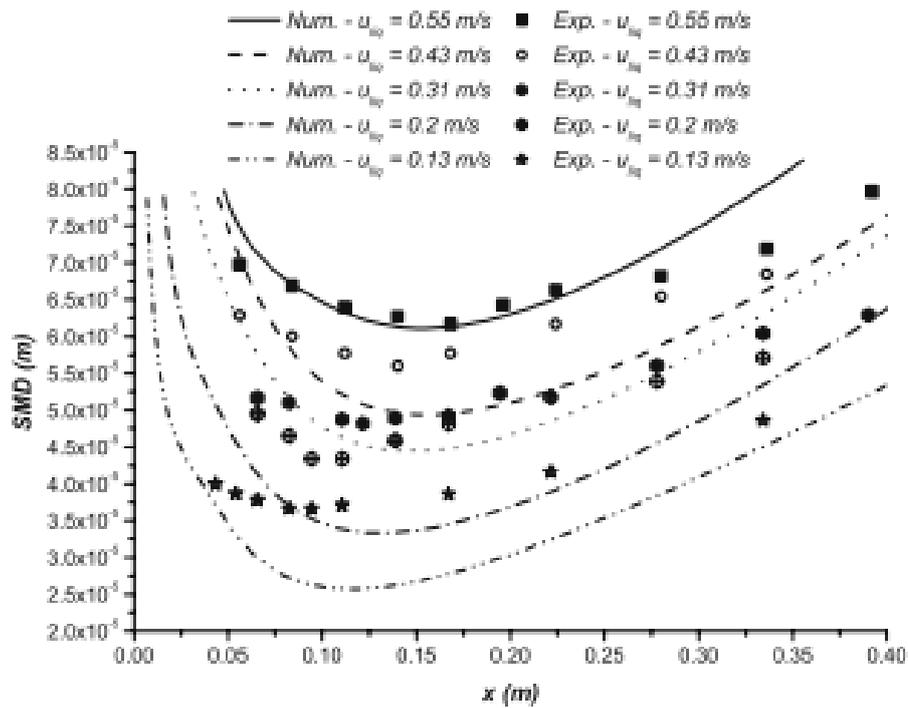
Figure 3.5 Spray SMD along symmetry axis for different liquid jet velocities and a fixed gas velocity of 140 m/s [40]
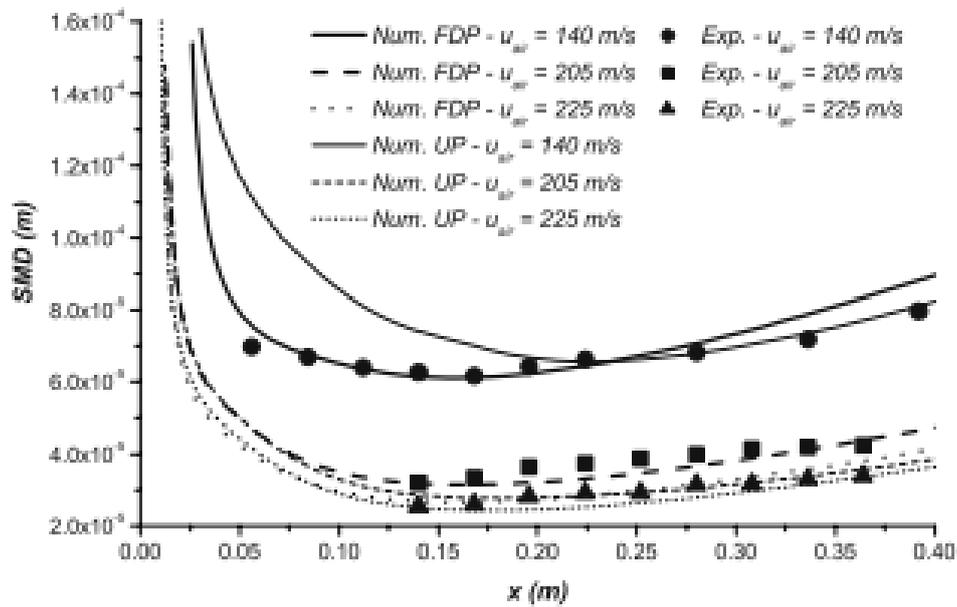


Figure 3.6 Spray SMD along symmetry axis for different gas jet velocities and a fixed liquid velocity of 0.5 m/s[40]

### 3.11.5 **Eulerian-Eulerian atomization models**

Eulerian-Eulerian models is originally devolved for internal duct flows, mono-disperse liquid-gas flows and for solid particle laden two-phase flows. They are classified based on atomization modelling [40, 157]:

1. Models (type 1) with two continuity and momentum equations, one for gas and one for liquid and with single constant droplet size. These are normally used for internal dilute two-phase flows or monodisperse laden flows.

2. Models (type 2) with different size groups, each group having its own momentum equation and velocity field. A droplet number balance equation for each group size containing source terms for production and destruction of droplets due to break-up and coalescence accounts for secondary break-up and its coalescence. This requires sub-models for these two processes. Models of Luo and Svendsen [157]

3. Model of type 1 above with addition of a model for calculation of the mean drops  SMD and distribution at each numerical element. Model of Platzer and Sommerfeld [158] which uses this approach to calculate the droplet size and its distribution.

The major challenge in using the Eulerian-Eulerian model is that it is not good in predicting the spray parameters in the dilute region where the spray liquid tends to a completely a dispersed phase[159]. This rises basically from the nature of the Eulerian momentum equations that are accurate only for a continuous phase[40].

**Capability of Eulerian-Eulerian (E-E) model in providing the spray characteristic parameters**

- These models have the ability to predict the following parameters
- Mean droplet size or distribution
- Spread angle
- Velocity profile
- Penetration depth with time

**Advantages**

- Can deal with primary break-up and the flow inside the nozzle
- Economic in computation time

**Disadvantages**

- Inaccurate in dilute spray region
- Computationally expensive for the model types 1 and 2

### 3.11.6 **Eulerian-Lagrangian Spray atomization (ELSA) model**

In this model, the Eulerian and the Lagrangian viewpoints are combined in modelling the atomization and separate the spray into the dense and dispersed regions due to the difference in its structure and atomization. The dense region is near the nozzle with complex and irregular topology of the spray and the dispersed phase is a far-field of the spray with a collection of droplets [160]. Since Lagrangian approach is more appropriate in the dispersed region of the spray and Eulerian modelling has been applied to the near-field by several researchers a combination of the two approaches have been used to resolve or model the primary and secondary atomization. The main assumption in this model is that the flow must be highly turbulent with high Reynolds and Weber numbers and Hoyas et al [161] indicate that the Reynolds and Weber number should be greater than 1500 and 350 respectively. The second assumption is that the liquid and the gas mixture is modelled as a single flow with mean properties.

The three distinct zones for ELSA model such as Eulerian mixture, transition and Lagrangian zone are shown in Figure 3.7.
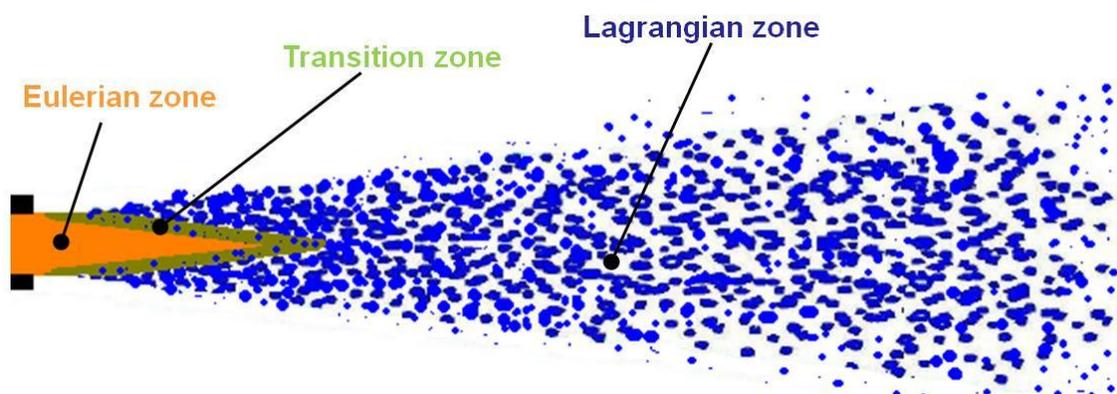


Figure 3.7 Three spray zones in ELSA model [152]

A drawback of this model is that the grid resolution close to the nozzle is sensitive and difficulty in adequately representing this near dense zone to capture the primary atomization as well as a serious imbalance load caused by large droplets created close to the near field [152].

### 3.11.7 **Model selection**

Since the cost of performing simulation with DNS/LES models is very expensive and Lagrangian approach is also very effective in predicting secondary atomization the $\Sigma$$-$Y model has been selected for use within this project for the following reasons

- It allows the use of standard numerical procedures based on a single continuity equation without source terms. The momentum conservation equation in this model is written in terms of a single velocity field which is the velocity of the centre of mass within a computational cell. In this way, one avoids the necessity to calculate the momentum exchange between the phases and uncertainties related to such calculation [162].

- Even in its original form, the model is capable of predicting droplet size and distributions with order-of-magnitude accuracy.

- There have been significantly more publications relating to this model suggesting that the model shows promise to many researchers and that as the model matures results will continue to increase in accuracy.

- The fully Eulerian formulation is naturally implemented in STAR-CD

### 3.11.8 **Model limitations**

The following are the limitations of the $\Sigma$$-$Y atomisation model

- The $\Sigma$$-$Y atomisation model in its only form can only predict the droplet Sauter Mean Diameter (SMD) and droplet number density in the primary atomization regime

- The model cannot characterise the droplet size distributions for polydispersed sprays

- The model is applicable to sprays with large Reynolds and Weber numbers [40, 163].

- The model uses standard k-$\varepsilon$ turbulence model which is developed for a single fluid flow though attempts have been made to extend the model for Large Eddy Simulation (LES) [164]. But in reality, k-$\varepsilon$ turbulence model is not the very best in predicting turbulence in two-phase flows. However, due to the absence of generally acceptable turbulence model for the two-phase flow standard k-$\varepsilon$ turbulence model is widely used in spite of its inadequacies.

### 3.12 Summary

This chapter reviews the computational numerical methods used in the STAR CD code and discusses the basic conservation equations of mass flow and momentum to obtain the velocity and pressure fields in the spray. The additional facility in STAR CD for solving an arbitrary number of transport equations for user-defined variables needed for special-purpose applications as well as solving the basic flow equations was also reviewed. Brief accounts of turbulence modelling techniques in the STAR CD such as the k-epsilon model, Renormalisation Group' (RNG) and realizable' k-ε model were also presented and the governing equations of the standard k-epsilon turbulence model analysed. In order to solve the basic conservation equations two pressure-velocity coupling SIMPLE and PISO algorithms were compared. This chapter also reviews how the geometry for the nozzle was designed and the type of mesh and parameters used for the computation. In addition, the discretization practices in the STAR-CD such upwind differencing (UD), linear upwind differencing (LUD), central differencing (CD) scheme, monotone advection and reconstruction scheme (MARS) and blended differencing were also discussed. The various boundary types employed in the STAR-CD and the specific boundary locations and conditions were also analysed and discussed. The review was also done on the two categories of spray modeling such as primary atomization and secondary atomization. Whilst primary atomization modelling makes assumptions about the physics inside the nozzle and computes an initial drop size in the region near the nozzle, secondary atomization models droplets that traverse the domain where they become hydrodynamically unstable and break into smaller droplets. Other types of atomization model such as Lagrangian atomization model, Eulerian model, Eulerian-Eulerian model and Eulerian-Lagrangian model were also reviewed. The $\Sigma-Y$ atomization model which is the main model used to predict the Saute Mean Diameter (SMD) was also thoroughly analysed and the merits and drawbacks of the model evaluated

# CHAPTER 4 EXPERIMENTAL ANALYSIS

## 4.1 Introduction

The experimental studies involved using a hollow cone nozzle to produce a spray in order to assess and validate an entirely Eulerian model involving mainly modelling of the liquid mass and surface density to predict the mean drop sizes. A laser-diffraction-based drop size analyser (Malvern Spraytec) was used to obtain drop size data from the free spray. The hydrodynamics structure was characterized by the spray drop size (Sauter Mean Diameter, SMD), number density and size distribution, and this was measured at various axial distances from the tip of the nozzle and radial distances from the spray centreline. The influence of injection pressure, volume flow rate and geometrical sizes on the mean drop sizes were also investigated. The Liquid sheet break up process was also visualised and analysed using a high speed camera. Spraytec software (version3.30) was used to analyse the raw data obtained from the experiments and convert them to drop size (SMD) values and size distribution information.

## 4.2 Apparatus

The apparatus was designed with the purpose of producing a continuous spray and to examine the spray characteristics quantitatively and qualitatively. The experimental layout is shown in Fig.4.1. Water, which was the working fluid, was initially collected in a 0.4$l$ container and fed into the main line by a pump (A TCS Micro pumpR pump (S/N: 16062755 TCS) controlled by 24V power supply. A 300W triple power source by TTiR (EX354Tv) was used to control the pump speed by varying the supplied voltage. The resulting pressure drop across the apparatus was measured using a pressure transducer ifmR (PT5414) which has a range of 0.16-40 bar (16-4000kPa). The pressure sensor detected the pressure in the system and converted it to an analogue signal which was read by a digital multimeter later converted to pressure. The set-up of the pressure measurement device was that of a typical 4-20mA circuit set up with a 500Ω resistor. In order to atomise the fluids, a stand was built whereby the fluid was atomised downwards into the laser beam as illustrated in Figure 4.1. The stand was built to allow for variation in the axial distance above the laser beam as well as in the other two perpendicular directions. A clamp was used to hold the nozzle to the stand allowing for the nozzle to be changed quickly. A plastic container was used to collect the fluid from the spray. Deflection of the sprayed liquid from the container back to the

measurement region initially caused problems during atomisation which affected the drop size measurement. In order to solve this problem absorbant tissue papers at the base of the collection chamber prevented splash back.
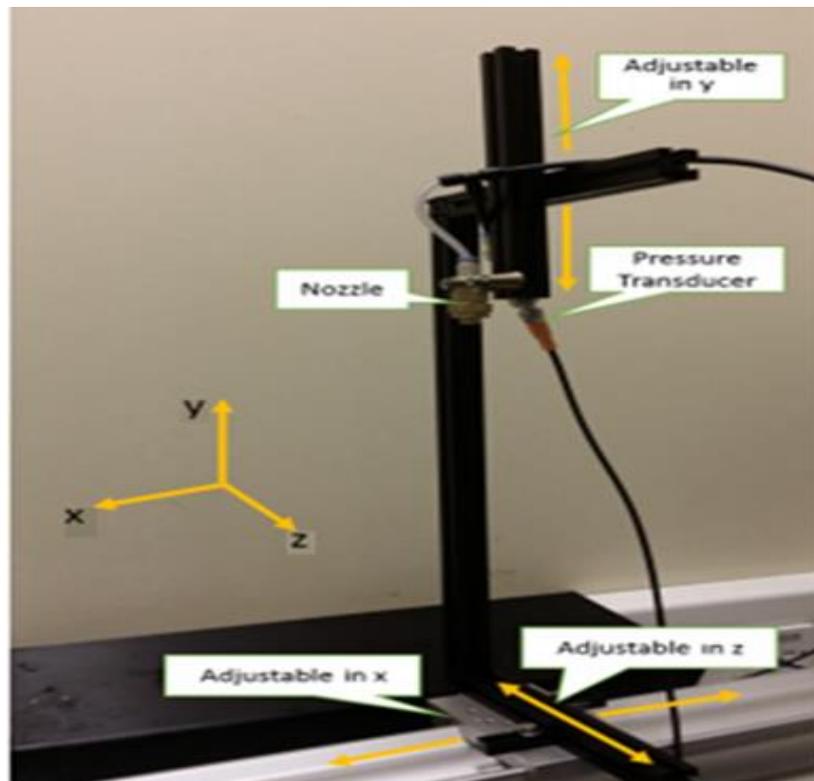


Figure 4.1 Photographs of the experimental setup

## 4.3 The Atomizer

The atomizers used for this study were pressure swirl nozzles PFS 1392B1 and RXT 0250TI manufactured by PNR Ltd which produce hollow cone sprays. This company manufactures various types of quality nozzles to precision. The tangential in-flow nozzle is made of AISI 303 stainless steel and in particular, the nozzle exit diameter is 3.5mm, the nominal spray angle is 70 degrees, the inlet diameter is 3.7mm, the nominal flow rate at 3.0 bar gauge pressure is 3.90 litre per minute. The other specifications of PFS1392B1 and RXT0250TI are shown in Table 4.1. The reason for selecting these particular nozzles is primarily because of the computational model developed by the researcher and to assess and validate the $\Sigma - Y$ atomization model for further improvement. In this nozzle, liquid under pressure is formed into finely atomized droplets and work on the tangential flow principle. Inside the nozzle, there is an axial groove that injects the liquid tangentially into the vortex chamber where the strong centrifugal force produces a high rotational velocity and generates a finely atomized liquid hollow cone sprays. The relevant characteristics which determine the performance of these nozzles are the following

1. The liquid flow delivered as a function of the feed pressure

2. The opening angle of the produced spray

3. The nozzle efficiency as the ratio between the energy of the spray and the energy used by the nozzle

4. The evenness of the flow distribution over the target and

5. The droplet size distribution of the spray.

Figure 4.2 shows schematic drawings of the atomizers used and Figure 4.2a shows the nozzle that will produce conical spray pattern at 900 with respect to feed pipe axis and Figure 4.2b showing the nozzle that will produce the hollow cone sprays in line with feed pipe axis. The physical measurements of the nozzles are shown in Table 4.1 [165].
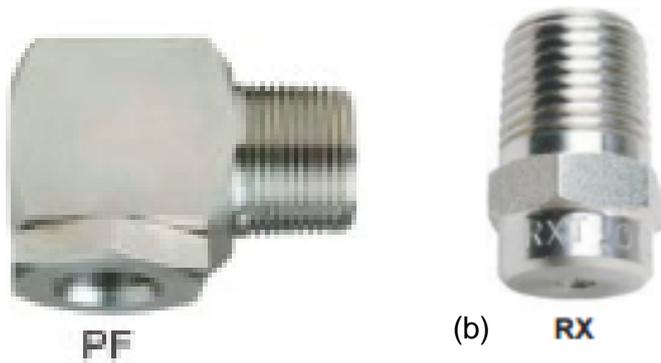
Figure 4.2 Schematic and pictorial drawing of the nozzle (dimensions in millimetres)

Table 4.1 Physical parameters of the nozzle

| (a) Nozzle with tangential flow | | | | |
| --- | --- | --- | --- | --- |
| Material | Nozzle length L (mm) | Height H (mm) | Nozzle exit diameter (mm) | Liquid inlet diameter (mm) |
| Stainless steel | 34 | 24 | 3.5 | 3.7 |
| (b) Nozzle with in-line flow | | | | |
| Material | Nozzle length L (mm) | Height  H (mm) | Nozzle diameter (mm) | Liquid inlet diameter (mm) |
| Brass | 6.35 | 24 | 1.500 | 3.0 |

## 4.4 The Test Liquid

The test liquid used for the spray experiment was soft tap water at an average temperature of 13 degrees Celsius. The test liquid property parameters are presented in Table 4.2.

Table 4.2 Test liquid properties

| Property | Mass density | Viscosity | Surface tension |
|---|---|---|---|
| Test liquid (water) | 1000 | 0.001 | 0.072 |
| Units | $kg/m^3$ | $kg/ms$ | $kg/s^2$ |
| Symbol | $\rho_L$ | $\mu_L$ | $\sigma_T$ |
| Source | Crowley et al [166] | Emekwuru et al [15] | Emekwuru et al [15] |

## 4.5 Spray Measurement Methods

The spray characteristics were measured using a Malvern Spraytec which is a non-intrusive, laser-diffraction-based drop analyser designed to continuously measure drop sizes and distribution information for continuous sprays Figure 4.3. This instrument is one of the most convenient and reliable spray analysers used in examining the global characteristics of sprays[167]. However, Hirleman et al [168] and Dodge [169] exposed some of the limitations of the instrument while several researchers have indicated that the variation in mean drop size and size distribution can be influenced by the effects of drop acceleration and deceleration [7]. The Malvern Spratec instrument is based on the Fraunhofer diffraction theory of a collimated laser beam scattering by moving drops. Light from the laser (1) is scattered by the spray droplets (3). The laser beam is expanded by the collimated optics (2) to provide a wide range parallel beam. The scattered light is focussed by a focusing lens (4) in a Fourier arrangement and picked up by the detector array (5). Unscattered light is focused by the focusing lens (4) so that it passes through the pinhole at the centre of the detector array. This is measured by the beam power detector to give the light transmission [170, 171].
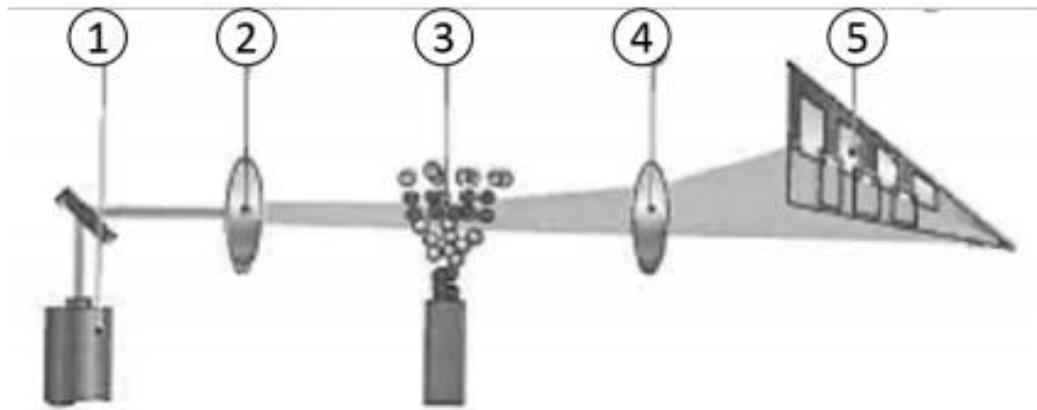
Figure 4.3 Measurement set-up of the Malvern Spraytec system[170]

The optical head had a He Ne 5 mW diode laser. To prevent particulate contamination of the optical apertures, there was a long base bridge with a 500 mm internal span between the transmitter and receiver optics (Figure 4.3), and a flow control panel provided clean and pressurised liquid to the centrally positioned nozzle between the transmitter and receiver optics. The electronics interface powered the optical head, acquired the raw scattering data, and processed and transmitted the signal information to the computer. The processed scattered data from the Spraytec was saved to the hard drive of a personal computer which had Spraytec software (version 3.30) installed on it and this software converted the raw data into useful mean drop sizes and distribution data [172]. The principles of laser diffraction drop size analysers have been discussed extensively (Lefebvre[1]; Malvern Spraytec Manual [170]; Emekwuru, [173]). When a parallel beam of light interacts with a drop, a diffraction pattern is formed such that some of the light is diffracted by an amount depending on the drop size. In general, large drops scatter light at small forward angles and small drops scatter light at large forward angles [170]. A lens focuses the diffraction pattern onto a photo detector, which measures the scattered light intensity. A curve-fitting program is used to convert the scattered light intensity into an empirical drop size distribution function, and this is displayed instantly.

The need to avoid making drop size measurements close to the nozzle has been stressed by Wittig et al [167]  and Lefebvre[7]. The rapid deceleration of the smallest drops in the spray in this region gives rise to readings of SMD appreciably lower than the true value. Chin et al [174] recommend a downstream distance of 25cm at air pressure of 100kPa as being the ideal plane at which to make the drop size measurements.

Lefebvre [7] indicated that their calculations take no account of evaporation and suggested that to minimize errors arising from this effect it is desirable to keep the distance as short as possible and estimated that 15cm was the best downstream distance at the pressure of 0.1MPa. For the nozzle size and the liquid used in the experiments of Lefebvre [6], 50 mm was the best minimum axial position beyond which the results were consistent and below which no meaningful information was obtained for mean drop size and size distribution and this also agrees with the downstream distance used by Emekwuru [172] at the atomizing air pressure of 138kPa. All measurements were taken with the laser beam passing through the centreline of the spray. The problems associated with such measurement have been discussed by various workers including Dodge [169] and Chin et al [174]. However, Lefebvre [7] indicated that centre measurements are generally preferred because they encompass both the smaller drops in the core of the spray as well as the larger drops at the spray periphery. Figure 4.4 shows the different distances from the nozzle tip for liquid sprays. The readings were taken only when the sprays were fully developed. The vertical and horizontal intervals between the measurement points were 20 and 5mm respectively.
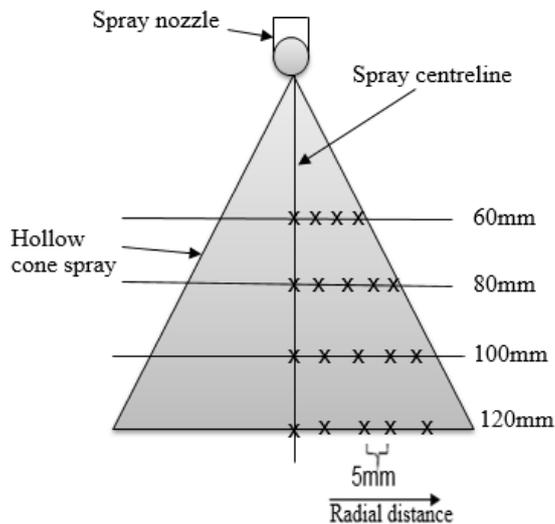


Figure 4.4 Measurement points relative to nozzle tip

Assuming that the sprays were almost symmetrical, measurements were conducted for only half portion of the sprays. In using the Spraytec, the liquid was sprayed at various flow rates and drop sizes measured. Since the flow rate supplied by the pump could not be directly controlled, the power supplied to the pump was controlled by varying the voltage instead. All samples were sprayed at voltages of (0.5, 1, 1.5, 2 and 2.5)V. The flow rate was measured by timing how much time 0.4ml takes to spray. The pressure drop measured by the transducer was also recorded in volts to be later converted to

pressure units. Spraytec was operated at 2.5 kHz for 10s per measurement. The parameters used during the experiment for the Malvern Spraytec system are presented in Table 4.3.

Table 4.3 Drop analyzer system parameters[170]

| Parameter | Units | Value |
|---|---|---|
| **Transmitting optics setup** | | |
| Laser power | mW | 5 |
| Beam waist diameter | mm | 10 |
| Laser wavelength | nm | 632.8 |
| Path length | mm | 30 |
| **Receiving optics setup** | | |
| Drop size range mean diameter ($D_{32}$) | µm | 0.1-2500 |
| Lens focal length | mm | 300 |
| Particle refractive index | - | 1.334 (water) |
| Medium refractive index | - | 1.000 (air) |

To visualize the liquid film break up, a high-speed resolution camera was utilized. Initially, a minimum exposure time and automatic flash were used to obtain the best possible instant picture as shown in Figure 4.5.
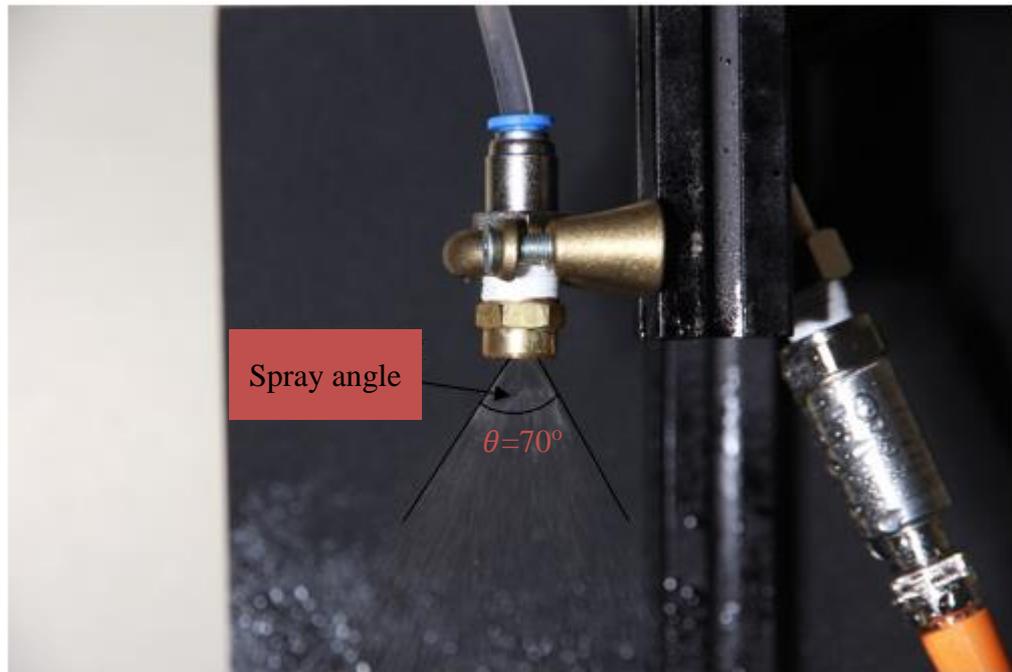


Figure 4.5 Image from fast-shutter camera

**4.6 Hydrodynamics Analysis**

The hydrodynamics features of the spray were analysed using the drop size and the distribution. The results for spray in close proximity are usually difficult to measure. The inconsistencies of the results in this region can be due to possibly multiple scattering from the dense spray [173]. In this study, only measurements beyond 50 mm along the spray centre line of the nozzle are found to be consistent. Measurements were taken at axial distances of 50-150 mm in 20 mm increments along the atomizer centre line. Also at the radial distances of 5-50 mm, measurements were taken at radial distance increments of 5 mm.

Measurement of droplet size on spray centreline enables insight into the distribution of drops along the nozzle symmetry and helps to validate theoretical studies or relations for determining droplet sizes which is easier to develop on this axis [173, 175]. The symmetrical pattern observed during the experiments can also be explained in terms of the balance of forces acting in a spray during the operating conditions. There is a vertical effect due to the aerodynamic and gravity forces, and these forces act the same on mirror drops on either side of the nozzle axis [7]. Figure 4.6 andFigure **4.7** show the

uncorrected light scattering data and alignment of the laser beam for corrections before capturing the raw data. The Malvern Spraytec software provides means for correction of the effects of multiple scattering during the experiments. In cases where the particle concentration is high, the measurement process is complicated by scattered light being re-scattered by other particles before it reaches the detector. These multiple scattering errors are corrected by a light scattering correction algorithm and the correction effects during the experiments are seen in the smoother transmission signal curves in Figure 4.7 compared to Figure 4.6 [170]. Figure 4.8 shows the drop size and transmission level time history which shows how the spray developed over time and plots the values of all derived parameters for each record against time. The illustration in Figure 4.8 was obtained when the spray was directed through the Malvern Spraytec measurement volume over a 10 second window.
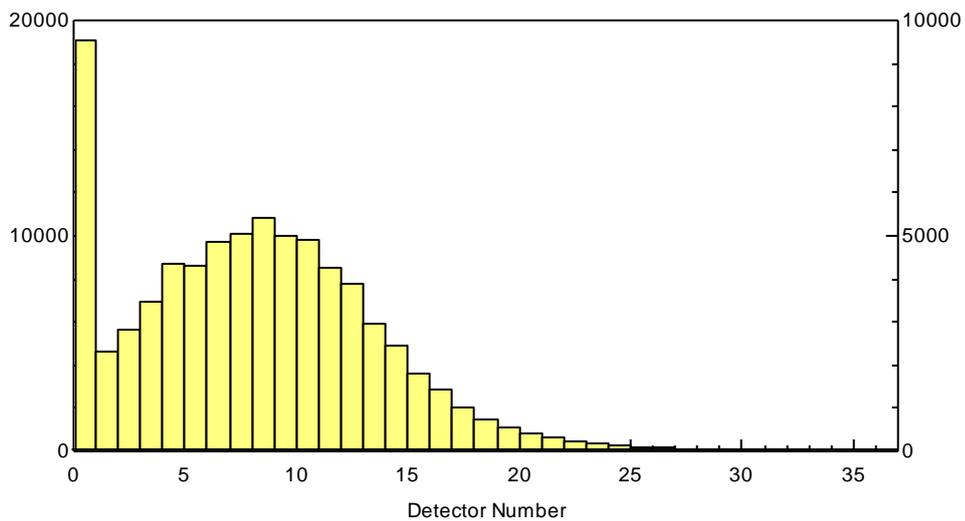


Figure 4.6 Uncorrected light scattering data. On transmission signal scale 1000 represents 1mW
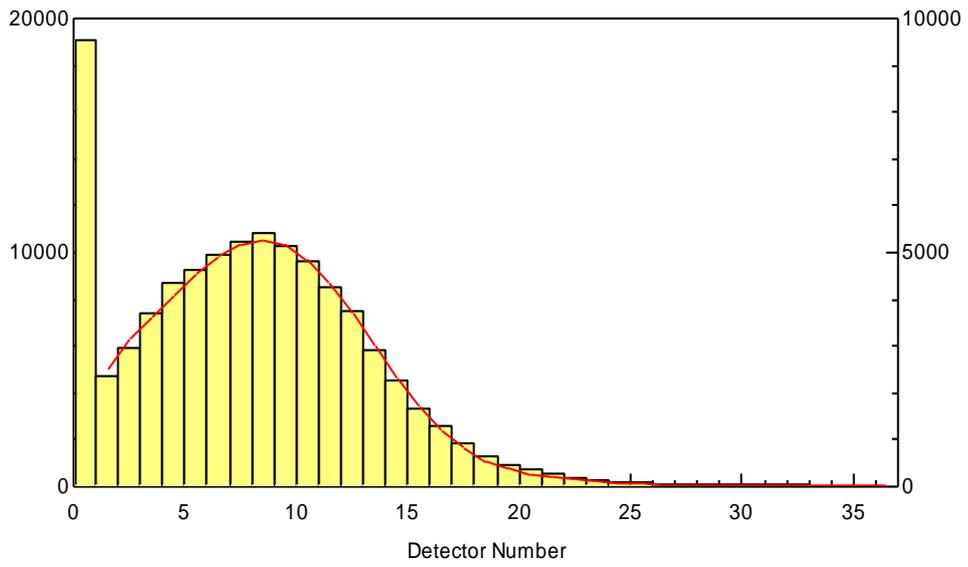
Figure 4.7 Corrected light scattering data. On transmission signal scale 1000 represents 1mW
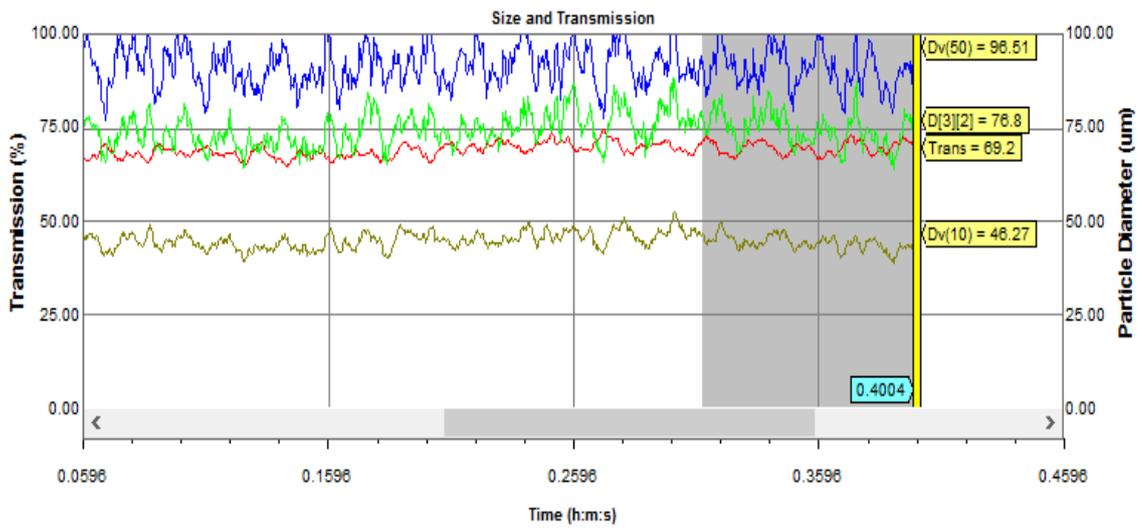


Figure 4.8 Drop size/transmission level time history

## 4.2 Summary

This chapter describes how a laser-diffraction-based drop size analyser (Malvern Spraytec) was used to obtain drop size data from the free spray. The apparatus was designed with the purpose of producing a continuous spray and to examine the spray characteristics quantitatively and qualitatively. The atomizers used for this study were pressure swirl nozzles PFS 1392B1 and RXT 0250TI manufactured by PNR Ltd which produce hollow cone sprays. The test liquid used  and its property parameters were presented. The spray measurement method for Malvern Spraytech which is mainly based on the Fraunhofer diffraction theory of a collimated laser beam scattering by moving drops was also described. The various locations where the droplet Sauter Mean Diameter (SMDs) and its distributions were measured for research work carried on hollow cone nozzle were evaluated and it was stated that only measurements beyond 50 mm along the spray centre line of the nozzle are found to be consistent. Measurements were taken at axial distances of 50-150 mm in 20 mm increments along the atomizer centre line as well as radial distance increments of 5 mm from the spray centreline in this study.

# CHAPTER 5 COMPUTATIONAL RESULTS AND DISCUSSION

## 5.1 Introduction

This chapter presents the modelling results for the flow fields on the cross section and vertical plane as well as the prediction of the Sauter Mean Diameter (SMD) at the spray centerline and radial positions for the $\Sigma - Y$ atomisation model. In order to have a better understanding of the flow and turbulence fields, the two-dimensional vertical plane is cut through the atomizer at $180^0$ and 3D view of the nozzle for the pressure distribution is shown in Figure 5.1. The two inlets or holes are symmetrically located at the side and in the middle of the atomizer so that the spray emerging from the nozzle can be adequately captured and analysed on the plane. The nozzle exit is located at the centre of the computational domain for an axisymmetric study to be carried out in the computational domain on the plane. Liquid through the outside jet and air through the middle jet are injected at a steady state and simulations were carried out using the Eulerian single-phase modelling methodology for the injected fluids with high-density variation, high Weber and Reynolds numbers. This Eulerian approach treats the liquid and air as a single continuous phase with large-scale features of the flow dependent only upon density variation. The Standard k-epsilon turbulence model was used to model the turbulence effect since it provided the best match in the validation after analysing other variants of k-epsilon turbulence models. The investigation of the turbulence models are presented in Chapter 6.
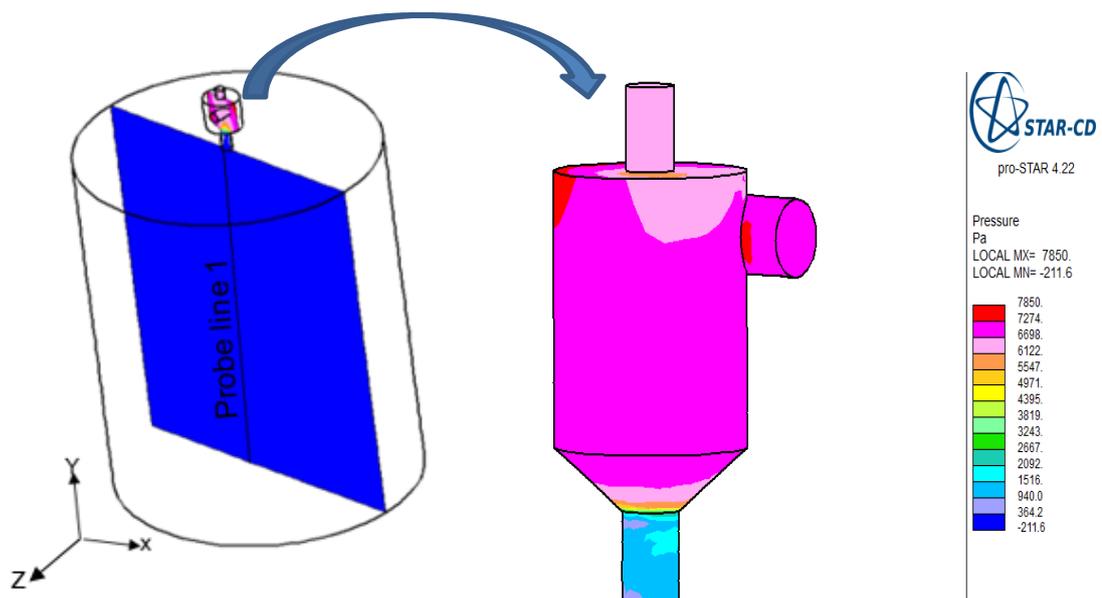


Figure 5.1  Vertical section plane and 3D plot of pressure distribution

The flow simulations were carried out with the boundary condition for the liquid inlet taken to be a specified velocity flow rate normal to the vertical plane and air velocity inlet parallel to the plane. The outlet of the computational domain is set to atmospheric pressure boundary. All wall boundaries are taken as no-slip. For gas and liquid respectively the densities are 1.20 and 997.5 kg/m$^3$. In order to compare the results of the flow and turbulence fields, two simulations were run for two pressure-velocity coupling algorithms (SIMPLE and PISO) and SIMPLE algorithm was used to enforce mass conservation and to obtain the pressure field. These simulations were run at steady state with maximum residual tolerance of $1\times10^{-4}$ for convergence to be achieved.

## 5.2 Grid independence test

Figure 5.2 presents the grid independence test using variation of pressure profile with cell sizes in the swirl chamber, contraction zone and exit orifice of the atomizer. The pressure variations are taken on the symmetry line inside the atomizer shown on the vertical plane in Figure 5.1 and the x-axis values are the positions on the symmetry line.
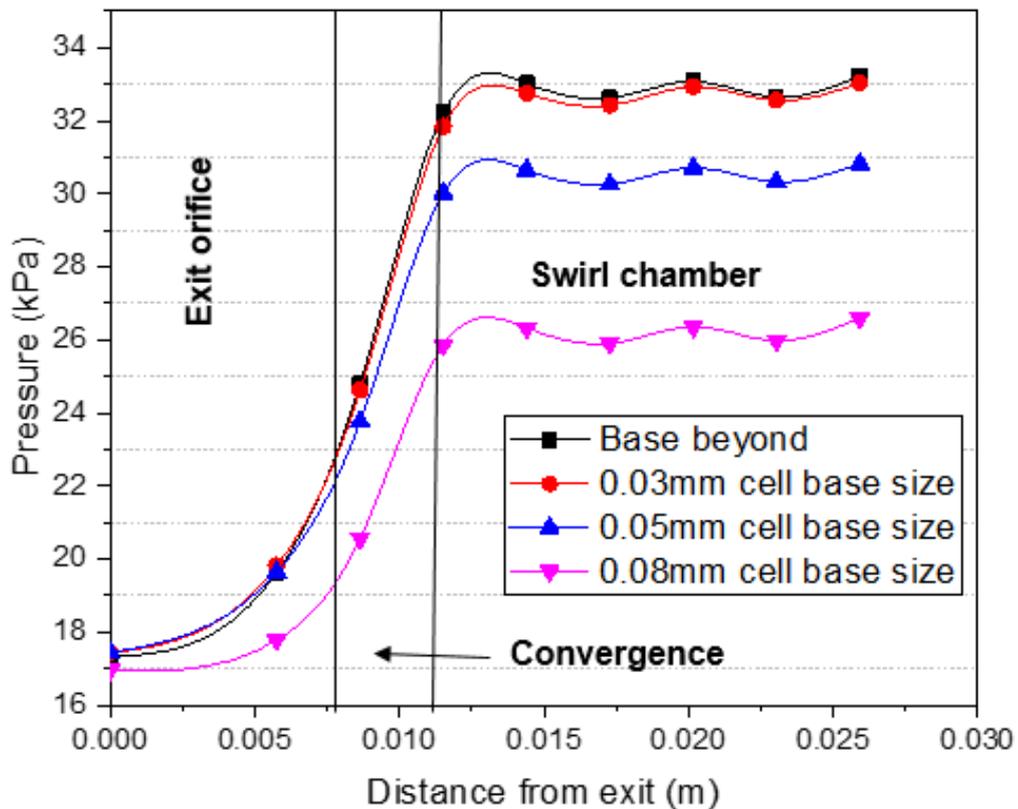


Figure 5.2 Grid independence test using variation of pressure profile with grid sizes

87

One significant observation with this result is that the pressure in the swirl chamber is almost constant, drops sharply in the contraction zone and further decreases in the exit orifice which is consistent with the experimental observation made by Horvay and Leukel [5] on the gauge pressure at the internal walls of the pressure swirl atomizer. The pink, blue and red lines represent the variation of pressure in the nozzle on the symmetry line for cells, from coarse to fine grid, with base sizes of 0.08 mm, 0.05 mm and 0.03 mm respectively. With simulation of cell size 0.08 mm the pressure profile has maximum value of 0.266 bars, the 0.05 mm cell size the maximum pressure profile corresponds to 0.308 bars and 0.330 bars was the maximum value for the pressure profile when the mesh base size was reduced to 0.03 mm. It was observed after carrying out this series of grid independence tests shown on Figure 5.2 that increasing the number of cells beyond 1,894,340 with a base size of 0.03 mm did not alter the pressure profile. Thus the numerical simulations are grid independent beyond 1,894,340 cells of base size 0.03 mm on the symmetry line. The discretisation error for the maximum pressure profile $P_{max}$ using the Grid Convergence Index (GCI) was calculated with these relations. The relative error,$e$, between successive grids is found by

$$e = \frac{f_2 - f_1}{f_1}$$

where $f_1$ is the fine grid and $f_2$ is the coarse grid

For each pair of successive grids, GCI is found from

$$GCI = \frac{F_s|e|}{(r^p - 1)}$$

where $F_s = 1.25$ is the factor of safety recommended for three grid studies, r is the grid refinement ratio of 1.6 , p is the order of discretisation assumed to be 2. The two errors for the three grids are shown in Table 5.1

Table 5.1 Grid statistics, pressure data and discretisation error estimates

| Grid size (mm) | $P_{max}$ (bar) | e | $GCI(\%)$ |
|---|---|---|---|
| 0.08 | 0.266 | - | - |
| 0.05 | 0.308 | 0.1579 | 19.74 |
| 0.03 | 0.330 | 0.0714 | 5.72 |

From Table 5.1 the results show that Grid Convergence Index (GCI) from the coarse to the fine grid is relatively low and therefore a grid independent solution is achieved.

## 5.3 Comparison of SIMPLE and PISO algorithms results

Figure 5.3 shows the contour plot for density with 15 levels on the colour map**.** In "one-fluid-two-phase" $\Sigma - Y_{\text{liq}}$ atomization model, high mean density variation is an important parameter and depends on the Favre averaged liquid mass fraction. Flow and turbulence fields depend heavily on the mean density variation and as such to get a complete picture of the model for further analysis to be conducted density variation for the two fluids treated as a single phase fluid must first and foremost be achieved for the simulation. From the figure, the blue colour corresponds to the lowest density and the red colour representing the maximum value for the density distribution can be observed in the vicinity of the liquid entry into the atomizer. The density variation can be seen in between these two limits and is large in relation to the maximum and minimum values of the density distributions. This is expected due to large density difference that exits between liquid and gases [176]. As can be seen in the spray the density variations effect is stronger upstream and becomes less extreme in the downward stream. This density variation may be due to the compressibility effects induced by high-velocity flows between the two fluids. In this model temperatures of the liquid and gas are not considered so the density variations cannot be related to temperature variations.

In order to assess whether or not these numerical results can be trusted for the density distribution, simulations were performed for two algorithms for pressure-velocity (SIMPLE and PISO) coupling. The residuals for the main parameters calculated, such as: continuity equation, momentum and turbulence model were compared for both algorithms. Under the same conditions, and low under-relaxation factors to avoid divergence of the iterations, the two algorithms showed appropriate convergence with the maximum residuals for continuity being $1\text{x}10^{-4}$. With regards to computational time, the PISO case expends less CPU time than the SIMPLE case and has greater stability. The results show that the maximum local density value is 997.5 kg/m$^3$ for both algorithms and minimum values of 1.184 kg/m$^3$ and 1.205 kg/m$^3$ for SIMPLE and PISO simulations respectively. The average density in the distribution is in the range between 499.3 and 570.5 kg/m$^3$. It can, therefore, be easily seen that there are negligible differences in the two results indicating the result for the density is good and acceptable since SIMPLE and PISO algorithms tend to produce almost the same results

under the same conditions, the only difference being the procedures for coupling the pressure and velocity are different[103].
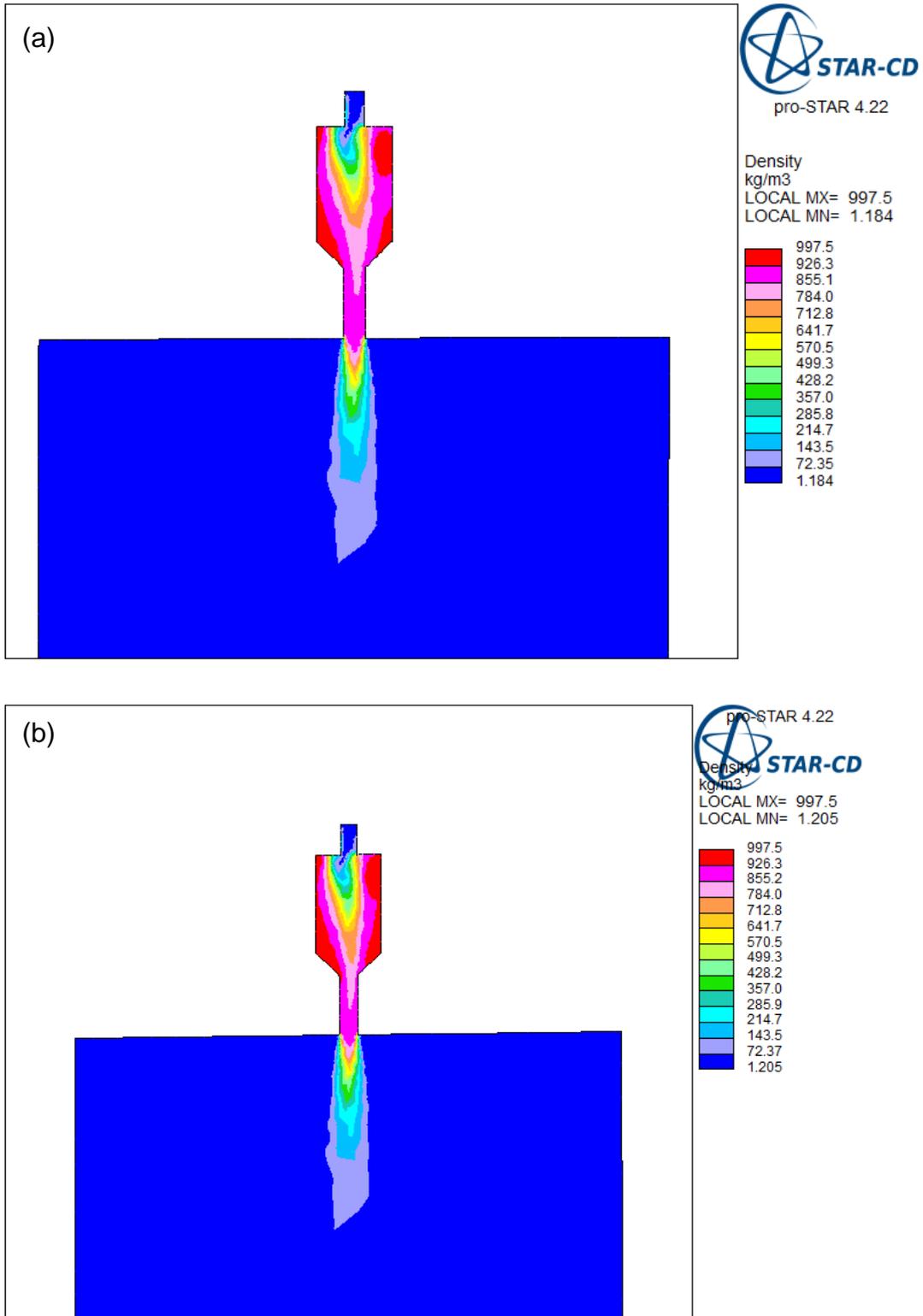


Figure 5.3 Comparison of density variations for (a) SIMPLE and (b) PISO algorithms

Figure 5.4 presents the velocity magnitude on the vertical plane for the PISO and SIMPLE algorithms. The blue colour on both results represents the lowest values on the velocity distribution, which also implies that outside the spray there is only air. The minimum values of the velocity magnitude for the SIMPLE and PISO simulations are 0.56 m/s and 0.54 m/s respectively. The red colour indicates the maximum values for the velocity on both contours and has values of 7.85 m/s and 7.61 m/s$^2$ respectively. The results indicate that the average velocity in the distribution is in the range of 3.905 m/s to 3.924 m/s. The high values of the velocity in close proximity to the liquid entry into the atomizer are expected since the liquid velocity is high. The results also show that the spray is symmetrical on the vertical plane and therefore the flow behaviour can be evaluated on the spray centreline. Conical spray is clearly visible and the minimum values are found downstream of the spray for both simulations. This is in conformity with the theory that the liquid sheet emanating from pressure-swirl atomizer outlet widens in the form of a cone after leaving the nozzle and disintegrates downstream into droplets[177] and are mostly confined in the core regions of the spray. It can also be found that the velocity in the centre spread of the liquid is greater than the speed of the droplets at the periphery of the spray. This is especially true because at the centre axis the air will drag the smaller droplets towards the centre while the larger droplets will remain at the outer periphery and as such the velocity distribution across the plane can vary appreciably from the centre to the outer radius. The phenomena at the tip of the spray may represent the break-up process of the spray sheet into droplets which may be induced by turbulent behaviour in the spray since in turbulent flows the turbulent transport terms are dependent on the mean velocity field. It can be observed that at the same colour locations for both the SIMPLE and PISO results, the velocity field values are slightly higher for SIMPLE than for PISO. These small discrepancies are acceptable since it lies within 1% and 3% as indicated by Barton [178] in his study to compare SIMPLE and PISO type algorithms for flow fields.
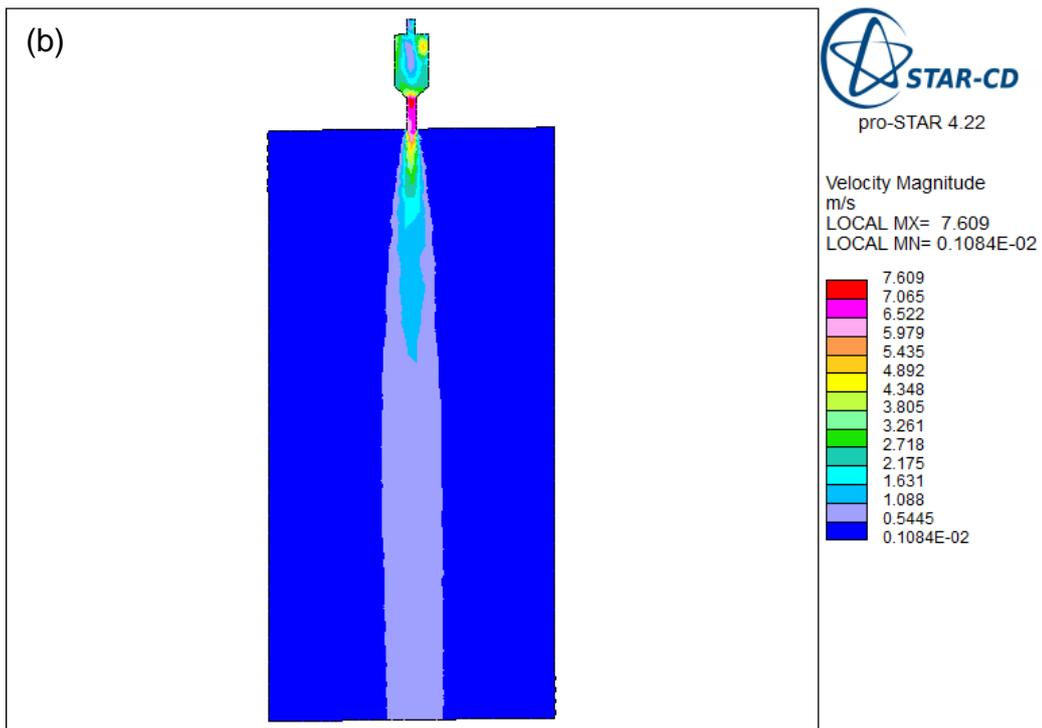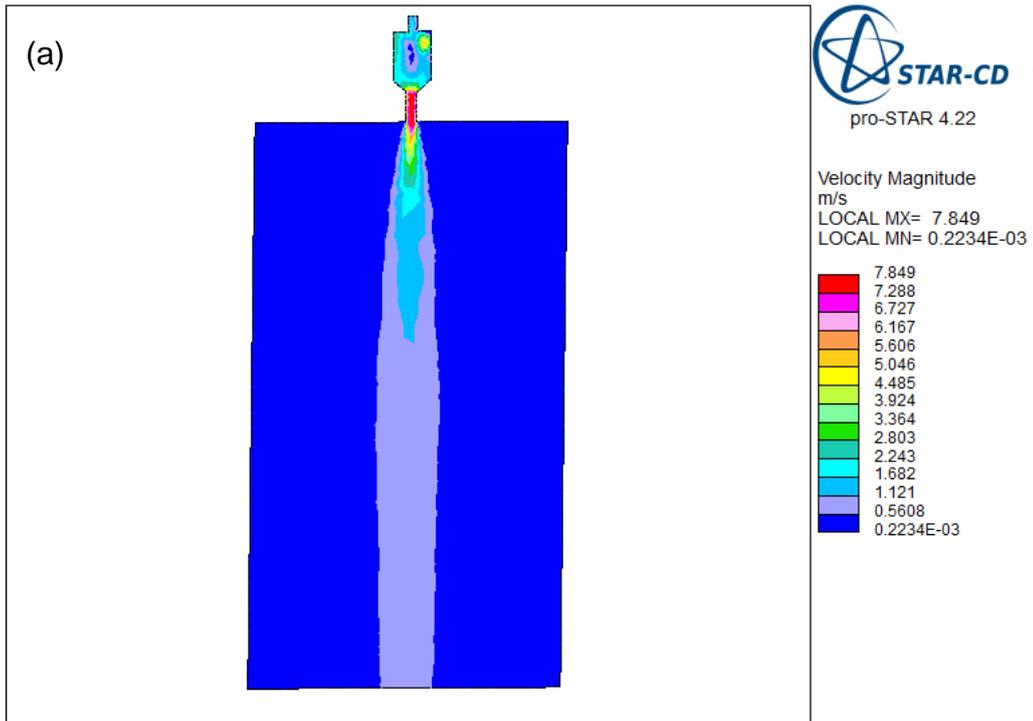
Figure 5.4 Comparison of velocity magnitudes on the vertical plane for (a) SIMPLE and (b) PISO algorithms

Figure 5.5 shows turbulent kinetic energy on the vertical plane when the simulations for the SIMPLE and PISO algorithms were compared. The turbulent kinetic energies are colour coded such that the various colours represent localised turbulent kinetic energy at various locations in the spray. As can be seen from the two results high turbulent kinetic energy increases in the vicinity of the atomizer exit and may be due to low liquid density at those locations. It can also be observed that low turbulent kinetic energy is found in the downstream of the spray which may be due to decrease in liquid velocity and high density variation. From the results, turbulent kinetic energy for PISO is slightly higher than the SIMPLE case when compared at the same colour locations with the maximum turbulent kinetic energy being 1.907 $m^2/s^2$ and 1.814 $m^2/s^2$ respectively and the least turbulent kinetic energy values of 0.074 $m^2/s^2$ and 0.0072 $m^2/s^2$ respectively. The results indicate that the average turbulent kinetic energy values in the distribution corresponding to the light yellow in the SIMPLE and PISO cases are 0.908 $m^2/s^2$ and 1.06 $m^2/s^2$ respectively. The very low turbulent kinetic energy observed in the centre spread of the atomizer may be caused by large liquid to gas ratio and may also be attributed to the inadequacies in standard k-epsilon turbulence model in predicting better turbulent kinetic energy in two phase flow. Turbulence fields depend on density variation in this atomization model [40] and as the density variation decreases greatly the standard k-epsilon turbulence model may not adequately capture this effect and might have accounted for some of these distortions or fluctuations in the turbulent kinetic energy. The fact is turbulence modelling, even for single phase flows, is an active area of research and the modelling of variable density flows particularly flows with large density ratio is currently an unsolved problem[40].

The results also show that some recirculation zones are observed close to the walls in the swirl chamber and again standard k-epsilon turbulence model may not be good in predicting variable density flows which experience recirculation zones. However, as indicated by Pandal et al [123] in optimizing diesel spray break-up using this Σ-Y atomization model and Beshesti et al.[40] in assessing this Σ-Y model in air-assisted atomisation, most applied numerical works are still based on this turbulence model due to its robustness and accuracy in modelling shear driven flows with minimally curved streamlines but recirculation flows are challenging for any turbulence model.
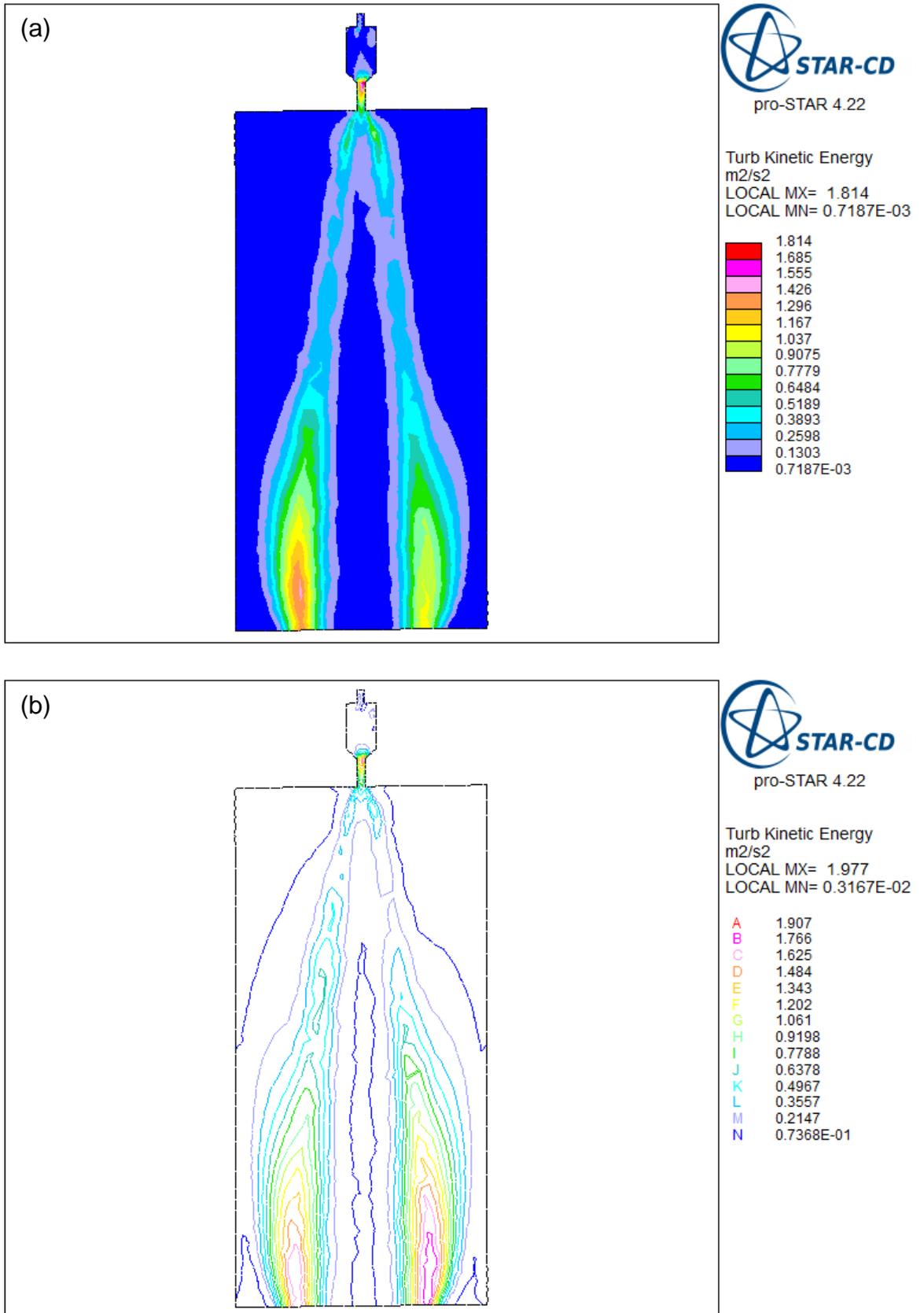
Figure 5.5 Comparison of turbulent kinetic energy on the vertical section plane for (a) SIMPLE and (b) PISO algorithms
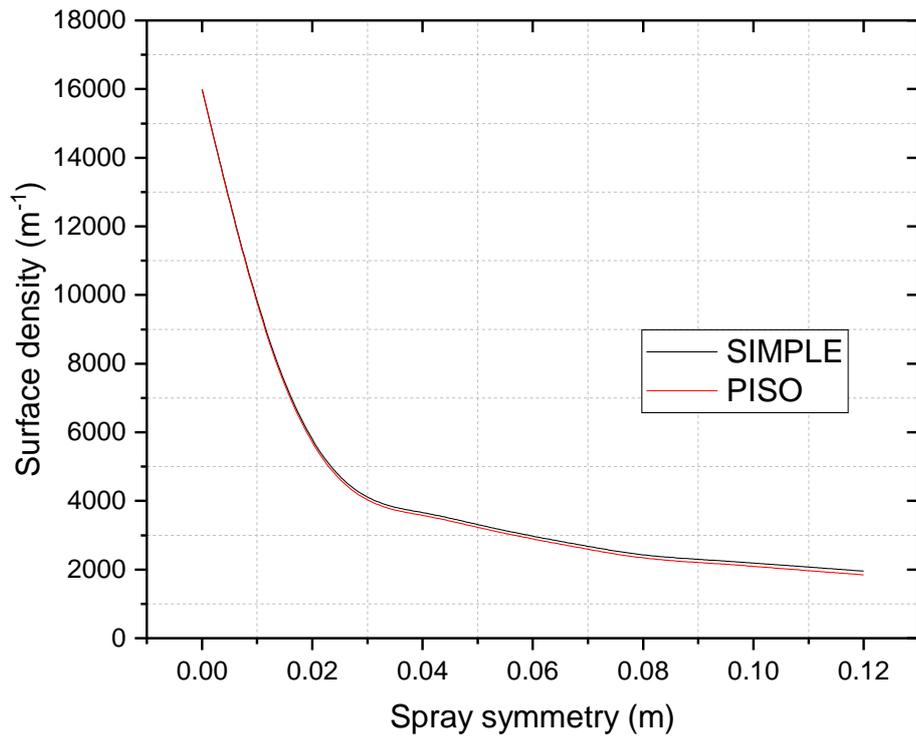
Figure 5.6 Contour plot of surface density for SIMPLE and PISO algorithm, axial positions
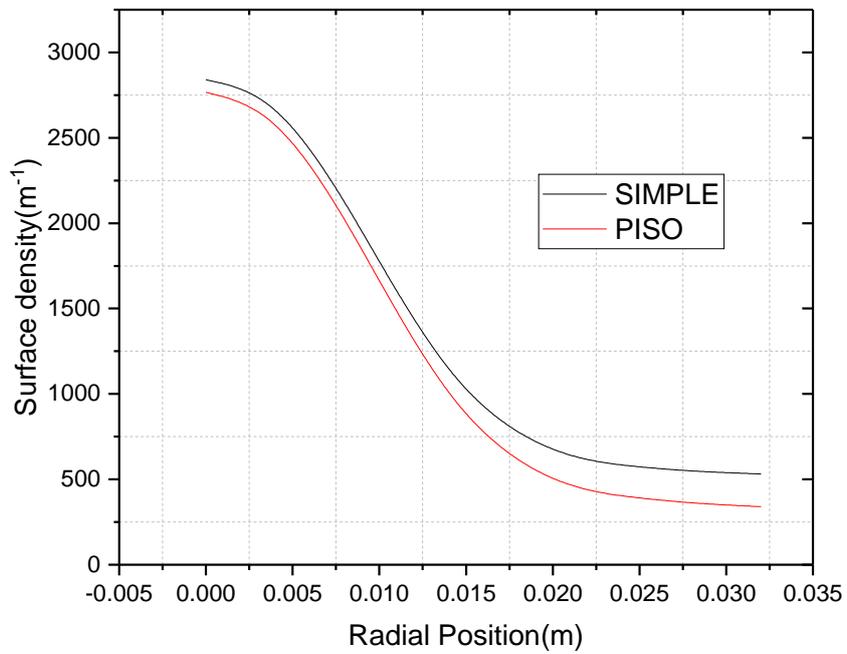


Figure 5.7 Contour plot of surface density for SIMPLE and PISO algorithms, radial at y = 60 mm

95

Figure 5.6 and Figure 5.7 show the comparison of the contour plots of predicted surface density for SIMPLE and PISO cases at y = 60 mm for the radial case and axial profile resulting from the locations on the spray centre line. The results show that the surface density is almost 2800 m$^{-1}$ for both SIMPLE and PISO at axial location x=0 and for the other locations the SIMPLE predicted surface density is slightly higher than the PISO for the radial case. It can be observed from the radial results that the least surface density values are 480 m$^{-1}$ and 505 m$^{-1}$ for PISO and SIMPLE respectively. The axial result also shows that the surface density decreases linearly on the spray centreline. These two results were used in the prediction of the Sauter mean diameter (SMD) on both axial and radial positions of the spray plume in the computational domain with SIMPLE algorithm used in all predictions.

## 5.4 Flow fields on the crossection plane

Figure 5.8 shows the predicted velocity magnitudes on the nozzle cross sections as shown on Figure 5.8a. The velocity magnitudes were generated in the sprays across the swirl chamber, contraction zone, mid section of the exit orifice and the tangential port into the swirl chamber. It was observed that the liquid velocity was very high in the tangential inlet to the atomizer as well as in the core of the exit orifice. Figure 5.9 shows the velocity distribution across the spray in the computational domain when the transport equation for the liquid mass fraction, interfacial surface density and average density were modelled. It was evaluated at the sections for y = 60, 80 100 and 120 mm from the tip of the nozzle. Hollow cone spray formation can be observed and this gets wider at the distance increases with the entrained air. The flow fields for the velocity magnitudes indicate that regions of relatively high velocities in the liquid were found to be in the atomizer compared to the velocity in the computational domain. Figure 5.10 shows the contour plots of pressure distribution, mean mass fraction of liquid, mass fraction of air and turbulent quantities such as turbulent viscosity, turbulent kinetic energy and its rate of dissipation at entry into the atomizer. Two-phase flow can clearly be seen between the mass fraction of liquid and air in the atomizer as shown in Figure 5.10b and Figure 5.10c and liquid dispersion is correctly captured. It can also be observed that turbulent kinetic energy was very higher near the internal walls in the swirl chamber and pressure was also seen to be high near the internal walls as well. The maximum value for the density distribution can be observed in the vicinity of the liquid entry into the atomizer.
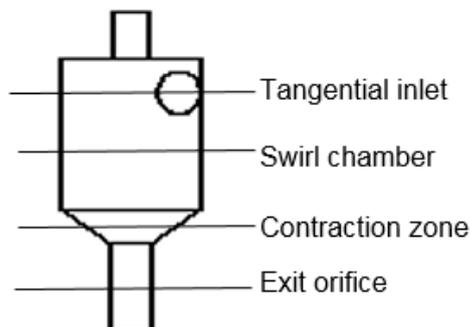


a.   Cross-section through the centres of parts of  the nozzle
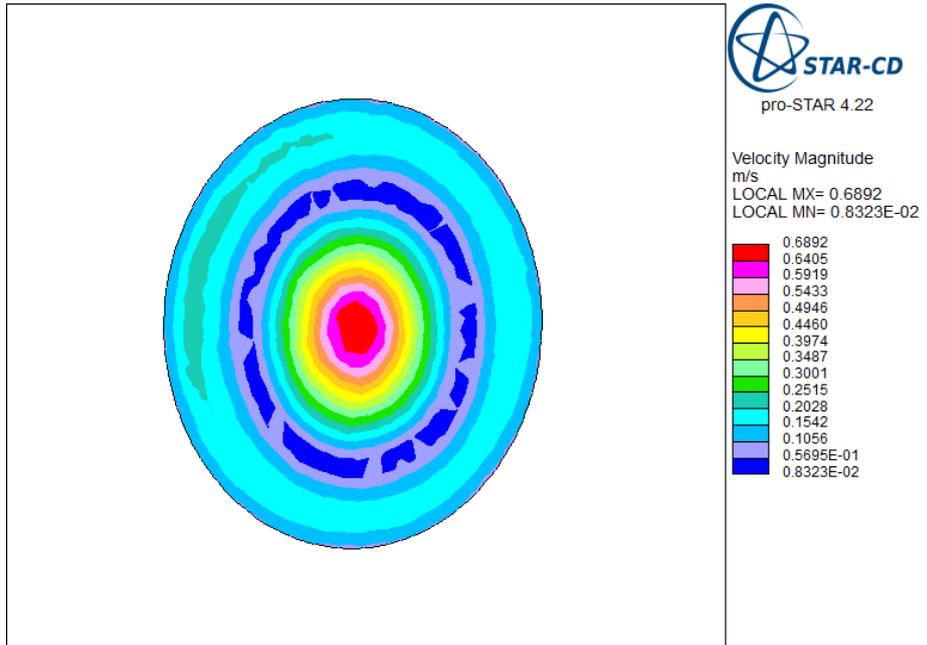
b. Swirl chamber
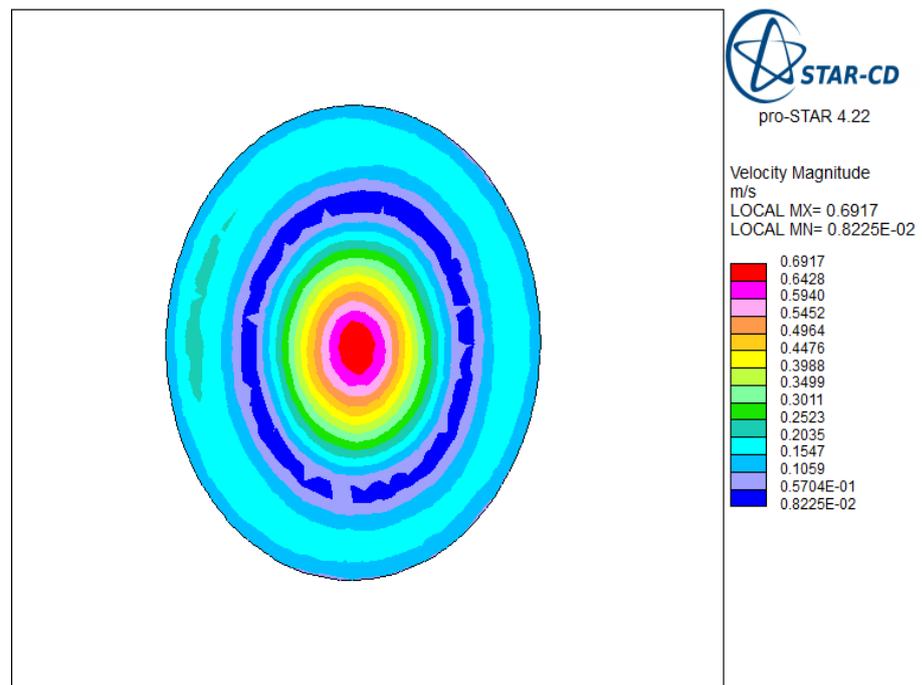


c. Contraction zone
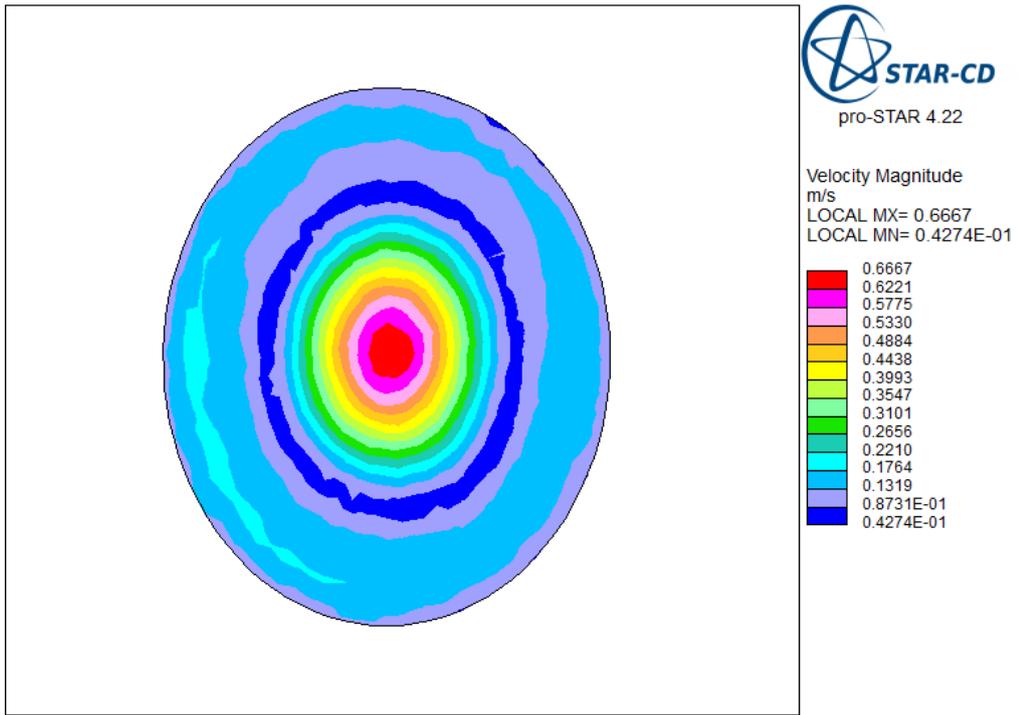
d. Nozzle exit orifice
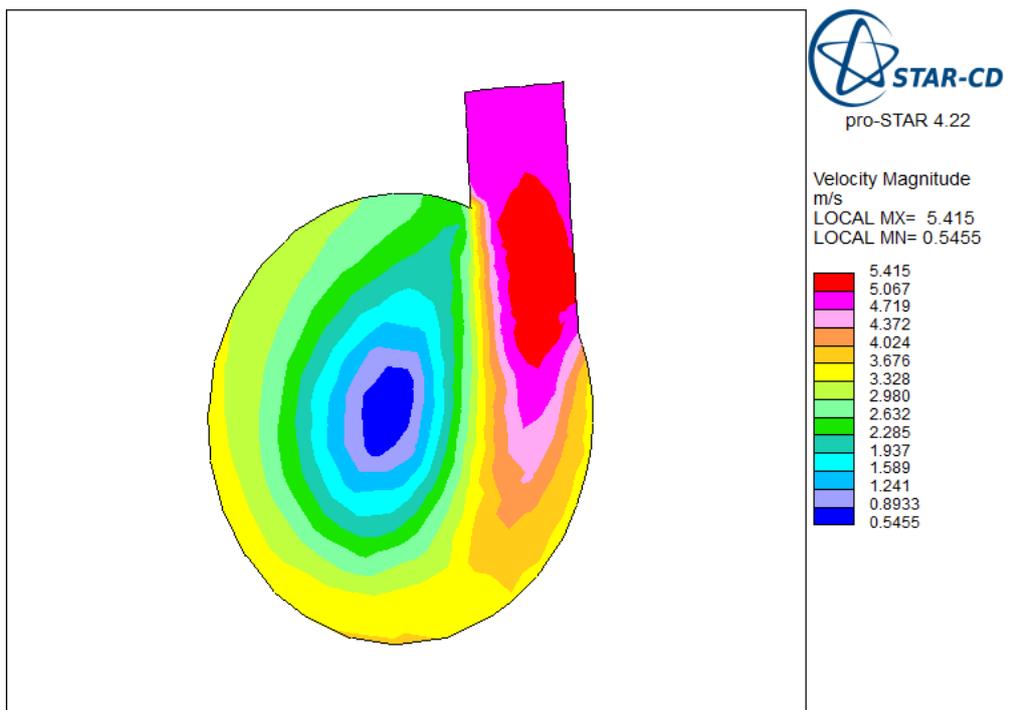


e. Tangential entry into nozzle

Figure 5.8 Velocity magnitudes at various nozzle sections
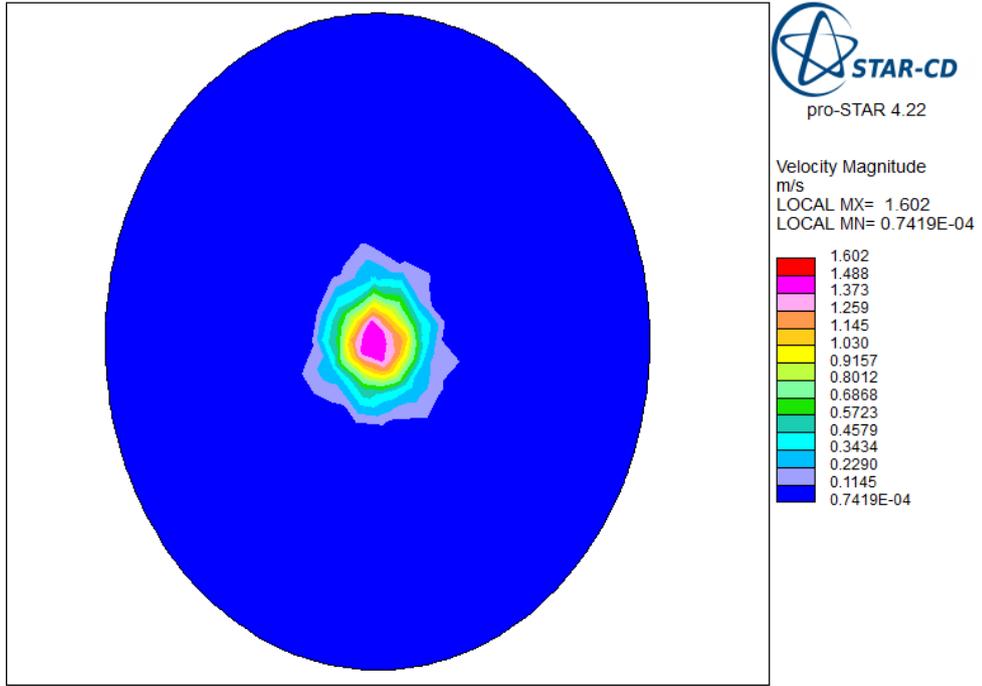
Velocity = 60 mm
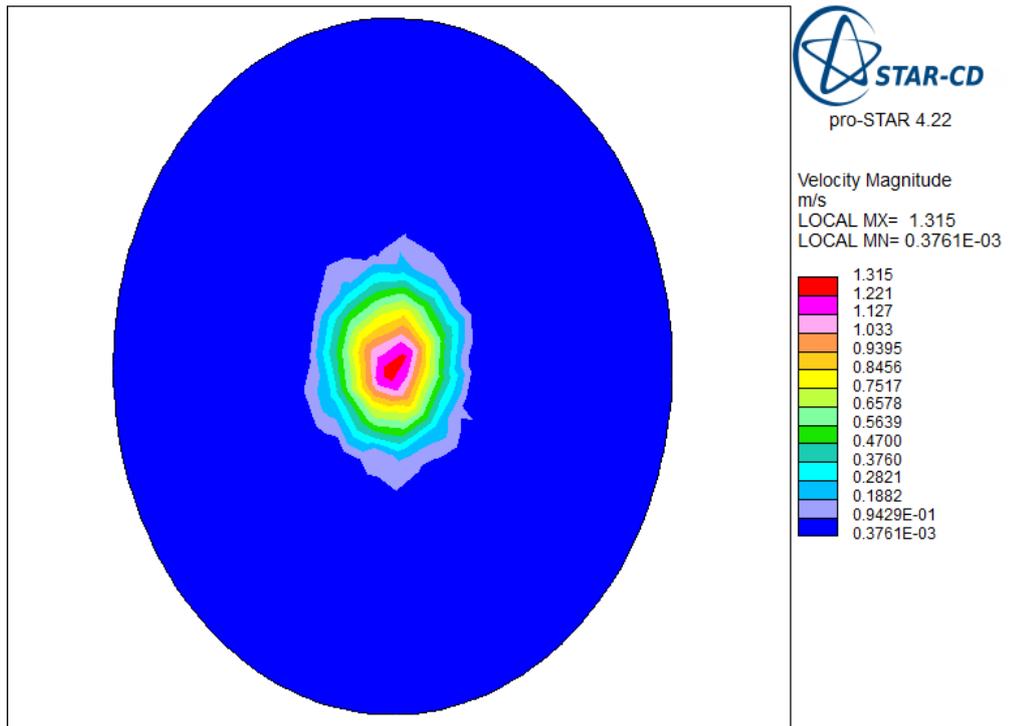


Velocity = 80 mm
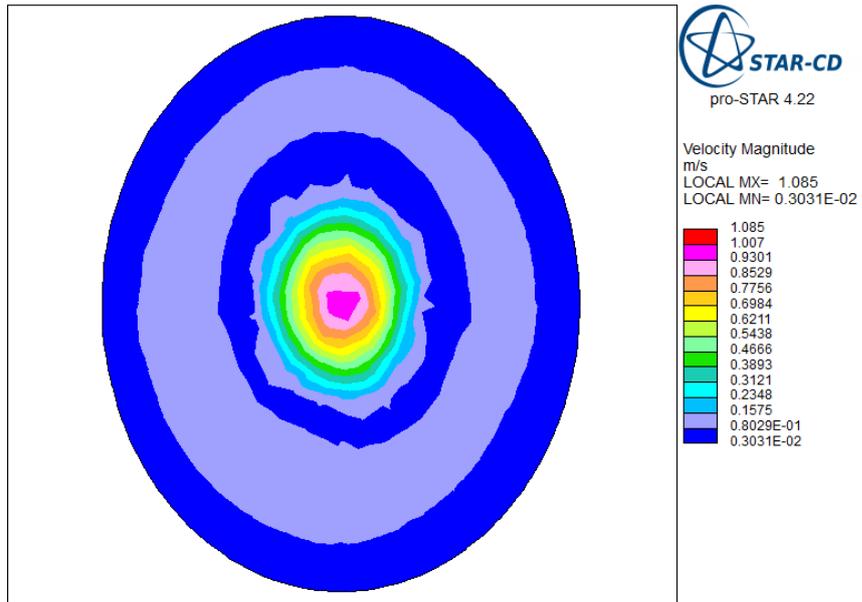
Velocity = 100 mm
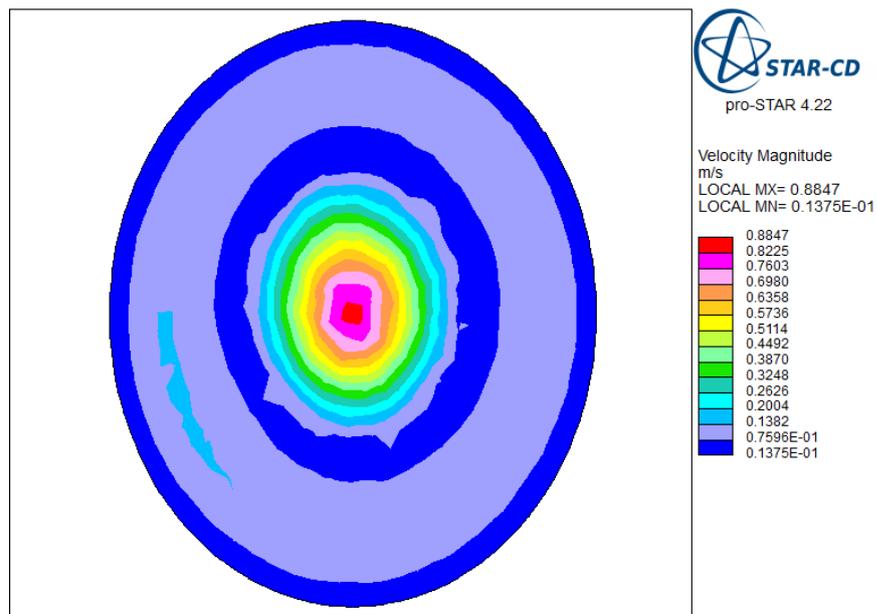


Velocity = 120 mm

Figure 5.9 Contour plot of velocity magnitude at various cross sections in the computational domain
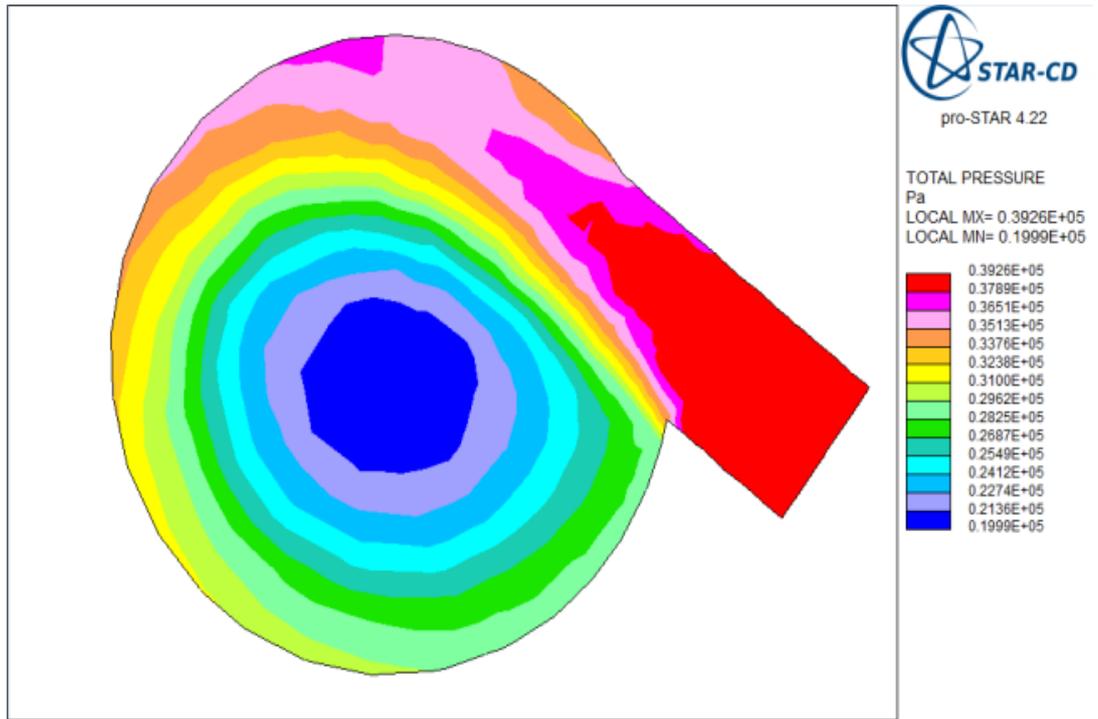
a. Pressure distribution
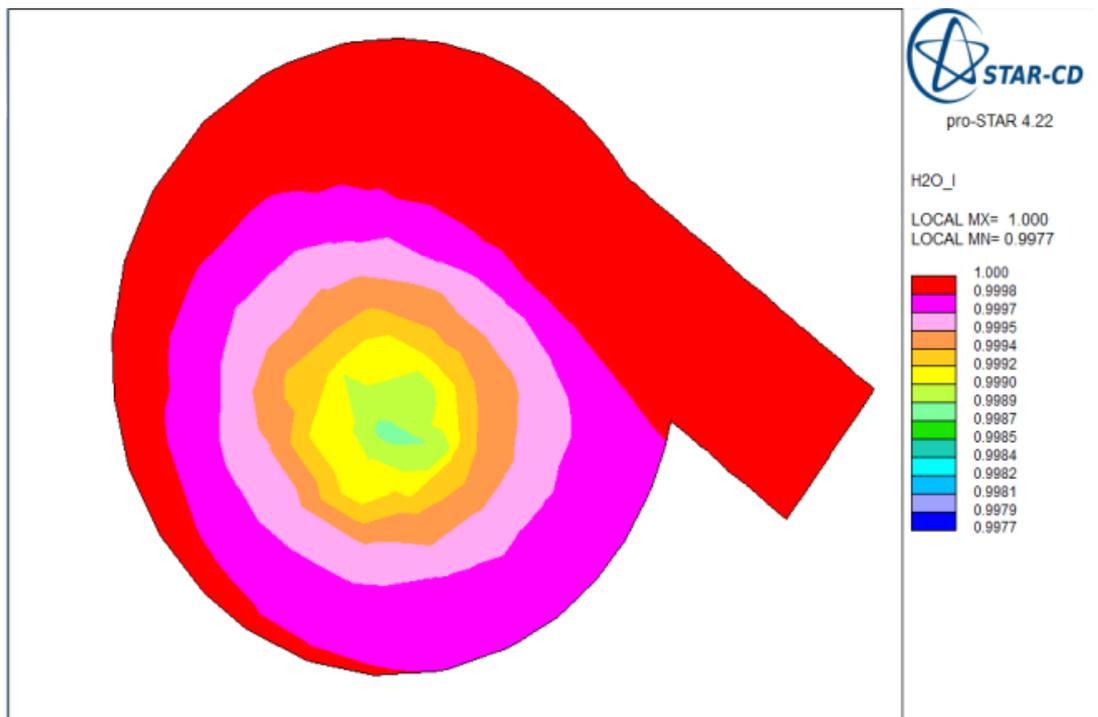


b. Mass fraction of liquid
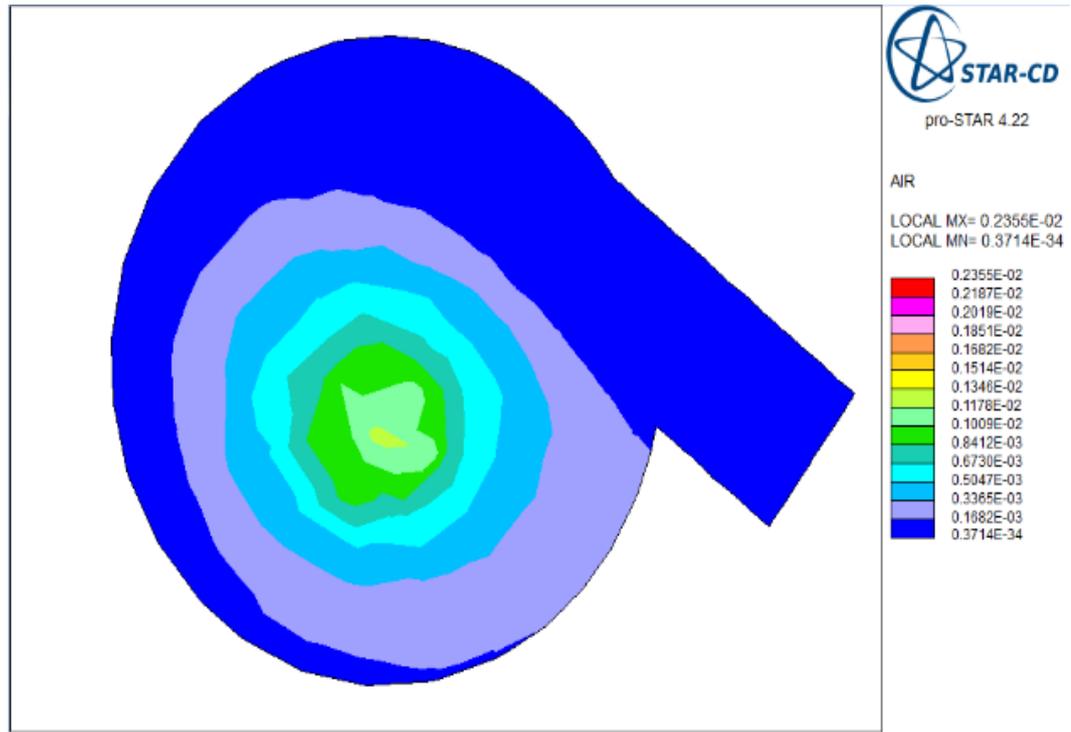
c. Mass fraction of air
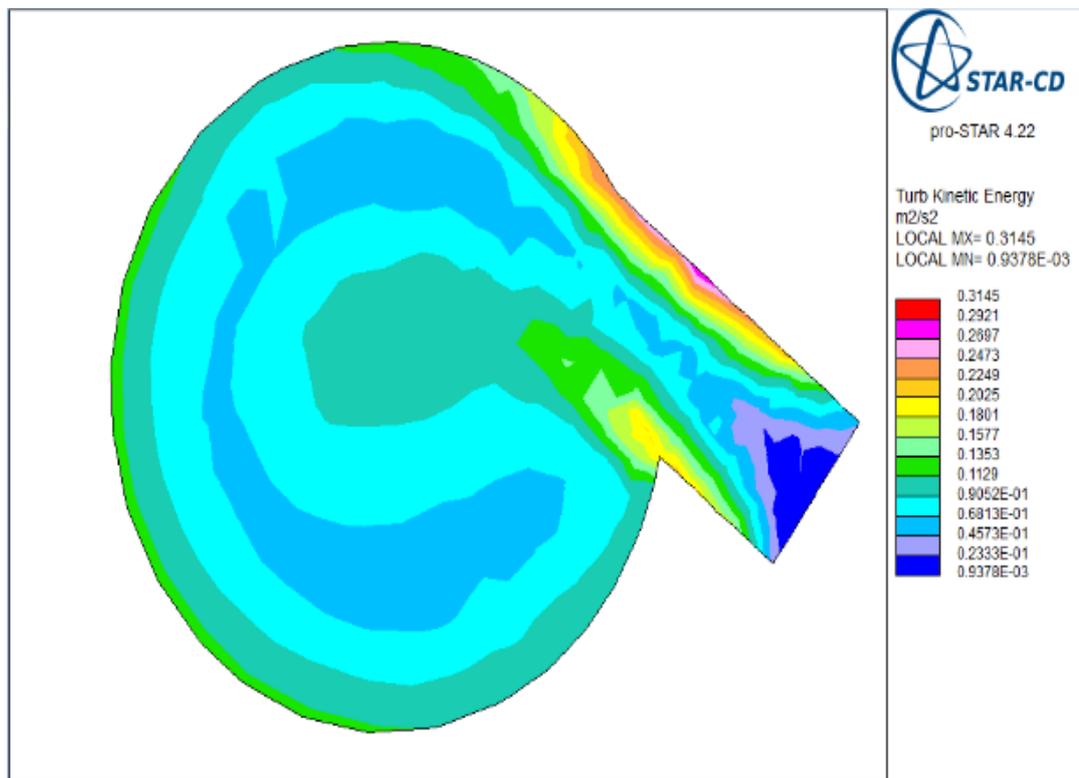


d. Turbulent kinetic energy
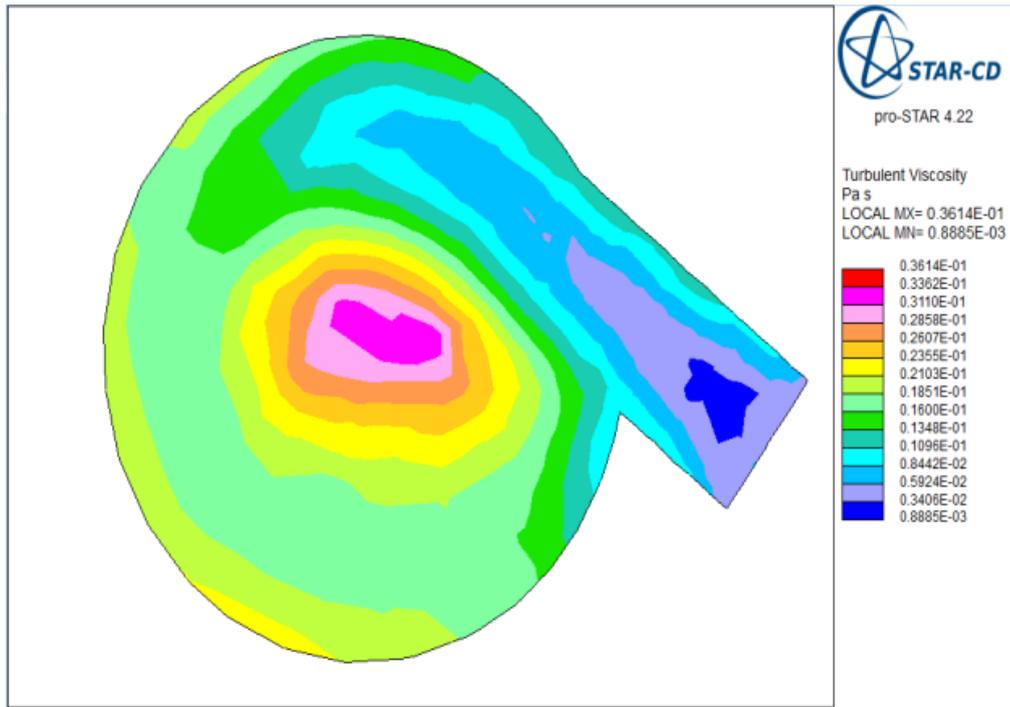
e. Turbulent viscosity
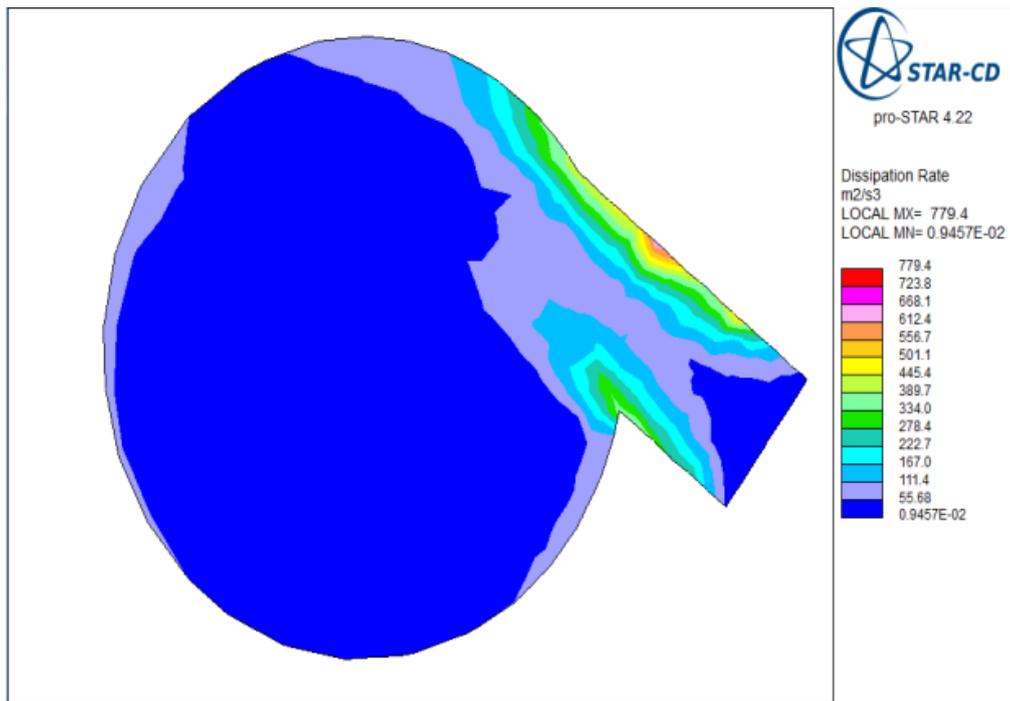


f. Turbulent dissipation rate

Figure 5.10 Contour plots of scalar quantities on the cross section plane at the entry into the nozzle
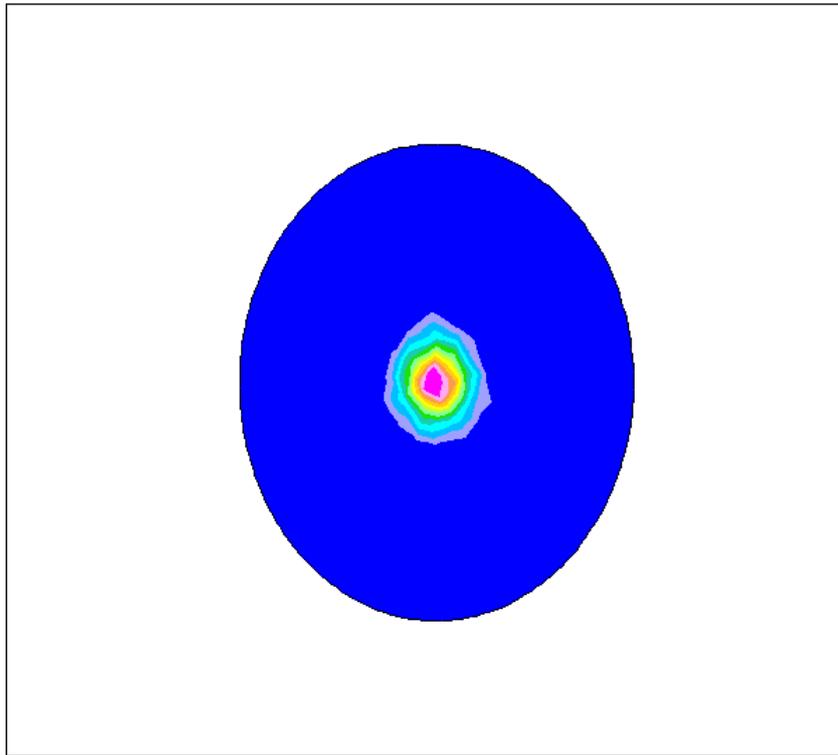
a. y=60mm
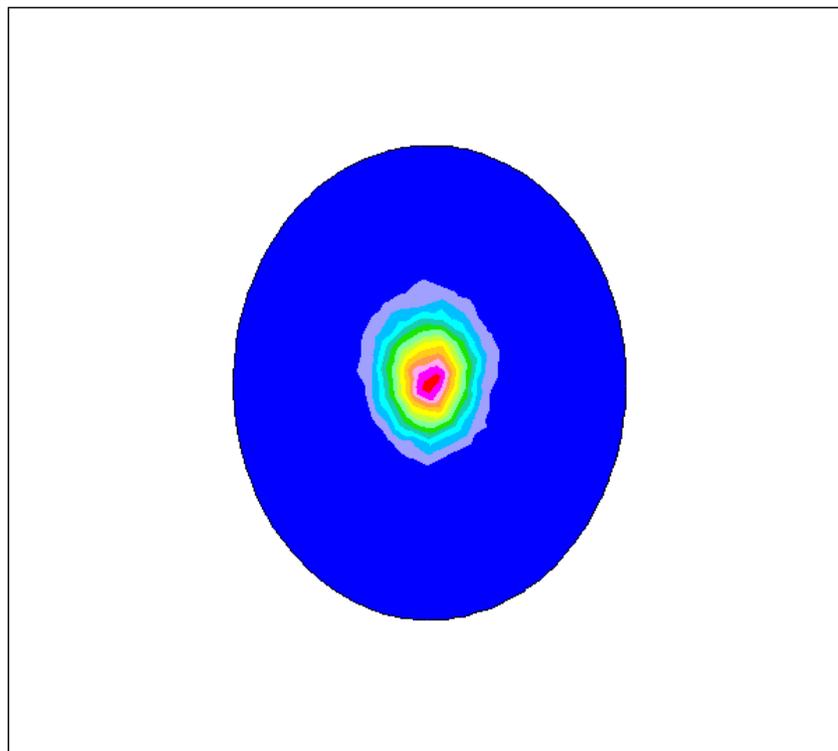


b. y=80mm
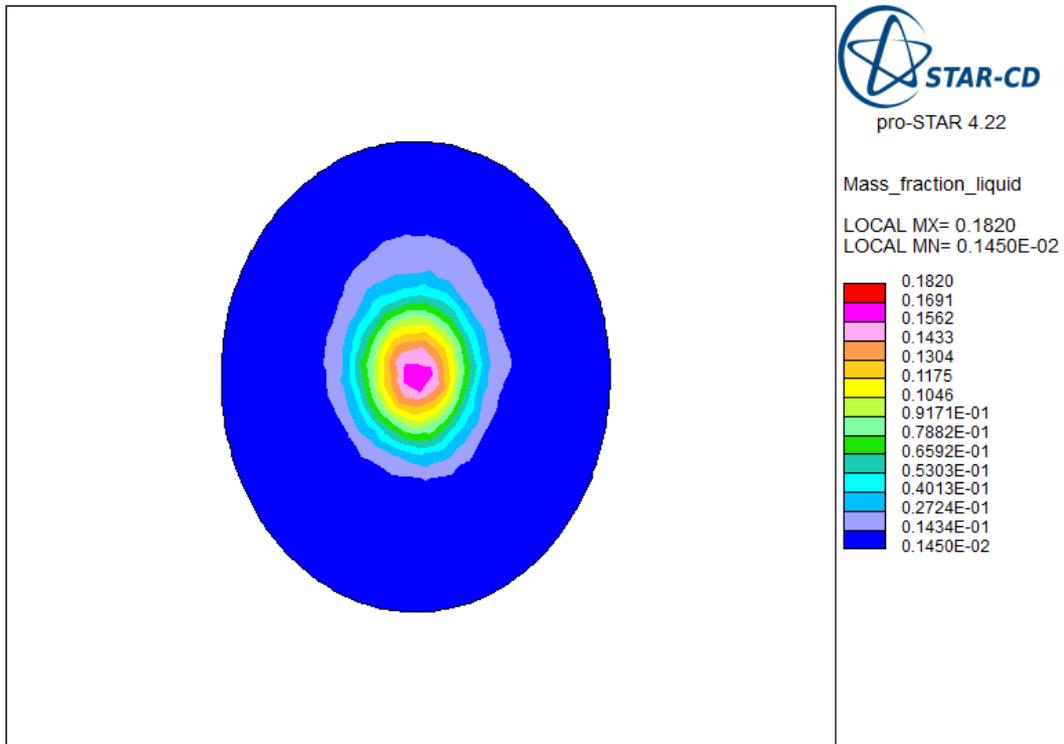
c. y=100mm
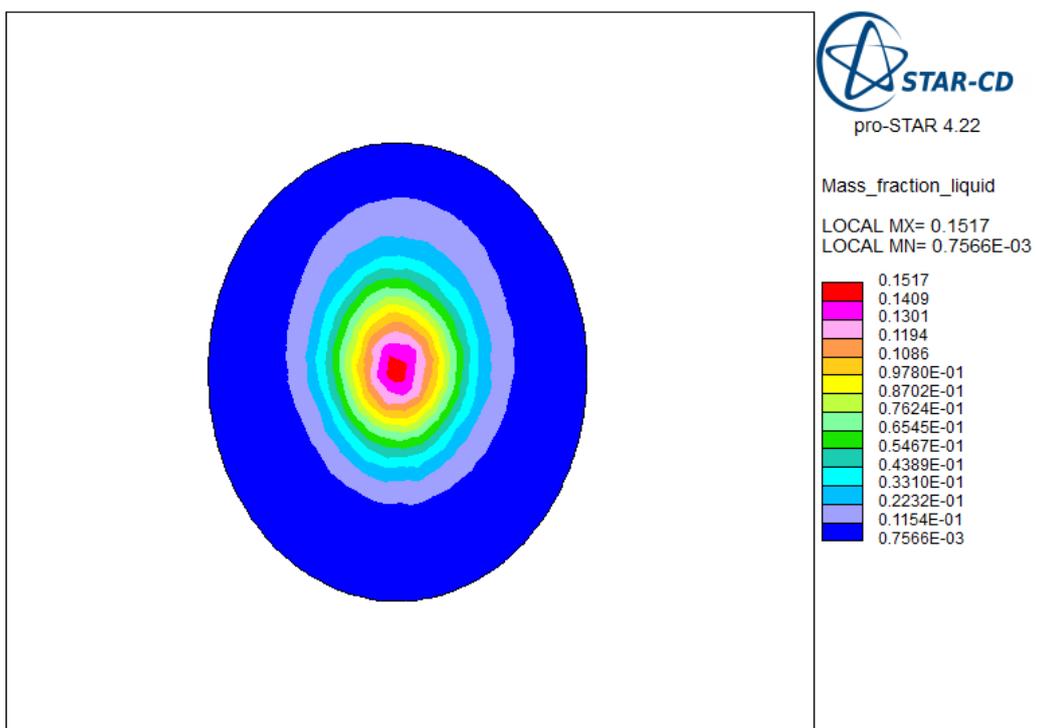


d. y=120mm

Figure 5.11 Mass fraction of liquid on various cross section planes at y=60, 80, 100 and 120 mm

Figure 5.11 presents the liquid mass fraction field *Y* at y=60, 80, 100 and 120 mm across the spray sections where droplet SMDs will be measured for validation of SMD at the radial positions. These results together with the corresponding interfacial surface density presented in Figure 5.12 were used to predict the SMD at radial locations in the spray. Spray spreading in radial direction is clearly observed and minimum values were found downstream the spray. This is because the mass fraction of the liquid decreases inside the spray as the liquid penetrates the air. The evolution of the interphase liquid surface density has the same behaviour as the mean liquid mass fraction. The minimum and maximum values of average interphase surface density correspond to the locations where the average liquid mass fraction is also minimum and maximum. This means the more liquid there is the more liquid and gas interface there is.
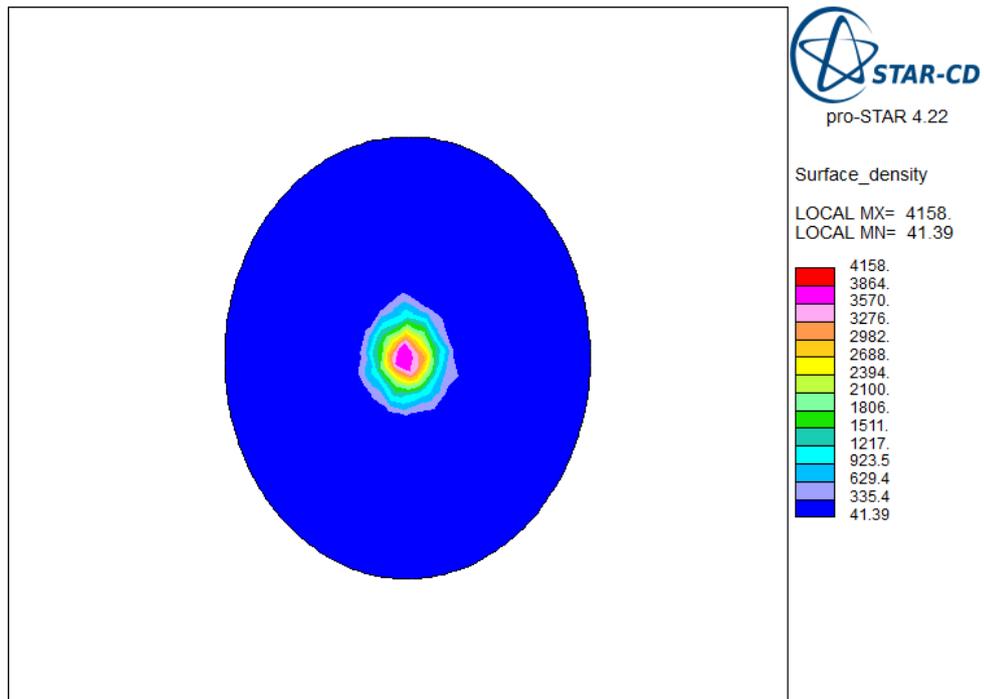


a.  y = 60 mm
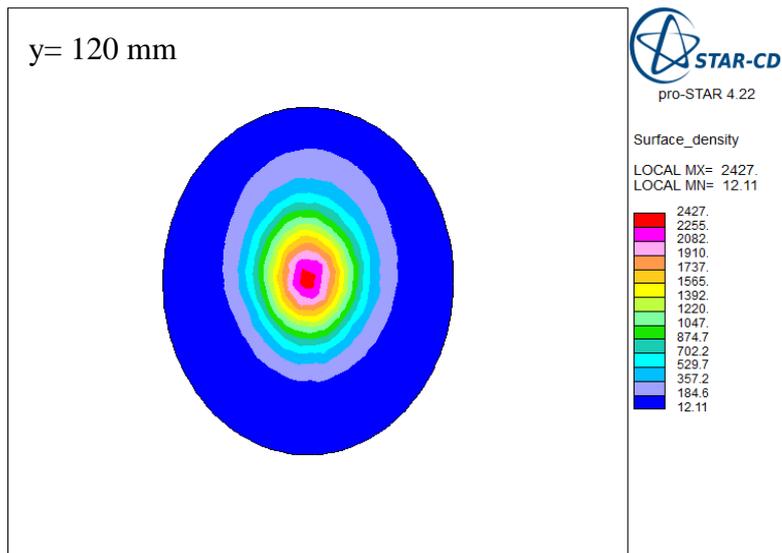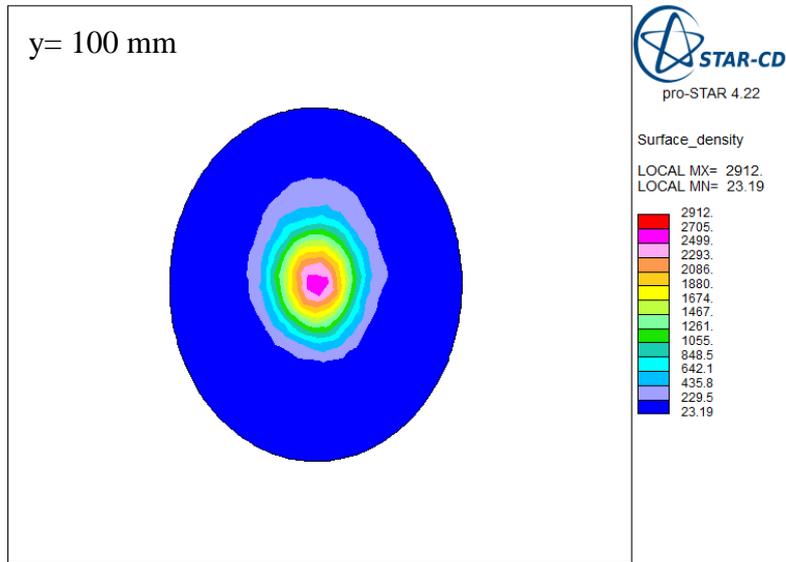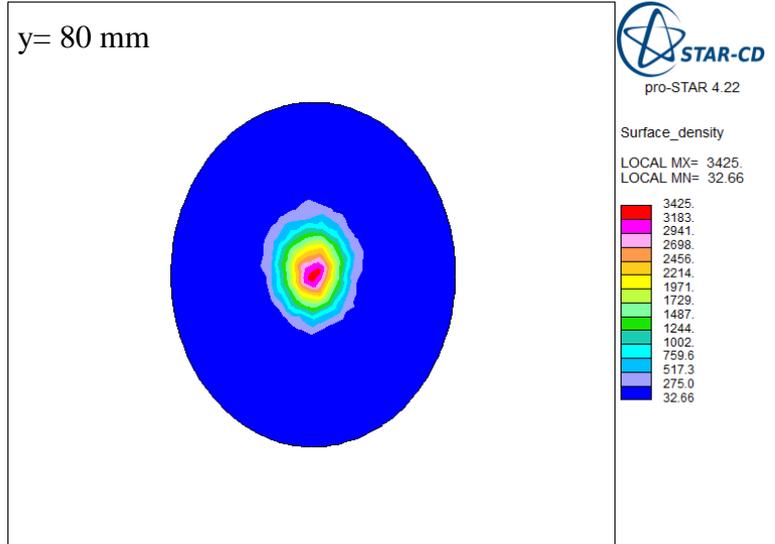
Figure 5.12 Surface density on various cross section planes at y=60, 80, 100 and 120 mm

### 5.5 Flow fields on the vertical plane

Figure 5.13a shows the axial profile of the droplet velocity obtained on the spray axis. The values on the y-axis represent the positions on the spray centre axis from the nozzle exit to the downstream in the computational domain. The vertical axis represents the velocity magnitude of the droplets at the various axial positions on the symmetry axis away from the nozzle exit. It can be seen that the maximum velocity at the vicinity of the nozzle exit is 6.5 m/s. The liquid velocity decreases quite sharply from the nozzle exit up to 20 mm to approximately 1.5 m/s. It further reduces to a low value and remains almost constant in the downstream part of the spray. Figure 5.13b shows the radial profile of the droplet velocity at the axial position y = 60mm. The result shows that higher mean velocity can be observed at the centre spread of the spray and it decreases towards the periphery of the spray.



(a)
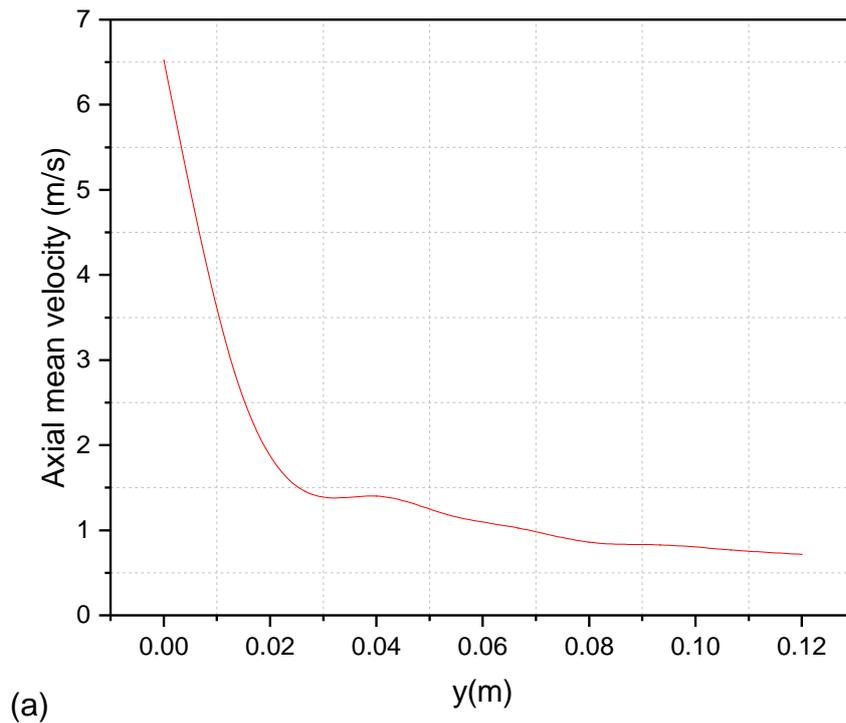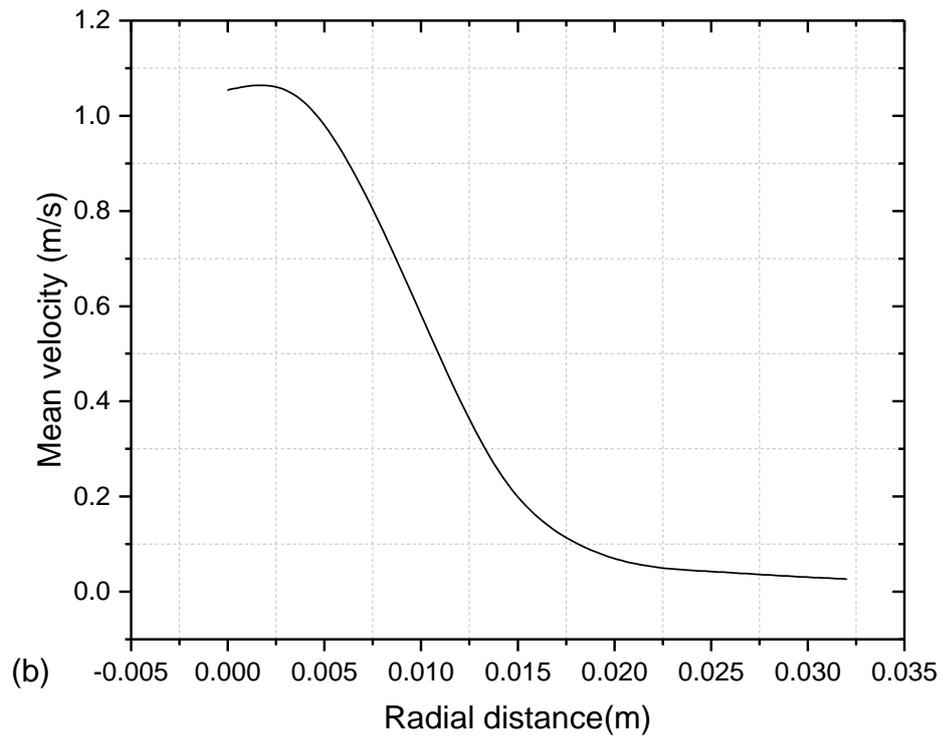
Figure 5.13 Droplet velocity on the (a) spary centreline and (b) radial positions at y = 60mm
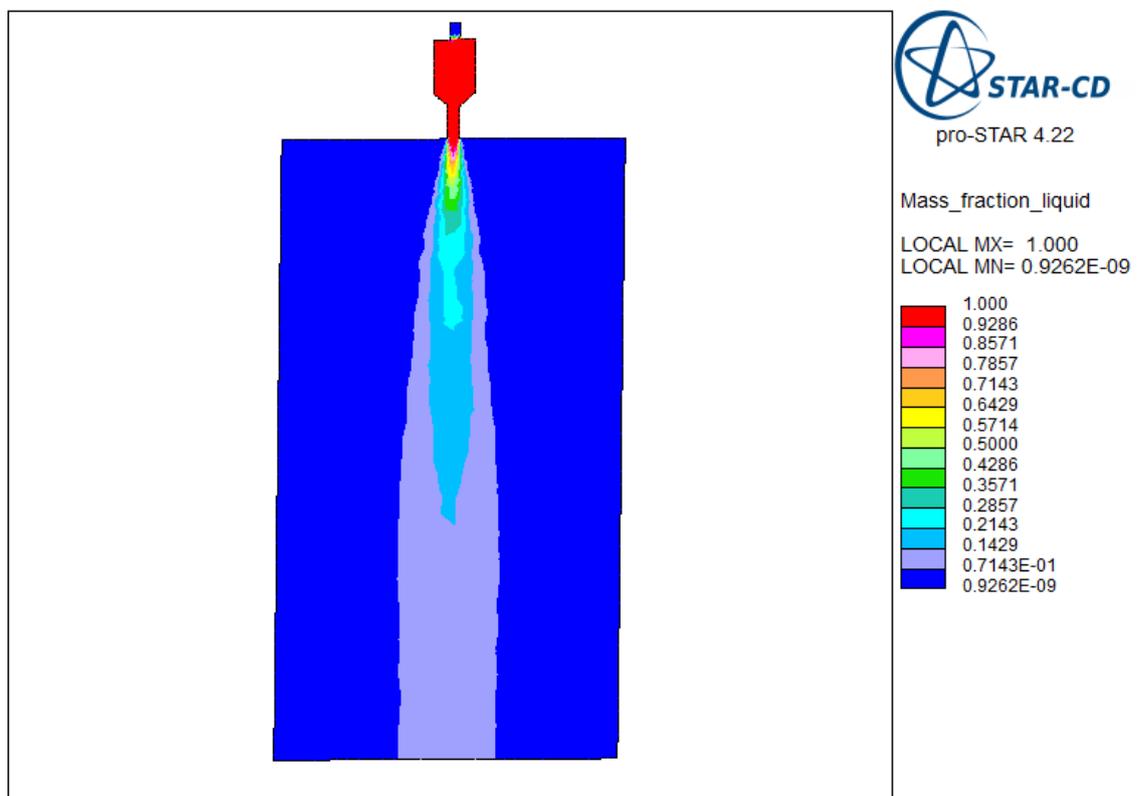


Figure 5.14 Contour plot of liquid mass fraction on the vertical plane
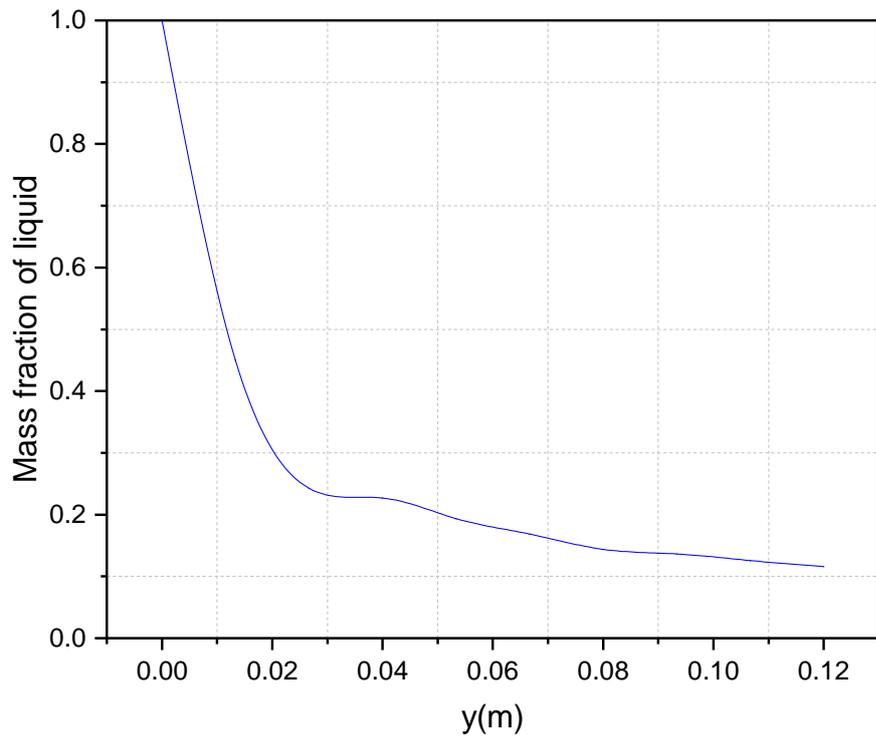
Figure 5.15 Liquid mass fraction on the spray centre line
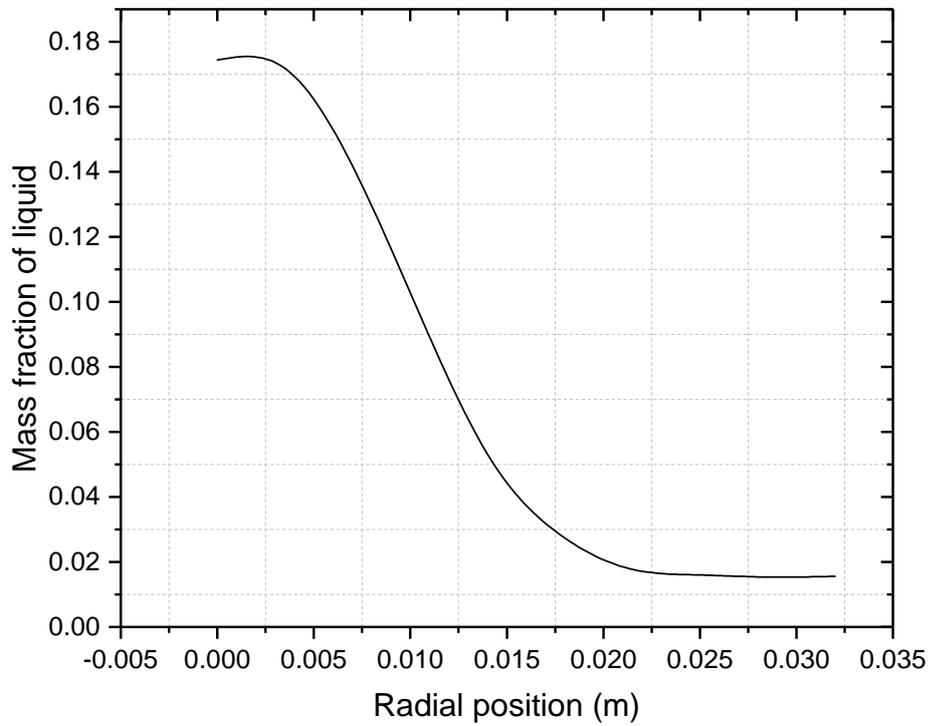


Figure 5.16 Mass fraction of liquid on the spray radial positions at y = 60 mm

Figure 5.14 illustrates the 2D field of the liquid mass fraction on the vertical plane. The liquid mass fraction lies between 0 and 1. The liquid mass fraction is 1 (in red) at the liquid phase and 0 at the air phase. Inside the domain of the atomizer, there is only liquid and as the liquid moves through the gas phase, the liquid mass fraction in the centre spread decreases. Outside the spray indicated by the blue colour, it is surrounded by only air. Conical spray is clearly visible and on the spray axis the mean liquid mass fraction decreases downstream the computational domain. Figure 5.15 presents the graph of the liquid mass fraction on the spray centre axis. The x-axis values represent the positions as shown on the probe line 1 in Figure 5.1. The liquid mass fraction on the vertical axis has a maximum value of 1. As can be seen from Figure 5.15 the value of the mass fraction of the liquid is high at the nozzle exit at x=0 and decreases downwards with the lowest value of 0.1. Figure 5.16 shows the liquid mass fraction distributions on the spray radial positions at y=60 mm which shows higher liquid mass fraction at the centre spread and decreasing sprays towards the atomizer walls. The high value of the liquid mass fraction at this location may be due to the initial impulse and high energy in the liquid as it leaves the exit orifice of the nozzle and attempting to penetrate the air. Liquid dispersion into the air may give rise to the decrease in the value of the liquid mass fraction.
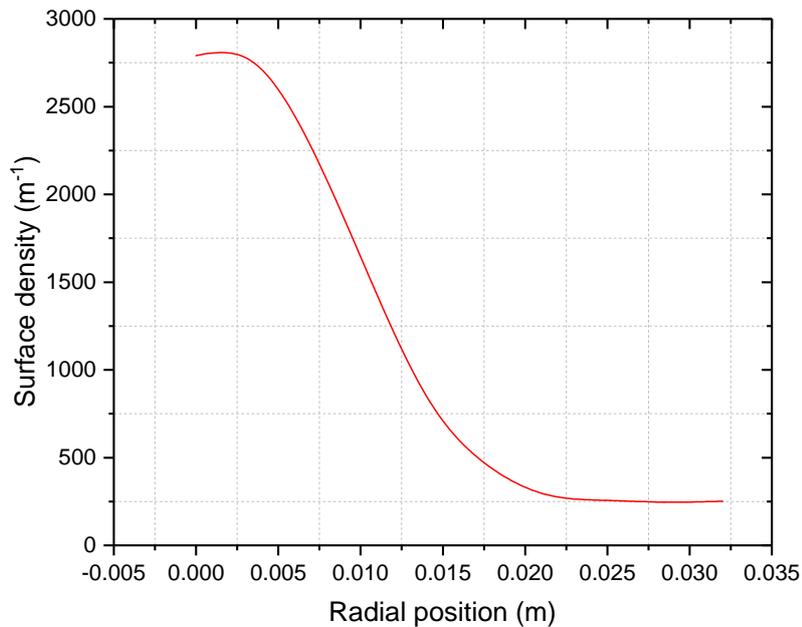


Figure 5.17 Predicted surface density on radial position at y =60 mm

The interfacial surface density being the key quantity characterising the atomization quality and droplet diameter in this model is predicted along and across the atomizer as shown in Figure 5.17, Figure 5.18 and Figure 5.19. In Figure 5.17 the radial positions are taken at y=60 mm from the tip of the atomizer. The vertical axis values represent the values of the interfacial surface density predicted on the radial positions. The axial position x=0 corresponds to a position on the spray centre axis. The y=60 mm is located with reference to the minimum distance away from the nozzle exit from which meaningful data can be obtained for spray drop size measurement. The results show that the interfacial surface density has the same shape profile as the mass fraction of the liquid. The minimal and maximum values of the surface density respectively are also at the point where the mass fraction values are also minimal and maximum respectively. This means that the more the liquid at a position in the field the more the surface density and vice versa. The maximum value for the surface density is 2800 m$^{-1}$ at axial position x=0. This increase in the surface area density may be due to the bulk turbulence of the liquid. It is supported by Beheshti et al [40] that the rate of liquid surface area increase is a weighted sum of rates determined by the bulk turbulence and the drop collision.
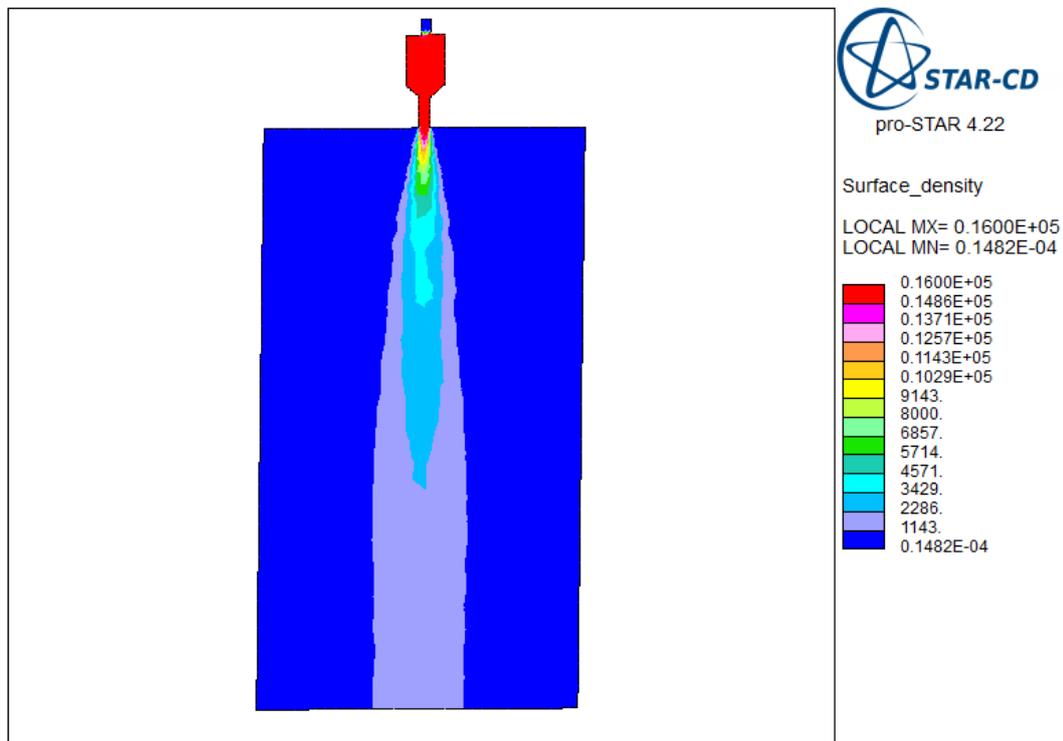


Figure 5.18 Contour plot of interfacial surface density on the vertical plane
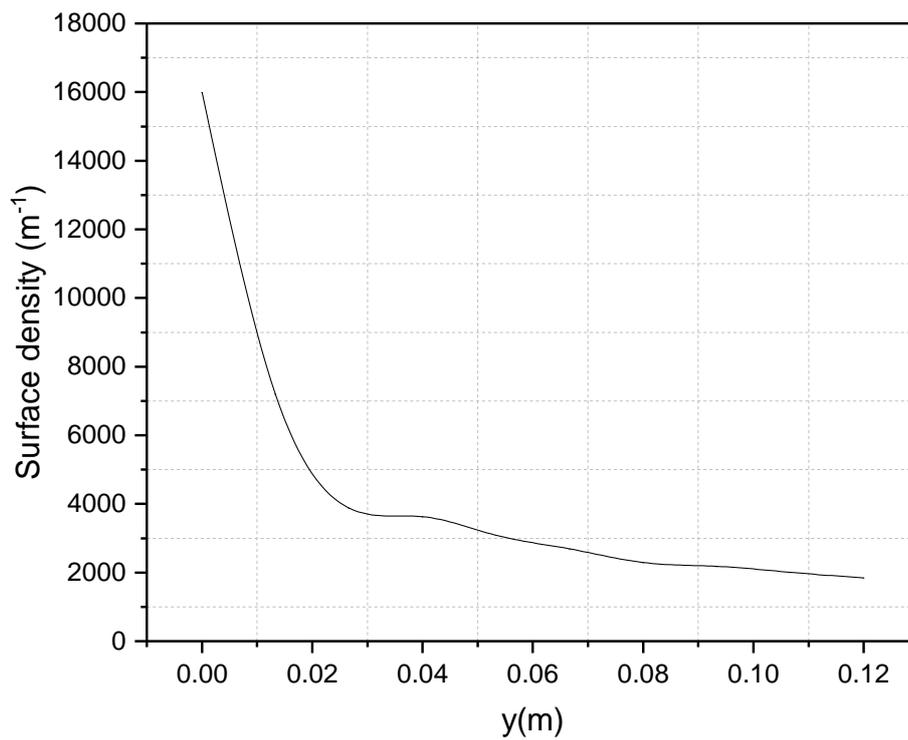
Figure 5.19 Predicted interfacial surface density on the spray centre line

Figure 5.19 shows predicted interfacial surface density on the spray centre line evaluated from the contour plot of surface density shown in Figure 5.18. It can be observed that the surface area density in the atomizer decreases sharply along the symmetry line (between axial position y=0 and 30 mm) from 16000 $m^{-1}$ to 4000 $m^{-1}$. The coordinates (x,y = 0,0) is located at the tip of the nozzle exit. Inside the computational domain, and on the spray centre line, the value of the predicted interfacial surface density decreases slowly as is almost constant (axial positions y = 30 mm and y = 120 mm) with a value of 2000 $m^{-1}$. This result is used to predict the Sauter Mean Diameter (SMD) on the spray centre axis.

### 5.6 Prediction of Sauter Mean Diameter (SMD)

Figure 5.20 presents the radial profile of numerical predicted Sauter Mean diameter (SMD) at axial positions y = 60 mm from the nozzle exit. The result shows that the SMDs are smaller in the vicinity of the spray centre axis (axial position = 0) and higher droplet SMD values can be seen at the periphery of the spray. Thus it can be deduced that the SMD depends on the radial distance. This may be due to the large droplets experiencing less drag than the smaller droplets and can also be due to droplet coalescence which is accounted for by the model. Outside the liquid sheet, the mass fraction and liquid surface density are zero and so the SMD calculated does not represent any droplet diameter. The result also shows that the droplet size has been predicted with correct order-of-magnitude when compared to the works of Beheshti[40] and Vallet et al[14] when assessing the same model.
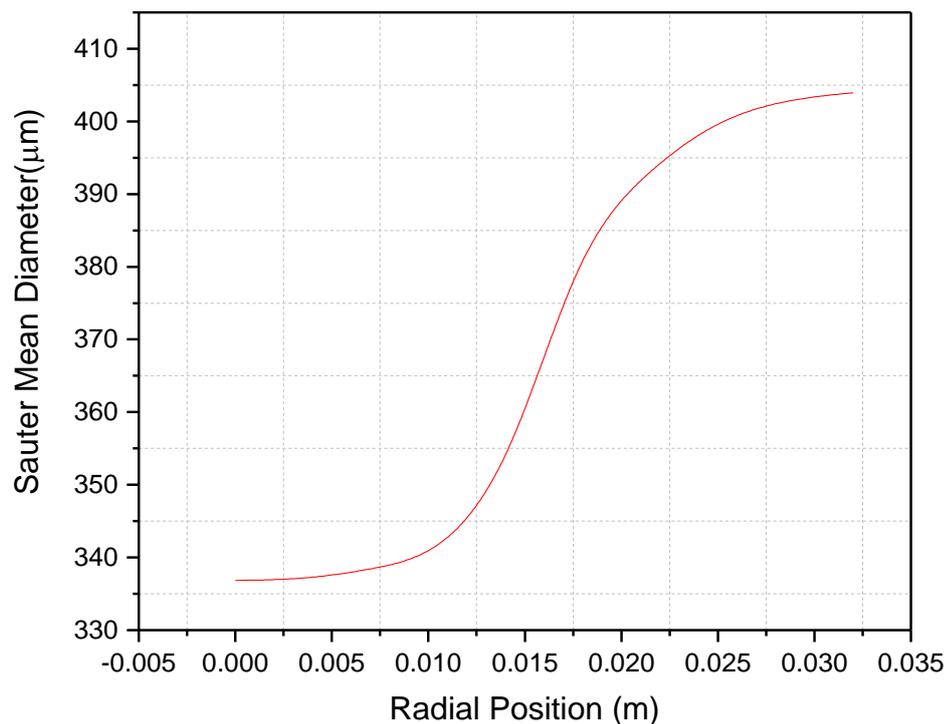


Figure 5.20 Sauter mean diameter (SMD) on radial positions at y= 60mm
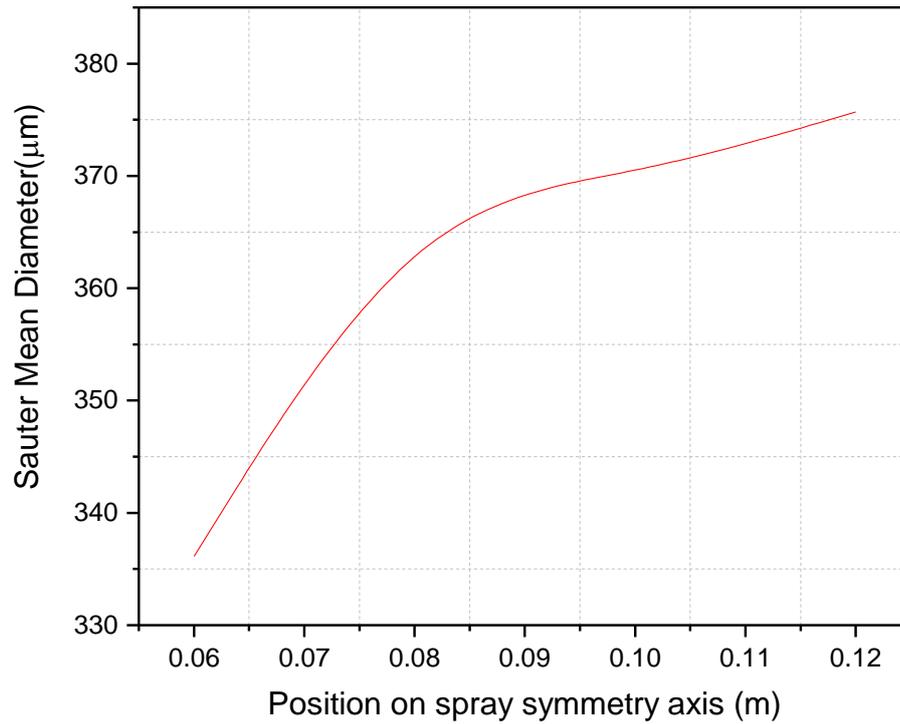
Figure 5.21. Spray Sauter mean diameter (SMD) predicted on the symmetry axis

Figure 5.21 shows the Sauter mean diameter predicted on the spray centre axis. The y-values are the positions on the symmetry axis away from the nozzle exit in the computational domain. The curved line shows the Sauter mean diameter (SMD) predicted at the various locations on the spray centre line. The results show that the Sauter mean diameters (SMDs) close to the nozzle exit are smaller than other positions on the symmetry line downwards the domain. Thus, it can be deduced that the SMD increases with increasing downstream distance. This phenomenon may be attributed to droplets collisions which may result in droplet coalescence. It can also be concluded that these SMD values were predicted with correct order of magnitude and therefore was compared with the experimental results.

## 5.7 Summary

The findings from this chapter show that across the various sections of the nozzle the pressure in the swirl chamber is almost constant, drop sharply in the contraction zone and further decreases in the exit orifice which is consistent with the experimental observations of many researchers. The flow fields for the velocity magnitudes indicate that regions of relatively high velocities in the liquid were found to be in the atomizer compared to the velocity magnitude  downstream the spray. It was deduced that the mass fraction of the liquid decreases inside the spray as the liquid penetrates the air and that the evolution of the liquid surface density has the same behaviour as the mean liquid mass fraction. The findings show that the SMDs are smaller in the vicinity of the spray centreline and higher droplet SMD values are seen at the periphery of the spray Thus the SMD depends on the radial positions in the spray. It was also observed that the SMDs close to the nozzle exit are smaller than other positions on the symmetry line downstream the spray.

# CHAPTER 6 EXPERIMENTAL RESULTS AND VALIDATION

## 6.1 Introduction

This experimental and validation section undertakes the measurements of the droplet SMD at different axial distances for the hollow-cone nozzle and different radial distances from the spray centreline using a laser-diffraction-based drop size analyser (Malvern Spraytec) and also investigates the influence of injection pressure and liquid flow rate on the SMD. In addition, the geometrical exit orifice diameters of 3.5mm and 1.5mm of the nozzle on the SMD are also analysed. The drop size distributions along the nozzle centreline 60, 80, 100 and 120mm as well as the radial drop distributions from spray centreline at 10, 15, 20 and 25mm are also discussed. The liquid film breakup as a function of the pressure differential is also presented. For the validation to be carried out variants of different turbulence models on the SMDs were first evaluated and the validation of SMD at spray centre axis and radial positions performed.

## 6.2 Spray symmetry and mean drop sizes

Figure 6.1 shows axial profiles of the arithmetic mean diameter $d_{10}$, Sauter mean diameter, SMD $d_{32}$, De Broukere diameter, $d_{43}$ and mass median diameter (MMD) $d_{50}$ evaluated at axial positions of $y = 60, 80, 100,$ and 120 mm for injection pressure of 3.0 bars. Since droplet sizing can only be made after the disintegration of the liquid sheet, measurements can only be taken at a certain distance from the liquid sheet breakup. Therefore comparisons at closer axial distances are meaningless and in particular measurements below 60 mm from the tip of the nozzle are neglected. The diameters $d_{10}$ and $d_{50}$ correspond, respectively, to drop diameters that encompass 10% and 50% of total volume of drops below the drop volume considered. It can be observed that the characteristic drop sizes increase in the axial direction downstream the nozzle. Arithmetic mean diameter $d_{10}$ shows the least drop size and lower than the Sauter mean diameter $d_{32}$ which is expected in most drop size distributions. De Broukere diameter, $d_{43}$ records the highest drop size values. The Sauter mean diameter $d_{32}$ which is described by Chin and Lefebvre [179] as the best measure of the fineness of sprays and mass median diameter $d_{50}$ fall in within this range with the Sauter mean diameter $d_{32}$ far lower than the mass median diameter $d_{50}$. The relative positions of the different diameters as shown in Figure 6.1 also conform to the observations made by Williams [180] where the Sauter mean diameter, $d_{32}$, is 18 μm and the other diameters $d_{10}$ and $d_{50}$

are 5.5 μm and 24 μm respectively. In Figure 6.2 the influence of pressure on mean drop size $d_{32}$ was analysed at the locations on the spray centreline. As expected, it is observed that an increase in the injection pressure of liquid leads to a decrease in SMDs on the spray centreline.
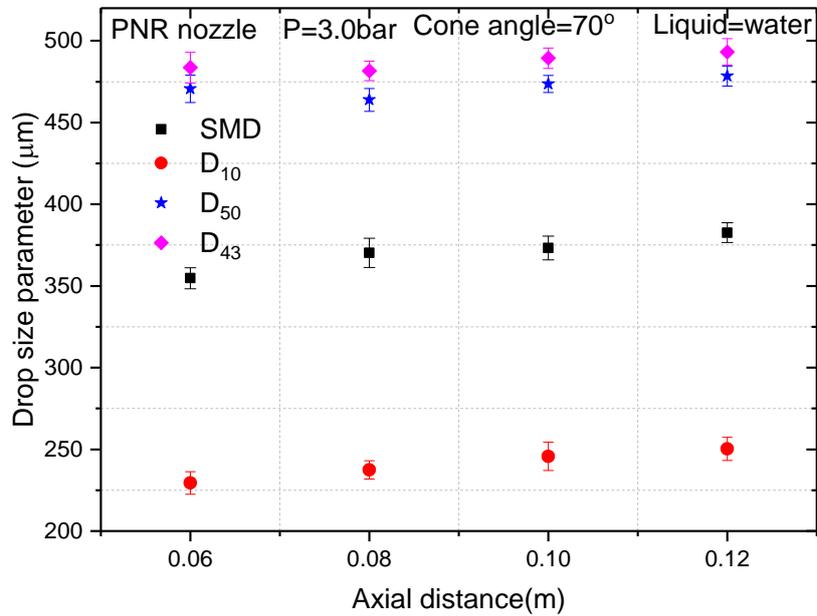


Figure 6.1 Drop size parameter profile along the spray centre line at atomizing pressure of 3.0bars, experimental. The error bars indicate the standard deviation of three measurements.
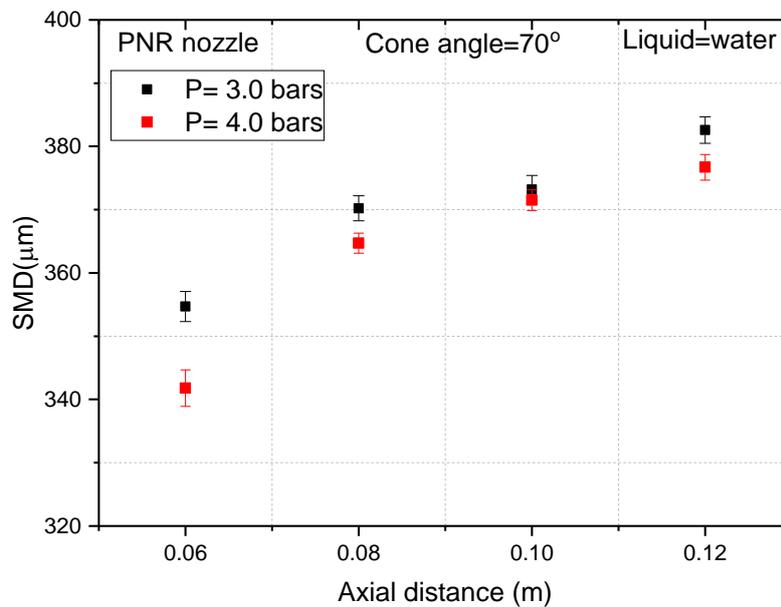


Figure 6.2 Sauter Mean Diameter (SMD) along the spray centre line at two different injection pressures, experimental
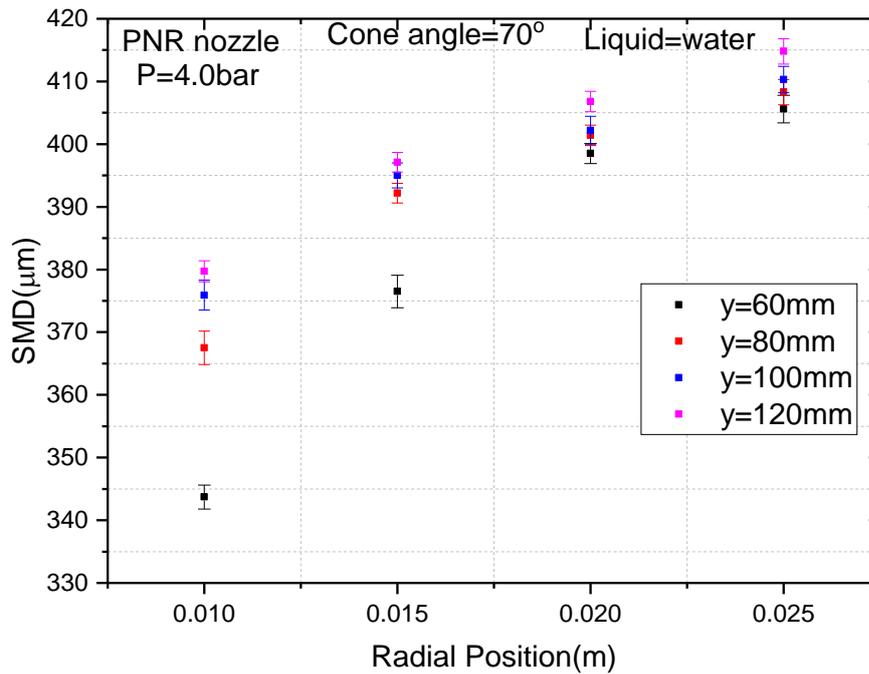
Figure 6.3 Radial Sauter Mean diameter (SMD) at axial positions y=60, 80, 100 and 120 mm from the nozzle exit at injection pressure of 4.0 bars. The error bars indicate the standard deviation of three measurements

Figure 6.3 show  the experimental results of Sauter Mean diameter (SMD) at radial positions 10, 15, 20 and 25mm from the spray centreline for axial positions y = 60, 80, 100 and 120 mm from the nozzle exit at injection pressure of 4.0 bars. It is found that the radial drop size profile from the spray center line shows an increase in the drop sizes as the axial distance increases from the spray centerline. At 60 mm from the nozzle, however, the drop sizes are as high as 402µm. The radial variation of the drop sizes is found to be dependent on both the injection pressure conditions and the spray measurement positions. It is evident that the higher the injection pressures, the smaller the drop sizes. From these spray profiles, it is also seen that larger sized drops occupy the spray periphery compared to those occupying the spray core. This is because they are less affected by the airflow entrained in the spray core that carries smaller drops.

## 6.3 Variation of inlet pressure on the Sauter Mean Diameter (SMD)

Figure 6.4 presents the influence of injection pressure on the Sauter Mean Diameter (SMD) at y = 90 mm. It can clearly be seen that the increase in pressure leads to a decrease in the mean drop size (SMD) and is due to the combined effect of stronger liquid sheet instability and the maximum growth of the surface wave as the pressure increases. This makes the liquid sheet breaks up more easily and produces smaller droplets. Flow rate as the only parameter concerning the quantity rather than quality of an atomised liquid is shown in Figure 6.6 and its influence on the droplet SMD is analysed. It can be seen that the droplet SMD also decreases with increasing liquid flow rate. Figure 6.5 shows the flow rate and the injection pressure and it can be observed that the flow rate and injection pressure increase in exponential form which is consistent with the flow rate calculation formula. This also agrees wth the findings by Emekwuru and Watkins [172] that an increase in liquid flow rate would usually decrease the drop size. This can be justified with the explanation that greater flow rate indicates greater velocity of the liquid and hence the relative velocity between air and the droplets is reduced. This helps in reducing the drag work required and thus a greater part of kinetic energy is available for the creation of new surfaces and consequently more droplets.
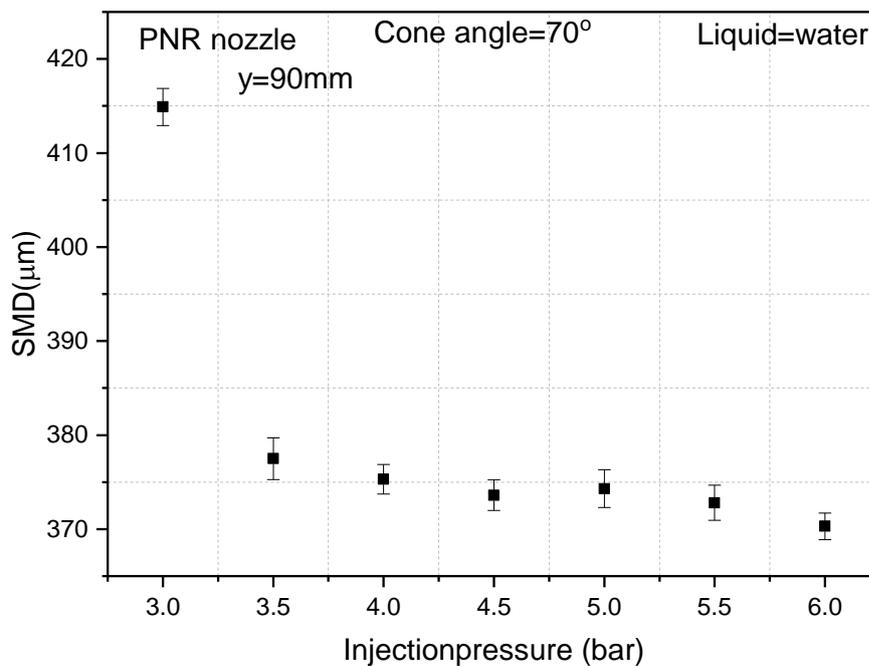


Figure 6.4 Influence of injection pressure on the Sauter Mean Diameter (SMD)
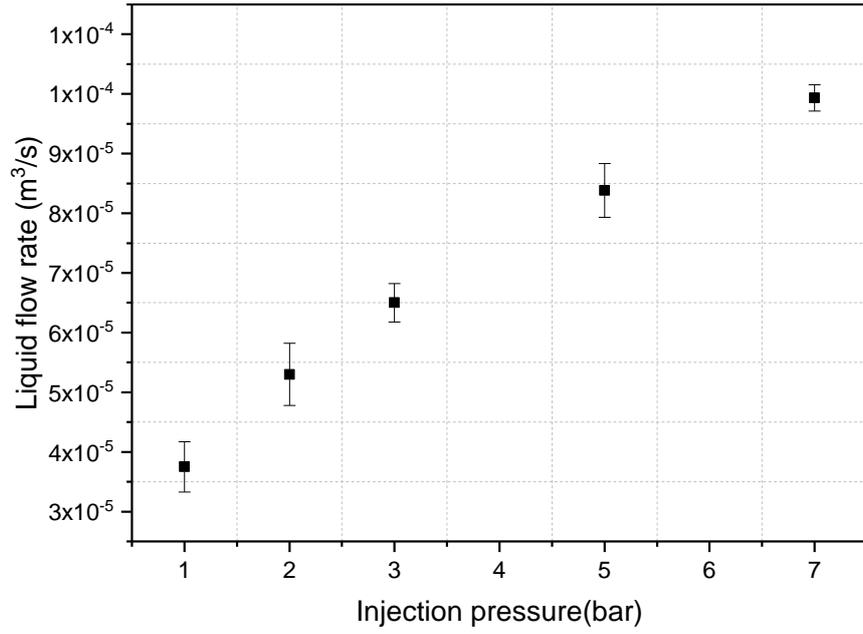
Figure 6.5 Liquid flow rate versus injection pressure
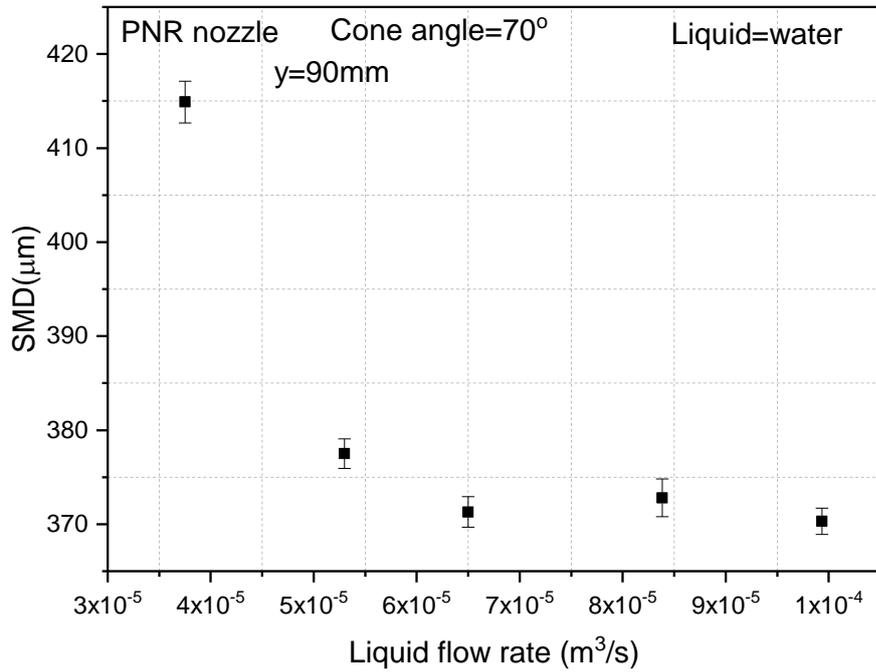


Figure 6.6 Effect of liquid flow rate on the Sauter Mean Diameter (SMD)

**6.4 Influence of geometrical dimensions on the Sauter Mean Diameter (SMD)**

Figure 6.7 shows the influence of nozzle exit orifice on the Sauter Mean Diameter (SMD) and can be observed that the nozzle exit orifice diameters 3.5 mm and 1.5 mm for big nozzle and small nozzle respectively have different SMD at the axial positions with small nozzle showing smaller SMDs than the big nozzle. Another significant observation is that break-up lengths are different for the two nozzles. When the 3.5 mm nozzle has droplet formation beyond 50mm  and the 1.5mm exit orifice nozzle has droplet SMD measured above 30mm.
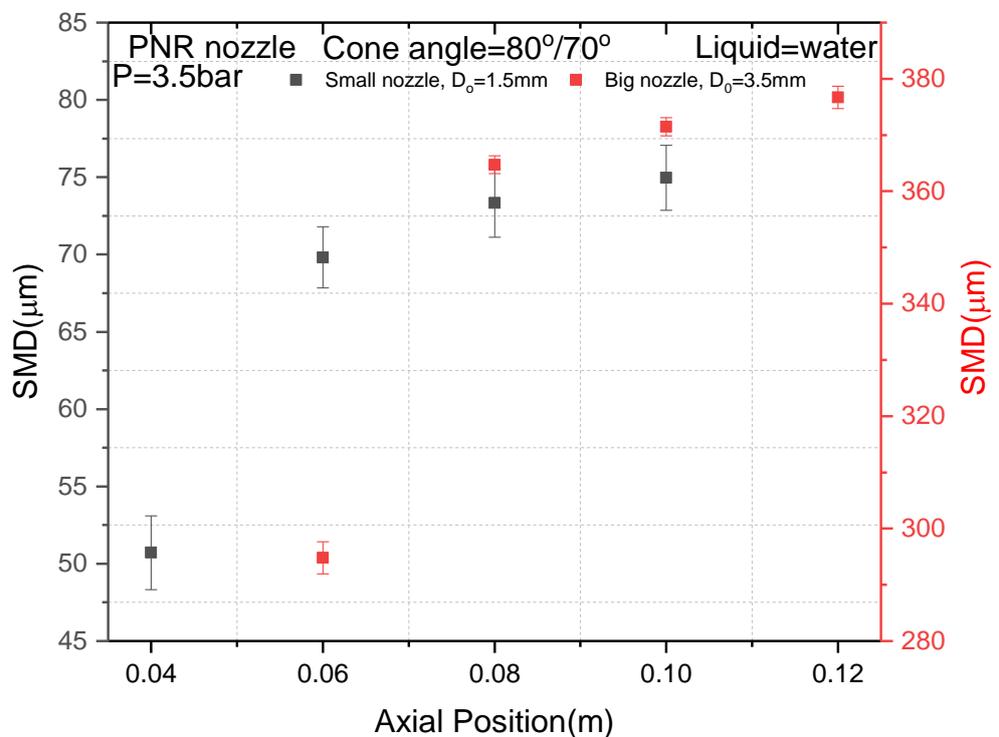


Figure 6.7 Effect of geometrical dimensions of the nozzle on the Sauter Mean Diameter (SMD)

**6.5 Drop size distributions along the nozzle centreline and from spray centreline**

The drop distributions or histogram displays the spray results in the form of 'in band' percentages. Each bar in the graph represents a size band of droplets and its height represents the percentage of the spray that is within that size band. The Figures below shows the histogram and graphs which are generated from the numeric values shown in Appendix 1. The cumulative undersize or result less than displays the percentage of the spray which is below a certain size [170].
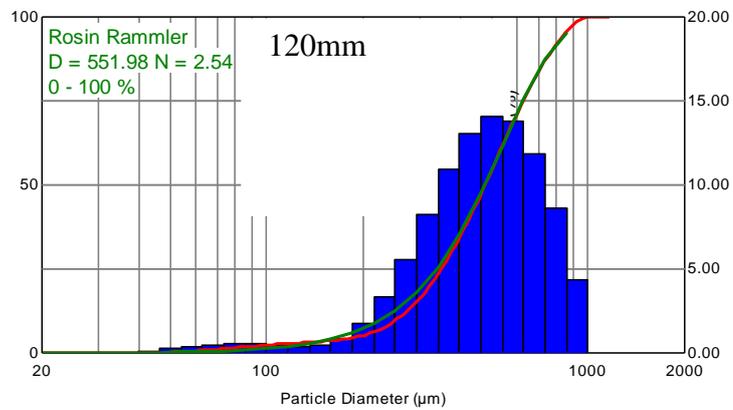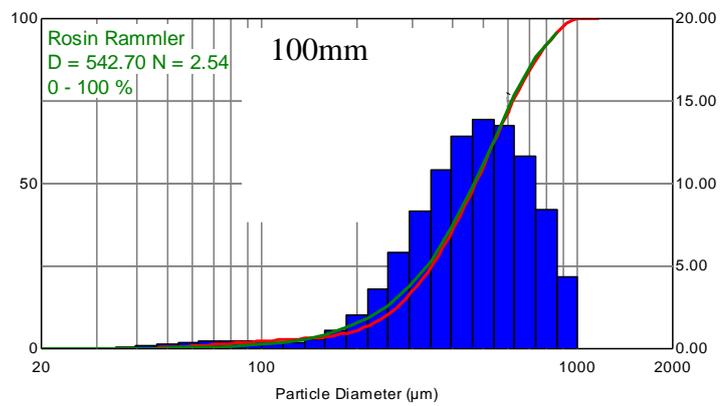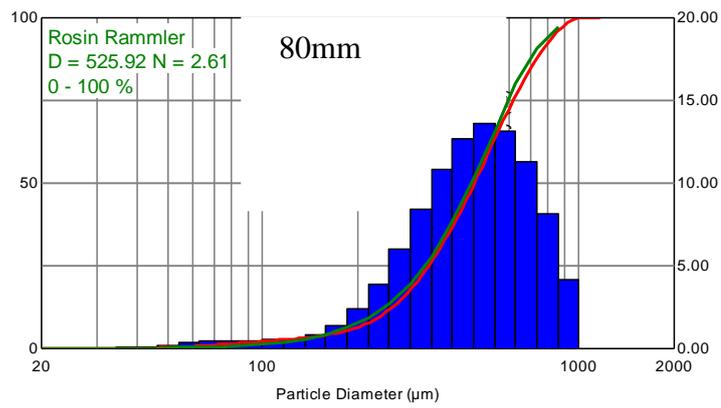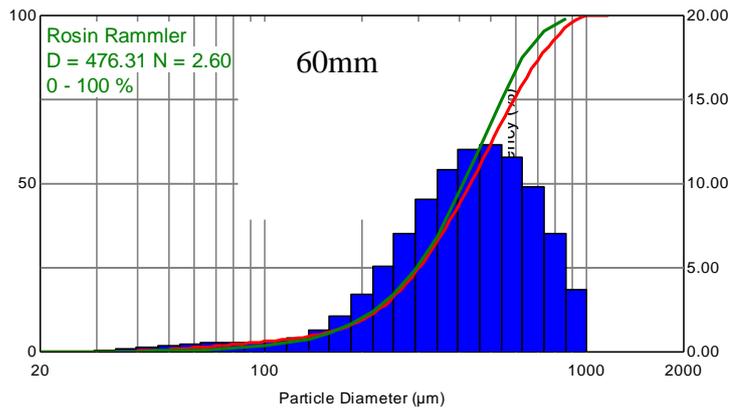
Figure 6.8 Drop size distributions for injection pressure value of 3.5bars at axial distance y= 60, 80, 100 and 120 mm along the 3.5mm exit orifice nozzle centre line
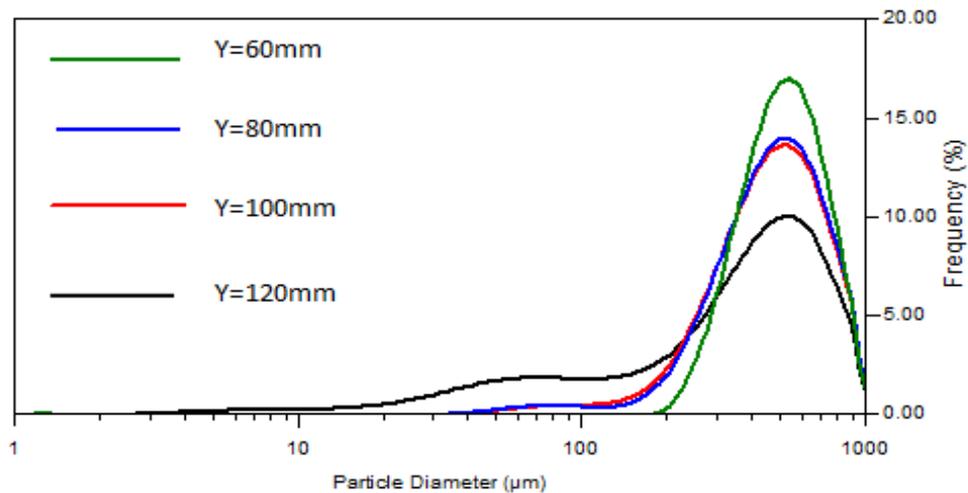
Figure 6.9 Particle Size Overlay (PSO) evaluated at axial sections along the 3.5mm exit orifice nozzle centre line for injection pressure value of 3.5bars

Figure 6.8 and Figure 6.9 present results of the drop size distributions and size overlay at various axial distances of 60, 80, 100 and 120 mm from the nozzle exit with the injection pressure value of 3.5 bars. It is observed that an increase in droplet formation through the spray downstream distances causes an increase in the drag force on droplets, so the distribution curves of droplets' size become more flat and its maximum value decreases and moves to bigger drop sizes. Hence, droplet size distributions become more homogenous. This could be explained by two primary processes. The first is the coalescence of the drops due to collisions. Small drops can merge to create larger droplets. The second reason is the *'selection by drag'* process [172, 181]. Large droplets suffer less braking than the smaller drops and hence there is a tendency to have more of them downstream. There is also a possibility of smaller droplets positioned far away from the nozzle evaporating thus shifting the measured spectrum towards the larger droplets [182]. In Figure 6.10 and Figure 6.11, it is seen that monomodal distributions have been observed and a lot of large-sized drops are present at the outer edges of the sprays. This happens because further downstream of the spray, larger drops experience less drag as the spray is more dilute and thus travels further outward**.** A study of hollow cone nozzles with water as the spraying fluid also observed this trend as the drop distribution was described as having two peaks with one higher than other [1, 172].

126
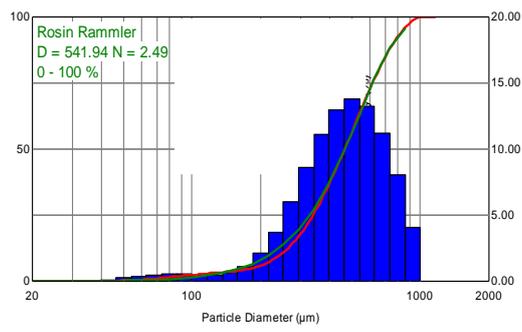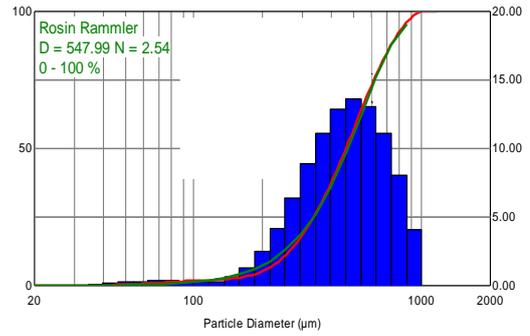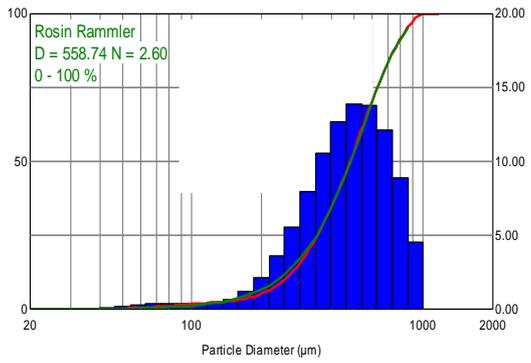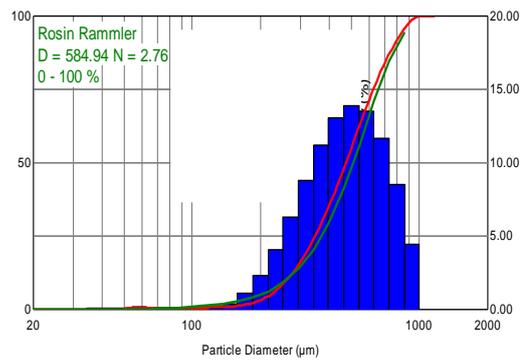
Figure 6.10 Drop size distributions for injection pressure of 3.5 bar at various radial positions and 80 mm axial distance from exit orifice
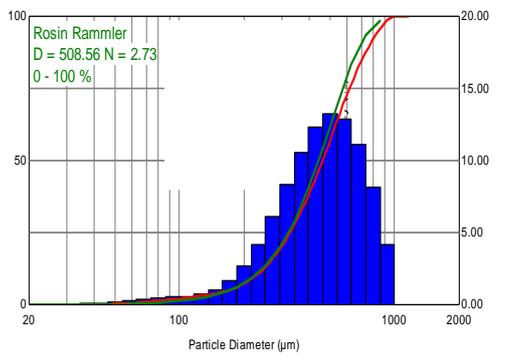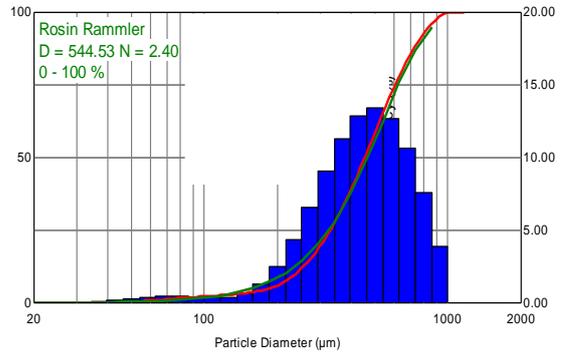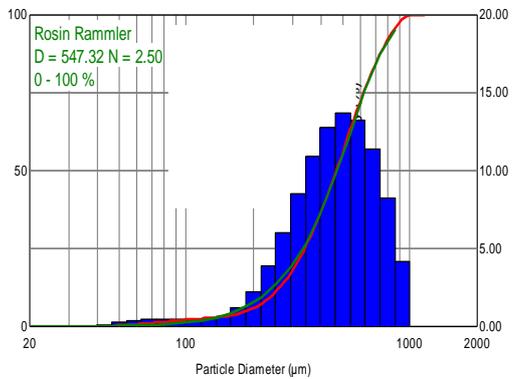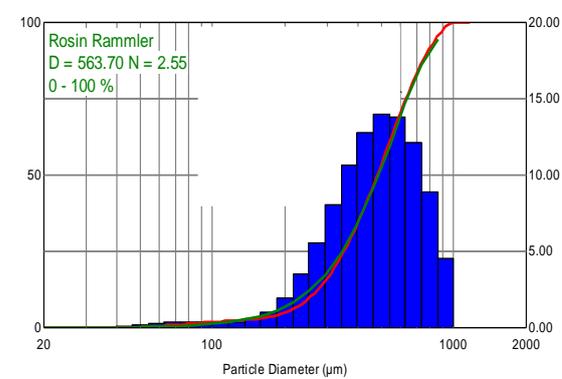


Figure 6.11 Drop size distributions for injection pressure of 3.5 bar at various radial positions and 120 mm axial distance from exit orifice

## 6.6 Liquid film breakup

The liquid film breakup as a function of the pressure differential can be visualized in the short exposure time pictures presented in Figure 6.12. It was observed in all the experiments carried out that a smooth liquid film around a hollow core was formed immediately after the atomizer nozzle exit orifice, ending in a ragged edge, and after that a well-defined hollow-cone spray was established. It can also be noticed from the pictures that the spray angle increases when the pressure differential increases, and the liquid film length is reduced.



|   2bar   |   3bar   |



|   4bar   |   5bar   |
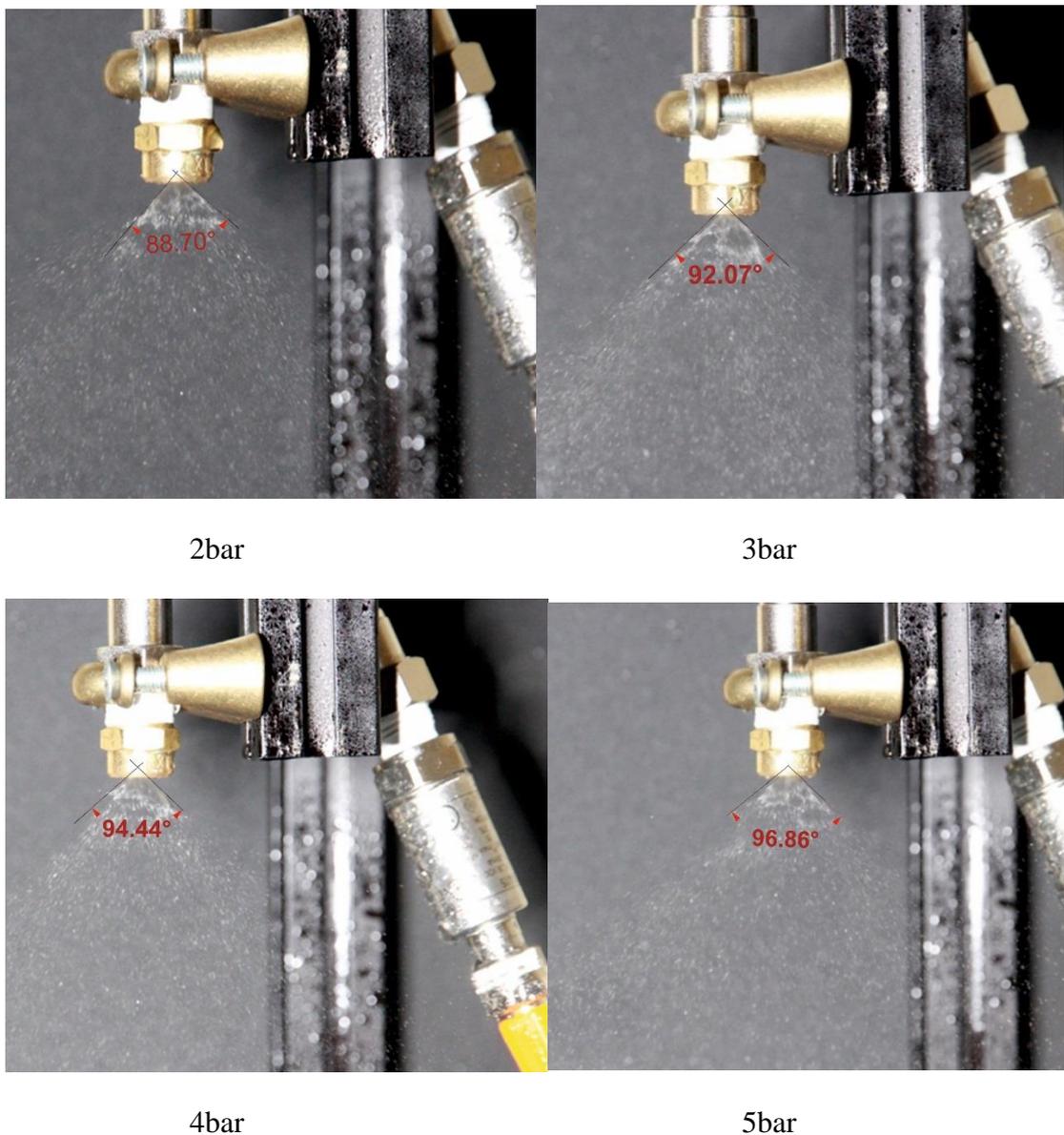
Figure 6.12 Liquid sheet break up images from the fast shutter-camera for different injection pressures

## 6.7 Validation of $\Sigma - Y$ atomisation model

In order to establish the performance of the $\Sigma - Y$ Eulerian atomization model in terms of Sauter Mean Diameter (SMD) predictions, validation is carried out by comparing modelling results to Malvern Spraytec measurements which provided unique SMD data within near dense spray region of the nozzle. To enable the best comparisons of simulated SMD predictions against experiments to be achieved, different turbulence models were first evaluated in order to choose and achieve the best possible match with measurements for the spray droplet Sauter Mean Diameters (SMDs). The RANS turbulence models investigated in the prediction of SMD predictions were the Standard k- ε, RNG k- ε and Realizable k-epsilon turbulence models and this investigation also helps to draw a more accurate conclusion about turbulence model for the $\Sigma - Y$ atomization model. The predicted Sauter Mean Diameter (SMD) of the liquid water at different axial distances along the nozzle and radial positions from the spray centreline and their corresponding data for the same locations and operating conditions from measurements were used for the validation as discussed later.

### 6.7.1 **Effect of variants of k-epsilon turbulence model on the Sauter mean diameter**

Figure 6.13 shows the graph of turbulent intensity decays along the axial position by comparing the standard k-epsilon and RNG k-epsilon turbulence models. It can be observed that the standard k-epsilon model predicted a higher decay in the average turbulent intensity as compared to RNG k-epsilon. Turbulent intensity is defined as the ratio of the root-mean-square turbulent velocity fluctuations to the mean flow velocity ($\acute{u}$/U), and is expressed as a percentage. The turbulent intensity is also related to the turbulent kinetic in the flow as $k = 3(UI)^2/2$ where I is the turbulent intensity. The turbulent kinetic energy and the mean flow velocity can easily be computed from the flow. In comparing the two $k - \varepsilon$ turbulence models, the inlet turbulent intensity was kept constant. In theory, turbulence is affected by swirl in the mean flow. Since the RNG model accounts for this rotational motion appropriately by modifying the turbulent viscosity, larger decay could be counted for and therefore the turbulence in the flow gets uniformly distributed in the swirl chamber and the computational domain as compared to standard $k - \varepsilon$ model. In Figure 6.14, it can be seen that 10% of turbulent intensity is closer to the experimental data points and standard k-epsilon model utilize in this atomization is the best because it tends to produce the smallest SMD and the best match and configurations with the experimental results when compared to the RNG and Realizable K-epsilon turbulence models (Figure 6.15). It can also be observed that the turbulent intensity is higher in the outside spray than the center spread of the nozzle and this in conformity to the observation made by Yoon et al [183]. The reason is that the droplet which decreases momentum in the outside spray makes a great impact by the inflow of surrounding air. The turbulent intensity is getting smaller towards the downstream because the momentum of relative velocity is dramatically fallen and there is less actions of air current for droplet which is related with the highly small amount of air brought by its surroundings. However, there was no significant changes in the droplet velocity when the three turbulent models were compared as shown in Figure 6.16.
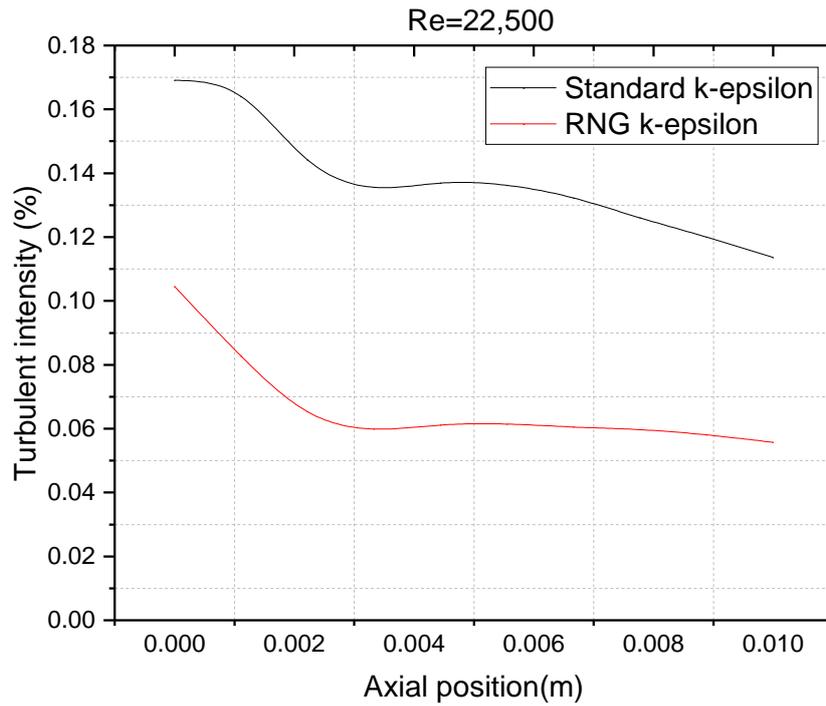
Figure 6.13 Turbulent intensity decays along the axial position by comparing the standard k-epsilon and RNG k-epsilon turbulence models
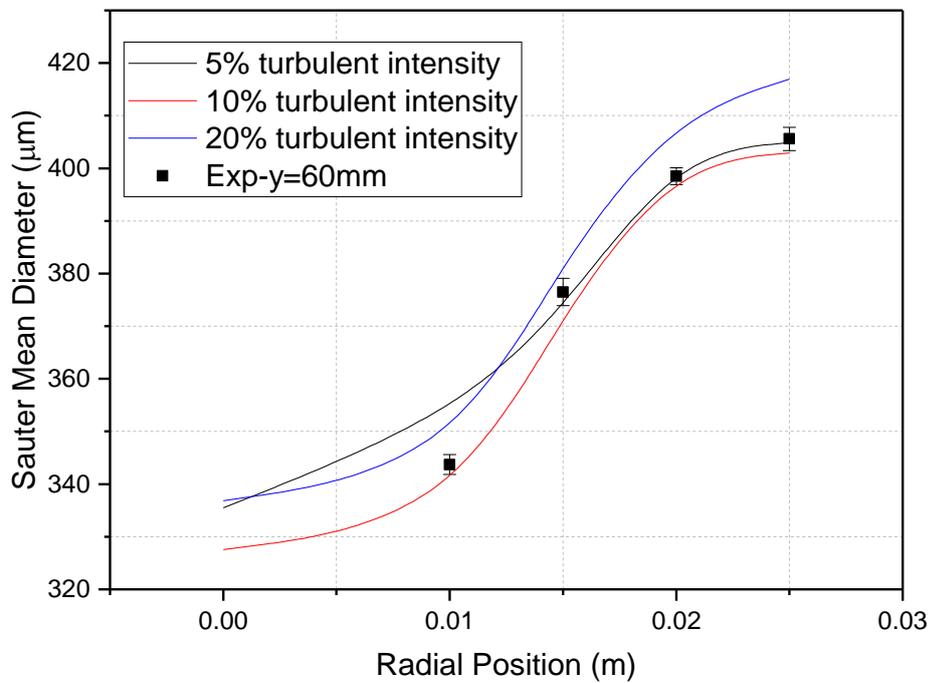


Figure 6.14 Effect of turbulent intensity on the Sauter mean diameter (SMD)

131
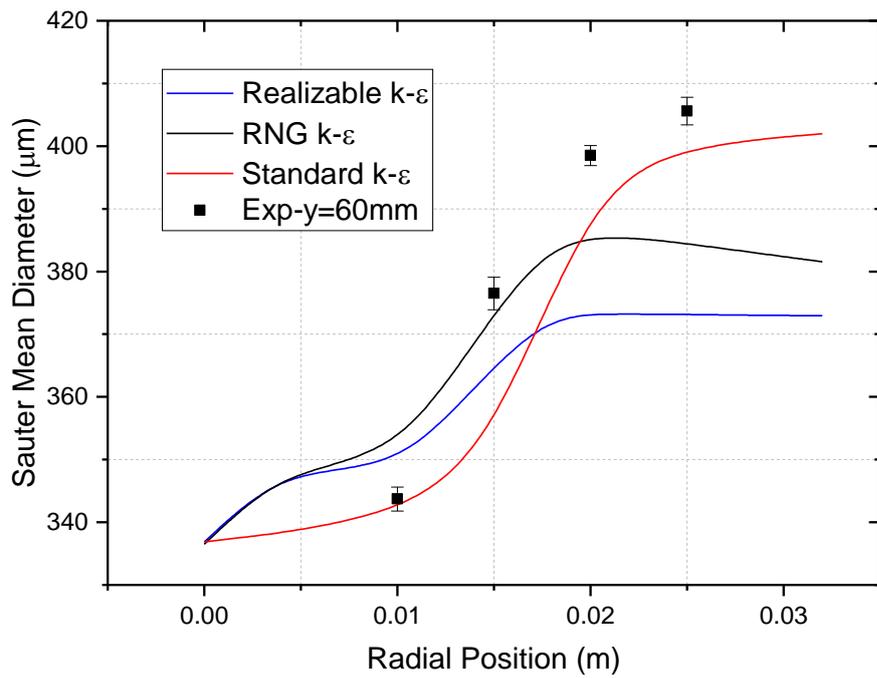
Figure 6.15 Effect of turbulence models on the Sauter mean diameter (SMD) at y=60mm
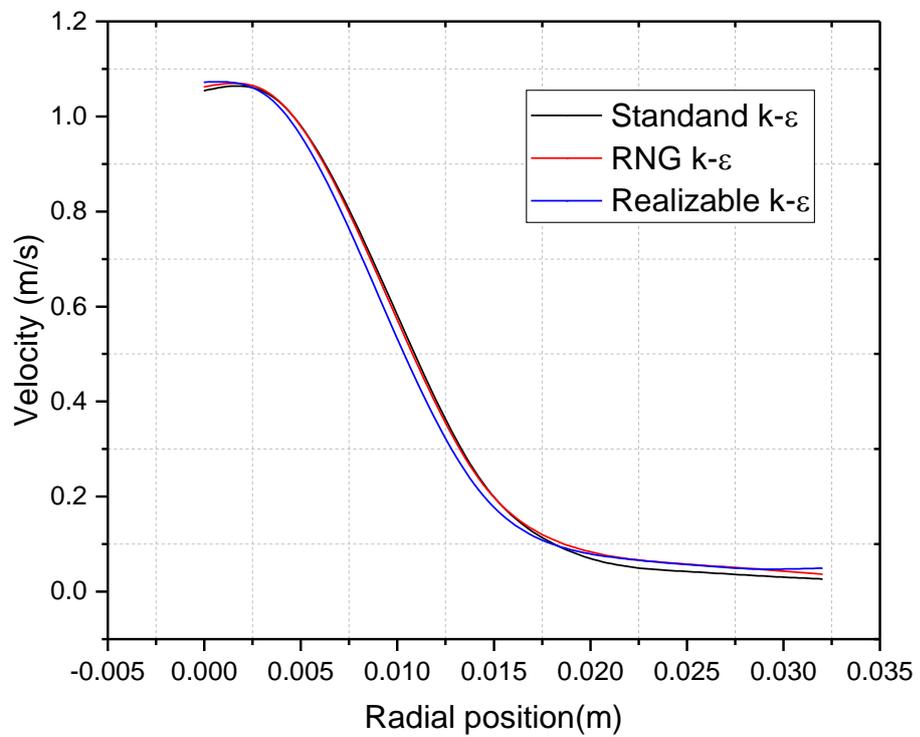


Figure 6.16 Effect of turbulence models on the mean liquid velocity, modelling

### 6.7.2 **Validation of Sauter Mean Diameter (SMD) at radial positions**

Figure 6.17 shows the comparison of the model with measurements for droplet Sauter Mean Diameter (SMD) at y=60, 80, 100 and 120 mm. The agreement between the model and experimental radial profiles at 60 mm downstream of the nozzle is good. The trend shows that the Sauter mean diameter SMD increases with increasing radial distances which is qualitatively correct but the rate of change is small with the mean diameter of the large droplets found on the periphery of the spray under predicted and the small mean drop size at the vicinity of the spray centreline perfectly predicted. At axial position of 80 mm from the exit of the nozzle, the agreement between the $\Sigma - Y_{liq}$ atomisation model and experimental radial droplet mean diameter distributions is satisfactory with good prediction of the droplet size at the spray periphery but higher than the value predicted at position 60 mm axial distance from the nozzle exit. The rate of increase of droplet size with radial distance is correct and the size of the largest droplet at the spray periphery is well predicted. There is also a good agreement between the radial positions at 100 mm downstream of the nozzle for the model and the measurement with the droplet SMD having slight under-prediction of less than an average of 3%. The results at this axial position also shows that most of the predicted SMDs near the inner region of the spray are below the experimental values. In addition, the SMD increases at similar rates with radial distances for both results at this axial position. The radial profiles for the mean droplet sizes (SMDs) between the calculations and the experiments at the axial position 120 mm from the exit of the nozzle are closer with the SMD being small near the centreline of the spray and SMD reasonably predicted. The trend of increasing droplet size with radial distance is observed and agrees with the work of many researchers in predicting the mean drop sizes from a pressure swirl atomizer [7, 15]. The mean drop diameter of the experimental results of the largest droplet at the periphery of the spray is higher than its predicted values. However, the SMD at radial distance near the spray centreline is closely predicted in relation to the measurements. The more uniform and continuously increasing Sauter mean diameter with radial distance may be attributed to the farthest axial distance from which the drop sizes were measured and may also due to the coalescence of smaller droplets and this have been accounted for in the model. The small drop sizes observed around the spray symmetry axis may be attributed to collisions between the liquid droplets and by aerodynamic drag interactions with the entrained air as result of the hollow cone spray pattern emanating from the nozzle [7].

The collisions result in unstable interactions between the drops and in turn lead to breaking down of droplets smaller than their original sizes. This is also supported by the observation made by Yoon et al [183] that the separation of small droplets near the centreline arises due to the competition between turbulent dispersion and entrainment of air by the spray and that droplets that are dispersed by turbulent eddies or fluctuations will move outwards from the inner region, but their outward motion will be opposed by the air entrainment. The air entrainment causes a radially inward velocity in conjunction with the spatial acceleration of the liquid jet. Small droplets will follow the mean gas motion which drives them to the spray centreline. Larger droplets are less affected by the air entrainment and will follow more ballistic trajectories subject to initial velocity vectors arising from the jet breakup process and turbulent dispersion. Further downstream the nozzle, the inward entrainment velocities are reduced to the point where smaller droplets are substantially dispersed from the centre line. Overall, the computational predictions of SMD for $\Sigma - Y_{liq}$ atomisation model shows a very good agreement with most of the experimental measurements in the radial positions when standard k-ε turbulence was used. However, more divergence was observed between the predictions and the experimental measurements when the RNG k-ε turbulence model and Realizable k-ε turbulence model were used in the predictions as shown in Figure 6.18 and Figure 6.19.
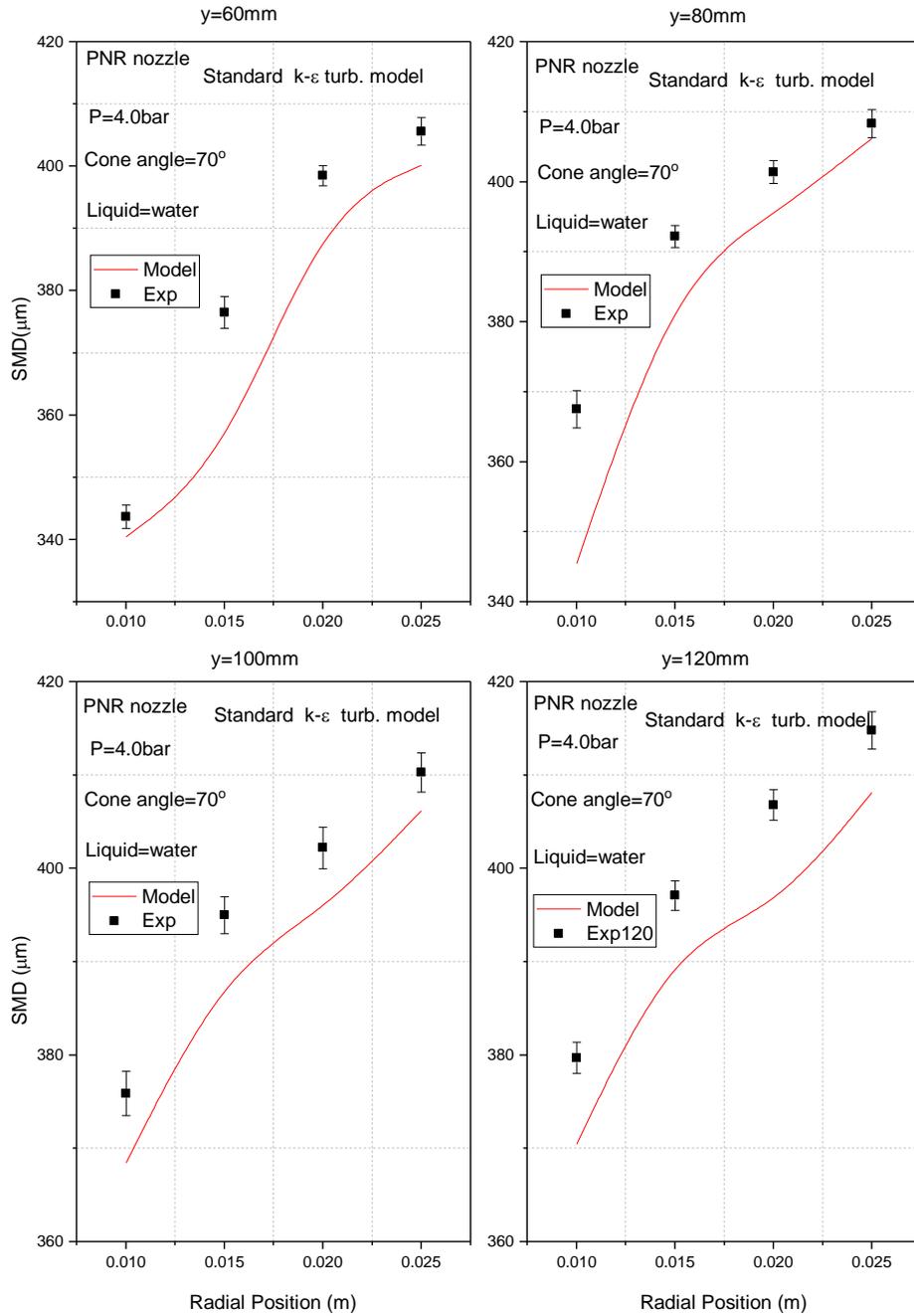
Figure 6.17 Validation of droplet Sauter Mean Diameter (SMD), model with experiment, standard k-ε turbulence model
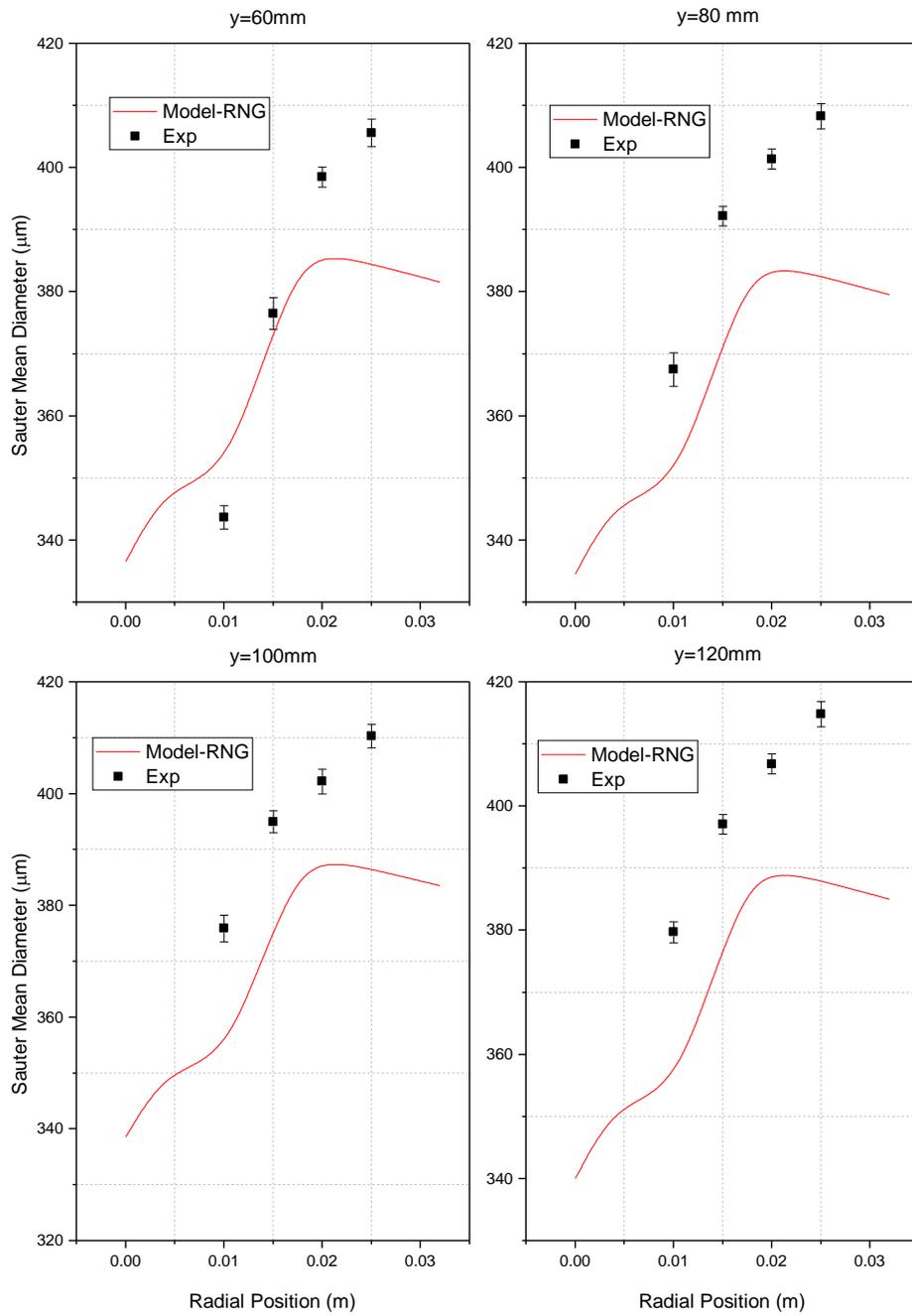
Figure 6.18 Validation of droplet Sauter Mean Diameter (SMD), model with experiment, RNG k-ε turbulence model
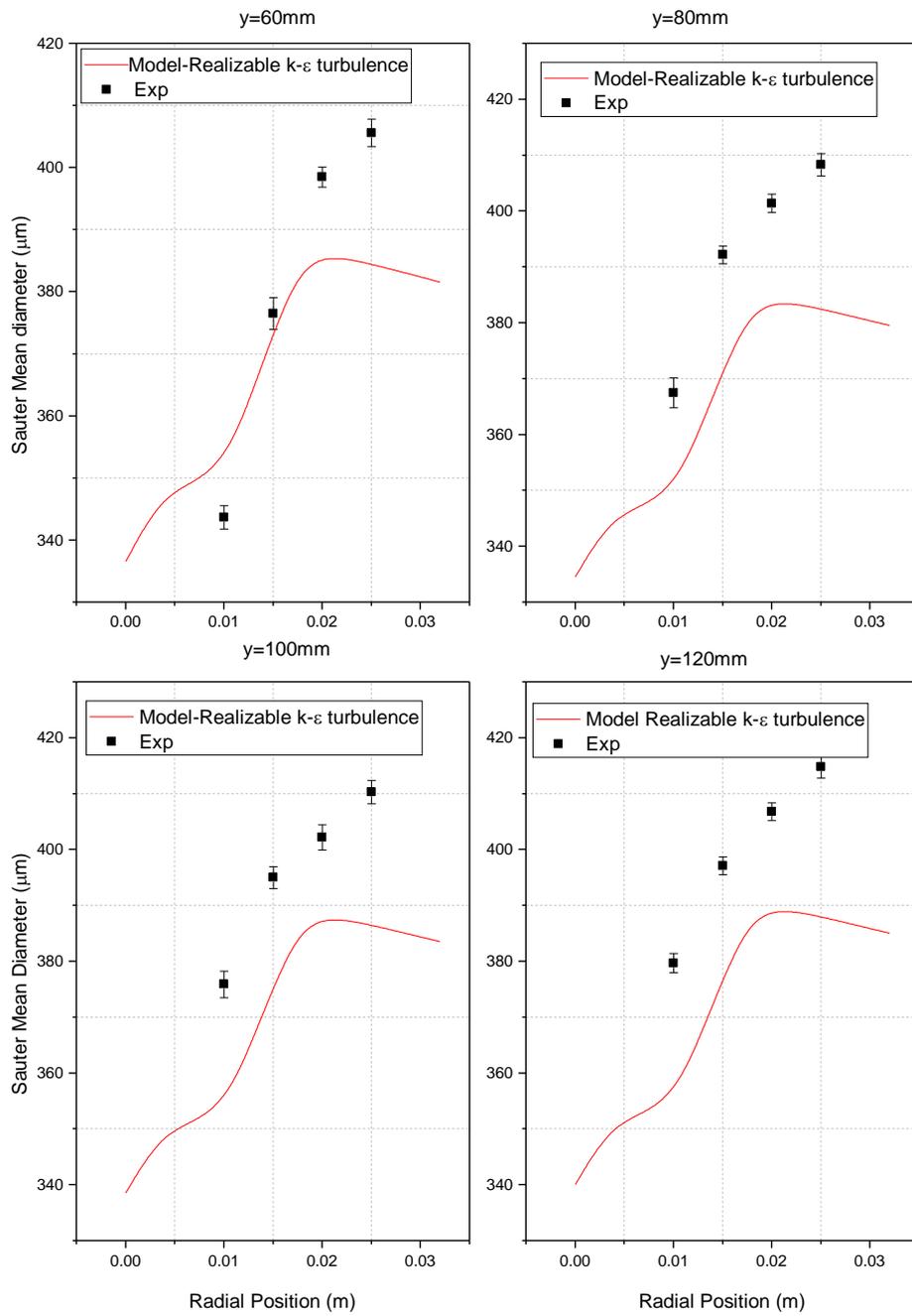
Figure 6.19 Validation of droplet Sauter Mean Diameter (SMD), model with experiment, Realizable k-ε turbulence model

### 6.7.3 Validation of Sauter Mean Diameter (SMD) at spray centre axis

Figure 6.20 illustrates the validation of Sauter mean diameter (SMD) for the model with the experiment results on the spray centreline. It can be observed that the model has good agreement with the measurements with percentage error of less than an average of 5% between the model and the experiements at axial distances 60mm and 120mm and better prediction at axial distances 80mm and 100mm. Figure 6.21 shows more clearly how sensitive SMD is to pressure differentials. This is because as pressure increases faster maximum growth rate of the liquid film occurs and will lead to the linear stability of the surface wave of the thread film getting worse. So the interaction between the liquid phase and the gas phase becomes stronger and the film can break up more easily. This will make the droplet SMD gets smaller.
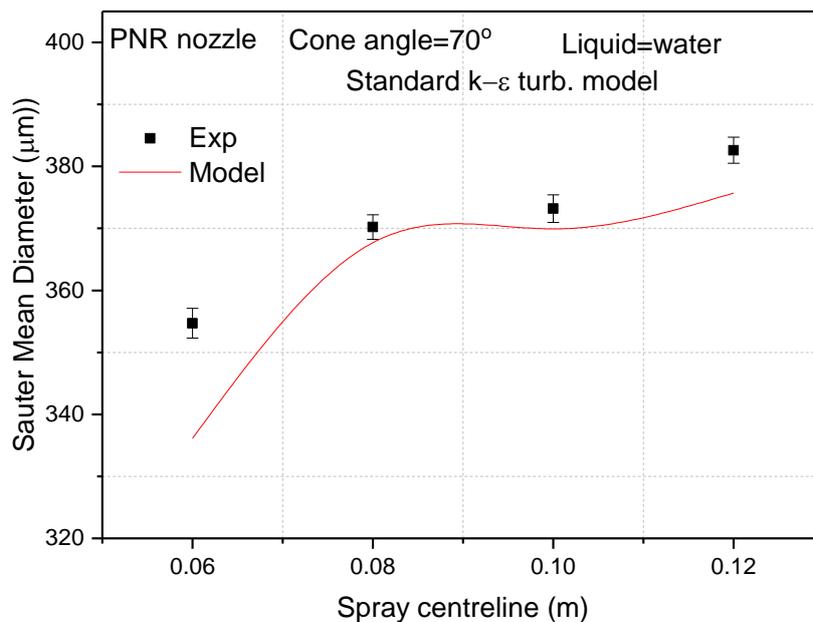


Figure 6.20 Validation of Sauter Mean Diameter (SMD) at spray centre axis, model and experiment
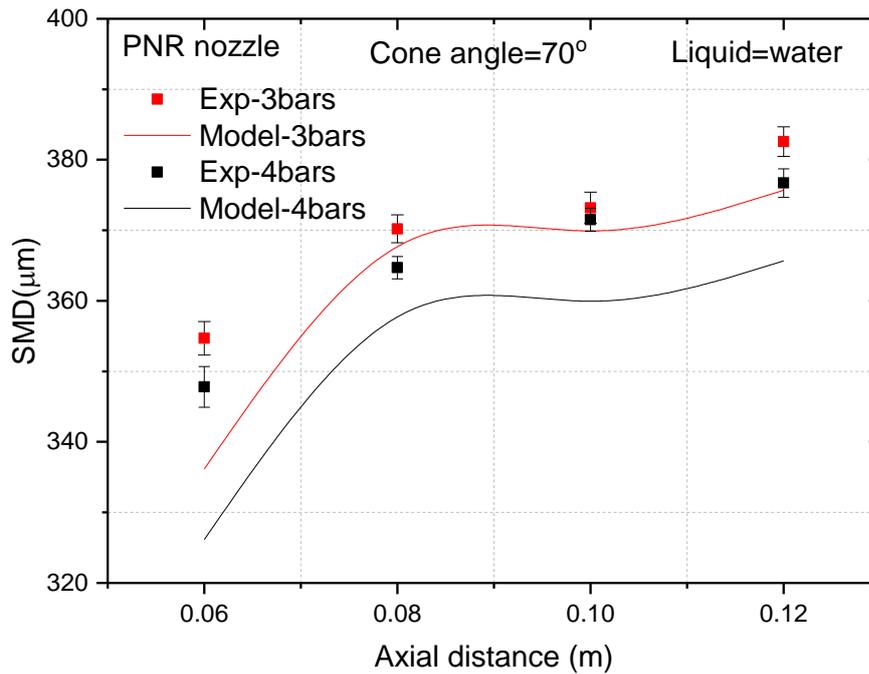
Figure 6.21 Influence of pressure on Sauter Mean Diameter, model and experiment

## 6.8 Summary

This chapter performed the validation of the model and the computational predictions of SMDs for $\Sigma - Y_{liq}$ atomisation model showed a very good agreement with most of the experimental measurements on the radial positions and the spray centreline with the percentage error of less than 5%. The results also showed that the standard k-epsilon turbulence model utilized in this model was the best model when compared to the RNG and Realizable K-epsilon turbulence models since it tends to produce the best match with the experimental results.

# CHAPTER 7 PARAMETRIC STUDY AND CFD-BASED DESIGN OPTIMIZATION

## 7.1 Introduction

These parametric studies investigate the dependence of the Sauter Mean Diameter (SMD) under various operating conditions, fluid properties and geometrical dimensions. The parameters varied are pressure, liquid and gas velocities, liquid and gas densities, liquid viscosity, surface tension and the geometrical orifice size of the nozzle and their effects on the SMD at axial positions along the spray and radial distances from the spray centre line of the pressure swirl atomizer.

The objective of the CFD-based design optimization is to obtain the nozzle exit orifice parameters, operating conditions and fluid properties that perform or give the most minimum droplet (SMD) at axial distances along the spray centerline. The design variables (DVs) used are liquid viscosity ($DV_1$) 0.00031 to 0.2 Pa.s, surface tension ($DV_2$) 0.02 to 0.075 mN/m, nozzle exit orifice diameter ($DV_3$) 0.0015 to 0.0035 m and liquid velocity ($DV_4$) from 1 to 6 m/s. The design cases were generated using a statistical Design of Experiments (DoE) technique known as Latin Hypercube Designs (LHD) using Matlab.

In order to establish relationship between design of experiments (DoE) variables such as liquid viscosity $\mu_l$, surface tension $\sigma$, liquid velocity $v$, and nozzle exit diameter $D_o$ and the resulting droplet SMD, and obtain a usable SMD correlation for the model, surface fitting of the data was carried out. The result was compared to two existing SMD correlations such as Jasuja [63] and Radcliffe [62] based on four design variables considered in their correlations.

To further analyse the new SMD correlation for the model, 3D surface plots of SMD against various combinations of liquid properties and operating conditions with hold values for the existing and the new SMD correlations were shown using meshgrid surface plot code in Matlab. The kinematic viscosity ranges from 1 mm$^2$/s to 1000 mm$^2$/s and the continuous variables for surface tension is between 20 mNm$^{-1}$ and 75 mNm$^{-1}$ to cover wide range of liquids properties. The pressure values are generated between 0.5 and 10 bars based on the operating conditions of pressure swirl nozzles indicated by PNR Ltd in the user manual. The minimum and maximum values for mass flow rate are 0.0017 kg/s and 0.1667 kg/s respectively and were taken from the user manual for nozzles by PNR Ltd at constant pressure of 3 bars

## 7.2 Dependency of Sauter mean diameter on radial distances

The Sauter Mean Diameter (SMD) of the liquid mass fraction predicted at the radial locations in the spray (i.e. between, x = 0 and 32 mm) is presented in Figure 7.1 and the corresponding interfacial surface density at the same positions is shown in Figure 7.2. The axial distance was taken at 60mm, 80mm, 100mm and 120mm below the nozzle exit. These were used to compute the SMD shown in Figure 7.3. It can be seen from the results that the SMD is smaller in the centre spread of the spray and increases with increasing radial distances which is consistent with the observation made by Milan[7, 42]. However, there is a critical value of SMD where the rate of increase changes. The relatively larger mean drop sizes were observed at increasing radial distances because larger droplets tend to travel farther due to their greater momentum. A change of droplet sizes in the radial direction as seen in all locations were due to different dynamic behaviour of small and large liquid droplet sizes. Large Sauter mean diameters (SMD) are dispersed by the spray initial cone angle and subsequent interactions with smaller droplets by coalescence and also with turbulent eddies in the entrained air. The smaller SMD's are generally increasingly swept toward the spray centre line by aerodynamic drag interactions with the entrained air[7]. The result clearly demonstrates that the farther the distance from the exit of the nozzle the larger the SMD on the spray centre line although the relative span is small.
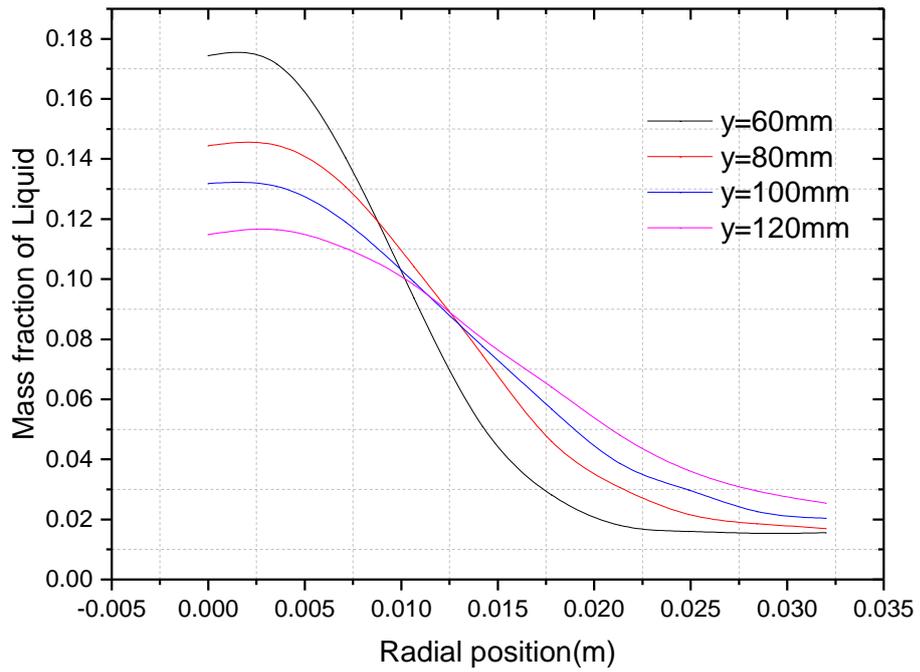
Figure 7.1 Radial profiles of the mean liquid mass fraction, predicted
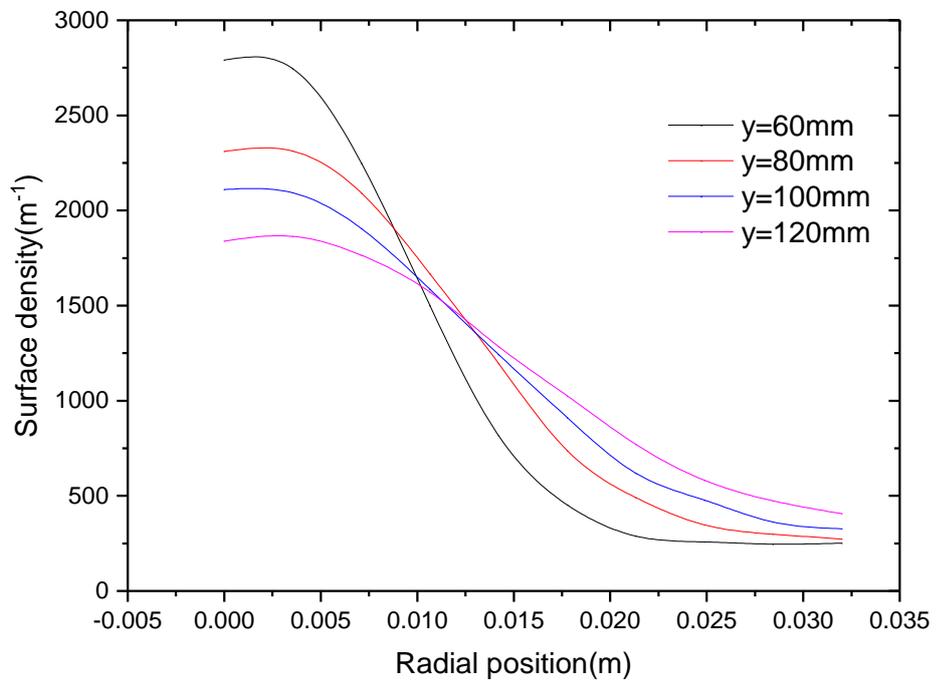


Figure 7.2 Radial profiles of the mean liquid surface density at various axial positions
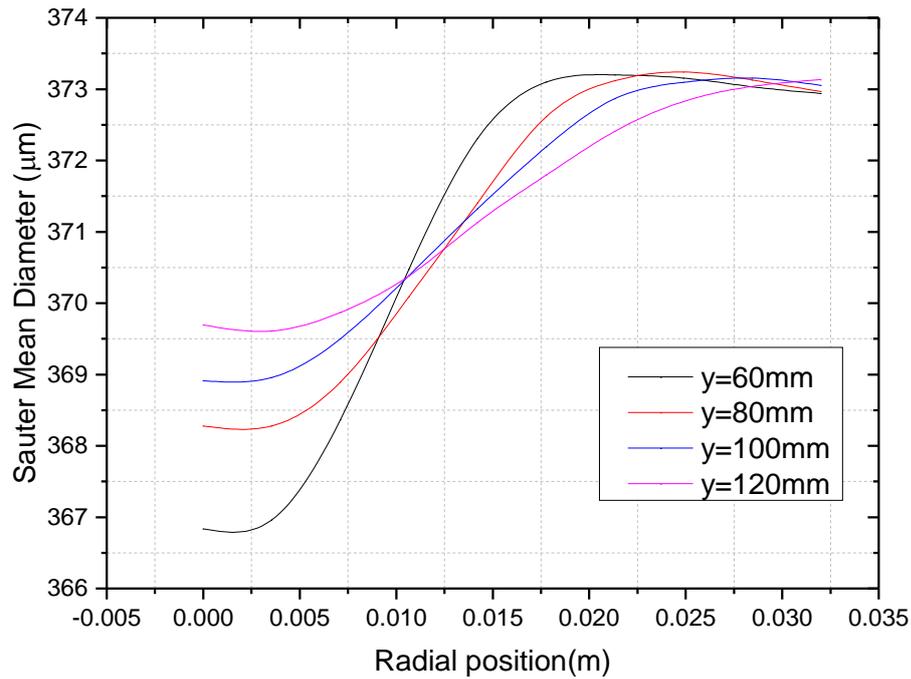
Figure 7.3 Predicted Sauter mean diameter (SMD) at various axial positions

## 7.3 Dependency of Sauter mean diameter on symmetric axis and pressure

The influence of pressure on the SMD at various axial positions was presented in Figure 7.4. The two injection pressure values were 3 and 4 bars and the SMD was analysed at these two values on the symmetry axis. It is very important to understand how the SMD emanating from pressure-swirl atomizer performs or behaves at different axial distances since this inter alia is critical in combustion applications especially in the internal combustion engines where space is limited and the atomizer needs to perform well at very short distances. The results show that the SMD decreases with increasing pressure but increases with axial distances. This has been explained that higher injection pressure leads to higher velocity of the liquid sheet and thus causes decreases in the droplet size[14] as shown in Figure 7.5. It can also be observed clearly on the radial profile of Sauter mean diameter on radial positions at y= 60 and 80 mm for two injection pressures shown in Figure 7.6 that the higher the pressure the smaller the Sauter mean diameter (SMD) and produces larger droplet velocity as shown in Figure 7.5. This result is consistent with Maly [42] where for 5, 10 and 15 bars the SMDs of 54.1µm, 46.1µm and 41.6µm were obtained respectively. The influence of

pressure differentials on the Sauter mean diameter at y = 50, 60, 70 and 80mm has also been presented in Figure 7.7. This result shows that the pressure differential increases with decreasing mean droplet size SMD. However, the SMD decreases sharply at the critical pressure value of 0.35bars.
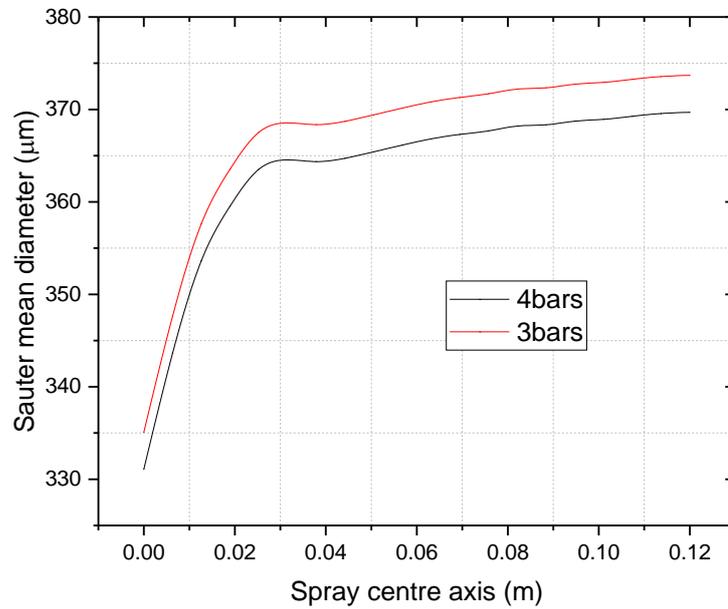


Figure 7.4 Dependency of Sauter mean diameter on pressure at spray symmetric axis
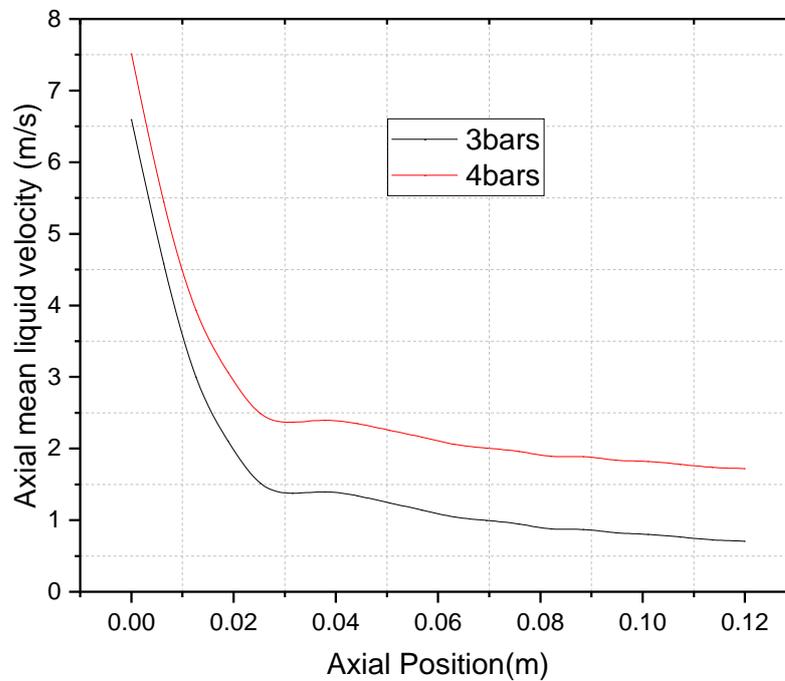


Figure 7.5 Axial profile of the axial mean liquid velocity for two injection pressure values
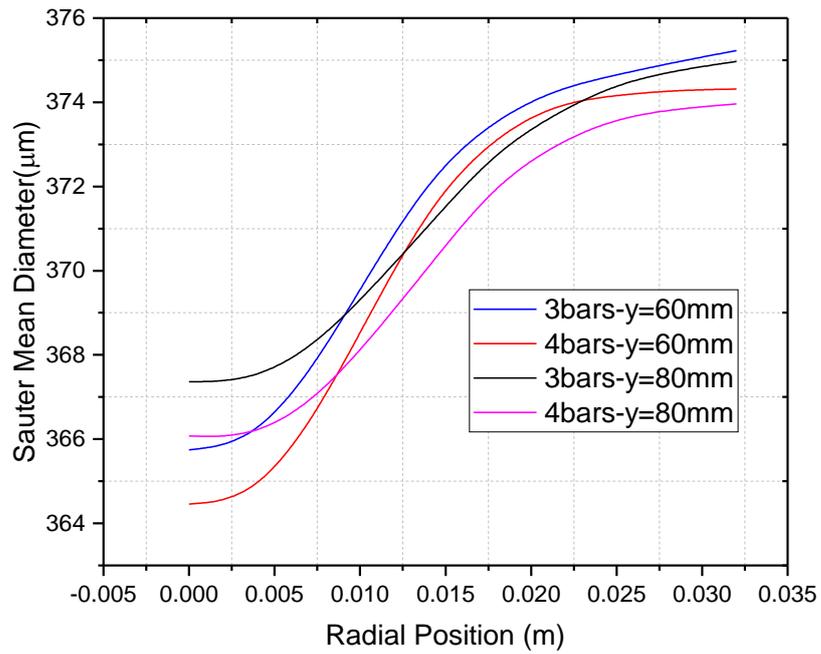
Figure 7.6 Dependency of Sauter mean diameter on radial positions at y= 60 and 80 mm for two injection pressures
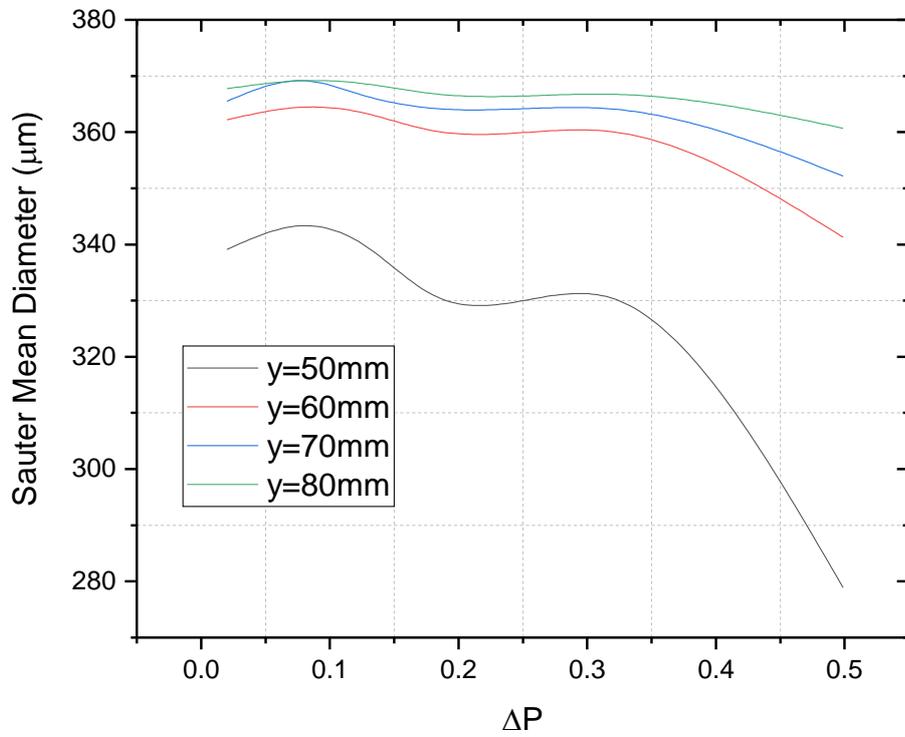


Figure 7.7 Influence of pressure on Sauter mean diameter SMD at y=50, 60, 70 and 80 mm

## 7.4 Dependency of Sauter mean diameter on liquid velocity

Figure 7.8 shows the effect of liquid velocity on the Sauter mean diameter on the spray centre axis. The liquid velocity values used are 1, 2, 4 and 6 m/s and are evaluated on the downward distance from the nozzle. The results show that the increase in liquid velocity leads to the increase in the droplet Sauter mean diameter (SMD). This is because when liquid velocity increases the total free surface energy increases making droplet coalescence into bigger droplet.
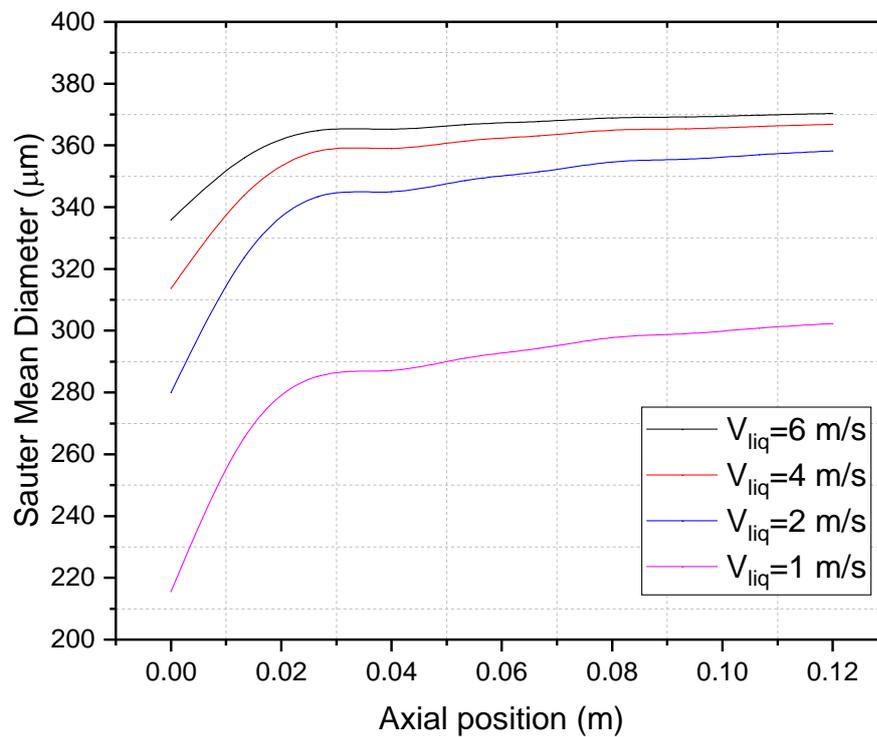


Figure 7.8 Dependency of Sauter mean diameter on liquid velocity at $V_g$ = 1.5 m/s

### 7.5 Dependency of sauter mean diameter on the gas velocity

Gas velocity was varied from 1 m/s to 5m/s with an increment of 1m/s as shown in Figure 7.9. The SMD was calculated on the spray centre axis with the axial distance interval of 20 mm to 120mm away from the nozzle exit. Plotting the predicted SMD values against the variations of axial positions for the various velocities show that the droplet SMD decreases with increasing gas velocities. This is because when gas velocity increases the total turbulent kinetic energy increases making droplet breakup into smaller droplets.
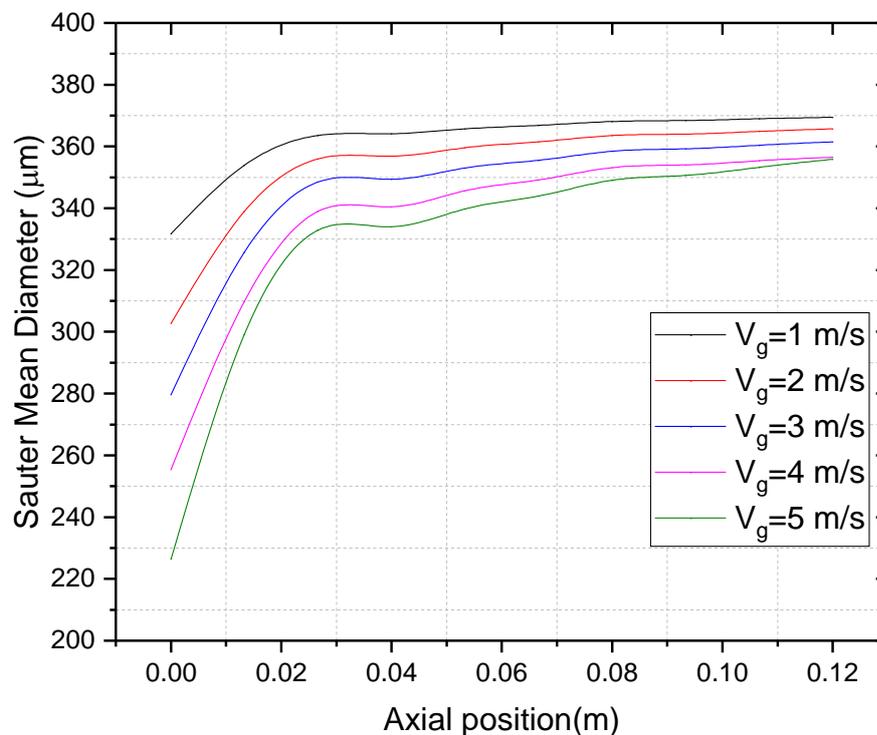


Figure 7.9 Dependency of Sauter mean diameter on the gas velocity at $V_{liq}$ = 5m/s

### 7.6 Dependency of Sauter mean diameter on the liquid density

Figure 7.10 shows the results of simulations for the dependency of Sauter mean diameter (SMD) on the liquid density. The density of liquid was varied from the range of 1000 to 50 kg/m$^3$ with the intermediate values of 600, 300, 150 and 100 kg/m$^3$. The simulations were run for each value and the results of the SMD were evaluated on the spray symmetry axis at different positions of 50, 60, 70, 80, 90 and 100 mm downstream the nozzle exit orifice shown in Figure 7.10. The general profile of the

results shows that for a particular position on the spray axis the SMD is lower for smaller liquid density value and increases with higher liquid density values as shown in Figure 7.11. Additionally, at y=50mm and $\rho_{liq}$= 1000 kg/m$^3$ the SMD is 47.08µm and for the same liquid density and at y=60mm the SMD is 184.90µm higher than the previous position. This clearly can be observed for the remaining cases and thus for the same liquid density value the SMD increases with increasing downstream distance below the tip of the nozzle exit on the symmetry axis.
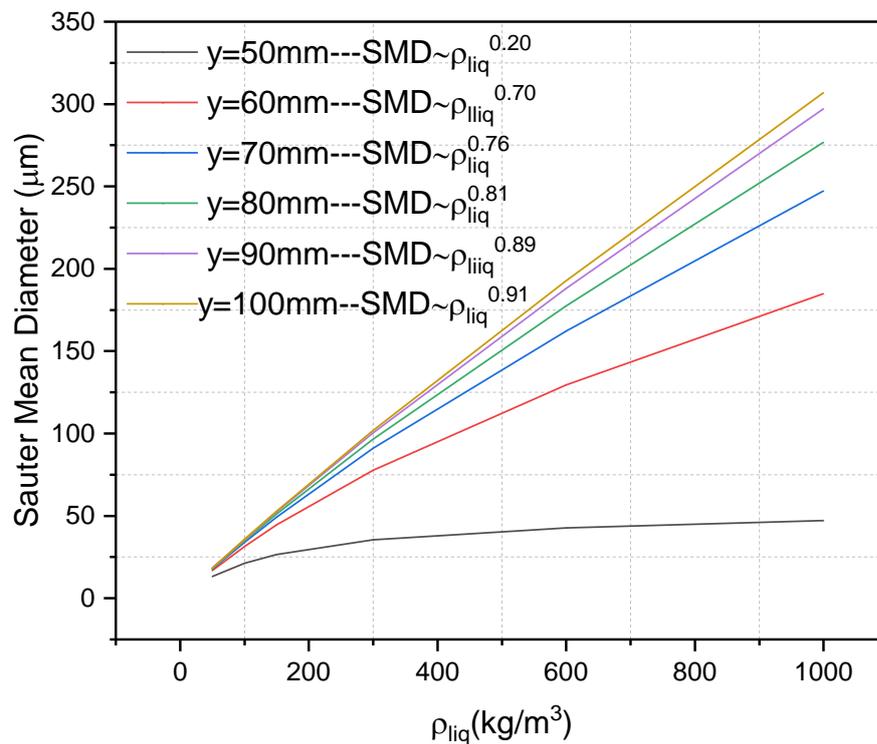


Figure 7.10 Dependency of Sauter mean diameter on the liquid density

When the log-log scale was analysed for the SMD and the liquid density in order to establish a correlation between these two quantities with other variables remaining constant, a line with a slope of 0.20 fits very well with the results at y =50mm. Maximum dependency of 0.91 ($SMD = \rho_{liq}{}^{0.91}$) was found for the result at y = 100 mm. The observed exponents are good agreement and within the range of correlations established by Lefebvre et al [7]. Another observation was that for various liquid density values the liquid core lengths are different thus for higher liquid density the length is longer and the vice versa. In order to show these, the contours of the average

density of the liquid and air superimposed with streamlines were plotted for the near and far fields for the liquid density at 1000, 600 and 300kg/m$^3$ shown in Figure 7.12.
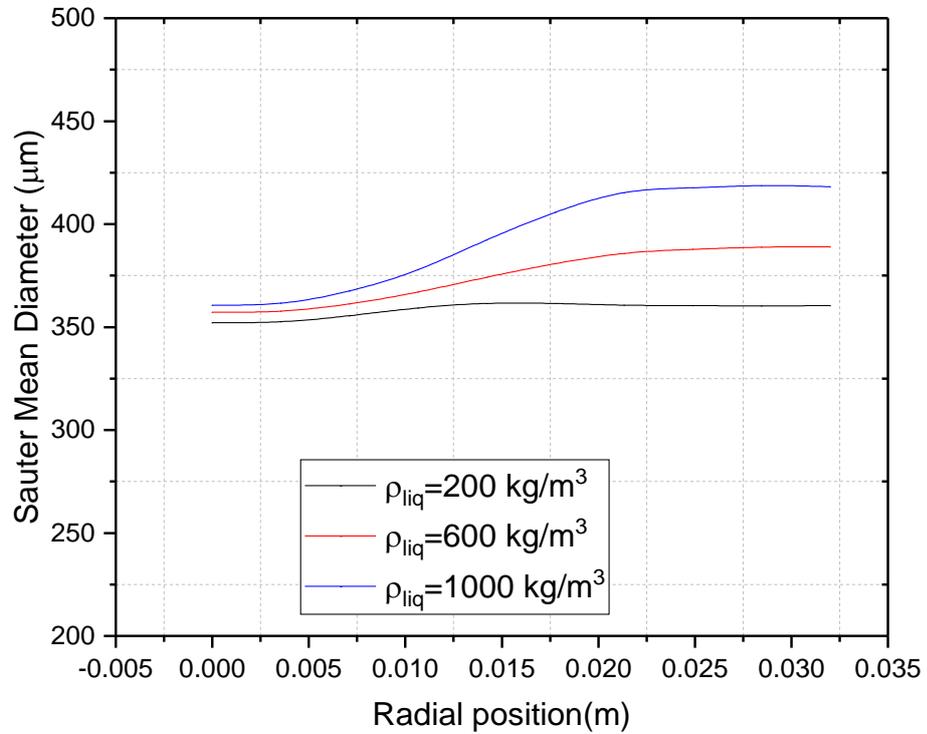


Figure 7.11 Radial profile of Sauter mean diameter(SMD) of liquid density at 200, 600 and 1000 kg/m$^3$
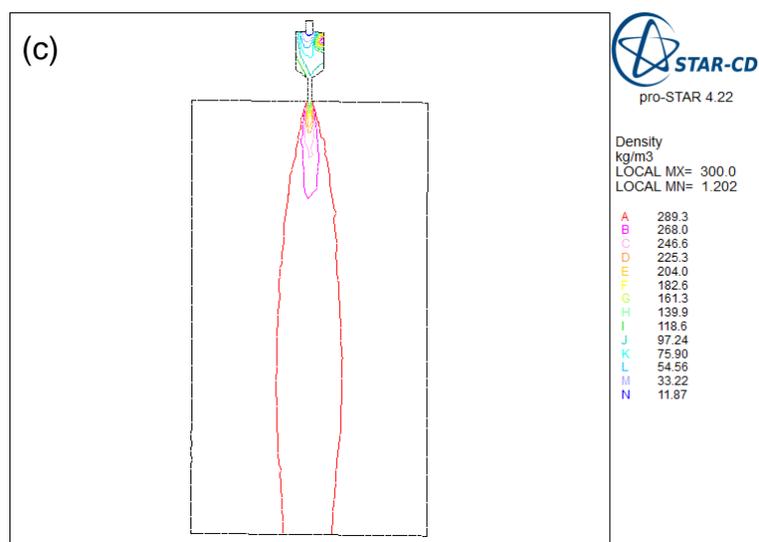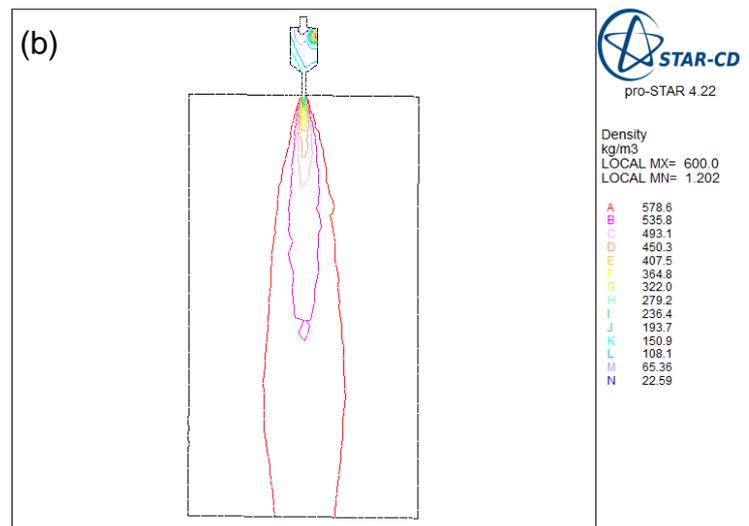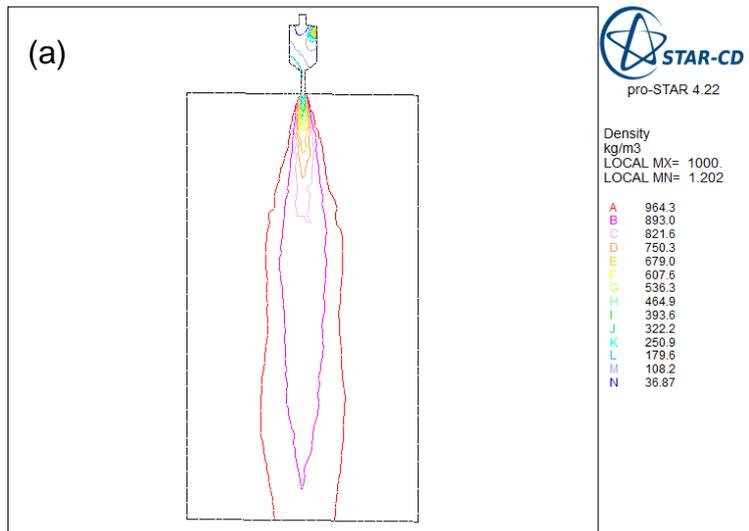
Figure 7.12 Contour plots of liquid densities of (a)1000 (b)600 (c) 300 kg/m$^3$ super-imposed with streamlines

### 7.7 Dependency of Sauter mean diameter on gas density

One of the important air properties influencing atomization is its density and as such the effect of the gas density on the SMD for the model was analysed as shown in Fig Figure 7.13. The gas density was varied from 0.6 kg/m$^3$ to the original value of 1.2 kg/m$^3$ and then to the highest value of 10 kg/m$^3$ in order to analyse the SMDs before and after the value of 1.2 kg/m$^3$. The air density values between these limits were 2, 4, 6 and 8 kg/m$^3$. The analysis was done at the axial positions on the spray centre at 50, 60, 70, 80, 90 and 100 mm downstream the nozzle. As can be seen from the figure, the dependency of SMD on the gas density increases with the droplet Sauter Mean Diameter. This is also in line with the observation made by Beheshti [40] and Lefebvre [1]. It can also be deduced from the graph that the SMD values increase with increasing axial distance on the spray symmetry axis and this is also in conformity to the observation made by Beheshti[40] in assessing this same atomization model. The variation of the gas density also has effect on the liquid core length as shown in Figure 7.14 and can be observed that the liquid core lengths decrease with increasing gas density.
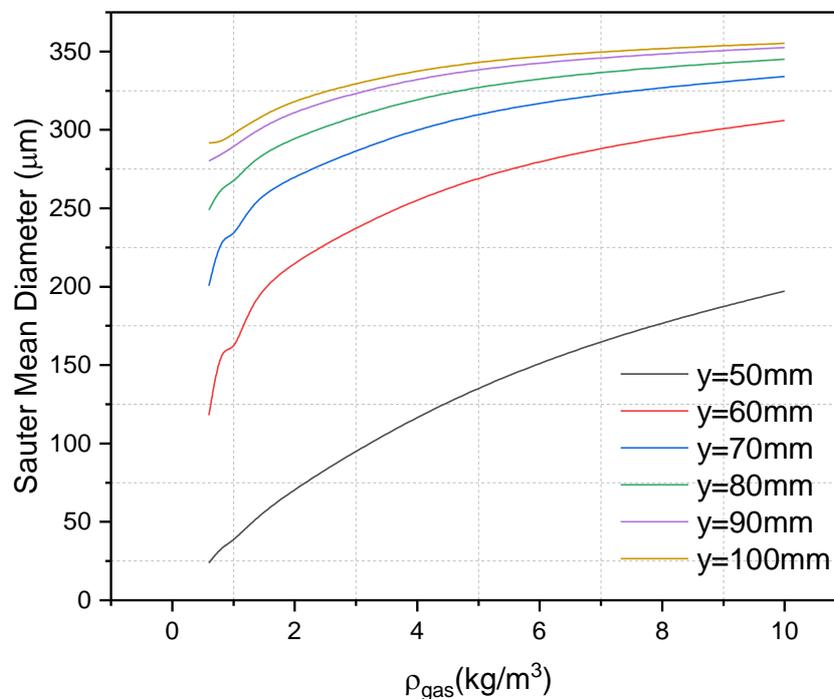


Figure 7.13 Dependency of Sauter mean diameter on gas density at different axial positions
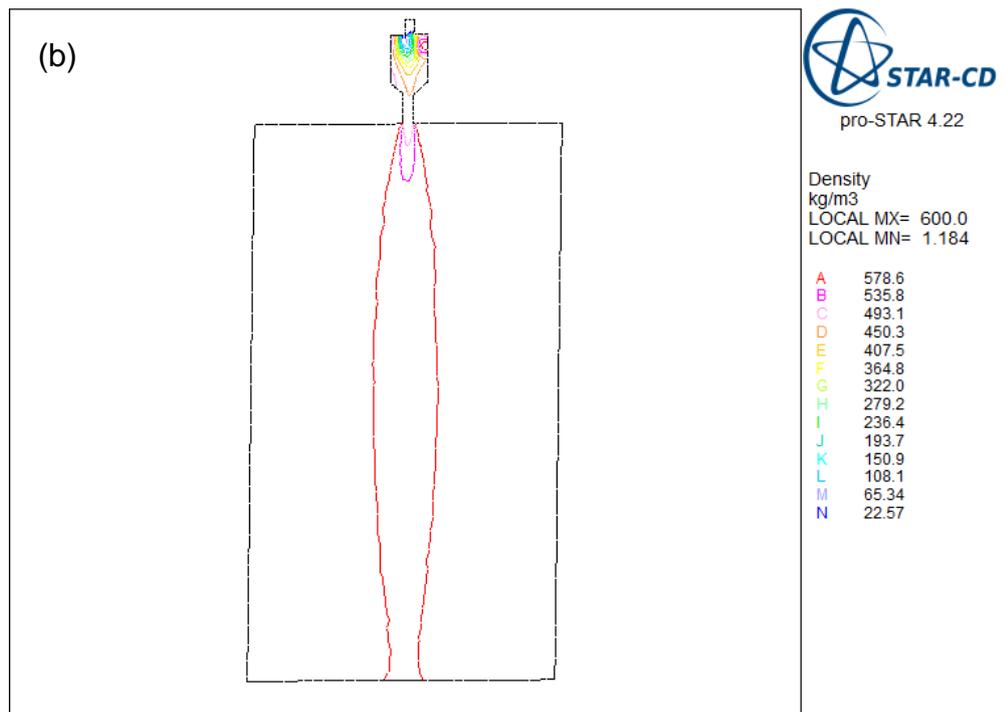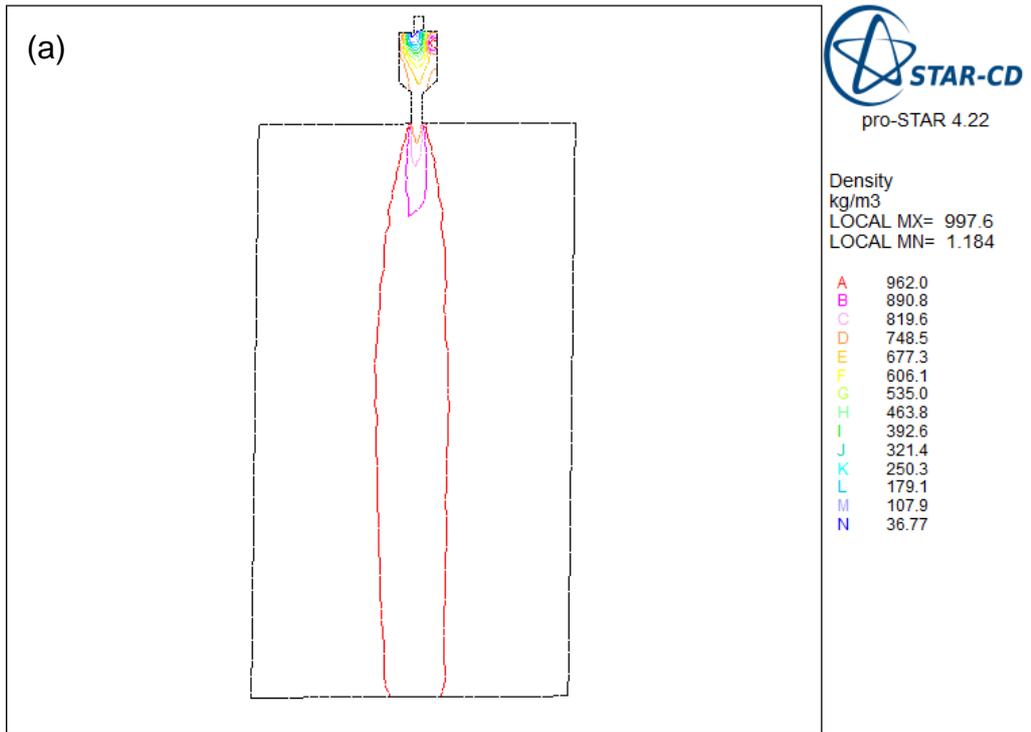
Figure 7.14 Influence of gas densities of (a) 1.2 (b) 2 kg/m$^3$ on the liquid core length

## 7.8 Dependency of Sauter mean diameter on the liquid viscosity

Figure 7.15 shows the variation of Sauter mean diameter (SMD) in relation to liquid viscosity on the axial positions. Three liquid viscosities of 0.001 Pa.s, 0.005 Pa.s and 0.009 Pa.s were selected and analysed beyond 50mm downstream of the nozzle. The results confirm the adverse effect of an increase in liquid viscosity on atomization quality in particular on the SMD and thus increase it. This also agrees with the observation made by Lefebvre[1] that an increase in the liquid viscosity will usually increase the Sauter Mean Diameter of the drops. The influence of liquid viscosities of water at various temperatures is shown more directly on Figure 7.16 which illustrates the dependency of SMD on the liquid viscosity and at the radial positions for pressure swirl nozzle. It can clearly be seen that at the temperature of 90 $^{\circ}$C for water its viscosity is smaller than its corresponding viscosity at the temperature of 20 $^{\circ}$C. This invariably affects the SMD and thus decreases the SMD at high temperatures for liquid water. When various percentages of glycerol were added to liquid water the viscosity also changes and shown in Figure 7.17. When this is plotted against the flow energy, the results show that viscosity with a higher percentage of glycerol increase the SMD at most flow energies. This result is also in agreement with the observation made by Eggers and Villermaux who, however, indicated that the increase in the SMD is more significant by adding viscoelasticity. In addition, all fluids produce finer droplets with higher flow energy. This is due to the high relative ambient gas speed which produces finer droplets [184].
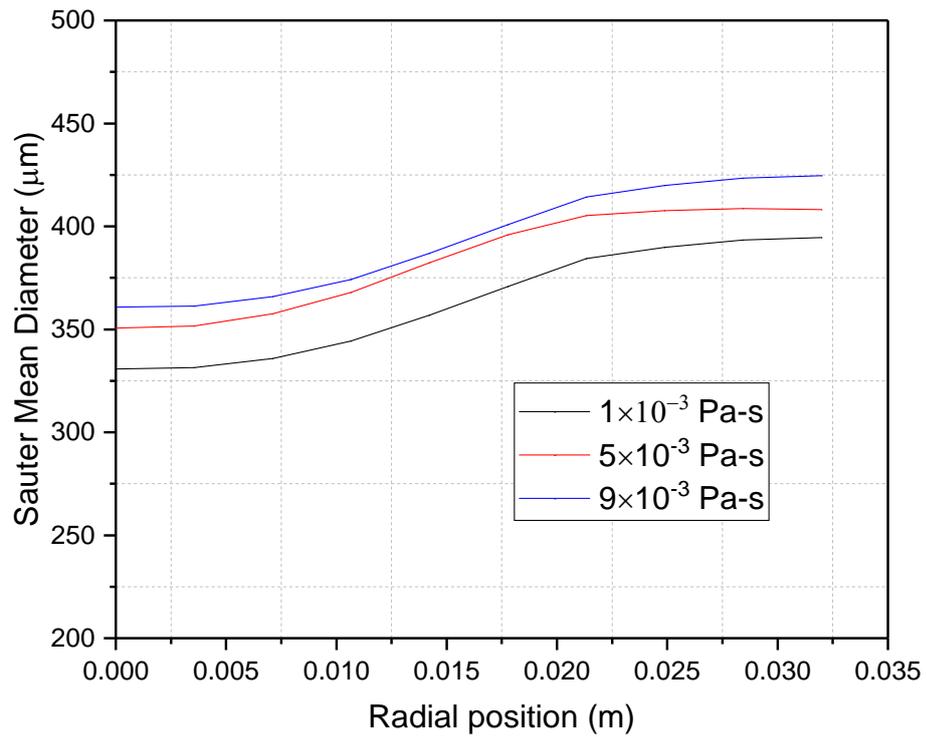
Figure 7.15 Radial profile of Sauter mean diameter at various liquid viscosities
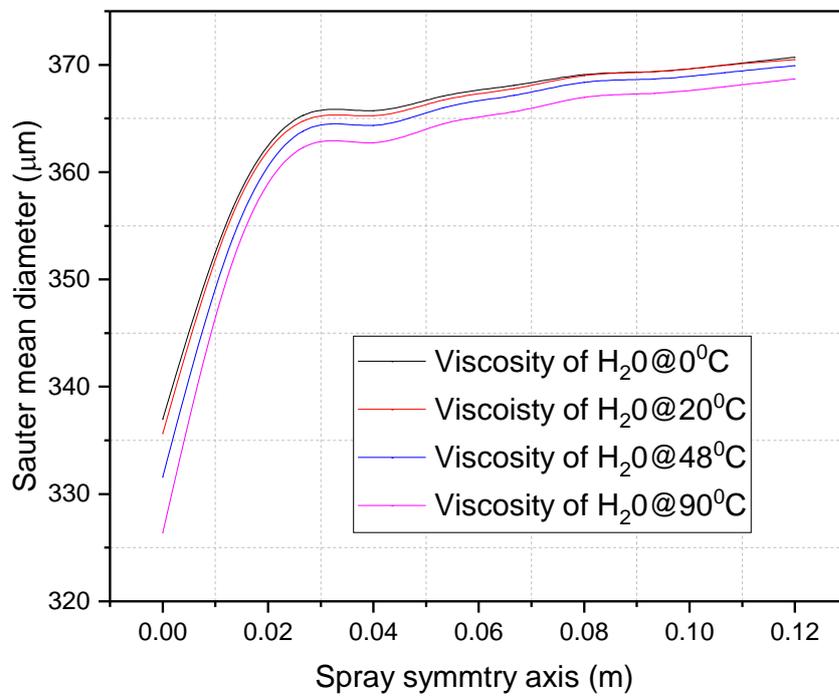


Figure 7.16 Variation of Sauter mean diameter (SMD) in relation to liquid viscosity on spray centre line
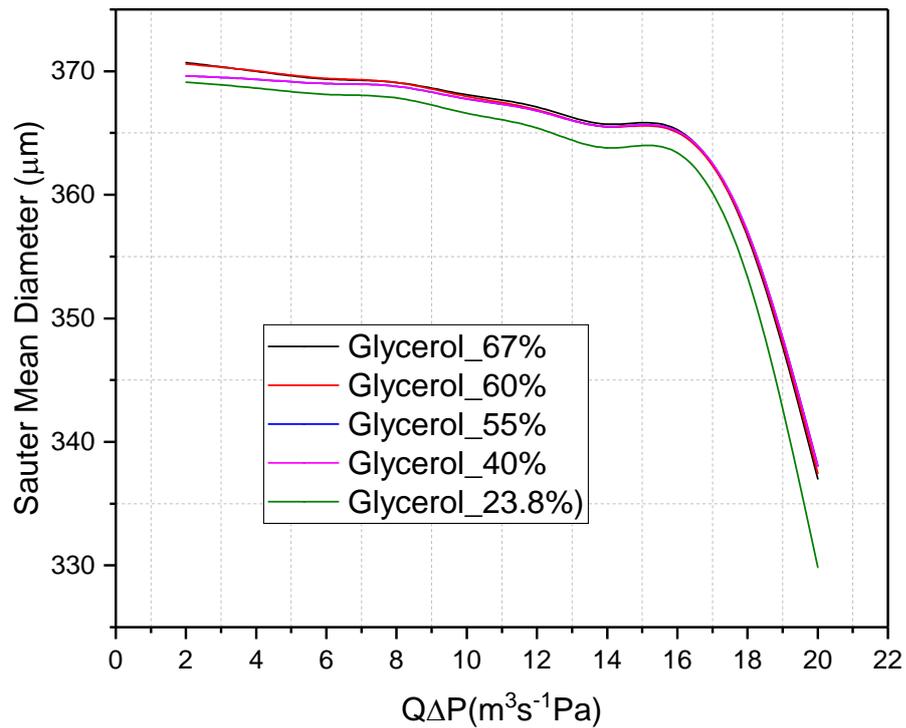
Figure 7.17 Drop size (SMD) for the fluids listed in the legend at flow energy

## 7.9 Dependency of Sauter mean diameter (SMD) on the surface tension

The effect of two surface tension forces on the Sauter mean diameter (SMD) is shown in Figure 7.18. The results show that higher surface tension values lead to larger value of the SMD. The surface tension coefficient shows up in the destruction term of the transport equation for the mean interfacial surface density. Therefore, the reduction of the surface tension force will cause destruction reduction in the mean liquid and gas interface density and as a result reduce the Sauter mean diameter (SMD) of the droplets. This result is also in agreement with the findings obtained by Belhadef et al [14] in assessing this model that the Sauter mean diameter is lower with a weaker surface tension. And this also agrees with the conclusions drawn by Lefebvre [7] that the higher SMD values exhibited by water compared to most liquids are due entirely to the higher surface tension of water.
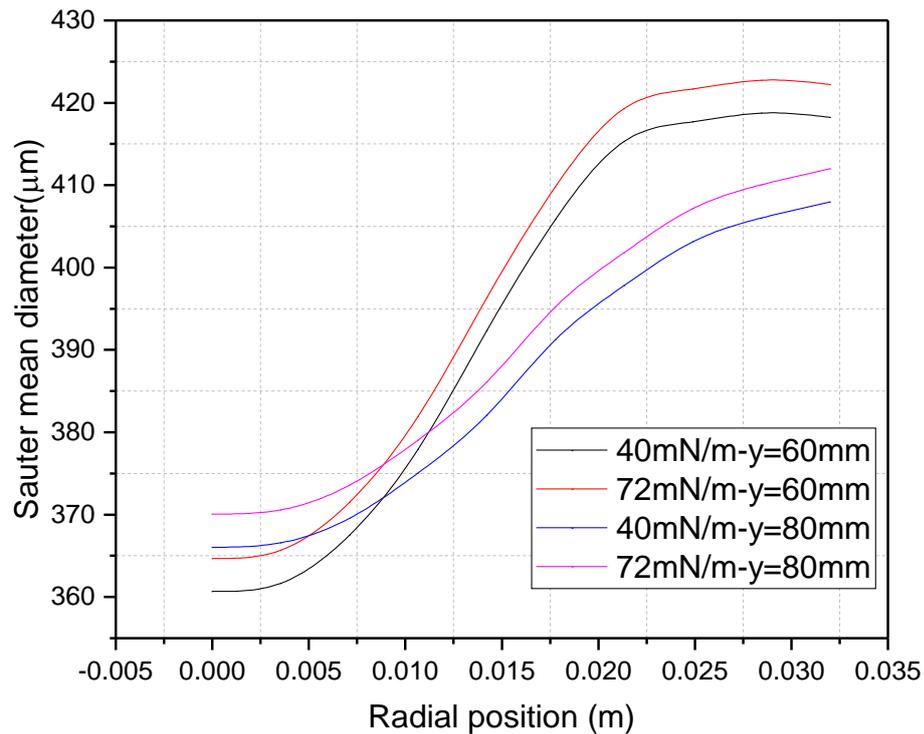
Figure 7.18 Radial profiles of Sauter mean diameter (SMD) for two surface tension values at y = 60 mm and y = 80 mm

### 7.10 Effect of nozzle exit orifice diameters on SMD at axial locations

One of the most critical geometric features of pressure swirl atomizer is the final discharge orifice since this is where the liquid attains its maximum velocity before it is ejected from the nozzle into the computational domain in the form of a conical spray. As viscous losses tend to be high in this region of maximum flow velocity, normal design practice is to make the length to diameter ratio of the final discharge orifice as small as possible without creating a sharp edge that would be difficult to manufacture. In addition, to characterise the size of a fuel nozzle for most modelling purposes, the dimensions normal to the axis of the nozzle and combustor are considered and in the pressure swirl atomizer the exit orifice diameter is the basic one considered by Giffen and Murasjew [74, 185]. The influence of final discharge orifice 1.5, 2.5 and 3.5 mm on the mean drop sizes (SMD) is presented in Figure 7.19. It is evident from the result that the SMD also tends to increase noticeably with increasing atomizer diameter. This result is expected because the larger the exit orifice the larger the initial sheet thickness

will be and SMD for pressure-swirl atomizers will tend to scale with the initial sheet thickness and therefore an increase in the discharge orifice increases the mean drop size (SMD) in the spray and reduces the spray angle.
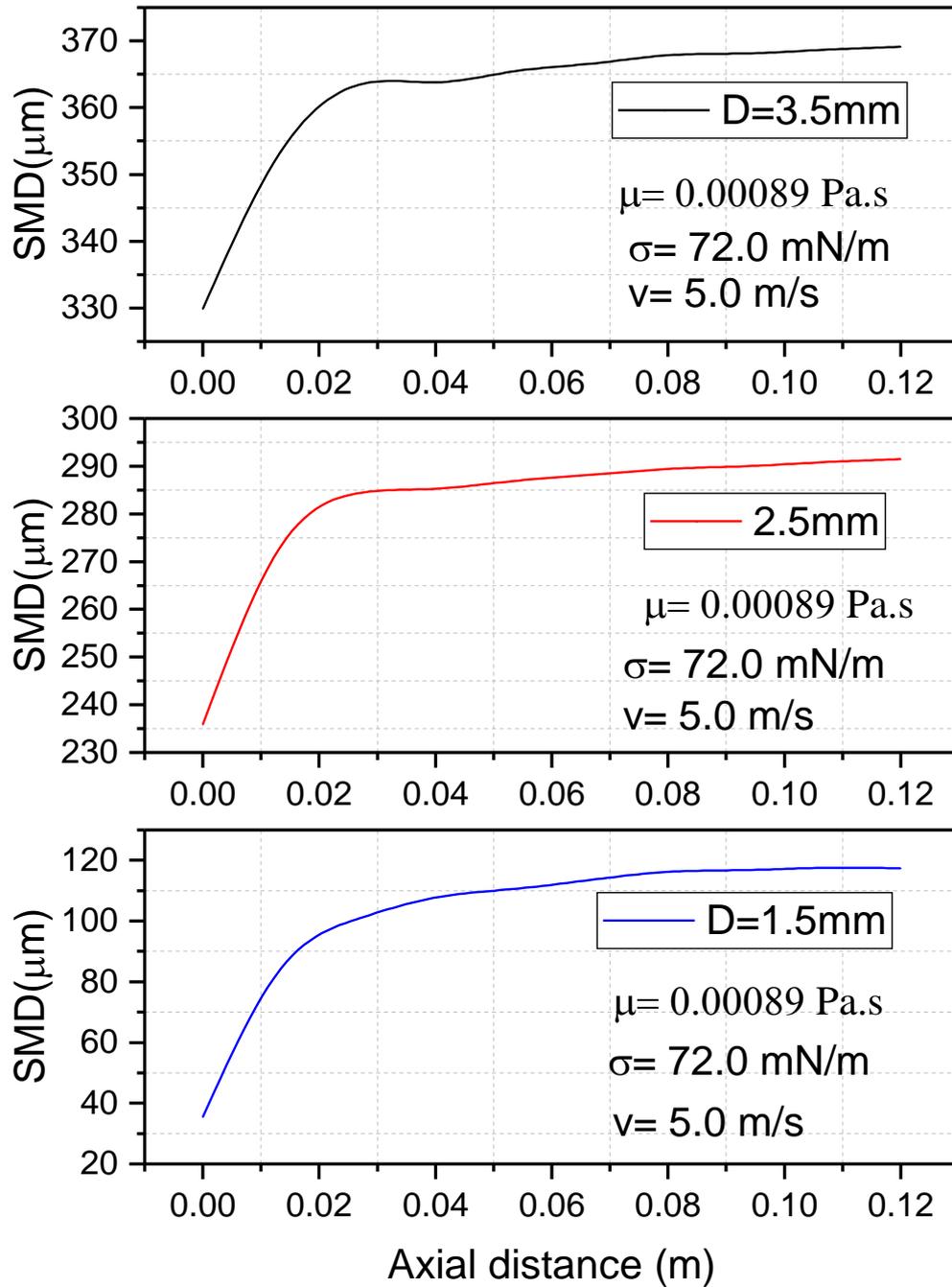


Figure 7.19 Axial variation of SMD for different exit orifice diameters

## 7.11 Sauter mean diameter (SMD) variation with injection velocity and density ratio

In Figure 7.20 and Figure 7.21 larger droplet velocities are seen in the centre spread of the spray than the concentration of droplets in the outer radial locations and this is generally due to the fact the larger size droplets are less affected by the air flow and tend to follow a more independent path, whereas smaller size droplets tend to follow the air flow field. The mean velocity profiles reveal the effect of air entrainment into the spray core and the resulting transport of small droplets. This entrainment causes the high droplet velocities on the spray centerline. Figure 7.22 presents the distribution of SMD for the injection velocity and density ratio. It is seen that the SMD decreases rapidly with increasing injection velocity. This behaviour is exhibited by all the density ratios. The rate at which the SMD drops is very small initially, but the values of 6 m/s tend to drop sharply for very high injection velocities. If the injection velocity is increased to even higher values, the flow will become highly turbulent and contain recirculation zones that will alter the droplet behaviour drastically. Based on this, to utilize this model for very high injection velocities proper physics must be accounted for. Another observation that is evident in Figure 7.22 is that as the gas density is increased (low $\rho_{liq}/\rho_g$), the SMD is drastically reduced. This may be attributed to the fact that with higher gas densities, the interaction between the droplets and the air is much higher, therefore the air does more work on the mean drop sizes and breaks the droplets apart.
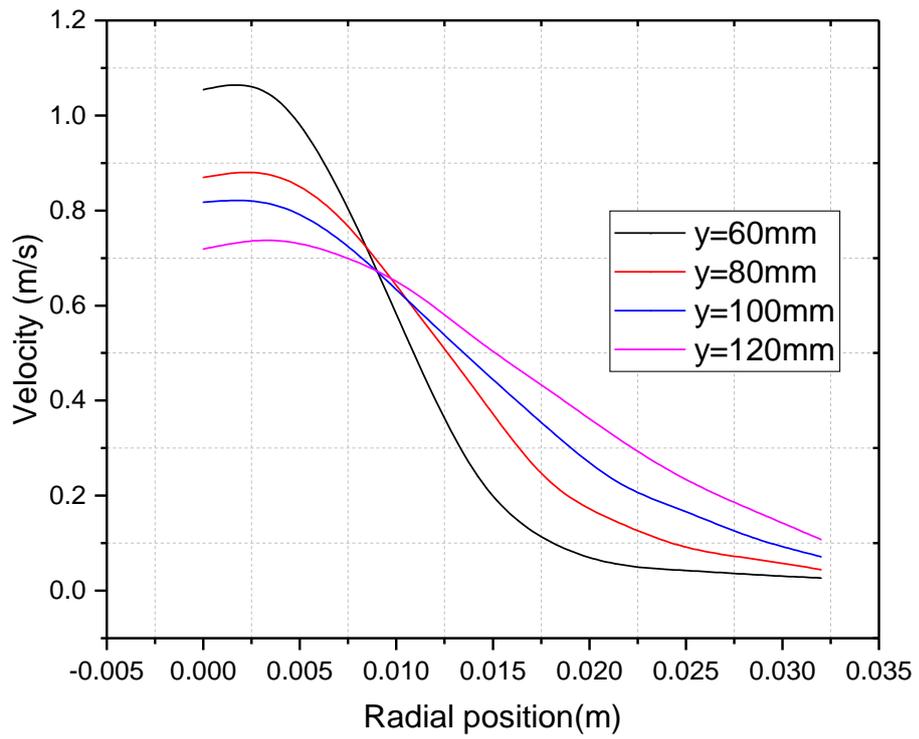
Figure 7.20 Radial profiles of mean liquid velocity at y = 60, 80, 100 and 120 mm
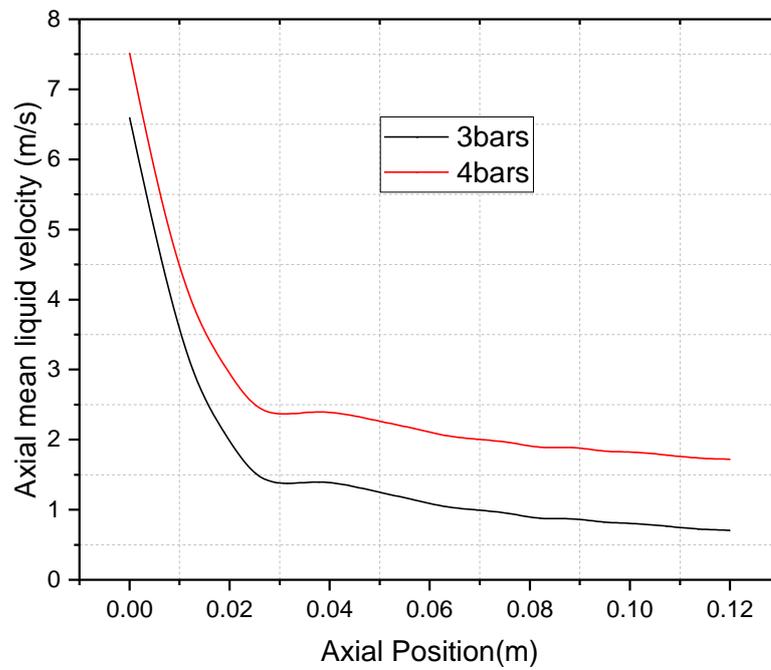


Figure 7.21 Axial profile of the axial mean liquid velocity for two injection pressure values
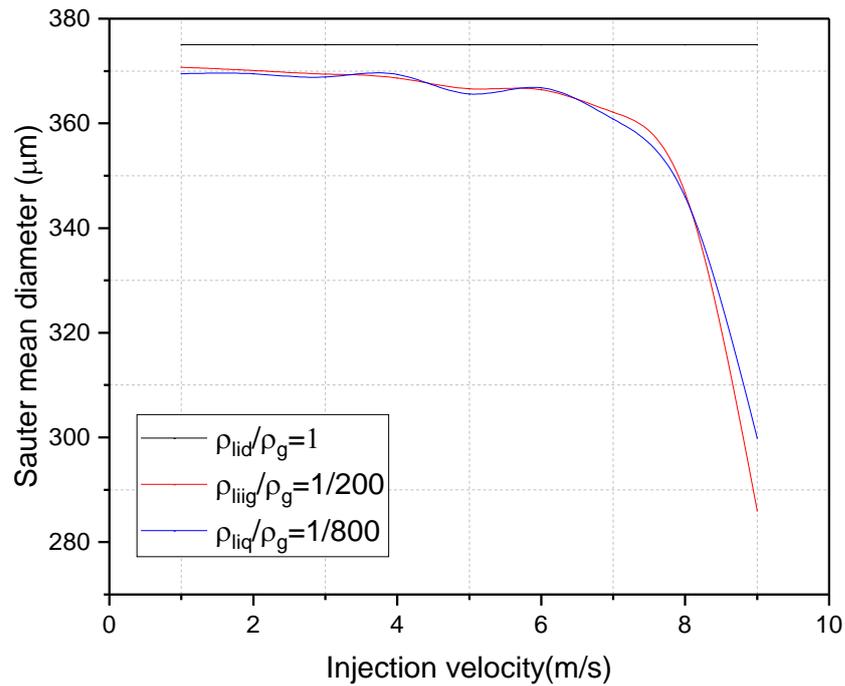
Figure 7.22 Sauter mean diameter (SMD) variation with injection velocity and density ratio

## 7.12 Effect of liquid density ratios on turbulent quantities

The graphs in Figure 7.23-Figure 7.27 show the influence of changes in the density ratios on the turbulent quantities for the model on a vertical section plane for the liquid and gas modelled as a single multicomponent species when all the transport equations and variables defined Three density ratios are (1) when $\rho_{liq} = \rho_{air}$ (2) when $\rho_{liq} = 200\rho_{air}$ and (3) when $\rho_{liq} = 800\rho_{air}$ were compared with all other flow variables remaining constant. It can be observed that the turbulent intensity increases with increasing density ratios but the turbulent length scale rather increases with decreasing density ratios. Large density variations on the length scale can be seen downstream of the spray on the spray centre line. The turbulent kinetic energy also shows increases when the liquid density varies from 1.30 kg/m$^3$ to 1040 kg/m$^3$. These high values of turbulent kinetic energies can be seen in the atomizer and low turbulent kinetic energies are noticeable few millimetres from the atomizer exit. The increase in density ratios also give rise to significantly increase in the turbulent viscosity as shown in Figure 7.26. High rates of dissipation of the turbulent kinetic energy are higher in the atomizer than the computation domain in relation to variations in density ratios. It can be

160

deduced clearly from the results that the increase in liquid density reveals changes in individual turbulent parameters and the changes are disproportionate.
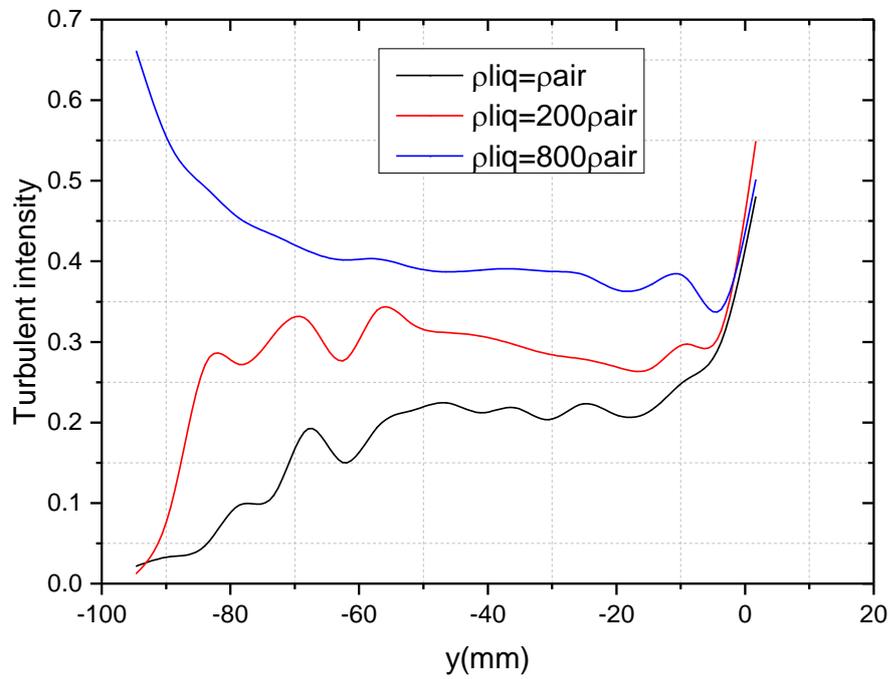


Figure 7.23 The effect of variation of liquid density on the turbulent intensity on the spray centreline
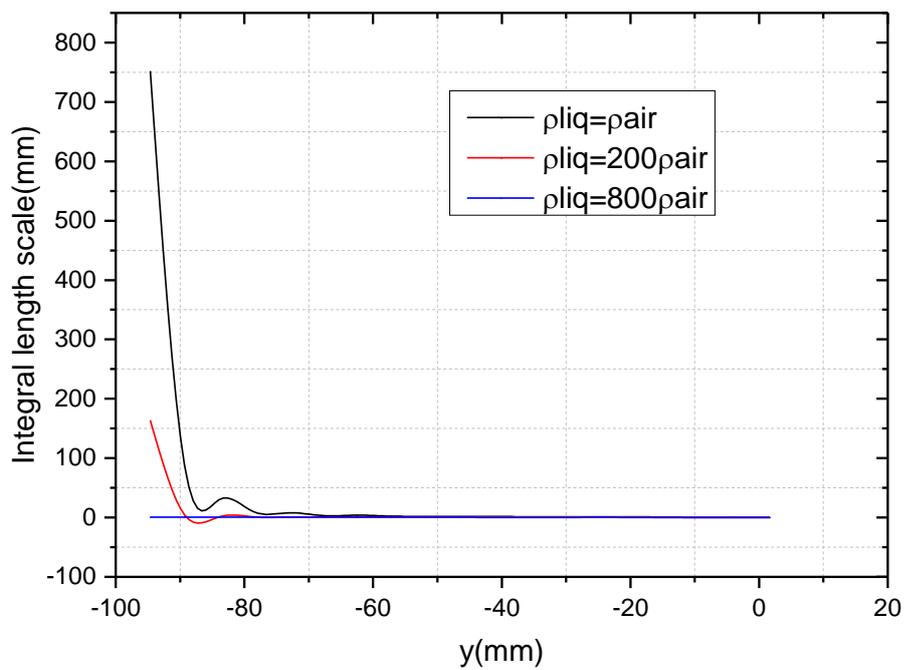


Figure 7.24 The effect of variation of liquid density on integral length scale
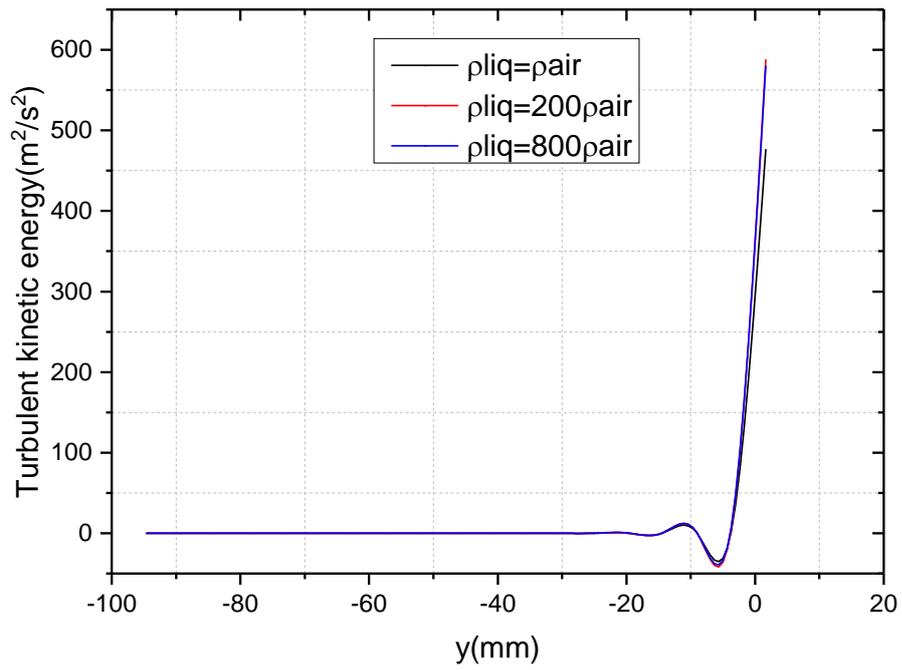
Figure 7.25 The effect of variation of liquid density on turbulent kinetic energy on spray centreline
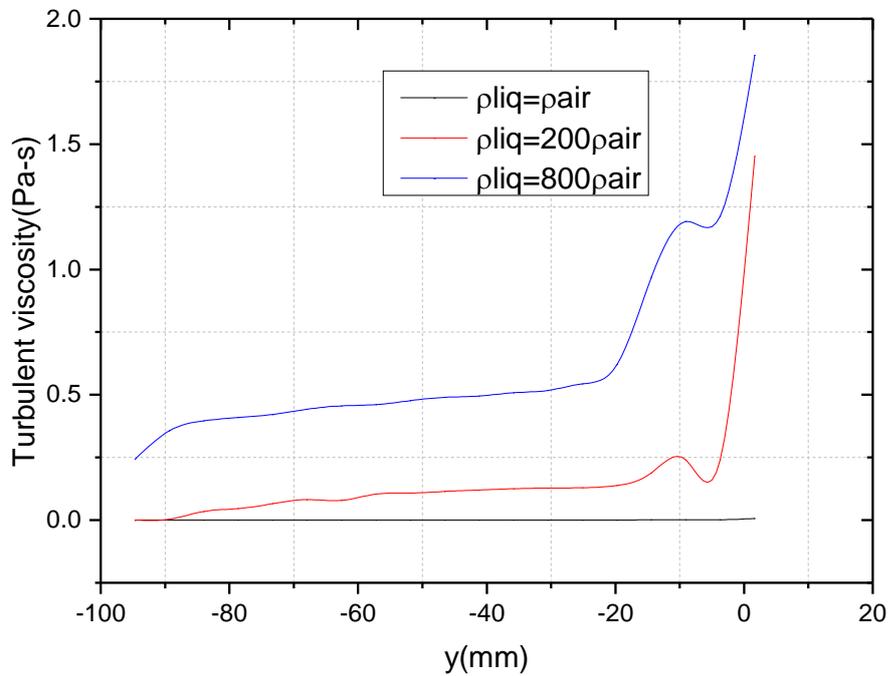


Figure 7.26 The effect of variation of liquid density on turbulent viscosity

162
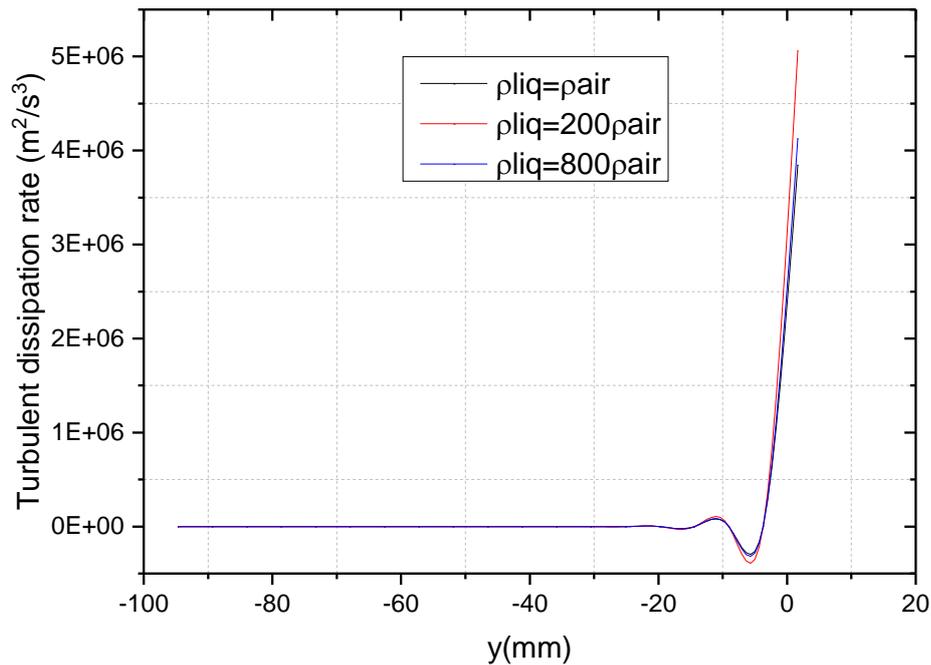
Figure 7.27 The effect of variation of liquid density on turbulent dissipation rate

## 7.13 Comparison of Sauter mean diameter (SMD) of diesel, gasoline and kerosene

Figure 7.28 shows the results of the comparison of SMDs for various liquids such as gasoline, diesel and kerosene for internal combustion engines applications with their properties shown in Table 2.1. The experimental study of sprays of liquid fuels such as gasoline and diesel can be hazardous and costly. This is the more reason liquid spray with non-flammable in nature such as water was used in the validation process and to reduce these problems  However, by modelling these liquid fuel sprays these problems are also overcome and the spray characteristics can easily be studied. Owing to a small disparity in liquids density of these fuels, it is assumed that only viscosity and surface tension are responsible for changes in SMD and axial velocity. Gasoline with the lowest viscosity has the highest axial velocity in the spray centre. On the other hand, diesel oil with the highest viscosity has the smallest axial velocity on the centre spread of the spray and the mean velocity of kerosene was found to be in the middle of the two liquids. Table 7.1 shows the level of dependence of SMD on three different liquids as is more clearly shown in Figure 7.29. Kerosene and gasoline both with low viscosities have significantly smaller SMD while more viscous diesel oil has considerably larger

SMD. This is also in conformity with the observation made by Maly [42] which shows a dependence of SMD on different liquids as shown on Table 7.2.

Table 7.1 Influence of liquid properties on SMD

| Liquid | Formula | Density kg/m3 | Surface Tension N/m | Dynamic Viscosity $\mu \cdot 10^6$ Pa$\cdot$s | SMD [$\mu$m] |
|--------|---------|---------|---------|---------|------|
| Diesel | $C_{12}H_{26}$ | 840 | 0.028 | 2400 | 400.0 |
| Kerosene | $C_{12}H_{24}$ | 800 | 0.026 | 1600 | 363.3 |
| Gasoline | $C_8H_{18}$ | 750 | 0.025 | 380 | 352.6 |

Table 7.2 Influence of liquid properties on SMD [42]

| Liquid | SMD [$\mu$m] |
|--------|--------------|
| Arctic diesel | 44.2 |
| Kerosene | 46.3 |
| Winter diesel | 46.9 |
| Kerosene + oil | 50.7 |
| Biodiesel | 50.7 |
| Palm oil | 52.6 |
| Aged winter diesel | 53.1 |
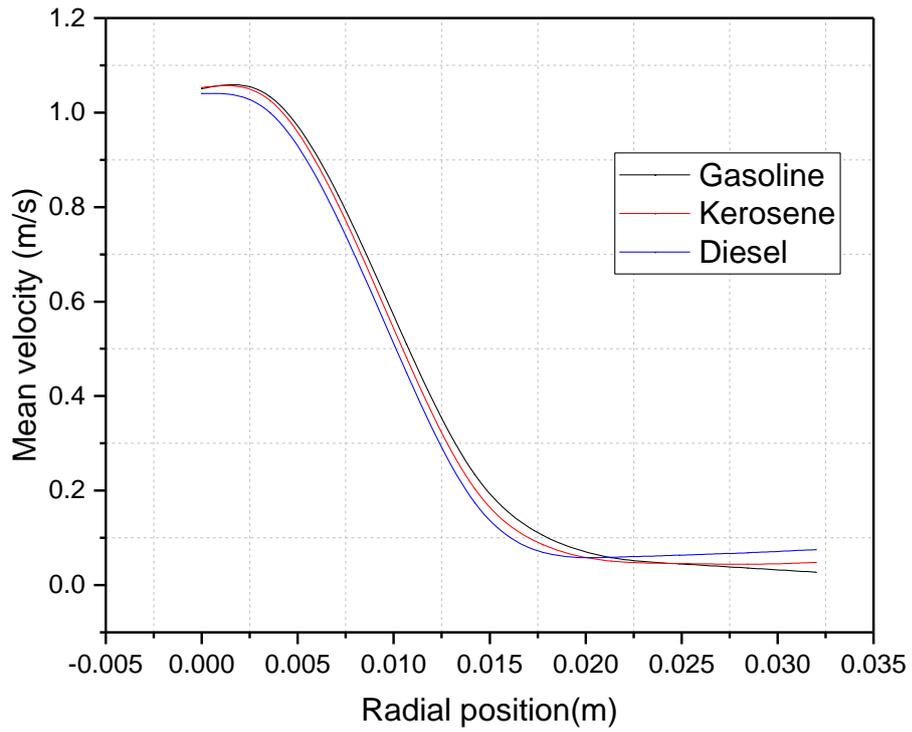
Figure 7.28 Comparison of droplet velocity for diesel, gasoline and kerosene liquid fuel, modelling at y=90mm
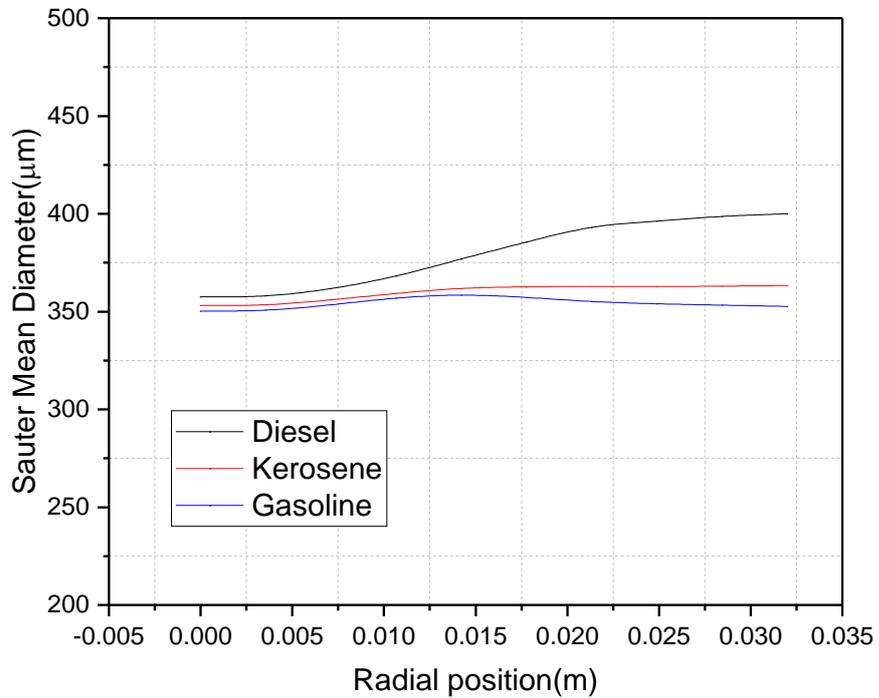


Figure 7.29 Comparison of Sauter mean diameter (SMD) of diesel, gasoline and kerosene, modelling at y=90mm

### 7.14 CFD based  design optimisation

The objective of this study is to obtain the optimal nozzle exit orifice parameters, operating conditions and fluid properties that perform or give the most  minimum droplet (SMD) at axial distances along the spray centerline. The design variables (DVs) used are liquid viscosity ($DV_1$) 0.00031 to 0.2 Pa.s, surface tension ($DV_2$) 0.02 to 0.075 mN/m, nozzle exit orifice diameter ($DV_3$) 0.0015 to 0.0035 m and liquid velocity ($DV_4$) from 1 to 6 m/s as shown in Table 7.3. The design cases were generated using a statistical Design of Experiments (DoE) technique known as Latin Hypercube Designs (LHD) in Matlab. This resulted in eighty-seven (87) design cases for CFD simulations shown in Table 8.1 in Appendix III. Felipe et al [133] indicate that for four (4) variables for medium designs using LHD a minimum of seventy (70) cases are required. A commercial Computational Fluid Dynamics (CFD) software STAR-CD code was used to simulate the two-phase flow for the eighty-seven (87) design cases for seventy-three (73) different nozzle exit diameters. The standard k-ε turbulence model was used to capture the turbulent behavior in the flow. The results were obtained for the average density, liquid mass fraction and interfacial surface density from the simulations, the  $\Sigma - Y_{liq}$ atomisation model was used to evaluate the Sauter mean diameter (SMD) at the axial  positions of the spray at 20, 40, 60, 80, 100 and 120 mm. Combinatorial optimization was performed in order to identify and obtain the minimum SMD at these locations.

Table 7.3 Definition of design of experiment (DoE) variables for optimization

| Design parameters | Description | Symbol | Range of values |
|---|---|---|---|
| Input variables | Liquid viscosity | $DV_1$ | 0.31 to 200 mPa.s |
| | surface tension | $DV_2$ | 20  to 75 mN/m |
| | Nozzle orifice diameter | $DV_3$ | 1.5 to 3.5 mm |
| | Liquid velocity | $DV_4$ | 1 to 6 m/s |
| Output variables | Average density distribution at the axial positions | $\bar{\rho}$ | $> 0$ |
| | Liquid mass fraction distribution at the axial positions | $Y_{liq}$ | $> 0$ |
| | Surface density | $\Sigma$ | $> 0$ |
| Objectives | Minimize the  Sauter Mean diameter (SMD)  at the axial positions | $d_{32}$ | - |
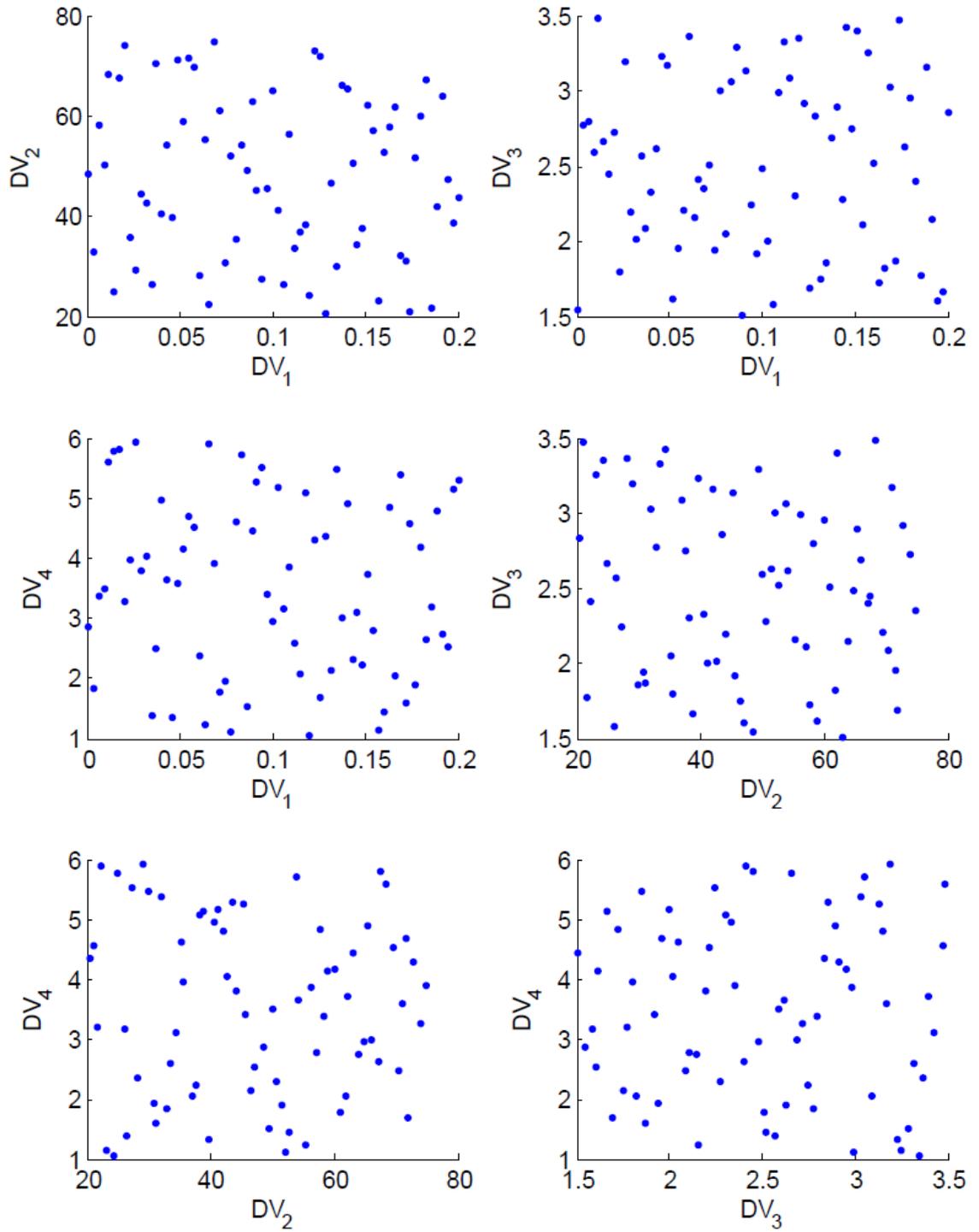
Figure 7.30 Combinations and distributions of design parameters for optimization

In order to map and show uniform distributions between the design variables as shown in Figure 7.30 the modified Latin hypercube Matlab code was used. This code can be found in Appendix III. The original code was created to generate random values between 0 and 1 but with the modified code the extreme limits can be varied and give options to specify user-defined values. In running this code, a total of 87 design cases were generated including the corner or factorial points for the correct combination of parameters such as liquid viscosity, surface tension, nozzle orifice diameter and liquid velocity as shown in Table 8.1 in Appendix III. It can be observed that the design points are uniformly distributed among the design variables and can accommodate and suffice for a wide range of fluid properties for liquids such as water, diesel, gasoline and kerosene fuels.

In performing the combinatorial optimization, eighty-seven (87) simulations were run in Star-CD CFD code using the standard k-ε turbulence model and their results for average density, mass fraction of liquid and interfacial surface density generated analysed. These were used to compute for the droplet Sauter Mean Diameter (SMD) at the axial positions on the spray centre line. With the 4-factor design of experiment (DoE) resulting in the simulations of eighty seven (87) cases, the results show the cases with the most minimum droplet Sauter mean diameter (SMD) at the various axial locations along the nozzle on the spray centreline for the combinations of liquid viscosity, surface tension, nozzle exit diameter and liquid velocity as shown in Table 7.4. The results show that case 17 generated the most minimum SMD at axial position 20 mm and 40 mm from the nozzle exit. Case 1 was the most minimum SMD at locations 60 mm, 80 mm and 100 mm from the nozzle exit and case 24 gives the best minimum from the nozzle exit at axial distance 120 mm. Figure 7.31 presents the results of the best minimum Sauter Mean diameters (SMDs) along the spray centre line for cases 1, 17 and 24 respectively.

Table 7.4 The best minimum Sauter Mean diameters (SMDs) on the spray centre line for cases 1, 17 and 24

| Case | DV1 Viscosity | DV2 Surface tension | DV3 Nozzle exit diameter | DV4 Liquid velocity | Sauter Mean Diameter, SMD (µm) | | | | | |
| | | | | | Axial positions (mm) | | | | | |
| | | | | | 20 | 40 | 60 | 80 | 100 | 120 |
| 1 | 0.00031 | 20 | 1.50 | 1.0 | 22.41 | 23.15 | 23.53 | 24.09 | 29.32 | 33.34 |
| 17 | 0.00031 | 35.71 | 2.7 | 1.07 | 19.10 | 20.58 | 24.56 | 26.62 | 31.79 | 35.36 |
| 24 | 0.02028 | 47.71 | 1.64 | 1.14 | 23.72 | 24.07 | 25.49 | 25.90 | 29.89 | 32.79 |
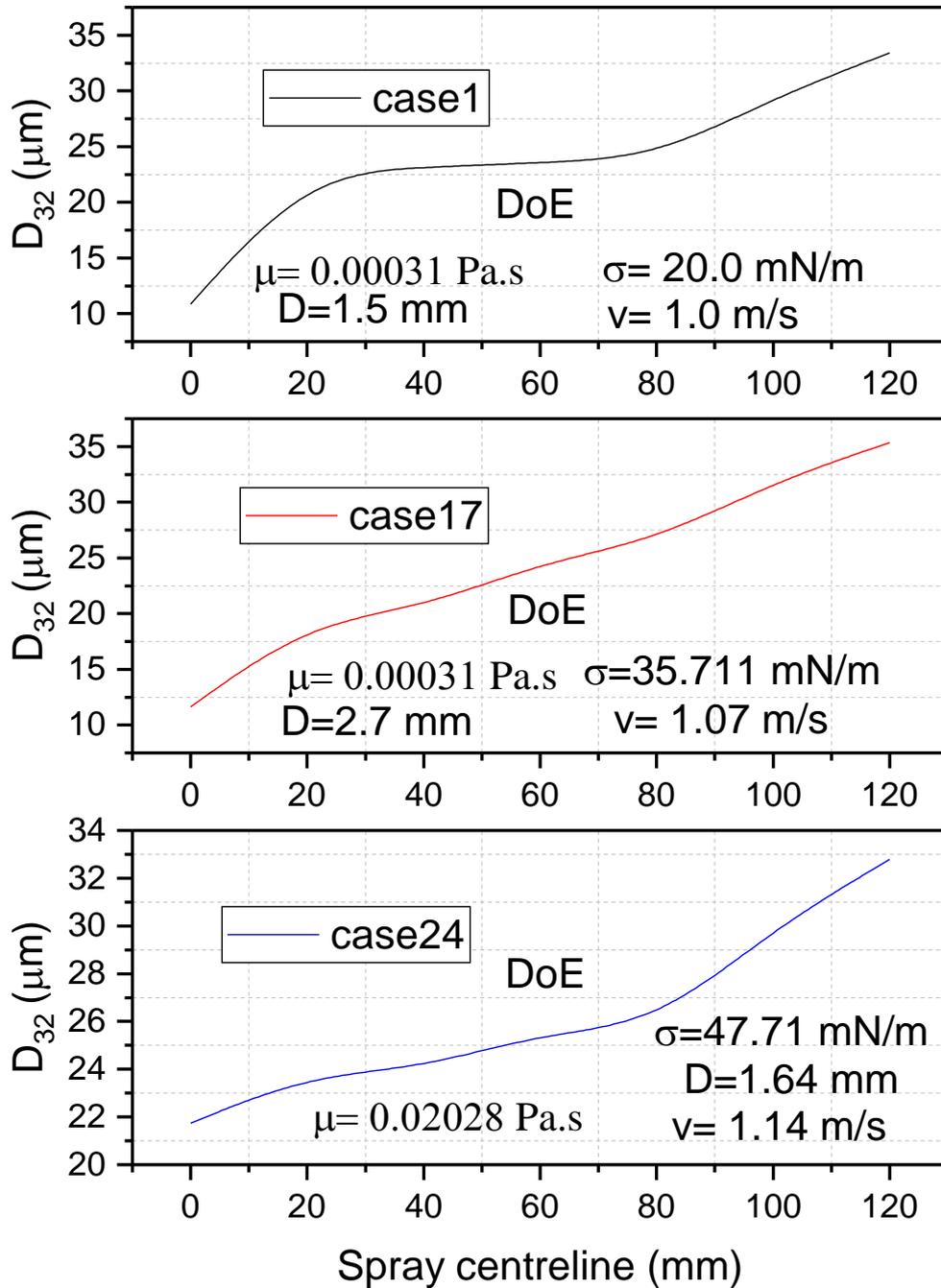
Figure 7.31 SMDs on the spray centreline for case 1, case 17 and case 24

### 7.14.1 **Optimization and evaluation of SMD for DoE variables**

The optimization of droplet Sauter Mean Diameter of a spray nozzle under different spray conditions was investigated numerically using $\Sigma - Y_{liq}$ atomization model. The optimal SMD was influenced greatly by the operating conditions, nozzle exit diameter and fluid properties as shown in Figure 7.31. In order to identify and obtain the most minimum SMDs, Figure 7.32 to Figure **7.35** present the bar charts for all the 87 cases including the corner or factorial points. The black, red, blue and pink depict the first, second, third and fourth cases respectively on a particular bar chart. The vertical axis represents the axial positions on the spray centreline and droplet Sauter Mean Diameter (SMDs) evaluated at that locations shown on the horizontal axis. These charts were optimized to generate the best three cases shown in Figure 7.31. The resultant graph in Figure 7.31 shows that the SMD increases with increasing axial distance on the spray centre line for all the best three cases. The curve up to 20 mm is considered the conical liquid sheet for which no meaningful SMD can be predicted or evaluated. This indication is also consistent with the experimental measurements observed by many researchers on pressure swirl nozzle [1, 7]. Beyond this point, atomization process starts which may either be caused by the disintegration of the liquid sheet by aerodynamic forces or turbulence forces within the liquid itself. This gives rise to the formation of droplets beyond this point and subsequent smaller droplets collisions resulting in coalescence downstream the spray. Coalescence results in one droplet of a larger size than that of the pre-collision droplets. Since these phenomena appear at low relative velocity, it is expected that their effect is significant in low-velocity regions of the spray where this causes an increase in droplet size. Another possible outcome of droplet collisions which may result in coalescence is when the relative velocity of the droplets is higher and the collisional kinetic energy is sufficient to expel the intervening layer of gas. If the collisional energy exceeds the value for permanent coalescence, then temporary coalescence occurs. Temporary coalescence may result in either disruption or fragmentation. In disruption, the collision product separates into the same number of droplets which existed prior to the collision. In fragmentation, the coalesced droplet breaks up into numerous satellite droplets [186]. Coalescence followed by disruption does not have any significant influence on droplet size. Even if some mass transfer occurs, the droplet diameters are not changed in any observable way. This model takes coalescence into account.

One other observation with the spray combination inputs with better performance in these limits by exhibiting most minimum Sauter Mean diameter is that the low values of operating conditions, nozzle exit diameters and fluid properties play significant effect in the remarkable improvement in the size of the droplet SMD at these positions. But more dominant is the liquid viscosity and the operating conditions. The significant reduction in size makes this atomization model more suited and applicable to a wide range of spray application areas especially in the internal combustion engines where small SMDs are desired and agricultural spraying where smallest droplets are essential to good plant cover.
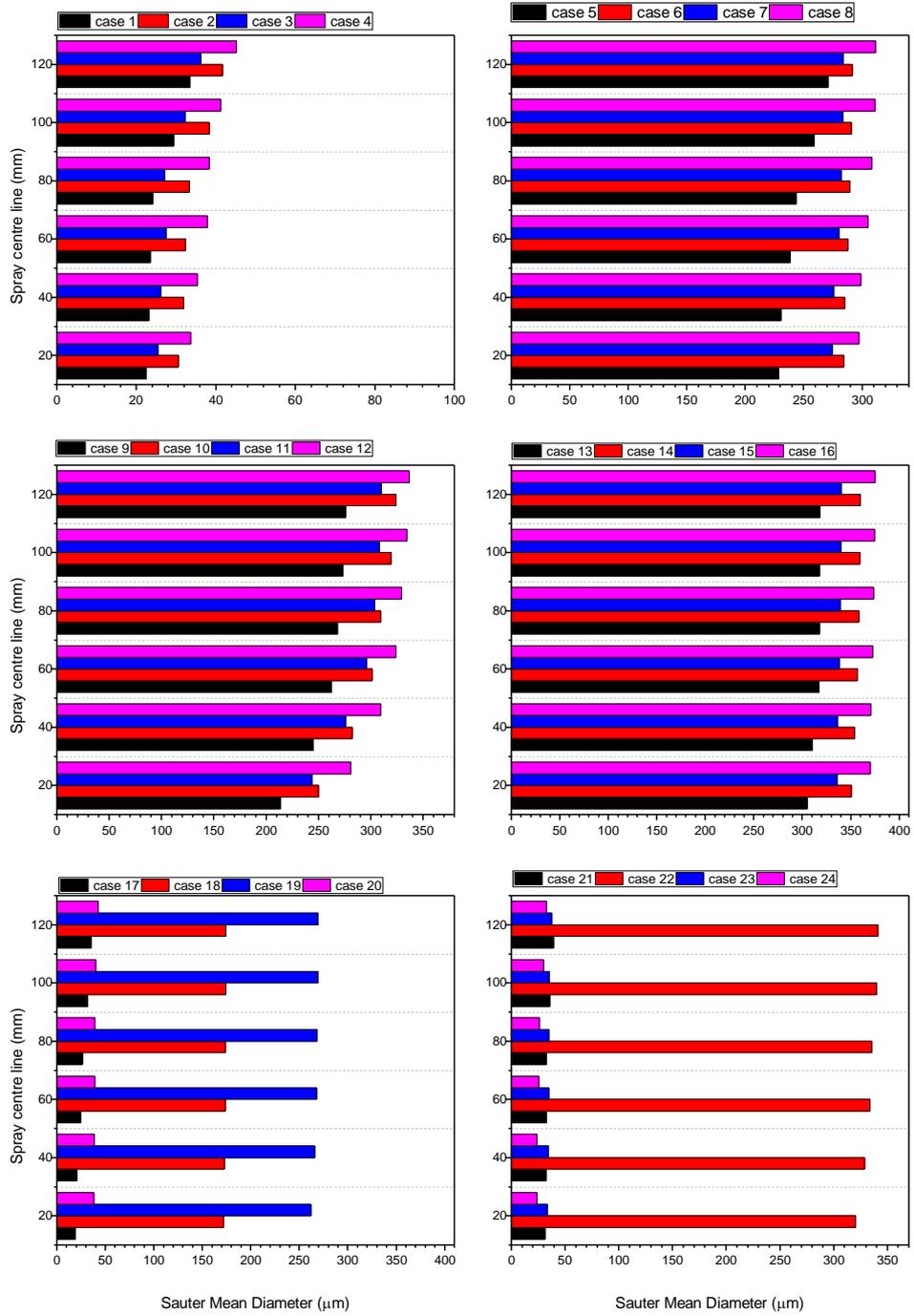
Figure 7.32 SMDs on the spray centre axis for case 1 to case 24
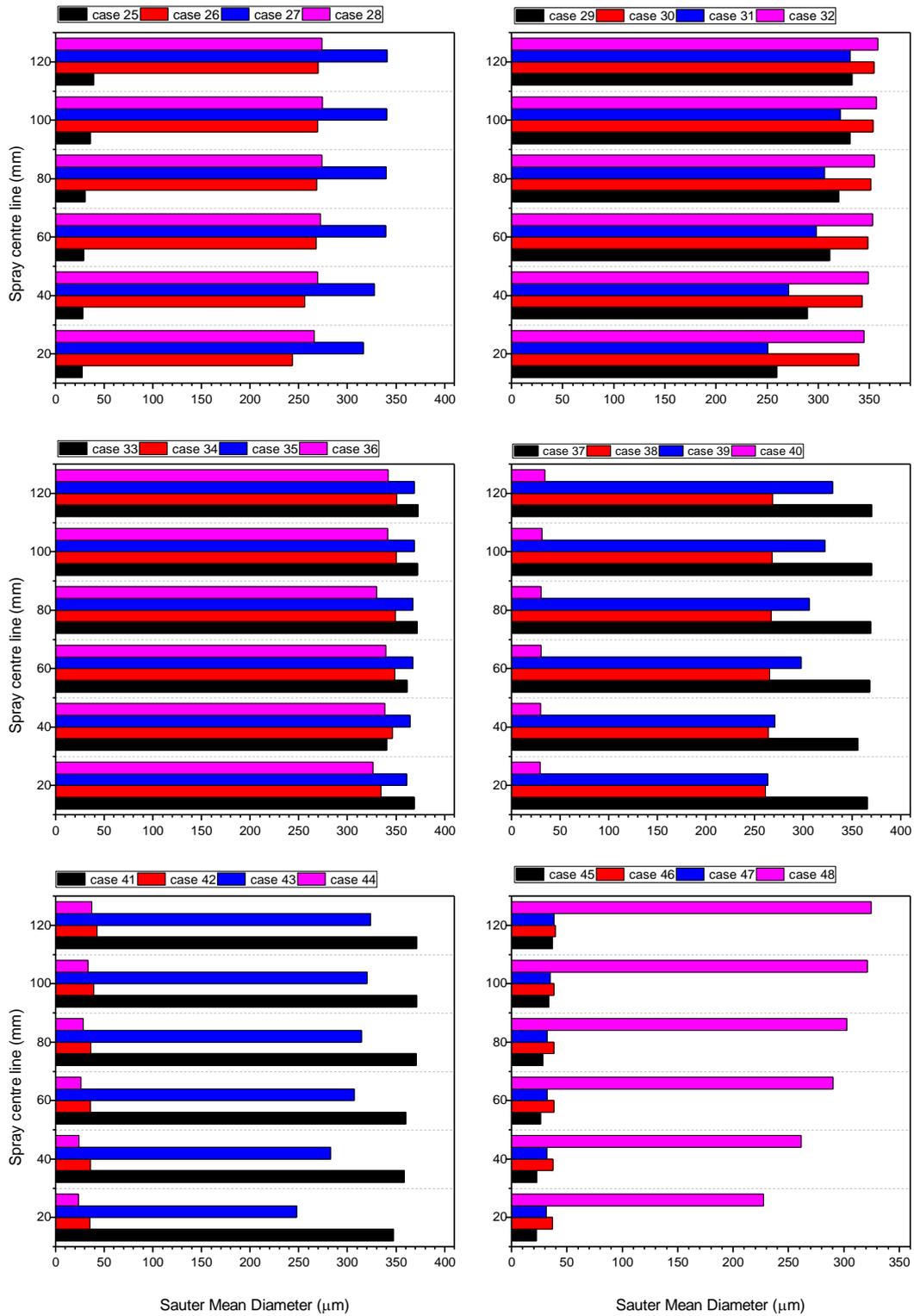
Figure 7.33 SMDs on the spray centre axis for case 25 to case 48
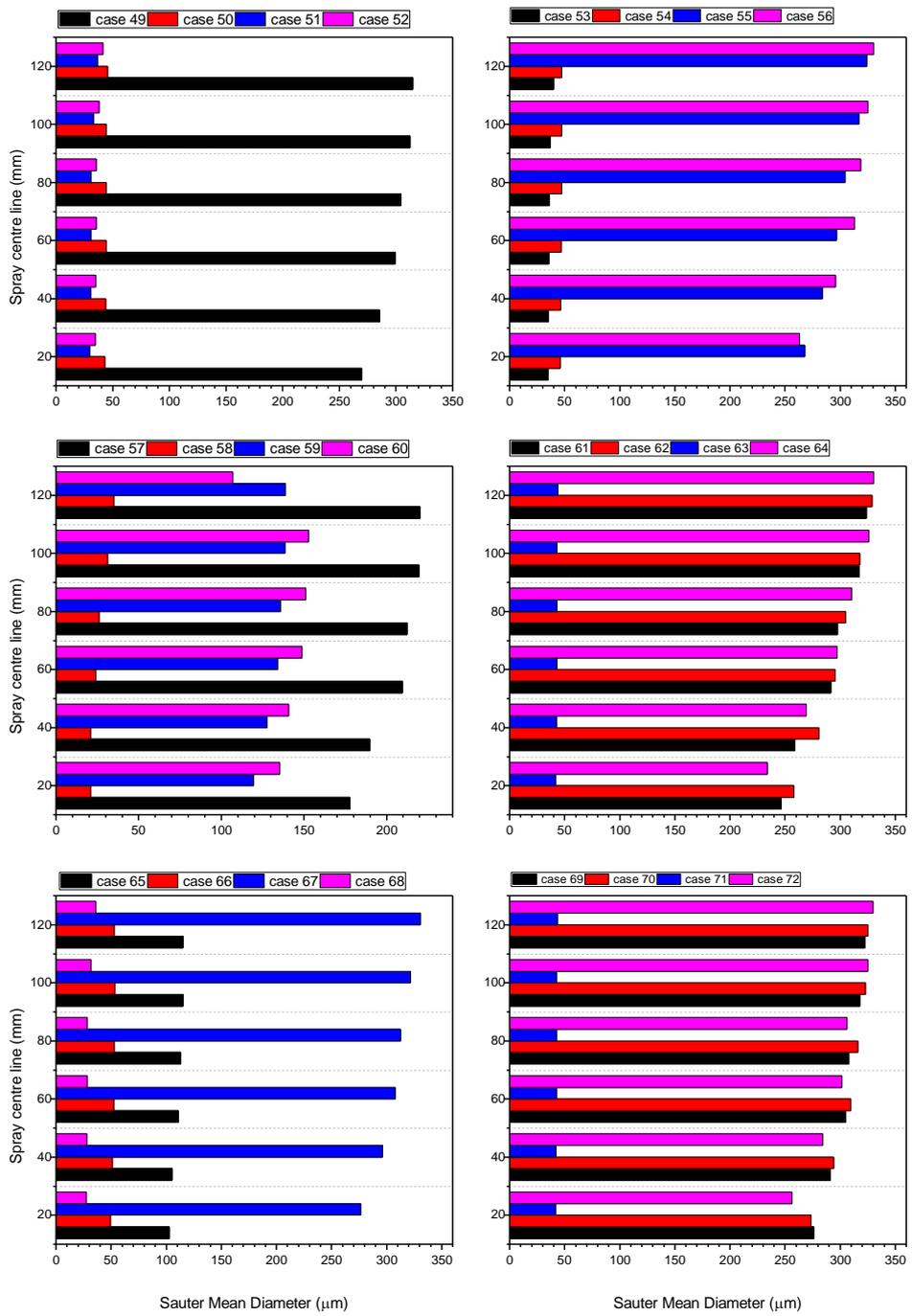
Figure 7.34 SMDs on the spray centre axis for case 49 to case 72
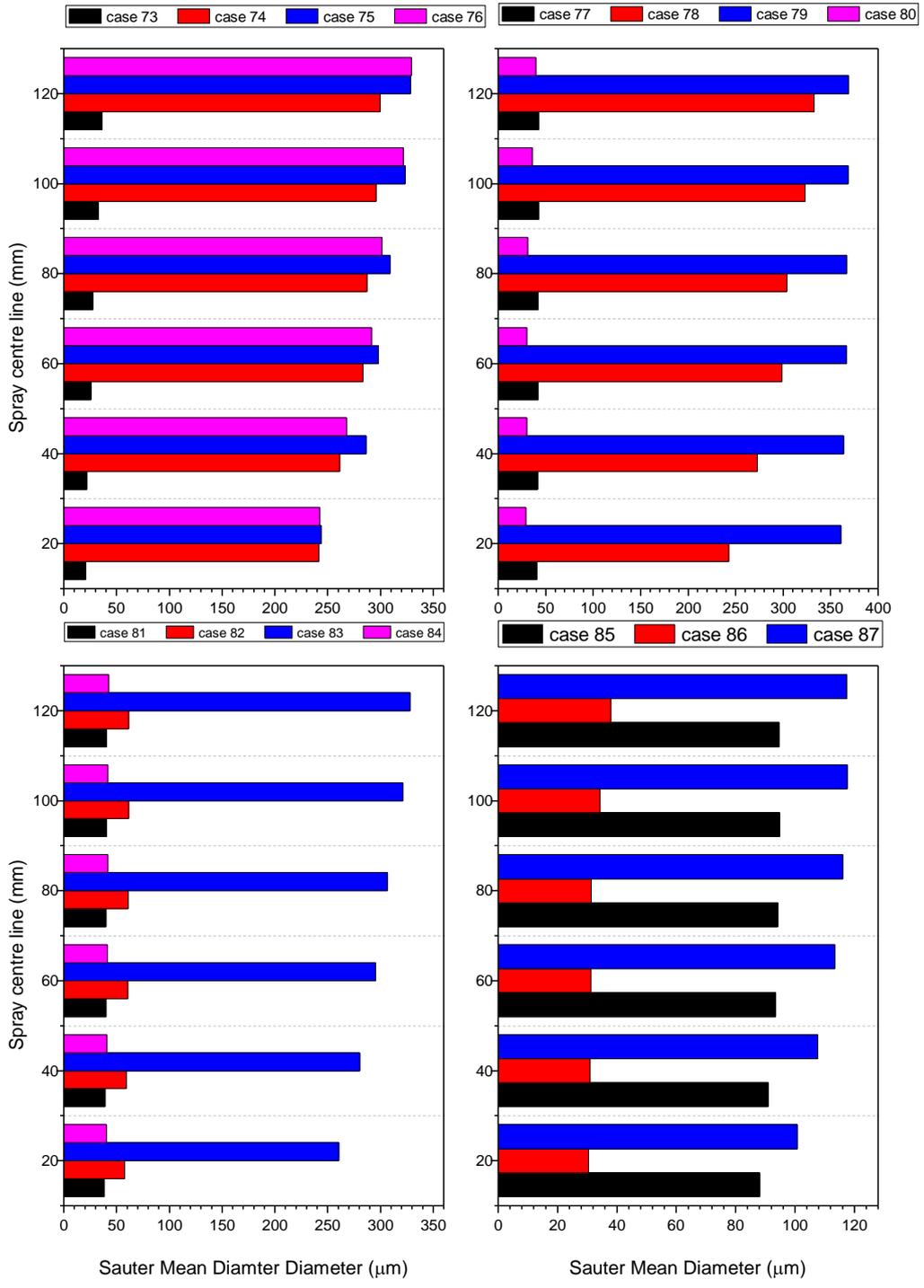
Figure 7.35 SMDs on the spray centre axis for case 73 to case 87

### 7.15 SMD correlation based on 4-factor DoE

In the Design of Experiments (DoE), the four (4) design variables are liquid viscosity $\mu_l$, surface tension $\sigma$, liquid velocity $v$, and nozzle exit diameter $D_o$. In order to establish relationship between these inputs and the resulting droplet Sauter Mean Diameter (SMD) and obtain usable SMD correlation for the model, surface fitting of the data was carried out. The result was compared to two existing SMD correlations such as Jasuja [63] and Radcliffe [62]. The following relations are used to transform some of the DOEs to the standard variables of kinematic viscosity $\vartheta$, surface tension $\sigma$, mass flow rate $\dot{m}_l$, and pressure differential $\Delta P_l$ in their correlations. The kinematic viscosity is obtained from $\vartheta = \frac{\mu_l}{\rho_l}$ where $\mu_l$ is the dynamic viscosity and $\rho_l$ the density of the liquid. The pressure differential $\Delta P_l$ is derived from $v = \sqrt{\frac{2\Delta P_l}{\rho_l}}$ where $v$ is the velocity. The mass flow rate $\dot{m}_l$ is also found from these relations

$$FN = \frac{\dot{m}_l}{\sqrt{\rho_l \Delta P_l}}$$

where flow number, $FN$, in terms of atomizer dimensions is defined by Maly [42] as $FN = 0.389 D_0^{1.25} A_i^{0.5} D_c^{-0.25}$ where $D_o$ is nozzle exit diameter from the DoE, the inlet area $A_o$ from the geometry of the nozzle and $D_c$, the diameter of the swirl chamber from the nozzle geometry.

Therefore, SMD correlation based on 4-factor DoE is formulated as shown below

$$SMD = \lambda \vartheta^a \sigma^b \dot{m}_l{}^c \Delta p_l{}^d$$

where $\lambda$, a, b, c and d are experimental constants determined from fitting the data. As indicated, the data for dependent variable SMD and independent variables $\vartheta$, $\sigma$, $\dot{m}_l$ and $\Delta P_l$ were generated from the DoE points shown in Appendix III using the appropriate relations demonstrated above. Using Matlab Isqcurvefit code in the optimization tool box shown in Appendix IV gives $\lambda = 2.025$, $a = 0.122$, $b = 0.078$, $c = 0.06$ and $d = -0.42$ with the normal of the residuals (resnorm) of the data representing the measure of the goodness of fit as 9.7261 which is less than the residual norm at the bad ending point. Hence, the fit is extremely good considering the variations in the liquid properties and operating conditions.

Therefore, the SMD correlation for model is

$$SMD = 2.03\vartheta^{0.12}\sigma^{0.08}\dot{m}_l{}^{0.06}\Delta p_l{}^{-0.42}$$

Comparing this correlation and the experimental constants to the two existing SMD correlations, Jasuja $SMD = 4.4\vartheta^{0.16}\sigma^{0.6}\dot{m}_l{}^{0.22}\Delta p_l{}^{-0.43}$ and Radcliffe $SMD = 7.3\vartheta^{0.2}\sigma^{0.6}\dot{m}_l{}^{0.25}\Delta p_l{}^{-0.4}$, show that the model under predicts all the constants but has high dependency on the viscosity and pressure differential. In the Radcliffe case, the pressure differential is the only variable that is over predicted in the new correlation. The slight disparities in the experimental constants predicted may be attributed to the range of values used for the kinematic viscosity and the difficulty in adequately capturing surface tension. Wang et al [7, 68] even assert that within the same limits of fluid properties and nozzle operating conditions is not possible to define one universal SMD correlation based on this formulation. To further analyse the new SMD correlation, surface plots for various combinations of predictor variables against the SMD with hold values were carried out.

Surface Plot of SMD vs Kinematic viscosity and Surface tension

Radcliffe $SMD = 7.3\vartheta^{0.2}\sigma^{0.6}\dot{m}_l{}^{0.25}\Delta p_l{}^{-0.4}$
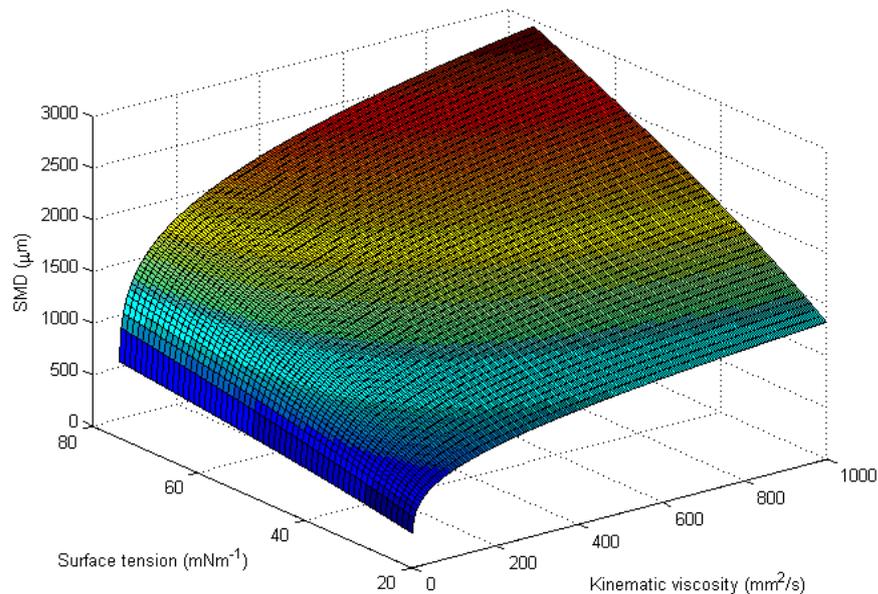
$$\text{Jasuja} \quad SMD = 4.4\vartheta^{0.16}\sigma^{0.6}\dot{m}_l^{0.22}\Delta p_l^{-0.43}$$
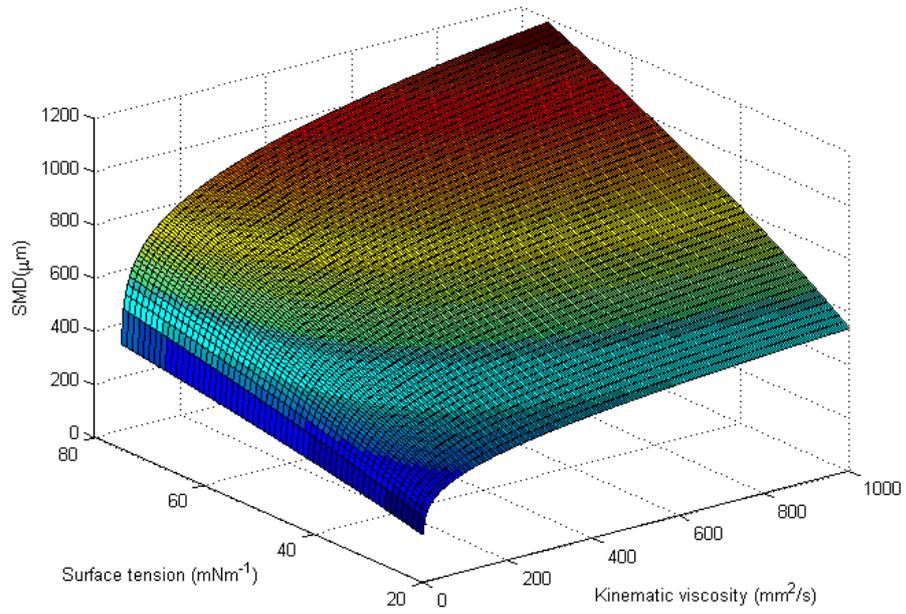


Figure 7.36 Surface plot of SMD against liquid properties with constant operating conditions for two existing SMD correlations

$$\text{New} \quad SMD = 2.03\vartheta^{0.12}\sigma^{0.08}\dot{m}_l^{0.06}\Delta p_l^{-0.42}$$
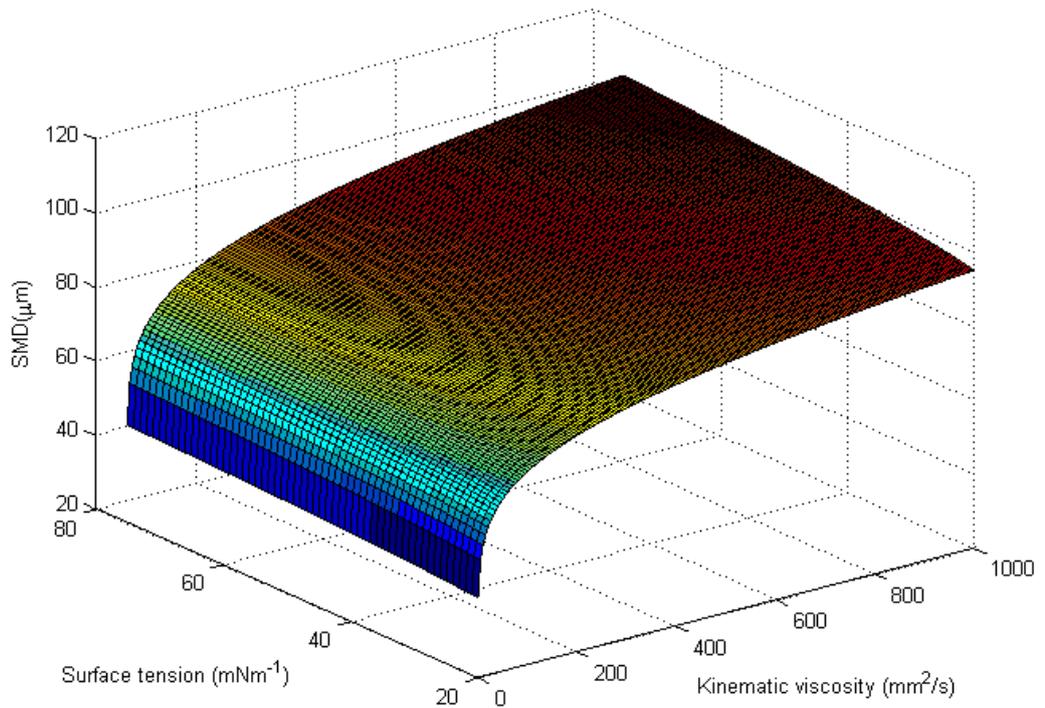


Figure 7.37 Surface plot of SMD against liquid properties with constant operating conditions for the new SMD correlation

Figure 7.36 and Figure **7.37** show the 3D surface plot of SMD against liquid properties with constant operating conditions for existing and new SMD correlations. The kinematic viscosity ranges from 1 mm²/s to 1000 mm²/s and the continuous variables for surface tension is between 20 mNm$^{-1}$ and 75 mNm$^{-1}$ to cover wide range liquids properties. The two operating conditions, pressure and mass flow rate, are held at constant levels in order to estimate the approximate SMDs or response variables for the correlations and also observe the relationship between these two predictor variables and SMD based on the fitted model SMD correlation. In this case, the possible SMDs are known from these two fluid properties within these input continuous variables and constraints. With meshgrid surface plot code in Matlab, the two continuous variables of kinematic viscosity and surface tension as well as the fitted model SMD correlation were defined with built-in functions and the response surface generated.

In order to analyse the response surface of the new fitted SMD correlation for the $\Sigma - Y_{liq}$ atomization model, the result was compared to two existing SMD correlations by Radcliffe and Jasuja based on the same four input variables. The results show the response surface or SMDs of the new model equation exhibit similar trend and shape with the existing correlations and the SMDs were smaller than those for the two existing correlations for the same conditions and constraints. This may be due to the smaller exponents or dependency of surface tension and the mass flow rate in the new SMD model which means the model could not adequately account for the surface tension.

The response surface shown in Figure 7.37 is curved because the new SMD correlation contains quadratic terms that are significant. The highest SMD approximately 110μm of the surface is seen in the upper left corner of the plot and corresponds with the combination of highest values of 1000 mm²/s and 75 mNm$^{-1}$ for kinematic viscosity and surface tension respectively. The lowest values of SMDs for the surface are observed in the lower left corner of the plot and this corresponds with low values of both kinematic viscosity and surface tension 1 mm²/s and 20 mNm$^{-1}$ respectively. The third and fourth predictor variables, mass flow rate and pressure differential, are not displayed in the surface plot since they are hold values. These results were obtained for the hold values for mass flow rate of 0.0074 kg/s with its experimental-power constant and pressure at 0.93MPa. The significance of this result is that liquids with lower fluid properties will give small droplet SMDs with other conditions remaining unchanged for a particular pressure swirl nozzle.

Surface Plot of SMD vs Kinematic viscosity and Pressure

Radcliffe $SMD = 7.3 \vartheta^{0.2} \sigma^{0.6} \dot{m}_l^{0.25} \Delta p_l^{-0.4}$
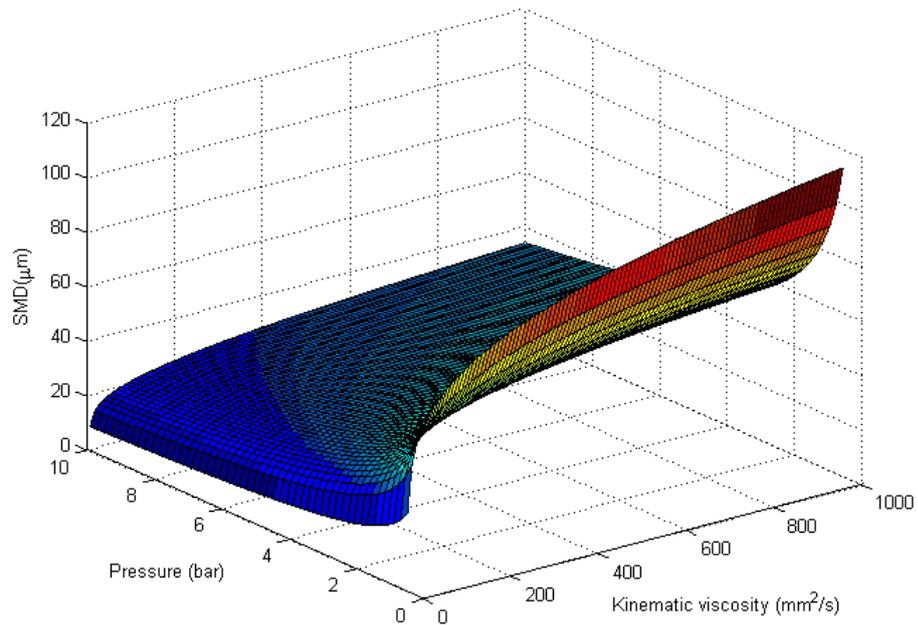


Jasuja $SMD = 4.4 \vartheta^{0.16} \sigma^{0.6} \dot{m}_l^{0.22} \Delta p_l^{-0.43}$
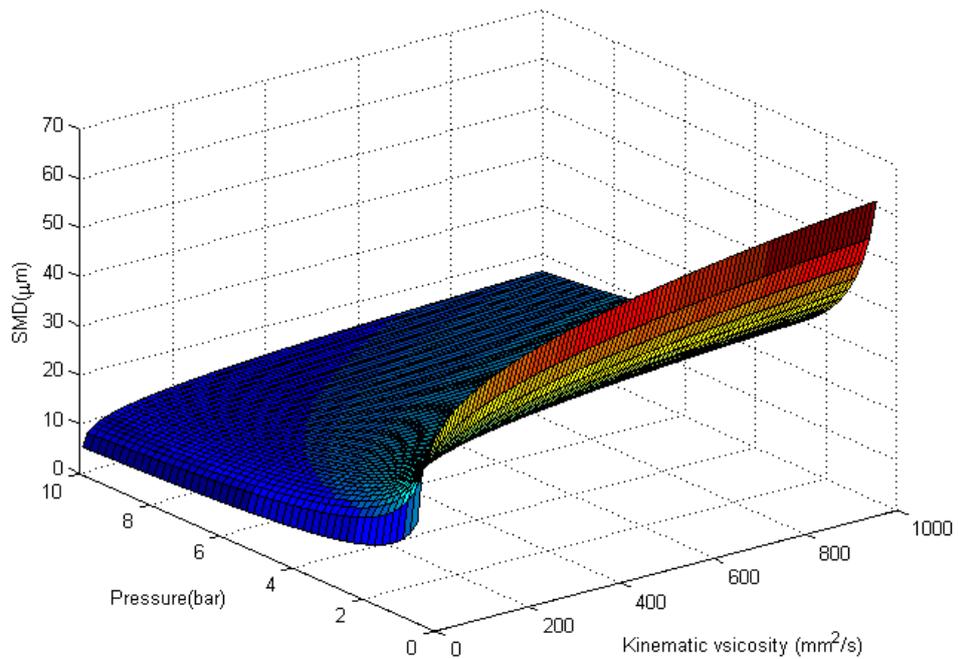


Figure 7.38 Surface plot of SMD against kinematic viscosity and pressure with constant mass flow rate and surface tension for two existing SMD correlations

$$SMD = 2.03\vartheta^{0.12}\sigma^{0.08}\dot{m}_l{}^{0.06}\Delta p_l{}^{-0.42}$$
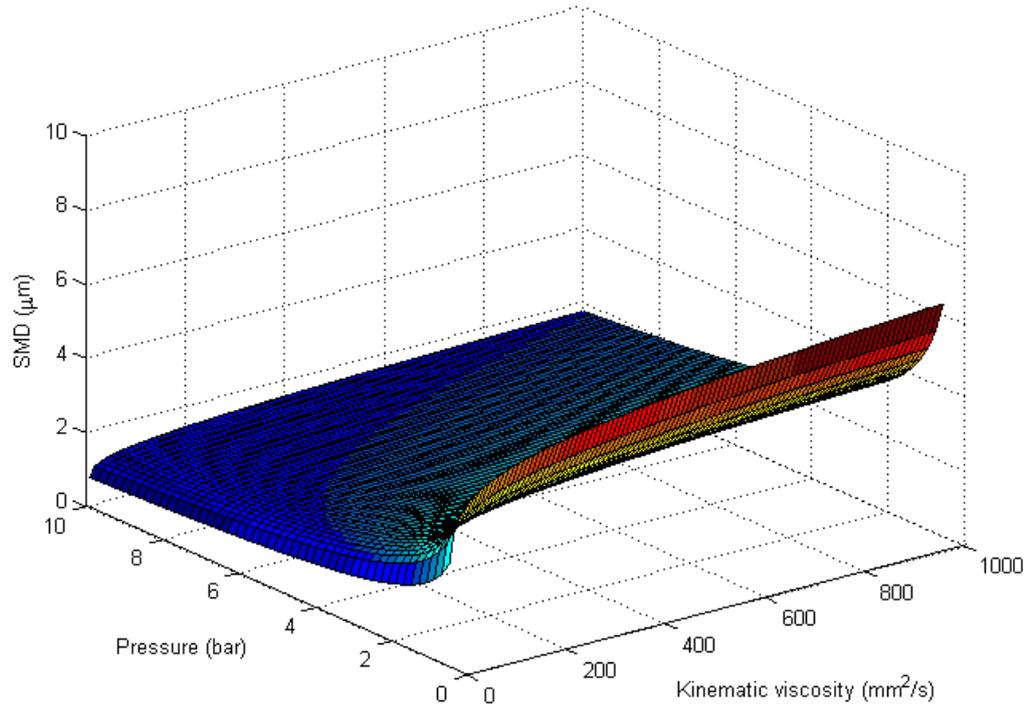


Figure 7.39 Surface plot of SMD against kinematic viscosity and pressure with constant mass flow rate and surface tension for the new SMD correlation

Figure 7.38 and Figure 7.39 present the surface plot of SMD against kinematic viscosity and pressure with holding the parameters of mass flow rate and surface tension in SMD correlations constant. The continuous variables for pressure are generated between 0.5 and 10 bars based on the operating conditions of pressure swirl nozzles indicated by PNR Ltd in the user manual and the kinematic viscosity lies within 1 mm²/s and 1000 mm²/s. The average constant surface tension value is taken as 47.5 mNm$^{-1}$ and the hold value for the mass flow rate is 0.0074 kg/s. From the three plots similar profiles were observed and the response surface for these predictors for the new fitted model was less than those in the existing SMD correlations. The results also show the peak SMD for this combination and conditions is in the upper right corner of the plot and occurs at lower value of pressure at 0.5 bar and highest value of 1000 mm²/s for the kinematic viscosity. With these results on these conditions, the local minimum SMDs are expected to emanate from pressure swirl nozzle with liquids with higher viscosity operating under lower pressure conditions.

182

Surface Plot of SMD vs Kinematic viscosity and Mass flow rate

Radcliffe $SMD = 7.3\vartheta^{0.2}\sigma^{0.6}\dot{m}_\mathrm{l}^{0.25}\Delta p_\mathrm{l}^{-0.4}$



Jasuja $SMD = 4.4\vartheta^{0.16}\sigma^{0.6}\dot{m}_\mathrm{l}^{0.22}\Delta p_\mathrm{l}^{-0.43}$



Figure 7.40 Surface plot of SMD against kinematic viscosity and mass flow rate with constant operating condition and surface tension for two existing SMD correlations

$$SMD = 2.03\vartheta^{0.12}\sigma^{0.08}\dot{m}_l{}^{0.06}\Delta p_l{}^{-0.42}$$
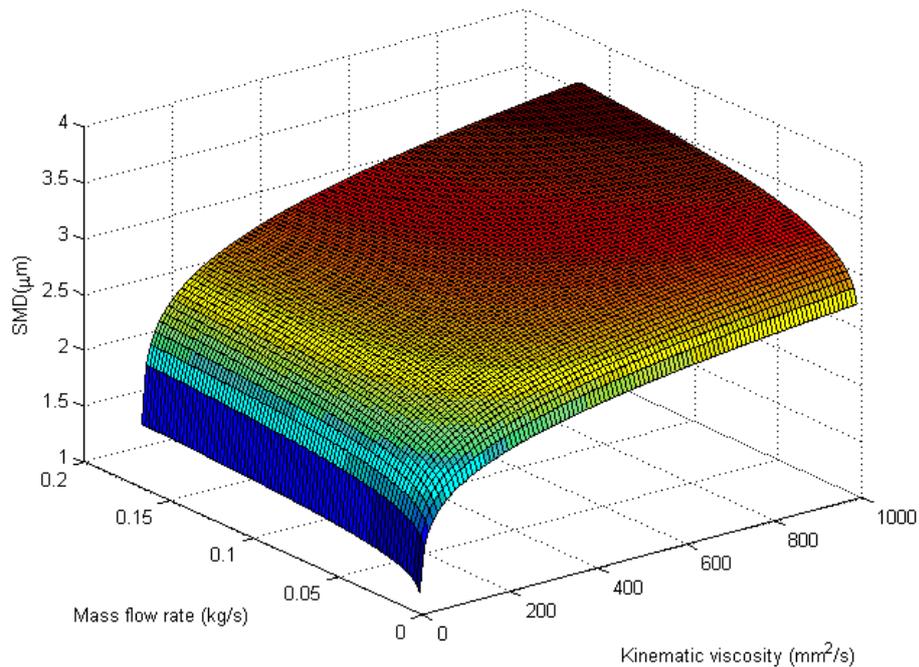


Figure 7.41 Surface plot of SMD against kinematic viscosity and mass flow rate with constant operating condition and surface tension for the new SMD correlation

Figure 7.40 and Figure 7.41 demonstrate the surface plot of SMD against kinematic viscosity and mass flow rate with constant pressure operating condition and surface tension for the new and existing SMD correlations. The minimum and maximum values for mass rate flow are 0.0017 kg/s and 0.1667 kg/s respectively and were taken from the user manual for nozzles by PNR Ltd at constant pressure of 3 bars. The hold value for the liquid property is assumed as 47.5 mNm$^{-1}$ for surface tension.and the boundary for the design space for kinematic viscosity ranges from 1 mm$^2$/s to 1000 mm$^2$/s.

The plot in Figure 7.41 shows how the response variable, the SMD, relates to two of the four predictors or components based on the new fitted model SMD correlation. As indicated, the surface plot can only show three variables at a time, while holding the other two components at a constant level. The SMD observed on the plots are only valid for these fixed levels of these input variables. The plots show the same general trends and profiles for the existing and new SMD correlations and maximum droplet sizes are expected from a nozzle of higher flow rate with denser liquids based on these input conditions.

Surface Plot of SMD vs Surface tension and Mass flow rate

Radcliffe $SMD = 7.3\vartheta^{0.2}\sigma^{0.6}\dot{m}_l^{0.25}\Delta p_l^{-0.4}$
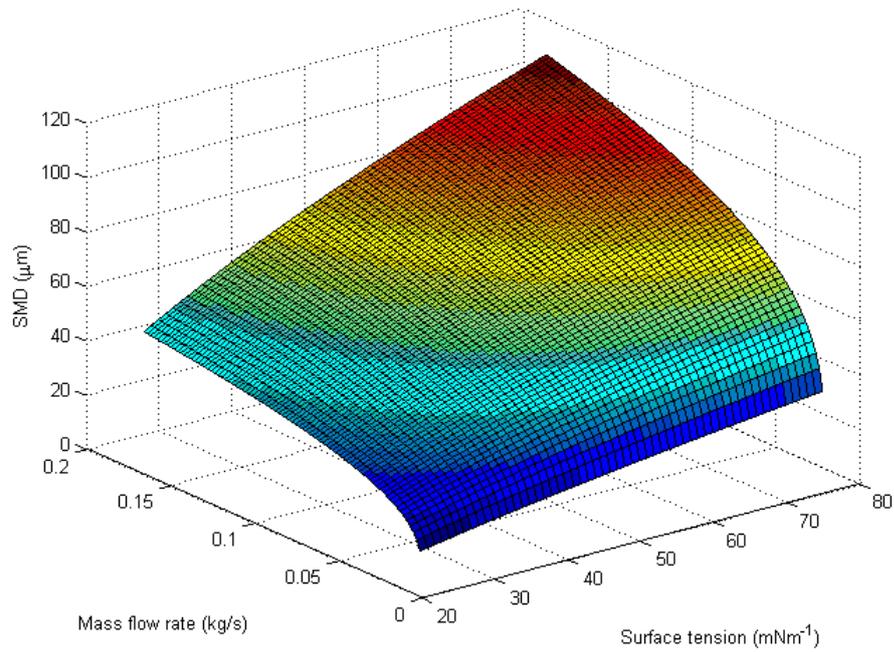


Jasuja $SMD = 4.4\vartheta^{0.16}\sigma^{0.6}\dot{m}_l^{0.22}\Delta p_l^{-0.43}$
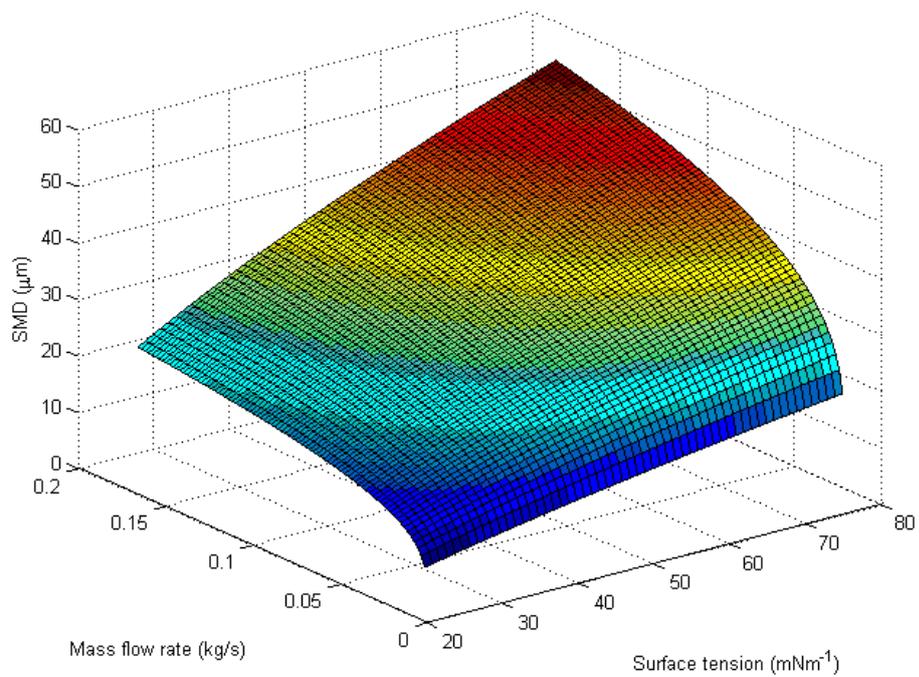


Figure 7.42 Surface plot of SMD against surface tension and mass flow rate with constant operating condition and kinematic viscosity for two existing SMD correlations

$$SMD = 2.03\vartheta^{0.12}\sigma^{0.08}\dot{m}_l{}^{0.06}\Delta p_l{}^{-0.42}$$
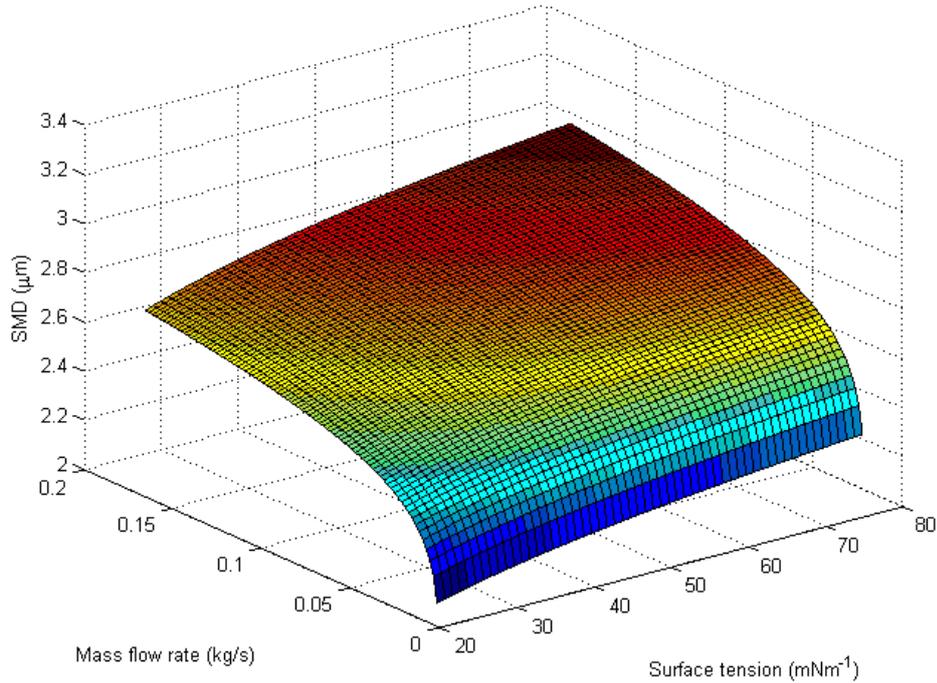


Figure 7.43 Surface plot of SMD against surface tension and mass flow rate with constant operating condition and kinematic viscosity for the new SMD correlation

The 3D surface plots of SMD against surface tension and mass flow rate with constant pressure operating condition and kinematic viscosity for SMD correlations are shown in Figure 7.42 and Figure 7.43. The Figures show a smooth curve response surface which were generated from these continuous predictors: $0.0017 \leq \dot{m} \leq 0.1667$ for mass flow rate, $20 \leq \sigma \leq 75$ for surface tension, hold values of 3 bars and 200 mm$^2$/s for pressure and viscosity respectively. The maximum value for the response surface is observed at the upper left corner of the plot and corresponds with highest combined input values for mass flow rate and surface tension. The lowest values of mass flow rate and surface tension based on the model constant parameters will result in producing smaller SMDs by pressure swirl nozzle. The resulting surface response for the new fitted model is lower than the SMD for the existing correlations as expected and consistent with the previous results and the general shape of the new model is similar to the existing ones.

Surface Plot of SMD vs Pressure and Surface tension

Radcliffe $SMD = 7.3\vartheta^{0.2}\sigma^{0.6}\dot{m}_{\mathrm{l}}^{0.25}\Delta p_{\mathrm{l}}^{-0.4}$
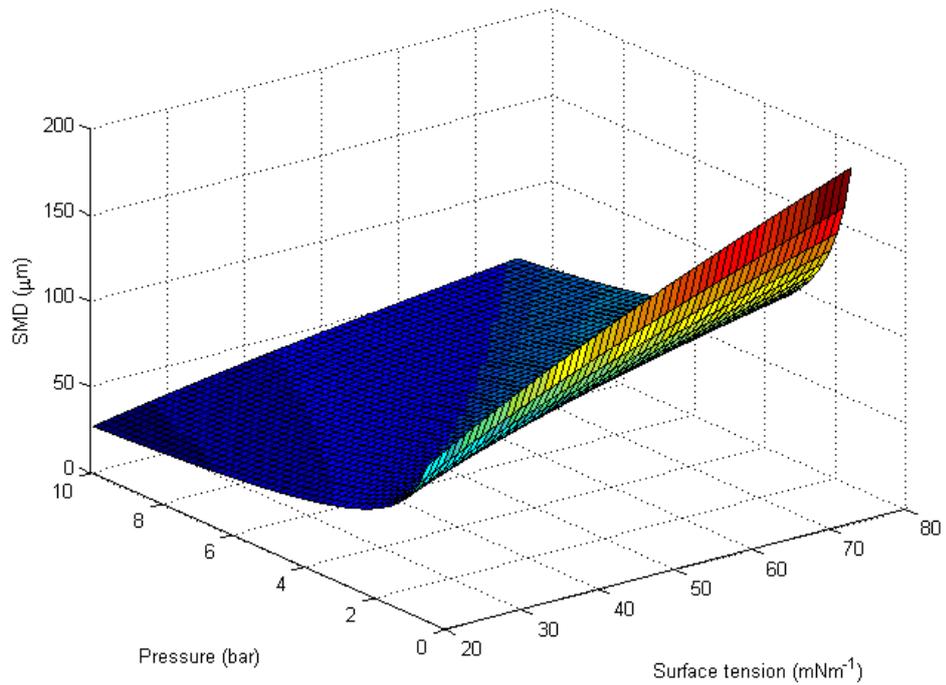


Jasuja $SMD = 4.4\vartheta^{0.16}\sigma^{0.6}\dot{m}_{\mathrm{l}}^{0.22}\Delta p_{\mathrm{l}}^{-0.43}$
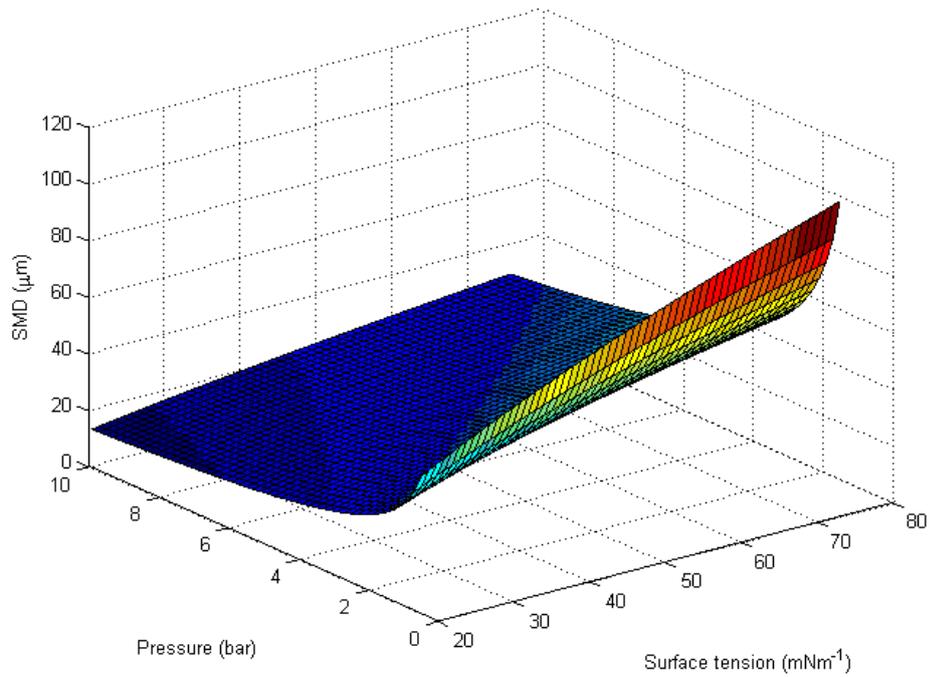


Figure 7.44 Surface plot of SMD against surface tension and pressure with constant mass flow rate and kinematic viscosity for two existing SMD correlations

187

$$SMD = 2.03\vartheta^{0.12}\sigma^{0.08}\dot{m}_l{}^{0.06}\Delta p_l{}^{-0.42}$$
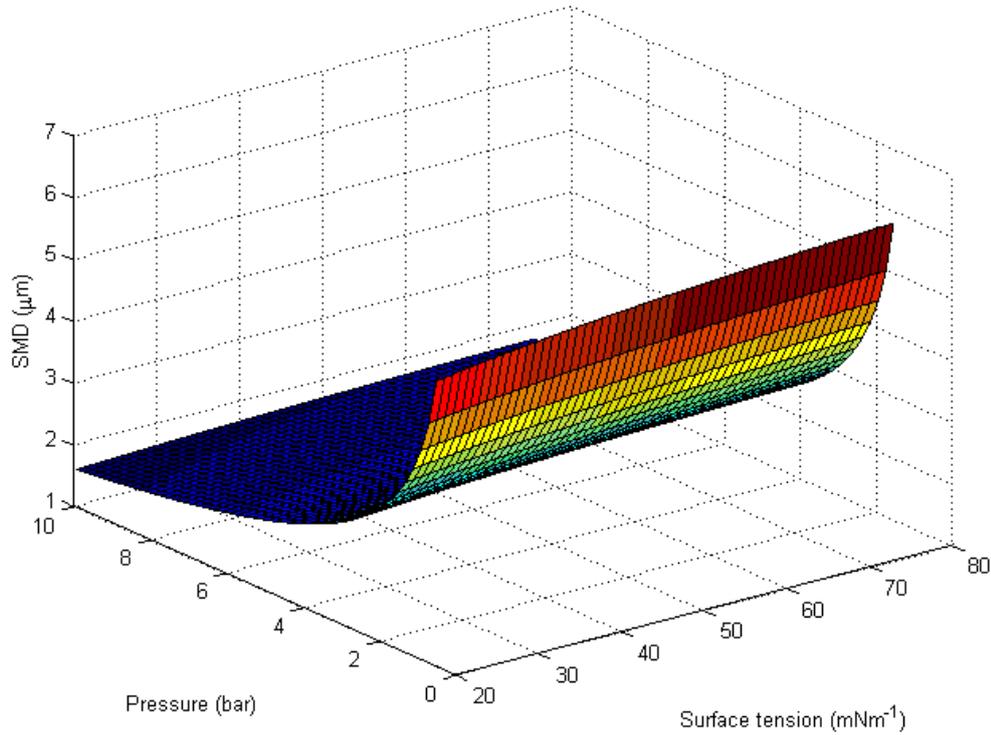


Figure 7.45 Surface plot of SMD against surface tension and pressure with constant mass flow rate and  kinematic viscosity for the new SMD correlation

Figure 7.44 and Figure 7.45 illustrate surface plot of SMD against surface tension and pressure with constant mass flow rate and kinematic viscosity for the SMD correlations. The boundaries of the design space are $0.5 \leq \Delta P \leq 10$ bars and $20 \leq \sigma \leq 75$ mNm$^{-1}$ for pressure and surface tension respectively and 3D surface plot hows how the response variable the droplet Saute Mean Diameter (SMD) relates to these two predictor variables. The results show that the peaks of the SMDs correspond with combinations of lower pressure operating condition and liquid with higher surface tension and verse versa for the local minimum for the SMDs. These optimum results were obtained for the fitted model equations with hold on values for average viscosity and flow rate as 200 mm$^2$/s and 0.084 kg/s respectively.

Surface Plot of SMD vs Pressure and Mass flow rate

Radcliffe $SMD = 7.3\vartheta^{0.2}\sigma^{0.6}\dot{m}_l^{0.25}\Delta p_l^{-0.4}$
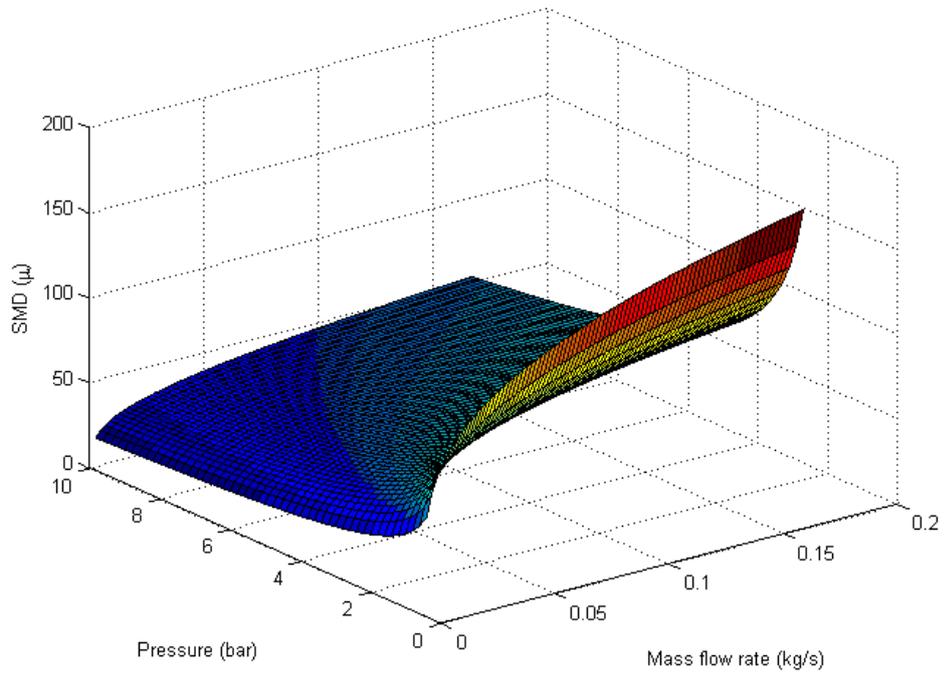


Jasuja $SMD = 4.4\vartheta^{0.16}\sigma^{0.6}\dot{m}_l^{0.22}\Delta p_l^{-0.43}$
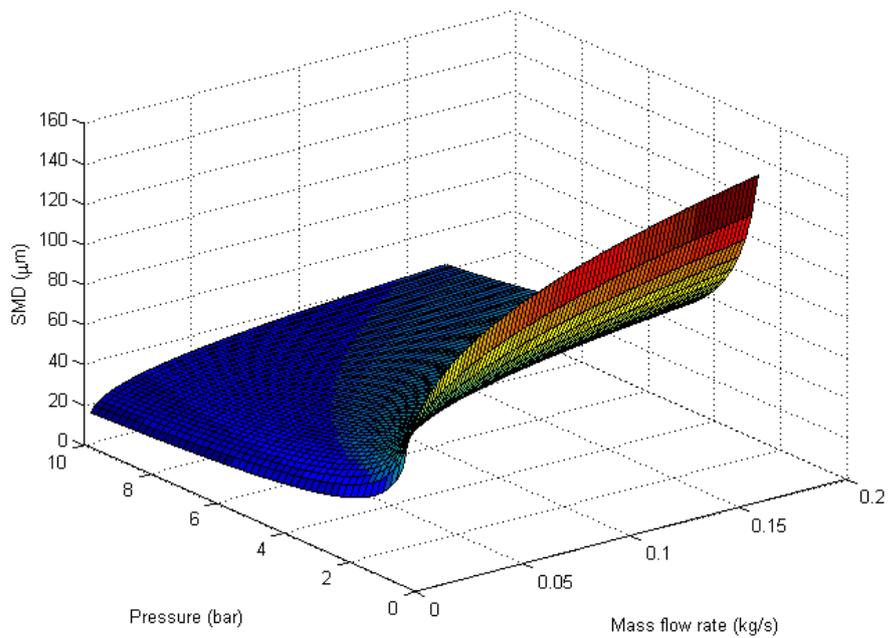


Figure 7.46 Surface plot of SMD against two operating conditions with constant liquid properties for two existing SMD correlations

$$SMD = 2.03\vartheta^{0.12}\sigma^{0.08}\dot{m}_l^{0.06}\Delta p_l^{-0.42}$$
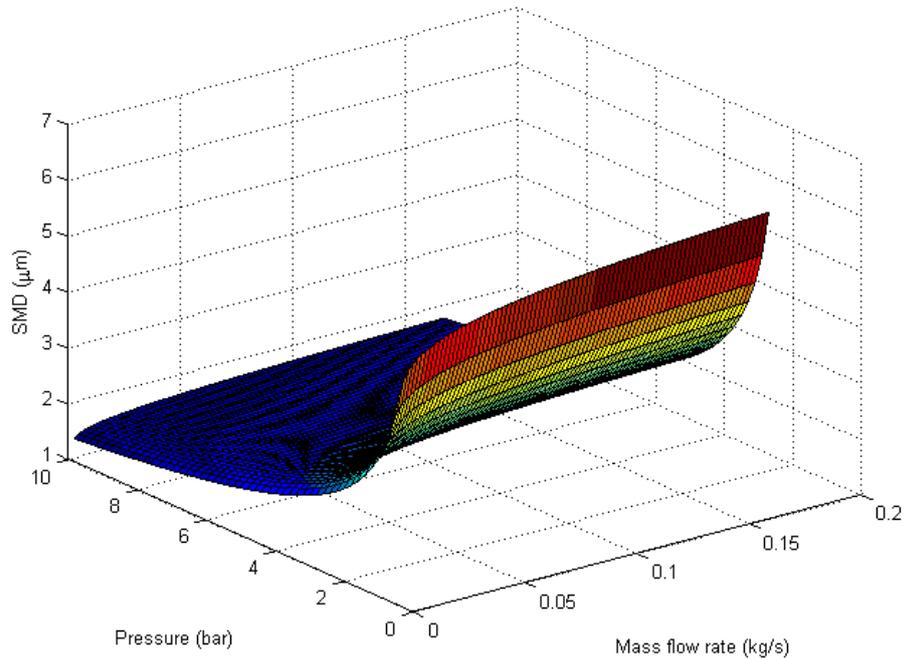


Figure 7.47 Surface plot of SMD against two operating conditions with constant liquid properties for the new SMD correlation

The surface plots in Figure 7.46 and Figure 7.47 show the relationship between two operating conditions, pressure and mass flow rate, which are one of the most parameters used in selecting a nozzle and the output SMDs or the response surface for these SMD correlations. The liquids properties such as viscosity and surface tension are the hold values. These combinations are worth analysing because for a particular liquid these liquid properties are known. It can be observed from the plots that high pressure differentials and low mass flow rates result in lower droplet SMDs. However, higher SMDs are expected at higher mass flow rates and lower pressure differentials. The maximum on the plots for the three cases are 150µm, 130µm and 5.3µm respectively for the two existing and new correlations respectively. The peak on the new correlation corresponds with the highest SMD value and occurs at approximate mass flow rate of 0.1667 kg/s and pressure of 3 bars. These results are possible with liquid properties assumed at 200 mm$^2$/s and 47.5 mNm$^{-1}$ for viscosity and surface tension respectively.

## 7.16 Summary

The findings show that the SMD is smaller in the centre spread of the spray and increases with increasing radial distances. It was observed that the SMD decreases with increasing pressure but increases with axial distances. The results also show that the increase in liquid velocity leads to the increase in the droplet Sauter mean diameter (SMD). The variation in the gas velocities on the axial positions shows that the droplet SMD decreases with increasing gas velocities and for the same liquid density value the SMD increases with increasing downstream distance. The mean droplet sizes (SMD) are also found to increase with ambient air density. The influence of liquid viscosities on SMD makes SMD exhibits decreasing trend with decreasing liquid viscosity on the spray centreline and radial position. The results also show that higher surface tension values lead to the larger value of the SMD. The influence of nozzle discharge orifice 1.5, 2.5 and 3.5 mm on the mean drop sizes (SMD) shows that the SMD also tends to increase noticeably with increasing atomizer exit diameter. It was deduced from the results that at low liquid density to gas density ratio ((low $\rho_{liq}/\rho_g$) the SMD is drastically reduced. When liquid fuels were analysed the findings show that kerosene and gasoline both with low viscosities have significantly smaller SMD while more viscous diesel oil has considerably larger SMD.

When optimization was performed in order to identify the optimal nozzle exit design parameter, operating conditions and fluid properties that perform at or give the most minimum drop sizes (SMD) at the spray centre line, the results show that case 17 generated the most minimum SMD at axial position 20 mm and 40 mm from the nozzle exit. Case 1 was the most minimum SMD at locations 60 mm, 80 mm and 100 mm from the nozzle exit and case 24 gives the best minimum from the nozzle exit at axial distance 120 mm. The findings reveal that low values of operating conditions, nozzle exit diameters and fluid properties play significant effect in the remarkable reduction in the size of the droplet SMDs at these positions. The findings also establish a new SMD correlation for the model which is found to be consistent with the existing correlations and has high dependencies on the liquid viscosity and pressure differential. The results also show that the response surfaces of the new correlation exhibit similar trend and shape with the existing correlations for the various combinations of liquid properties and operating conditions and thus the SMDs were smaller than those for the two existing correlations for the same conditions and constraints

# CHAPTER 8 CONCLUSIONS AND DETAILED ASSESSMENT OF MODEL

## 8.1 Introduction

In this chapter, a summary of the major points is presented and then thoroughly discussed in more details.

## 8.2 Summary of the major points

In this work, $\Sigma - Y_{liq}$ atomisation model has been validated and applied to sprays from pressure-swirl atomizer using the CFD commercial code STAR-CD. This entirely Eulerian model proposed by Vallet et al [23] has some unique features and capabilities. This model can characterise the atomization from the inside of the atomizer through to its primary break-up and secondary atomization by providing information on the mean velocities, fluid properties, turbulence properties droplet size $d_{32}$, droplet number density, liquid mass fraction and the interphase surface density between the liquid and gas. These properties are achieved by using a single set of equations for the conservation of mass, momentum and turbulence model treating both phases as a single continuum with high density variation, large Weber and Reynolds numbers. Thus the model is quite easier than the Lagrangian spray model which requires the knowledge and the input of velocity profile, droplet size and distributions of the spray before it can be modelled for further atomization especially the secondary break-up to be analysed. This means that Lagrangian model is not good in predicting the atomization characteristics at the primary break-up regime. In addition, the two-fluid Eulerian-Eulerian model where different sets of equations are used to describe the continuity, momentum and turbulence model both the dispersed and continuous phase is also difficult to model and computationally expensive. Therefore, the need for validation and assessment of the atomization capabilities of the $\Sigma - Y_{liq}$ atomization model.

The model principally makes use of transport equation for the development of surface tension density ($\Sigma$) to characterize the rate at which surface tension energy is created. A second transport equation tracking the transport of liquid mass fraction ($Y_{liq}$) models the turbulent mixing of liquid. With knowledge of a local interfacial surface area and liquid mass fraction, the Sauter mean diameter SMD is then characterized. The predictive potential of the model has been evaluated by performing simulations in a designed pressure swirl atomizer which show results for turbulence, flow fields and droplet size (SMD) with reasonable order-of-magnitude.

In order to achieve the desired outcome for better understanding of the physics behind the model, the SIMPLE and PISO algorithms in the CFD code to achieve appropriate pressure-velocity coupling were analysed and the properties and scalars such as average density, local velocity and turbulence model were compared. The standard k-epsilon turbulence in the code was also utilised since it gives the best match with the experimental results.

The validation of this model was performed by the experimental data obtained from the measurements carried out using the Malvern Spraytec for drop size measurement and characterization. A very good agreement was achieved between the model prediction and experimental measurements of the droplet sizes (SMD) at the near-field of the nozzle. The validations confirmed the model capabilities of predicting the droplet Sauter mean diameter (SMD) with the correct order of magnitudes.

In addition, parametric studies were also carried out to explore and analyse some exponential dependency and the influence of Sauter Mean diameter (SMD) on liquid and gas densities, liquid and gas velocities. These were also found to be in reasonably good agreement with some of the empirical correlations for Sauter Mean Diameter (SMD) for pressure swirl atomizer along the spray centreline. In addition, different liquid viscosities, surface tension forces, and nozzle exit orifice sizes were also simulated and analysed for the $\Sigma - Y_{liq}$ atomisation model in order to observe their effects on the SMD. Typical ranges of values found in a wide range of spray applications or conditions were used. It was noted that these three parameters viscosity, surface tension and nozzle exit orifice have reduction effects on the SMD as their values decreased for the range of values considered.

There was also analysis on variants of RANS-based turbulence models such as the standard, RNG, and realizable k-epsilon turbulence models and it was observed that the standard k-epsilon turbulence model has the best configuration or match with the experimental results. This also confirms the usage and adoption of this variant of k-epsilon turbulence model in developing this atomization model. In the same analysis, 10% of turbulent intensity was utilised after comparing it with the effect of 5% and 20% intensities on the SMD at the axial positions along the spray.

Liquid core lengths were also analysed to give the qualitative view of the break-up length in the primary atomization regime and it was observed that the core lengths decrease with increasing liquid density for pressure swirl atomizer.

To further assess the capabilities of this $\Sigma - Y_{liq}$ atomization model, optimization technique was performed on the model in the pressure swirl atomizer to achieve the objective of the combination of geometrical designed variables, fluid properties and operating conditions that produce or give the most minimum Sauter Mean diameter (SMD) at the axial positions on the spray centre line. These 4-factor Design of Experiments (DoE) points were mapped and uniformly distributed using the modified Latin hypercube designs (LHD) code resulting in eighty seven (87) design cases. It was realised after simulating that lower fluid properties and exit orifice diameter were the design variables that produced the most minimum and remarkable reduction in the SMD at the axial locations downstream the nozzle.

In order to establish a usable and new SMD correlation for the model based on 4-factor Design of Experiments (DoE), Matlab Isqcurvefit code in the optimization tool box was used to fit the data with experimental constants approximately obtained with the normal of the residuals (resnorm) representing the measure of the goodness of fit.

The SMD correlation for the model showed that for given fluid properties and nozzle operating conditions the SMD could easily be computed and known. This would also serve as a reference or benchmark for researchers working to improve on this model and within these fluid properties, operating conditions and nozzle geometrical regimes considered.

## 8.3 Conclusions in detail and Assessment of Model

In chapter 5, $\Sigma - Y_{liq}$ atomization model was applied to sprays emanating from pressure swirl atomizer using finite volume method implemented in the Star-CD code to capture the features and atomization characteristics of the spray. It was shown that high-density variation between the liquid and the gas, which is one of the critical requirements of this model, was achieved and the contour plots of these variations on the vertical plane in the computational domain for the SIMPLE and PISO algorithms showed negligible difference between the two results. It was also observed qualitatively that the contour plots of the velocity on the vertical plane in both cases showed that the velocity in the centre spread of the spray decreases with the downstream distance and varies appreciably from the centre to the outer radius of the spray. It was also shown that the standard k-epsilon turbulence model was adequate for this model though some recirculation zones are observed close to the walls in the swirl chamber and as such the turbulent kinetic energy resulted in very low turbulent kinetic energy observed in the centre spread of the spray. The interfacial surface density modelled across four sections in the spray qualitatively showed similar scalar scenes of the liquid mass fraction at the same axial locations and hollow cone sprays were clearly visible. It was observed on the spray axis that the mean liquid mass fraction decreases downstream the sprays.

**SMD on axial distances**: Many features of atomization characteristics especially the SMD which is the main output of this model was analysed since its determination is an important input parameter for efficient combustion for internal combustion engines related applications as larger SMD will produce more pollutants (oxides of nitrogen, carbon monoxide) in the exhaust emissions. As such when the SMDs were predicted at the axial positions on the spray centre line, it was observed that SMDs in close proximity to the nozzle exit after the disintegration of the liquid sheet were smaller than the ones near the far field of the spray. Thus it was deduced that the SMDs increase with increasing axial distances on the spray symmetry line. This was attributed to the collisions of smaller droplets giving rise to droplet coalescing at the downstream of the spray which was accounted for in the model. It was also observed that the model predicted droplet size with the correct order of magnitudes.

**SMD on radial positions**: In the case of prediction of SMD on the radial positions in the spray, it was observed that higher droplet SMDs were seen at the periphery of the

spray while the smaller ones were more dominant in the vicinity of the centre portion of the spray. It was concluded that SMDs vary with the radial positions of the sprays emanating from the pressure swirl atomizer. This was attributed to the aerodynamic force which tends to drag the smaller droplets towards the centre while the larger droplets resulting from the droplet coalescence which are less affected by this force remain at the outer periphery of the spray.

In terms of experimental measurement in order to obtain unique data to validate the numerical results, the findings showed after measurements were taken beyond 50 mm from the tip of the nozzle that arithmetic mean diameter $d_{10}$ showed the least drop size and lower than the Sauter mean diameter $d_{32}$ while the De Broukere diameter, $d_{43}$ recorded the highest drop size values measured in the four axial distances consider in the spray centre line. It was also noted in the mean drop size characterization that the Sauter mean diameter $d_{32}$ was far lower than the mass median diameter $d_{50}$ and increase with the axial positions of the spray.

When the experimental data was obtained for the SMDs in the radial positions it was also noted that the SMD from the spray centre line showed an increase in the drop sizes as the radial distance increases towards the periphery. This is because small droplets will follow the mean gas motion which drives them to the spray centreline. Larger droplets are less affected by the air entrainment. In terms of variation of injection pressure on the SMD at the axial positions, the SMD was found to have decreased with increase in pressure. This was due to the faster maximum growth rate of the liquid film as the pressure increases and which will lead to the linear stability of the surface wave of the thread film getting worse. This will eventually give rise to stronger interaction between the liquid phase and the gas phase and therefore make the film breaks up more easily. This will make the droplet SMD smaller. The same finding was observed for the increase in the liquid flow rate and was concluded that there was a linear relationship between the pressure and the flow rate of the nozzle and the two have the same effect on the SMD. With regard to the experimental observation of the effect of two different nozzle exit orifice diameters on the SMD at the spray centre locations, the findings showed that the nozzle with small orifice diameter exhibited smaller SMDs than the big nozzle and the liquid sheet lengths beyond which meaningful drops measurement could be obtained were different for the two nozzles with the length of the smaller one far below the big one.

In terms of drop size distributions at radial positions as measured and processed by Malvern Spraytech software, it was noted that the drop size distribution showed an increase in droplet formation through the spray downstream distances and become more uniform. The distribution curves of droplets' size become more flat and its maximum value decreased and moved to bigger drop sizes.

To enhance the understanding of the liquid sheet instability and liquid film breakup mechanisms against the pressure differential, visualisation was done using fast shutter camera and it was noted that a well-defined hollow-cone spray was captured and that the spray angle increased when the pressure differential increased and the liquid film length was reduced.

**K-epsilon turbulence models on SMD:** It was observed that the standard k-epsilon turbulence model utilized in this model was the best model when compared to the RNG and Realizable K-epsilon turbulence models since it tends to produce the smallest SMD and the best match with the experimental results. However, when the turbulent intensity decay was observed along the axial position by comparing the standard k-epsilon and RNG k-epsilon turbulence models, the standard k-epsilon model predicted a higher decay in the average turbulent intensity as compared to RNG k-epsilon model. In addition, it was noted however that the model could not show much difference in the droplet velocity when the three k-epsilon turbulence models were compared.

**Validation of SMD:** When the validation of Sauter Mean Diameter (SMD) at radial positions was performed at y=60 mm it was realised that a very good agreement was achieved but the rate of change was too small with the SMD of the large droplets found on the periphery of the spray under predicted and the small mean drop sizes at the vicinity of the spray centreline perfectly predicted. At axial position of 80 mm from the exit of the nozzle, the agreement between the model and experimental results was satisfactory with a good prediction of the droplet size at the spray periphery. There was also a good agreement between the model and the measurement at 100 mm downstream of the nozzle with the predicted SMD having an average of 3% under prediction at the radial position. In addition, it was observed that the radial profiles for the SMDs at the axial position 120 mm from the exit of the nozzle were closer between the calculations and the experiments with the SMD being smaller near the spray centre line which was attributed to the competition between turbulent dispersion and entrainment of air by the hollow cone spray.

It was also demonstrated and shown that the model also agreed with measurements when the validation of SMD was evaluated on the spray centreline of the nozzle. In all, it was concluded that the computational predictions of SMD for the $\Sigma - Y_{liq}$ atomization model showed good validation with the experimental measurements.

When the parametric study was performed to investigate and confirm the dependency of SMD on radial distances, it was observed that the results of SMD was smaller in the centre spread of the spray and increased with increasing radial distances. This observation was consistent at the axial distances 60mm, 80mm, 100mm and 120mm downstream the nozzle exit. It was also noted with the same vertical heights and at x = 0 that the farther the distance from the exit of the nozzle the larger the SMD on the spray centre line.

When the dependency of SMD was observed on the vertical positions in the spray, since this is very critical in combustion applications especially in the internal combustion engines where space is limited and the atomizer needs to perform well at very short distances, it was observed that the SMD increased with axial distances but decreased with increasing pressure and flow rate. However, this higher pressure produced or increased the droplet velocity.

**Injection velocity on SMD**: When the liquid velocity was increased from 1 m/s to a maximum of 6 m/s at a constant gas velocity, it was found to have a corresponding increment in the SMD evaluated in the spray centreline. However, the dependency of SMD on the gas velocity was observed to be decreasing with increasing gas velocities. This was because when gas velocity increases the total turbulent kinetic energy increases making droplet breakup into smaller droplet.

**Exponential dependency of SMD on fluid properties**: The density of the liquid was varied from the range of 1000 to 50 kg/m³. The general profile of the results showed that for a particular position on the spray centreline the SMD was lower for smaller liquid density values and increased with higher liquid densities. It was also noted that the calculated exponent was found to have a reasonably close agreement with the empirical correlations for the pressure swirl atomizer at the spray centre line. For the effect of gas density on SMD, it was observed that the gas density increases with the droplet Sauter Mean Diameter (SMD) and was this consistent with the observation made by Lefebvre in analysing this parameter on centreline of sprays from pressure swirl atomizers. It was also found that for various liquid densities the liquid core

lengths was different and thus for higher liquid density the length was longer and vice versa.

**Dependency of Sauter mean diameter (SMD) on the liquid viscosity.** The results confirmed the adverse effect of an increase in liquid viscosity on atomization quality in particular on the SMD and thus decrease with decreasing SMD. When the influence of liquid viscosities of water at various temperatures were observed, it was clearly seen that at the temperature of 90°C for water, its viscosity was smaller than its corresponding viscosity at the temperature of 20 °C. This invariably affected the SMD and thus decreased it at high temperatures for the liquid water.

**Dependency of Sauter mean diameter (SMD) on the surface tension:** When the effect of surface tension on the Sauter mean diameter (SMD) was observed, it was found that higher surface tension values led to larger value of the SMD. Since the surface tension coefficient shows up in the destruction term of the transport equation for the mean interfacial surface density the reduction of the surface tension force will cause destruction reduction in the mean liquid and gas interface density and as a result reduce the Sauter mean diameter (SMD) of the droplets.

**SMD variation with injection velocity and density ratio:** It was seen that the SMD decreased rapidly with increasing injection velocity for low density ratios. This was attributed to the fact that with higher gas densities  the interaction between the droplets and the air is much higher, therefore the air does more work on the mean drop sizes (SMDs)  and breaks the droplets apart.

**SMD on nozzle exit diameter:** It was evident from the result that the SMD also tended to increase noticeably with increase in atomizer exit orifice diameter. This result was expected because the larger the exit orifice the larger the initial sheet thickness and SMD for pressure-swirl atomizers will tend to scale with the initial sheet thickness and therefore increase the droplet (SMD).

**Effect of density ratios on turbulent quantities:** It was observed that the turbulent intensity increased with increasing density ratios but the turbulent length scale rather increased with decreasing density ratios. Large density variations on the integral length scale were  seen downstream of the spray on the spray centre line.

**SMD of diesel, gasoline and kerosene:** It was noted that gasoline with the lowest viscosity has the highest axial velocity in the spray centre. On the other hand, diesel fuel with the highest viscosity has the smallest axial velocity on the centre spread of the

spray and the mean velocity of kerosene was found to be in the middle of the two liquids. Kerosene and gasoline both with low viscosities have significantly smaller SMD while more viscous diesel fuel has considerably larger SMD.

**Optimization for minimum SMD on spray centreline:** In achieving this result, 4-factor design of experiment (DoE) resulting in eighty-seven (87) cases were generated using Latin Hypercube Designs (LHD). When the combinatorial optimization was performed in order to obtain the most minimum droplet Sauter mean diameter (SMD) at the various locations on the spray centre line for a wide range of variations and combinations of liquid viscosity, surface tension, nozzle exit diameter and liquid velocity, it was observed that case 17 generated the most minimum SMD at axial positions 20 mm and 40 mm from the nozzle exit, case 1 was the most minimum SMD at locations 60 mm, 80 mm and 100 mm from the nozzle exit and case 24 gave the best minimum from the nozzle exit at axial distance 120 mm. It was concluded that this optimization led to significant reduction in the size of the droplet SMD and makes this atomization model more suited and applicable to a wide range of spray application areas.

**SMD correlation for $\Sigma - Y_{liq}$ atomisation model:** In order to establish a novel SMD correlation of the model and compare the experimental constants in the correlation with the existing SMD correlations such as Jasuja and Radcliffe based on 4-factor design of experiments (DoE), Matlab Isqcurvefit code in the optimization tool box was used to fit the data. The experimental constants on the kinematic viscosity and pressure differential were well predicted but disparities were observed in the experimental constants on the surface tension and mass flow rate when compared to the two existing correlations. These differences were attributed to the range of values used for the liquid properties and the difficulties in adequately capturing surface tension in the model.

To further assess the new SMD correlation for $\Sigma - Y_{liq}$ atomisation model, surface plots of various combinations of the predictor variables against SMD with typical values were performed. It was observed that in all cases the response variables for the new SMD model were smaller when compared to the two existing SMD correlations.

In all based on computational assessment and experimental validation performed, the $\Sigma - Y_{liq}$ atomisation model is very good in predicting and capturing most important features of the primary atomization such as droplet SMDs, mean velocities, turbulent kinetic energy and liquid core length. The model also proves to be a versatile one since

it can accommodate a wide range of variations for spray input parameters and generate any size of the output atomization characteristics in particular SMD so desired and required. The model is able to establish a usable SMD correlation which is consistent with existing correlations and will serve as a reference or benchmark for further assessment of this model by researchers.

**Reference**

1.     Lefebvre, A. and V. McDonell, *Atomization and sprays*. second ed. Vol. 1040. 2017: CRC press.

2.     Lefebvre, A.H. and D. Hallal, *Gas Turbine Alternative Fuels and Emissions*. CRC, Boca Raton, FL, 2010.

3.     Bayvel, L. and Z. Orzechowski, *Liquid Atomization, Combustion: An International Series*. 1993, Taylor & Francis.

4.     Dombrowski, N. and D. Hasson, *The flow characteristics of swirl (centrifugal) spray pressure nozzles with low viscosity liquids*. AIChE Journal, 1969. **15**(4): p. 604-611.

5.     Horvay, M. and W. Leuckel, *Experimental and theoretical investigation of swirl nozzles for pressure-jet atomization*. German chemical engineering, 1986. **9**(5): p. 276-283.

6.     Park, K.S. and S.D. Heister, *Nonlinear modeling of drop size distributions produced by pressure-swirl atomizers*. International Journal of Multiphase Flow, 2010. **36**(1): p. 1-12.

7.     Lefebvre, A. and X. Wang, *Mean drop sizes from pressure-swirl nozzles*. Journal of propulsion and power, 1987. **3**(1): p. 11-18.

8.     Rizk, N. and A.H. Lefebvre, *Internal flow characteristics of simplex swirl atomizers*. Journal of Propulsion and Power, 1985. **1**(3): p. 193-199.

9.     Rho, B.-J., S.-J. Kang, J.-H. Oh, and S.-G. Lee, *Swirl effect on the spray characteristics of a twin-fluid jet*. KSME International Journal, 1998. **12**(5): p. 899-906.

10.    De Corso, S. and G. Kemeny, *Effect of ambient and fuel pressure on nozzle spray angle*. Trans. ASME, 1957. **79**(3): p. 607-615.

11.    Neya, K. and S. Satô, *Effect of ambient air pressure on the spray characteristics of swirl atomizers*. 1968: Ship Research Institute.

12.    Ortman, J. and A. Lefebvre, *Fuel distributions from pressure-swirl atomizers*. AIAA Journal of Propulsion and Power, 1985. **1**(1): p. 11-15.

13. Dodge, L. and J. Biaglow, *Effect of elevated temperature and pressure on sprays from simplex swirl atomizers.* ASME, Transactions, Journal of Engineering for Gas Turbines and Power, 1986. **108**: p. 209-215.

14. Belhadef, A., A. Vallet, M. Amielh, and F. Anselmet, *Pressure-swirl atomization: Modeling and experimental approaches.* International Journal of Multiphase Flow, 2012. **39**: p. 13-20.

15. Emekwuru, N. and A.P. Watkins, *Analysis of a two-fluid sprayer and its use to develop the number size distribution moments spray model, Part II: Computational Analysis.* Atomization and Sprays, 2010. **20**(8): p. 653-672.

16. Datta, A. and S. Som, *Numerical prediction of air core diameter, coefficient of discharge and spray cone angle of a swirl spray pressure nozzle.* International journal of heat and fluid flow, 2000. **21**(4): p. 412-419.

17. Lefebvre, A.H., *Gas turbine combustion.* 1998: CRC press.

18. Trinh, H.P., C. Chen, and M. Balasubramanyam, *Numerical simulation of liquid jet atomization including turbulence effects.* Journal of engineering for gas turbines and power, 2007. **129**(4): p. 920-928.

19. Lin, J., L. Qian, H. Xiong, and T.L. Chan, *Effects of operating conditions on droplet deposition onto surface of atomization impinging spray.* Surface and Coatings Technology, 2009. **203**(12): p. 1733-1740.

20. Xiong, H.-B., J. Lin, and Z.-F. Zhu, *Three-dimensional simulation of effervescent atomization spray.* Atomization and Sprays, 2009. **19**(1): p. 75-90.

21. Bishop, R., *Thermo-fluid dynamic theory of two-phase flow.* 1975, IOP Publishing.

22. Drew, D.A., *Mathematical modeling of two-phase flow.* Annual review of fluid mechanics, 1983. **15**(1): p. 261-291.

23. Vallet, A., Burluka, AA and R. Borghi, *Development of a Eulerian model for the "atomization" of a liquid jet.* Atomization and sprays, 2001. **11**(6): p. 619-642.

24. Khavkin, Y.I., *Theory and practice of swirl atomizers.* 2003: CRC Press.

25. Lefebvre, A.H., *Fifty years of gas turbine fuel injection.* Atomization and Sprays, 2000. **10**(3-5).

26.     Ashgriz, N., *Handbook of atomization and sprays: theory and applications.* 2011: Springer Science & Business Media.

27.     He, Z., G. Guo, X. Tao, W. Zhong, X. Leng, and Q. Wang, *Study of the effect of nozzle hole shape on internal flow and spray characteristics.* International Communications in Heat and Mass Transfer, 2016. **71**: p. 1-8.

28.     Durdina, L., J. Jedelsky, and M. Jicha, *Investigation and comparison of spray characteristics of pressure-swirl atomizers for a small-sized aircraft turbine engine.* International Journal of Heat and Mass Transfer, 2014. **78**: p. 892-900.

29.     Davanlou, A., J.D. Lee, S. Basu, and R. Kumar, *Effect of viscosity and surface tension on breakup and coalescence of bicomponent sprays.* Chemical Engineering Science, 2015. **131**: p. 243-255.

30.     Payri, R., J. Salvador, J. Gimeno, and J. De la Morena, *Analysis of diesel spray atomization by means of a near-nozzle field visualization technique.* Atomization and Sprays, 2011. **21**(9).

31.     Strutt, J.W. and L. Rayleigh, *On the instability of jets.* Proc. London Math. Soc, 1878. **10**: p. 4-13.

32.     Weber, C., *Disintegration of liquid jets.* Z. Angew. Math. Mech, 1931. **11**(2): p. 136-159.

33.     Hoyt, J.W. and J. Taylor, *Waves on water jets.* Journal of Fluid Mechanics, 1977. **83**(1): p. 119-127.

34.     Reitz, R. and F. Bracco, *Mechanism of atomization of a liquid jet.* The Physics of Fluids, 1982. **25**(10): p. 1730-1742.

35.     Reitz, R.D., *Atomization and other breakup regimes of a liquid jet.* 1978.

36.     Dumouchel, C., *On the experimental investigation on primary atomization of liquid streams.* Experiments in fluids, 2008. **45**(3): p. 371-422.

37.     Sterling, A.M. and C. Sleicher, *The instability of capillary jets.* Journal of Fluid Mechanics, 1975. **68**(3): p. 477-495.

38.     Miesse, C., *Correlation of experimental data on the disintegration of liquid jets.* Industrial & Engineering Chemistry, 1955. **47**(9): p. 1690-1701.

39. Dan, T., T. Yamamoto, J. Senda, and H. Fujimoto, *Effect of nozzle configurations for characteristics of non-reacting diesel fuel spray*. 1997, SAE Technical Paper.

40. Beheshti, N., A.A. Burluka, and M. Fairweather, *Assessment of $\Sigma- Y$ liq model predictions for air-assisted atomisation*. Theoretical and Computational Fluid Dynamics, 2007. **21**(5): p. 381-397.

41. Fraser, R., N. Dombrowski, and J. Routley, *The production of uniform liquid sheets from spinning cups*. Chemical Engineering Science, 1963. **18**(6): p. 315-321.

42. Maly, M., *Quality of Fuel Atomization from Small Pressure-Swirl Atomizers*. 2014, PhD Thesis, Brno University of Technology, Faculty of Mechanical Engineering

43. Grant, R.P. and S. Middleman, *Newtonian jet stability*. AIChE Journal, 1966. **12**(4): p. 669-678.

44. Shimizu, M., M. Arai, and H. Hiroyasu, *Measurements of breakup length in high speed jet*. Bulletin of JSME, 1984. **27**(230): p. 1709-1715.

45. Chehroudi, B., S.-H. Chen, F.V. Bracco, and Y. Onuma, *On the intact core of full-cone sprays*. 1985, SAE Technical Paper.

46. Andrews, M.J., *The large-scale fragmentation of the intact liquid core of a spray jet*. Atomization and Sprays, 1993. **3**(1).

47. Taylor, G., *Generation of ripples by wind blowing over a viscous fluid. Reprinted in The Scientific Papers of Sir Geoffrey Ingram Taylor, Vol. 3*. 1963, Cambridge Univ. Press, London.

48. Tseng, L., G. Ruff, P. Wu, and G. Faeth, *Continuous- and dispersed-phase structure of pressure-atomized sprays*. Recent advances in spray combustion: Spray combustion measurements and model simulation., 1996. **2**: p. 3-30.

49. Lefebvre, A., *The role of fuel preparation in low-emission combustion*. Journal of engineering for gas turbines and power, 1995. **117**(4): p. 617-654.

50. Rosin, P. and E. Rammler, *Regularities in the distribution of cement particles*. J Inst Fuel, 1933. **7**: p. 29-33.

51.     Rosin, P., *The laws governing the fineness of powdered coal.* J. Inst. Fuel., 1933. **7**: p. 29-36.

52.     Babinsky, E. and P. Sojka, *Modeling drop size distributions.* Progress in energy and combustion science, 2002. **28**(4): p. 303-329.

53.     Sellens, R. and T. Brzustowski, *A prediction of the drop size distribution in a spray from first principles.* Atomisation Spray Technology, 1985. **1**: p. 89-102.

54.     Xianguo, L. and R.S. TANKIN0, *Droplet size distribution: A derivation of a Nukiyama-Tanasawa type distribution function.* Combustion Science and Technology, 1987. **56**(1-3): p. 65-76.

55.     Sovani, S.D., P.E. Sojka, and Y.R. Sivathanu, *Prediction of drop size distributions from first principles: the influence of fluctuations in relative velocity and liquid physical properties.* Atomization and Sprays, 1999. **9**(2).

56.     Sovani, S.D., P.E. Sojka, and Y.R. Sivathanu, *Prediction of drop size distributions from first principles: Joint PDF effects.* Atomization and Sprays, 2000. **10**(6): p. 587-602.

57.     Sivathanu, Y. and J. Gore, *A discrete probability function method for the equation of radiative transfer.* Journal of Quantitative Spectroscopy and Radiative Transfer, 1993. **49**(3): p. 269-280.

58.     Rayleigh, L., *On the instability of jets.* Proceedings of the London mathematical society, 1878. **1**(1): p. 4-13.

59.     Goren, S.L. and M. Gottlieb, *Surface-tension-driven breakup of viscoelastic liquid threads.* Journal of Fluid Mechanics, 1982. **120**: p. 245-266.

60.     Panchagnula, M.V., P.E. Sojka, and P.J. Santangelo, *On the three-dimensional instability of a swirling, annular, inviscid liquid sheet subject to unequal gas velocities.* Physics of Fluids, 1996. **8**(12): p. 3300-3312.

61.     Ohnesorge, W.v., *Formation of drops by nozzles and the breakup of liquid jets.* Z. Angew. Math. Mech, 1936. **16**(4): p. 355-358.

62.     Radcliffe, A., *The Performance of a Type of Swirl Atomizer*.* Proceedings of the Institution of Mechanical engineers, 1955. **169**(1): p. 93-106.

63.     Jasuja, A., *Atomization of crude and residual fuel oils.* Journal of Engineering for Gas Turbines and Power, 1979. **101**(2): p. 250-258.

64.     Simmons, H., *The prediction of Sauter mean diameter for gas turbine fuel nozzles of different types.* Journal of Engineering for Gas Turbines and Power, 1980. **102**(3): p. 646-652.

65.     Babu, K.R., M. Narasimhan, and K. Narayanaswamy, *Prediction of mean drop size of fuel sprays from swirl spray atomizers.* International Journal of Turbo and Jet Engines, 1989. **6**: p. 133-141.

66.     Kennedy, J., *High Weber number SMD correlations for pressure atomizers.* Journal of engineering for gas turbines and power, 1986. **108**(1): p. 191-195.

67.     Lefebvre, A.H., *The prediction of Sauter mean diameter for simplex pressure-swirl atomisers.* Atomisation Spray Technology, 1987. **3**: p. 37-51.

68.     Wang, X. and A. Lefebvre. *Influence of ambient air pressure on pressure-swirl atomization.* in *ASME 1987 International Gas Turbine Conference and Exhibition.* 1987. American Society of Mechanical Engineers.

69.     Couto, H., J. Carvalho, and D. Bastos-Netto, *Theoretical formulation for Sauter mean diameter of pressure-swirl atomizers.* Journal of Propulsion and Power, 1997. **13**(5): p. 691-696.

70.     Musemic, E. and P. Walzel, *Swirl Atomizers with Coanda Deflection Outlets.*

71.     Elkotb, M., *Fuel atomization for spray modelling.* Progress in Energy and Combustion Science, 1982. **8**(1): p. 61-91.

72.     Tanasawa, Y., Y. Miyasaka, and M. Umehara. *Effect of shape of rotating disks and cups on liquid atomization.* in *Proceedings of the 1st International Conference on Liquid Atomization and Spray Systems.* 1978.

73.     El-Shanawany, M. and A. Lefebvre. *Airblast atomization: the effect of linear scale on mean drop size.* in *ASME 1980 International Gas Turbine Conference and Products Show.* 1980. American Society of Mechanical Engineers.

74.     Giffen, E. and A. Muraszew, *The Atomization of Liquid FuelsChapman and Hall.* 1953, London.

75.     Som, S. and G. Biswas, *Initiation of air core in a swirl nozzle using time-independent power-law fluids.* Acta mechanica, 1984. **51**(3-4): p. 179-197.

76.     Moradi, A., *Theoretical Prediction of Sauter Mean Diameter for Pressure-Swirl Atomizers through Integral Conservation Methods*. 2013: Arizona State University.

77.     Wei, X. and H. Yong, *Improved Semiempirical Correlation to Predict Sauter Mean Diameter for Pressure-Swirl Atomizer*. Journal of Propulsion and Power, 2014. **30**(6): p. 1628-1635.

78.     De Keukelaere, H., *The Internal Flow in a Swirl Atomizer Nozzle*. 1995.

79.     Hsieh, K. and R. Rajamani, *Mathematical model of the hydrocyclone based on physics of fluid flow*. AIChE Journal, 1991. **37**(5): p. 735-746.

80.     Rizk, N. and A. Lefebvre, *Influence of liquid properties on the internal flow characteristics of simplex swirl atomizers*. American Society of Mechanical Engineers, 1986. **1**.

81.     Jones, A. *Design optimization of a large pressure-jet atomizer for power plant*. in *Proceedings of the Second International Conference on Liquid Atomization and Spray Systems*. 1982.

82.     Simmons, H. and C. Harding, *Some effects of using water as a test fluid in fuel nozzle spray analysis*. Journal of Engineering for Gas Turbines and Power, 1981. **103**(1): p. 118-123.

83.     Saha, A., J.D. Lee, S. Basu, and R. Kumar, *Breakup and coalescence characteristics of a hollow cone swirling spray*. Physics of Fluids 2012. **24**(12): p. 124103.

84.     Muhammad, R., Y. Huang, and Z. Zheng, *Effect of geometric parameters on spray characteristics of pressure swirl atomizers*. International Journal of Hydrogen Energy, 2016. **41**(35): p. 15790-15799.

85.     Chinn, J., A.J. Yule, and H. De Keukelaere. *Swirl Atomizer Internal Flow: A Computational and Experimental Study*. in *12th Annual Conference of ILASS-Europe, Lund, Sweden*. 1996.

86.     Cooper, D., A. Yule, and J. Chinn. *Experimental measurements and computational predictions of the internal flow field in a pressure swirl atomizer*. in *Proc. ILASS-Europe*. 1999.

87. Yule, A. and J. Chinn, *The internal flow and exit conditions of pressure swirl atomizers.* Atomization and Sprays, 2000. **10**(2): p. 121-146.

88. Nouri-Borujerdi, A. and A. Kebriaee, *Numerical simulation of laminar and turbulent two-phase flow in pressure-swirl atomizers.* AIAA journal, 2012. **50**(10): p. 2091-2101.

89. Taylor, G.I. *The mechanics of swirl atomizers.* in *Proceedings of the Seventh International Congress for Applied Mechanics.* 1948.

90. Rizk, N. and A. Lefebvre, *Prediction of velocity coefficient and spray cone angle for simplex swirl atomizers.* International Journal of Turbo and Jet Engines, 1987. **4**(1-2): p. 65-74.

91. Lefebvre, A. and M. Suyari, *Film thickness measurements in a simplex swirl atomizer.* Journal of Propulsion and Power, 1986. **2**(6): p. 528-533.

92. Hansen, K., J. Madsen, C. Trinh, C. Ibsen, T. Solberg, and B. Hjertager, *A computational and experimental study of the internal flow in a scaled pressure-swirl atomizer.* Zaragoza, 2002. **9**: p. 11.

93. Jacobsen, C.B., *Large eddy simulation of confined swirling flow: a numerical and experimental investigation of isothermal combustion chamber flows.* 1997, Aalborg : Aalborg University: Institut for Energiteknik, Aalborg Universitet.

94. Yule, A. and J. Chinn. *Pressure swirl atomizer internal flow and performance.* in *Proceedings of the 10th annual conference on liquid atomization and spray systems ILASS, Americas.* 1997.

95. Steinthorsson, E. and D. Lee. *Numerical simulations of internal flow in a simplex atomizer.* in *ICLASS-2000.* 2000.

96. Wang, D., Z. Ma, S.-M. Jeng, and M.A. Benjamin. *Experimental study on large-scale simplex nozzle.* in *the 35th AIAA/ASME/SAE/ASEE Joint Propulsion Conference and Exhibit.* 1999.

97. Sakman, A.T., S. Jha, M. Jog, S. Jeng, and M. Benjamin, *A numerical parametric study of simplex fuel nozzle internal flow and performance.* 1998, University of Cincinnati.

98. Saha, K., S. Som, M. Battistoni, Y. Li, E. Pomraning, and P.K. Senecal, *Numerical investigation of two-phase flow evolution of in-and near-nozzle*

*regions of a gasoline direct injection engine during needle transients.* SAE International Journal of Engines, 2016. **9**(2): p. 1230-1240.

99. Arun Vijay, G., N. Shenbaga Vinayaga Moorthi, and A. Manivannan, *Internal And External Flow Characteristics Of Swirl Atomizers: A Review.* Atomization and Sprays, 2015. **25** (2): p. 153–188

100. Qin, C. and E. Loth, *Numerical description of a pressure-swirl nozzle spray.* Chemical Engineering and Processing: Process Intensification, 2016. **107**: p. 68-79.

101. Stevenin, C., A. Vallet, S. Tomas, M. Amielh, and F. Anselmet, *Eulerian atomization modeling of a pressure-atomized spray for sprinkler irrigation.* International Journal of Heat and Fluid Flow, 2016. **57**: p. 142-149.

102. Reynolds, O., *On the dynamical theory of incompressible viscous fluids and the determination of the criterion.* Philosophical Transactions of the Royal Society of London. A, 1895: p. 123-164.

103. Versteeg, H.K. and W. Malalasekera, *An introduction to computational fluid dynamics: the finite volume method*. 2007: Pearson Education.

104. Spalart, P., W. Jou, M. Strelets, and S. Allmaras, *Comments on the feasibility of LES for wings, and on a hybrid RANS/LES approach.* Advances in DNS/LES, 1997. **1**: p. 4-8.

105. Smith, A. and T. Cebeci, *Numerical Solution of the Turbulent-boundary-layer Equations*. 1967, DTIC Document.

106. Launder, B. and B. Sharma, *Application of the energy-dissipation model of turbulence to the calculation of flow near a spinning disc.* Letters in heat and mass transfer, 1974. **1**(2): p. 131-137.

107. Jones, W. and B. Launder, *The prediction of laminarization with a two-equation model of turbulence.* International journal of heat and mass transfer, 1972. **15**(2): p. 301-314.

108. Launder, B.E. and D. Spalding, *The numerical computation of turbulent flows.* Computer methods in applied mechanics and engineering, 1974. **3**(2): p. 269-289.

109.    Yakhot, V., S. Orszag, S. Thangam, T. Gatski, and C. Speziale, *Development of turbulence models for shear flows by a double expansion technique.* Physics of Fluids A: Fluid Dynamics (1989-1993), 1992. **4**(7): p. 1510-1520.

110.    Wilcox, D.C., *Reassessment of the scale-determining equation for advanced turbulence models.* AIAA journal, 1988. **26**(11): p. 1299-1310.

111.    Wilcox, D., *Turbulence Modelling for CFD, DCW Industries Inc., La Canada, California.* 1993, IBSN 0-9636051-0-0.

112.    Baharanchi, A.A., S. Gokaltun, and S. Eshraghi. *A numerical approach for the simulation of internal nozzle flow in a pressure swirl atomizer using different turbulent models and towards an effective inlet weber number.* in *ASME 2013 International Mechanical Engineering Congress and Exposition.* 2013. American Society of Mechanical Engineers.

113.    Trask, N.A., *Implementation of an eulerian atomization model to characterize primary spray formation*, in *Masters Thesis.* 2010, University of Massachusetts Amherst. p. 434.

114.    Gorokhovski, M. and M. Herrmann, *Modeling primary atomization.* Annu. Rev. Fluid Mech., 2008. **40**: p. 343-366.

115.    Elghobashi, S. and T. Abou‐Arab, *A two‐equation turbulence model for two‐phase flows.* Physics of Fluids (1958-1988), 1983. **26**(4): p. 931-938.

116.    Quintao, K.K., *Design Optimization of Nozzle Shapes for Maximum Uniformity of Exit Flow*, in *Masters thesis,  Mechanical Engineering Department.* 2012, Florida International University.

117.    Colaço, M.J. and G.S. Dulikravich, *A survey of basic deterministic, heuristic and hybrid methods for single-objective optimization and response surface generation.* Thermal Measurements and Inverse Techniques, 2009. **1**: p. 355-406.

118.    Colaço, M.J., G.S. Dulikravich, and D. Sahoo, *A response surface method-based hybrid optimizer.* Inverse Problems in Science and Engineering; Formerly Inverse Problems in Engineering, 2008. **16**(6): p. 717-741.

119.    Atmanlı, A., B. Yüksel, E. Ileri, and A.D. Karaoglan, *Response surface methodology based optimization of diesel–n-butanol–cotton oil ternary blend*

ratios to improve engine performance and exhaust emission characteristics. Energy Conversion and Management, 2015. **90**: p. 383-394.

120. Benajes, J., R. Novella, J.M. Pastor, A. Hernández-López, M. Hasegawa, N. Tsuji, M. Emi, I. Uehara, J. Martorell, and M. Alonso, *Optimization of the combustion system of a medium duty direct injection diesel engine by combining CFD modeling with experimental validation.* Energy Conversion and Management, 2016. **110**: p. 212-229.

121. Hatami, M., M. Cuijpers, and M. Boot, *Experimental optimization of the vanes geometry for a variable geometry turbocharger (VGT) using a Design of Experiment (DoE) approach.* Energy Conversion and Management, 2015. **106**: p. 1057-1070.

122. Silva, V. and A. Rouboa, *Combining a 2-D multiphase CFD model with a Response Surface Methodology to optimize the gasification of Portuguese biomasses.* Energy Conversion and Management, 2015. **99**: p. 28-40.

123. Pandal, A., R. Payri, J. García-Oliver, and J. Pastor, *Optimization of spray break-up CFD simulations by combining Σ-Y Eulerian atomization model with a response surface methodology under diesel engine-like conditions (ECN Spray A).* Computers & Fluids, 2017. **156**: p. 9-20.

124. Colaço, M., W. Silva, A. Magalhães, and G. Dulikravich. *Response surface methods applied to scarce and small sets of training points A comparative study.* in *EngOpt 2008-international conference on engineering optimization, Rio de Janeiro, Brazil.* 2008.

125. Moral, R.J. and G.S. Dulikravich, *Multi-objective hybrid evolutionary optimization with automatic switching among constituent algorithms.* AIAA journal, 2008. **46**(3): p. 673.

126. Jeong, S., M. Murayama, and K. Yamamoto, *Efficient optimization design method using kriging model.* Journal of aircraft, 2005. **42**(2): p. 413-420.

127. McKay, M.D., R.J. Beckman, and W.J. Conover, *Comparison of three methods for selecting values of input variables in the analysis of output from a computer code.* Technometrics, 1979. **21**(2): p. 239-245.

128. Iman, R.L. and W. Conover, *Small sample sensitivity analysis techniques for computer models. with an application to risk assessment.* Communications in statistics-theory and methods, 1980. **9**(17): p. 1749-1842.

129. Stein, M., *Large sample properties of simulations using Latin hypercube sampling.* Technometrics, 1987. **29**(2): p. 143-151.

130. Simpson, T.W., J. Poplinski, P.N. Koch, and J.K. Allen, *Metamodels for computer-based engineering design: survey and recommendations.* Engineering with computers, 2001. **17**(2): p. 129-150.

131. Kleijnen, J.P., S.M. Sanchez, T.W. Lucas, and T.M. Cioppa, *State-of-the-art review: a user's guide to the brave new world of designing simulation experiments.* INFORMS Journal on Computing, 2005. **17**(3): p. 263-289.

132. Viana, F.A. *Things you wanted to know about the Latin hypercube design and were afraid to ask.* in *10th World Congress on Structural and Multidisciplinary Optimization*. 2013. sn.

133. Viana, F.A., G. Venter, and V. Balabanov, *An algorithm for fast optimal Latin hypercube design of experiments.* International journal for numerical methods in engineering, 2010. **82**(2): p. 135-156.

134. Rajaram, A., V. Subash, K. Surendar, and P. Raghu, *Optimization Of Spray Characteristics By Response Surface Methodology.* International Journal of Modern Trends in Engineering and Science, 2018. **5**(3): p. 1-3.

135. CD-adapco, *User Guide ,Star-CCM+ Version 11.02.* 2016.

136. Fluent, A., *ANSYS Fluent User's Guide.* Ansys Inc, 2011.

137. Guide, C.U., *Release 4.4, 2001.* Computational Fluid Dynamics Services, AEA Industrial Technology, Harwell Laboratory, Oxfordshire, UK.

138. Ltd, O.F., *Openfoam user guide.* 2016.

139. CD-Adapco, *User Guide, Star-CD Version 4.16.* 2016.

140. Warsi, Z., *Conservation form of the Navier-Stokes equations in general nonsteady coordinates.* AIAA Journal, 1981. **19**(2): p. 240-242.

141. Rodi, W. *Influence of buoyancy and rotation on equations for the turbulent length scale.* in *2nd symposium on turbulent shear flows*. 1979. London, Imperial College of Science and Technology.

142. EL TAHRY, S., *k-epsilon equation for compressible reciprocating engine flows.* Journal of Energy, 1983. **7**(4): p. 345-353.

143. Yakhot, V. and S.A. Orszag, *Renormalization group analysis of turbulence. I. Basic theory.* Journal of scientific computing, 1986. **1**(1): p. 3-51.

144. Shih, T.-H., W.W. Liou, A. Shabbir, Z. Yang, and J. Zhu, *A new k-ϵ eddy viscosity model for high reynolds number turbulent flows.* Computers & Fluids, 1995. **24**(3): p. 227-238.

145. Issa, R.I., *Solution of the implicitly discretised fluid flow equations by operator-splitting.* Journal of computational physics, 1986. **62**(1): p. 40-65.

146. Gosman, A.D., W. Pun, A. Runchal, D. Spalding, and M. Wolfshtein, *Heat and mass transfer in recirculating flows.* 1969: Academic press London.

147. Patankar, S., *Numerical heat transfer and fluid flow.* 1980: CRC Press.

148. Lai, K.Y.M., *Numerical analysis of fluid transport phenomena.* 1983, Imperial College London (University of London).

149. Leschziner, M., *Practical evaluation of three finite difference schemes for the computation of steady-state recirculating flows.* Computer Methods in Applied Mechanics and Engineering, 1980. **23**(3): p. 293-312.

150. Senecal, P., K. Richards, E. Pomraning, T. Yang, M. Dai, R. McDavid, M. Patterson, S. Hou, and T. Shethaji, *A new parallel cut-cell Cartesian CFD code for rapid grid generation applied to in-cylinder diesel engine simulations.* 2007, SAE Technical Paper 2007-01-0159.

151. Ning, W., R.D. Reitz, A.M. Lippert, and R. Diwakar, *Development of a next-generation spray and atomization model using an Eulerian-Lagrangian methodology.* 2007, University of Wisconsin--Madison.

152. Khuong, A.D., *The Eulerian-Lagrangian Spray Atomization (ELSA) model of the jet atomization in CFD simulations: evaluation and validation.* 2012.

153. Gorokhovski, M., J. Jouanguy, and A. Chtab. *Simulation of air-blast atomization:'floating guard'statistic particle method for conditioning of LES computation; stochastic models of break-up and coalescence.* in *Proc. Int. Conf. Liq. Atom. Spray Syst., 10th (ICLASS-2006).* 2006.

154.     Kadem, N., A. Tchiftchibachian, and R. Borghi, *Experimental and numerical modeling study for irrigation gun water jet.* Atomization and Sprays, 2008. **18**(4).

155.     Beheshti, N., A. Burluka, and M. Fairweather. *Atomisation In Turbulent Flows: Modelling For Application.* In *Tsfp Digital Library Online*. 2003. Begel House Inc.

156.     Gharbi, A., E. Ruffin, F. Anselmet, and R. Schiestel, *Numerical modelling of variable density turbulent jets.* International journal of heat and mass transfer, 1996. **39**(9): p. 1865-1882.

157.     Luo, H. and H.F. Svendsen, *Theoretical model for drop and bubble breakup in turbulent dispersions.* AIChE Journal, 1996. **42**(5): p. 1225-1233.

158.     Platzer, E. and M. Sommerfeld. *Modelling of turbulent atomisation with and Euler/Euler approach including the drop size prediction.* in *9th International Conference on Liquid Atomization and Spray Systems*. 2003.

159.     Deux, E. and M. Sommerfeld, *Modelling of spray atomisation and dispersion.* Proc. ILASS-Europe 2004, 2004: p. 195-200.

160.     Leung, T.F., C.P. Groth, and J. Hu. *Evaluation of an eulerian-lagrangian spray atomization (elsa) model for nozzle flow: Modeling of coupling between dense and disperse regions.* in *47th AIAA Thermophysics Conference*. 2017.

161.     Hoyas, S., A. Gil, X. Margot, D. Khuong-Anh, and F. Ravet, *Evaluation of the Eulerian–Lagrangian Spray Atomization (ELSA) model in spray simulations: 2D cases.* Mathematical and Computer Modelling, 2013. **57**(7): p. 1686-1693.

162.     Mashayek, F. and R. Pandya, *Analytical description of particle/droplet-laden turbulent flows.* Progress in energy and combustion science, 2003. **29**(4): p. 329-378.

163.     Reitz, R. and F. Bracco, *Mechanism of atomization of a liquid jet.* Physics of Fluids (1958-1988), 1982. **25**(10): p. 1730-1742.

164.     Chesnel, J., J. Reveillon, T. Menard, and F.-X. Demoulin, *Large eddy simulation of liquid jet atomization.* Atomization and Sprays, 2011. **21**(9).

165.     PNR UK, L., *General Purpose Spray Nozzles, CTG UG20 BR.* 6 July 2017.

166.     Crowley, J.M., G.S. Wright, and J.C. Chato, *Selecting a working fluid to increase the efficiency and flow rate of an EHD pump.* IEEE Transactions on Industry Applications, 1990. **26**(1): p. 42-49.

167.     Wittig, S., M. Aigner, K. Sakbani, and T. Sattelmayer, *Optical measurements of droplet size distributions: Special considerations in the parameter definition for fuel atomizers*. 1984, Karlsruhe Univ (Germany Fr) Inst Fuer Thermische Stroemungsmaschinen.

168.     Hirleman, E.D., V. Oechsle, and N. Chigier, *Response characteristics of laser diffraction particle size analyzers: optical sample volume extent and lens effects.* Optical Engineering, 1984. **23**(5): p. 235610-235610-.

169.     Dodge, L.G., *Change of calibration of diffraction-based particle sizers in dense sprays.* Optical Engineering, 1984. **23**(5): p. 626-630.

170.     Malvern-Instruments, *Spraytec User Manual MAN0368*. 2007, Issue.

171.     Malvern/INSITEC, *Method for measuring particle size in the presence of multiple scattering*. 1997, Google Patents: US.

172.     Emekwuru, N. and A.P. Watkins, *Analysis of a two-fluid sprayer and its use to develop the number size distribution moments spray model, Part I: Experimental Analysis.* Atomization and Sprays, 2010. **20**(6): p. 467–484.

173.     Emekwuru, N.G. and P. Watkins, *Statistical Experimental Analysis of a Two-Fluid Sprayer and Its Use to Develop the Number Size Distribution Moments Model of Sprays*. 2007: University of Manchester.

174.     Chin, J.S., Nickolaus, D., and Lefebvre, A.H, *Influence of Downstream Distance on the Spray Characteristics of Pressure-Swirl Atomizers.* Journal of Engineering for Gas Turbines and Power, 1986. **108**(1): p. 224-224.

175.     Jahannama, M.R., A. Paul Watkins, and A.J. Yule, *Electrostatic Effects On Agricultural Air-Atomized Sprays And Deposition. Part I: An Experimental Study.* Atomization and Sprays, 2005. **15**: p. 603-628.

176.     Demoulin, F.-X., P.-A. Beau, G. Blokkeel, A. Mura, and R. Borghi, *A new model for turbulent flows with large density fluctuations: application to liquid atomization.* Atomization and Sprays, 2007. **17**(4).

177. Nonnenmacher, S. and M. Piesche, *Design of hollow cone pressure swirl nozzles to atomize Newtonian fluids.* Chemical Engineering Science, 2000. **55**(19): p. 4339-4348.

178. Barton, I., *Comparison of SIMPLE‐and PISO‐type algorithms for transient flows.* International Journal for numerical methods in fluids, 1998. **26**(4): p. 459-483.

179. Chin, J. and A. Lefebvre, *The role of the heat-up period in fuel drop evaporation.* International Journal of Turbo and Jet Engines, 1985. **2**(4): p. 315-326.

180. Williams, L.R., *Effect of pipe diameter on horizontal annular two-phase flow*. 1990, PhD thesis, University of Illinois at Urbana-Champaign.

181. Levy, N., S. Amara, J.-C. Champoussin, and N. Guerrassi, *Non-reactive diesel spray computations supported by PDA measurements*. 1997, SAE Technical Paper.

182. Schürmann, P., Forsyth, J., Padrutt, R., and Heiniger, K. C., *Spray characterization downstream of swirl pressure nozzle in gas turbine fogging and high fogging applications*, in *Power-Gen International, Power-Gen International Conf. and Exhibition*. 2003, PennWell Corporation:Tulsa: Las Vegas, USA.

183. Yoon, S.H., D.K. Kim, and B.H. Kim, *Effect of nozzle geometry for swirl type twin-fluid water mist nozzle on the spray characteristic.* Journal of mechanical science and technology, 2011. **25**(7): p. 1761.

184. Eggers, J. and E. Villermaux, *Physics of liquid jets.* Reports on progress in physics, 2008. **71**(3): p. 036601.

185. Simmons, H., *The prediction of Sauter mean diameter for gas turbine fuel nozzles of different types.* ASME paper, 1980. **102**: p. 646-652.

186. Orme, M., *Experiments on droplet collisions, bounce, coalescence and disruption.* Progress in Energy and Combustion Science, 1997. **23**(1): p. 65-79.

**APPENDICES**

Appendix I      **Sample experimental raw data**

## a. Axial distance Drop size and DSD measurement at 60 mm

**! Average Measurement Parameters**           **28 Oct 2016 - 11:06:24.3600**

(average size distribution, weighted)
Example results555.smea\Import\Averages\V6 1 1.psd
Sample : watersherry
Start+0.0004 (s) :: +0.3600 (s)

---

**Standard Values:**

| | | |
|---|---|---|
| Trans = 41.4 (%) | Dv(10) = 229.5 (µm) | Span = 1.051 |
| Cv = 2820 (PPM) | Dv(50) = 485.1 (µm) | D[3][2] = 294.8 (µm) |
| SSA = 0.0204 (m²/cc) | Dv(90) = 739.3 (µm) | D[4][3] = 483.6 (µm) |

---

**Notes:**
using catheter nozzle

---

**Average (average size distribution, weighted):**
Source file: V6 1
868 Records Averaged                         31 Records Skipped
Average Range = 28 Oct 2016 - 11:06:24.0004 :: 11:06:24.3600

---

**Measurement Values and Settings**
Instrument = Spraytec - Open Spray

| | |
|---|---|
| Lens = 300mm | Path Length = 30.0 (mm) |
| Particulate Refractive Index = 1.33 + 0.000i | Scatter start = 1 |
| Dispersant Refractive Index = 1.00 | Scatter end = 36 |
| Particle Density = 1.00 (gm/cc) | Scattering threshold = 1 |
| Residual = 0.00 (%) | Minimum size = 0.10 (µm) |
| Extinction analysis = Off | Maximum size = 2500.00 (µm) |
| | Multiple Scatter = On |

---

**Identification**

| | |
|---|---|
| Operator = mnska | S/W = v3.20.006 |
| Serial Numbers: Instrument = MAL1118761 | Detector = 10FT-CDL |
| SOP Name = -MANUAL 4- -IMPORTED MEASUREMENT- | |
| Last Edited = Not Edited | |

---

**Rapid Measurement**
Trigger = Manual
Trigger Delay = 0.0 msecs

---

! Low Light Transmission

Example results555.smea\Import\V6 1 1.psc
Sample : watersherry
Start+0.0024 (s)
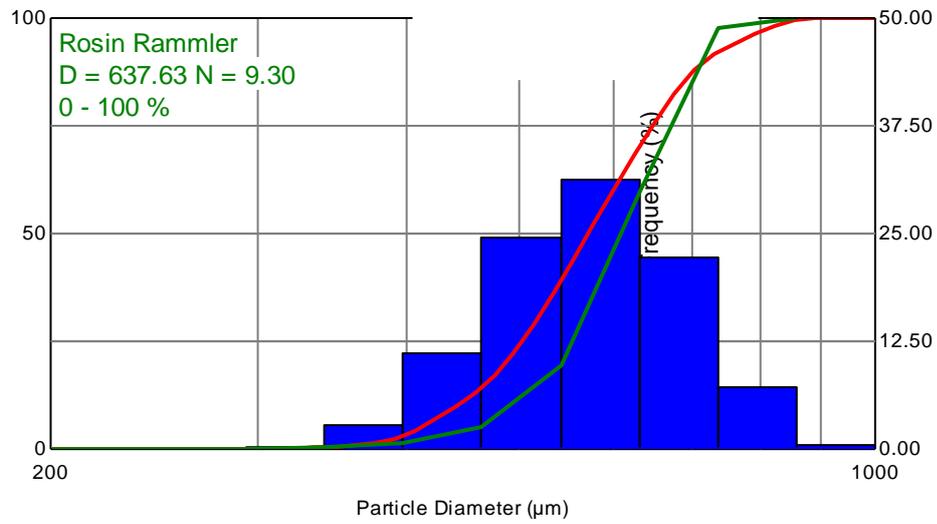


Rosin Rammler
D = 637.63 N = 9.30
0 - 100 %

Particle Diameter (µm)

| Size (µm) | % V < | % V | Size (µm) | % V < | % V | Size (µm) | % V < | % V |
|---|---|---|---|---|---|---|---|---|
| 0.117 | 0.00 | 0.00 | 2.51 | 0.00 | 0.00 | 54.12 | 0.00 | 0.00 |
| 0.136 | 0.00 | 0.00 | 2.93 | 0.00 | 0.00 | 63.10 | 0.00 | 0.00 |
| 0.158 | 0.00 | 0.00 | 3.41 | 0.00 | 0.00 | 73.56 | 0.00 | 0.00 |
| 0.185 | 0.00 | 0.00 | 3.98 | 0.00 | 0.00 | 85.77 | 0.00 | 0.00 |
| 0.215 | 0.00 | 0.00 | 4.64 | 0.00 | 0.00 | 100.00 | 0.00 | 0.00 |
| 0.251 | 0.00 | 0.00 | 5.41 | 0.00 | 0.00 | 116.59 | 0.00 | 0.00 |
| 0.293 | 0.00 | 0.00 | 6.31 | 0.00 | 0.00 | 135.94 | 0.00 | 0.00 |
| 0.341 | 0.00 | 0.00 | 7.36 | 0.00 | 0.00 | 158.49 | 0.00 | 0.00 |
| 0.398 | 0.00 | 0.00 | 8.58 | 0.00 | 0.00 | 184.79 | 0.00 | 0.00 |
| 0.464 | 0.00 | 0.00 | 10.00 | 0.00 | 0.00 | 215.44 | 0.00 | 0.00 |
| 0.541 | 0.00 | 0.00 | 11.66 | 0.00 | 0.00 | 251.19 | 0.00 | 0.00 |
| 0.631 | 0.00 | 0.00 | 13.59 | 0.00 | 0.00 | 292.87 | 0.01 | 0.01 |
| 0.736 | 0.00 | 0.00 | 15.85 | 0.00 | 0.00 | 341.46 | 0.35 | 0.34 |
| 0.858 | 0.00 | 0.00 | 18.48 | 0.00 | 0.00 | 398.11 | 3.19 | 2.84 |
| 1.00 | 0.00 | 0.00 | 21.54 | 0.00 | 0.00 | 464.16 | 14.35 | 11.16 |
| 1.17 | 0.00 | 0.00 | 25.12 | 0.00 | 0.00 | 541.17 | 38.86 | 24.51 |
| 1.36 | 0.00 | 0.00 | 29.29 | 0.00 | 0.00 | 630.96 | 70.14 | 31.28 |
| 1.58 | 0.00 | 0.00 | 34.15 | 0.00 | 0.00 | 735.64 | 92.29 | 22.15 |
| 1.85 | 0.00 | 0.00 | 39.81 | 0.00 | 0.00 | 857.70 | 99.47 | 7.18 |
| 2.15 | 0.00 | 0.00 | 46.42 | 0.00 | 0.00 | 1000.00 | 100.00 | 0.53 |

**! Average Measurement Parameters**                    **28 Oct 2016 - 11:08:25.3500**

(average size distribution, weighted)
Example results555.smea\Import\Averages\V6a 1 1.psd
Sample : watersherry
Start+0.0004 (s) :: +0.3500 (s)

---

**Standard Values:**

| | | |
|---|---|---|
| Trans = 39.9 (%) | Dv(10) = 233.8 (µm) | Span = 1.073 |
| Cv = 3042 (PPM) | Dv(50) = 474.6 (µm) | D[3][2] = 304.7 (µm) |
| SSA = 0.0197 (m²/cc) | Dv(90) = 743.3 (µm) | D[4][3] = 481 (µm) |

---

**Notes:**
using catheter nozzle

---

**Average (average size distribution, weighted):**
Source file: V6a 1
835 Records Averaged                              39 Records Skipped
Average Range =  28 Oct 2016 - 11:08:25.0004 :: 11:08:25.3500

---

**Measurement Values and Settings**
Instrument = Spraytec - Open Spray

| | |
|---|---|
| Lens = 300mm | Path Length = 30.0 (mm) |
| Particulate Refractive Index = 1.33 + 0.000i | Scatter start = 1 |
| Dispersant Refractive Index = 1.00 | Scatter end = 36 |
| Particle Density = 1.00 (gm/cc) | Scattering threshold = 1 |
| Residual = 0.00   (%) | Minimum size = 0.10 (µm) |
| Extinction analysis = Off | Maximum size = 2500.00 (µm) |
| | Multiple Scatter = On |

---

**Identification**

| | |
|---|---|
| Operator = mnska | S/W =  v3.20.006 |
| Serial Numbers: Instrument = MAL1118761 | Detector = 10FT-CDL |
| SOP Name = -MANUAL 5- -IMPORTED MEASUREMENT- | |
| Last Edited = Not Edited | |

---

**Rapid Measurement**
Trigger = Manual
Trigger Delay = 0.0 msecs

---

! Low Light Transmission

Example results555.smea\Import\V6a 1 1.ps
Sample : watersherry
Start+0.1140 (s)



Rosin Rammler
D = 377.47 N = 1.27
0 - 100 %
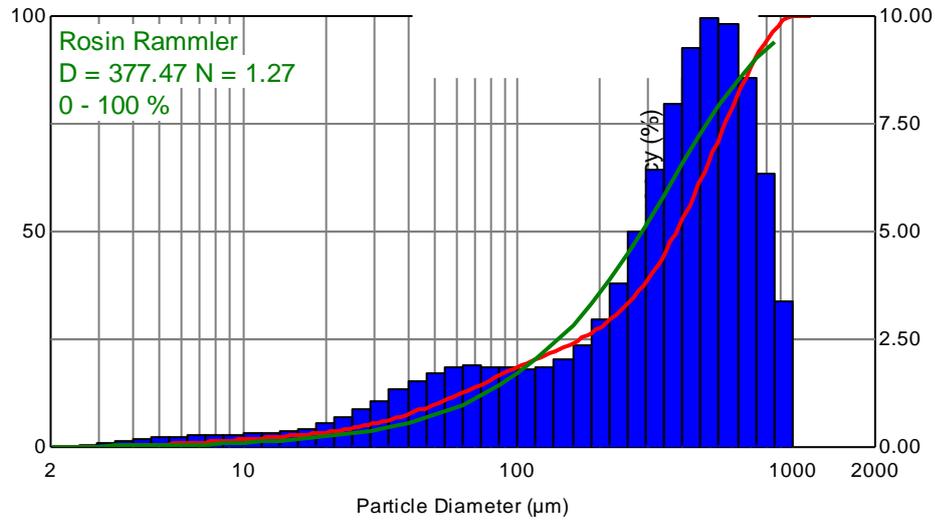
| Size (µm) | % V < | % V | Size (µm) | % V < | % V | Size (µm) | % V < | % V |
|---|---|---|---|---|---|---|---|---|
| 0.117 | 0.00 | 0.00 | 2.51 | 0.01 | 0.01 | 54.12 | 10.91 | 1.73 |
| 0.136 | 0.00 | 0.00 | 2.93 | 0.06 | 0.05 | 63.10 | 12.76 | 1.84 |
| 0.158 | 0.00 | 0.00 | 3.41 | 0.15 | 0.09 | 73.56 | 14.64 | 1.88 |
| 0.185 | 0.00 | 0.00 | 3.98 | 0.27 | 0.13 | 85.77 | 16.51 | 1.87 |
| 0.215 | 0.00 | 0.00 | 4.64 | 0.44 | 0.17 | 100.00 | 18.34 | 1.84 |
| 0.251 | 0.00 | 0.00 | 5.41 | 0.65 | 0.21 | 116.59 | 20.17 | 1.82 |
| 0.293 | 0.00 | 0.00 | 6.31 | 0.90 | 0.24 | 135.94 | 22.04 | 1.87 |
| 0.341 | 0.00 | 0.00 | 7.36 | 1.16 | 0.27 | 158.49 | 24.07 | 2.03 |
| 0.398 | 0.00 | 0.00 | 8.58 | 1.45 | 0.28 | 184.79 | 26.43 | 2.37 |
| 0.464 | 0.00 | 0.00 | 10.00 | 1.74 | 0.29 | 215.44 | 29.38 | 2.94 |
| 0.541 | 0.00 | 0.00 | 11.66 | 2.04 | 0.30 | 251.19 | 33.20 | 3.82 |
| 0.631 | 0.00 | 0.00 | 13.59 | 2.37 | 0.32 | 292.87 | 38.21 | 5.01 |
| 0.736 | 0.00 | 0.00 | 15.85 | 2.73 | 0.36 | 341.46 | 44.67 | 6.46 |
| 0.858 | 0.00 | 0.00 | 18.48 | 3.16 | 0.43 | 398.11 | 52.64 | 7.97 |
| 1.00 | 0.00 | 0.00 | 21.54 | 3.69 | 0.53 | 464.16 | 61.90 | 9.26 |
| 1.17 | 0.00 | 0.00 | 25.12 | 4.37 | 0.68 | 541.17 | 71.87 | 9.97 |
| 1.36 | 0.00 | 0.00 | 29.29 | 5.23 | 0.86 | 630.96 | 81.67 | 9.80 |
| 1.58 | 0.00 | 0.00 | 34.15 | 6.32 | 1.08 | 735.64 | 90.26 | 8.58 |
| 1.85 | 0.00 | 0.00 | 39.81 | 7.64 | 1.32 | 857.70 | 96.62 | 6.36 |
| 2.15 | 0.00 | 0.00 | 46.42 | 9.18 | 1.55 | 1000.00 | 100.00 | 3.38 |

### b. Axial distance Drop size and DSD measurement at 80 mm

**Average Measurement Parameters**　　　　　**28 Oct 2016 - 10:58:53.3000**
(average size distribution, weighted)
Example results555.smea\Import\Averages\V8 1 1.psd
Sample : watersherry
Start+0.0004 (s) :: +0.3000 (s)

---

**Standard Values:**

| | | |
|---|---|---|
| Trans = 65.9 (%) | Dv(10) = 237.4 (µm) | Span = 1.134 |
| Cv = 1677 (PPM) | Dv(50) = 463.9 (µm) | D[3][2] = 364.7 (µm) |
| SSA = 0.0165 (m²/cc) | Dv(90) = 763.3 (µm) | D[4][3] = 481.6 (µm) |

---

**Notes:**
using catheter nozzle

---

**Average (average size distribution, weighted):**
Source file: V8 1
749 Records Averaged　　　　　　　　　　　0 Records Skipped
Average Range =  28 Oct 2016 - 10:58:53.0004 :: 10:58:53.3000

---

**Measurement Values and Settings**
Instrument = Spraytec - Open Spray

| | |
|---|---|
| Lens = 300mm | Path Length = 30.0 (mm) |
| Particulate Refractive Index = 1.33 + 0.000i | Scatter start = 1 |
| Dispersant Refractive Index = 1.00 | Scatter end = 35 |
| Particle Density = 1.00 (gm/cc) | Scattering threshold = 1 |
| Residual = 0.00   (%) | Minimum size = 0.10 (µm) |
| Extinction analysis = Off | Maximum size = 2500.00 (µm) |
| | Multiple Scatter = On |

---

**Identification**

| | |
|---|---|
| Operator = mnska | S/W =  v3.20.006 |
| Serial Numbers: Instrument = MAL1118761 | Detector = 10FT-CDL |
| SOP Name = -MANUAL 2- -IMPORTED MEASUREMENT- | |
| Last Edited = Not Edited | |

---

**Rapid Measurement**
Trigger = Manual
Trigger Delay = 0.0 msecs

Example results555.smea\Import\V8 1 1.psc
Sample : watersherry
Start+0.0024 (s)
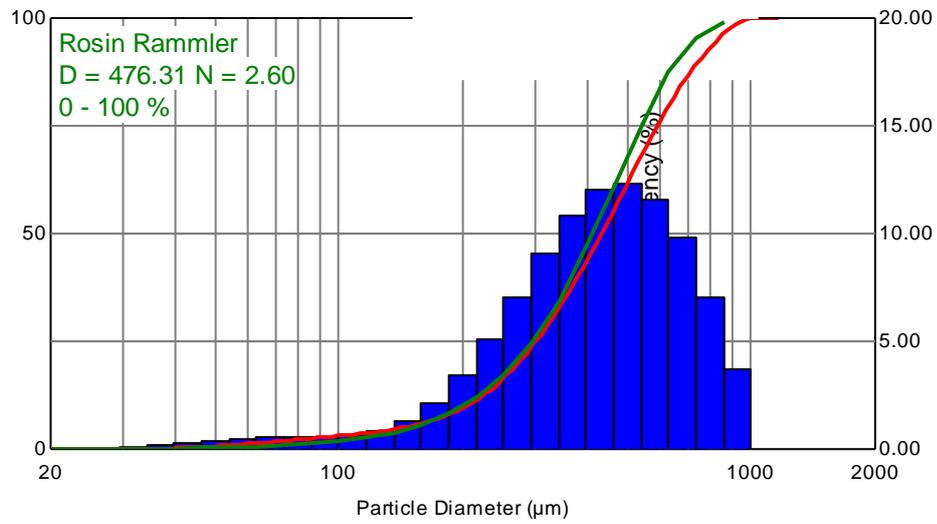


| Size (µm) | % V < | % V | Size (µm) | % V < | % V | Size (µm) | % V < | % V |
|---|---|---|---|---|---|---|---|---|
| 0.117 | 0.00 | 0.00 | 2.51 | 0.00 | 0.00 | 54.12 | 0.85 | 0.38 |
| 0.136 | 0.00 | 0.00 | 2.93 | 0.00 | 0.00 | 63.10 | 1.34 | 0.48 |
| 0.158 | 0.00 | 0.00 | 3.41 | 0.00 | 0.00 | 73.56 | 1.89 | 0.55 |
| 0.185 | 0.00 | 0.00 | 3.98 | 0.00 | 0.00 | 85.77 | 2.48 | 0.58 |
| 0.215 | 0.00 | 0.00 | 4.64 | 0.00 | 0.00 | 100.00 | 3.07 | 0.60 |
| 0.251 | 0.00 | 0.00 | 5.41 | 0.00 | 0.00 | 116.59 | 3.72 | 0.65 |
| 0.293 | 0.00 | 0.00 | 6.31 | 0.00 | 0.00 | 135.94 | 4.57 | 0.84 |
| 0.341 | 0.00 | 0.00 | 7.36 | 0.00 | 0.00 | 158.49 | 5.86 | 1.29 |
| 0.398 | 0.00 | 0.00 | 8.58 | 0.00 | 0.00 | 184.79 | 7.98 | 2.12 |
| 0.464 | 0.00 | 0.00 | 10.00 | 0.00 | 0.00 | 215.44 | 11.36 | 3.38 |
| 0.541 | 0.00 | 0.00 | 11.66 | 0.00 | 0.00 | 251.19 | 16.43 | 5.07 |
| 0.631 | 0.00 | 0.00 | 13.59 | 0.00 | 0.00 | 292.87 | 23.48 | 7.06 |
| 0.736 | 0.00 | 0.00 | 15.85 | 0.00 | 0.00 | 341.46 | 32.58 | 9.10 |
| 0.858 | 0.00 | 0.00 | 18.48 | 0.00 | 0.00 | 398.11 | 43.46 | 10.87 |
| 1.00 | 0.00 | 0.00 | 21.54 | 0.00 | 0.00 | 464.16 | 55.50 | 12.05 |
| 1.17 | 0.00 | 0.00 | 25.12 | 0.00 | 0.00 | 541.17 | 67.84 | 12.34 |
| 1.36 | 0.00 | 0.00 | 29.29 | 0.00 | 0.00 | 630.96 | 79.42 | 11.58 |
| 1.58 | 0.00 | 0.00 | 34.15 | 0.06 | 0.06 | 735.64 | 89.21 | 9.79 |
| 1.85 | 0.00 | 0.00 | 39.81 | 0.21 | 0.15 | 857.70 | 96.29 | 7.08 |
| 2.15 | 0.00 | 0.00 | 46.42 | 0.47 | 0.26 | 1000.00 | 100.00 | 3.71 |

(average size distribution, weighted)
Example results555.smea\Import\Averages\V8a 1 1.psd
Sample : watersherry
Start+0.1996 (s) ::  +0.4004 (s)

---

**Standard Values:**

| | | |
|---|---|---|
| Trans = 67.3 (%) | Dv(10) = 243 (µm) | Span = 1.115 |
| Cv = 1615 (PPM) | Dv(50) = 469.7 (µm) | D[3][2] = 371.2 (µm) |
| SSA = 0.0162 (m²/cc) | Dv(90) = 766.7 (µm) | D[4][3] = 486.6 (µm) |

---

**Notes:**
using catheter nozzle

---

**Average (average size distribution, weighted):**
Source file: V8a 1
502 Records Averaged                        0 Records Skipped
Average Range =  28 Oct 2016 - 11:01:22.1996 :: 11:01:22.4004

---

**Measurement Values and Settings**
Instrument = Spraytec - Open Spray

| | |
|---|---|
| Lens = 300mm | Path Length = 30.0 (mm) |
| Particulate Refractive Index = 1.33 + 0.000i | Scatter start = 1 |
| Dispersant Refractive Index = 1.00 | Scatter end = 34 |
| Particle Density = 1.00 (gm/cc) | Scattering threshold = 1 |
| Residual = 0.00   (%) | Minimum size = 0.10 (µm) |
| Extinction analysis = Off | Maximum size = 2500.00 (µm) |
| | Multiple Scatter = On |

---

**Identification**

| | |
|---|---|
| Operator = mnska | S/W =  v3.20.006 |
| Serial Numbers: Instrument = MAL1118761 | Detector = 10FT-CDL |
| SOP Name = -MANUAL 3- -IMPORTED MEASUREMENT- | |
| Last Edited = Not Edited | |

---

**Rapid Measurement**
Trigger = Manual
Trigger Delay = 0.0 msecs

Example results555.smea\lmport\V8a 1 1.ps
Sample : watersherry
Start+0.1240 (s)
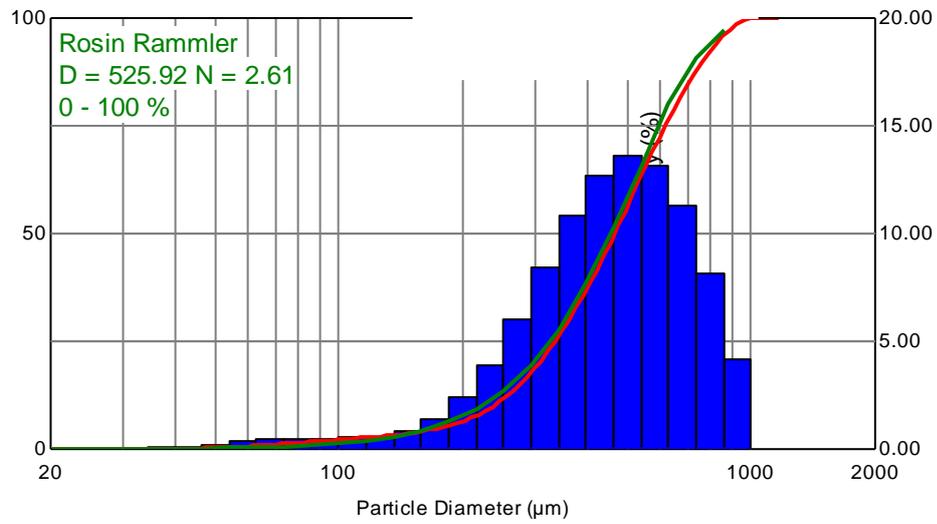


| Size (µm) | % V < | % V | Size (µm) | % V < | % V | Size (µm) | % V < | % V |
|---|---|---|---|---|---|---|---|---|
| 0.117 | 0.00 | 0.00 | 2.51 | 0.00 | 0.00 | 54.12 | 0.43 | 0.23 |
| 0.136 | 0.00 | 0.00 | 2.93 | 0.00 | 0.00 | 63.10 | 0.76 | 0.33 |
| 0.158 | 0.00 | 0.00 | 3.41 | 0.00 | 0.00 | 73.56 | 1.18 | 0.42 |
| 0.185 | 0.00 | 0.00 | 3.98 | 0.00 | 0.00 | 85.77 | 1.66 | 0.48 |
| 0.215 | 0.00 | 0.00 | 4.64 | 0.00 | 0.00 | 100.00 | 2.16 | 0.50 |
| 0.251 | 0.00 | 0.00 | 5.41 | 0.00 | 0.00 | 116.59 | 2.68 | 0.52 |
| 0.293 | 0.00 | 0.00 | 6.31 | 0.00 | 0.00 | 135.94 | 3.27 | 0.59 |
| 0.341 | 0.00 | 0.00 | 7.36 | 0.00 | 0.00 | 158.49 | 4.10 | 0.83 |
| 0.398 | 0.00 | 0.00 | 8.58 | 0.00 | 0.00 | 184.79 | 5.47 | 1.37 |
| 0.464 | 0.00 | 0.00 | 10.00 | 0.00 | 0.00 | 215.44 | 7.84 | 2.37 |
| 0.541 | 0.00 | 0.00 | 11.66 | 0.00 | 0.00 | 251.19 | 11.75 | 3.91 |
| 0.631 | 0.00 | 0.00 | 13.59 | 0.00 | 0.00 | 292.87 | 17.73 | 5.98 |
| 0.736 | 0.00 | 0.00 | 15.85 | 0.00 | 0.00 | 341.46 | 26.13 | 8.40 |
| 0.858 | 0.00 | 0.00 | 18.48 | 0.00 | 0.00 | 398.11 | 36.93 | 10.79 |
| 1.00 | 0.00 | 0.00 | 21.54 | 0.00 | 0.00 | 464.16 | 49.62 | 12.69 |
| 1.17 | 0.00 | 0.00 | 25.12 | 0.00 | 0.00 | 541.17 | 63.22 | 13.60 |
| 1.36 | 0.00 | 0.00 | 29.29 | 0.00 | 0.00 | 630.96 | 76.39 | 13.17 |
| 1.58 | 0.00 | 0.00 | 34.15 | 0.01 | 0.01 | 735.64 | 87.69 | 11.29 |
| 1.85 | 0.00 | 0.00 | 39.81 | 0.07 | 0.06 | 857.70 | 95.84 | 8.15 |
| 2.15 | 0.00 | 0.00 | 46.42 | 0.20 | 0.13 | 1000.00 | 100.00 | 4.16 |

### c. Axial distance Drop size and DSD measurements at 100 mm

**Average Measurement Parameters**          **28 Oct 2016 - 10:51:42.4004**

(average size distribution, weighted)
Example results555.smea\Import\Averages\V10 1 2.psd
Sample : watersherry
Start+0.1996 (s) ::  +0.4004 (s)

---

**Standard Values:**

| | | |
|---|---|---|
| Trans = 67.5 (%) | Dv(10) = 245.7 (µm) | Span = 1.104 |
| Cv = 1607 (PPM) | Dv(50) = 473.6 (µm) | D[3][2] = 371.5 (µm) |
| SSA = 0.0161 (m²/cc) | Dv(90) = 768.6 (µm) | D[4][3] = 489.4 (µm) |

---

**Notes:**
using catheter nozzle

---

**Average (average size distribution, weighted):**
Source file: V10 1
502 Records Averaged                          0 Records Skipped
Average Range =  28 Oct 2016 - 10:51:42.1996 :: 10:51:42.4004

---

**Measurement Values and Settings**
Instrument = Spraytec - Open Spray

| | |
|---|---|
| Lens = 300mm | Path Length = 30.0 (mm) |
| Particulate Refractive Index = 1.33 + 0.000i | Scatter start = 1 |
| Dispersant Refractive Index = 1.00 | Scatter end = 35 |
| Particle Density = 1.00 (gm/cc) | Scattering threshold = 1 |
| Residual = 0.00  (%) | Minimum size = 0.10 (µm) |
| Extinction analysis = Off | Maximum size = 2500.00 (µm) |
| | Multiple Scatter = On |

---

**Identification**

| | |
|---|---|
| Operator = mnska | S/W =  v3.20.006 |
| Serial Numbers: Instrument = MAL1118761 | Detector = 10FT-CDL |
| SOP Name = -MANUAL 3- -IMPORTED MEASUREMENT- | |
| Last Edited = Not Edited | |

---

**Rapid Measurement**
Trigger = Manual
Trigger Delay = 0.0 msecs

Example results555.smea\Import\V10 1 1.ps
Sample : watersherry
Start+0.1000 (s)
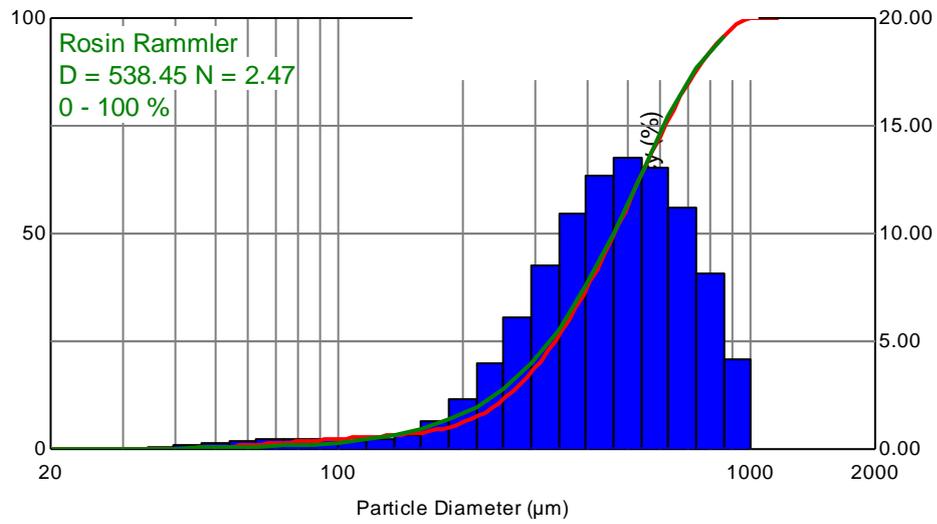


| Size (µm) | % V < | % V | Size (µm) | % V < | % V | Size (µm) | % V < | % V |
|-----------|-------|------|-----------|-------|------|-----------|--------|-------|
| 0.117 | 0.00 | 0.00 | 2.51 | 0.00 | 0.00 | 54.12 | 0.59 | 0.30 |
| 0.136 | 0.00 | 0.00 | 2.93 | 0.00 | 0.00 | 63.10 | 0.99 | 0.40 |
| 0.158 | 0.00 | 0.00 | 3.41 | 0.00 | 0.00 | 73.56 | 1.46 | 0.47 |
| 0.185 | 0.00 | 0.00 | 3.98 | 0.00 | 0.00 | 85.77 | 1.94 | 0.48 |
| 0.215 | 0.00 | 0.00 | 4.64 | 0.00 | 0.00 | 100.00 | 2.37 | 0.44 |
| 0.251 | 0.00 | 0.00 | 5.41 | 0.00 | 0.00 | 116.59 | 2.76 | 0.39 |
| 0.293 | 0.00 | 0.00 | 6.31 | 0.00 | 0.00 | 135.94 | 3.19 | 0.43 |
| 0.341 | 0.00 | 0.00 | 7.36 | 0.00 | 0.00 | 158.49 | 3.86 | 0.67 |
| 0.398 | 0.00 | 0.00 | 8.58 | 0.00 | 0.00 | 184.79 | 5.12 | 1.26 |
| 0.464 | 0.00 | 0.00 | 10.00 | 0.00 | 0.00 | 215.44 | 7.47 | 2.35 |
| 0.541 | 0.00 | 0.00 | 11.66 | 0.00 | 0.00 | 251.19 | 11.46 | 4.00 |
| 0.631 | 0.00 | 0.00 | 13.59 | 0.00 | 0.00 | 292.87 | 17.60 | 6.14 |
| 0.736 | 0.00 | 0.00 | 15.85 | 0.00 | 0.00 | 341.46 | 26.17 | 8.56 |
| 0.858 | 0.00 | 0.00 | 18.48 | 0.00 | 0.00 | 398.11 | 37.07 | 10.91 |
| 1.00 | 0.00 | 0.00 | 21.54 | 0.00 | 0.00 | 464.16 | 49.79 | 12.72 |
| 1.17 | 0.00 | 0.00 | 25.12 | 0.00 | 0.00 | 541.17 | 63.34 | 13.55 |
| 1.36 | 0.00 | 0.00 | 29.29 | 0.00 | 0.00 | 630.96 | 76.44 | 13.10 |
| 1.58 | 0.00 | 0.00 | 34.15 | 0.02 | 0.02 | 735.64 | 87.68 | 11.24 |
| 1.85 | 0.00 | 0.00 | 39.81 | 0.11 | 0.09 | 857.70 | 95.83 | 8.14 |
| 2.15 | 0.00 | 0.00 | 46.42 | 0.29 | 0.19 | 1000.00 | 100.00 | 4.17 |

**Average Measurement Parameters**          **28 Oct 2016 - 10:54:59.4004**

(average size distribution, weighted)
Example results555.smea\Import\Averages\V10a 1 1.psd
Sample : watersherry
Start+0.1996 (s) :: +0.4004 (s)

---

**Standard Values:**

| | | |
|---|---|---|
| Trans = 66.0 (%) | Dv(10) = 235.1 (µm) | Span = 1.138 |
| Cv = 1655 (PPM) | Dv(50) = 466.8 (µm) | D[3][2] = 361.2 (µm) |
| SSA = 0.0166 (m²/cc) | Dv(90) = 766.2 (µm) | D[4][3] = 482.9 (µm) |

---

**Notes:**
using catheter nozzle

---

**Average (average size distribution, weighted):**
Source file: V10a 1
502 Records Averaged                              0 Records Skipped
Average Range =  28 Oct 2016 - 10:54:59.1996 :: 10:54:59.4004

---

**Measurement Values and Settings**
Instrument = Spraytec - Open Spray

| | |
|---|---|
| Lens = 300mm | Path Length = 30.0 (mm) |
| Particulate Refractive Index = 1.33 + 0.000i | Scatter start = 1 |
| Dispersant Refractive Index = 1.00 | Scatter end = 35 |
| Particle Density = 1.00 (gm/cc) | Scattering threshold = 1 |
| Residual = 0.00  (%) | Minimum size = 0.10 (µm) |
| Extinction analysis = Off | Maximum size = 2500.00 (µm) |
| | Multiple Scatter = On |

---

**Identification**

| | |
|---|---|
| Operator = mnska | S/W =  v3.20.006 |
| Serial Numbers: Instrument = MAL1118761 | Detector = 10FT-CDL |
| SOP Name = -MANUAL 1- -IMPORTED MEASUREMENT- | |
| Last Edited = Not Edited | |

---

**Rapid Measurement**
Trigger = Manual
Trigger Delay = 0.0 msecs

Example results555.smea\Import\V10a 1 1.p
Sample : watersherry
Start+0.1000 (s)



Particle Diameter (µm)

| Size (µm) | % V < | % V | Size (µm) | % V < | % V | Size (µm) | % V < | % V |
|---|---|---|---|---|---|---|---|---|
| 0.117 | 0.00 | 0.00 | 2.51 | 0.00 | 0.00 | 54.12 | 0.52 | 0.27 |
| 0.136 | 0.00 | 0.00 | 2.93 | 0.00 | 0.00 | 63.10 | 0.89 | 0.38 |
| 0.158 | 0.00 | 0.00 | 3.41 | 0.00 | 0.00 | 73.56 | 1.34 | 0.45 |
| 0.185 | 0.00 | 0.00 | 3.98 | 0.00 | 0.00 | 85.77 | 1.82 | 0.48 |
| 0.215 | 0.00 | 0.00 | 4.64 | 0.00 | 0.00 | 100.00 | 2.27 | 0.45 |
| 0.251 | 0.00 | 0.00 | 5.41 | 0.00 | 0.00 | 116.59 | 2.66 | 0.39 |
| 0.293 | 0.00 | 0.00 | 6.31 | 0.00 | 0.00 | 135.94 | 3.05 | 0.39 |
| 0.341 | 0.00 | 0.00 | 7.36 | 0.00 | 0.00 | 158.49 | 3.62 | 0.57 |
| 0.398 | 0.00 | 0.00 | 8.58 | 0.00 | 0.00 | 184.79 | 4.69 | 1.07 |
| 0.464 | 0.00 | 0.00 | 10.00 | 0.00 | 0.00 | 215.44 | 6.74 | 2.05 |
| 0.541 | 0.00 | 0.00 | 11.66 | 0.00 | 0.00 | 251.19 | 10.38 | 3.64 |
| 0.631 | 0.00 | 0.00 | 13.59 | 0.00 | 0.00 | 292.87 | 16.17 | 5.79 |
| 0.736 | 0.00 | 0.00 | 15.85 | 0.00 | 0.00 | 341.46 | 24.49 | 8.32 |
| 0.858 | 0.00 | 0.00 | 18.48 | 0.00 | 0.00 | 398.11 | 35.34 | 10.86 |
| 1.00 | 0.00 | 0.00 | 21.54 | 0.00 | 0.00 | 464.16 | 48.23 | 12.88 |
| 1.17 | 0.00 | 0.00 | 25.12 | 0.00 | 0.00 | 541.17 | 62.13 | 13.90 |
| 1.36 | 0.00 | 0.00 | 29.29 | 0.00 | 0.00 | 630.96 | 75.65 | 13.52 |
| 1.58 | 0.00 | 0.00 | 34.15 | 0.01 | 0.01 | 735.64 | 87.28 | 11.63 |
| 1.85 | 0.00 | 0.00 | 39.81 | 0.08 | 0.07 | 857.70 | 95.69 | 8.42 |
| 2.15 | 0.00 | 0.00 | 46.42 | 0.25 | 0.16 | 1000.00 | 100.00 | 4.31 |

230

## d. Axial distance Drop size and DSD measurements at 120 mm

**Average Measurement Parameters**        **28 Oct 2016 - 10:46:09.4004**
(average size distribution, weighted)
Example results555.smea\Import\Averages\V12 1 1.psd
Sample : watersherry
Start+0.1996 (s) :: +0.4004 (s)

---

**Standard Values:**

| | | |
|---|---|---|
| Trans = 67.0 (%) | Dv(10) = 250.3 (µm) | Span = 1.086 |
| Cv = 1655 (PPM) | Dv(50) = 478.4 (µm) | D[3][2] = 376.7 (µm) |
| SSA = 0.0159 (m²/cc) | Dv(90) = 769.9 (µm) | D[4][3] = 493.2 (µm) |

---

**Notes:**
using catheter nozzle

---

**Average (average size distribution, weighted):**
Source file: V12 1
502 Records Averaged        0 Records Skipped
Average Range = 28 Oct 2016 - 10:46:09.1996 :: 10:46:09.4004

---

**Measurement Values and Settings**
Instrument = Spraytec - Open Spray

| | |
|---|---|
| Lens = 300mm | Path Length = 30.0 (mm) |
| Particulate Refractive Index = 1.33 + 0.000i | Scatter start = 1 |
| Dispersant Refractive Index = 1.00 | Scatter end = 36 |
| Particle Density = 1.00 (gm/cc) | Scattering threshold = 1 |
| Residual = 0.00 (%) | Minimum size = 0.10 (µm) |
| Extinction analysis = Off | Maximum size = 2500.00 (µm) |
| | Multiple Scatter = On |

---

**Identification**

| | |
|---|---|
| Operator = mnska | S/W = v3.20.006 |
| Serial Numbers: Instrument = MAL1118761 | Detector = 10FT-CDL |
| SOP Name = -MANUAL 2- -IMPORTED MEASUREMENT- | |
| Last Edited = Not Edited | |

---

**Rapid Measurement**
Trigger = Manual
Trigger Delay = 0.0 msecs

---

231

Example results555.smea\Import\V12 1 1.ps
Sample : watersherry
Start+0.1000 (s)



Rosin Rammler
D = 551.98 N = 2.54
0 - 100 %

Particle Diameter (µm)
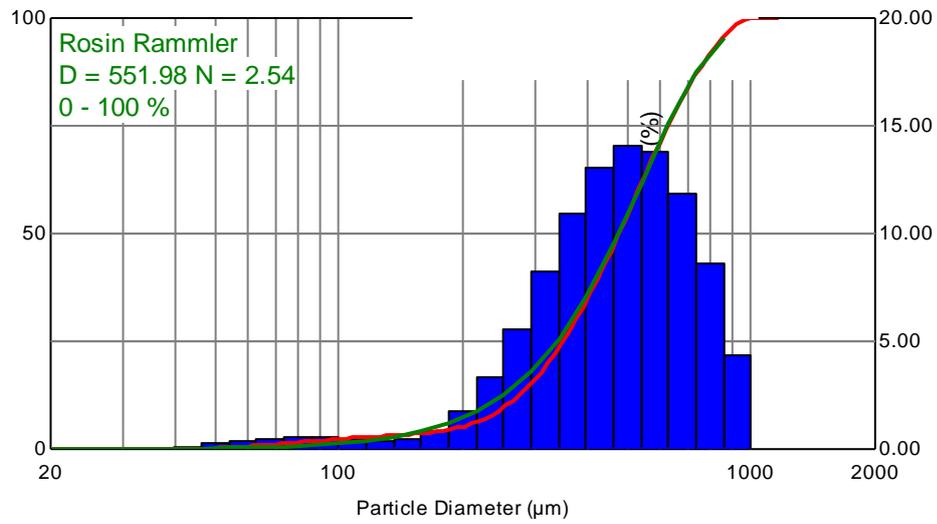
| Size (µm) | % V < | % V | Size (µm) | % V < | % V | Size (µm) | % V < | % V |
|---|---|---|---|---|---|---|---|---|
| 0.117 | 0.00 | 0.00 | 2.51 | 0.00 | 0.00 | 54.12 | 0.38 | 0.25 |
| 0.136 | 0.00 | 0.00 | 2.93 | 0.00 | 0.00 | 63.10 | 0.77 | 0.38 |
| 0.158 | 0.00 | 0.00 | 3.41 | 0.00 | 0.00 | 73.56 | 1.26 | 0.50 |
| 0.185 | 0.00 | 0.00 | 3.98 | 0.00 | 0.00 | 85.77 | 1.81 | 0.55 |
| 0.215 | 0.00 | 0.00 | 4.64 | 0.00 | 0.00 | 100.00 | 2.33 | 0.52 |
| 0.251 | 0.00 | 0.00 | 5.41 | 0.00 | 0.00 | 116.59 | 2.77 | 0.44 |
| 0.293 | 0.00 | 0.00 | 6.31 | 0.00 | 0.00 | 135.94 | 3.14 | 0.37 |
| 0.341 | 0.00 | 0.00 | 7.36 | 0.00 | 0.00 | 158.49 | 3.60 | 0.46 |
| 0.398 | 0.00 | 0.00 | 8.58 | 0.00 | 0.00 | 184.79 | 4.47 | 0.87 |
| 0.464 | 0.00 | 0.00 | 10.00 | 0.00 | 0.00 | 215.44 | 6.26 | 1.79 |
| 0.541 | 0.00 | 0.00 | 11.66 | 0.00 | 0.00 | 251.19 | 9.61 | 3.36 |
| 0.631 | 0.00 | 0.00 | 13.59 | 0.00 | 0.00 | 292.87 | 15.18 | 5.57 |
| 0.736 | 0.00 | 0.00 | 15.85 | 0.00 | 0.00 | 341.46 | 23.39 | 8.21 |
| 0.858 | 0.00 | 0.00 | 18.48 | 0.00 | 0.00 | 398.11 | 34.27 | 10.88 |
| 1.00 | 0.00 | 0.00 | 21.54 | 0.00 | 0.00 | 464.16 | 47.30 | 13.03 |
| 1.17 | 0.00 | 0.00 | 25.12 | 0.00 | 0.00 | 541.17 | 61.42 | 14.12 |
| 1.36 | 0.00 | 0.00 | 29.29 | 0.00 | 0.00 | 630.96 | 75.18 | 13.76 |
| 1.58 | 0.00 | 0.00 | 34.15 | 0.00 | 0.00 | 735.64 | 87.03 | 11.85 |
| 1.85 | 0.00 | 0.00 | 39.81 | 0.02 | 0.02 | 857.70 | 95.61 | 8.58 |
| 2.15 | 0.00 | 0.00 | 46.42 | 0.14 | 0.12 | 1000.00 | 100.00 | 4.39 |

**Average Measurement Parameters**  **28 Oct 2016 - 10:41:35.4004**

(average size distribution, weighted)
Example results555.smea\Import\Averages\V12a 1 1.psd
Sample : watersherry
Start+0.0696 (s) :: +0.4004 (s)

---

**Standard Values:**

| | | |
|---|---|---|
| Trans = 68.0 (%) | Dv(10) = 262.1 (µm) | Span = 1.048 |
| Cv = 1634 (PPM) | Dv(50) = 488.9 (µm) | D[3][2] = 387.6 (µm) |
| SSA = 0.0155 (m²/cc) | Dv(90) = 774.5 (µm) | D[4][3] = 502.4 (µm) |

---

**Notes:**
using catheter nozzle

---

**Average (average size distribution, weighted):**
Source file: V12a 1
827 Records Averaged                                         0 Records Skipped
Average Range =  28 Oct 2016 - 10:41:35.0696 :: 10:41:35.4004

---

**Measurement Values and Settings**
Instrument = Spraytec - Open Spray

| | |
|---|---|
| Lens = 300mm | Path Length = 30.0 (mm) |
| Particulate Refractive Index = 1.33 + 0.000i | Scatter start = 1 |
| Dispersant Refractive Index = 1.00 | Scatter end = 36 |
| Particle Density = 1.00 (gm/cc) | Scattering threshold = 1 |
| Residual = 0.00  (%) | Minimum size = 0.10 (µm) |
| Extinction analysis = Off | Maximum size = 2500.00 (µm) |
| | Multiple Scatter = On |

---

**Identification**

| | |
|---|---|
| Operator = mnska | S/W =  v3.20.006 |
| Serial Numbers: Instrument = MAL1118761 | Detector = 10FT-CDL |
| SOP Name = -MANUAL 1- -IMPORTED MEASUREMENT- | |
| Last Edited = Not Edited | |

---

**Rapid Measurement**
Trigger = Manual
Trigger Delay = 0.0 msecs

---

Example results555.smea\Import\V12a 1 1.p
Sample : watersherry
Start+0.1500 (s)



| Size (µm) | % V < | % V | Size (µm) | % V < | % V | Size (µm) | % V < | % V |
|---|---|---|---|---|---|---|---|---|
| 0.117 | 0.00 | 0.00 | 2.51 | 0.07 | 0.00 | 54.12 | 0.07 | 0.00 |
| 0.136 | 0.00 | 0.00 | 2.93 | 0.07 | 0.00 | 63.10 | 0.07 | 0.00 |
| 0.158 | 0.00 | 0.00 | 3.41 | 0.07 | 0.00 | 73.56 | 0.07 | 0.00 |
| 0.185 | 0.00 | 0.00 | 3.98 | 0.07 | 0.00 | 85.77 | 0.07 | 0.00 |
| 0.215 | 0.00 | 0.00 | 4.64 | 0.07 | 0.00 | 100.00 | 0.07 | 0.00 |
| 0.251 | 0.00 | 0.00 | 5.41 | 0.07 | 0.00 | 116.59 | 0.07 | 0.00 |
| 0.293 | 0.00 | 0.00 | 6.31 | 0.07 | 0.00 | 135.94 | 0.07 | 0.00 |
| 0.341 | 0.00 | 0.00 | 7.36 | 0.07 | 0.00 | 158.49 | 0.07 | 0.00 |
| 0.398 | 0.00 | 0.00 | 8.58 | 0.07 | 0.00 | 184.79 | 0.07 | 0.00 |
| 0.464 | 0.00 | 0.00 | 10.00 | 0.07 | 0.00 | 215.44 | 0.44 | 0.37 |
| 0.541 | 0.00 | 0.00 | 11.66 | 0.07 | 0.00 | 251.19 | 2.10 | 1.66 |
| 0.631 | 0.00 | 0.00 | 13.59 | 0.07 | 0.00 | 292.87 | 6.14 | 4.04 |
| 0.736 | 0.00 | 0.00 | 15.85 | 0.07 | 0.00 | 341.46 | 13.57 | 7.42 |
| 0.858 | 0.00 | 0.00 | 18.48 | 0.07 | 0.00 | 398.11 | 24.86 | 11.29 |
| 1.00 | 0.00 | 0.00 | 21.54 | 0.07 | 0.00 | 464.16 | 39.60 | 14.74 |
| 1.17 | 0.00 | 0.00 | 25.12 | 0.07 | 0.00 | 541.17 | 56.35 | 16.75 |
| 1.36 | 0.07 | 0.07 | 29.29 | 0.07 | 0.00 | 630.96 | 72.87 | 16.52 |
| 1.58 | 0.07 | 0.00 | 34.15 | 0.07 | 0.00 | 735.64 | 86.73 | 13.86 |
| 1.85 | 0.07 | 0.00 | 39.81 | 0.07 | 0.00 | 857.70 | 96.02 | 9.29 |
| 2.15 | 0.07 | 0.00 | 46.42 | 0.07 | 0.00 | 1000.00 | 100.00 | 3.98 |

| | Date-Time | File | Sample | Dx(10) | Dx(50) | Dx(90) |
|---|---|---|---|---|---|---|
| [V] | 28 Oct 2016... | V6a 1 1 | watersherry | 49.98 | 379.47 | 731.90 |
| [V] | 28 Oct 2016... | V8a 1 1 | watersherry | 236.49 | 466.16 | 764.36 |
| [V] | 28 Oct 2016... | V10a 1 1 | watersherry | 247.88 | 473.47 | 768.78 |
| [V] | 28 Oct 2016... | V12a 1 1 | watersherry | 320.12 | 511.04 | 770.51 |

[V]=Volume [N]=Number

**Frequency**

Example results555.smea\Overlays\V6a 1 1 1.pso

**9 Nov 2016 - 01:51:09**



| | Date-Time | File | Sample | Dx(10) | Dx(50) | Dx(90) |
|---|---|---|---|---|---|---|
| [V] | 28 Oct 2016... | V6a 1 1 | watersherry | 49.98 | 379.47 | 731.90 |
| [V] | 28 Oct 2016... | V8a 1 1 | watersherry | 236.49 | 466.16 | 764.36 |
| [V] | 28 Oct 2016... | V10a 1 1 | watersherry | 247.88 | 473.47 | 768.78 |
| [V] | 28 Oct 2016... | V12a 1 1 | watersherry | 320.12 | 511.04 | 770.51 |

[V]=Volume [N]=Number

235

## Cumulative

Example results555.smea\Overlays\V6 1
6cm away
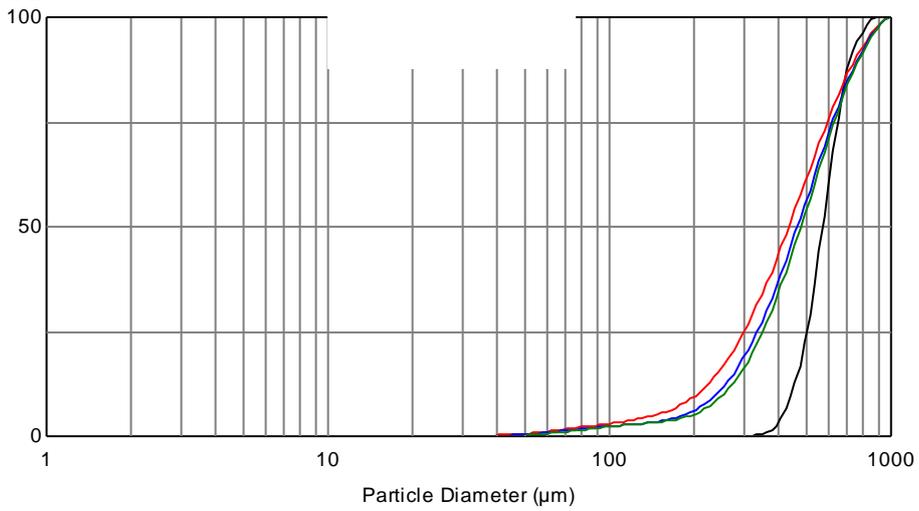


Particle Diameter (µm)

| | Date-Time | File | Sample | Dx(10) | Dx(50) | Dx(90) |
|---|---|---|---|---|---|---|
| [V] | 28 Oct 2016... | V6 1 1 | watersherry | 441.02 | 571.43 | 717.72 |
| [V] | 28 Oct 2016... | V8 1 1 | watersherry | 204.06 | 433.22 | 746.86 |
| [V] | 28 Oct 2016... | V10 1 1 | watersherry | 239.25 | 465.25 | 764.46 |
| [V] | 28 Oct 2016... | V12 1 1 | watersherry | 254.54 | 478.18 | 771.34 |

[V]=Volume [N]=Number

## Frequency

Example results555.smea\Overlays\V6 1 1 1.pso
6cm away
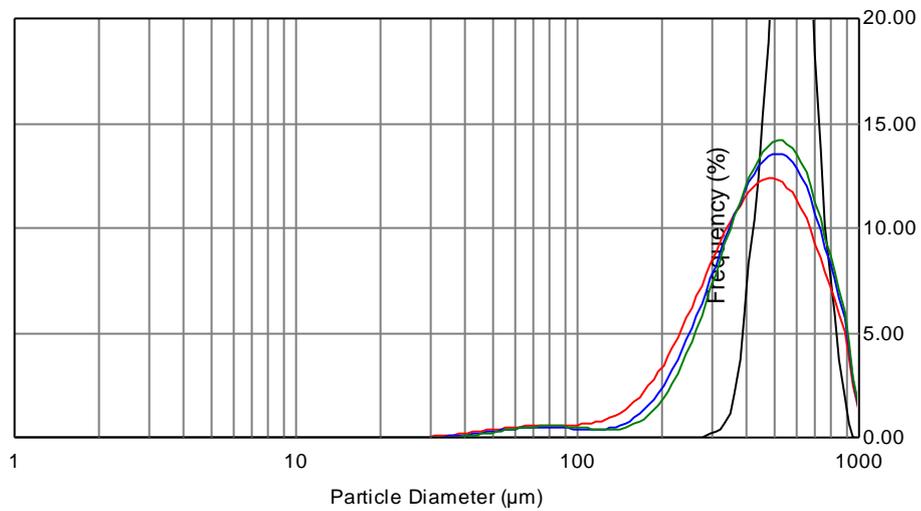


Particle Diameter (µm)

| | Date-Time | File | Sample | Dx(10) | Dx(50) | Dx(90) |
|---|---|---|---|---|---|---|
| [V] | 28 Oct 2016... | V6 1 1 | watersherry | 441.02 | 571.43 | 717.72 |
| [V] | 28 Oct 2016... | V8 1 1 | watersherry | 204.06 | 433.22 | 746.86 |
| [V] | 28 Oct 2016... | V10 1 1 | watersherry | 239.25 | 465.25 | 764.46 |
| [V] | 28 Oct 2016... | V12 1 1 | watersherry | 254.54 | 478.18 | 771.34 |

[V]=Volume [N]=Number

## e. Radial distances Drop sizes and DSD experimental results at y=60mm, x=10mm

| ! Average Measurement Parameters | 28 Oct 2016 - 11:24:16.2400 |
|---|---|

(average size distribution, weighted)
Example results666.smea\Import\Averages\V6_R10a_Proper 1 1.psd
Sample : watersherry
Start+0.0004 (s) :: +0.2400 (s)

**Standard Values:**

| | | |
|---|---|---|
| Trans = 44.9 (%) | Dv(10) = 262.2 (µm) | Span = 1.009 |
| Cv = 2966 (PPM) | Dv(50) = 488.4 (µm) | D[3][2] = 341.7 (µm) |
| SSA = 0.0176 (m²/cc) | Dv(90) = 755.1 (µm) | D[4][3] = 497.4 (µm) |

**Notes:**
using catheter nozzle

**Average (average size distribution, weighted):**
Source file: V6_R10a_Proper 1
586 Records Averaged                          13 Records Skipped
Average Range =  28 Oct 2016 - 11:24:16.0004 :: 11:24:16.2400

**Measurement Values and Settings**
Instrument = Spraytec - Open Spray

| | |
|---|---|
| Lens = 300mm | Path Length = 30.0 (mm) |
| Particulate Refractive Index = 1.33 + 0.000i | Scatter start = 1 |
| Dispersant Refractive Index = 1.00 | Scatter end = 36 |
| Particle Density = 1.00 (gm/cc) | Scattering threshold = 1 |
| Residual = 0.00   (%) | Minimum size = 0.10 (µm) |
| Extinction analysis = Off | Maximum size = 2500.00 (µm) |
| | Multiple Scatter = On |

**Identification**

| | |
|---|---|
| Operator = mnska | S/W =  v3.20.006 |
| Serial Numbers: Instrument = MAL1118761 | Detector = 10FT-CDL |
| SOP Name = -MANUAL 8- -IMPORTED MEASUREMENT- | |
| Last Edited = Not Edited | |

**Rapid Measurement**
Trigger = Manual
Trigger Delay = 0.0 msecs

! Low Light Transmission

Example results666.smea\Import\V6_R10a
Sample : watersherry
Start+0.2324 (s)



Rosin Rammler
D = 517.16 N = 2.37
0 - 100 %
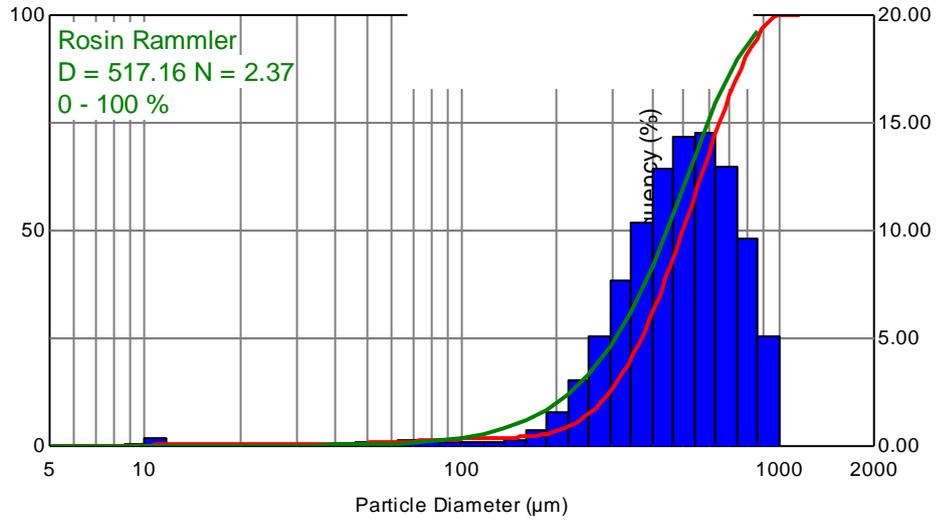
| Size (µm) | % V < | % V | Size (µm) | % V < | % V | Size (µm) | % V < | % V |
|-----------|-------|-----|-----------|-------|-----|-----------|-------|-----|
| 0.117 | 0.00 | 0.00 | 2.51 | 0.00 | 0.00 | 54.12 | 0.77 | 0.15 |
| 0.136 | 0.00 | 0.00 | 2.93 | 0.00 | 0.00 | 63.10 | 0.97 | 0.20 |
| 0.158 | 0.00 | 0.00 | 3.41 | 0.00 | 0.00 | 73.56 | 1.21 | 0.24 |
| 0.185 | 0.00 | 0.00 | 3.98 | 0.00 | 0.00 | 85.77 | 1.44 | 0.24 |
| 0.215 | 0.00 | 0.00 | 4.64 | 0.00 | 0.00 | 100.00 | 1.64 | 0.20 |
| 0.251 | 0.00 | 0.00 | 5.41 | 0.00 | 0.00 | 116.59 | 1.79 | 0.15 |
| 0.293 | 0.00 | 0.00 | 6.31 | 0.00 | 0.00 | 135.94 | 1.93 | 0.14 |
| 0.341 | 0.00 | 0.00 | 7.36 | 0.00 | 0.00 | 158.49 | 2.21 | 0.28 |
| 0.398 | 0.00 | 0.00 | 8.58 | 0.00 | 0.00 | 184.79 | 2.91 | 0.70 |
| 0.464 | 0.00 | 0.00 | 10.00 | 0.10 | 0.10 | 215.44 | 4.47 | 1.57 |
| 0.541 | 0.00 | 0.00 | 11.66 | 0.47 | 0.37 | 251.19 | 7.49 | 3.02 |
| 0.631 | 0.00 | 0.00 | 13.59 | 0.50 | 0.03 | 292.87 | 12.58 | 5.09 |
| 0.736 | 0.00 | 0.00 | 15.85 | 0.50 | 0.00 | 341.46 | 20.24 | 7.65 |
| 0.858 | 0.00 | 0.00 | 18.48 | 0.50 | 0.00 | 398.11 | 30.63 | 10.40 |
| 1.00 | 0.00 | 0.00 | 21.54 | 0.50 | 0.00 | 464.16 | 43.47 | 12.83 |
| 1.17 | 0.00 | 0.00 | 25.12 | 0.50 | 0.00 | 541.17 | 57.85 | 14.38 |
| 1.36 | 0.00 | 0.00 | 29.29 | 0.50 | 0.00 | 630.96 | 72.37 | 14.52 |
| 1.58 | 0.00 | 0.00 | 34.15 | 0.50 | 0.00 | 735.64 | 85.31 | 12.93 |
| 1.85 | 0.00 | 0.00 | 39.81 | 0.54 | 0.03 | 857.70 | 94.95 | 9.64 |
| 2.15 | 0.00 | 0.00 | 46.42 | 0.62 | 0.08 | 1000.00 | 100.00 | 5.05 |

238

e. **Radial distances Drop sizes and DSD experimental results at y=60mm, x=20mm**

| **Average Measurement Parameters** | **28 Oct 2016 - 12:06:33.4004** |
|---|---|

(average size distribution, weighted)
Example results666.smea\Import\Averages\V6_R20 1 1.psd
Sample : watersherry
Start+0.1996 (s) :: +0.4004 (s)

**Standard Values:**

| | | |
|---|---|---|
| Trans = 62.5 (%) | Dv(10) = 286.6 (µm) | Span = 0.9753 |
| Cv = 2016 (PPM) | Dv(50) = 497.5 (µm) | D[3][2] = 401.4 (µm) |
| SSA = 0.0149 (m²/cc) | Dv(90) = 771.8 (µm) | D[4][3] = 513 (µm) |

**Notes:**
using catheter nozzle

**Average (average size distribution, weighted):**
Source file: V6_R20 1
502 Records Averaged                    0 Records Skipped
Average Range = 28 Oct 2016 - 12:06:33.1996 :: 12:06:33.4004

**Measurement Values and Settings**
Instrument = Spraytec - Open Spray

| | |
|---|---|
| Lens = 300mm | Path Length = 30.0 (mm) |
| Particulate Refractive Index = 1.33 + 0.000i | Scatter start = 1 |
| Dispersant Refractive Index = 1.00 | Scatter end = 36 |
| Particle Density = 1.00 (gm/cc) | Scattering threshold = 1 |
| Residual = 0.00  (%) | Minimum size = 0.10 (µm) |
| Extinction analysis = Off | Maximum size = 2500.00 (µm) |
| | Multiple Scatter = On |

**Identification**

| | |
|---|---|
| Operator = mnska | S/W = v3.20.006 |
| Serial Numbers: Instrument = MAL1118761 | Detector = 10FT-CDL |
| SOP Name = -MANUAL 4- -IMPORTED MEASUREMENT- | |
| Last Edited = Not Edited | |

**Rapid Measurement**
Trigger = Manual
Trigger Delay = 0.0 msecs

Example results666.smea\Import\V6_R20 1
Sample : watersherry
Start+0.0996 (s)



Rosin Rammler
D = 584.94 N = 2.76
0 - 100 %

Particle Diameter (µm)
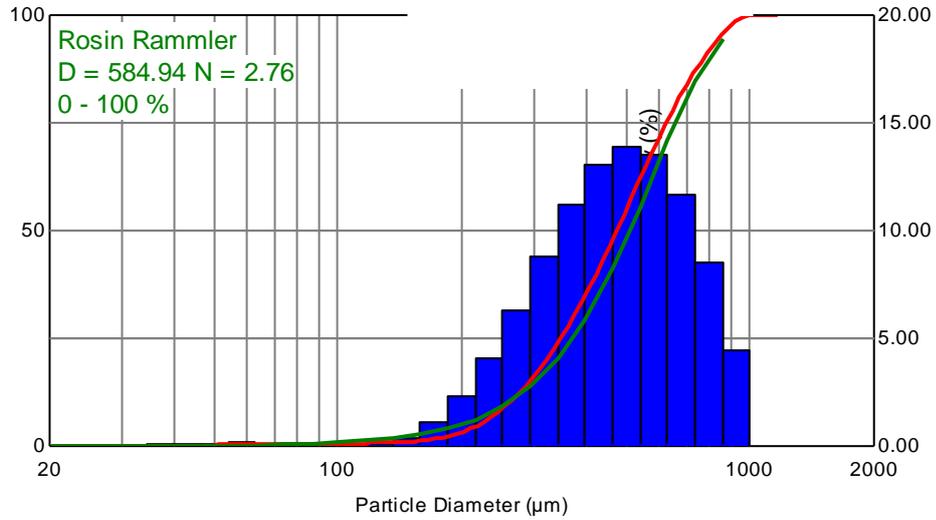
| Size (µm) | % V < | % V | Size (µm) | % V < | % V | Size (µm) | % V < | % V |
|---|---|---|---|---|---|---|---|---|
| 0.117 | 0.00 | 0.00 | 2.51 | 0.00 | 0.00 | 54.12 | 0.29 | 0.13 |
| 0.136 | 0.00 | 0.00 | 2.93 | 0.00 | 0.00 | 63.10 | 0.44 | 0.15 |
| 0.158 | 0.00 | 0.00 | 3.41 | 0.00 | 0.00 | 73.56 | 0.58 | 0.14 |
| 0.185 | 0.00 | 0.00 | 3.98 | 0.00 | 0.00 | 85.77 | 0.66 | 0.09 |
| 0.215 | 0.00 | 0.00 | 4.64 | 0.00 | 0.00 | 100.00 | 0.69 | 0.03 |
| 0.251 | 0.00 | 0.00 | 5.41 | 0.00 | 0.00 | 116.59 | 0.69 | 0.00 |
| 0.293 | 0.00 | 0.00 | 6.31 | 0.00 | 0.00 | 135.94 | 0.78 | 0.09 |
| 0.341 | 0.00 | 0.00 | 7.36 | 0.00 | 0.00 | 158.49 | 1.19 | 0.41 |
| 0.398 | 0.00 | 0.00 | 8.58 | 0.00 | 0.00 | 184.79 | 2.30 | 1.11 |
| 0.464 | 0.00 | 0.00 | 10.00 | 0.00 | 0.00 | 215.44 | 4.62 | 2.32 |
| 0.541 | 0.00 | 0.00 | 11.66 | 0.00 | 0.00 | 251.19 | 8.70 | 4.07 |
| 0.631 | 0.00 | 0.00 | 13.59 | 0.00 | 0.00 | 292.87 | 15.00 | 6.31 |
| 0.736 | 0.00 | 0.00 | 15.85 | 0.00 | 0.00 | 341.46 | 23.80 | 8.79 |
| 0.858 | 0.00 | 0.00 | 18.48 | 0.00 | 0.00 | 398.11 | 34.98 | 11.18 |
| 1.00 | 0.00 | 0.00 | 21.54 | 0.00 | 0.00 | 464.16 | 48.02 | 13.04 |
| 1.17 | 0.00 | 0.00 | 25.12 | 0.00 | 0.00 | 541.17 | 61.93 | 13.91 |
| 1.36 | 0.00 | 0.00 | 29.29 | 0.00 | 0.00 | 630.96 | 75.43 | 13.50 |
| 1.58 | 0.00 | 0.00 | 34.15 | 0.02 | 0.02 | 735.64 | 87.08 | 11.66 |
| 1.85 | 0.00 | 0.00 | 39.81 | 0.07 | 0.05 | 857.70 | 95.59 | 8.51 |
| 2.15 | 0.00 | 0.00 | 46.42 | 0.16 | 0.09 | 1000.00 | 100.00 | 4.41 |

240

**f. Radial distances Drop sizes and DSD experimental results at y=60mm, x=30mm**

---

**! Average Measurement Parameters**                    **28 Oct 2016 - 12:09:22.3000**

(average size distribution, weighted)
Example results666.smea\Import\Averages\V6_R30 1 1.psd
Sample : watersherry
Start+0.0004 (s) :: +0.3000 (s)

---

**Standard Values:**

| | | |
|---|---|---|
| Trans = 84.6 (%) | Dv(10) = 244 (µm) | Span = 1.095 |
| Cv = 656.2 (PPM) | Dv(50) = 479.3 (µm) | D[3][2] = 361.6 (µm) |
| SSA = 0.0166 (m²/cc) | Dv(90) = 768.6 (µm) | D[4][3] = 491.8 (µm) |

---

**Notes:**
using catheter nozzle

---

**Average (average size distribution, weighted):**
Source file: V6_R30 1
747 Records Averaged                         2 Records Skipped
Average Range = 28 Oct 2016 - 12:09:22.0004 :: 12:09:22.3000

---

**Measurement Values and Settings**
Instrument = Spraytec - Open Spray

| | |
|---|---|
| Lens = 300mm | Path Length = 30.0 (mm) |
| Particulate Refractive Index = 1.33 + 0.000i | Scatter start = 1 |
| Dispersant Refractive Index = 1.00 | Scatter end = 36 |
| Particle Density = 1.00 (gm/cc) | Scattering threshold = 1 |
| Residual = 0.00 (%) | Minimum size = 0.10 (µm) |
| Extinction analysis = Off | Maximum size = 2500.00 (µm) |
| | Multiple Scatter = On |

---

**Identification**

| | |
|---|---|
| Operator = mnska | S/W = v3.20.006 |
| Serial Numbers: Instrument = MAL1118761 | Detector = 10FT-CDL |
| SOP Name = -MANUAL 5- -IMPORTED MEASUREMENT- | |
| Last Edited = Not Edited | |

---

**Rapid Measurement**
Trigger = Manual
Trigger Delay = 0.0 msecs

---

! Low Scattering Signal

241

## Particle Size Distribution

Example results666.smea\Import\V6_R30 1
Sample : watersherry
Start+0.0996 (s)



Rosin Rammler
D = 541.94 N = 2.49
0 - 100 %
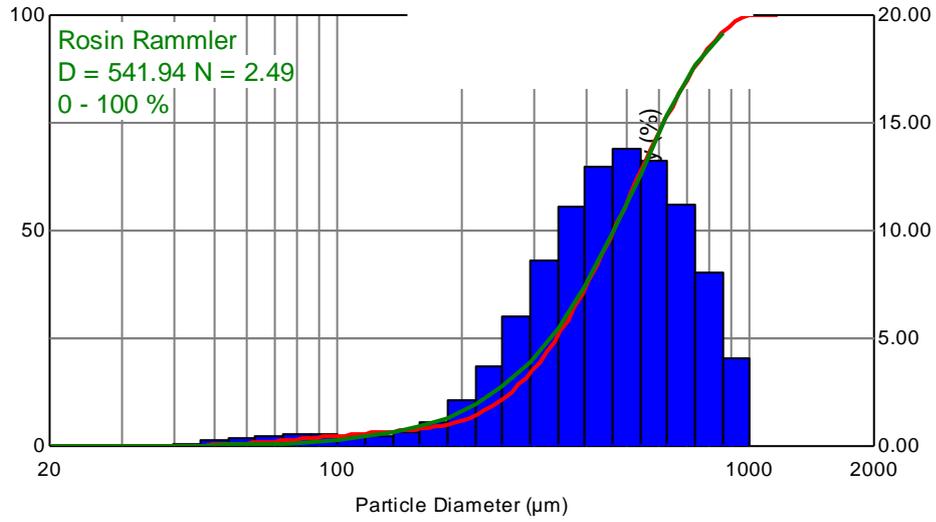
| Size (µm) | % V < | % V | Size (µm) | % V < | % V | Size (µm) | % V < | % V |
|---|---|---|---|---|---|---|---|---|
| 0.117 | 0.00 | 0.00 | 2.51 | 0.00 | 0.00 | 54.12 | 0.42 | 0.26 |
| 0.136 | 0.00 | 0.00 | 2.93 | 0.00 | 0.00 | 63.10 | 0.81 | 0.39 |
| 0.158 | 0.00 | 0.00 | 3.41 | 0.00 | 0.00 | 73.56 | 1.32 | 0.51 |
| 0.185 | 0.00 | 0.00 | 3.98 | 0.00 | 0.00 | 85.77 | 1.88 | 0.56 |
| 0.215 | 0.00 | 0.00 | 4.64 | 0.00 | 0.00 | 100.00 | 2.42 | 0.54 |
| 0.251 | 0.00 | 0.00 | 5.41 | 0.00 | 0.00 | 116.59 | 2.91 | 0.49 |
| 0.293 | 0.00 | 0.00 | 6.31 | 0.00 | 0.00 | 135.94 | 3.37 | 0.46 |
| 0.341 | 0.00 | 0.00 | 7.36 | 0.00 | 0.00 | 158.49 | 3.97 | 0.60 |
| 0.398 | 0.00 | 0.00 | 8.58 | 0.00 | 0.00 | 184.79 | 5.06 | 1.09 |
| 0.464 | 0.00 | 0.00 | 10.00 | 0.00 | 0.00 | 215.44 | 7.16 | 2.10 |
| 0.541 | 0.00 | 0.00 | 11.66 | 0.00 | 0.00 | 251.19 | 10.91 | 3.75 |
| 0.631 | 0.00 | 0.00 | 13.59 | 0.00 | 0.00 | 292.87 | 16.90 | 5.99 |
| 0.736 | 0.00 | 0.00 | 15.85 | 0.00 | 0.00 | 341.46 | 25.48 | 8.58 |
| 0.858 | 0.00 | 0.00 | 18.48 | 0.00 | 0.00 | 398.11 | 36.56 | 11.08 |
| 1.00 | 0.00 | 0.00 | 21.54 | 0.00 | 0.00 | 464.16 | 49.55 | 12.99 |
| 1.17 | 0.00 | 0.00 | 25.12 | 0.00 | 0.00 | 541.17 | 63.35 | 13.80 |
| 1.36 | 0.00 | 0.00 | 29.29 | 0.00 | 0.00 | 630.96 | 76.59 | 13.24 |
| 1.58 | 0.00 | 0.00 | 34.15 | 0.00 | 0.00 | 735.64 | 87.83 | 11.25 |
| 1.85 | 0.00 | 0.00 | 39.81 | 0.03 | 0.03 | 857.70 | 95.90 | 8.06 |
| 2.15 | 0.00 | 0.00 | 46.42 | 0.16 | 0.13 | 1000.00 | 100.00 | 4.10 |

242

### g. Radial distances Drop sizes and DSD experimental results at y=80mm, x=10mm

**Average Measurement Parameters**                    **28 Oct 2016 - 12:23:18.4004**

(average size distribution, weighted)
Example results666.smea\Import\Averages\V8_R10 1 1.psd
Sample : watersherry
Start+0.1996 (s) :: +0.4004 (s)

---

**Standard Values:**

| | | |
|---|---|---|
| Trans = 68.5 (%) | Dv(10) = 285.6 (µm) | Span = 0.9809 |
| Cv = 1646 (PPM) | Dv(50) = 496.9 (µm) | D[3][2] = 407.5 (µm) |
| SSA = 0.0147 (m²/cc) | Dv(90) = 773 (µm) | D[4][3] = 512.8 (µm) |

---

**Notes:**
using catheter nozzle

---

**Average (average size distribution, weighted):**
Source file: V8_R10 1
502 Records Averaged                              0 Records Skipped
Average Range =  28 Oct 2016 - 12:23:18.1996 :: 12:23:18.4004

---

**Measurement Values and Settings**
Instrument = Spraytec - Open Spray

| | |
|---|---|
| Lens = 300mm | Path Length = 30.0 (mm) |
| Particulate Refractive Index = 1.33 + 0.000i | Scatter start = 1 |
| Dispersant Refractive Index = 1.00 | Scatter end = 36 |
| Particle Density = 1.00 (gm/cc) | Scattering threshold = 1 |
| Residual = 0.00   (%) | Minimum size = 0.10 (µm) |
| Extinction analysis = Off | Maximum size = 2500.00 (µm) |
| | Multiple Scatter = On |

---

**Identification**

| | |
|---|---|
| Operator = mnska | S/W =  v3.20.006 |
| Serial Numbers: Instrument = MAL1118761 | Detector = 10FT-CDL |

SOP Name = -MANUAL 12- -IMPORTED MEASUREMENT-
Last Edited = Not Edited

---

**Rapid Measurement**
Trigger = Manual
Trigger Delay = 0.0 msecs

## Particle Size Distribution

Example results666.smea\Import\V8_R10 1
Sample : watersherry
Start+0.0996 (s)



Rosin Rammler
D = 547.99 N = 2.54
0 - 100 %

Particle Diameter (µm)
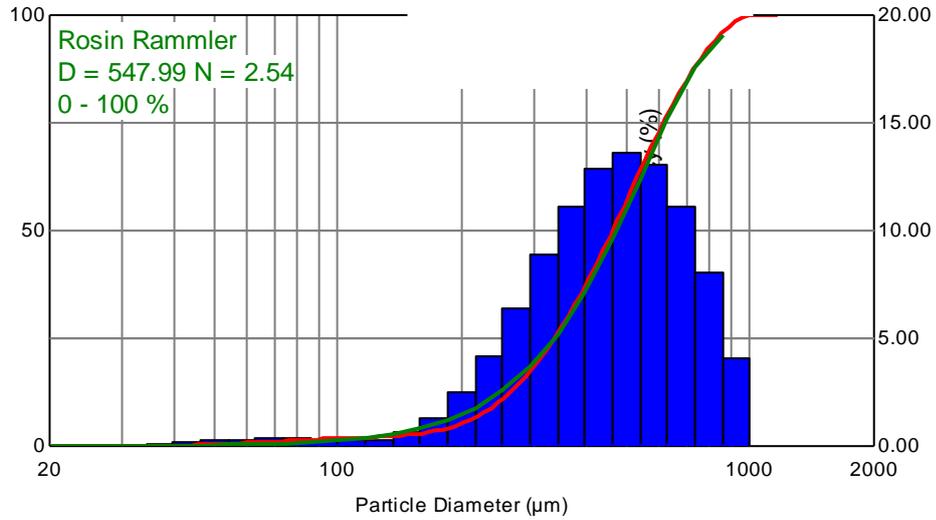
| Size (µm) | % V < | % V | Size (µm) | % V < | % V | Size (µm) | % V < | % V |
|---|---|---|---|---|---|---|---|---|
| 0.117 | 0.00 | 0.00 | 2.51 | 0.00 | 0.00 | 54.12 | 0.50 | 0.24 |
| 0.136 | 0.00 | 0.00 | 2.93 | 0.00 | 0.00 | 63.10 | 0.81 | 0.31 |
| 0.158 | 0.00 | 0.00 | 3.41 | 0.00 | 0.00 | 73.56 | 1.16 | 0.34 |
| 0.185 | 0.00 | 0.00 | 3.98 | 0.00 | 0.00 | 85.77 | 1.49 | 0.33 |
| 0.215 | 0.00 | 0.00 | 4.64 | 0.00 | 0.00 | 100.00 | 1.76 | 0.28 |
| 0.251 | 0.00 | 0.00 | 5.41 | 0.00 | 0.00 | 116.59 | 2.00 | 0.24 |
| 0.293 | 0.00 | 0.00 | 6.31 | 0.00 | 0.00 | 135.94 | 2.31 | 0.31 |
| 0.341 | 0.00 | 0.00 | 7.36 | 0.00 | 0.00 | 158.49 | 2.92 | 0.61 |
| 0.398 | 0.00 | 0.00 | 8.58 | 0.00 | 0.00 | 184.79 | 4.20 | 1.28 |
| 0.464 | 0.00 | 0.00 | 10.00 | 0.00 | 0.00 | 215.44 | 6.66 | 2.46 |
| 0.541 | 0.00 | 0.00 | 11.66 | 0.00 | 0.00 | 251.19 | 10.86 | 4.20 |
| 0.631 | 0.00 | 0.00 | 13.59 | 0.00 | 0.00 | 292.87 | 17.26 | 6.41 |
| 0.736 | 0.00 | 0.00 | 15.85 | 0.00 | 0.00 | 341.46 | 26.11 | 8.85 |
| 0.858 | 0.00 | 0.00 | 18.48 | 0.00 | 0.00 | 398.11 | 37.26 | 11.15 |
| 1.00 | 0.00 | 0.00 | 21.54 | 0.00 | 0.00 | 464.16 | 50.12 | 12.86 |
| 1.17 | 0.00 | 0.00 | 25.12 | 0.00 | 0.00 | 541.17 | 63.70 | 13.58 |
| 1.36 | 0.00 | 0.00 | 29.29 | 0.00 | 0.00 | 630.96 | 76.72 | 13.02 |
| 1.58 | 0.00 | 0.00 | 34.15 | 0.02 | 0.02 | 735.64 | 87.85 | 11.13 |
| 1.85 | 0.00 | 0.00 | 39.81 | 0.10 | 0.08 | 857.70 | 95.88 | 8.04 |
| 2.15 | 0.00 | 0.00 | 46.42 | 0.26 | 0.16 | 1000.00 | 100.00 | 4.12 |

244

### h. Radial distances Drop sizes and DSD experimental results at y=80mm, x=15mm

**Average Measurement Parameters**        **28 Oct 2016 - 11:44:01.4004**

(average size distribution, weighted)
Example results666.smea\Import\Averages\V8_R15a_Proper 1 1.psd
Sample : watersherry
Start+0.1996 (s) :: +0.4004 (s)

---

**Standard Values:**

| | | |
|---|---|---|
| Trans = 64.8 (%) | Dv(10) = 274.2 (µm) | Span = 1.015 |
| Cv = 1870 (PPM) | Dv(50) = 489.5 (µm) | D[3][2] = 397.1 (µm) |
| SSA = 0.0151 (m²/cc) | Dv(90) = 771 (µm) | D[4][3] = 505.3 (µm) |

---

**Notes:**
using catheter nozzle

---

**Average (average size distribution, weighted):**
Source file: V8_R15a_Proper 1
502 Records Averaged        0 Records Skipped
Average Range =  28 Oct 2016 - 11:44:01.1996 :: 11:44:01.4004

---

**Measurement Values and Settings**
Instrument = Spraytec - Open Spray

| | |
|---|---|
| Lens = 300mm | Path Length = 30.0 (mm) |
| Particulate Refractive Index = 1.33 + 0.000i | Scatter start = 1 |
| Dispersant Refractive Index = 1.00 | Scatter end = 36 |
| Particle Density = 1.00 (gm/cc) | Scattering threshold = 1 |
| Residual = 0.00   (%) | Minimum size = 0.10 (µm) |
| Extinction analysis = Off | Maximum size = 2500.00 (µm) |
| | Multiple Scatter = On |

---

**Identification**

| | |
|---|---|
| Operator = mnska | S/W =  v3.20.006 |
| Serial Numbers: Instrument = MAL1118761 | Detector = 10FT-CDL |
| SOP Name = -MANUAL 10- -IMPORTED MEASUREMENT- | |
| Last Edited = Not Edited | |

---

**Rapid Measurement**
Trigger = Manual
Trigger Delay = 0.0 msecs

---

# Particle Size Distribution

Example results666.smea\Import\V8_R15a
Sample : watersherry
Start+0.0996 (s)



Rosin Rammler
D = 558.74 N = 2.60
0 - 100 %

Particle Diameter (μm)
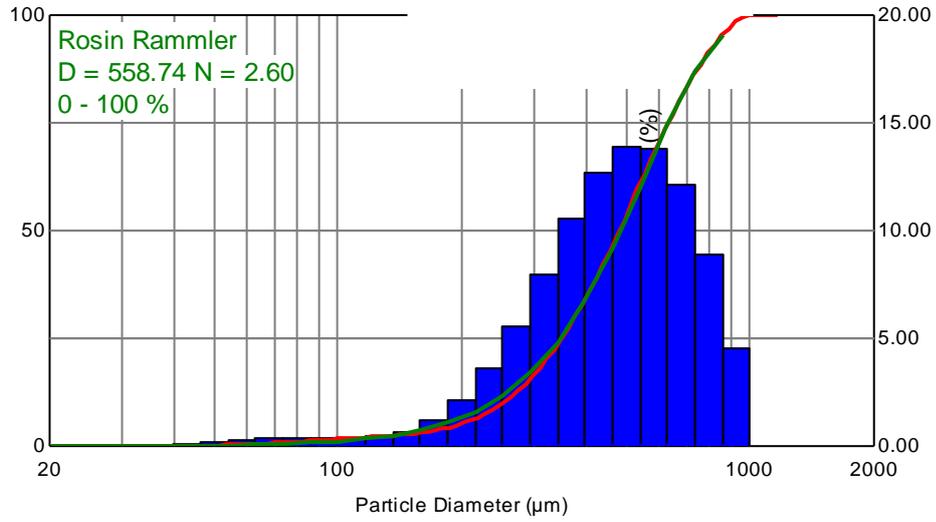
| Size (μm) | % V < | % V | Size (μm) | % V < | % V | Size (μm) | % V < | % V |
|---|---|---|---|---|---|---|---|---|
| 0.117 | 0.00 | 0.00 | 2.51 | 0.00 | 0.00 | 54.12 | 0.30 | 0.17 |
| 0.136 | 0.00 | 0.00 | 2.93 | 0.00 | 0.00 | 63.10 | 0.55 | 0.26 |
| 0.158 | 0.00 | 0.00 | 3.41 | 0.00 | 0.00 | 73.56 | 0.88 | 0.33 |
| 0.185 | 0.00 | 0.00 | 3.98 | 0.00 | 0.00 | 85.77 | 1.25 | 0.37 |
| 0.215 | 0.00 | 0.00 | 4.64 | 0.00 | 0.00 | 100.00 | 1.63 | 0.38 |
| 0.251 | 0.00 | 0.00 | 5.41 | 0.00 | 0.00 | 116.59 | 2.02 | 0.39 |
| 0.293 | 0.00 | 0.00 | 6.31 | 0.00 | 0.00 | 135.94 | 2.47 | 0.45 |
| 0.341 | 0.00 | 0.00 | 7.36 | 0.00 | 0.00 | 158.49 | 3.14 | 0.67 |
| 0.398 | 0.00 | 0.00 | 8.58 | 0.00 | 0.00 | 184.79 | 4.31 | 1.17 |
| 0.464 | 0.00 | 0.00 | 10.00 | 0.00 | 0.00 | 215.44 | 6.41 | 2.10 |
| 0.541 | 0.00 | 0.00 | 11.66 | 0.00 | 0.00 | 251.19 | 9.98 | 3.57 |
| 0.631 | 0.00 | 0.00 | 13.59 | 0.00 | 0.00 | 292.87 | 15.56 | 5.58 |
| 0.736 | 0.00 | 0.00 | 15.85 | 0.00 | 0.00 | 341.46 | 23.56 | 8.00 |
| 0.858 | 0.00 | 0.00 | 18.48 | 0.00 | 0.00 | 398.11 | 34.07 | 10.52 |
| 1.00 | 0.00 | 0.00 | 21.54 | 0.00 | 0.00 | 464.16 | 46.75 | 12.67 |
| 1.17 | 0.00 | 0.00 | 25.12 | 0.00 | 0.00 | 541.17 | 60.67 | 13.92 |
| 1.36 | 0.00 | 0.00 | 29.29 | 0.00 | 0.00 | 630.96 | 74.47 | 13.81 |
| 1.58 | 0.00 | 0.00 | 34.15 | 0.00 | 0.00 | 735.64 | 86.56 | 12.09 |
| 1.85 | 0.00 | 0.00 | 39.81 | 0.03 | 0.03 | 857.70 | 95.42 | 8.87 |
| 2.15 | 0.00 | 0.00 | 46.42 | 0.12 | 0.09 | 1000.00 | 100.00 | 4.58 |

246

### i. Radial distances Drop sizes and DSD experimental results at y=80mm, x=20mm

**Average Measurement Parameters**       **28 Oct 2016 - 12:05:02.4004**

(average size distribution, weighted)
Example results666.smea\Import\Averages\V8_R20 1 1.psd
Sample : watersherry
Start+0.1996 (s) :: +0.4004 (s)

---

**Standard Values:**

| | | |
|---|---|---|
| Trans = 68.5 (%) | Dv(10) = 287.9 (µm) | Span = 0.9735 |
| Cv = 1644 (PPM) | Dv(50) = 498.8 (µm) | D[3][2] = 406.8 (µm) |
| SSA = 0.0147 (m²/cc) | Dv(90) = 773.5 (µm) | D[4][3] = 514.3 (µm) |

---

**Notes:**
using catheter nozzle

---

**Average (average size distribution, weighted):**
Source file: V8_R20 1
502 Records Averaged      0 Records Skipped
Average Range = 28 Oct 2016 - 12:05:02.1996 :: 12:05:02.4004

---

**Measurement Values and Settings**
Instrument = Spraytec - Open Spray

| | |
|---|---|
| Lens = 300mm | Path Length = 30.0 (mm) |
| Particulate Refractive Index = 1.33 + 0.000i | Scatter start = 1 |
| Dispersant Refractive Index = 1.00 | Scatter end = 36 |
| Particle Density = 1.00 (gm/cc) | Scattering threshold = 1 |
| Residual = 0.00 (%) | Minimum size = 0.10 (µm) |
| Extinction analysis = Off | Maximum size = 2500.00 (µm) |
| | Multiple Scatter = On |

---

**Identification**

| | |
|---|---|
| Operator = mnska | S/W = v3.20.006 |
| Serial Numbers: Instrument = MAL1118761 | Detector = 10FT-CDL |
| SOP Name = -MANUAL 3- -IMPORTED MEASUREMENT- | |
| Last Edited = Not Edited | |

---

**Rapid Measurement**
Trigger = Manual
Trigger Delay = 0.0 msecs

Example results666.smea\Import\V8_R20 1
Sample : watersherry
Start+0.0996 (s)
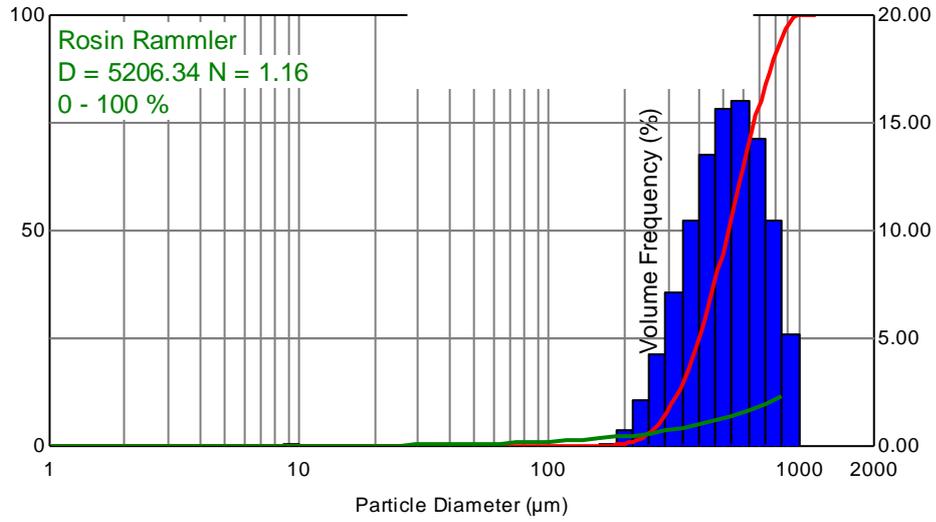


| Size (µm) | % V < | % V | Size (µm) | % V < | % V | Size (µm) | % V < | % V |
|-----------|-------|-----|-----------|-------|-----|-----------|-------|-----|
| 0.117 | 0.00 | 0.00 | 2.51 | 0.04 | 0.00 | 54.12 | 0.11 | 0.00 |
| 0.136 | 0.00 | 0.00 | 2.93 | 0.04 | 0.00 | 63.10 | 0.11 | 0.00 |
| 0.158 | 0.00 | 0.00 | 3.41 | 0.04 | 0.00 | 73.56 | 0.11 | 0.00 |
| 0.185 | 0.00 | 0.00 | 3.98 | 0.04 | 0.00 | 85.77 | 0.11 | 0.00 |
| 0.215 | 0.00 | 0.00 | 4.64 | 0.04 | 0.00 | 100.00 | 0.11 | 0.00 |
| 0.251 | 0.00 | 0.00 | 5.41 | 0.04 | 0.00 | 116.59 | 0.11 | 0.00 |
| 0.293 | 0.00 | 0.00 | 6.31 | 0.04 | 0.00 | 135.94 | 0.11 | 0.00 |
| 0.341 | 0.00 | 0.00 | 7.36 | 0.04 | 0.00 | 158.49 | 0.11 | 0.00 |
| 0.398 | 0.00 | 0.00 | 8.58 | 0.04 | 0.00 | 184.79 | 0.22 | 0.10 |
| 0.464 | 0.00 | 0.00 | 10.00 | 0.11 | 0.08 | 215.44 | 0.98 | 0.76 |
| 0.541 | 0.00 | 0.00 | 11.66 | 0.11 | 0.00 | 251.19 | 3.07 | 2.10 |
| 0.631 | 0.00 | 0.00 | 13.59 | 0.11 | 0.00 | 292.87 | 7.33 | 4.25 |
| 0.736 | 0.00 | 0.00 | 15.85 | 0.11 | 0.00 | 341.46 | 14.47 | 7.14 |
| 0.858 | 0.00 | 0.00 | 18.48 | 0.11 | 0.00 | 398.11 | 24.89 | 10.43 |
| 1.00 | 0.00 | 0.00 | 21.54 | 0.11 | 0.00 | 464.16 | 38.40 | 13.51 |
| 1.17 | 0.00 | 0.00 | 25.12 | 0.11 | 0.00 | 541.17 | 54.01 | 15.61 |
| 1.36 | 0.04 | 0.04 | 29.29 | 0.11 | 0.00 | 630.96 | 70.03 | 16.02 |
| 1.58 | 0.04 | 0.00 | 34.15 | 0.11 | 0.00 | 735.64 | 84.31 | 14.29 |
| 1.85 | 0.04 | 0.00 | 39.81 | 0.11 | 0.00 | 857.70 | 94.79 | 10.48 |
| 2.15 | 0.04 | 0.00 | 46.42 | 0.11 | 0.00 | 1000.00 | 100.00 | 5.21 |

### j. Radial distances Drop sizes and DSD experimental results at y=80mm, x=30mm

**Average Measurement Parameters**               **28 Oct 2016 - 12:11:41.4004**

(average size distribution, weighted)
Example results666.smea\Import\Averages\V8_R30 1 1.psd
Sample : watersherry
Start+0.1996 (s) :: +0.4004 (s)

---

**Standard Values:**

| | | |
|---|---|---|
| Trans = 75.9 (%) | Dv(10) = 251.8 (µm) | Span = 1.082 |
| Cv = 1120 (PPM) | Dv(50) = 473.2 (µm) | D[3][2] = 374.3 (µm) |
| SSA = 0.0160 (m²/cc) | Dv(90) = 763.7 (µm) | D[4][3] = 489.9 (µm) |

---

**Notes:**
using catheter nozzle

---

**Average (average size distribution, weighted):**
Source file: V8_R30 1
502 Records Averaged                                    0 Records Skipped
Average Range = 28 Oct 2016 - 12:11:41.1996 :: 12:11:41.4004

---

**Measurement Values and Settings**
Instrument = Spraytec - Open Spray

| | |
|---|---|
| Lens = 300mm | Path Length = 30.0 (mm) |
| Particulate Refractive Index = 1.33 + 0.000i | Scatter start = 1 |
| Dispersant Refractive Index = 1.00 | Scatter end = 36 |
| Particle Density = 1.00 (gm/cc) | Scattering threshold = 1 |
| Residual = 0.00  (%) | Minimum size = 0.10 (µm) |
| Extinction analysis = Off | Maximum size = 2500.00 (µm) |
| | Multiple Scatter = On |

---

**Identification**

| | |
|---|---|
| Operator = mnska | S/W = v3.20.006 |
| Serial Numbers: Instrument = MAL1118761 | Detector = 10FT-CDL |
| SOP Name = -MANUAL 6- -IMPORTED MEASUREMENT- | |
| Last Edited = Not Edited | |

---

**Rapid Measurement**
Trigger = Manual
Trigger Delay = 0.0 msecs

Example results666.smea\Import\V8_R30 1
Sample : watersherry
Start+0.0996 (s)
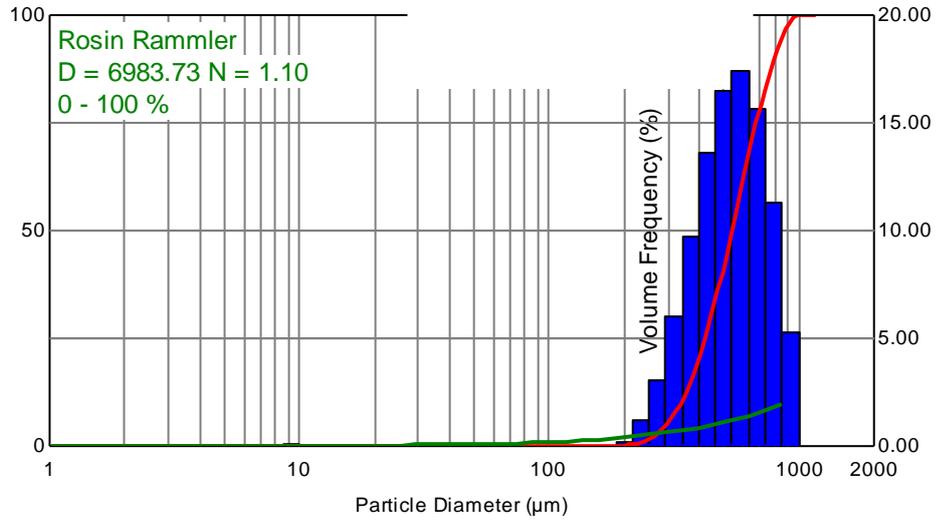


| Size (µm) | % V < | % V | Size (µm) | % V < | % V | Size (µm) | % V < | % V |
|---|---|---|---|---|---|---|---|---|
| 0.117 | 0.00 | 0.00 | 2.51 | 0.04 | 0.00 | 54.12 | 0.12 | 0.00 |
| 0.136 | 0.00 | 0.00 | 2.93 | 0.04 | 0.00 | 63.10 | 0.12 | 0.00 |
| 0.158 | 0.00 | 0.00 | 3.41 | 0.04 | 0.00 | 73.56 | 0.12 | 0.00 |
| 0.185 | 0.00 | 0.00 | 3.98 | 0.04 | 0.00 | 85.77 | 0.12 | 0.00 |
| 0.215 | 0.00 | 0.00 | 4.64 | 0.04 | 0.00 | 100.00 | 0.12 | 0.00 |
| 0.251 | 0.00 | 0.00 | 5.41 | 0.04 | 0.00 | 116.59 | 0.12 | 0.00 |
| 0.293 | 0.00 | 0.00 | 6.31 | 0.04 | 0.00 | 135.94 | 0.12 | 0.00 |
| 0.341 | 0.00 | 0.00 | 7.36 | 0.04 | 0.00 | 158.49 | 0.12 | 0.00 |
| 0.398 | 0.00 | 0.00 | 8.58 | 0.04 | 0.00 | 184.79 | 0.12 | 0.00 |
| 0.464 | 0.00 | 0.00 | 10.00 | 0.12 | 0.08 | 215.44 | 0.35 | 0.23 |
| 0.541 | 0.00 | 0.00 | 11.66 | 0.12 | 0.00 | 251.19 | 1.53 | 1.18 |
| 0.631 | 0.00 | 0.00 | 13.59 | 0.12 | 0.00 | 292.87 | 4.60 | 3.07 |
| 0.736 | 0.00 | 0.00 | 15.85 | 0.12 | 0.00 | 341.46 | 10.60 | 6.00 |
| 0.858 | 0.00 | 0.00 | 18.48 | 0.12 | 0.00 | 398.11 | 20.33 | 9.73 |
| 1.00 | 0.00 | 0.00 | 21.54 | 0.12 | 0.00 | 464.16 | 33.90 | 13.57 |
| 1.17 | 0.00 | 0.00 | 25.12 | 0.12 | 0.00 | 541.17 | 50.40 | 16.50 |
| 1.36 | 0.04 | 0.04 | 29.29 | 0.12 | 0.00 | 630.96 | 67.82 | 17.43 |
| 1.58 | 0.04 | 0.00 | 34.15 | 0.12 | 0.00 | 735.64 | 83.48 | 15.66 |
| 1.85 | 0.04 | 0.00 | 39.81 | 0.12 | 0.00 | 857.70 | 94.75 | 11.26 |
| 2.15 | 0.04 | 0.00 | 46.42 | 0.12 | 0.00 | 1000.00 | 100.00 | 5.25 |

250

### k. Radial distances Drop sizes and DSD experimental results at y=100mm, x=10mm

**Average Measurement Parameters**                    **28 Oct 2016 - 12:20:16.4004**

(average size distribution, weighted)
Example results777.smea\Import\Averages\V10_R10 1 1.psd
Sample : watersherry
Start+0.1996 (s) :: +0.4004 (s)

---

**Standard Values:**

| | | |
|---|---|---|
| Trans = 70.4 (%) | Dv(10) = 278.9 (µm) | Span = 0.9982 |
| Cv = 1520 (PPM) | Dv(50) = 497 (µm) | D[3][2] = 400 (µm) |
| SSA = 0.0150 (m²/cc) | Dv(90) = 775 (µm) | D[4][3] = 510.8 (µm) |

---

**Notes:**
using catheter nozzle

---

**Average (average size distribution, weighted):**
Source file: V10_R10 1
502 Records Averaged                                   0 Records Skipped
Average Range = 28 Oct 2016 - 12:20:16.1996 :: 12:20:16.4004

---

**Measurement Values and Settings**
Instrument = Spraytec - Open Spray

| | |
|---|---|
| Lens = 300mm | Path Length = 30.0 (mm) |
| Particulate Refractive Index = 1.33 + 0.000i | Scatter start = 1 |
| Dispersant Refractive Index = 1.00 | Scatter end = 36 |
| Particle Density = 1.00 (gm/cc) | Scattering threshold = 1 |
| Residual = 0.00  (%) | Minimum size = 0.10 (µm) |
| Extinction analysis = Off | Maximum size = 2500.00 (µm) |
| | Multiple Scatter = On |

---

**Identification**

| | |
|---|---|
| Operator = mnska | S/W = v3.20.006 |
| Serial Numbers: Instrument = MAL1118761 | Detector = 10FT-CDL |
| SOP Name = -MANUAL 11- -IMPORTED MEASUREMENT- | |
| Last Edited = Not Edited | |

---

**Rapid Measurement**
Trigger = Manual
Trigger Delay = 0.0 msecs

---

# Particle Size Distribution

Example results777.smea\Import\V10_R10
Sample : watersherry
Start+0.0996 (s)



Rosin Rammler
D = 563.70 N = 2.55
0 - 100 %

Particle Diameter (µm)
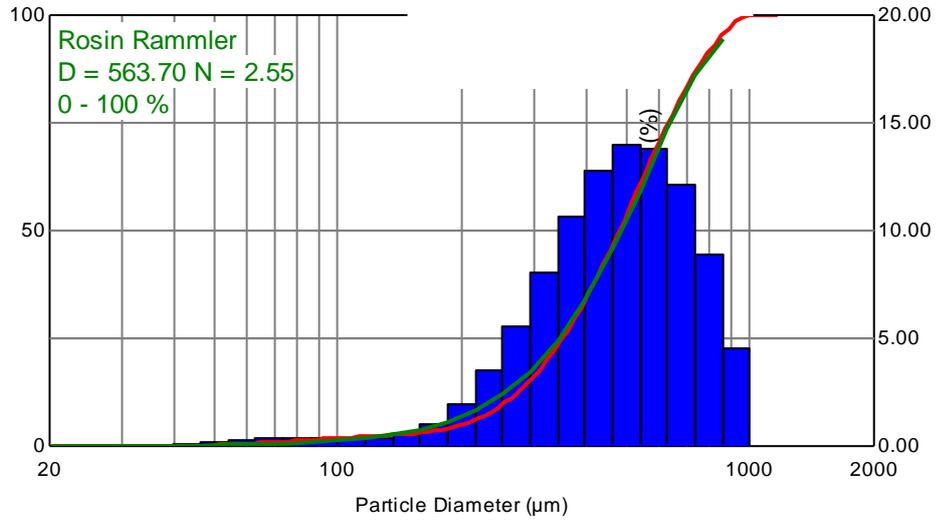
| Size (µm) | % V < | % V | Size (µm) | % V < | % V | Size (µm) | % V < | % V |
|---|---|---|---|---|---|---|---|---|
| 0.117 | 0.00 | 0.00 | 2.51 | 0.00 | 0.00 | 54.12 | 0.35 | 0.21 |
| 0.136 | 0.00 | 0.00 | 2.93 | 0.00 | 0.00 | 63.10 | 0.66 | 0.31 |
| 0.158 | 0.00 | 0.00 | 3.41 | 0.00 | 0.00 | 73.56 | 1.04 | 0.38 |
| 0.185 | 0.00 | 0.00 | 3.98 | 0.00 | 0.00 | 85.77 | 1.45 | 0.41 |
| 0.215 | 0.00 | 0.00 | 4.64 | 0.00 | 0.00 | 100.00 | 1.84 | 0.39 |
| 0.251 | 0.00 | 0.00 | 5.41 | 0.00 | 0.00 | 116.59 | 2.19 | 0.35 |
| 0.293 | 0.00 | 0.00 | 6.31 | 0.00 | 0.00 | 135.94 | 2.56 | 0.36 |
| 0.341 | 0.00 | 0.00 | 7.36 | 0.00 | 0.00 | 158.49 | 3.10 | 0.54 |
| 0.398 | 0.00 | 0.00 | 8.58 | 0.00 | 0.00 | 184.79 | 4.12 | 1.02 |
| 0.464 | 0.00 | 0.00 | 10.00 | 0.00 | 0.00 | 215.44 | 6.10 | 1.97 |
| 0.541 | 0.00 | 0.00 | 11.66 | 0.00 | 0.00 | 251.19 | 9.59 | 3.49 |
| 0.631 | 0.00 | 0.00 | 13.59 | 0.00 | 0.00 | 292.87 | 15.17 | 5.58 |
| 0.736 | 0.00 | 0.00 | 15.85 | 0.00 | 0.00 | 341.46 | 23.24 | 8.07 |
| 0.858 | 0.00 | 0.00 | 18.48 | 0.00 | 0.00 | 398.11 | 33.88 | 10.63 |
| 1.00 | 0.00 | 0.00 | 21.54 | 0.00 | 0.00 | 464.16 | 46.66 | 12.78 |
| 1.17 | 0.00 | 0.00 | 25.12 | 0.00 | 0.00 | 541.17 | 60.65 | 14.00 |
| 1.36 | 0.00 | 0.00 | 29.29 | 0.00 | 0.00 | 630.96 | 74.49 | 13.84 |
| 1.58 | 0.00 | 0.00 | 34.15 | 0.00 | 0.00 | 735.64 | 86.58 | 12.09 |
| 1.85 | 0.00 | 0.00 | 39.81 | 0.03 | 0.03 | 857.70 | 95.43 | 8.85 |
| 2.15 | 0.00 | 0.00 | 46.42 | 0.14 | 0.11 | 1000.00 | 100.00 | 4.57 |

252

## l. Radial distances Drop sizes and DSD experimental results at y=100mm, x=10mm

**Average Measurement Parameters**                    **28 Oct 2016 - 11:50:09.4004**

(average size distribution, weighted)
Example results777.smea\Import\Averages\V10_R15c 1 1.psd
Sample : watersherry
Start+0.1996 (s) :: +0.4004 (s)

---

**Standard Values:**

| | | |
|---|---|---|
| Trans = 72.5 (%) | Dv(10) = 281.3 (µm) | Span = 0.9898 |
| Cv = 1408 (PPM) | Dv(50) = 499.8 (µm) | D[3][2] = 404.2 (µm) |
| SSA = 0.0148 (m²/cc) | Dv(90) = 776 (µm) | D[4][3] = 513.7 (µm) |

---

**Notes:**
using catheter nozzle

---

**Average (average size distribution, weighted):**
Source file: V10_R15c 1
502 Records Averaged                         0 Records Skipped
Average Range = 28 Oct 2016 - 11:50:09.1996 :: 11:50:09.4004

---

**Measurement Values and Settings**
Instrument = Spraytec - Open Spray

| | |
|---|---|
| Lens = 300mm | Path Length = 30.0 (mm) |
| Particulate Refractive Index = 1.33 + 0.000i | Scatter start = 1 |
| Dispersant Refractive Index = 1.00 | Scatter end = 36 |
| Particle Density = 1.00 (gm/cc) | Scattering threshold = 1 |
| Residual = 0.00  (%) | Minimum size = 0.10 (µm) |
| Extinction analysis = Off | Maximum size = 2500.00 (µm) |
| | Multiple Scatter = On |

---

**Identification**

| | |
|---|---|
| Operator = mnska | S/W =  v3.20.006 |
| Serial Numbers: Instrument = MAL1118761 | Detector = 10FT-CDL |
| SOP Name = -MANUAL 13- -IMPORTED MEASUREMENT- | |
| Last Edited = Not Edited | |

---

**Rapid Measurement**
Trigger = Manual
Trigger Delay = 0.0 msecs

---

### m. Radial distances Drop sizes and DSD experimental results at y=100mm, x=15mm

**Particle Size Distribution**                                      16 - 11:50:09.0996

Example results777.smea\Import\V10_R15
Sample : watersherry
Start+0.0996 (s)
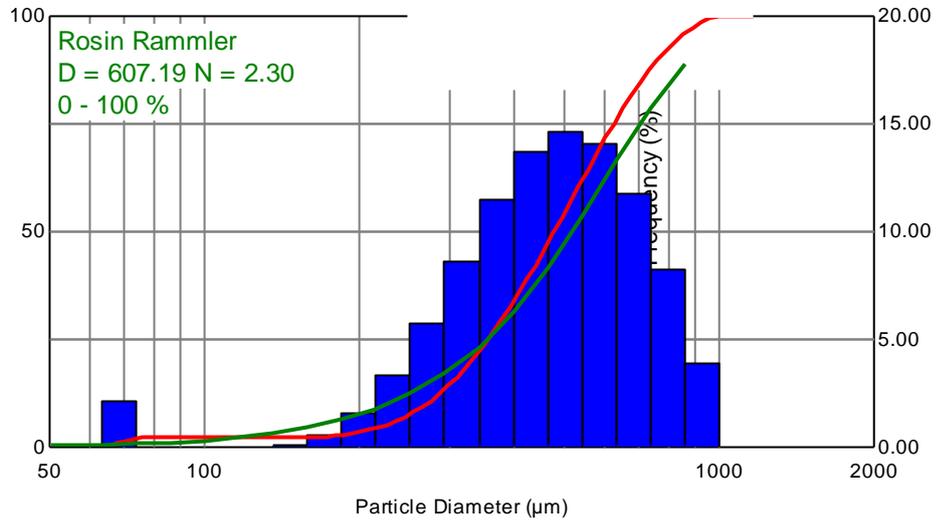


| Size (µm) | % V < | % V | Size (µm) | % V < | % V | Size (µm) | % V < | % V |
|---|---|---|---|---|---|---|---|---|
| 0.117 | 0.00 | 0.00 | 2.51 | 0.00 | 0.00 | 54.12 | 0.00 | 0.00 |
| 0.136 | 0.00 | 0.00 | 2.93 | 0.00 | 0.00 | 63.10 | 0.00 | 0.00 |
| 0.158 | 0.00 | 0.00 | 3.41 | 0.00 | 0.00 | 73.56 | 2.14 | 2.14 |
| 0.185 | 0.00 | 0.00 | 3.98 | 0.00 | 0.00 | 85.77 | 2.14 | 0.00 |
| 0.215 | 0.00 | 0.00 | 4.64 | 0.00 | 0.00 | 100.00 | 2.14 | 0.00 |
| 0.251 | 0.00 | 0.00 | 5.41 | 0.00 | 0.00 | 116.59 | 2.14 | 0.00 |
| 0.293 | 0.00 | 0.00 | 6.31 | 0.00 | 0.00 | 135.94 | 2.14 | 0.00 |
| 0.341 | 0.00 | 0.00 | 7.36 | 0.00 | 0.00 | 158.49 | 2.25 | 0.11 |
| 0.398 | 0.00 | 0.00 | 8.58 | 0.00 | 0.00 | 184.79 | 2.82 | 0.57 |
| 0.464 | 0.00 | 0.00 | 10.00 | 0.00 | 0.00 | 215.44 | 4.42 | 1.60 |
| 0.541 | 0.00 | 0.00 | 11.66 | 0.00 | 0.00 | 251.19 | 7.76 | 3.34 |
| 0.631 | 0.00 | 0.00 | 13.59 | 0.00 | 0.00 | 292.87 | 13.54 | 5.78 |
| 0.736 | 0.00 | 0.00 | 15.85 | 0.00 | 0.00 | 341.46 | 22.19 | 8.65 |
| 0.858 | 0.00 | 0.00 | 18.48 | 0.00 | 0.00 | 398.11 | 33.69 | 11.50 |
| 1.00 | 0.00 | 0.00 | 21.54 | 0.00 | 0.00 | 464.16 | 47.38 | 13.69 |
| 1.17 | 0.00 | 0.00 | 25.12 | 0.00 | 0.00 | 541.17 | 62.05 | 14.67 |
| 1.36 | 0.00 | 0.00 | 29.29 | 0.00 | 0.00 | 630.96 | 76.10 | 14.05 |
| 1.58 | 0.00 | 0.00 | 34.15 | 0.00 | 0.00 | 735.64 | 87.89 | 11.79 |
| 1.85 | 0.00 | 0.00 | 39.81 | 0.00 | 0.00 | 857.70 | 96.09 | 8.20 |
| 2.15 | 0.00 | 0.00 | 46.42 | 0.00 | 0.00 | 1000.00 | 100.00 | 3.91 |

254

### n. Radial distances Drop sizes and DSD experimental results at y=100mm, x=15mm

**Average Measurement Parameters**                    **28 Oct 2016 - 12:02:02.4004**

(average size distribution, weighted)
Example results777.smea\Import\Averages\V10_R20 1 1.psd
Sample : watersherry
Start+0.1996 (s) :: +0.4004 (s)

---

**Standard Values:**

| | | |
|---|---|---|
| Trans = 73.1 (%) | Dv(10) = 268.9 (µm) | Span = 1.028 |
| Cv = 1345 (PPM) | Dv(50) = 492.4 (µm) | D[3][2] = 394.2 (µm) |
| SSA = 0.0152 (m²/cc) | Dv(90) = 775.1 (µm) | D[4][3] = 506.1 (µm) |

---

**Notes:**
using catheter nozzle

---

**Average (average size distribution, weighted):**
Source file: V10_R20 1
502 Records Averaged                              0 Records Skipped
Average Range = 28 Oct 2016 - 12:02:02.1996 :: 12:02:02.4004

---

**Measurement Values and Settings**
Instrument = Spraytec - Open Spray

| | |
|---|---|
| Lens = 300mm | Path Length = 30.0 (mm) |
| Particulate Refractive Index = 1.33 + 0.000i | Scatter start = 1 |
| Dispersant Refractive Index = 1.00 | Scatter end = 36 |
| Particle Density = 1.00 (gm/cc) | Scattering threshold = 1 |
| Residual = 0.00 (%) | Minimum size = 0.10 (µm) |
| Extinction analysis = Off | Maximum size = 2500.00 (µm) |
| | Multiple Scatter = On |

---

**Identification**

| | |
|---|---|
| Operator = mnska | S/W = v3.20.006 |
| Serial Numbers: Instrument = MAL1118761 | Detector = 10FT-CDL |
| SOP Name = -MANUAL 2- -IMPORTED MEASUREMENT- | |
| Last Edited = Not Edited | |

---

**Rapid Measurement**
Trigger = Manual
Trigger Delay = 0.0 msecs

---

## o. Radial distances Drop sizes and DSD experimental results at y=100mm, x=20mm

**Particle Size Distribution**                                        16 - 12:02:02.1232

Example results777.smea\Import\V10_R20
Sample : watersherry
Start+0.1232 (s)



Rosin Rammler
D = 605.22 N = 2.62
0 - 100 %
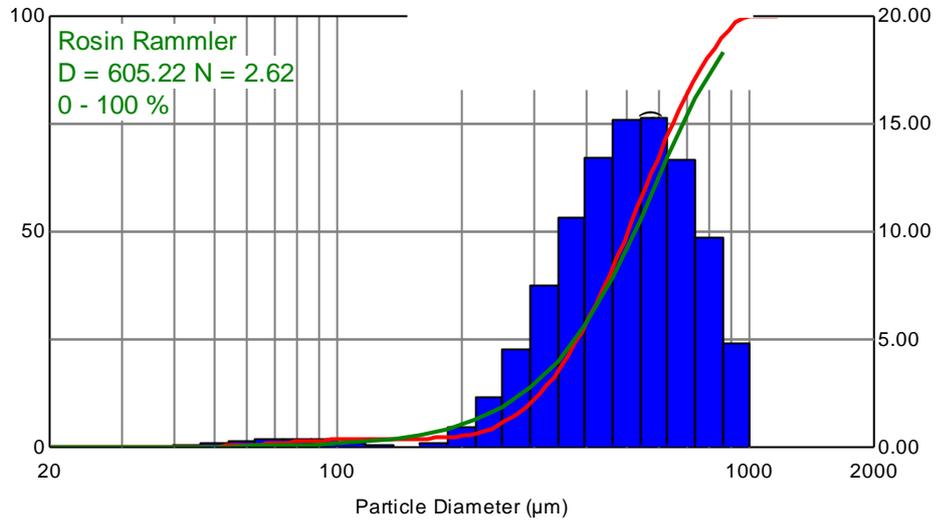
| Size (µm) | % V < | % V | Size (µm) | % V < | % V | Size (µm) | % V < | % V |
|---|---|---|---|---|---|---|---|---|
| 0.117 | 0.00 | 0.00 | 2.51 | 0.00 | 0.00 | 54.12 | 0.30 | 0.20 |
| 0.136 | 0.00 | 0.00 | 2.93 | 0.00 | 0.00 | 63.10 | 0.62 | 0.32 |
| 0.158 | 0.00 | 0.00 | 3.41 | 0.00 | 0.00 | 73.56 | 1.02 | 0.40 |
| 0.185 | 0.00 | 0.00 | 3.98 | 0.00 | 0.00 | 85.77 | 1.43 | 0.42 |
| 0.215 | 0.00 | 0.00 | 4.64 | 0.00 | 0.00 | 100.00 | 1.77 | 0.34 |
| 0.251 | 0.00 | 0.00 | 5.41 | 0.00 | 0.00 | 116.59 | 1.97 | 0.19 |
| 0.293 | 0.00 | 0.00 | 6.31 | 0.00 | 0.00 | 135.94 | 2.02 | 0.05 |
| 0.341 | 0.00 | 0.00 | 7.36 | 0.00 | 0.00 | 158.49 | 2.03 | 0.02 |
| 0.398 | 0.00 | 0.00 | 8.58 | 0.00 | 0.00 | 184.79 | 2.25 | 0.22 |
| 0.464 | 0.00 | 0.00 | 10.00 | 0.00 | 0.00 | 215.44 | 3.18 | 0.92 |
| 0.541 | 0.00 | 0.00 | 11.66 | 0.00 | 0.00 | 251.19 | 5.52 | 2.34 |
| 0.631 | 0.00 | 0.00 | 13.59 | 0.00 | 0.00 | 292.87 | 10.10 | 4.57 |
| 0.736 | 0.00 | 0.00 | 15.85 | 0.00 | 0.00 | 341.46 | 17.57 | 7.48 |
| 0.858 | 0.00 | 0.00 | 18.48 | 0.00 | 0.00 | 398.11 | 28.22 | 10.65 |
| 1.00 | 0.00 | 0.00 | 21.54 | 0.00 | 0.00 | 464.16 | 41.68 | 13.46 |
| 1.17 | 0.00 | 0.00 | 25.12 | 0.00 | 0.00 | 541.17 | 56.88 | 15.19 |
| 1.36 | 0.00 | 0.00 | 29.29 | 0.00 | 0.00 | 630.96 | 72.12 | 15.25 |
| 1.58 | 0.00 | 0.00 | 34.15 | 0.00 | 0.00 | 735.64 | 85.48 | 13.35 |
| 1.85 | 0.00 | 0.00 | 39.81 | 0.01 | 0.01 | 857.70 | 95.16 | 9.68 |
| 2.15 | 0.00 | 0.00 | 46.42 | 0.10 | 0.09 | 1000.00 | 100.00 | 4.84 |

256

**p. Radial distances Drop sizes and DSD experimental results at y=100mm, x=30mm**

| **Average Measurement Parameters** | **28 Oct 2016 - 12:13:02.4004** |
|---|---|

(average size distribution, weighted)
Example results777.smea\Import\Averages\V10_R30 1 1.psd
Sample : watersherry
Start+0.1996 (s) :: +0.4004 (s)

**Standard Values:**

| | | |
|---|---|---|
| Trans = 77.5 (%) | Dv(10) = 255.5 (μm) | Span = 1.066 |
| Cv = 1051 (PPM) | Dv(50) = 483.7 (μm) | D[3][2] = 378.9 (μm) |
| SSA = 0.0158 (m²/cc) | Dv(90) = 771 (μm) | D[4][3] = 497.4 (μm) |

**Notes:**
using catheter nozzle

**Average (average size distribution, weighted):**
Source file: V10_R30 1
502 Records Averaged                                   0 Records Skipped
Average Range =  28 Oct 2016 - 12:13:02.1996 :: 12:13:02.4004

**Measurement Values and Settings**
Instrument = Spraytec - Open Spray

| | |
|---|---|
| Lens = 300mm | Path Length = 30.0 (mm) |
| Particulate Refractive Index = 1.33 + 0.000i | Scatter start = 1 |
| Dispersant Refractive Index = 1.00 | Scatter end = 36 |
| Particle Density = 1.00 (gm/cc) | Scattering threshold = 1 |
| Residual = 0.00   (%) | Minimum size = 0.10  (μm) |
| Extinction analysis = Off | Maximum size = 2500.00 (μm) |
| | Multiple Scatter = On |

**Identification**

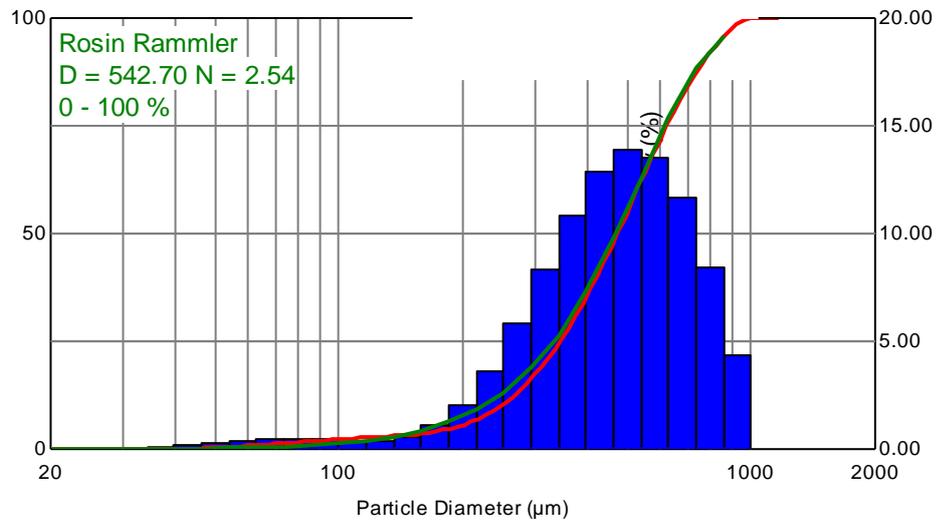| | |
|---|---|
| Operator = mnska | S/W =  v3.20.006 |
| Serial Numbers: Instrument = MAL1118761 | Detector = 10FT-CDL |
| SOP Name = -MANUAL 7- -IMPORTED MEASUREMENT- | |
| Last Edited = Not Edited | |

**Rapid Measurement**
Trigger = Manual
Trigger Delay = 0.0 msecs

Example results777.smea\Import\V10_R30
Sample : watersherry
Start+0.0996 (s)

Rosin Rammler
D = 544.53 N = 2.40
0 - 100 %



Particle Diameter (μm)
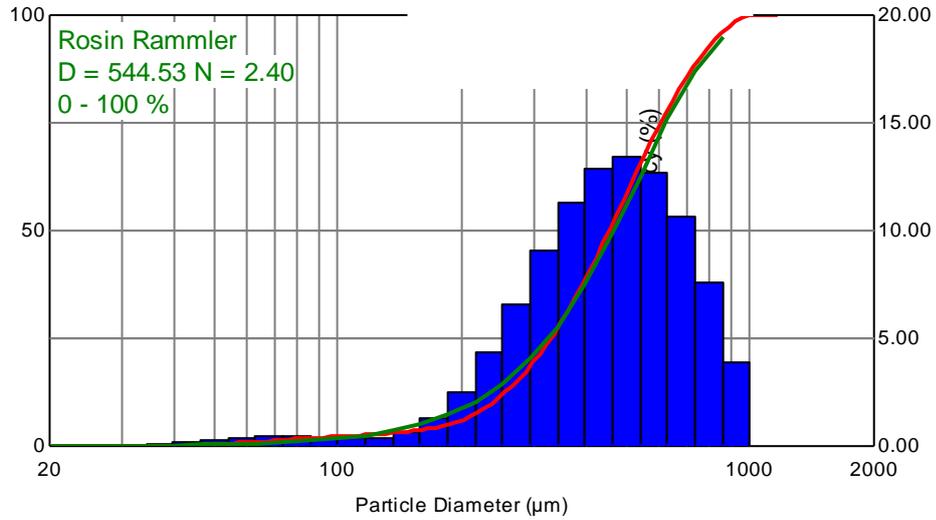
| Size (μm) | % V < | % V | Size (μm) | % V < | % V | Size (μm) | % V < | % V |
|---|---|---|---|---|---|---|---|---|
| 0.117 | 0.00 | 0.00 | 2.51 | 0.00 | 0.00 | 54.12 | 0.54 | 0.30 |
| 0.136 | 0.00 | 0.00 | 2.93 | 0.00 | 0.00 | 63.10 | 0.94 | 0.40 |
| 0.158 | 0.00 | 0.00 | 3.41 | 0.00 | 0.00 | 73.56 | 1.40 | 0.46 |
| 0.185 | 0.00 | 0.00 | 3.98 | 0.00 | 0.00 | 85.77 | 1.86 | 0.46 |
| 0.215 | 0.00 | 0.00 | 4.64 | 0.00 | 0.00 | 100.00 | 2.27 | 0.40 |
| 0.251 | 0.00 | 0.00 | 5.41 | 0.00 | 0.00 | 116.59 | 2.62 | 0.35 |
| 0.293 | 0.00 | 0.00 | 6.31 | 0.00 | 0.00 | 135.94 | 3.01 | 0.39 |
| 0.341 | 0.00 | 0.00 | 7.36 | 0.00 | 0.00 | 158.49 | 3.67 | 0.66 |
| 0.398 | 0.00 | 0.00 | 8.58 | 0.00 | 0.00 | 184.79 | 5.00 | 1.33 |
| 0.464 | 0.00 | 0.00 | 10.00 | 0.00 | 0.00 | 215.44 | 7.54 | 2.54 |
| 0.541 | 0.00 | 0.00 | 11.66 | 0.00 | 0.00 | 251.19 | 11.86 | 4.32 |
| 0.631 | 0.00 | 0.00 | 13.59 | 0.00 | 0.00 | 292.87 | 18.44 | 6.58 |
| 0.736 | 0.00 | 0.00 | 15.85 | 0.00 | 0.00 | 341.46 | 27.49 | 9.05 |
| 0.858 | 0.00 | 0.00 | 18.48 | 0.00 | 0.00 | 398.11 | 38.79 | 11.31 |
| 1.00 | 0.00 | 0.00 | 21.54 | 0.00 | 0.00 | 464.16 | 51.69 | 12.90 |
| 1.17 | 0.00 | 0.00 | 25.12 | 0.00 | 0.00 | 541.17 | 65.12 | 13.43 |
| 1.36 | 0.00 | 0.00 | 29.29 | 0.00 | 0.00 | 630.96 | 77.81 | 12.69 |
| 1.58 | 0.00 | 0.00 | 34.15 | 0.00 | 0.00 | 735.64 | 88.50 | 10.69 |
| 1.85 | 0.00 | 0.00 | 39.81 | 0.07 | 0.07 | 857.70 | 96.12 | 7.63 |
| 2.15 | 0.00 | 0.00 | 46.42 | 0.24 | 0.17 | 1000.00 | 100.00 | 3.88 |

258

### q. Radial distances Drop sizes and DSD experimental results at y=120mm, x=10mm

| **Average Measurement Parameters** | **28 Oct 2016 - 12:17:39.4004** |
|---|---|

(average size distribution, weighted)
Example results777.smea\Import\Averages\V12_R10 1 1.psd
Sample : watersherry
Start+0.1996 (s) ::  +0.4004 (s)

---

**Standard Values:**

| | | |
|---|---|---|
| Trans = 76.3 (%) | Dv(10) = 252.5 (µm) | Span = 1.081 |
| Cv = 1129 (PPM) | Dv(50) = 478.8 (µm) | D[3][2] = 379.7 (µm) |
| SSA = 0.0158 (m²/cc) | Dv(90) = 770 (µm) | D[4][3] = 494 (µm) |

---

**Notes:**
using catheter nozzle

---

**Average (average size distribution, weighted):**
Source file: V12_R10 1

| | |
|---|---|
| 502 Records Averaged | 0 Records Skipped |

Average Range =  28 Oct 2016 - 12:17:39.1996 :: 12:17:39.4004

---

**Measurement Values and Settings**
Instrument = Spraytec - Open Spray

| | |
|---|---|
| Lens = 300mm | Path Length = 30.0 (mm) |
| Particulate Refractive Index = 1.33 + 0.000i | Scatter start = 1 |
| Dispersant Refractive Index = 1.00 | Scatter end = 36 |
| Particle Density = 1.00 (gm/cc) | Scattering threshold = 1 |
| Residual = 0.00   (%) | Minimum size = 0.10 (µm) |
| Extinction analysis = Off | Maximum size = 2500.00 (µm) |
| | Multiple Scatter = On |

---

**Identification**

| | |
|---|---|
| Operator = mnska | S/W =  v3.20.006 |
| Serial Numbers: Instrument = MAL1118761 | Detector = 10FT-CDL |

SOP Name = -MANUAL 9- -IMPORTED MEASUREMENT-
Last Edited = Not Edited

---

**Rapid Measurement**
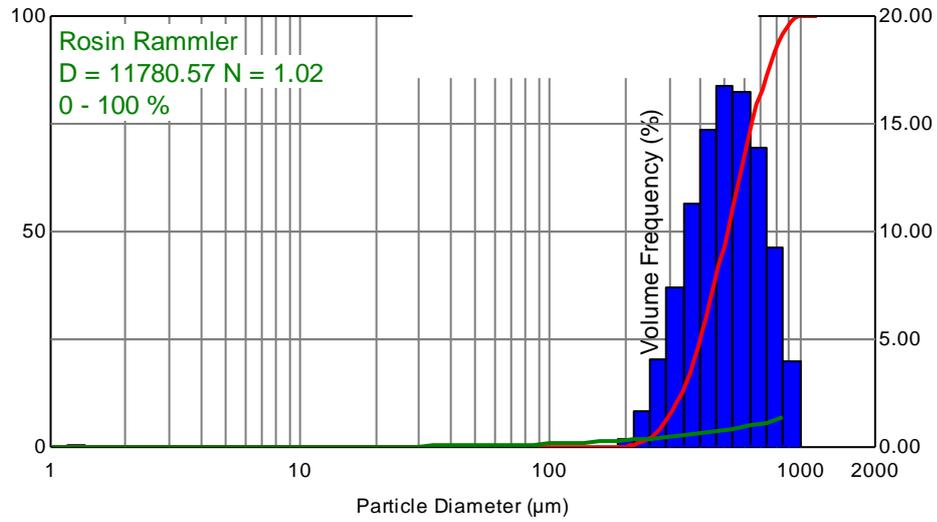Trigger = Manual
Trigger Delay = 0.0 msecs

Example results777.smea\Import\V12_R10
Sample : watersherry
Start+0.0996 (s)

Rosin Rammler
D = 508.56 N = 2.73
0 - 100 %

Particle Diameter (µm)
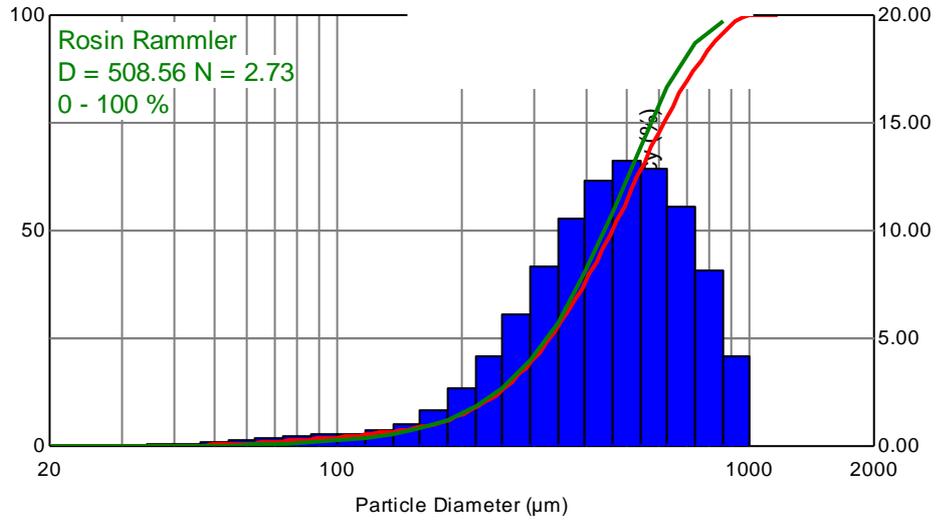
| Size (µm) | % V < | % V | Size (µm) | % V < | % V | Size (µm) | % V < | % V |
|-----------|-------|------|-----------|-------|------|-----------|--------|-------|
| 0.117 | 0.00 | 0.00 | 2.51 | 0.00 | 0.00 | 54.12 | 0.39 | 0.21 |
| 0.136 | 0.00 | 0.00 | 2.93 | 0.00 | 0.00 | 63.10 | 0.70 | 0.31 |
| 0.158 | 0.00 | 0.00 | 3.41 | 0.00 | 0.00 | 73.56 | 1.10 | 0.40 |
| 0.185 | 0.00 | 0.00 | 3.98 | 0.00 | 0.00 | 85.77 | 1.57 | 0.47 |
| 0.215 | 0.00 | 0.00 | 4.64 | 0.00 | 0.00 | 100.00 | 2.08 | 0.52 |
| 0.251 | 0.00 | 0.00 | 5.41 | 0.00 | 0.00 | 116.59 | 2.66 | 0.58 |
| 0.293 | 0.00 | 0.00 | 6.31 | 0.00 | 0.00 | 135.94 | 3.39 | 0.73 |
| 0.341 | 0.00 | 0.00 | 7.36 | 0.00 | 0.00 | 158.49 | 4.44 | 1.05 |
| 0.398 | 0.00 | 0.00 | 8.58 | 0.00 | 0.00 | 184.79 | 6.12 | 1.67 |
| 0.464 | 0.00 | 0.00 | 10.00 | 0.00 | 0.00 | 215.44 | 8.82 | 2.70 |
| 0.541 | 0.00 | 0.00 | 11.66 | 0.00 | 0.00 | 251.19 | 13.03 | 4.21 |
| 0.631 | 0.00 | 0.00 | 13.59 | 0.00 | 0.00 | 292.87 | 19.19 | 6.16 |
| 0.736 | 0.00 | 0.00 | 15.85 | 0.00 | 0.00 | 341.46 | 27.56 | 8.37 |
| 0.858 | 0.00 | 0.00 | 18.48 | 0.00 | 0.00 | 398.11 | 38.12 | 10.56 |
| 1.00 | 0.00 | 0.00 | 21.54 | 0.00 | 0.00 | 464.16 | 50.43 | 12.31 |
| 1.17 | 0.00 | 0.00 | 25.12 | 0.00 | 0.00 | 541.17 | 63.63 | 13.20 |
| 1.36 | 0.00 | 0.00 | 29.29 | 0.00 | 0.00 | 630.96 | 76.50 | 12.87 |
| 1.58 | 0.00 | 0.00 | 34.15 | 0.00 | 0.00 | 735.64 | 87.66 | 11.16 |
| 1.85 | 0.00 | 0.00 | 39.81 | 0.06 | 0.05 | 857.70 | 95.80 | 8.14 |
| 2.15 | 0.00 | 0.00 | 46.42 | 0.18 | 0.12 | 1000.00 | 100.00 | 4.20 |

### r. Radial distances Drop sizes and DSD experimental results at y=120mm, x=15mm

**Average Measurement Parameters**                    **28 Oct 2016 - 11:55:08.4004**

(average size distribution, weighted)
Example results777.smea\Import\Averages\V12_R15b 1 1.psd
Sample : watersherry
Start+0.1996 (s) :: +0.4004 (s)

---

**Standard Values:**

| | | |
|---|---|---|
| Trans = 74.7 (%) | Dv(10) = 270.4 (µm) | Span = 1.023 |
| Cv = 1251 (PPM) | Dv(50) = 493.7 (µm) | D[3][2] = 395 (µm) |
| SSA = 0.0152 (m²/cc) | Dv(90) = 775.4 (µm) | D[4][3] = 507.1 (µm) |

---

**Notes:**
using catheter nozzle

---

**Average (average size distribution, weighted):**
Source file: V12_R15b 1
502 Records Averaged                                   0 Records Skipped
Average Range =  28 Oct 2016 - 11:55:08.1996 :: 11:55:08.4004

---

**Measurement Values and Settings**
Instrument = Spraytec - Open Spray

| | |
|---|---|
| Lens = 300mm | Path Length = 30.0 (mm) |
| Particulate Refractive Index = 1.33 + 0.000i | Scatter start = 1 |
| Dispersant Refractive Index = 1.00 | Scatter end = 36 |
| Particle Density = 1.00 (gm/cc) | Scattering threshold = 1 |
| Residual = 0.00   (%) | Minimum size = 0.10 (µm) |
| Extinction analysis = Off | Maximum size = 2500.00 (µm) |
| | Multiple Scatter = On |

---

**Identification**

| | |
|---|---|
| Operator = mnska | S/W =  v3.20.006 |
| Serial Numbers: Instrument = MAL1118761 | Detector = 10FT-CDL |
| SOP Name = -MANUAL 15- -IMPORTED MEASUREMENT- | |
| Last Edited = Not Edited | |

---

**Rapid Measurement**
Trigger = Manual
Trigger Delay = 0.0 msecs

---

Example results777.smea\Import\V12_R15l
Sample : watersherry
Start+0.0996 (s)

Rosin Rammler
D = 8413.00 N = 1.02
0 - 100 %
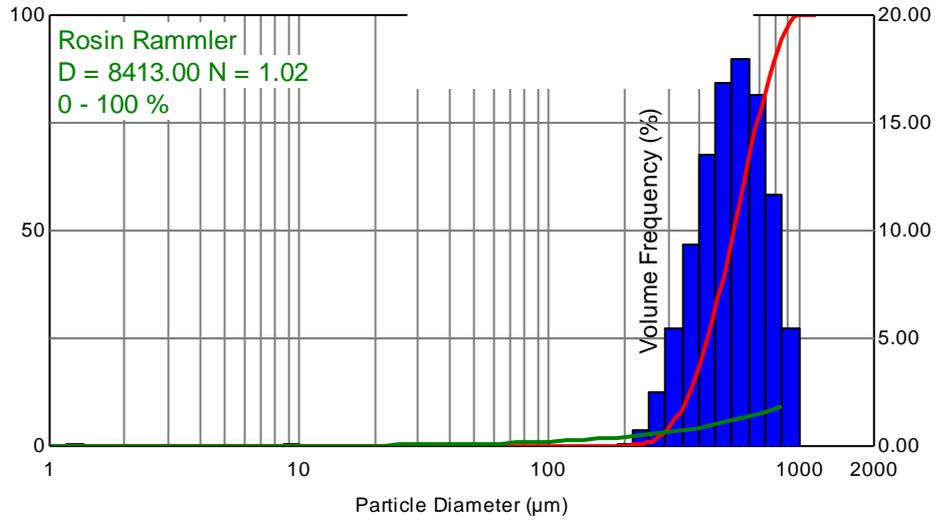


| Size (µm) | % V < | % V | Size (µm) | % V < | % V | Size (µm) | % V < | % V |
|---|---|---|---|---|---|---|---|---|
| 0.117 | 0.00 | 0.00 | 2.51 | 0.06 | 0.00 | 54.12 | 0.18 | 0.00 |
| 0.136 | 0.00 | 0.00 | 2.93 | 0.06 | 0.00 | 63.10 | 0.18 | 0.00 |
| 0.158 | 0.00 | 0.00 | 3.41 | 0.06 | 0.00 | 73.56 | 0.18 | 0.00 |
| 0.185 | 0.00 | 0.00 | 3.98 | 0.06 | 0.00 | 85.77 | 0.18 | 0.00 |
| 0.215 | 0.00 | 0.00 | 4.64 | 0.06 | 0.00 | 100.00 | 0.18 | 0.00 |
| 0.251 | 0.00 | 0.00 | 5.41 | 0.06 | 0.00 | 116.59 | 0.18 | 0.00 |
| 0.293 | 0.00 | 0.00 | 6.31 | 0.06 | 0.00 | 135.94 | 0.18 | 0.00 |
| 0.341 | 0.00 | 0.00 | 7.36 | 0.06 | 0.00 | 158.49 | 0.18 | 0.00 |
| 0.398 | 0.00 | 0.00 | 8.58 | 0.06 | 0.00 | 184.79 | 0.18 | 0.00 |
| 0.464 | 0.00 | 0.00 | 10.00 | 0.18 | 0.12 | 215.44 | 0.23 | 0.05 |
| 0.541 | 0.00 | 0.00 | 11.66 | 0.18 | 0.00 | 251.19 | 1.00 | 0.77 |
| 0.631 | 0.00 | 0.00 | 13.59 | 0.18 | 0.00 | 292.87 | 3.50 | 2.50 |
| 0.736 | 0.00 | 0.00 | 15.85 | 0.18 | 0.00 | 341.46 | 8.92 | 5.42 |
| 0.858 | 0.00 | 0.00 | 18.48 | 0.18 | 0.00 | 398.11 | 18.25 | 9.33 |
| 1.00 | 0.00 | 0.00 | 21.54 | 0.18 | 0.00 | 464.16 | 31.77 | 13.52 |
| 1.17 | 0.00 | 0.00 | 25.12 | 0.18 | 0.00 | 541.17 | 48.59 | 16.82 |
| 1.36 | 0.06 | 0.06 | 29.29 | 0.18 | 0.00 | 630.96 | 66.58 | 17.99 |
| 1.58 | 0.06 | 0.00 | 34.15 | 0.18 | 0.00 | 735.64 | 82.83 | 16.26 |
| 1.85 | 0.06 | 0.00 | 39.81 | 0.18 | 0.00 | 857.70 | 94.54 | 11.71 |
| 2.15 | 0.06 | 0.00 | 46.42 | 0.18 | 0.00 | 1000.00 | 100.00 | 5.46 |

### s. Radial distances Drop sizes and DSD experimental results at y=120mm, x=20mm

**Average Measurement Parameters**       **28 Oct 2016 - 12:00:31.4004**

(average size distribution, weighted)
Example results777.smea\Import\Averages\V12_R20 1 1.psd
Sample : watersherry
Start+0.1996 (s) :: +0.4004 (s)

---

**Standard Values:**

| | | |
|---|---|---|
| Trans = 74.6 (%) | Dv(10) = 268.2 (µm) | Span = 1.03 |
| Cv = 1267 (PPM) | Dv(50) = 492.4 (µm) | D[3][2] = 395.5 (µm) |
| SSA = 0.0152 (m²/cc) | Dv(90) = 775.3 (µm) | D[4][3] = 505.9 (µm) |

---

**Notes:**
using catheter nozzle

---

**Average (average size distribution, weighted):**
Source file: V12_R20 1
502 Records Averaged          0 Records Skipped
Average Range = 28 Oct 2016 - 12:00:31.1996 :: 12:00:31.4004

---

**Measurement Values and Settings**
Instrument = Spraytec - Open Spray

| | |
|---|---|
| Lens = 300mm | Path Length = 30.0 (mm) |
| Particulate Refractive Index = 1.33 + 0.000i | Scatter start = 1 |
| Dispersant Refractive Index = 1.00 | Scatter end = 36 |
| Particle Density = 1.00 (gm/cc) | Scattering threshold = 1 |
| Residual = 0.00  (%) | Minimum size = 0.10 (µm) |
| Extinction analysis = Off | Maximum size = 2500.00 (µm) |
| | Multiple Scatter = On |

---

**Identification**

| | |
|---|---|
| Operator = mnska | S/W = v3.20.006 |
| Serial Numbers: Instrument = MAL1118761 | Detector = 10FT-CDL |
| SOP Name = -MANUAL 1- -IMPORTED MEASUREMENT- | |
| Last Edited = Not Edited | |

---

**Rapid Measurement**
Trigger = Manual
Trigger Delay = 0.0 msecs

Example results777.smea\Import\V12_R20
Sample : watersherry
Start+0.0996 (s)
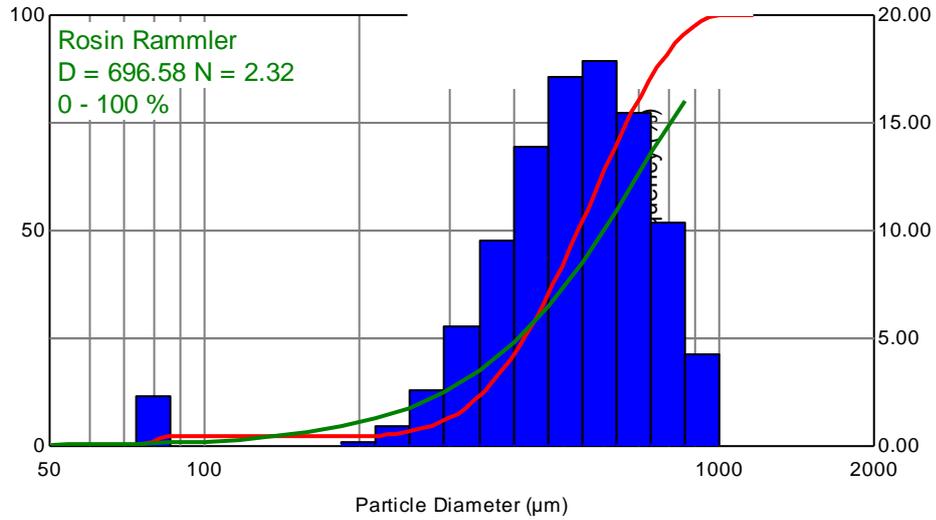


Rosin Rammler
D = 696.58 N = 2.32
0 - 100 %

| Size (µm) | % V < | % V | Size (µm) | % V < | % V | Size (µm) | % V < | % V |
|---|---|---|---|---|---|---|---|---|
| 0.117 | 0.00 | 0.00 | 2.51 | 0.00 | 0.00 | 54.12 | 0.00 | 0.00 |
| 0.136 | 0.00 | 0.00 | 2.93 | 0.00 | 0.00 | 63.10 | 0.00 | 0.00 |
| 0.158 | 0.00 | 0.00 | 3.41 | 0.00 | 0.00 | 73.56 | 0.00 | 0.00 |
| 0.185 | 0.00 | 0.00 | 3.98 | 0.00 | 0.00 | 85.77 | 2.33 | 2.33 |
| 0.215 | 0.00 | 0.00 | 4.64 | 0.00 | 0.00 | 100.00 | 2.33 | 0.00 |
| 0.251 | 0.00 | 0.00 | 5.41 | 0.00 | 0.00 | 116.59 | 2.33 | 0.00 |
| 0.293 | 0.00 | 0.00 | 6.31 | 0.00 | 0.00 | 135.94 | 2.33 | 0.00 |
| 0.341 | 0.00 | 0.00 | 7.36 | 0.00 | 0.00 | 158.49 | 2.33 | 0.00 |
| 0.398 | 0.00 | 0.00 | 8.58 | 0.00 | 0.00 | 184.79 | 2.33 | 0.00 |
| 0.464 | 0.00 | 0.00 | 10.00 | 0.00 | 0.00 | 215.44 | 2.51 | 0.18 |
| 0.541 | 0.00 | 0.00 | 11.66 | 0.00 | 0.00 | 251.19 | 3.41 | 0.90 |
| 0.631 | 0.00 | 0.00 | 13.59 | 0.00 | 0.00 | 292.87 | 6.00 | 2.58 |
| 0.736 | 0.00 | 0.00 | 15.85 | 0.00 | 0.00 | 341.46 | 11.52 | 5.53 |
| 0.858 | 0.00 | 0.00 | 18.48 | 0.00 | 0.00 | 398.11 | 21.08 | 9.56 |
| 1.00 | 0.00 | 0.00 | 21.54 | 0.00 | 0.00 | 464.16 | 34.96 | 13.88 |
| 1.17 | 0.00 | 0.00 | 25.12 | 0.00 | 0.00 | 541.17 | 52.07 | 17.11 |
| 1.36 | 0.00 | 0.00 | 29.29 | 0.00 | 0.00 | 630.96 | 69.95 | 17.87 |
| 1.58 | 0.00 | 0.00 | 34.15 | 0.00 | 0.00 | 735.64 | 85.42 | 15.47 |
| 1.85 | 0.00 | 0.00 | 39.81 | 0.00 | 0.00 | 857.70 | 95.78 | 10.36 |
| 2.15 | 0.00 | 0.00 | 46.42 | 0.00 | 0.00 | 1000.00 | 100.00 | 4.22 |

### t. Radial distances Drop sizes and DSD experimental results at y=120mm, x=20mm

| **Average Measurement Parameters** | **28 Oct 2016 - 12:14:42.4004** |
|---|---|

(average size distribution, weighted)
Example results777.smea\Import\Averages\V12_R30 1 1.psd
Sample : watersherry
Start+0.1996 (s) ::  +0.4004 (s)

---

**Standard Values:**

| | | |
|---|---|---|
| Trans = 72.5 (%) | Dv(10) = 270 (µm) | Span = 1.027 |
| Cv = 1386 (PPM) | Dv(50) = 490.2 (µm) | D[3][2] = 394.8 (µm) |
| SSA = 0.0152 (m²/cc) | Dv(90) = 773.2 (µm) | D[4][3] = 504.8 (µm) |

---

**Notes:**
using catheter nozzle

---

**Average (average size distribution, weighted):**
Source file: V12_R30 1
502 Records Averaged                    0 Records Skipped
Average Range =  28 Oct 2016 - 12:14:42.1996 :: 12:14:42.4004

---

**Measurement Values and Settings**
Instrument = Spraytec - Open Spray

| | |
|---|---|
| Lens = 300mm | Path Length = 30.0 (mm) |
| Particulate Refractive Index = 1.33 + 0.000i | Scatter start = 1 |
| Dispersant Refractive Index = 1.00 | Scatter end = 36 |
| Particle Density = 1.00 (gm/cc) | Scattering threshold = 1 |
| Residual = 0.00   (%) | Minimum size = 0.10 (µm) |
| Extinction analysis = Off | Maximum size = 2500.00 (µm) |
| | Multiple Scatter = On |

---

**Identification**

| | |
|---|---|
| Operator = mnska | S/W =  v3.20.006 |
| Serial Numbers: Instrument = MAL1118761 | Detector = 10FT-CDL |
| SOP Name = -MANUAL 8- -IMPORTED MEASUREMENT- | |
| Last Edited = Not Edited | |

---

**Rapid Measurement**
Trigger = Manual
Trigger Delay = 0.0 msecs

### u. Radial distances Drop sizes and DSD experimental results at y=120mm, x=30mm

**Particle Size Distribution**                                        16 - 12:14:42.0996

Example results777.smea\Import\V12_R30
Sample : watersherry
Start+0.0996 (s)
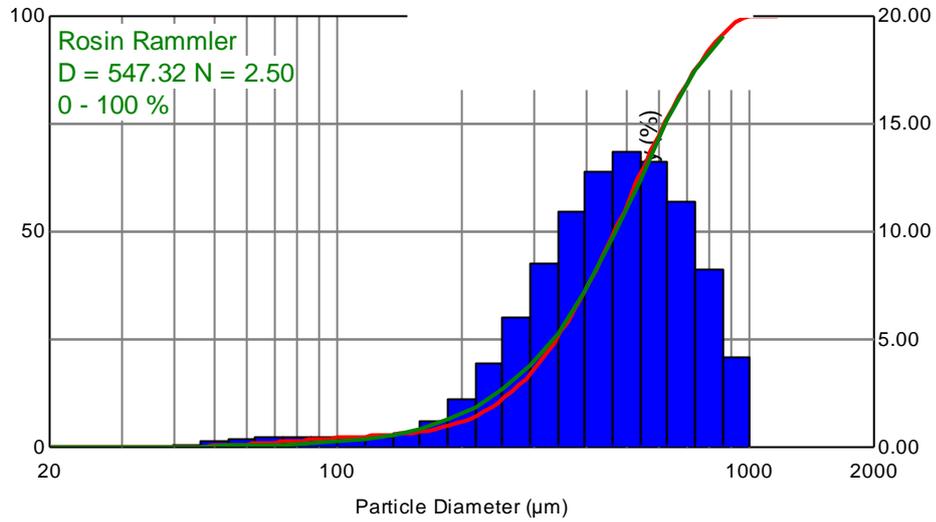


| Size (µm) | % V < | % V | Size (µm) | % V < | % V | Size (µm) | % V < | % V |
|---|---|---|---|---|---|---|---|---|
| 0.117 | 0.00 | 0.00 | 2.51 | 0.00 | 0.00 | 54.12 | 0.41 | 0.24 |
| 0.136 | 0.00 | 0.00 | 2.93 | 0.00 | 0.00 | 63.10 | 0.76 | 0.35 |
| 0.158 | 0.00 | 0.00 | 3.41 | 0.00 | 0.00 | 73.56 | 1.19 | 0.43 |
| 0.185 | 0.00 | 0.00 | 3.98 | 0.00 | 0.00 | 85.77 | 1.65 | 0.46 |
| 0.215 | 0.00 | 0.00 | 4.64 | 0.00 | 0.00 | 100.00 | 2.10 | 0.45 |
| 0.251 | 0.00 | 0.00 | 5.41 | 0.00 | 0.00 | 116.59 | 2.51 | 0.41 |
| 0.293 | 0.00 | 0.00 | 6.31 | 0.00 | 0.00 | 135.94 | 2.95 | 0.44 |
| 0.341 | 0.00 | 0.00 | 7.36 | 0.00 | 0.00 | 158.49 | 3.60 | 0.65 |
| 0.398 | 0.00 | 0.00 | 8.58 | 0.00 | 0.00 | 184.79 | 4.81 | 1.21 |
| 0.464 | 0.00 | 0.00 | 10.00 | 0.00 | 0.00 | 215.44 | 7.07 | 2.26 |
| 0.541 | 0.00 | 0.00 | 11.66 | 0.00 | 0.00 | 251.19 | 10.96 | 3.89 |
| 0.631 | 0.00 | 0.00 | 13.59 | 0.00 | 0.00 | 292.87 | 17.00 | 6.05 |
| 0.736 | 0.00 | 0.00 | 15.85 | 0.00 | 0.00 | 341.46 | 25.53 | 8.52 |
| 0.858 | 0.00 | 0.00 | 18.48 | 0.00 | 0.00 | 398.11 | 36.47 | 10.94 |
| 1.00 | 0.00 | 0.00 | 21.54 | 0.00 | 0.00 | 464.16 | 49.29 | 12.82 |
| 1.17 | 0.00 | 0.00 | 25.12 | 0.00 | 0.00 | 541.17 | 63.00 | 13.70 |
| 1.36 | 0.00 | 0.00 | 29.29 | 0.00 | 0.00 | 630.96 | 76.24 | 13.25 |
| 1.58 | 0.00 | 0.00 | 34.15 | 0.00 | 0.00 | 735.64 | 87.60 | 11.36 |
| 1.85 | 0.00 | 0.00 | 39.81 | 0.04 | 0.04 | 857.70 | 95.80 | 8.20 |
| 2.15 | 0.00 | 0.00 | 46.42 | 0.17 | 0.13 | 1000.00 | 100.00 | 4.20 |

Appendix II       **Sample Raw data from computational**

**velocity**

| velocity | density | fraction | surface | top | bottom | d32 |
|---|---|---|---|---|---|---|
| 0 | 753.323 | 0.404755 | 6439.69 | 1829.468 | 6100447 | 0.000299891 |
| 3.56E-03 | 754.159 | 0.40249 | 6403.39 | 1821.249 | 6066059 | 0.000300236 |
| 7.11E-03 | 761.038 | 0.383639 | 6102.41 | 1751.783 | 5780935 | 0.000303028 |
| 1.07E-02 | 771.091 | 0.356492 | 5668.83 | 1649.327 | 5370196 | 0.000307126 |
| 1.42E-02 | 780.424 | 0.33177 | 5273.68 | 1553.528 | 4995863 | 0.000310963 |
| 1.78E-02 | 786.421 | 0.316246 | 5025.32 | 1492.215 | 4760586 | 0.000313452 |
| 2.13E-02 | 790.134 | 0.306962 | 4876.24 | 1455.247 | 4619360 | 0.000315032 |
| 2.49E-02 | 791.701 | 0.303219 | 4815.86 | 1440.353 | 4562160 | 0.000315717 |
| 2.84E-02 | 792.81 | 0.300627 | 4773.74 | 1430.041 | 4522259 | 0.000316223 |
| 3.20E-02 | 793.524 | 0.299065 | 4748.05 | 1423.892 | 4497923 | 0.000316566 |

**2**

| velocity | density | fraction | surface | top | bottom | d32 |
|---|---|---|---|---|---|---|
| 0 | 874.861 | 0.195688 | 3134.06 | 1027.199 | 2968958 | 0.00034598 |
| 3.56E-03 | 876.486 | 0.190746 | 3055.09 | 1003.117 | 2894148 | 0.000346602 |
| 7.11E-03 | 886.858 | 0.160536 | 2571.34 | 854.2358 | 2435882 | 0.000350689 |
| 1.07E-02 | 901.595 | 0.118736 | 1901.4 | 642.3107 | 1801234 | 0.000356595 |
| 1.42E-02 | 914.687 | 8.28E-02 | 1325.11 | 454.5564 | 1255303 | 0.000362109 |
| 1.78E-02 | 921.805 | 6.38E-02 | 1019.45 | 352.9206 | 965745.4 | 0.000365439 |
| 2.13E-02 | 925.201 | 5.51E-02 | 879.673 | 305.9514 | 833331.8 | 0.000367142 |
| 2.49E-02 | 926.128 | 5.29E-02 | 843.88 | 293.968 | 799424.4 | 0.000367725 |
| 2.84E-02 | 926.675 | 5.16E-02 | 822.585 | 286.7485 | 779251.2 | 0.000367979 |
| 3.20E-02 | 926.968 | 5.09E-02 | 811.863 | 283.0849 | 769094.1 | 0.000368076 |

**3**

| velocity | density | fraction | surface | top | botto | d32 |
|---|---|---|---|---|---|---|
| 0 | 911.925 | 0.17304 | 2770.04 | 946.797 | 2624114 | 0.000360806 |
| 3.56E-03 | 912.789 | 0.168287 | 2694.18 | 921.6631 | 2552251 | 0.000361118 |
| 7.11E-03 | 918.896 | 0.13672 | 2189.35 | 753.7888 | 2074015 | 0.000363444 |
| 1.07E-02 | 927.802 |  | 1465.56 | 509.2787 | 1388354 | 0.000366822 |
| 1.42E-02 | 935.988 | 5.07E-02 | 812.716 | 284.832 | 769902.1 | 0.000369959 |
| 1.78E-02 | 940.545 | 2.84E-02 | 454.209 | 160.0437 | 430281.3 | 0.000371951 |
| 2.13E-02 | 942.818 | 1.75E-02 | 280.225 | 99.13562 | 265462.7 | 0.000373445 |
| 2.49E-02 | 943.435 | 1.47E-02 | 234.51 | 83.207 | 222156 | 0.000374543 |
| 2.84E-02 | 943.83 | 1.29E-02 | 206.221 | 73.33389 | 195357.3 | 0.000375383 |
| 3.20E-02 | 944.017 | 1.22E-02 | 193.885 | 69.059 | 183671.1 | 0.000375993 |

**4**

| velocity | density | fraction | surface | top | bottom | d32 |
|---|---|---|---|---|---|---|
| 0 | 926.556 | 0.172752 | 2764.02 | 960.3864 | 2618411 | 0.000366782 |
| 3.56E-03 | 927.133 | 0.167411 | 2681.41 | 932.2638 | 2540153 | 0.000367011 |
| 7.11E-03 | 930.954 | 0.134738 | 2155.77 | 752.6093 | 2042204 | 0.000368528 |
| 1.07E-02 | 936.493 | 8.76E-02 | 1401.06 | 492.0668 | 1327252 | 0.000370741 |
| 1.42E-02 | 941.536 | 4.51E-02 | 721.355 | 254.7486 | 683354 | 0.000372792 |
| 1.78E-02 | 944.249 | 2.25E-02 | 359.255 | 127.2753 | 340329.4 | 0.000373977 |
| 2.13E-02 | 945.507 | 1.22E-02 | 194.555 | 69.04886 | 184305.8 | 0.000374643 |
| 2.49E-02 | 945.807 | 9.79E-03 | 156.435 | 55.5466 | 148194 | 0.000374824 |
| 2.84E-02 | 945.992 | 8.37E-03 | 133.786 | 47.51612 | 126738.2 | 0.000374916 |
| 3.20E-02 | 946.075 | 7.77E-03 | 124.236 | 44.12333 | 117691.2 | 0.000374907 |

**5**

| velocity | density | fractio | surface | top | bottom | d32 |
|---|---|---|---|---|---|---|
| 0 | 923.654 | 0.176788 | 2828.88 | 979.7457 | 2679855 | 0.000365597 |
| 3.56E-03 | 924.067 | 0.174109 | 2786.08 | 965.3303 | 2639309 | 0.000365751 |
| 7.11E-03 | 928.465 | 0.141616 | 2266.26 | 788.913 | 2146873 | 0.000367471 |
| 1.07E-02 | 935.054 | 9.29E-02 | 1487.31 | 521.3545 | 1408959 | 0.000370028 |
| 1.42E-02 | 941.028 | 4.91E-02 | 786.576 | 277.3804 | 745139.2 | 0.000372253 |
| 1.78E-02 | 944.141 | 2.63E-02 | 421.324 | 148.9656 | 399128.7 | 0.000373227 |
| 2.13E-02 | 945.485 | 1.65E-02 | 264.043 | 93.40049 | 250133.2 | 0.000373403 |
| 2.49E-02 | 945.741 | 1.47E-02 | 235.092 | 83.14652 | 222707.4 | 0.000373344 |
| 2.84E-02 | 945.834 | 1.41E-02 | 225.929 | 79.89044 | 214027.1 | 0.000373273 |
| 3.20E-02 | 945.828 | 1.42E-02 | 228.279 | 80.70996 | 216253.3 | 0.00037322 |

**6**

| velocity | density | fract | surface | top | bottom | d32 |
|---|---|---|---|---|---|---|
| 0 | 932.928 | 0.175136 | 2801.6 | 980.3357 | 2654012 | 0.000369379 |
| 3.56E-03 | 933.11 | 0.1725 | 2759.18 | 965.7689 | 2613826 | 0.000369485 |
| 7.11E-03 | 935.616 | 0.140897 | 2253.31 | 790.9529 | 2134606 | 0.000370538 |
| 1.07E-02 | 939.412 | 9.33E-02 | 1491.87 | 525.9646 | 1413278 | 0.000372159 |
| 1.42E-02 | 942.861 | 5.01E-02 | 800.377 | 283.4212 | 758213.1 | 0.000373801 |
| 1.78E-02 | 944.652 | 2.76E-02 | 440.749 | 156.5557 | 417530.3 | 0.000374956 |
| 2.13E-02 | 945.42 | 1.79E-02 | 285.161 | 101.4984 | 270138.7 | 0.000375727 |
| 2.49E-02 | 945.542 | 1.63E-02 | 259.367 | 92.3248 | 245703.5 | 0.000375757 |
| 2.84E-02 | 945.554 | 1.59E-02 | 253.162 | 90.11167 | 239825.4 | 0.000375739 |
| 3.20E-02 | 945.513 | 1.62E-02 | 258.743 | 92.06782 | 245112.4 | 0.000375615 |

**7**

| velocity | density | frac | surface | top | bottom | d32 |
|---|---|---|---|---|---|---|
| 0 | 931.831 | 0.176976 | 2831.51 | 989.4703 | 2682346 | 0.000368882 |
| 3.56E-03 | 931.814 | 0.177013 | 2832.05 | 989.6591 | 2682858 | 0.000368882 |
| 7.11E-03 | 934.402 | 0.147118 | 2353.72 | 824.8041 | 2229726 | 0.000369913 |
| 1.07E-02 | 938.547 | 9.93E-02 | 1588.84 | 559.2623 | 1505140 | 0.000371568 |
| 1.42E-02 | 942.501 | 5.35E-02 | 855.435 | 302.4122 | 810370.7 | 0.000373178 |
| 1.78E-02 | 944.681 | 2.78E-02 | 444.429 | 157.5223 | 421016.5 | 0.000374148 |
| 2.13E-02 | 945.814 | 1.42E-02 | 227.032 | 80.62024 | 215072 | 0.000374852 |
| 2.49E-02 | 946.109 | 1.06E-02 | 169.515 | 60.24236 | 160584.9 | 0.000375143 |
| 2.84E-02 | 946.293 | 8.35E-03 | 133.207 | 47.41274 | 126189.7 | 0.000375726 |
| 3.20E-02 | 946.406 | 7.23E-03 | 115.172 | 41.043 | 109104.7 | 0.00037618 |

**8**

| velocity | density | frac | surface | top | bot | d32 |
|---|---|---|---|---|---|---|
| 0 | 933.281 | 0.174703 | 2795.19 | 978.2819 | 2647939 | 0.00036945 |
| 3.56E-03 | 933.239 | 0.175192 | 2803.13 | 980.976 | 2655461 | 0.000369418 |
| 7.11E-03 | 935.66 | 0.144515 | 2312.43 | 811.3014 | 2190611 | 0.000370354 |
| 1.07E-02 | 939.524 | 9.56E-02 | 1530.47 | 539.0744 | 1449845 | 0.000371815 |
| 1.42E-02 | 943.194 | 4.93E-02 | 789.581 | 279.0172 | 747985.9 | 0.000373025 |
| 1.78E-02 | 945.188 | 2.41E-02 | 386.638 | 136.7054 | 366269.9 | 0.000373237 |
| 2.13E-02 | 946.214 | 1.13E-02 | 181.811 | 64.11414 | 172233.2 | 0.000372252 |
| 2.49E-02 | 946.454 | 8.36E-03 | 134.936 | 47.4726 | 127827.6 | 0.00037138 |
| 2.84E-02 | 946.652 | 6.07E-03 | 98.4109 | 34.50461 | 93226.61 | 0.000370115 |
| 3.20E-02 | 946.761 | 4.97E-03 | 80.664 | 28.23843 | 76414.62 | 0.000369542 |

**9**

| velocity | density | fraction | surface | top | bottom | d32 |
|---|---|---|---|---|---|---|
| 0 | 933.36 | 0.17692 | 2830.62 | 990.7803 | 2681503 | 0.000369487 |
| 3.56E-03 | 933.138 | 0.179811 | 2876.98 | 1006.731 | 2725421 | 0.000369385 |
| 7.11E-03 | 935.421 | 0.151005 | 2416.21 | 847.5195 | 2288924 | 0.00037027 |
| 1.07E-02 | 939.247 | 0.102757 | 1644.39 | 579.0852 | 1557764 | 0.000371741 |
| 1.42E-02 | 942.989 | 5.55E-02 | 887.846 | 313.7681 | 841074.3 | 0.000373056 |
| 1.78E-02 | 945.117 | 2.81E-02 | 451.156 | 159.615 | 427389.1 | 0.000373465 |
| 2.13E-02 | 946.282 | 1.29E-02 | 207.986 | 73.44322 | 197029.3 | 0.000372753 |
| 2.49E-02 | 946.582 | 8.91E-03 | 143.613 | 50.58246 | 136047.5 | 0.0003718 |
| 2.84E-02 | 946.802 | 6.02E-03 | 97.5909 | 34.20701 | 92449.81 | 0.000370006 |
| 3.20E-02 | 946.906 | 4.77E-03 | 77.5849 | 27.10863 | 73497.73 | 0.000368836 |

| liquid | | | denisty | | | fraction | | | surface | top | bot | d32 |
|---|---|---|---|---|---|---|---|---|---|---|---|---|
| viscosity | | 0 | 939.221 | | 0 | 0.194935 | | 0 | 3085.51 | 1098.522 | 3077984 | 0.000357 |
| axial | | 0.01 | 946.857 | | 0.01 | 0.166941 | | 0.01 | 2635.66 | 948.4155 | 2629232 | 0.000361 |
| 2 | | 0.02 | 949.804 | | 0.02 | 0.156474 | | 0.02 | 2467.11 | 891.7178 | 2461093 | 0.000362 |
| | | 0.03 | 954.619 | | 0.03 | 0.13941 | | 0.03 | 2192.82 | 798.5006 | 2187472 | 0.000363 |
| | | 0.04 | 955.593 | | 0.04 | 0.136402 | | 0.04 | 2144.34 | 782.0688 | 2139110 | 0.000366 |
| | | 0.05 | 958.226 | | 0.05 | 0.127617 | | 0.05 | 2002.79 | 733.7156 | 1997905 | 0.000367 |

| | | | density | | | fraction | | | surface | top | bot | bottom |
|---|---|---|---|---|---|---|---|---|---|---|---|---|
| 4 | | 0 | 943.693 | | 0 | 0.194814 | | 0 | 3086.66 | 997.561 | 1103.068 | 3079132 |
| | | 0.01 | 949.167 | | 0.01 | 0.169664 | | 0.01 | 2684.18 | 997.561 | 966.2368 | 2677633 |
| | | 0.02 | 951.082 | | 0.02 | 0.160355 | | 0.02 | 2535.68 | 997.561 | 915.0645 | 2529495 |
| | | 0.03 | 954.539 | | 0.03 | 0.145312 | | 0.03 | 2296.11 | 997.561 | 832.2358 | 2290510 |
| | | 0.04 | 955.037 | | 0.04 | 0.142576 | | 0.04 | 2252.61 | 997.561 | 816.9921 | 2247116 |
| | | 0.05 | 956.783 | | 0.05 | 0.134827 | | 0.05 | 2129.5 | 997.561 | 774.0011 | 2124306 |

| | | | density | | | fraction | | | surface | top | bott | d32 |
|---|---|---|---|---|---|---|---|---|---|---|---|---|
| 6 | | 0 | 926.366 | | 0 | 0.209291 | | 0 | 3358.49 | 1163.28 | 3350299 | 0.000347 |
| | | 0.01 | 934.649 | | 0.01 | 0.181237 | | 0.01 | 2910.99 | 1016.358 | 2903860 | 0.00035 |
| | | 0.02 | 938.08 | | 0.02 | 0.170038 | | 0.02 | 2732.26 | 957.0555 | 2725596 | 0.000351 |
| | | 0.03 | 943.707 | | 0.03 | 0.152152 | | 0.03 | 2446.66 | 861.5214 | 2440693 | 0.000353 |
| | | 0.04 | 944.863 | | 0.04 | 0.148602 | | 0.04 | 2389.91 | 842.4512 | 2384081 | 0.000353 |
| | | 0.05 | 947.999 | | 0.05 | 0.138968 | | 0.05 | 2235.92 | 790.4492 | 2230467 | 0.000354 |

| | | | density | | | fraction | | | surface | top | bot | d32 |
|---|---|---|---|---|---|---|---|---|---|---|---|---|
| 8 | | 0 | 931.342 | | 0 | 0.209682 | | 0 | 3299.99 | 1171.714 | 3291941 | 0.000356 |
| | | 0.01 | 939.704 | | 0.01 | 0.181181 | | 0.01 | 2839.23 | 1021.539 | 2832305 | 0.000361 |
| | | 0.02 | 943.11 | | 0.02 | 0.170025 | | 0.02 | 2658.88 | 962.1137 | 2652395 | 0.000363 |
| | | 0.03 | 948.306 | | 0.03 | 0.152896 | | 0.03 | 2382.4 | 869.9532 | 2376589 | 0.000366 |
| | | 0.04 | 949.393 | | 0.04 | 0.149718 | | 0.04 | 2331.26 | 852.8473 | 2325574 | 0.000367 |
| | | 0.05 | 952.217 | | 0.05 | 0.140888 | | 0.05 | 2189.08 | 804.9357 | 2183741 | 0.000369 |

| | | | density | | | fraction | | | surface | ton | bot | |
|---|---|---|---|---|---|---|---|---|---|---|---|---|
| 10 | | 0 | 935.691 | | 0 | 0.210339 | | 0 | 3379.72 | 1180.874 | 3371477 | 0.00035 |
| | | 0.01 | 942.322 | | 0.01 | 0.183386 | | 0.01 | 2948.04 | 1036.852 | 2940850 | 0.000353 |
| | | 0.02 | 945.177 | | 0.02 | 0.172403 | | 0.02 | 2772.03 | 977.7081 | 2765269 | 0.000354 |
| | | 0.03 | 949.82 | | 0.03 | 0.154718 | | 0.03 | 2488.47 | 881.7255 | 2482401 | 0.000355 |
| | | 0.04 | 950.831 | | 0.04 | 0.151003 | | 0.04 | 2428.92 | 861.47 | 2422996 | 0.000356 |
| | | 0.05 | 953.43 | | 0.05 | 0.141314 | | 0.05 | 2273.54 | 808.398 | 2267995 | 0.000356 |

| | | | density | | | fraction | | | surface | top | bot | d32 |
|---|---|---|---|---|---|---|---|---|---|---|---|---|
| 15 | | 0 | 936.146 | | 0 | 0.20336 | | 0 | 3292.84 | 1142.248 | 3284809 | 0.000348 |
| | | 0.01 | 942.922 | | 0.01 | 0.176509 | | 0.01 | 2864.42 | 998.6053 | 2857434 | 0.000349 |
| | | 0.02 | 945.541 | | 0.02 | 0.166236 | | 0.02 | 2700.41 | 943.0977 | 2693824 | 0.00035 |
| | | 0.03 | 949.875 | | 0.03 | 0.149848 | | 0.03 | 2438.12 | 854.0212 | 2432173 | 0.000351 |
| | | 0.04 | 950.711 | | 0.04 | 0.146544 | | 0.04 | 2385.38 | 835.926 | 2379562 | 0.000351 |
| | | 0.05 | 953.088 | | 0.05 | 0.137592 | | 0.05 | 2242.09 | 786.8237 | 2236622 | 0.000352 |

| | 0.05 | 6 | 7 | 8 | 9 | 0.1 |
|---|---|---|---|---|---|---|
| visc | | | | | | |
| 2 | 0.000367 | 0.000366 | 0.000363 | 0.000362 | 0.000361 | 0.000357 |
| 4 | 0.000364 | 0.000364 | 0.000363 | 0.000362 | 0.000361 | 0.000358 |
| 6 | 0.000354 | 0.000353 | 0.000353 | 0.000351 | 0.00035 | 0.000347 |
| 8 | 0.000369 | 0.000367 | 0.000366 | 0.000363 | 0.000361 | 0.000356 |
| 10 | 0.000356 | 0.000356 | 0.000355 | 0.000354 | 0.000353 | 0.00035 |
| 15 | 0.000352 | 0.000351 | 0.000351 | 0.00035 | 0.000349 | 0.000348 |

| viscosity | | | | | | |
|---|---|---|---|---|---|---|
| 0.000289 | 367.2424 | 365.6048 | 363.3409 | 362.326 | 360.7197 | 356.8966 |
| 0.000489 | 364.3548 | 363.5737 | 363.3409 | 361.7577 | 360.8548 | 358.2398 |
| 0.000689 | 354.3874 | 353.3652 | 352.9824 | 351.1362 | 349.9987 | 347.2169 |
| 0.000889 | 368.604 | 366.7255 | 366.0511 | 362.7339 | 360.6741 | 355.934 |
| 0.001089 | 356.4373 | 355.5392 | 355.1907 | 353.5671 | 352.5688 | 350.2542 |
| 0.001589 | 351.7912 | 351.294 | 351.135 | 350.0963 | 349.4763 | 347.7365 |

**Block 1**

| surface tension | | density | | | fraction | | | surface | top | bot | d32 | |
|---|---|---|---|---|---|---|---|---|---|---|---|---|
| 40 | 0 | 939.704 | | 0 | 0.181181 | | 0 | 2839.23 | 1021.539 | 2832305 | 0.000361 | 360.6741 |
| y=60 | 0.003556 | 941.079 | | 0.003556 | 0.176454 | | 0.003556 | 2761.52 | 996.3429 | 2754785 | 0.000362 | 361.6772 |
| | 0.007111 | 949.687 | | 0.007111 | 0.147683 | | 0.007111 | 2295.28 | 841.5158 | 2289682 | 0.000368 | 367.5252 |
| | 0.010667 | 962.025 | | 0.010667 | 0.107501 | | 0.010667 | 1645.82 | 620.5119 | 1641806 | 0.000378 | 377.9447 |
| | 0.014222 | 973.322 | | 0.014222 | 0.072141 | | 0.014222 | 1076.46 | 421.3009 | 1073835 | 0.000392 | 392.3331 |
| | 0.017778 | 979.728 | | 0.017778 | 0.052691 | | 0.017778 | 765.045 | 309.7371 | 763179.1 | 0.000406 | 405.8511 |
| | 0.021333 | 983.003 | | 0.021333 | 0.043194 | | 0.021333 | 614.903 | 254.7578 | 613403.3 | 0.000415 | 415.3186 |
| | 0.024889 | 984.025 | | 0.024889 | 0.04042 | | 0.024889 | 572.748 | 238.6475 | 571351.1 | 0.000418 | 417.6898 |
| | 0.028444 | 984.731 | | 0.028444 | 0.038538 | | 0.028444 | 545.104 | 227.6992 | 543774.5 | 0.000419 | 418.7382 |
| | 0.032 | 985.139 | | 0.032 | 0.037491 | | 0.032 | 531.157 | 221.6007 | 529861.5 | 0.000418 | 418.2238 |

**Block 2**

| | | density | | | density | | | surface | liq dens | | d32 | |
|---|---|---|---|---|---|---|---|---|---|---|---|---|
| 72 | 0 | 939.704 | | 0 | 0.181181 | | 0 | 2839.23 | 997.561 | | 360.6741 | 364.6741 |
| y=60 | 0.003556 | 941.079 | | 0.003556 | 0.176454 | | 0.003556 | 2761.52 | 997.561 | | 361.6772 | 365.6772 |
| | 0.007111 | 949.687 | | 0.007111 | 0.147683 | | 0.007111 | 2295.28 | 997.561 | | 367.5252 | 371.5252 |
| | 0.010667 | 962.025 | | 0.010667 | 0.107501 | | 0.010667 | 1645.82 | 997.561 | | 377.9447 | 381.9447 |
| | 0.014222 | 973.322 | | 0.014222 | 0.072141 | | 0.014222 | 1076.46 | 997.561 | | 392.3331 | 396.3331 |
| | 0.017778 | 979.728 | | 0.017778 | 0.052691 | | 0.017778 | 765.045 | 997.561 | | 405.8511 | 409.8511 |
| | 0.021333 | 983.003 | | 0.021333 | 0.043194 | | 0.021333 | 614.903 | 997.561 | | 415.3186 | 419.3186 |
| | 0.024889 | 984.025 | | 0.024889 | 0.04042 | | 0.024889 | 572.748 | 997.561 | | 417.6898 | 421.6898 |
| | 0.028444 | 984.731 | | 0.028444 | 0.038538 | | 0.028444 | 545.104 | 997.561 | | 418.7382 | 422.7382 |
| | 0.032 | 985.139 | | 0.032 | 0.037491 | | 0.032 | 531.157 | 997.561 | | 418.2238 | 422.2238 |

**Block 3**

| | | density | | | fraction | | | surface | top | bott | | |
|---|---|---|---|---|---|---|---|---|---|---|---|---|
| 40 | 0 | 948.306 | | 0 | 0.152896 | | 0 | 2382.4 | 869.9532 | 2376589 | 0.000366 | 366.0511 |
| y=80 | 0.003556 | 948.833 | | 0.003556 | 0.151213 | | 0.003556 | 2354.09 | 860.8553 | 2348348 | 0.000367 | 366.579 |
| | 0.007111 | 952.828 | | 0.007111 | 0.137867 | | 0.007111 | 2137.91 | 788.1812 | 2132696 | 0.00037 | 369.5704 |
| | 0.010667 | 959.712 | | 0.010667 | 0.115522 | | 0.010667 | 1777.92 | 665.2071 | 1773584 | 0.000375 | 375.0638 |
| | 0.014222 | 967.205 | | 0.014222 | 0.091921 | | 0.014222 | 1399.5 | 533.4381 | 1396087 | 0.000382 | 382.0953 |
| | 0.017778 | 974.516 | | 0.017778 | 0.069384 | | 0.017778 | 1039.47 | 405.6961 | 1036935 | 0.000391 | 391.2455 |
| | 0.021333 | 978.83 | | 0.021333 | 0.056553 | | 0.021333 | 836.948 | 332.1346 | 834906.7 | 0.000398 | 397.8105 |
| | 0.024889 | 981.688 | | 0.024889 | 0.04813 | | 0.024889 | 704.903 | 283.4889 | 703183.7 | 0.000403 | 403.1506 |
| | 0.028444 | 983.197 | | 0.028444 | 0.043643 | | 0.028444 | 635.627 | 257.4574 | 634076.7 | 0.000406 | 406.0351 |
| | 0.032 | 984.26 | | 0.032 | 0.04045 | | 0.032 | 586.939 | 238.8781 | 585507.5 | 0.000408 | 407.9848 |

**Block 4**

| | | density | | | fraction | | | surface | d32 | | | |
|---|---|---|---|---|---|---|---|---|---|---|---|---|
| 72 | 0 | 948.306 | | 0 | 0.152896 | | 0 | 2382.4 | 366.0511 | 370.0511 | | |
| y=80 | 0.003556 | 948.833 | | 0.003556 | 0.151213 | | 0.003556 | 2354.09 | 366.579 | 370.579 | | |
| | 0.007111 | 952.828 | | 0.007111 | 0.137867 | | 0.007111 | 2137.91 | 369.5704 | 373.5704 | | |
| | 0.010667 | 959.712 | | 0.010667 | 0.115522 | | 0.010667 | 1777.92 | 375.0638 | 379.0638 | | |
| | 0.014222 | 967.205 | | 0.014222 | 0.091921 | | 0.014222 | 1399.5 | 382.0953 | 386.0953 | | |
| | 0.017778 | 974.516 | | 0.017778 | 0.069384 | | 0.017778 | 1039.47 | 391.2455 | 395.2455 | | |
| | 0.021333 | 978.83 | | 0.021333 | 0.056553 | | 0.021333 | 836.948 | 397.8105 | 401.8105 | | |
| | 0.024889 | 981.688 | | 0.024889 | 0.04813 | | 0.024889 | 704.903 | 403.1506 | 407.1506 | | |
| | 0.028444 | 983.197 | | 0.028444 | 0.043643 | | 0.028444 | 635.627 | 406.0351 | 410.0351 | | |
| | 0.032 | 984.26 | | 0.032 | 0.04045 | | 0.032 | 586.939 | 407.9848 | 411.9848 | | |

**air density = 0.6**

| | density | | fraction | | surface | top | bottom | d32 |
|---|---|---|---|---|---|---|---|---|
| 0 | 929.571 | 0 | 0.200054 | 0 | 3146.22 | 1115.786 | 3138546 | 0.000356 |
| 1.00E-02 | 937.264 | 1.00E-02 | 0.175675 | 1.00E-02 | 2757.02 | 987.9231 | 2750296 | 0.000359 |
| 2.00E-02 | 940.559 | 2.00E-02 | 0.165883 | 2.00E-02 | 2600.89 | 936.1365 | 2594546 | 0.000361 |
| 3.00E-02 | 945.99 | 3.00E-02 | 0.149896 | 3.00E-02 | 2346.19 | 850.8007 | 2340468 | 0.000364 |
| 4.00E-02 | 947.127 | 4.00E-02 | 0.14662 | 4.00E-02 | 2294.06 | 833.2066 | 2288465 | 0.000364 |
| 5.00E-02 | 950.132 | 5.00E-02 | 0.138006 | 5.00E-02 | 2157.03 | 786.7435 | 2151769 | 0.000366 |

**air density = 0.8**

| | density | | fraction | | surface | top | bot | d32 |
|---|---|---|---|---|---|---|---|---|
| 0 | 938.177 | 0 | 0.211705 | 0 | 3388.12 | 1191.701 | 3379856 | 0.000353 |
| 1.00E-02 | 945.216 | 1.00E-02 | 0.184775 | 1.00E-02 | 2957.4 | 1047.914 | 2950187 | 0.000355 |
| 2.00E-02 | 948.122 | 2.00E-02 | 0.173781 | 2.00E-02 | 2781.51 | 988.5935 | 2774726 | 0.000356 |
| 3.00E-02 | 952.728 | 3.00E-02 | 0.156381 | 3.00E-02 | 2503.18 | 893.9313 | 2497075 | 0.000358 |
| 4.00E-02 | 953.658 | 4.00E-02 | 0.152975 | 4.00E-02 | 2448.65 | 875.315 | 2442678 | 0.000358 |
| 5.00E-02 | 956.208 | 5.00E-02 | 0.14337 | 5.00E-02 | 2294.92 | 822.5492 | 2289323 | 0.000359 |

**air density = 1**

| | density | | fraction | | surface | | top | bottom |
|---|---|---|---|---|---|---|---|---|
| 0 | 928.114 | 0 | 0.219453 | 0 | 3492.1 | 997.561 | 1222.064 | 3483583 |
| 1.00E-02 | 936.837 | 1.00E-02 | 0.187082 | 1.00E-02 | 2974.93 | 997.561 | 1051.592 | 2967674 |
| 2.00E-02 | 940.207 | 2.00E-02 | 0.174307 | 2.00E-02 | 2770.49 | 997.561 | 983.308 | 2763733 |
| 3.00E-02 | 945.551 | 3.00E-02 | 0.154829 | 3.00E-02 | 2458.65 | 997.561 | 878.3923 | 2452653 |
| 4.00E-02 | 946.477 | 4.00E-02 | 0.151262 | 4.00E-02 | 2401.59 | 997.561 | 858.996 | 2395733 |
| 5.00E-02 | 949.146 | 5.00E-02 | 0.141529 | 5.00E-02 | 2245.75 | 997.561 | 805.9901 | 2240273 |

**air density = 1.3**

| | density | | fraction | | surface | top | bot | d3 |
|---|---|---|---|---|---|---|---|---|
| 0 | 944.932 | 0 | 0.203362 | 0 | 3278.68 | 1152.98 | 3270683 | 0.000353 |
| 1.00E-02 | 950.958 | 1.00E-02 | 0.176052 | 1.00E-02 | 2840.31 | 1004.508 | 2833382 | 0.000355 |
| 2.00E-02 | 953.519 | 2.00E-02 | 0.164558 | 2.00E-02 | 2655.32 | 941.4551 | 2648844 | 0.000355 |
| 3.00E-02 | 957.538 | 3.00E-02 | 0.146764 | 3.00E-02 | 2368.65 | 843.1926 | 2362873 | 0.000357 |
| 4.00E-02 | 958.289 | 4.00E-02 | 0.14343 | 4.00E-02 | 2314.94 | 824.6843 | 2309294 | 0.000357 |
| 5.00E-02 | 960.371 | 5.00E-02 | 0.134291 | 5.00E-02 | 2167.59 | 773.8151 | 2162303 | 0.000358 |

**air density = 2**

| density | | | fraction | | surface | top | bot | d32 |
|---|---|---|---|---|---|---|---|---|
| 0 | 945.091 | | 0 | 0.197388 | 0 | 3163.61 | 1119.298 | 3155894 | 0.000355 |
| 1.00E-02 | 950.545 | | 1.00E-02 | 0.172056 | 1.00E-02 | 2756.57 | 981.2818 | 2749847 | 0.000357 |
| 2.00E-02 | 952.615 | | 2.00E-02 | 0.162346 | 2.00E-02 | 2600.32 | 927.9194 | 2593978 | 0.000358 |
| 3.00E-02 | 956.204 | | 3.00E-02 | 0.146645 | 3.00E-02 | 2347.67 | 841.3352 | 2341944 | 0.000359 |
| 4.00E-02 | 956.842 | | 4.00E-02 | 0.14353 | 4.00E-02 | 2297.58 | 824.0132 | 2291976 | 0.00036 |
| 5.00E-02 | 958.763 | | 5.00E-02 | 0.135064 | 5.00E-02 | 2161.37 | 776.9662 | 2156098 | 0.00036 |

**air density = 4**

| density | | | fraction | | surface | top | bottom | d32 |
|---|---|---|---|---|---|---|---|---|
| 0 | 931.309 | | | | 0 | 3240.73 | 1127.422 | 3232826 | 0.000349 |
| 1.00E-02 | 939.327 | | 0 | 0.201763 | 1.00E-02 | 2794.18 | 979.6936 | 2787365 | 0.000351 |
| 2.00E-02 | 942.569 | | 1.00E-02 | 0.173829 | 2.00E-02 | 2618.01 | 920.7693 | 2611625 | 0.000353 |
| 3.00E-02 | 947.714 | | 2.00E-02 | 0.162812 | 3.00E-02 | 2340.98 | 827.3373 | 2335270 | 0.000354 |
| 4.00E-02 | 948.706 | | 3.00E-02 | 0.145497 | 4.00E-02 | 2289.91 | 810.0166 | 2284325 | 0.000355 |
| 5.00E-02 | 951.403 | | 4.00E-02 | 0.142302 | 5.00E-02 | 2148.59 | 761.8911 | 2143350 | 0.000355 |
| | | | 5.00E-02 | 0.133468 | | | | |

**air density = 6**

| | density | | fraction | | surface | top | bottom | d32 |
|---|---|---|---|---|---|---|---|---|
| 0 | 931.82 | 0 | 0.2043 | 0 | 3273.49 | 1142.225 | 3265506 | 0.00035 |
| 1.00E-02 | 939.284 | 1.00E-02 | 0.177425 | 1.00E-02 | 2843.55 | 999.9148 | 2836615 | 0.000353 |
| 2.00E-02 | 942.365 | 2.00E-02 | 0.166618 | 2.00E-02 | 2670.71 | 942.0898 | 2664196 | 0.000354 |
| 3.00E-02 | 947.39 | 3.00E-02 | 0.149302 | 3.00E-02 | 2393.72 | 848.6833 | 2387882 | 0.000355 |
| 4.00E-02 | 948.396 | 4.00E-02 | 0.145843 | 4.00E-02 | 2338.39 | 829.9015 | 2332687 | 0.000356 |
| 5.00E-02 | 951.107 | 5.00E-02 | 0.136597 | 5.00E-02 | 2190.51 | 779.5102 | 2185167 | 0.000357 |

**air density = 8**

| density | | | fraction | | surface | top | bott | d32 |
|---|---|---|---|---|---|---|---|---|
| 0 | 929.847 | | 0 | 0.206921 | 0 | 3299.99 | 1154.429 | 3291941 | 0.000351 |
| 1.00E-02 | 938.009 | | 1.00E-02 | 0.179113 | 1.00E-02 | 2854.96 | 1008.058 | 2847997 | 0.000354 |
| 2.00E-02 | 941.413 | | 2.00E-02 | 0.16794 | 2.00E-02 | 2676.27 | 948.6054 | 2669743 | 0.000355 |
| 3.00E-02 | 946.765 | | 3.00E-02 | 0.150356 | 3.00E-02 | 2395.01 | 854.1108 | 2389169 | 0.000357 |
| 4.00E-02 | 947.864 | | 4.00E-02 | 0.146979 | 4.00E-02 | 2341.04 | 835.8966 | 2335330 | 0.000358 |
| 5.00E-02 | 950.744 | | 5.00E-02 | 0.137804 | 5.00E-02 | 2194.29 | 786.098 | 2188938 | 0.000359 |

**air density = 10**

| density | | | fraction | | surface | top | bottom | d32 |
|---|---|---|---|---|---|---|---|---|
| 0 | 932.871 | | 0 | 0.207272 | 0 | 3316.9 | 1160.148 | 3308810 | 0.000351 |
| 1.00E-02 | 940.521 | | 1.00E-02 | 0.179205 | 1.00E-02 | 2867.55 | 1011.276 | 2860556 | 0.000354 |
| 2.00E-02 | 943.622 | | 2.00E-02 | 0.167958 | 2.00E-02 | 2687.38 | 950.9332 | 2680825 | 0.000355 |
| 3.00E-02 | 948.604 | | 3.00E-02 | 0.150189 | 3.00E-02 | 2402.68 | 854.8193 | 2396820 | 0.000357 |
| 4.00E-02 | 949.547 | | 4.00E-02 | 0.146831 | 4.00E-02 | 2348.88 | 836.5376 | 2343151 | 0.000357 |
| 5.00E-02 | 952.158 | | 5.00E-02 | 0.137617 | 5.00E-02 | 2201.2 | 786.1988 | 2195831 | 0.000358 |

| liquid | | density | | | fraction | | | surface | | top | bottom | d32 | |
|---|---|---|---|---|---|---|---|---|---|---|---|---|---|
| density | 0.1 | 968.732 | | 0.1 | 0.206545 | | 0.1 | 3317.43 | 1000 | 1200.521 | 3317430 | 0.00036188 | 361.882694 |
| | 9.00E-02 | 970.796 | | 9.00E-02 | 0.180996 | | 9.00E-02 | 2907.85 | 1000 | 1054.261 | 2907850 | 0.00036256 | 362.5569259 |
| 1000 | 8.00E-02 | 971.451 | | 8.00E-02 | 0.170693 | | 8.00E-02 | 2742.29 | 1000 | 994.9193 | 2742290 | 0.00036281 | 362.8060173 |
| | 7.00E-02 | 972.879 | | 7.00E-02 | 0.154327 | | 7.00E-02 | 2479.09 | 1000 | 900.849 | 2479090 | 0.00036338 | 363.3788949 |
| | 6.00E-02 | 972.902 | | 6.00E-02 | 0.151225 | | 6.00E-02 | 2429.17 | 1000 | 882.7626 | 2429170 | 0.0003634 | 363.4009269 |
| | 5.00E-02 | 973.484 | | 5.00E-02 | 0.142571 | | 5.00E-02 | 2289.81 | 1000 | 832.7435 | 2289810 | 0.00036367 | 363.6736341 |
| | | | | | | | | | | | | | |
| | | density | | | fraction | | | | | top | bottom | d32 | |
| 600 | 0 | 562.46 | | 0 | 0.205866 | | 0 | 3268.92 | 600 | 694.7483 | 1961352 | 0.00035422 | 354.219101 |
| | 1.00E-02 | 566.747 | | 1.00E-02 | 0.17853 | | 1.00E-02 | 2832.08 | 600 | 607.0881 | 1699248 | 0.00035727 | 357.2686573 |
| | 2.00E-02 | 568.472 | | 2.00E-02 | 0.167666 | | 2.00E-02 | 2658.39 | 600 | 571.8806 | 1595034 | 0.00035854 | 358.5381616 |
| | 3.00E-02 | 571.266 | | 3.00E-02 | 0.150481 | | 3.00E-02 | 2383.49 | 600 | 515.7881 | 1430094 | 0.00036067 | 360.6672524 |
| | 4.00E-02 | 571.788 | | 4.00E-02 | 0.147216 | | 4.00E-02 | 2331.3 | 600 | 505.0581 | 1398780 | 0.00036107 | 361.0703994 |
| | 5.00E-02 | 573.258 | | 5.00E-02 | 0.13825 | | 5.00E-02 | 2187.89 | 600 | 475.5175 | 1312734 | 0.00036223 | 362.2344748 |
| | | | | | | | | | | | | | |
| 300 | | density | | | fraction | | | surface | | top | bottom | d32 | |
| | 0 | 279.432 | | 0 | 0.211466 | | 0 | 3363.69 | 300 | 354.5422 | 1009107 | 0.00035134 | 351.3425275 |
| | 1.00E-02 | 281.911 | | 1.00E-02 | 0.18272 | | 1.00E-02 | 2905.89 | 300 | 309.0647 | 871767 | 0.00035453 | 354.5266883 |
| | 2.00E-02 | 282.924 | | 2.00E-02 | 0.171271 | | 2.00E-02 | 2723.58 | 300 | 290.7401 | 817074 | 0.00035583 | 355.8307551 |
| | 3.00E-02 | 284.509 | | 3.00E-02 | 0.153449 | | 3.00E-02 | 2439.62 | 300 | 261.9457 | 731886 | 0.00035791 | 357.9050962 |
| | 4.00E-02 | 284.813 | | 4.00E-02 | 0.1502 | | 4.00E-02 | 2387.82 | 300 | 256.6735 | 716346 | 0.00035831 | 358.3093583 |
| | 5.00E-02 | 285.652 | | 5.00E-02 | 0.141048 | | 5.00E-02 | 2241.98 | 300 | 241.7439 | 672594 | 0.00035942 | 359.4201848 |
| | | | | | | | | | | | | | |
| | | density | | | fraction | | | surface | | top | bottom | d32 | |
| 150 | 0 | 140.171 | | 0 | 0.211285 | | 0 | 3362.91 | 150 | 177.6962 | 504436.5 | 0.00035227 | 352.2666944 |
| | 1.00E-02 | 141.376 | | 1.00E-02 | 0.183537 | | 1.00E-02 | 2917.67 | 150 | 155.6864 | 437650.5 | 0.00035573 | 355.7321686 |
| | 2.00E-02 | 141.85 | | 2.00E-02 | 0.17271 | | 2.00E-02 | 2743.73 | 150 | 146.9935 | 411559.5 | 0.00035716 | 357.1621625 |
| | 3.00E-02 | 142.618 | | 3.00E-02 | 0.155392 | | 3.00E-02 | 2465.53 | 150 | 132.9702 | 369829.5 | 0.00035954 | 359.5445402 |
| | 4.00E-02 | 142.756 | | 4.00E-02 | 0.152273 | | 4.00E-02 | 2415.54 | 150 | 130.4273 | 362331 | 0.00035997 | 359.967285 |
| | 5.00E-02 | 143.159 | | 5.00E-02 | 0.143256 | | 5.00E-02 | 2270.76 | 150 | 123.0503 | 340614 | 0.00036126 | 361.2602953 |
| | | | | | | | | | | | | | |
| 100 | | density | | | fraction | | | surface | | | | d32 | |
| | 0 | 93.4276 | | 0 | 0.213805 | | 0 | 3425.03 | 100 | 119.8517 | 342503 | 0.00034993 | 349.9289878 |
| | 1.00E-02 | 94.2134 | | 1.00E-02 | 0.186161 | | 1.00E-02 | 2980.21 | 100 | 105.2332 | 298021 | 0.00035311 | 353.1065413 |
| | 2.00E-02 | 94.5216 | | 2.00E-02 | 0.175411 | | 2.00E-02 | 2807.22 | 100 | 99.48077 | 280722 | 0.00035437 | 352.6618546 |
| | 3.00E-02 | 95.0213 | | 3.00E-02 | 0.158173 | | 3.00E-02 | 2530.03 | 100 | 90.17882 | 253003 | 0.00035643 | 356.4338151 |
| | 4.00E-02 | 95.1089 | | 4.00E-02 | 0.155155 | | 4.00E-02 | 2481.5 | 100 | 88.53973 | 248150 | 0.0003568 | 356.7992274 |
| | 5.00E-02 | 95.371 | | 5.00E-02 | 0.146212 | | 5.00E-02 | 2337.8 | 100 | 83.66631 | 233780 | 0.00035788 | 357.8847973 |
| | | | | | | | | | | | | | |
| | | density | | | fraction | | | surface | | | | | |
| 50 | 0 | 46.5502 | | 0 | 0.223157 | | 0 | 3575.52 | 50 | 62.32802 | 178776 | 0.00034864 | 348.6375011 |
| | 1.00E-02 | 46.9328 | | 1.00E-02 | 0.19605 | | 1.00E-02 | 3141.02 | 50 | 55.20705 | 157051 | 0.00035152 | 351.5230889 |
| | 2.00E-02 | 47.0811 | | 2.00E-02 | 0.185655 | | 2.00E-02 | 2974.24 | 50 | 52.44505 | 148712 | 0.00035266 | 352.6618546 |
| | 3.00E-02 | 47.3234 | | 3.00E-02 | 0.168866 | | 3.00E-02 | 2704.58 | 50 | 47.94788 | 135229 | 0.00035457 | 354.568026 |
| | 4.00E-02 | 47.3621 | | 4.00E-02 | 0.166151 | | 4.00E-02 | 2660.93 | 50 | 47.21556 | 133046.5 | 0.00035488 | 354.8801484 |
| | 5.00E-02 | 47.4869 | | 5.00E-02 | 0.157581 | | 5.00E-02 | 2523.12 | 50 | 44.8982 | 126156 | 0.00035589 | 355.8942827 |

**smd for various air velocity**

**1**

| | x | density | x | fraction | x | surface | top | bottom | d32 | d32 |
|---|---|---|---|---|---|---|---|---|---|---|
| various | 0 | 838.013 | 0 | 0.999821 | 0 | 15997.2 | 5027.178 | 15154468 | 0.000332 | 331.7291071 |
| air veloicty | 1.33E-02 | 894.069 | 1.33E-02 | 0.466615 | 1.33E-02 | 7466.31 | 2503.116 | 7072985 | 0.000354 | 353.8981227 |
| 1 | 2.67E-02 | 918.577 | 2.67E-02 | 0.245178 | 2.67E-02 | 3923.32 | 1351.289 | 3716640 | 0.000364 | 363.578235 |
| | 4.00E-02 | 919.889 | 4.00E-02 | 0.233043 | 4.00E-02 | 3729.08 | 1286.242 | 3532632 | 0.000364 | 364.1030624 |
| | 5.33E-02 | 923.941 | 5.33E-02 | 0.197798 | 5.33E-02 | 3165.05 | 1096.522 | 2998315 | 0.000366 | 365.7127523 |
| | 6.67E-02 | 926.845 | 6.67E-02 | 0.172896 | 6.67E-02 | 2766.68 | 961.4868 | 2620931 | 0.000367 | 366.8492797 |
| | 8.00E-02 | 930.065 | 8.00E-02 | 0.145569 | 8.00E-02 | 2329.46 | 812.3318 | 2206744 | 0.000368 | 368.1132812 |
| | 9.33E-02 | 930.887 | 9.33E-02 | 0.138629 | 9.33E-02 | 2218.38 | 774.2876 | 2101516 | 0.000368 | 368.4424476 |
| | 0.106667 | 932.243 | 0.106667 | 0.12728 | 0.106667 | 2036.76 | 711.9353 | 1929463 | 0.000369 | 368.9809838 |
| | 0.12 | 933.615 | 0.12 | 0.115935 | 0.12 | 1855.43 | 649.4319 | 1757686 | 0.000369 | 369.4812097 |

**2**

| | x | denisty | x | fraction | x | surface | density C | top | bottom | d32 |
|---|---|---|---|---|---|---|---|---|---|---|
| | 0 | 764.844 | 0 | 0.99976 | 0 | 15996.1 | 947.32 | 4587.963 | 15153425 | 0.000302767 |
| 2 | 1.33E-02 | 856.26 | 1.33E-02 | 0.458865 | 1.33E-02 | 7341.68 | 947.32 | 2357.446 | 6954920 | 0.000338961 |
| | 2.67E-02 | 899.31 | 2.67E-02 | 0.231971 | 2.67E-02 | 3711.35 | 947.32 | 1251.683 | 3515836 | 0.000356013 |
| | 4.00E-02 | 901.462 | 4.00E-02 | 0.219264 | 4.00E-02 | 3508.05 | 947.32 | 1185.949 | 3323246 | 0.000356865 |
| | 5.33E-02 | 908.482 | 5.33E-02 | 0.183591 | 5.33E-02 | 2937.3 | 947.32 | 1000.735 | 2782563 | 0.000359645 |
| | 6.67E-02 | 913.208 | 6.67E-02 | 0.159769 | 6.67E-02 | 2556.14 | 947.32 | 875.414 | 2421483 | 0.00036152 |
| | 8.00E-02 | 918.302 | 8.00E-02 | 0.134746 | 8.00E-02 | 2155.8 | 947.32 | 742.4251 | 2042232 | 0.000363536 |
| | 9.33E-02 | 919.576 | 9.33E-02 | 0.128719 | 9.33E-02 | 2059.45 | 947.32 | 710.2014 | 1950958 | 0.000364027 |
| | 0.106667 | 921.743 | 0.106667 | 0.118563 | 0.106667 | 1897.08 | 947.32 | 655.7077 | 1797142 | 0.000364861 |
| | 0.12 | 924.02 | 0.12 | 0.108128 | 0.12 | 1730.19 | 947.32 | 599.4746 | 1639044 | 0.000365747 |

**3**

| | x | density | x | fraction | x | surface | top | bottom | d32 | |
|---|---|---|---|---|---|---|---|---|---|---|
| 3 | 0 | 706.657 | 0 | 0.999572 | 0 | 15993.6 | 4238.127 | 15151057 | 0.00028 | 279.7248576 |
| | 1.33E-02 | 822.833 | 1.33E-02 | 0.449593 | 1.33E-02 | 7193.98 | 2219.64 | 6815001 | 0.000326 | 325.6991009 |
| | 2.67E-02 | 880.465 | 2.67E-02 | 0.224982 | 2.67E-02 | 3600.2 | 1188.533 | 3410541 | 0.000348 | 348.4879666 |
| | 4.00E-02 | 882.799 | 4.00E-02 | 0.21427 | 4.00E-02 | 3428.73 | 1134.944 | 3248105 | 0.000349 | 349.4173445 |
| | 5.33E-02 | 891.899 | 5.33E-02 | 0.181009 | 5.33E-02 | 2896.4 | 968.6505 | 2743818 | 0.000353 | 353.030194 |
| | 6.67E-02 | 898.104 | 6.67E-02 | 0.158794 | 6.67E-02 | 2540.81 | 855.6812 | 2406960 | 0.000356 | 355.5028391 |
| | 8.00E-02 | 905.413 | 8.00E-02 | 0.133925 | 8.00E-02 | 2142.74 | 727.5446 | 2029860 | 0.000358 | 358.4210007 |
| | 9.33E-02 | 907.357 | 9.33E-02 | 0.127053 | 9.33E-02 | 2032.64 | 691.6946 | 1925561 | 0.000359 | 359.2172589 |
| | 0.106667 | 910.564 | 0.106667 | 0.115971 | 0.106667 | 1855.62 | 633.5941 | 1757866 | 0.00036 | 360.4336895 |
| | 0.12 | 913.928 | 0.12 | 0.104303 | 0.12 | 1670.32 | 571.9526 | 1582328 | 0.000361 | 361.462831 |

**4**

| | x | density | x | fraction | x | surface | top | bottom | d32 | |
|---|---|---|---|---|---|---|---|---|---|---|
| 4 | 0 | 645.434 | 0 | 0.999462 | 0 | 15991.4 | 3870.521 | 15148973 | 0.000255 | 255.4972226 |
| | 1.33E-02 | 782.533 | 1.33E-02 | 0.440709 | 1.33E-02 | 7051.44 | 2069.216 | 6679970 | 0.00031 | 309.7642612 |
| | 2.67E-02 | 856.24 | 2.67E-02 | 0.227103 | 2.67E-02 | 3633.71 | 1166.728 | 3442286 | 0.000339 | 338.939874 |
| | 4.00E-02 | 860 | 4.00E-02 | 0.215439 | 4.00E-02 | 3447.08 | 1111.665 | 3265488 | 0.00034 | 340.4285361 |
| | 5.33E-02 | 873.342 | 5.33E-02 | 0.179695 | 5.33E-02 | 2875.26 | 941.6111 | 2723791 | 0.000346 | 345.6987116 |
| | 6.67E-02 | 882.181 | 6.67E-02 | 0.156033 | 6.67E-02 | 2497 | 825.8961 | 2365458 | 0.000349 | 349.1484837 |
| | 8.00E-02 | 892.635 | 8.00E-02 | 0.128957 | 8.00E-02 | 2064.37 | 690.6692 | 1955619 | 0.000353 | 353.1716527 |
| | 9.33E-02 | 895.107 | 9.33E-02 | 0.122176 | 9.33E-02 | 1956.63 | 656.1636 | 1853555 | 0.000354 | 354.0027957 |
| | 0.106667 | 899.25 | 0.106667 | 0.111152 | 0.106667 | 1781.49 | 599.7206 | 1687641 | 0.000355 | 355.3602799 |
| | 0.12 | 903.89 | 0.12 | 9.88E-02 | 0.12 | 1586.5 | 535.9236 | 1502923 | 0.000357 | 356.5874951 |

**5**

| | x | density | x | fraction | x | surface | top | bottom | d32 | |
|---|---|---|---|---|---|---|---|---|---|---|
| 5 | 0 | 572.128 | 0 | 0.999297 | 0 | 15988.9 | 3430.355 | 15146605 | 0.000226 | 226.4768125 |
| | 1.33E-02 | 755.84 | 1.33E-02 | 0.42519 | 1.33E-02 | 6803.27 | 1928.254 | 6444874 | 0.000299 | 299.191844 |
| | 2.67E-02 | 841.17 | 2.67E-02 | 0.208907 | 2.67E-02 | 3343.1 | 1054.358 | 3166985 | 0.000333 | 332.9215779 |
| | 4.00E-02 | 843.882 | 4.00E-02 | 0.199941 | 4.00E-02 | 3199.75 | 1012.36 | 3031187 | 0.000334 | 333.9812453 |
| | 5.33E-02 | 858.443 | 5.33E-02 | 0.168556 | 5.33E-02 | 2697.2 | 868.1743 | 2555112 | 0.00034 | 339.779422 |
| | 6.67E-02 | 868.422 | 6.67E-02 | 0.148555 | 6.67E-02 | 2375.69 | 774.0506 | 2250539 | 0.000344 | 343.9401412 |
| | 8.00E-02 | 880.648 | 8.00E-02 | 0.124848 | 8.00E-02 | 1994.97 | 659.6828 | 1889875 | 0.000349 | 349.0616342 |
| | 9.33E-02 | 884.191 | 9.33E-02 | 0.118358 | 9.33E-02 | 1890.31 | 627.9065 | 1790728 | 0.000351 | 350.6430378 |
| | 0.106667 | 890.833 | 0.106667 | 0.106105 | 0.106667 | 1694.52 | 567.131 | 1605253 | 0.000353 | 353.2970339 |
| | 0.12 | 898.016 | 0.12 | 9.27E-02 | 0.12 | 1480.8 | 499.2109 | 1402791 | 0.000356 | 355.8696226 |

| | density | | fraction | | surface | constdens | top | bottom | d32 |
|---|---|---|---|---|---|---|---|---|---|
| smd on | 0 | 848.634 | 0 | 0.999848 | 0 | 15997.6 | 947.32 | 5091.03 | 15154846 | 0.000335934 |
| symmetry | 1.33E-02 | 899.227 | 1.33E-02 | 0.470883 | 1.33E-02 | 7534.19 | 947.32 | 2540.584 | 7137289 | 0.000355959 |
| axis at | 2.67E-02 | 921.65 | 2.67E-02 | 0.244974 | 2.67E-02 | 3919.64 | 947.32 | 1354.682 | 3713153 | 0.000364833 |
| various | 4.00E-02 | 922.766 | 4.00E-02 | 0.233583 | 4.00E-02 | 3737.39 | 947.32 | 1293.255 | 3540504 | 0.000365274 |
| velocities | 5.33E-02 | 926.446 | 5.33E-02 | 0.197803 | 5.33E-02 | 3164.96 | 947.32 | 1099.523 | 2998230 | 0.000366724 |
| 6 m/s | 6.67E-02 | 929.07 | 6.67E-02 | 0.17253 | 6.67E-02 | 2760.69 | 947.32 | 961.7547 | 2615257 | 0.000367748 |
| | 8.00E-02 | 931.912 | 8.00E-02 | 0.145361 | 8.00E-02 | 2325.94 | 947.32 | 812.782 | 2203409 | 0.000368875 |
| | 9.33E-02 | 932.61 | 9.33E-02 | 0.13875 | 9.33E-02 | 2220.01 | 947.32 | 776.3978 | 2103060 | 0.000369175 |
| | 0.106667 | 933.793 | 0.106667 | 0.127609 | 0.106667 | 2041.24 | 947.32 | 714.9623 | 1933707 | 0.000369737 |
| | 0.12 | 934.974 | 0.12 | 0.116577 | 0.12 | 1864.25 | 947.32 | 653.9788 | 1766041 | 0.000370308 |

| | | densit | | fraction | | surface | top | bottom | d32 | |
|---|---|---|---|---|---|---|---|---|---|---|
| 4 | 0 | 792.695 | 0 | 0.999836 | 0 | 15997.5 | 4755.39 | 15154752 | 0.000314 | 313.7887101 |
| | 1.33E-02 | 868.657 | 1.33E-02 | 0.474828 | 1.33E-02 | 7597.28 | 2474.776 | 7197055 | 0.000344 | 343.8595226 |
| | 2.67E-02 | 904.682 | 2.67E-02 | 0.246959 | 2.67E-02 | 3951.3 | 1340.516 | 3743146 | 0.000358 | 358.1255835 |
| | 4.00E-02 | 906.828 | 4.00E-02 | 0.232926 | 4.00E-02 | 3726.75 | 1267.343 | 3530425 | 0.000359 | 358.9774547 |
| | 5.33E-02 | 912.818 | 5.33E-02 | 0.197086 | 5.33E-02 | 3153.27 | 1079.422 | 2987156 | 0.000361 | 361.3544071 |
| | 6.67E-02 | 917.257 | 6.67E-02 | 0.170903 | 6.67E-02 | 2734.35 | 940.5718 | 2590304 | 0.000363 | 363.1124679 |
| | 8.00E-02 | 921.906 | 8.00E-02 | 0.143916 | 8.00E-02 | 2302.74 | 796.0621 | 2181432 | 0.000365 | 364.9264651 |
| | 9.33E-02 | 923.115 | 9.33E-02 | 0.136882 | 9.33E-02 | 2190.38 | 758.147 | 2074991 | 0.000365 | 365.3736543 |
| | 0.106667 | 925.101 | 0.106667 | 0.125522 | 0.106667 | 2008.81 | 696.7232 | 1902986 | 0.000366 | 366.1210366 |
| | 0.12 | 927.045 | 0.12 | 0.114551 | 0.12 | 1833.28 | 637.1636 | 1736703 | 0.000367 | 366.8811884 |

| | | density | | fraction | | surface | top | bottom | d32 | |
|---|---|---|---|---|---|---|---|---|---|---|
| 2 | 0 | 707.328 | 0 | 0.999305 | 0 | 15988.2 | 4241.018 | 15145942 | 0.00028 | 280.0102197 |
| | 1.33E-02 | 818.263 | 1.33E-02 | 0.459217 | 1.33E-02 | 7351.44 | 2254.562 | 6964166 | 0.000324 | 323.737492 |
| | 2.67E-02 | 868.573 | 2.67E-02 | 0.254579 | 2.67E-02 | 4078.21 | 1326.723 | 3863370 | 0.000343 | 343.4107295 |
| | 4.00E-02 | 872.508 | 4.00E-02 | 0.238663 | 4.00E-02 | 3823.34 | 1249.412 | 3621926 | 0.000345 | 344.9579329 |
| | 5.33E-02 | 881.74 | 5.33E-02 | 0.204912 | 5.33E-02 | 3282.85 | 1084.075 | 3109909 | 0.000349 | 348.5872031 |
| | 6.67E-02 | 888.934 | 6.67E-02 | 0.179404 | 6.67E-02 | 2874 | 956.8699 | 2722598 | 0.000351 | 351.4547519 |
| | 8.00E-02 | 896.697 | 8.00E-02 | 0.152778 | 8.00E-02 | 2446.85 | 821.9734 | 2317950 | 0.000355 | 354.6122506 |
| | 9.33E-02 | 898.999 | 9.33E-02 | 0.144831 | 9.33E-02 | 2319.35 | 781.2175 | 2197167 | 0.000356 | 355.5568021 |
| | 0.106667 | 902.375 | 0.106667 | 0.133491 | 0.106667 | 2137.4 | 722.7536 | 2024802 | 0.000357 | 356.9503238 |
| | 0.12 | 905.458 | 0.12 | 0.12337 | 0.12 | 1975.06 | 670.2381 | 1871014 | 0.000358 | 358.2218938 |

| | | density | | fraction | | surface | top | bottom | | |
|---|---|---|---|---|---|---|---|---|---|---|
| 1 | 0 | 544.727 | 0 | 0.999524 | 0 | 15993 | 3266.806 | 15150489 | 0.000216 | 215.6238199 |
| | 1.33E-02 | 674.509 | 1.33E-02 | 0.579034 | 1.33E-02 | 9319.95 | 2343.382 | 8828975 | 0.000265 | 265.4194691 |
| | 2.67E-02 | 728.266 | 2.67E-02 | 0.425538 | 2.67E-02 | 6881.4 | 1859.429 | 6518888 | 0.000285 | 285.2371733 |
| | 4.00E-02 | 733.609 | 4.00E-02 | 0.411325 | 4.00E-02 | 6654.58 | 1810.51 | 6304017 | 0.000287 | 287.199481 |
| | 5.33E-02 | 744.306 | 5.33E-02 | 0.385885 | 5.33E-02 | 6248.46 | 1723.299 | 5919291 | 0.000291 | 291.132686 |
| | 6.67E-02 | 752.695 | 6.67E-02 | 0.367311 | 6.67E-02 | 5950.2 | 1658.839 | 5636743 | 0.000294 | 294.2902989 |
| | 8.00E-02 | 761.605 | 8.00E-02 | 0.348253 | 8.00E-02 | 5642.15 | 1591.387 | 5344922 | 0.000298 | 297.7382072 |
| | 9.33E-02 | 765.015 | 9.33E-02 | 0.341551 | 9.33E-02 | 5533.35 | 1567.75 | 5241853 | 0.000299 | 299.0831283 |
| | 0.106667 | 769.542 | 0.106667 | 0.332956 | 0.106667 | 5393.42 | 1537.342 | 5109295 | 0.000301 | 300.8911928 |
| | 0.12 | 773.152 | 0.12 | 0.32656 | 0.12 | 5289.76 | 1514.883 | 5011095 | 0.000302 | 302.3057772 |

**petrol**

| | | density | | fraction | | surface | | bot | | |
|---|---|---|---|---|---|---|---|---|---|---|
| fuel | 696.135 | 0 | 660.243 | 0 | 0.17474 | 0 | 2781.22 | 692.237 | 1936105 | 0.000358 | 357.5411477 |
| Radial | 696.135 | 3.56E-03 | 660.812 | 3.56E-03 | 0.17127 | 3.56E-03 | 2724.65 | 679.056 | 1896724 | 0.000358 | 358.0149859 |
| | 696.135 | 7.11E-03 | 665.853 | 7.11E-03 | 0.14388 | 7.11E-03 | 2282.75 | 574.818 | 1589102 | 0.000362 | 361.7247451 |
| | 696.135 | 1.07E-02 | 673.276 | 1.07E-02 | 0.10442 | 1.07E-02 | 1645.76 | 421.821 | 1145671 | 0.000368 | 368.1867036 |
| | 696.135 | 1.42E-02 | 680.131 | 1.42E-02 | 6.89E-02 | 1.42E-02 | 1071.79 | 281.196 | 746110.5 | 0.000377 | 376.8818763 |
| | 696.135 | 1.78E-02 | 684.151 | 1.78E-02 | 4.86E-02 | 1.78E-02 | 743.91 | 199.65 | 517861.8 | 0.000386 | 385.5273884 |
| | 696.135 | 2.13E-02 | 686.315 | 2.13E-02 | 3.81E-02 | 2.13E-02 | 573.253 | 156.847 | 399061.5 | 0.000393 | 393.0390002 |
| | 696.135 | 2.49E-02 | 687.006 | 2.49E-02 | 3.49E-02 | 2.49E-02 | 520.831 | 143.68 | 362568.7 | 0.000396 | 396.2839724 |
| | 696.135 | 2.84E-02 | 687.448 | 2.84E-02 | 3.28E-02 | 2.84E-02 | 487.377 | 135.244 | 339280.2 | 0.000399 | 398.6215513 |
| | 696.135 | 3.20E-02 | 687.691 | 3.20E-02 | 3.17E-02 | 3.20E-02 | 469.714 | 130.791 | 326984.4 | 0.0004 | 399.9928406 |

**diesel**

| | | | | fraction | | surface | | bot | | |
|---|---|---|---|---|---|---|---|---|---|---|
| | 786.088 | 0 | 737.801 | 0 | 0.18243 | 0 | 2933.33 | 807.56 | 2305856 | 0.00035 | 350.2214601 |
| | 786.088 | 3.56E-03 | 738.977 | 3.56E-03 | 0.17733 | 3.56E-03 | 2852.17 | 786.252 | 2242057 | 0.000351 | 350.6835246 |
| | 786.088 | 7.11E-03 | 746.088 | 7.11E-03 | 0.1475 | 7.11E-03 | 2376.23 | 660.279 | 1867926 | 0.000353 | 353.4824005 |
| | 786.088 | 1.07E-02 | 756.293 | 1.07E-02 | 0.10566 | 1.07E-02 | 1709.02 | 479.45 | 1343440 | 0.000357 | 356.8826253 |
| | 786.088 | 1.42E-02 | 765.64 | 1.42E-02 | 6.85E-02 | 1.42E-02 | 1117.3 | 314.772 | 878296.1 | 0.000358 | 358.3896202 |
| | 786.088 | 1.78E-02 | 770.969 | 1.78E-02 | 4.78E-02 | 1.78E-02 | 786.989 | 220.968 | 618642.6 | 0.000357 | 357.1815621 |
| | 786.088 | 2.13E-02 | 773.721 | 2.13E-02 | 3.74E-02 | 2.13E-02 | 621.758 | 173.606 | 488756.5 | 0.000355 | 355.1999392 |
| | 786.088 | 2.49E-02 | 774.601 | 2.49E-02 | 3.42E-02 | 2.49E-02 | 571.463 | 159.027 | 449220.2 | 0.000354 | 354.0070819 |
| | 786.088 | 2.84E-02 | 775.214 | 2.84E-02 | 3.21E-02 | 2.84E-02 | 537.437 | 149.257 | 422472.8 | 0.000353 | 353.2946647 |
| | 786.088 | 3.20E-02 | 775.582 | 3.20E-02 | 3.09E-02 | 3.20E-02 | 518.449 | 143.699 | 407546.5 | 0.000353 | 352.5950757 |

| | | density | | fraction | | surface | | bot | d32 | |
|---|---|---|---|---|---|---|---|---|---|---|
| | 745.756 | 0 | 704.075 | 0 | 0.18323 | 0 | 2939.14 | 774.063 | 2191881 | 0.000353 | 353.1499972 |
| | 745.756 | 3.56E-03 | 704.887 | 3.56E-03 | 0.1786 | 3.56E-03 | 2865.16 | 755.336 | 2136710 | 0.000353 | 353.5040648 |
| kerose | 745.756 | 7.11E-03 | 710.292 | 7.11E-03 | 0.14964 | 7.11E-03 | 2402.38 | 637.712 | 1791589 | 0.000356 | 355.9473829 |
| | 745.756 | 1.07E-02 | 718.148 | 1.07E-02 | 0.10847 | 1.07E-02 | 1744.31 | 467.372 | 1300830 | 0.000359 | 359.2877479 |
| | 745.756 | 1.42E-02 | 725.421 | 1.42E-02 | 7.15E-02 | 1.42E-02 | 1152.8 | 311.079 | 859707.5 | 0.000362 | 361.8427714 |
| | 745.756 | 1.78E-02 | 729.607 | 1.78E-02 | 5.07E-02 | 1.78E-02 | 820.566 | 221.927 | 611942 | 0.000363 | 362.6597676 |
| | 745.756 | 2.13E-02 | 731.768 | 2.13E-02 | 4.03E-02 | 2.13E-02 | 654.727 | 177.137 | 488266.6 | 0.000363 | 362.7872326 |
| | 745.756 | 2.49E-02 | 732.451 | 2.49E-02 | 3.73E-02 | 2.49E-02 | 606.294 | 164.052 | 452147.4 | 0.000363 | 362.8280123 |
| | 745.756 | 2.84E-02 | 732.926 | 2.84E-02 | 3.54E-02 | 2.84E-02 | 574.923 | 155.638 | 428752.3 | 0.000363 | 363.0028582 |
| | 745.756 | 3.20E-02 | 733.223 | 3.20E-02 | 3.44E-02 | 3.20E-02 | 558.478 | 151.291 | 416488.3 | 0.000363 | 363.2529105 |

symmetry below

| Symmtery | | density | | fraction | | surface | top | bot | |
|---|---|---|---|---|---|---|---|---|---|
| Petrol | 696.135 | 0 | 534.375 | 0 | 0.9994 | 0 | 15990.7 | 3204.31 | 11131686 | 0.000287855 |
| | 696.135 | 1.33E-02 | 610.763 | 1.33E-02 | 0.46566 | 1.33E-02 | 7443.41 | 1706.462 | 5181618 | 0.00032933 |
| | 696.135 | 2.67E-02 | 647.861 | 2.67E-02 | 0.24511 | 2.67E-02 | 3911.54 | 952.7716 | 2722960 | 0.000349903 |
| | 696.135 | 4.00E-02 | 650.518 | 4.00E-02 | 0.22882 | 4.00E-02 | 3649.87 | 893.1209 | 2540802 | 0.000351511 |
| | 696.135 | 5.33E-02 | 656.66 | 5.33E-02 | 0.19453 | 5.33E-02 | 3099.28 | 766.4286 | 2157517 | 0.000355236 |
| | 696.135 | 6.67E-02 | 660.97 | 6.67E-02 | 0.17068 | 6.67E-02 | 2715.72 | 676.8862 | 1890508 | 0.000358045 |
| | 696.135 | 8.00E-02 | 665.393 | 8.00E-02 | 0.14676 | 8.00E-02 | 2330.62 | 585.9264 | 1622426 | 0.000361142 |
| | 696.135 | 9.33E-02 | 666.635 | 9.33E-02 | 0.14007 | 9.33E-02 | 2222.78 | 560.2374 | 1547355 | 0.000362061 |
| | 696.135 | 0.106667 | 668.498 | 0.10667 | 0.13003 | 0.106667 | 2061 | 521.5327 | 1434734 | 0.000363505 |
| | 696.135 | 0.12 | 670.259 | 0.12 | 0.12047 | 0.12 | 1907.05 | 484.4806 | 1327564 | 0.000364939 |

| | | kero | | fraction | | surface | | | |
|---|---|---|---|---|---|---|---|---|---|
| Kerosen | 745.756 | 0 | 579.195 | 0 | 0.99945 | 0 | 15991.4 | 3473.273 | 11925682 | 0.000291243 |
| | 745.756 | 1.33E-02 | 657.93 | 1.33E-02 | 0.4592 | 1.33E-02 | 7350.47 | 1812.717 | 5481657 | 0.000330688 |
| | 745.756 | 2.67E-02 | 692.095 | 2.67E-02 | 0.25058 | 2.67E-02 | 4015.61 | 1040.563 | 2994665 | 0.000347472 |
| | 745.756 | 4.00E-02 | 694.538 | 4.00E-02 | 0.23594 | 4.00E-02 | 3781.68 | 983.2283 | 2820211 | 0.000348636 |
| | 745.756 | 5.33E-02 | 700.459 | 5.33E-02 | 0.20294 | 5.33E-02 | 3254.18 | 852.9195 | 2426824 | 0.000351455 |
| | 745.756 | 6.67E-02 | 704.891 | 6.67E-02 | 0.17898 | 6.67E-02 | 2871.14 | 756.9726 | 2141170 | 0.000353532 |
| | 745.756 | 8.00E-02 | 709.533 | 8.00E-02 | 0.15437 | 8.00E-02 | 2477.58 | 657.1624 | 1847670 | 0.000355671 |
| | 745.756 | 9.33E-02 | 710.921 | 9.33E-02 | 0.14719 | 9.33E-02 | 2362.75 | 627.8342 | 1762035 | 0.000356312 |
| | 745.756 | 0.106667 | 712.999 | 0.10667 | 0.13641 | 0.106667 | 2190.27 | 583.544 | 1633407 | 0.000357256 |
| | 745.756 | 0.12 | 714.881 | 0.12 | 0.12659 | 0.12 | 2033.06 | 542.9593 | 1516167 | 0.000358113 |

| Diesel | | density | | fraction | | surface | | | |
|---|---|---|---|---|---|---|---|---|---|
| | 786.088 | 0 | 583.471 | 0 | 0.99934 | 0 | 15992.3 | 3498.515 | 12571355 | 0.000278293 |
| | 786.088 | 1.33E-02 | 681.092 | 1.33E-02 | 0.45646 | 1.33E-02 | 7314.7 | 1865.356 | 5749998 | 0.00032441 |
| | 786.088 | 2.67E-02 | 722.869 | 2.67E-02 | 0.25032 | 2.67E-02 | 4018.68 | 1085.683 | 3159036 | 0.000343675 |
| | 786.088 | 4.00E-02 | 725.747 | 4.00E-02 | 0.23585 | 4.00E-02 | 3787.29 | 1027.005 | 2977143 | 0.000344963 |
| | 786.088 | 5.33E-02 | 733.181 | 5.33E-02 | 0.20256 | 5.33E-02 | 3255.12 | 891.0921 | 2558811 | 0.000348245 |
| | 786.088 | 6.67E-02 | 738.794 | 6.67E-02 | 0.17815 | 6.67E-02 | 2865.15 | 789.7146 | 2252260 | 0.000350632 |
| | 786.088 | 8.00E-02 | 744.679 | 8.00E-02 | 0.1532 | 8.00E-02 | 2466.7 | 684.5134 | 1939043 | 0.000353016 |
| | 786.088 | 9.33E-02 | 746.4 | 9.33E-02 | 0.14596 | 9.33E-02 | 2351.04 | 653.6494 | 1848124 | 0.000353683 |
| | 786.088 | 0.106667 | 749.052 | 0.10667 | 0.13505 | 0.106667 | 2176.87 | 606.9703 | 1711211 | 0.000354702 |
| | 786.088 | 0.12 | 751.523 | 0.12 | 0.125 | 0.12 | 2016.24 | 563.6603 | 1584942 | 0.000355635 |

| Gasoline | axial velocity | | | radial | | |
|---|---|---|---|---|---|---|
| | | 0 | 6.62145 | radial | 0 | 1.05041 |
| | | 1.33E-02 | 2.89025 | velocity | 3.56E-03 | 1.03396 |
| | | 2.67E-02 | 1.4671 | | 7.11E-03 | 0.82458 |
| | | 4.00E-02 | 1.41232 | | 1.07E-02 | 0.50975 |
| | | 5.33E-02 | 1.18984 | | 1.42E-02 | 0.23389 |
| | | 6.67E-02 | 1.03824 | | 1.78E-02 | 0.10543 |
| | | 8.00E-02 | 0.878122 | | 2.13E-02 | 5.83E-02 |
| | | 9.33E-02 | 0.846455 | | 2.49E-02 | 4.47E-02 |
| | | 0.106667 | 0.776184 | | 2.84E-02 | 3.60E-02 |
| | | 0.12 | 0.705049 | | 3.20E-02 | 2.76E-02 |

| Kerosene | axial velocity | | | radial | | |
|---|---|---|---|---|---|---|
| | | 0 | 6.73353 | radial | 0 | 1.05319 |
| | | 1.33E-02 | 2.89513 | velocity | 3.56E-03 | 1.02584 |
| | | 2.67E-02 | 1.46739 | | 7.11E-03 | 0.80442 |
| | | 4.00E-02 | 1.41084 | | 1.07E-02 | 0.48132 |
| | | 5.33E-02 | 1.19199 | | 1.42E-02 | 0.20407 |
| | | 6.67E-02 | 1.04242 | | 1.78E-02 | 8.50E-02 |
| | | 8.00E-02 | 0.881629 | | 2.13E-02 | 5.07E-02 |
| | | 9.33E-02 | 0.844905 | | 2.49E-02 | 4.56E-02 |
| | | 0.106667 | 0.776463 | | 2.84E-02 | 4.40E-02 |
| | | 0.12 | 0.719946 | | 3.20E-02 | 4.80E-02 |

| Diesel oil | axial | | | radial | | |
|---|---|---|---|---|---|---|
| | | 0 | 6.66167 | radial | 0 | 1.04043 |
| | velocity | 1.33E-02 | 2.90639 | velocity | 3.56E-03 | 1.00016 |
| | | 2.67E-02 | 1.47293 | | 7.11E-03 | 0.772273 |
| | | 4.00E-02 | 1.41322 | | 1.07E-02 | 0.449882 |
| | | 5.33E-02 | 1.18655 | | 1.42E-02 | 0.17407 |
| | | 6.67E-02 | 1.0216 | | 1.78E-02 | 6.90E-02 |
| | | 8.00E-02 | 0.859777 | | 2.13E-02 | 5.90E-02 |
| | | 9.33E-02 | 0.831317 | | 2.49E-02 | 6.33E-02 |
| | | 0.106667 | 0.770896 | | 2.84E-02 | 6.85E-02 |
| | | 0.12 | 0.71867 | | 3.20E-02 | 7.48E-02 |

**2 Velocity**

| | density | | fraction | | surface | top | bottom | d32 | |
|---|---|---|---|---|---|---|---|---|---|
| 0 | 741.814 | 0 | 0.999561 | 0 | 15992.2 | 4448.93 | 15953195 | 0.000278874 | 278.8739218 |
| 2.00E-02 | 900.773 | 2.00E-02 | 0.322559 | 2.00E-02 | 5120.68 | 1743.315 | 5108191 | 0.000341278 | 341.2783007 |
| 4.00E-02 | 924.162 | 4.00E-02 | 0.234907 | 4.00E-02 | 3707.33 | 1302.553 | 3698288 | 0.000352204 | 352.2042632 |
| 6.00E-02 | 939.704 | 6.00E-02 | 0.181181 | 6.00E-02 | 2839.23 | 1021.539 | 2832305 | 0.000360674 | 360.674087 |
| 8.00E-02 | 948.306 | 8.00E-02 | 0.152896 | 8.00E-02 | 2382.4 | 869.9532 | 2376589 | 0.000366051 | 366.0511117 |
| 0.1 | 952.217 | 0.1 | 0.140888 | 0.1 | 2189.08 | 804.9357 | 2183741 | 0.000368604 | 368.6040393 |

**4V**

| | density | | fraction | | | surface | top | bottom | d32 | |
|---|---|---|---|---|---|---|---|---|---|---|
| 0 | 879.021 | 0 | 0.999824 | 997.561 | 0 | 15997.2 | 5273.198 | 15958183 | 0.000330438 | 330.4384848 |
| 2.00E-02 | 957.837 | 2.00E-02 | 0.318608 | 997.561 | 2.00E-02 | 5097.74 | 1831.047 | 5085307 | 0.000360066 | 360.066231 |
| 4.00E-02 | 968.604 | 4.00E-02 | 0.229813 | 997.561 | 4.00E-02 | 3677.02 | 1335.587 | 3668052 | 0.000364113 | 364.1133872 |
| 6.00E-02 | 975.624 | 6.00E-02 | 0.173739 | 997.561 | 6.00E-02 | 2779.83 | 1017.024 | 2773050 | 0.000366753 | 366.7527202 |
| 8.00E-02 | 979.48 | 8.00E-02 | 0.143604 | 997.561 | 8.00E-02 | 2297.69 | 843.9435 | 2292086 | 0.000368199 | 368.1988808 |
| 0.1 | 981.157 | 0.1 | 0.131077 | 997.561 | 0.1 | 2097.24 | 771.6427 | 2092125 | 0.000368832 | 368.8320529 |

**5V**

| | density | | fraction | | surface | top | bottom | d32 | |
|---|---|---|---|---|---|---|---|---|---|
| 0 | 880.725 | 0 | 0.999822 | 0 | 15997.2 | 5283.409 | 15958183 | 0.000331078 | 331.0783842 |
| 2.00E-02 | 958.455 | 2.00E-02 | 0.320637 | 2.00E-02 | 5130.55 | 1843.897 | 5118037 | 0.000360274 | 360.2742542 |
| 4.00E-02 | 969.046 | 4.00E-02 | 0.230839 | 4.00E-02 | 3693.81 | 1342.162 | 3684801 | 0.000364243 | 364.2426637 |
| 6.00E-02 | 975.945 | 6.00E-02 | 0.17446 | 6.00E-02 | 2791.64 | 1021.58 | 2784831 | 0.000366837 | 366.8373838 |
| 8.00E-02 | 979.722 | 8.00E-02 | 0.144426 | 8.00E-02 | 2310.9 | 848.984 | 2305264 | 0.000368281 | 368.2806318 |
| 0.1 | 981.36 | 0.1 | 0.131873 | 0.1 | 2109.95 | 776.4893 | 2104804 | 0.000368913 | 368.9129181 |

**6V**

| | density | | fraction | | surface | top | bottom | d32 | |
|---|---|---|---|---|---|---|---|---|---|
| 0 | 904.935 | 0 | 0.999867 | 0 | 15997.9 | 5428.888 | 15958881 | 0.00034018 | 340.1797294 |
| 2.00E-02 | 966.9 | 2.00E-02 | 0.320378 | 2.00E-02 | 5125.87 | 1858.641 | 5113368 | 0.000363487 | 363.486635 |
| 4.00E-02 | 975.256 | 4.00E-02 | 0.230915 | 4.00E-02 | 3694.44 | 1351.207 | 3685429 | 0.000366635 | 366.6350213 |
| 6.00E-02 | 980.711 | 6.00E-02 | 0.174062 | 6.00E-02 | 2784.73 | 1024.227 | 2777938 | 0.0003687 | 368.7004866 |
| 8.00E-02 | 983.664 | 8.00E-02 | 0.143941 | 8.00E-02 | 2302.54 | 849.5375 | 2296924 | 0.000369859 | 369.8587503 |
| 0.1 | 984.896 | 0.1 | 0.131852 | 0.1 | 2109.07 | 779.163 | 2103926 | 0.000370338 | 370.3376699 |

**8V**

| | density | | fraction | | surface | top | bottom | d32 | |
|---|---|---|---|---|---|---|---|---|---|
| 0 | 913.337 | 0 | 0.999874 | 0 | 15997.9 | 5479.332 | 15958183 | 0.000343341 | 343.340581 |
| 2.00E-02 | 969.477 | 2.00E-02 | 0.320676 | 2.00E-02 | 5130.84 | 1865.328 | 5118326 | 0.000364441 | 364.4410462 |
| 4.00E-02 | 977.098 | 4.00E-02 | 0.230114 | 4.00E-02 | 3681.81 | 1349.064 | 3672830 | 0.000367309 | 367.3090099 |
| 6.00E-02 | 981.979 | 6.00E-02 | 0.173078 | 6.00E-02 | 2769.21 | 1019.754 | 2762456 | 0.000369148 | 369.147529 |
| 8.00E-02 | 984.513 | 8.00E-02 | 0.143929 | 8.00E-02 | 2302.8 | 850.1998 | 2297183 | 0.000370105 | 370.1053226 |
| 0.1 | 985.526 | 0.1 | 0.132289 | 0.1 | 2116.48 | 782.2455 | 2111318 | 0.000370501 | 370.5010468 |

**10V**

| | density | | fraction | | surface | top | bot | d32 | |
|---|---|---|---|---|---|---|---|---|---|
| 0 | 901.966 | 0 | 0.999863 | 0 | 15997.4 | 5411.055 | 15958382 | 0.000339073 | 339.0728752 |
| 2.00E-02 | 963.522 | 2.00E-02 | 0.330659 | 2.00E-02 | 5291.08 | 1911.583 | 5278175 | 0.000362167 | 362.1674737 |
| 4.00E-02 | 972.46 | 4.00E-02 | 0.240162 | 4.00E-02 | 3843.29 | 1401.288 | 3833916 | 0.000365498 | 365.4977189 |
| 6.00E-02 | 978.537 | 6.00E-02 | 0.179483 | 6.00E-02 | 2872.55 | 1053.785 | 2865544 | 0.000367743 | 367.7432952 |
| 8.00E-02 | 981.791 | 8.00E-02 | 0.146713 | 8.00E-02 | 2349.13 | 864.249 | 2343400 | 0.000368801 | 368.8012477 |
| 0.1 | 983.007 | 0.1 | 0.133742 | 0.1 | 2140.7 | 788.8159 | 2135479 | 0.000369386 | 369.3850764 |

| turbulent | | density | | Fraction | | surface | constat | top | bottom | d32 |
|---|---|---|---|---|---|---|---|---|---|---|
| intensity | 0 | 972.765 | 0 | 0.174728 | 0 | 2796.88 | 997.561 | 1019.816 | 2790058 | 0.000366 |
| 0.2 | 0.003556 | 973.306 | 0.003556 | 0.171359 | 0.003556 | 2743.42 | 997.561 | 1000.708 | 2736729 | 0.000366 |
| | 0.007111 | 977.753 | 0.007111 | 0.140006 | 0.007111 | 2242 | 997.561 | 821.3477 | 2236532 | 0.000367 |
| | 0.010667 | 984.425 | 0.010667 | 0.093188 | 0.010667 | 1492.8 | 997.561 | 550.4172 | 1489159 | 0.00037 |
| | 0.014222 | 990.672 | 0.014222 | 0.05019 | 0.014222 | 804.67 | 997.561 | 298.3316 | 802707.4 | 0.000372 |
| | 0.017778 | 994.083 | 0.017778 | 0.027038 | 0.017778 | 433.97 | 997.561 | 161.2693 | 432911.5 | 0.000373 |
| | 0.021333 | 995.702 | 0.021333 | 0.016281 | 0.021333 | 261.627 | 997.561 | 97.26615 | 260988.9 | 0.000373 |
| | 0.024889 | 996.059 | 0.024889 | 0.014012 | 0.024889 | 225.163 | 997.561 | 83.74127 | 224613.8 | 0.000373 |
| | 0.028444 | 996.23 | 0.028444 | 0.013016 | 0.028444 | 209.197 | 997.561 | 77.79919 | 208686.8 | 0.000373 |
| | 0.032 | 996.246 | 0.032 | 0.013027 | 0.032 | 209.335 | 997.561 | 77.86798 | 208824.4 | 0.000373 |

| 0.05 | | density | | fraction | | surface | top | bottom | d32 | |
|---|---|---|---|---|---|---|---|---|---|---|
| | 0 | 977.994 | 0 | 0.174832 | 0 | 2797.87 | 1025.908 | 2791046 | 0.000368 | 367.5711 |
| | 0.003556 | 978.52 | 0.003556 | 0.169942 | 0.003556 | 2719.72 | 997.7499 | 2713087 | 0.000368 | 367.7545 |
| | 0.007111 | 982.217 | 0.007111 | 0.1365 | 0.007111 | 2184.69 | 804.4357 | 2179362 | 0.000369 | 369.1153 |
| | 0.010667 | 987.619 | 0.010667 | 0.087915 | 0.010667 | 1407.34 | 520.9574 | 1403907 | 0.000371 | 371.0767 |
| | 0.014222 | 992.487 | 0.014222 | 0.044334 | 0.014222 | 710.048 | 264.0055 | 708316.2 | 0.000373 | 372.7227 |
| | 0.017778 | 995.013 | 0.017778 | 0.02174 | 0.017778 | 348.527 | 129.7871 | 347676.9 | 0.000373 | 373.298 |
| | 0.021333 | 996.093 | 0.021333 | 0.012146 | 0.021333 | 195.017 | 72.58888 | 194541.4 | 0.000373 | 373.1283 |
| | 0.024889 | 996.302 | 0.024889 | 0.0103 | 0.024889 | 165.48 | 61.57326 | 165076.4 | 0.000373 | 372.9986 |
| | 0.028444 | 996.405 | 0.028444 | 0.009396 | 0.028444 | 151.01 | 56.17542 | 150641.7 | 0.000373 | 372.9075 |
| | 0.032 | 996.431 | 0.032 | 0.009168 | 0.032 | 147.345 | 54.81299 | 146985.6 | 0.000373 | 372.914 |

| | | 0deg | 20 deg | 48 deg | 90 deg | | turb models | | |
|---|---|---|---|---|---|---|---|---|---|
| viscosity | 0 | 336.9887 | 335.6467 | 331.6081 | 326.4109 | | d32 sand | d32RNG | d32Rea |
| | 0.01333 | 356.6421 | 356.0862 | 353.8198 | 351.6905 | | 366.8374 | 366.3536 | 366.5126 |
| | 0.02667 | 365.2742 | 364.7548 | 363.8227 | 362.2942 | | 366.9629 | 366.6964 | 366.8289 |
| | 0.04 | 365.7252 | 365.2445 | 364.3508 | 362.7392 | | 368.3691 | 368.8797 | 369.3086 |
| | 0.05333 | 367.1033 | 366.7104 | 365.9947 | 364.5096 | | 370.4769 | 372.6332 | 373.8087 |
| | 0.06667 | 368.082 | 367.7937 | 367.1465 | 365.6176 | | 372.3123 | 378.1795 | 379.8437 |
| | 0.08 | 369.0978 | 368.9885 | 368.3737 | 366.972 | | 373.1004 | 384.7203 | 384.5633 |
| | 0.09333 | 369.377 | 369.351 | 368.6933 | 367.3525 | | 373.2012 | 390.5352 | 385.7258 |
| | 0.10667 | 369.9858 | 369.9471 | 369.264 | 367.9531 | | 373.1552 | 391.6598 | 384.4988 |
| | 0.12 | 370.7039 | 370.4944 | 369.9142 | 368.6889 | | 373.033 | 392.3261 | 383.0019 |
| | | | | | | | 372.9397 | 391.9642 | 381.5263 |

| Q and P | 0.238 | 0.4 | 0.55 | 0.6 | 0.67 |
|---|---|---|---|---|---|
| 2 | 370.7039 | 370.5746 | 369.6154 | 369.6154 | 369.1131 |
| 4 | 369.9858 | 370.0275 | 369.3351 | 369.3351 | 368.627 |
| 6 | 369.377 | 369.436 | 369.0007 | 369.0007 | 368.1205 |
| 8 | 369.0978 | 369.0823 | 368.7849 | 368.7849 | 367.8286 |
| 10 | 368.082 | 367.9461 | 367.7605 | 367.7605 | 366.5889 |
| 12 | 367.1033 | 366.8899 | 366.8075 | 366.8075 | 365.4155 |
| 14 | 365.7252 | 365.5019 | 365.5178 | 365.5178 | 363.8062 |
| 16 | 365.2742 | 365.0367 | 365.1658 | 365.1658 | 363.3898 |
| 18 | 356.6421 | 356.7697 | 357.019 | 357.019 | 353.3401 |
| 20 | 336.9887 | 337.4461 | 338.0476 | 338.0476 | 329.8275 |

**60mm section**

| denisty | | | fraction | 0 | 0.17446 | surface | 0 | 2791.64 | d32 | top | DensityLi | bottom | |
|---|---|---|---|---|---|---|---|---|---|---|---|---|---|
| 60mm | 0 | 975.945 | | 3.56E-03 | 0.171617 | | 3.56E-03 | 2746.26 | | 1021.58 | 997.561 | 2784831.19 | 0.000366837 |
| | 3.56E-03 | 976.319 | | 7.11E-03 | 0.140484 | | 7.11E-03 | 2248.27 | | 1005.318 | 997.561 | 2739561.872 | 0.000366963 |
| | 7.11E-03 | 980.151 | | 1.07E-02 | 9.37E-02 | | 1.07E-02 | 1.50E+03 | | 826.1732 | 997.561 | 2242786.469 | 0.000368369 |
| | 1.07E-02 | 985.931 | | 1.42E-02 | 5.09E-02 | | 1.42E-02 | 8.16E+02 | | 554.2786 | 997.561 | 1496122.037 | 0.000370477 |
| | 1.42E-02 | 991.27 | | 1.78E-02 | 2.82E-02 | | 1.78E-02 | 4.52E+02 | | 303.0086 | 997.561 | 813856.1516 | 0.000372312 |
| | 1.78E-02 | 994.126 | | 2.13E-02 | 1.80E-02 | | 2.13E-02 | 2.89E+02 | | 168.3678 | 997.561 | 451266.6696 | 0.0003731 |
| | 2.13E-02 | 995.424 | | 2.49E-02 | 1.60E-02 | | 2.49E-02 | 2.57E+02 | | 107.4502 | 997.561 | 287915.0583 | 0.000373201 |
| | 2.49E-02 | 995.68 | | 2.84E-02 | 1.54E-02 | | 2.84E-02 | 2.47E+02 | | 95.7191 | 997.561 | 256512.8355 | 0.000373155 |
| | 2.84E-02 | 995.769 | | 3.20E-02 | 1.56E-02 | | 3.20E-02 | 2.50E+02 | | 91.80353 | 997.561 | 246100.2938 | 0.000373033 |
| | 3.20E-02 | 995.746 | | | | | | | | 93.17195 | 997.561 | 249831.172 | 0.00037294 |
| | | | | | | | | | | 0 | | | |

**80mm section**

| | | | | | | | | | | top | bottom | | |
|---|---|---|---|---|---|---|---|---|---|---|---|---|---|
| denisty | 0 | 979.722 | fraction | 0 | 0.144426 | surface | 0 | 2310.9 | | 848.984 | 2305264 | 0.000368281 | 368.2806318 |
| 80mm | 3.56E-03 | 979.737 | | 3.56E-03 | 0.14452 | | 3.56E-03 | 2312.46 | | 849.5495 | 2306820 | 0.000368277 | 368.2773604 |
| | 7.11E-03 | 981.438 | | 7.11E-03 | 0.130726 | | 7.11E-03 | 2091.88 | | 769.7968 | 2086778 | 0.000368893 | 368.8925315 |
| | 1.07E-02 | 984.72 | | 1.07E-02 | 0.104152 | | 1.07E-02 | 1666.8 | | 615.3633 | 1662735 | 0.000370091 | 370.091124 |
| | 1.42E-02 | 988.39 | | 1.42E-02 | 7.46E-02 | | 1.42E-02 | 1194.17 | | 442.4431 | 1191257 | 0.000371408 | 371.4084715 |
| | 1.78E-02 | 991.963 | | 1.78E-02 | 4.60E-02 | | 1.78E-02 | 736.033 | | 273.5878 | 734237.8 | 0.000372615 | 372.614641 |
| | 2.13E-02 | 993.884 | | 2.13E-02 | 3.06E-02 | | 2.13E-02 | 490.899 | | 182.7174 | 489701.7 | 0.00037312 | 373.1198494 |
| | 2.49E-02 | 995.009 | | 2.49E-02 | 2.17E-02 | | 2.49E-02 | 347.608 | | 129.4242 | 346760.2 | 0.000373238 | 373.2383636 |
| | 2.84E-02 | 995.395 | | 2.84E-02 | 1.86E-02 | | 2.84E-02 | 298.168 | | 110.9834 | 297440.8 | 0.000373128 | 373.1275907 |
| | 3.20E-02 | 995.596 | | 3.20E-02 | 1.70E-02 | | 3.20E-02 | 272.664 | | 101.4463 | 271999 | 0.000372966 | 372.9655796 |

**100mm section**

| | | | | | | | | | | top | bottom | | |
|---|---|---|---|---|---|---|---|---|---|---|---|---|---|
| density | 0 | 981.36 | Fraction | 0 | 0.131873 | surface | 0 | 2109.95 | | 776.4893 | 2104804 | 0.000368913 | 368.9129181 |
| 100mm | 3.56E-03 | 981.519 | | 3.56E-03 | 0.130858 | | 3.56E-03 | 2093.79 | | 770.6377 | 2088683 | 0.000368959 | 368.958616 |
| | 7.11E-03 | 983.012 | | 7.11E-03 | 0.118973 | | 7.11E-03 | 1903.73 | | 701.7113 | 1899087 | 0.000369499 | 369.49934 |
| | 1.07E-02 | 985.479 | | 1.07E-02 | 9.91E-02 | | 1.07E-02 | 1585.4 | | 585.7766 | 1581533 | 0.000370385 | 370.3852679 |
| | 1.42E-02 | 988.135 | | 1.42E-02 | 7.76E-02 | | 1.42E-02 | 1242.59 | | 460.2814 | 1239559 | 0.000371327 | 371.3266297 |
| | 1.78E-02 | 990.718 | | 1.78E-02 | 5.68E-02 | | 1.78E-02 | 909.797 | | 337.796 | 907578 | 0.000372195 | 372.2195069 |
| | 2.13E-02 | 992.973 | | 2.13E-02 | 3.86E-02 | | 2.13E-02 | 618.312 | | 229.9868 | 616803.9 | 0.000372869 | 372.8686408 |
| | 2.49E-02 | 994.057 | | 2.49E-02 | 2.98E-02 | | 2.49E-02 | 477.302 | | 177.6449 | 476137.9 | 0.000373096 | 373.0956075 |
| | 2.84E-02 | 994.936 | | 2.84E-02 | 2.26E-02 | | 2.84E-02 | 362.459 | | 134.9241 | 361575 | 0.000373157 | 373.1565537 |
| | 3.20E-02 | 995.204 | | 3.20E-02 | 2.04E-02 | | 3.20E-02 | 327.03 | | 121.7013 | 326232.4 | 0.000373051 | 373.0509829 |

**120mm section**

| | | | | | | | | | | top | bottom | | |
|---|---|---|---|---|---|---|---|---|---|---|---|---|---|
| density | 0 | 983.565 | Fraction | 0 | 0.114866 | surface | 0 | 1838.07 | | 677.8691 | 1833587 | 0.000369696 | 369.6956202 |
| 120 | 3.56E-03 | 983.375 | | 3.56E-03 | 0.116469 | | 3.56E-03 | 1863.8 | | 687.1962 | 1859254 | 0.000369609 | 369.6085346 |
| | 7.11E-03 | 984.151 | | 7.11E-03 | 0.110259 | | 7.11E-03 | 1764.58 | | 651.069 | 1760276 | 0.000369868 | 369.8675438 |
| | 1.07E-02 | 985.651 | | 1.07E-02 | 9.81E-02 | | 1.07E-02 | 1570.46 | | 580.2494 | 1566630 | 0.000370381 | 370.3807043 |
| | 1.42E-02 | 987.85 | | 1.42E-02 | 8.02E-02 | | 1.42E-02 | 1284.05 | | 475.3908 | 1280918 | 0.000371133 | 371.1328014 |
| | 1.78E-02 | 989.839 | | 1.78E-02 | 6.40E-02 | | 1.78E-02 | 1025.01 | | 380.1689 | 1022510 | 0.0003718 | 371.7996404 |
| | 2.13E-02 | 991.8 | | 2.13E-02 | 4.81E-02 | | 2.13E-02 | 769.957 | | 286.0395 | 768079.1 | 0.000372409 | 372.4089007 |
| | 2.49E-02 | 993.251 | | 2.49E-02 | 3.63E-02 | | 2.49E-02 | 582.291 | | 216.5637 | 580870.8 | 0.000372826 | 372.8259078 |
| | 2.84E-02 | 994.098 | | 2.84E-02 | 2.95E-02 | | 2.84E-02 | 472.757 | | 175.9255 | 471603.9 | 0.000373037 | 373.0365801 |
| | 3.20E-02 | 994.606 | | 3.20E-02 | 2.54E-02 | | 3.20E-02 | 406.652 | | 151.3649 | 405660.2 | 0.000373132 | 373.1322886 |

**mass fraction**

| radial | mass fraction 60mm | radial | mass fraction 80mm | radial | massfraction 100mm | radial | mass fraction 120mm |
|---|---|---|---|---|---|---|---|
| 0 | 0.17446 | 0 | 0.144426 | 0 | 0.131873 | 0 | 0.114866 |
| 0.003556 | 0.171617 | 0.003556 | 0.14452 | 0.003556 | 0.130858 | 0.003556 | 0.116469 |
| 0.007111 | 0.140484 | 0.007111 | 0.130726 | 0.007111 | 0.118973 | 0.007111 | 0.110259 |
| 0.010667 | 0.093698 | 0.010667 | 0.104152 | 0.010667 | 0.099068 | 0.010667 | 0.0981161 |
| 0.014222 | 0.050946 | 0.014222 | 0.074607 | 0.014222 | 0.077635 | 0.014222 | 0.0802063 |
| 0.017778 | 0.028227 | 0.017778 | 0.045967 | 0.017778 | 0.056827 | 0.017778 | 0.0640119 |
| 0.021333 | 0.017991 | 0.021333 | 0.03064 | 0.021333 | 0.038602 | 0.021333 | 0.0480674 |
| 0.024889 | 0.016022 | 0.024889 | 0.021679 | 0.024889 | 0.029785 | 0.024889 | 0.0363392 |
| 0.028444 | 0.015366 | 0.028444 | 0.018583 | 0.028444 | 0.022602 | 0.028444 | 0.029495 |
| 0.032 | 0.015595 | 0.032 | 0.016983 | 0.032 | 0.020381 | 0.032 | 0.0253643 |

**Surface density**

| radial | surface 60mm | radial | surface 80mm | radial | surface 100mm | radial | surface 120mm |
|---|---|---|---|---|---|---|---|
| 0 | 2791.64 | 0 | 2310.9 | 0 | 2109.95 | 0 | 1838.07 |
| 0.003556 | 2746.26 | 0.003556 | 2312.46 | 0.003556 | 2093.79 | 0.003556 | 1863.8 |
| 0.007111 | 2248.27 | 0.007111 | 2091.88 | 0.007111 | 1903.73 | 0.007111 | 1764.58 |
| 0.010667 | 1499.78 | 0.010667 | 1666.8 | 0.010667 | 1585.4 | 0.010667 | 1570.46 |
| 0.014222 | 815.846 | 0.014222 | 1194.17 | 0.014222 | 1242.59 | 0.014222 | 1284.05 |
| 0.017778 | 452.37 | 0.017778 | 736.033 | 0.017778 | 909.797 | 0.017778 | 1025.01 |
| 0.021333 | 288.619 | 0.021333 | 490.899 | 0.021333 | 618.312 | 0.021333 | 769.957 |
| 0.024889 | 257.14 | 0.024889 | 347.608 | 0.024889 | 477.302 | 0.024889 | 582.291 |
| 0.028444 | 246.702 | 0.028444 | 298.168 | 0.028444 | 362.459 | 0.028444 | 472.757 |
| 0.032 | 250.442 | 0.032 | 272.664 | 0.032 | 327.03 | 0.032 | 406.652 |

**60 mm mean drop size SMD**

| radial | d32 60mm | radial | d32 80mm | rdaial | d32 100mm | radial | d32 120mm |
|---|---|---|---|---|---|---|---|
| 0 | 366.8374 | 0 | 368.2806 | 0 | 368.9129 | 0 | 369.6956202 |
| 0.003556 | 366.9629 | 0.003556 | 368.2774 | 0.003556 | 368.9586 | 0.003556 | 369.6085346 |
| 0.007111 | 368.3691 | 0.007111 | 368.8925 | 0.007111 | 369.4993 | 0.007111 | 369.8675438 |
| 0.010667 | 370.4768 | 0.010667 | 370.0911 | 0.010667 | 370.3853 | 0.010667 | 370.3807043 |
| 0.014222 | 372.3123 | 0.014222 | 371.4085 | 0.014222 | 371.3266 | 0.014222 | 371.1328014 |
| 0.017778 | 373.1004 | 0.017778 | 372.6146 | 0.017778 | 372.195 | 0.017778 | 371.7996404 |
| 0.021333 | 373.2012 | 0.021333 | 373.1198 | 0.021333 | 372.8686 | 0.021333 | 372.4089007 |
| 0.024889 | 373.1552 | 0.024889 | 373.2384 | 0.024889 | 373.0956 | 0.024889 | 372.8259078 |
| 0.028444 | 373.033 | 0.028444 | 373.1276 | 0.028444 | 373.1566 | 0.028444 | 373.0365801 |
| 0.032 | 372.9397 | 0.032 | 372.9656 | 0.032 | 373.051 | 0.032 | 373.1322886 |

279

Appendix III       **Modified LHD Matlab Code and DoE Cases**

**Modified Latin Hypercube Matlab code for Design of Experiments(DoE)**
```
function
[X_scaled,X_normalized]=lhsdesign_modified(n,min_ranges_p,max_ranges_p)
%lhsdesign_modified is a modification of the Matlab Statistics function lhsdesign.
%It might be a good idea to jump straight to the example to see what does
%this function do.
%The following is the description of lhsdesign from Mathworks documentation
% X = lhsdesign(n,p) returns an n-by-p matrix, X, containing a latin hypercube sample
of n values on each of p variables.
%For each column of X, the n values are randomly distributed with one from each
interval (0,1/n), (1/n,2/n), ..., (1-1/n,1), and they are randomly permuted.
%lhsdesign_modified provides a latin hypercube sample of n values of
%each of p variables but unlike lhsdesign, the variables can range between
%any minimum and maximum number specified by the user, where as lhsdesign
%only provide data between 0 and 1 which might not be very helpful in many
%practical problems where the range is not bound to 0 and 1
%Inputs:
%      n: number of radomly generated data points
%      min_ranges_p: [1xp] or [px1] vector that contains p values that correspond to the
minimum value of each variable
%      max_ranges_p: [1xp] or [px1] vector that contains p values that correspond to the
maximum value of each variable
%Outputs
%      X_scaled: [nxp] matrix of randomly generated variables within the
%      min/max range that the user specified
%      X_normalized: [nxp] matrix of randomly generated variables within the
%      0/1 range
%      figure
%      subplot(2,1,1),plot(X_scaled(:,1),X_scaled(:,2),'*')
%      title('Random Variables')

%      xlabel('X1')

%      ylabel('X2')

%      grid on

%      subplot(2,1,2),plot(X_normalized(:,1),X_normalized(:,2),'r*')

%      title('Normalized Random Variables')

%      xlabel('Normalized X1')

%      ylabel('Normalized X2')

%      grid on

p=length(min_ranges_p);
[M,N]=size(min_ranges_p);
if M<N
    min_ranges_p=min_ranges_p';
end

[M,N]=size(max_ranges_p);
if M<N
    max_ranges_p=max_ranges_p';
```

```
end

slope=max_ranges_p-min_ranges_p;
offset=min_ranges_p;

SLOPE=ones(n,p);
OFFSET=ones(n,p);

for i=1:p
   SLOPE(:,i)=ones(n,1).*slope(i);
   OFFSET(:,i)=ones(n,1).*offset(i);
end
X_normalized = lhsdesign(n,p);

X_scaled=SLOPE.*X_normalized+OFFSET;
```

**Corner points**
```
DOE2 =[];
for x4 = [min, max]
   % the fouth parameter
   for x3 = [min, max]
      % third parameter
      for x2 = [min, max]
         % second parameter
         for x = [min, max]
      % first parameter
      DOE2 = [DOE2; x,x2,x3,x4];
      % the number of x should be equal to the number parameters
         end
      end
   end
end
```

**Intermediary points**
```
steps = n
doe(:,1) = linspace(min, max, steps);  %first parameter contains increment
% linspace(min value, max value, steps)
doe(:,2) = lhsdesign_modified(steps, min, max); %second parameter random
distribution
%lhsdesign_modified(steps,min value,max value)
doe(:,3)= lhsdesign_modified(n, min, max);
doe(:,4) = lhsdesign_modified(n, min, max);

%subplot creat figure matrix (mxn) figure number  m columns, n rows
% subplot(m,n,figure number)
subplot(3,2,1)
plot(doe(:,1),doe(:,2),'b.')
 xlabel('DV_1');ylabel('DV_2');

% Distributions
subplot(3,2,2)
```

```
plot(doe(:,1),doe(:,3),'b.')
 xlabel('DV_1');ylabel('DV_3');

subplot(3,2,3)
plot(doe(:,1),doe(:,4),'b.')
xlabel('DV_1');ylabel('DV_4');

subplot(3,2,4)
plot(doe(:,2),doe(:,3),'b.')
xlabel('DV_2');ylabel('DV_3');

subplot(3,2,5)
plot(doe(:,2),doe(:,4),'.')
xlabel('DV_2');ylabel('DV_4');

subplot(3,2,6)
plot(doe(:,3),doe(:,4),'b.')
 xlabel('DV_3');ylabel('DV_4');
```

**Table 8.1 4-Factor Design of Experiment(DoE) Points**

| | DV1(viscosity) | DV2(Surf.Tension) | DV3(NozzleDia) | DV4(Liq.Vel) |
|---|---|---|---|---|
| | Design of Experiment (DoE) points for CFD Based Design Optimization | | | |
| 1 | 0.00031 | 20 | 1.5 | 1 |
| 2 | 0.2 | 20 | 1.5 | 1 |
| 3 | 0.00031 | 75 | 1.5 | 1 |
| 4 | 0.2 | 75 | 1.5 | 1 |
| 5 | 0.00031 | 20 | 3.5 | 1 |
| 6 | 0.2 | 20 | 3.5 | 1 |
| 7 | 0.00031 | 75 | 3.5 | 1 |
| 8 | 0.2 | 75 | 3.5 | 1 |
| 9 | 0.00031 | 20 | 1.5 | 6 |
| 10 | 0.2 | 20 | 1.5 | 6 |
| 11 | 0.00031 | 75 | 1.5 | 6 |
| 12 | 0.2 | 75 | 1.5 | 6 |
| 13 | 0.00031 | 20 | 3.5 | 6 |
| 14 | 0.2 | 20 | 3.5 | 6 |
| 15 | 0.00031 | 75 | 3.5 | 6 |
| 16 | 0.2 | 75 | 3.5 | 6 |
| 17 | 0.00031 | 35.71429 | 2.7 | 1.07143 |
| 18 | 0.003163 | 49.07143 | 1.67143 | 4.21429 |
| 19 | 0.006015 | 27.85714 | 2.1 | 3 |
| 20 | 0.008868 | 30.21429 | 3.24286 | 3.14286 |
| 21 | 0.011721 | 61.64286 | 2.75714 | 2.28571 |
| 22 | 0.014574 | 50.64286 | 3.38571 | 1.21429 |
| 23 | 0.017426 | 45.14286 | 2.38571 | 2.35714 |
| 24 | 0.020279 | 46.71429 | 1.64286 | 1.14286 |
| 25 | 0.023132 | 37.28571 | 3.35714 | 2 |
| 26 | 0.025984 | 53 | 3.47143 | 3.71429 |
| 27 | 0.028837 | 42.78571 | 2.9 | 5.64286 |
| 28 | 0.03169 | 45.92857 | 2.35714 | 5.71429 |
| 29 | 0.034543 | 63.21429 | 1.95714 | 3.57143 |
| 30 | 0.037395 | 65.57143 | 3.32857 | 1.57143 |
| 31 | 0.040248 | 34.14286 | 2.01429 | 5.28571 |
| 32 | 0.043101 | 69.5 | 2.5 | 1.35714 |
| 33 | 0.045953 | 60.07143 | 2.04286 | 5.85714 |

| 34 | 0.048806 | 22.35714 | 2.32857 | 4.85714 |
|----|----------|----------|---------|---------|
| 35 | 0.051659 | 71.07143 | 3.15714 | 3.35714 |
| 36 | 0.054512 | 34.92857 | 1.75714 | 3.07143 |
| 37 | 0.057364 | 48.28571 | 3.5 | 5.57143 |
| 38 | 0.060217 | 21.57143 | 2.67143 | 2.42857 |
| 39 | 0.06307 | 72.64286 | 1.87143 | 4.57143 |
| 40 | 0.065922 | 60.85714 | 1.84286 | 1.71429 |
| 41 | 0.068775 | 67.14286 | 2.44286 | 5 |
| 42 | 0.071628 | 24.71429 | 3.41429 | 2.85714 |
| 43 | 0.074481 | 44.35714 | 1.5 | 4.92857 |
| 44 | 0.077333 | 52.21429 | 2.87143 | 1.5 |
| 45 | 0.080186 | 28.64286 | 3.07143 | 1.42857 |
| 46 | 0.083039 | 57.71429 | 2.41429 | 2.71429 |
| 47 | 0.085891 | 74.21429 | 2.64286 | 2.21429 |
| 48 | 0.088744 | 33.35714 | 2.72857 | 5.92857 |
| 49 | 0.091597 | 36.5 | 2.24286 | 4 |
| 50 | 0.09445 | 39.64286 | 3.44286 | 3.78571 |
| 51 | 0.097302 | 25.5 | 2.21429 | 1.92857 |
| 52 | 0.100155 | 56.92857 | 3.3 | 2.78571 |
| 53 | 0.103008 | 38.07143 | 2.78571 | 2.64286 |
| 54 | 0.10586 | 20.78571 | 3.01429 | 3.92857 |
| 55 | 0.108713 | 23.92857 | 1.92857 | 5.21429 |
| 56 | 0.111566 | 59.28571 | 1.81429 | 6 |
| 57 | 0.114419 | 66.35714 | 3.21429 | 5.5 |
| 58 | 0.117271 | 58.5 | 2.3 | 1 |
| 59 | 0.120124 | 75 | 2.84286 | 4.42857 |
| 60 | 0.122977 | 32.57143 | 3.27143 | 5.35714 |
| 61 | 0.125829 | 73.42857 | 2.18571 | 5.07143 |
| 62 | 0.128682 | 70.28571 | 1.7 | 3.85714 |
| 63 | 0.131535 | 67.92857 | 3.04286 | 3.5 |
| 64 | 0.134388 | 53.78571 | 2.58571 | 5.42857 |
| 65 | 0.13724 | 51.42857 | 3.18571 | 4.78571 |
| 66 | 0.140093 | 56.14286 | 1.55714 | 1.85714 |
| 67 | 0.142946 | 54.57143 | 1.52857 | 4.35714 |

| | | | | |
|---|---|---|---|---|
| 68 | 0.145798 | 68.71429 | 2.07143 | 1.64286 |
| 69 | 0.148651 | 41.21429 | 1.9 | 5.78571 |
| 70 | 0.151504 | 29.42857 | 1.58571 | 2.57143 |
| 71 | 0.154357 | 31.78571 | 2.98571 | 3.42857 |
| 72 | 0.157209 | 23.14286 | 1.72857 | 4.14286 |
| 73 | 0.160062 | 38.85714 | 3.12857 | 1.28571 |
| 74 | 0.162915 | 26.28571 | 2.81429 | 5.14286 |
| 75 | 0.165767 | 49.85714 | 2.27143 | 4.28571 |
| 76 | 0.16862 | 27.07143 | 2.12857 | 4.71429 |
| 77 | 0.171473 | 20 | 2.61429 | 3.21429 |
| 78 | 0.174326 | 40.42857 | 1.78571 | 4.07143 |
| 79 | 0.177178 | 47.5 | 2.55714 | 2.5 |
| 80 | 0.180031 | 64 | 3.1 | 2.14286 |
| 81 | 0.182884 | 43.57143 | 1.61429 | 1.78571 |
| 82 | 0.185736 | 62.42857 | 2.15714 | 2.92857 |
| 83 | 0.188589 | 64.78571 | 1.98571 | 4.64286 |
| 84 | 0.191442 | 55.35714 | 2.95714 | 3.28571 |
| 85 | 0.194295 | 42 | 2.92857 | 4.5 |
| 86 | 0.197147 | 31 | 2.47143 | 2.07143 |
| 87 | 0.2 | 71.85714 | 2.52857 | 3.64286 |

Appendix IV      **MATLAB CODE FOR LSQCURVEFIT**

**MATLAB CODE FOR LSQCURVEFIT**

function [x,resnorm,residual,exitflag,output,lambda,jacobian] =
ascona(x0,xdata,ydata,PrecondBandWidth_Data)

%    xdata1 Input : DV1viscosity

%    xdata2 Input : DV2SurfTension

%    xdata3 Input : DV3Massflow

%    xdata4 Input : DV4Pressure

%    ydata Output : SMD

options = optimoptions('lsqcurvefit');

%% Modify options setting

options = optimoptions(options,'Display', 'off');

options = optimoptions(options,'PrecondBandWidth', PrecondBandWidth_Data);

[x,resnorm,residual,exitflag,output,lambda,jacobian] = ...

lsqcurvefit(@(x,xdata)x(1)*xdata1.^x(2).*xdata2.^x(3).*xdata3.^x(4).*xdata4.^x(5),x0
,xdata,ydata,[],[],options);

% x(1)= λ, x(2)= a, x(3)= b, x(4)= c, x(5)= d

xdata = [xdata1, xdata2, xdata3, xdata4];

ydata = [ydata];

% x = [x(1), x(2), x(3), x(4), x(5)]

x0 = [Initial point];

end